Creep lifing methods for components under high temperature creep.

Abdallah, Zakaria

Swansea University
Prifysgol Abertawe

CREEP LIFING METHODS

FOR

COMPONENTS UNDER HIGH TEMPERATURE CREEP

ZAKARIA A. M. ABDALLAH
(B.SC MECHANICAL ENGINEERING, M.Res MATERIALS ENGINEERING)

Thesis submitted to the Faculty of
Materials Engineering at Swansea University
in partial fulfilment of the requirements for the degree of

DOCTOR OF PHILOSOPHY, Ph.D
IN
(POWER/AEROSPACE) MATERIALS ENGINEERING

MAJOR SUPERVISORS

Swansea University
Prifysgol Abertawe

Dr. Karen Perkins
(Academic Supervisor)

Mr. Steve Williams
(Industrial Supervisor)

30th September 2010
Swansea, United Kingdom

ProQuest LLC.
789 East Eisenhower Parkway
P.O. Box 1346
Ann Arbor, MI 48106 – 1346

DECLARATION

I hereby certify that this work has not previously been accepted in substance for any degree and is not being concurrently submitted in candidature for any degree.

Signed: ... . (Candidate)

Date: .....30th September 2010……..

STATEMENT 1

I hereby certify that this thesis is the result of my own investigations, except where otherwise stated. Where correction services have been used, the extent and nature of the correction is clearly marked in a footnote(s). Other sources are acknowledged by giving explicit references. For this purpose, a bibliography is appended.

Signed: ... . (Candidate)

Date: ..... 30th September 2010……..

STATEMENT 2

I hereby give consent for my thesis, if accepted, to be available for photocopying and for inter-library loan, and for the title and summary to be made available to outside organisations.

Signed: ... . (Candidate)

Date: ..... 30th September 2010……..

STATEMENT 3

I hereby give consent for my thesis, if accepted, to be available for photocopying and for inter-library loans after expiry of a bar on access approved by Swansea University.

Signed: .... (Candidate)

Date: ..... 30th September 2010……..

CREEP LIFING METHODS
FOR
COMPONENTS UNDER HIGH TEMPERATURE CREEP

ZAKARIA A. M. ABDALLAH

(ABSTRACT)

Structural alloys applied to Aerospace and Power Generation applications are expected to operate at temperatures exceeding those originally envisaged during design to meet the tightening regulations on emissions, satisfy the 'green lobby' and improve the efficiency of operation. Extended periods of high stresses over time will induce creep deformation and eventually static failure in such alloys. Current empirical methods to predict creep performance are restricted by the amount of long-term creep data generated on the international stage, as such generation of data is a matter of time and cost. To alleviate this shortfall in measured data, a novel extrapolation methodology, the Wilshire equations, has been developed at Swansea University for long-term creep predictions. In the current research work, this new methodology has been widely studied and successfully used to predict the long-term creep behaviour of a selected aerospace alloy. Titanium IMI834, currently employed in aerospace industry, has been used as the model material to enable sensitivity studies, examine and correlate creep performance to the microstructure and deformation mechanisms using this technique. For this purpose, tensile, stress relaxation, creep, creep-step or cyclic creep, and creep-vacuum tests have been carried out on Titanium IMI834 in order to study the deformation behaviour of this alloy and to run the new model. The Metallurgical work involved studying the behaviour of this alloy under creep and cyclic creep conditions (in both air and vacuum) and the oxidising layer developed on the surface of this alloy, the alpha-case, has also been thoroughly studied under different conditions of stresses and temperatures. Besides, the surface cracks were studied and predictions based on the actual measurements were obtained. Other parametric techniques have been critically reviewed, examined and compared to the Wilshire technique creep predictions. As a milestone of this project, full creep curves were accurately re-constructed, based on this technique, at all stresses and temperatures and compared with the available creep curves.

ACKNOWLEDGMENTS

I would like to thank many people without whom this project would not have been successfully completed. First, I would like to express my deep gratitude to ***Dr. Karen Perkins***, my academic supervisor at Swansea University, for her guidance, encouragement and support. I do appreciate the time she has devoted for me to make this project successful and the knowledge that I had from her which will stay with me always, wherever and whenever I work in the future. I would also like to thank and extend my gratitude to ***Mr. Steve Williams***, my industrial supervisor at Rolls-Royce plc, who was always there to support and guide me throughout my project. His ideas and knowledge have enriched my experience in this field of science and his efforts and suggestions were behind the success of this project. I would like to thank ***Prof. Brian Wilshire*** for selecting me to carry out this project using the new methodology that he developed. My deepest gratitude goes to ***Prof. Martin Bache*** for his continuous support and help on many occasions along the period of my project without which I would never be able to start my PhD at Swansea University. My gratitude and special thanks must be expressed to ***Dr. Mark Whittaker*** for his help and advice always during my project. His support in the early stages of my project is very highly appreciated which gave me a great motivation to carry out the necessary practical work in the labs. Also, I would like to thank ***Dr. Elizabeth Sackett*** and ***Dr. William Harrison*** for their continuous assistance and support in many occasions and particularly in the practical and analytical work of my project. My thanks also go to ***Mrs. Veronica Holding*** for her efforts in the school of materials engineering at Swansea University and Rolls-Royce plc University Technology Centre (UTC).

My special and deepest thanks go to my ***Mother***, for her love, care and blessings, and all my brothers, especially ***Dr. Khaled***, for his continuous and unforgettable support during my study, ***Ali***, who was the first person who supported and encouraged me after my first degree and ***Allam***, who was the main person who motivated me to pursue my study in the UK. I present this degree to my ***Father***, whom I wish was alive to celebrate this achievement with me, for his encouragement to us always to study and succeed.

I would also like to thank my ***Officemates***, ***Colleagues*** and ***Friends*** who have directly or indirectly influenced my stay in Swansea. The Materials Engineering Department at ***Swansea University*** and ***Rolls-Royce plc*** deserve my sincere appreciation for providing me the opportunity to pursue my study in Swansea.

TABLE OF CONTENTS

APPENDIX (A): CONTENTS

APPENDIX (B): CONTENTS

APPENDIX (C): CONTENTS

APPENDIX (D): CONTENTS

CHAPTER 1

INTRODUCTION

The drive towards more efficient gas turbines and the associated reductions in greenhouse emissions require the existing gas turbines to operate under higher severe temperatures. However, this aim is restricted by the limitation of the materials used in such harsh environments which may, eventually, lead to the deformation and failure of these components. In order to avoid such catastrophic failures and increase the efficiency, future designs must utilise novel or improved alloy systems with an enhanced temperature capability. One key material property that governs the life of many components within the gas turbine is creep. A detailed understanding of the creep behaviour of materials is seen as an essential requirement. However, understanding and predicting the creep properties is a very important challenge for researchers, which is the basis of this study. Therefore, the current research will thoroughly concentrate and investigate the long-term creep predictions of materials as well as their behavioural attributes under the applied stresses and temperatures.

1.1 GENERAL

There are many applications where materials are required to survive, without failure, for long periods in severe environments characterised by high stresses and temperatures. The best practical application which exemplifies this aim is the gas turbine where many components are subjected to very high temperatures, resulting from the hot gas stream, and stresses, resulting from the rotational speeds. Therefore, when selecting materials for high temperature components, the resistance of these materials to deformation and failure over long periods of time must be assessed and evaluated in order to avoid creep failures [1].

Creep is defined as the plastic deformation of materials under the effect of high stresses and temperatures for long durations of time which, eventually, leads to fracture. Generally speaking, problems of creep failure and excessive distortion are experienced at temperatures equal, or just above, to the half of the melting temperature, T_M, of a material. It might be possible to avoid creep problems by either selecting materials of high melting temperatures or maintaining the operation temperatures far away from those at which creep could take place, typically less than the third of the melting point of a material. However, these simple solutions do not provide a comprehensive and convincing answer to the problem. On one hand, materials of

high melting temperatures can be developed and employed but will still show creep deformation under the high stresses and temperatures encountered in such applications. On the other hand, if temperatures are lowered to less than the third of the melting temperature, this will, in return, lower the efficiency, which is undesirable in these applications. Therefore, the design stage is the crucial part of the industrial process where decisions should be taken so as to avoid the long-term creep failures [1].

During the design stage, a comprehensive study and analysis of a material's behaviour should be made before this material is considered for a particular application. For certain applications, this might be adequate but for fundamental studies of creep behaviour, full creep curves must be available. For this purpose, creep tests can be carried out at different stresses and temperatures in order to provide the designer with the necessary information to study and analyse the long-term behaviour of materials under the applied stresses and temperatures. Various types of tests were developed for such purposes wherein a specimen is subjected to a tensile load, at a specified temperature, and its elongation over time is recorded [1]. The 'Stress-Rupture' test is one of the creep tests in which the specimen's time to fracture, t_f, and its creep ductility at fracture, ε_f, are measured. This test defines only the fracture point of a material without providing any information about the shape of the creep curve, i.e. no creep curves are recorded in such tests. Whereas the 'Normal Creep' test provides not only the previous fracture coordinates, but also the whole plot of the full creep curve at the selected stress and temperature. However, as the cross sectional area of the specimen continuously decreases while the creep test is ongoing under a constant load, the stress on the specimen will, thus, vary accordingly. To avoid this variation, the 'Constant-Stress' creep test was introduced in order to keep the stress constant during creep by using a profiled cam mechanism [1, 2].

It is also well known that large variations, or scatter, might exist in the generated data. Many sources of scatter might exist, such as: inaccurate measurements of the diameter of the specimens, the applied load and thus, the applied stresses, the gauge length, the specimen's temperature if the thermocouples were not accurately calibrated and the extension, or the strain, if the extensometers were not well calibrated. Moreover, scatter might be a result of the existence of surface defects and scratches which can become possible sources of surface cracks leading to a premature failure of the material. Therefore, a designer must consider this fact when using such information for practical purposes. However, as long as the data are available, studies can be carried out in order to predict the creep behaviour under different applied conditions. Since it is impractical to perform creep tests for the entire lifetime of some real applications, particularly when lifetimes can range, for instance, from 20,000 to 120,000 hours as in the power generation applications, determining a conservative and an acceptable method for extrapolating the short-term measurements is a

significant goal. Alternatively, for aerospace applications, where the time to a certain percentage strain is more desirable, this method should also provide accurate predictions of the creep behaviour based on this criterion. Starting from this point, many extrapolation techniques were devised for the purpose of predicting the long-term creep behaviour of materials without the need to carry out practical tests which could last for many years before being able to size and manufacture the required components. Minimising the scale of these larger tests will, in return, reduce the cost and save the time needed for such long-term tests. Hence, these predictions require short-term data to be available from the various types of creep tests at the same conditions as the actual application. Extrapolation methods must take into consideration that creep is a critical function of stress and temperature, i.e. a relatively small change in either of these quantities can drastically affect the material's lifetime. These methods are being used to predict both creep-rupture and creep-deformation behaviours, in which the former has received a greater attention than the latter as a result of the more drastic consequences of brittle failures, i.e. sudden rupture, compared with ductile failures, i.e. excess deformation [2].

1.2 Project Highlights

The first part of this research will review the traditional parametric models, most of which proved their invalidity in predicting the creep properties based on short-term measurements, indicating the flaws and limitations involved in their use for such purposes which, thus, led to overestimations of the real lifetime of many materials and could have caused potentially catastrophic consequences. Furthermore, it will show that the inaccuracy involved with these techniques is a result of ignoring some parameters and factors affecting the real creep behaviour of practical applications. In addition, it will prove that many of these techniques were based on individual assumptions which are not necessarily taking place during creep deformation and led, thus, to many errors and overestimations in the long-term predictions. For this reason, any lifing technique should be accurate, acceptable and generally conservative.

An overview of a new methodology will be presented taking into consideration the flaws and the errors involved in the previous proposed techniques. It will be shown that this new methodology was based on parameters that have physical meaning in contrast to most of the traditional techniques that have only involved 'variable constants' or 'fitting parameters' which did not necessarily have any physical explanations.

The research will then detail the practical work that has been carried out on the aerospace alloy, Titanium IMI834, which included: tensile, stress relaxation, creep, creep-step and creep-vacuum tests. Besides, the metallurgical work that has been done on each fractured specimen, which included metallographic and

fractographic work using the Optical and the Scanning Electron Microscopy (SEM), will also be discussed so as to understand the microstructural behaviour under the different types of testing. The oxidation of the surface layer, i.e. the alpha-case, encountered at high temperatures will be thoroughly studied and related to the initiation of the surface cracks from which the depth of these cracks can be predicted based on the actual measurements.

The analytical part will compare the results of the new technique with those of the other traditional methods and relate them to the microstructural studies that have been carried out in order to understand the physical meaning of this new technique. For the first time, as a major step forward in creep predictions, the new technique will be extended to provide full creep curves at all stresses and temperatures which will be compared with the actual creep curves previously obtained under the same conditions.

CHAPTER 2

BACKGROUND & LITERATURE REVIEW

The deformation of metals due to creep mechanisms presents a huge problem in power plants and aeroengine applications where higher temperatures are required to achieve higher efficiencies. However, this increase in efficiency is encountered by the limitation of materials to withstand such an increase in temperatures. Therefore, the design stage is very critical and essential in order to offset the possibilities of failure by excessive deformation. This aim can be achieved by predicting the creep behaviour under the applied stresses and temperatures. For this purpose, a variety of parametric methods for extrapolating short-term creep data were developed to quantify creep and creep fracture in the high temperature components. These approaches will be discussed and critically reviewed illustrating their limitations by reference to information openly available for many materials.

2.1 REVIEW OF CREEP PHENOMENON

Creep is defined as the plastic deformation of materials under the effect of a constant load and temperature for a long duration of time [3]. Applying a constant tensile load to a specimen that is maintained under a constant temperature, i.e. a constant-load test, enables us to determine the engineering creep properties of a material by recording its strain, ε, as a function of time, t [4]. However, during this constant-load test, the specimen's cross sectional area decreases continuously and hence, the stress increases. Therefore, a constant-stress test has been introduced to maintain a constant stress on the specimen throughout the test using a profiled cam, Figure (2.1), that makes a balance between the decreasing cross sectional area and the applied load [1]. This type of test is very widely used to obtain more accurate results of the creep behaviour of materials for basic fundamental studies [1, 4].

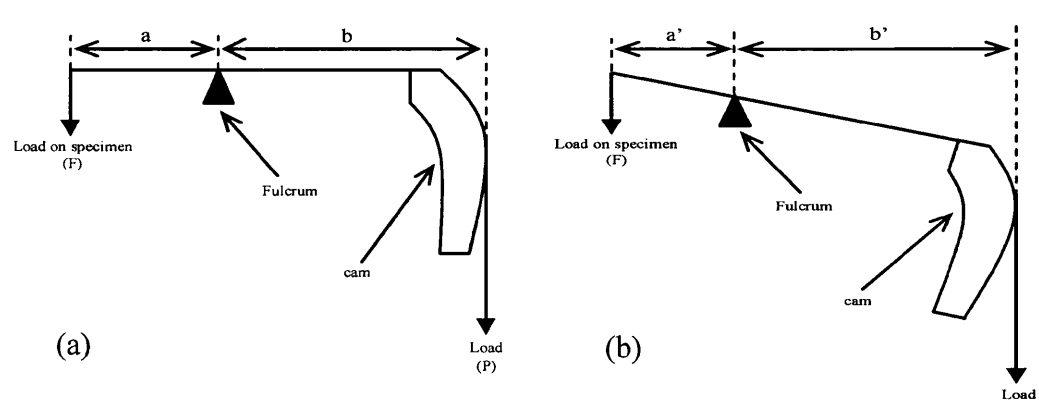

Figure (2.1): A sketch of the profiled cam used in creep machines; (a) before and (b) after loading [1].

Two types of creep behaviour can be defined, namely: the high temperature creep, Figure 2.2 (a), which occurs at temperatures higher than $0.4T_m$, where T_m is the melting point of a material, and the low temperature creep (or the logarithmic creep), Figure 2.2 (b), which occurs at temperatures around or lower than $0.3T_m$. The former type of creep has a more significant effect since it involves re-arrangement of atoms by diffusion inside the crystal lattice leading to fracture whereas the latter has dimensional changes which are extremely small, i.e. can be ignored, and rarely leads to fracture [1].

At the beginning of the creep test, i.e. at time equals zero, an instantaneous increase in strain, ε_o, takes place, elastically and plastically depending on the stress level, followed by a time dependent increase in strain, ε_c, due to creep deformation. As the temperature and/or stress increases, larger values of ε_o and ε_c are, thus, obtained as the material becomes more ductile at higher temperatures [1].

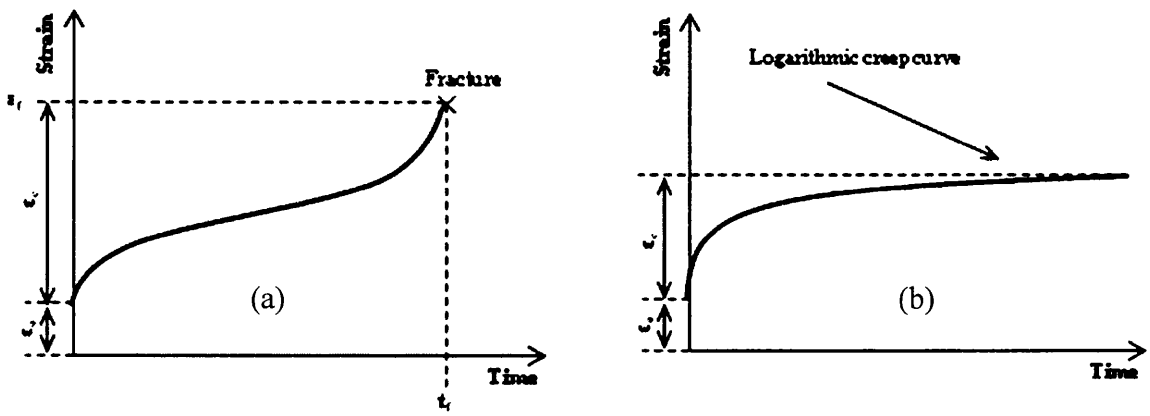

Figure (2.2): A schematic representation of the; (a) high and the; (b) low temperature creep [1].

Creep of crystalline materials occurs as a result of either migration of dislocations, grain boundary diffusion and shearing, or diffusion of vacancies, which can take place at all temperatures above absolute zero [3]. Hence, the main creep mechanisms can be classified as: Dislocation Glide or Creep (i.e. dislocation motion along slip planes under high stresses by thermal activation or dislocation motion by vacancy diffusion under intermediate stresses, respectively), Diffusional Creep (vacancy flow under low stresses) and finally, Grain Boundary Sliding [4].

The curve of the high temperature creep, Figure 2.2 (a), can be divided into three main stages, namely: Primary, Secondary (linear or steady-state) and Tertiary stage that ends with fracture, as illustrated in Figure (2.3). The slope at any point on this curve ($\dot{\varepsilon} = d\varepsilon/dt$) represents the strain rate at that point. The primary stage represents a region of a decreasing strain rate wherein the creep resistance of the material increases by its own deformation (this process is the predominant at low creep temperatures). In the secondary stage, a constant strain rate is observed and hence, it is sometimes called the 'steady-state' stage as the strain rate

becomes independent of time. The minimum value of the strain rate during the secondary stage is called the minimum creep rate, $\dot{\varepsilon}_m$. The final stage is the tertiary stage during which the strain rate increases continuously leading to fracture [1].

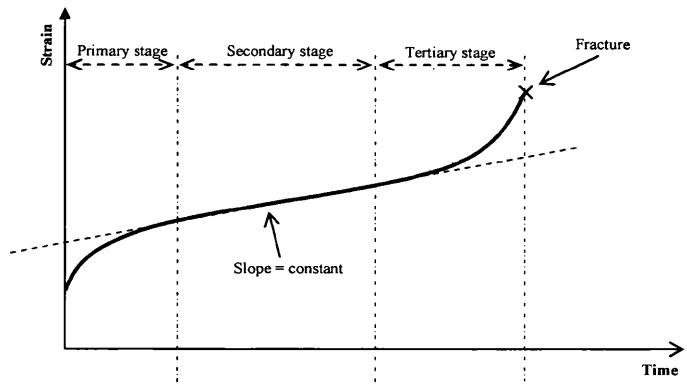

Figure (2.3): A schematic representation of the high temperature creep stages [1].

The secondary stage is usually used to determine the creep properties of any material. Mainly, the steady-state creep rate ($\dot{\varepsilon}_s$) and the time to fracture (t_f) are used to represent the design criteria of any material. They are related through the Monkman-Grant relation [2]:

$$M = \dot{\varepsilon}_s \, t_f \qquad \text{..... (2.1)}$$

where M is known as the Monkman-Grant constant. It is worthwhile noting that different needs for $\dot{\varepsilon}_s$ or t_f are involved according to each application. In other words, for short-time and high-temperature applications, the time to fracture is the appropriate design parameter since the steady-creep rate is difficult to be measured under such conditions. Whereas for long-time and high-temperature applications, the steady-creep rate is the critical design parameter [4, 5]. Another important observation that is to be mentioned is the effect of increasing the stress, σ, at a constant temperature, T, or vice versa. As the stress and/or temperature increases, higher values of creep rates are obtained with lower values of time to fracture where the curve becomes more tertiary dominated, i.e. primary stage diminishes, as illustrated in Figure (2.4). This is a result of the increased number of voids and cracks with increasing the stress and/or temperature [4, 5, 6].

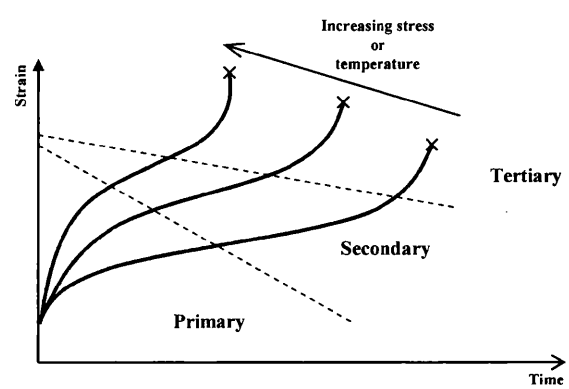

Figure (2.4): The effect of increasing the stress (temperature) at a constant temperature (stress) on creep [1].

2.2 Review of Creep Mechanisms

Three types of mechanisms are likely to take place during creep of materials, namely: Dislocation Glide or Creep, Diffusional Creep and Grain Boundary Sliding (GBS).

2.2.1 Dislocation Creep

Dislocation Creep is defined as the deformation controlled and characterised by dislocation slip in the grain lattice associated with glide on slip planes and climb over physical obstacles [7], as shown in Figure (2.5). This type of creep is regulated by climb-controlled dislocation motion in the grain interiors without affecting the dislocation density with stress and thus, it is independent of grain size. At intermediate stresses, the power law creep is observed with n = 3 for solid solutions, and n = 4 - 5 for pure metals.

In the case where solid solutions are involved, creep is controlled by the glide-step in glide/climb mechanism as dislocation motion is restricted by solute atoms. In this case, the creep rate is given by [8, 9]:

$$\dot{\varepsilon} = K D_s \sigma^n \qquad \text{..... (2.2)}$$

where D_s is the solute atoms' diffusion coefficient, and n = 3.

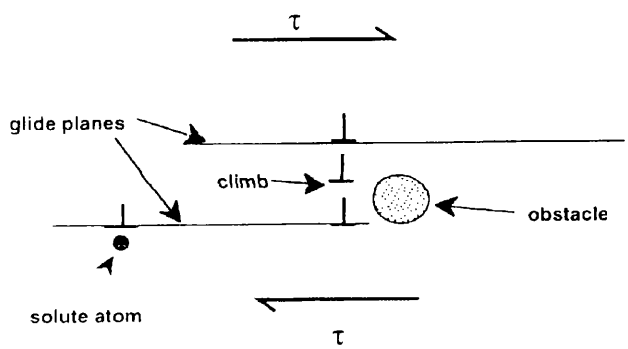

Figure (2.5): Dislocation Creep associated with climb and glide of dislocations [9].

In pure metals, where more energy is required for dislocation climb, creep takes place by an upward movement of dislocations over physical obstacles, as illustrated in Figure (2.6). In this case, the creep rate is given by [9, 10]:

$$\dot{\varepsilon} = K D_L \sigma^n \qquad \text{..... (2.3)}$$

where D_L is the lattice diffusion coefficient, and n = 4 - 5.

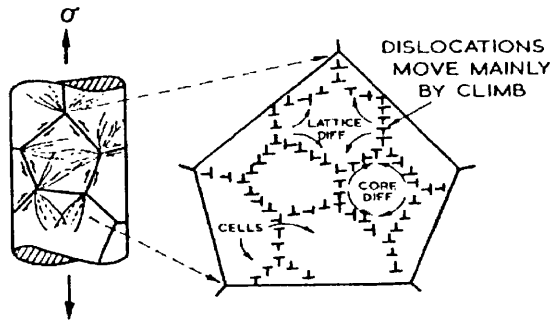

Figure (2.6): Power law creep and cell formation by climb [11].

At higher stresses, the power law fails to predict the strain rate values as the measured values of stresses are greater than those it can predict, which is known as the 'power law breakdown'. The process in such a case is a glide-controlled flow instead of a climb-controlled, as illustrated in Figure (2.7).

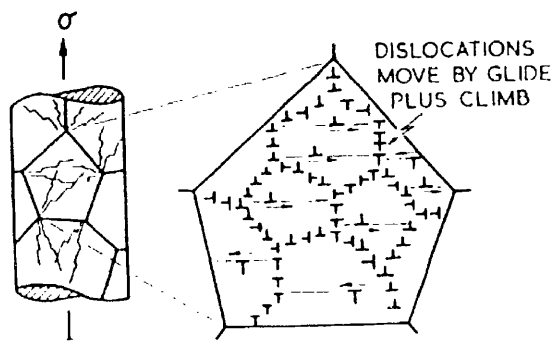

Figure (2.7): The Power law breakdown [11].

At very high temperatures, recrystallisation, along with the power law creep, occurs which induces new areas of primary creep in newly formed grains, as shown in Figure (2.8). This mechanism leads to a huge change in the dislocations substructure and leads to a drastic increase in strain rates [3, 9, 11].

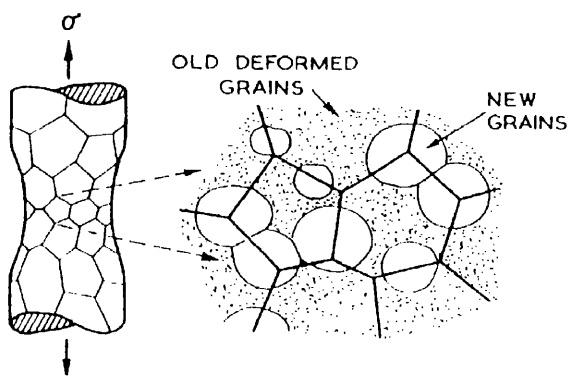

Figure (2.8): Recrystallisation at high temperatures [11].

2.2.2 Diffusional Creep

Diffusion of atoms is facilitated by either the presence of vacancies within the crystal lattice or by the thermal energy an atom can sufficiently have in order to move. Inside the lattice, as atoms vibrate, energy is transferred from one atom to another as they collide and thus, the energy is not uniformly distributed within the lattice [1]. Diffusion mainly occurs at very low stresses where dislocation movement is slow and could, thus, be negligible and ignored [12]. This type of creep leads to an elongation of the individual grains along the tensile axis, as shown in Figure (2.9).

At lower temperatures, creep is dominated by diffusion of vacancies and can be either called 'Nabarro-Herring' creep if the vacancies flow from grain boundaries in tension to grain boundaries in compression, or 'Coble' creep if the diffusion of vacancies takes place along the grain boundaries. However, at higher temperatures, these two types of creep do not provide accurate estimates of the minimum creep rate since work hardening and recovery take place and thus, creep is dominated by dislocation movement [1].

If the transport of matter is controlled by diffusion through the grain lattice, then it is a 'Nabarro-Herring' creep. The strain rate of 'Nabarro-Herring' creep ($\dot{\varepsilon}_{NH}$) is given by [1]:

$$\dot{\varepsilon}_{NH} \alpha 1/d^2 \qquad \text{..... (2.4)}$$

where d is the mean grain diameter. On the other hand, 'Coble' creep is similar to 'Nabarro-Herring' creep but it suggests that the mass transport occurs not only through the lattice, but also along the grain boundaries. It is described by [1]:

$$\dot{\varepsilon}_{C} \alpha 1/d^3 \qquad \text{..... (2.5)}$$

From these two relations, it is obvious that the dependence of Coble creep on grain size ($\sim 1/d^3$) is stronger than the dependence of Nabarro-Herring creep ($\sim 1/d^2$) and has, thus, a greater influence in very fine-grained materials which are more likely to be subjected to grain boundary sliding due to the overall increase in the grain boundary area.

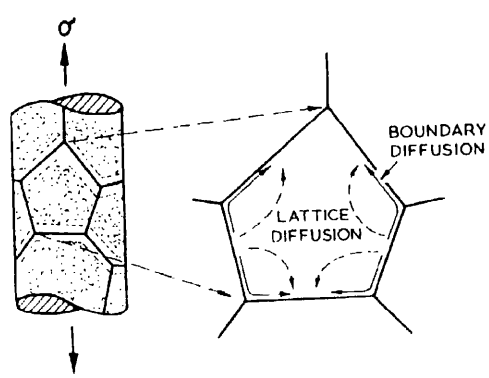

Figure (2.9): An illustration of the diffusional creep [11].

2.2.3 Grain Boundary Sliding

Grain boundary sliding (GBS) occurs during creep when the grain boundaries are not perfectly bonded together and are, thus, weaker than the ordered crystalline structure of the grains. The nearby regions relative to the grain boundaries can deform plastically at stresses lower than those required for the deformation of the interior regions of the lattice [9]. At lower stresses, grain boundary sliding becomes more dominant and helps in the initiation of intergranular fracture by facilitating the formation of wedge or triple-point cracks and voids growth on the grain boundaries which are normal to the tensile axis [4]. (N.B. this process is thoroughly discussed in section 2.3).

Many models were proposed to describe the grain boundary sliding process. A model set by Gifkins [13] describes the grains as if they are made of a separate core and mantle. In this model, the plastic flow consists of two independent slip processes that control the grain boundary sliding, namely: a slip that occurs in the mantle region and another slip that takes place within the core of each grain. When the former process dominates, superplasticity occurs [12, 14]. As the material is lost from longitudinal boundaries, diffusional creep requires grain boundary sliding to occur so as to keep the grains in contact. However, in order to avoid cracks or voids formation, additional mass-transfer must, therefore, occur at these grain boundaries. In other words, this means that the grain boundary sliding is an accommodating process which is necessary to maintain the structural integrity [12, 14]. It has been reported by Todd [15] that the Lifshitz model, Figure 2.10 (a), was also used to describe the process of grain boundary sliding in high-temperature diffusion viscous flow of polycrystalline materials at low stresses. In this model, it was deduced that sliding is a relative grain motion in which each grain keeps its neighbours throughout the deformation process. In contrast, Rachinger's model, Figure 2.10 (b), defines the grain boundary sliding as a creep process in which no significant elongation is exhibited by the grains, but a displacement with respect to each other takes place so that there is a net increase in their number lying along the tensile axis [15]. In other words, this model measures the contribution of grain boundary sliding to the axial strain by modeling the relative grain translations during plastic flow [15].

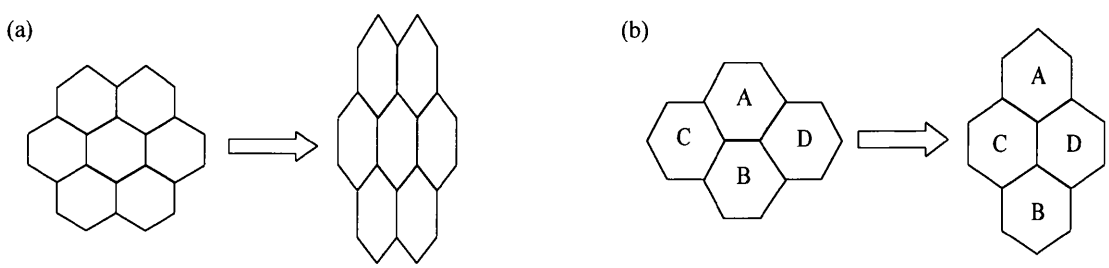

Figure (2.10): Grain boundary sliding models [15]; (a) Lifshitz's and (b) Rachinger's model.

2.3 Review of Creep Fracture

In general, high temperature creep leads to fracture at the end of the tertiary stage as a result of microcracks formation and growth along grain boundaries which are 90° oriented relative to the tensile stress axis. This kind of fracture is called 'intergranular' fracture since it involves cracks initiated and spread along the grain boundaries. Two general types of intergranular fracture can take place, namely: wedge or triple-point cracks and grain boundary cavities [1].

2.3.1 Wedge (Triple Point) Cracks

Under the effect of high stresses and temperatures, atoms move relative to each other causing a shear movement at the grain boundaries as each grain tries to pull apart from its neighbouring grains, as illustrated in Figure (2.11). This mechanism occurs as a result of the applied tensile stresses causing the grains to slide above each other [1]. It has been shown elsewhere [14] that grain boundary sliding is necessary for void nucleation. This is a common mechanism in fine-grained alloys where the overall grain boundary areas are increased.

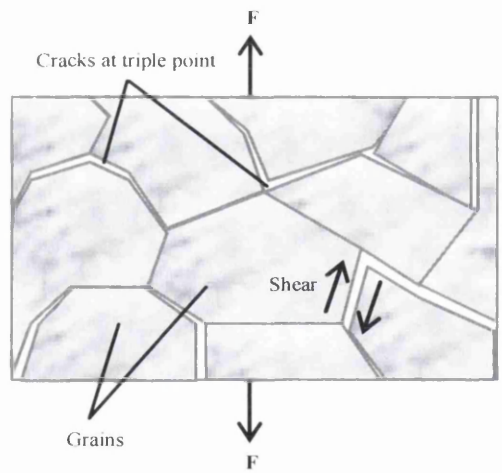

Figure (2.11): Grain boundary sliding and triple point cracks.

2.3.2 Cavities Formation at Grain Boundaries

At low stresses, cavities form at grain boundaries by nucleation and growth [14]. They are found at the early stages of creep and they increase, link-up and propagate under the effect of the applied tensile stresses, as shown in Figure (2.12). Once cavities are formed, they tend to absorb other vacancies from the surrounding grain boundaries. Cavities can absorb and link-up with other vacancies only when the grains are able to pull apart other adjacent grains, Figure (2.13), which is a constrained cavity growth and thus, it depends on the overall creep of atoms [1, 14].

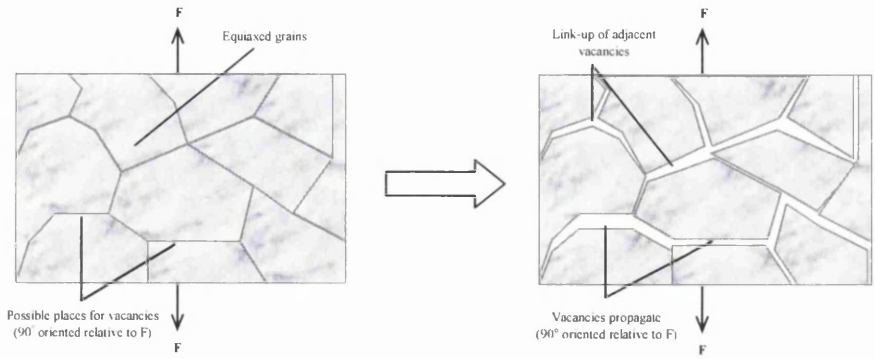

Figure (2.12): Cavities link-up and propagation.

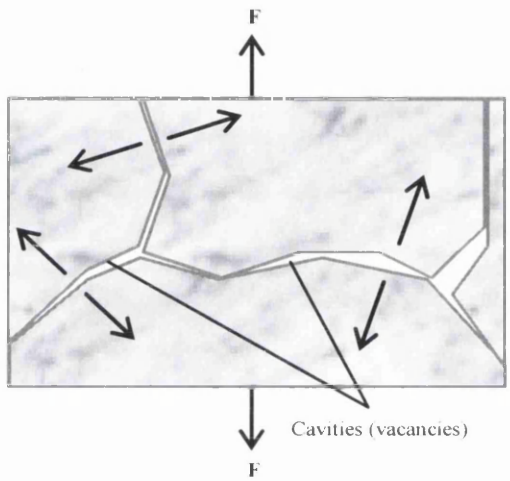

Figure (2.13): Cavities absorb other cavities as grains try to pull apart from each other.

Equiaxed grain structures, or the conventionally casted (CC), can be more easily pulled apart or separated by crack link-up than the elongated grains, or the directionally solidified (DS), as can be seen in Figure 2.14 (a) and (b), respectively. Therefore, the difficulty with which link-up between the internally cracked regions in the DS alloys accounts for the fact that rupture lives and creep ductilities exhibited are considerably greater than those recorded for the CC materials [16, 17].

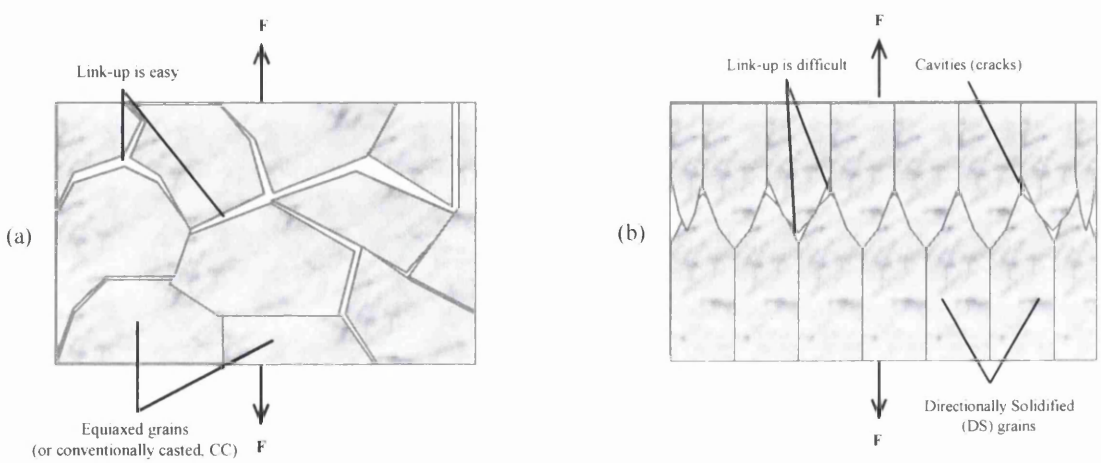

Figure (2.14): Equiaxed and directionally solidified grains behaviour.

Moreover, the improved creep lives and ductilities of the DS materials can be explained on the basis that when cracks eventually initiate on the short transverse grain boundary segments of a columnar grain, they can not spread very far without intersecting a longitudinal boundary which has a low component of normal stress across it [18]. As the CC and DS materials creep initially at the same manner, i.e. start with primary creep followed by consequent stages, the CC materials tend to fracture earlier than the DS materials, Figure (2.15), without going through the tertiary stage in some cases [16].

However, the most practical solution to avoid cracks development in a material is the elimination of grain boundaries by introducing the single crystal (SC) phenomenon where, in this case, the whole bulk of a material consists only of a single grain and thus, no neighbouring grains or grain boundaries exist [16].

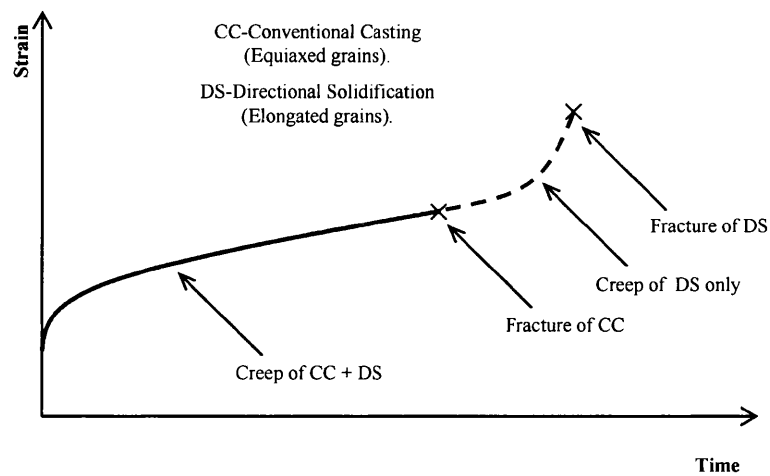

Figure (2.15): A comparison between equiaxed and directionally solidified grains behaviour [1].

2.4 Review of Creep Parametric Methods

Many approaches were proposed in an effort to predict the long-term creep properties based on short-term creep measurements so as to reduce the time scales and costs required to obtain such long-term data. Each of these approaches represents a technique through which the short-term creep-rupture data can be extrapolated using a time-temperature parameter. This concept is based on the assumption that all creep-rupture data, for a given material, can be superimposed to produce a single 'master curve' wherein the stress is plotted against a parameter that contains and combines time and temperature. Based on this master curve, that can only be constructed using available short-term measurements, extrapolation to longer times can then be obtained [19]. These parametric methods play a key role during the design stage in which the high temperature components are designed to codes that are intended to assure a specific life. Generally, these design codes define a maximum allowable stress that can exist in a component during the anticipated design life [19]. This

allowable design stress, which is a combined function of time, temperature and material, is usually based on the rupture stress required to give the expected design life. It is tempting to infer that the plant will give a satisfactory service up to, but not much beyond, the design life. For this reason, two distinct parts of the service life can be defined, namely: (a) the original design life which can typically be 100,000 hours, and (b) the safe economic life. Although the latter is normally outside the influence of the design codes, it can be considered as a significant fraction of the overall service life. Moreover, due to the time-dependent nature of materials' properties at high temperatures and the fact that ultimate failure is, thus, implicit, consideration must be always given to a 'beyond design' end-of-life criterion. Since the time required for a crack to grow can be very short, life extension is only safe within the time scale for crack initiation unless defect growth is being monitored [19].

In general, current methods normally involve two approaches, namely: (1) those which involve the acquisition and monitoring of operational parameters, the use of standard materials data, and the life fraction rule, and (2) those based on post-service examination and testing which require direct access to the component being examined for sampling and measurement [19]. These parametric methods have a great advantage, at least in theory, of requiring only a relatively small amount of data to establish the required master curve. Some of these approaches proved their validity for creep predictions by providing satisfactory results whereas others failed to give precise long-term predictions.

2.4.1 Review of the Power Law

The power law represents a combination of the temperature and stress dependences of creep rate which are described by, respectively, Arrhenius's and Norton's laws (N.B. These creep rate dependences are explained in Figure (2.4), page 7). In these two laws, the secondary strain rate, $\acute{\varepsilon}_s$, is used to describe the creep rate of materials, as follows [1]:

- **Arrhenius Law**: As the strain rate, $\acute{\varepsilon}_s$, increases with increasing the temperature, T, a straight line relationship can be obtained when plotting ($\ln \acute{\varepsilon}_s$) against (1/T), as shown in Figure 2.16 (a). Thus;

$$\acute{\varepsilon}_s \alpha \exp(-Qc/RT) \quad \ldots\ldots\ldots\ldots\ldots\ldots (2.6)$$

where Qc is the activation energy for creep and R is the gas constant.

- **Norton's Law**: As the strain rate, $\acute{\varepsilon}_s$, also increases with increasing the stress, σ, another straight line relationship can be obtained when plotting ($\ln \acute{\varepsilon}_s$) against ($\ln \sigma$), as shown in Figure 2.16 (b). Thus;

$$\acute{\varepsilon}_s \alpha \sigma^n \quad \ldots\ldots\ldots\ldots\ldots\ldots (2.7)$$

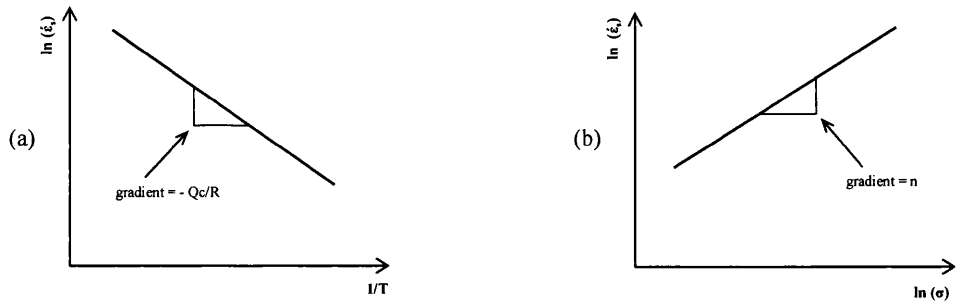

Figure (2.16): The secondary creep rate dependence of (a) temperature and (b) stress, respectively.

where n is the stress exponent. Combining these two laws together, i.e. equation 2.6 and 2.7, gives the power law equation as [1]:

$$\dot{\varepsilon}_s = A\,\sigma^n \exp(-Qc/RT) \qquad \text{..... (2.8)}$$

where A is a constant. It was also assumed that the value of Qc and n is constant but, in fact, after further research, it was found that their values vary according to the creep mechanism in different stress and temperature regimes [20]. The value of Qc is related to temperature, according to equation (2.6) and Figure 2.17 (a), such that Q_1 and Q_2 represent the value of Qc at high temperatures (due to vacancy flow through the lattice) and low temperatures (due to vacancy flow along grain boundaries), respectively [1]. On the other hand, the value of n is related to stress, according to equation (2.7) and Figure 2.17 (b), such that n_1 and n_2 represent the value of n at high stresses (due to dislocation creep) and low stresses (due to diffusional creep), respectively [1].

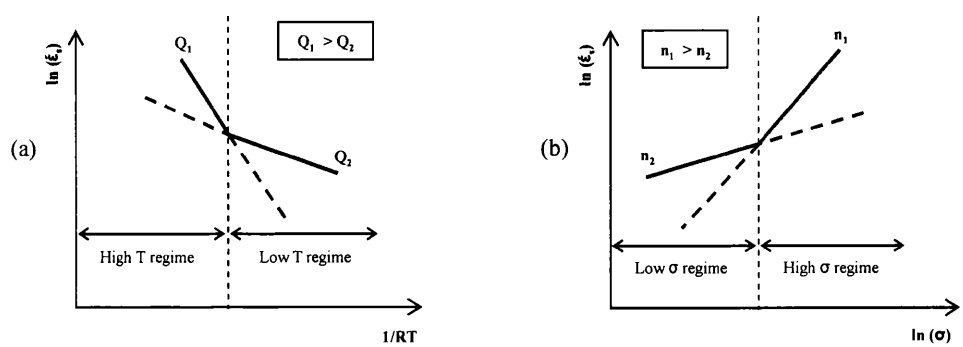

Figure (2.17): Transition of (a) Qc and (b) n, relative to temperature and stress, respectively.

According to Wilshire and Scharning [21], when creep tests were carried out on the 9-12% chromium steels, it was found that the value of Qc and n was changing with increasing the temperature and decreasing the stress. Therefore, it can be deduced that there is a variation in the value of Qc and n used in the power law equation depending, respectively, on temperature and stress regimes during the creep process. For this reason, and since these values vary in an unpredictable manner, the power law equation does not allow

accurate estimation of the long-term rupture strengths by extrapolating the short-term measurements [22]. Furthermore, using these relationships for extrapolation will overestimate the actual long-term performance, Figure (2.18), which might lead to considerable errors in the prediction of creep behaviour and thus, catastrophic consequences. If a certain method is unable to accurately predict the creep behaviour, the consequences will be less severe if the method underestimates the actual measurements rather than overestimates them as underestimation will keep the component life within the safe operational conditions.

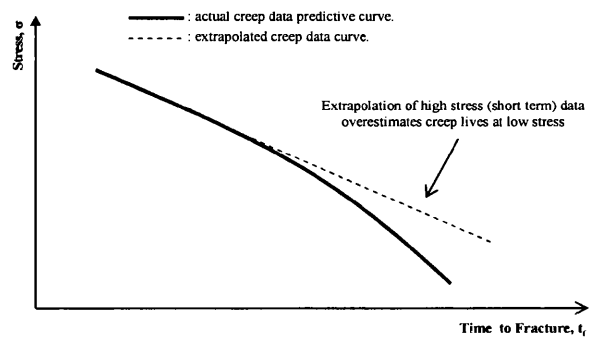

Figure (2.18): Extrapolation using the power law overestimates actual results.

2.4.2 Review of the Larson-Miller (LM) Methodology

This parametric approach is one of the methods used to predict the stress rupture data of metals. It has been originally derived from Arrhenius relation (equation 2.6 and 2.8) at a constant stress and thus, a constant stress exponent n, but at a variable value of T and Qc, which gave the final form of this relation as [23]:

$$P_{LM} = f(\sigma) = T (C_{LM} + \log t_f) \quad \text{..... (2.9)}$$

where C_{LM} and P_{LM} are the Larson-Miller constant and parameter, respectively. The parameter, P_{LM}, can be used to superimpose the family of rupture curves into a single master curve [2]. The constant, C_{LM}, includes the Monkman-Grant constant M, described in equation (2.1), which is a function of Qc that was proved elsewhere [2, 21] to be a function of stress. Plotting ($\log t_f$) against (1/T) at constant stresses, Figure (2.19), for some experimental data gave straight lines of slope P_{LM} and an intercept of - C_{LM} [24].

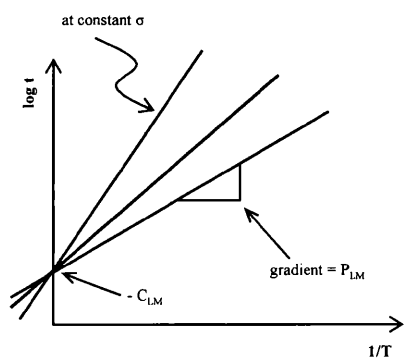

Figure (2.19): Determination of the Larson-Miller constant [24].

This method was further studied by Krivenyuk and Mamuzic [25], who described the constant C_{LM}, as:

$$C_{LM} = (T/\Delta T)\, m' \log (\sigma_1/\sigma_2) \quad \text{..... (2.10)}$$

where σ_1 and σ_2 are the corresponding stresses at a constant time value from two rectilinear stress-rupture (SR) curves tested at T_1 and T_2 (where $T_2 = T_1 + \Delta T$), and m′ is the reciprocal of the slope, at the selected time value, of the SR curve at temperature T_1. When the value of C_{LM} was estimated based on the data of two rectilinear SR curves at temperature T_1 and T_2, it was found that the value of C_{LM} depends on the position of the two curves relative to each other. In other words, if the curves were parallel then, this means that C_{LM} is constant. But, if the slope changed from one curve to another then, as the time to rupture increases, the value of the logarithm in equation (2.10) increases leading to a significant dependence of C_{LM} on time. Hence, for equidistant curves, the time dependence of the constant C_{LM} is weak, whereas it might become sharp for curves that are distinguished by their slopes [25].

Larson and Miller took one step further in their original proposal, suggesting that the value of the constant C_{LM} could be taken as 20 for many metallic materials [23, 26]. However, it was found that the value of this constant varies from one alloy to another and is also influenced by factors such as cold-working, thermo-mechanical processing, phase transitions and/or other structural modifications [26]. Moreover, most applications of the Larson-Miller parameter are made by first calculating the value of C_{LM} that provides the best fit of the raw data, which means that C_{LM} is treated as a 'fitting constant' based on a 'trial and error' method instead of being a physically meaningful constant. For instance, a certain study [26] showed that the value of this constant for specific aluminum alloys ranged from about 13 to 27.

In studies of refractory and heat-resistant steels and alloys by Krivenyuk and Mamuzic [25], calculations often gave rather lower values of the constant C_{LM} than the common used value of 20. In these investigations, the difference in the values of this constant was mainly a result of the time dependence of this constant. In addition, the refractory metals were primarily studied at short loading times whereas the heat-resistant materials were investigated at longer loading times which led to higher values of C_{LM} for the latter, according to formula (2.10). In agreement with these findings, Cipolla and Gabrel [27] found a huge stress overestimation when the Larson-Miller equation was used on the high chromium steel (Grade 91) at all temperatures, especially at 600°C. Therefore, the requirement of a physical realism of extrapolation was not completely fulfilled by this method which is less conservative and seems to be less able to describe the strong curvature between the low and the high stress regimes.

The equation of Larson and Miller was reviewed by Wilshire and Scharning [21] on the 9-12% chromium steels. Although it was generally accepted that C_{LM} should be taken as 20, the data fit with the curving LM plots was, frequently, better with other values, where, in the case of chromium steels, the best fit was obtained when C_{LM} was 36 instead of 20. This difference in the value of C_{LM} was attributed to the fact that it is a function of Qc which is, itself, a 'variable'. Thus, Larson and Miller's results were only in agreement with the theoretical equation for low temperature deformation, and could not accurately describe the high temperature properties.

A very logical explanation was given by Larke and Inglis [28] who assumed that if two different materials were tested at the same temperature, T, and fractured at the same time, t_f, then if the value of C_{LM} was the same for both materials, equation (2.9) would give the same value for P_{LM}, even though, as would in general be so, the stress to cause fracture is different for each material. Therefore, if the value of C_{LM} is considered 'presumably' as 20, as Larson and Miller suggested, then this suggestion will imply that, for the same conditions of testing, the fracture time would be the same for all materials, which is apparently unacceptable. In addition, this suggestion also means that if, for a given material, a set of stress-rupture curves at different temperatures are established, then, over the same temperature range, these curves would be valid for any other material provided that only the stress scale is altered [28].

The graphical method, Figure (2.19), recommended by Larson and Miller for determining the numerical value of C_{LM} was proved to be quite unsatisfactory [28]. This was based on the fact that, at least, one pair of lines intersects at a significantly different value of log t_f than the other pairs, and this, coupled with the fact that personal choice enters into the drawing of the curves associated with the basic log σ/log t_f data, increases the doubts on the acceptability of this method for determining the value of C_{LM} [28]. Another critical assessment of this method documented in Murry [29] concluded that the different curves which represent the variations of the Larson-Miller parameter with the initial stress, at different temperatures, very rarely coincided. It was also observed that the value of C_{LM} could vary from 2 to 55, very often in relation to the initial stress. In agreement with this assessment, another study also documented in Murry [29] found that the constant C_{LM} varied with the material, the test temperature and the initial stress. Along with these studies, another extensive work carried out by Penny and Marriott [2] on the Larson-Miller method stated that this method stands alone as the least accurate of all methods, both in correlation and extrapolation, where errors resulting from its use are significant even when good quality data are available.

Therefore, this parametric formula could only be used to a very limited extent to extrapolate time, temperature, stress and elongation since the value of C_{LM} was found to be variable. Moreover, the unknown

curvature of the parametric plots of the Larson-Miller equation makes data extrapolation unreliable. Hence, even when tests lasting up to 30,000 hours have been completed, this parametric method does not allow unambiguous determination of the 100,000 hours rupture strengths.

2.4.3 Review of the Manson-Haferd (MH) Methodology

Manson and Haferd [30] developed a linear time-temperature relationship for extrapolating creep and stress-rupture data. The Manson-Haferd (MH) methodology was developed in order to eliminate the errors introduced by the Larson-Miller technique which assumed a fixed value of the constant used in its equation that led to inaccuracies in predicting the creep life [2, 30]. This technique assumes the same starting point of steady-state creep dominated by a power law behaviour but considers, later on, that the logarithm of the time varies linearly with the test temperature at a constant initial stress, according to [29, 30]:

$$\log t = a - P_{MH}\, T \qquad \text{..... (2.11)}$$

where t is the time (either the time to fracture, t_f, or to a certain strain level, t_ε), $a = \log t_a + P_{MH}\, T_a$ (where t_a, P_{MH} and T_a are the Manson-Haferd time, parameter, and temperature constants, respectively), T is the absolute creep test temperature, and the point (T_a, t_a) is the point of intersection of the straight lines corresponding to the various iso-stress lines. Therefore, the Manson-Haferd parameter, P_{MH}, determines two constants compared to the Larson-Miller parameter that involves only one constant. Rearranging equation (2.11) gives [29, 30]:

$$P_{MH} = f(\sigma) = (\log t - \log t_a) / (T - T_a) \qquad \text{..... (2.12)}$$

According to Manson and Haferd's suggestion, the parameter P_{MH} can, thus, be derived graphically from the intersection point of the extrapolated iso-stress lines when plotting log t_f against T. Moreover, plotting P_{MH} versus stress, σ, will force all creep data to collapse onto a single 'master curve'. The equation of this curve can then be determined by a curve fitting technique, which yields an equation relating time to a given percent creep, temperature, and stress [30].

In agreement with Manson and Haferd, it was postulated elsewhere [29] that the parameter P_{MH} was derived from the approximately linear relationship found experimentally between log t_f and T as well as from the trend of the data that converge at a common point (T_a, t_a). This parameter, therefore, measures the slopes of the straight lines obtained for given values of stress. Values of T_a and log t_a which best fit the data vary for different materials [29]. Manson and Haferd showed that the values of T_a for most materials ranged from 0°F (-17.78°C) to 200°F (93.3°C) whereas the values of t_a varied appreciably [30]. Although single values of T_a

and log t_a might be found and universally agreed and used with satisfactory results, this possibility has not as yet been demonstrated. They also added that accurate results could be expected with this parameter, as with the LM parameter, only if the proper values of the constants were used for each material. However, the variation in the value of T_a and log t_a introduced many errors in extrapolating the short-term data, as it was found with the LM approach. Murray and Truman [31] also reviewed the MH technique and obtained new values of T_a and log t_a which accurately fitted the data of the Austenitic steels used in the experiment. They also found that the values of the constants obtained were different from the standard values proposed by Manson and Haferd. Along with Murray and Truman, different values of these two constants were obtained elsewhere [32, 33] when experiments were carried out on different steels.

An advantage of the MH parameter is that it can be used for various materials and different times which could be either the time to a certain percent creep strain or the time to rupture. However, the numerical values of the MH constants read from the plots of log t_f against T are not precise enough unless very comprehensive experimental data are available. Furthermore, by using this technique, predicting the stress and the time values outside the temperature range on which the magnitudes of the constants are based can lead to significant errors [28]. An assessment carried out by Pink [34] stated that none of the methods had a consistent physical basis and that the apparent success of a certain procedure has only resulted from its applications in just circumstantial conditions. Furthermore, it was added that on one hand, the method of Larson and Miller, for instance, shows better consistency with the deformation processes occurring at low temperatures and thus, offers better results in the extrapolation of this type of data. Whereas on the other hand, the method of Manson and Haferd does not present any physical meaning, but coincidentally describes the complex pattern of deformation controlled by several mechanisms and is, thus, more reliable for long-term predictions of data generated at higher temperatures.

All of these methods were only proposed to analyse creep testing data since there is no mention in the literature of using the hot-tensile testing data, for example, in the analysis using these techniques [32]. Therefore, and based on these facts, the validity of this method is limited based on the conditions according to which the test is being carried out and thus, further research should be done in order to improve its capability of predicting the long-term creep properties before adopting its results.

2.4.4 Review of the Orr-Sherby-Dorn (OSD) Methodology

The Orr-Sherby-Dorn (OSD) technique [35] involves a time-temperature parameter based on the parallelism of the iso-stress lines of a slope that represents the Orr-Sherby-Dorn Constant, C_{OSD}. In this methodology, the

assumptions of the Larson-Miller technique have been interchanged. In other words, the constant of the Larson-Miller equation, C_{LM}, became a function of stress whereas the parameter, P_{LM}, became a constant [2, 29]. Based on these new assumptions, the LM relation (equation 2.9) can be re-arranged to give the OSD equation as [35]:

$$P_{OSD} = f(\sigma) = \log t_f - C_{OSD} / T \quad \text{..... (2.13)}$$

where P_{OSD} and C_{OSD} are the Orr-Sherby-Dorn parameter and constant, respectively, T is the absolute creep test temperature and t_f is the time to fracture.

The basis of the OSD life prediction methodology is that the activation energy, Qc, remains constant over the entire creep curve, with relatively sparse supporting data [35]. However, since the constant C_{OSD} includes the activation energy, Qc, then any variations in Qc will, thus, ensure that the superimposed parametric plots will be non-linear [21]. Indeed, there is evidence that in some cases, the creep activation energy seems to increase systematically through the primary region [36].

In order to prove the variation in the value of C_{OSD}, tests were carried out by Murray and Truman [31] and graphs of log t_f against 1/T at constant stress values were plotted. The gradients of these plots, i.e. the values of C_{OSD}, were also calculated. Eventually, it was found that in spite of the difference between the values of C_{OSD} obtained experimentally and the values proposed by Orr, Sherby and Dorn, the data were fitted with reasonable accuracy [31]. Since the slope of the resulting log t_f against 1/T line will be the numerical value of C_{OSD}, it was proposed by Orr, Sherby and Dorn that the adjacent log σ/log t_f curves will be equidistant from each other along the time scale [28]. Therefore, in principle, only one line of log t_f against 1/T at a constant stress needs to be drawn in order to determine the value of the constant C_{OSD}, although in practice, the average slope of lines corresponding to different stress levels would be determined. However, it was found quite impracticable to obtain such lines and, in consequence, another method for determining the value of C_{OSD} has been employed elsewhere [28]. A paper published by Mullendore et al [37] revealed certain limitations in methods that employ only a single time-temperature parameter, as with the OSD method, and this became particularly obvious in cases where structural instabilities were involved. It was also added that due to the multiplicity of rate processes affecting the creep strength of complex alloys at high temperatures, it is absolutely impossible for a single parameter to describe precisely all creep properties involved. A review was also carried out on some high temperature alloys in which it was observed that the criterion of a constant slope of the lines specified by the ODS methodology was even less accurate than the assumption of the LM technique [37]. Another critical assessment documented in Murry [29] and carried out by Garofalo et al [38] revealed that at each test temperature, a separate curve could have been found in relation to the initial stress,

which represents the variations of this method as well as the other two methods of Larson-Miller and Manson-Haferd. This leads to the conclusion that the parameters studied were not only functions of stress, but also of other parameters involved in the process. Therefore, this method is found to be indirect and not taking sufficient account for longer tests [39]. According to Brozzo [40], a plot of the logarithm of the minimum creep rate against the reciprocal of the absolute temperature, at constant stresses, should give a series of straight lines. The same results should be obtained if the logarithm of the time to fracture is plotted against the same variable, since it is linearly related to the minimum creep rate. Therefore, it was possible to interpret the ODS and the LM parameters in terms of these plots. However, appreciable deviations from the claimed linearity were generally exhibited, except possibly for a limited range of temperatures. The reasons behind the failure of the rate-process equation in solving this problem can be readily recognised from the possibility of the metal, or the alloy, to deform according to various creep mechanisms accompanied by different activation energies and the likelihood of occurrence of some metallurgical changes during creep. Along with these findings, a direct evidence has been obtained by many investigators that metals and solid solution alloys can undergo a plastic deformation in different ways depending on the temperature and straining-rate conditions [40].

Therefore, based on these investigations, this methodology needs to include more materials and different processes in order to construct a complete and a comprehensive agreement about the value of its constants and the linearity of the plots that its equation implies.

2.4.5 Review of the Manson-Succop (MS) Methodology

The Manson and Succop (MS) methodology [41] is identified by the analysis of the iso-stress lines in the plot of log t_f versus T. The Manson-Succop parameter, P_{MS}, was based on the parallelism of these lines of a slope that represents the Manson-Succop constant, C_{MS}, and is given by [41]:

$$P_{MS} = f(\sigma) = \log t_f + C_{MS}\, T \qquad \text{..... (2.14)}$$

This method, in addition to other methods, was reviewed by Zharkova and Botvina [42] who confirmed that during long-term creep tests, fracture mechanisms changed according to the applied stress and the loading time. In this regard, they stated that fracture under high applied stresses was purely intergranular, under medium applied stresses it was also intergranular but resulted from wedge cracks formation and was also intergranular under low stresses but resulted from the formation and development of pores along grain boundaries. The change of fracture mechanisms was responsible for the appearance of the kink points in the

long-term strength curves [42]. The known timee-temperature parametric methods such as the Larson-Miller, Dorn, Manson-Succop, Manson-Haferd and mmany others, were based on relations with fixed values of constants in a wide range of temperatures and f fracture durations which, in return, ignored the changes of fracture mechanisms and led to many errors andd overestimations of the long-term creep life. For this reason, these methods are not necessarily reliable for creeep life predictions [42].

2.4.6 Review of the Manson-Brown (MIB) Methodology

In general, as generated data do not necessarily show a linear trend in their behaviour, it is then necessary to use more complex functions to fit these data. The simplest function with an adjustable degree of curvature is the power function. Consequently, it is actuallyy not surprising to find a generation of non-linear parameters containing the functional forms of the previous linear parameters raised to some power. The parameter which best illustrates this progression in complexity is the Manson-Brown Parameter, P_{MB}, of the form [43, 44]:

$$P_{MB} = f(\sigma) = (\log t - \log t_a) / (T - T_a)^q \quad \text{..... (2.15)}$$

In this expression, there are three constants (t_a,, T_a and the exponent q) which can be determined by a 'trial and error' graphical method. This equation reppresents the general form of the previously mentioned linear parameters such that, it represents [44]:

(a) Manson-Haferd equation when q = 1, (b) Laarson-Miller equation when q = -1 and T_a = 0, (c) Orr-Sherby-Dorn equation when log t_a and $1/T_a$ are both takken to be arbitrarily very large numbers with the condition that $T_a \log t_a = Qc$, (d) Manson-Succop equation whaen q = 1 and log t_a and T_a are both taken to be arbitrarily very large numbers such that $\log t_a / T_a = - C_{MS}$. This generalised technique is very beneficial and much better than the individual proposed methods in such that thhe data would dictate the specific form of the equation instead of trying to force any equation to fit the data [444].

Later on, Manson along with Roberts and Menddelson proposed a generalised parameter of the form [45]:

$$P_{Manson} = f(\sigma) = \sigma^v (\log t - \log t_a) / (T - T_a)^q \quad \text{..... (2.16)}$$

where v is an additional stress exponent consstant. This equation presents a more generalised form of the previous methods where more linear parameterrs can be derived just with a slight change in the values of the constants involved. These generalised equationss, i.e. equation (2.15) and (2.16), provide better techniques to predict the creep behaviour since they encompaass most of the known parametric approaches under different test conditions.

2.4.7 Review of the Monkman-Grant (MG) Methodology

The Monkman-Grant (MG) parametric method [46] uses the minimum strain rate, $\dot{\varepsilon}_{min}$, as a key variable to assess the time to fracture, t_f [47]. Monkman and Grant [46] noticed that the rupture time in the long-term creep tests could be related to the minimum strain rate by a power function of the form [46, 47]:

$$C_{MG} = \dot{\varepsilon}_{min} t_f^{\,m} \quad \text{..... (2.17)}$$

where C_{MG} is the Monkman-Grant constant and m is the time to fracture exponent. This equation suggests that the mechanisms that control creep deformation and creep rupture are, to a great extent, the same [46]. The constant, C_{MG}, in this relation usually depends on temperature [47]. The practical advantage of the Monkman-Grant rule is that the minimum strain rate, $\dot{\varepsilon}_{min}$, can be measured early in a creep test which, in return, facilitates the prediction of the long-term time to fracture, t_f. In other words, if the value of C_{MG} is determined, which is possible from short-term tests, the lifetime of a long-term test can be predicted once the minimum strain rate has been reached and recorded [47]. On the other hand, another study which was carried out by Borisenko et al [48] argued that the product of the minimum creep rate and the time to fracture is a constant value, C_{MG}, which is independent of stress and temperature. They also added that the value of this constant ranges between 0.03 and 0.3 for all materials and that the value of m should be 1.0, which eliminates the exponent from this equation. But later, and after some experiments that were carried out on tungsten, they found that the relation must be of the exponential form described in equation (2.17).

Another interpretation presented by Davies and Wilshire [14], which was based on experiments carried out on pure nickel, suggested that the constant, C_{MG}, was only independent of stress and temperature under high-temperature creep conditions, i.e. above $0.45T_m$, where T_m is the absolute melting temperature of a material, whereas higher values of this constant were recorded at temperatures below $0.45T_m$. Moreover, they found that the value of the exponent m was not varying appreciably from unity and thus, can be ignored.

Baldan and Kaftelen [49] observed that proportionality was generally found between t_f and $\dot{\varepsilon}_{min}$ when the material was strained. This observation was based on the long-term creep tensile tests where it was found that the time to fracture was inversely proportional to the power function of the minimum creep rate for relatively simple alloys such as pure metals and single phase alloys. Their equation is given by [49]:

$$C_{MG} = \dot{\varepsilon}_{min}^{\,m} t_f \quad \text{..... (2.18)}$$

where the value of the exponent m ranged between ~ 0.8 and ~ 0.95. Besides, it was found that the value of the constant, C_{MG}, ranged from ~ 2 to ~ 15, depending on the material and the microstructural variables as

this constant represents the contribution of the secondary creep strain to the total failure strain [49]. This equation was based on that when the material was strained, cavities and cracks grew, linked-up and led, eventually, to an intergranular creep fracture. Assuming that creep fracture is actually controlled by the creep growth of cavities at grain boundaries, this result would then be consistent with the Monkman-Grant equation as, from the very beginning, the fracture process is always linked to the creep process [49].

Dobes and Milicka [50] argued that the value of C_{MG} and m changed according to the applied stress in contrast to the studies of Davies and Wilshire [14] and Chih-Kuang Lin et al [47] who previously found that the value of C_{MG} was dependent on stress and/or temperature. Therefore, Dobes and Milicka modified the Monkman-Grant relation into the form [50]:

$$C_{MG}\ \varepsilon_f = \dot{\varepsilon}_{min}^{\ m}\ t_f \qquad \text{..... (2.19)}$$

where ε_f is the fracture strain recorded at t_f. This relation accounts for a possible stress dependence of the product ($\dot{\varepsilon}_{min}^{\ m}\ t_f$) due to changes in the fracture strain, ε_f, according to the applied stress. However, this modification of the equation does not improve the prediction capability since, instead of only one long-term creep parameter, i.e. t_f, their relationship requires also the knowledge of the second long-term parameter, i.e. ε_f. This is actually impractical since having known the values of these two parameters eliminates, in return, the need for any predictions which is mainly the aim of such approaches [51].

Some other studies [52] added that if continuous nucleation occurs, a modeling of the fracture process might lead to the Monkman-Grant relationship provided that diffusive and plastic coupling of cavity growth and cavity interactions are considered. Besides, this relationship might offer the possibility of long-term extrapolation if the same creep deformation mechanism operates during the whole creep life [53].

A research done by Menon et al [54] on silicon nitride examined the applicability of the Monkman-Grant relationship in predicting the stress rupture life. The data showed that the Monkman-Grant lines relating the rupture life to the minimum creep rate were stratified with respect to temperature. For this reason, a modification to the known expression of the Monkman-Grant equation was proposed to accommodate this temperature dependence [54]. Following this modification, another generalised form of the equation was proposed by Evans [55] who stated that the standard Monkman-Grant relation, equation (2.17), has the advantage of the easy estimate of the life of a material once the minimum creep rate is known. This ability of estimating the life of a material can be practically achieved by testing specimens at specified operating conditions until the minimum creep rate, which typically occurs well before the material's end-of-life, is reached and then, the test can be interrupted. This creep rate can then be used to predict the long-term creep

life using the Monkman-Grant equation. However, one important disadvantage of using this relation to predict the creep life is that at operating conditions, it can still take tens of thousands of hours to reach the minimum creep rate and tests of this length are often not viable from the practical and the economical perspectives [55].

Therefore, although the Monkman-Grant relationship is applicable in some situations, there is still a disagreement about a few details such as the values of the constants used in this relationship and whether they are stress and/or temperature dependents and thus, more materials have to be tested and examined using this technique in order to generalise its use.

2.4.8 Review of the θ-Projection Methodology

The θ-projection method is one of the extrapolation methods which proved its applicability, in some situations, in predicting the creep life. It can be summarised in that creep curves under uniaxial constant stress are measured over a range of stresses and temperatures and their shapes are recorded. These shapes are then 'projected' to other stresses and temperatures at which full creep curves can be re-constructed. The required properties are then read off the constructed curves [56]. Thus, the θ-Projection concept, in its most general form, the 4-θ equation, describes the variation of creep strain, ε, with time, t, according to [57]:

$$\varepsilon = \theta_1 [1 - \exp(-\theta_2 t)] - \theta_3 [1 - \exp(\theta_4 t)] \quad \text{..... (2.20)}$$

where t and T are the time and temperature, respectively, θ_1 and θ_3 are scaling parameters defining the extent of the primary and tertiary stages with respect to strain, while θ_2 and θ_4 are rate parameters characterising the curvature of the primary and tertiary creep curves, respectively [58]. In this equation, the two terms on the right hand side describe the normal primary and tertiary components in which a deceleration in creep rate is observed during the primary stage whereas an acceleration is recorded during the tertiary stage [59, 60]. This method was extensively studied by Evans [57] who argued that this technique has an added advantage over the other traditional parametric procedures in that creep predictions are not only limited to the rupture time. However, it was found that the interpolation and/or the extrapolation of the θ-function, traditionally used by this method, was not really the best predictor of the long-term life as more accurate results were obtained using simpler functional forms. Moreover, this equation was quite poor in fitting the experimental creep curve at small strain values [57]. Deviations from the actual creep measurements were also found when this equation was used, particularly in the late tertiary stage, by Evans and Wilshire [60] who attributed these deviations to the intergranular cracks that present immediately prior to fracture.

Another study carried out by Evans [61] was in agreement with one done by Evans [57] in that the θ-projection method gave the poorest projections of creep properties at low strains. Therefore, a modification to this equation has been suggested by Evans [61] in order to improve the fit of the experimental data at the very small strain values. This has been achieved by adding another two extra parameters to equation (2.20), which gave the (6-θ equation) as [61]:

$$\varepsilon = \theta_1 [1 - \exp(-\theta_2 t)] - \theta_3 [1 - \exp(\theta_4 t)] + \theta_5 [1 - \exp(-\theta_6 t)] \quad \text{..... (2.21)}$$

Now, in this equation, the first two right hand terms have the same physical meaning as in equation (2.20), whereas the third term describes the early primary creep behaviour that results from the initial sliding relaxation across grain boundaries [58]. According to Evans [57, 58, 61], this modified equation provided more precise results when it was used to fit experimental creep data, especially at the early stages of the primary creep. This was a result of the third term that has been added which took into account the effect of grain boundaries relaxation during the primary creep that was completely neglected by equation (2.20).

In comparison to the previous parametric methods, the θ-projection method was considered to be more reliable and more accurate in estimating the long-term creep life and thus, it has been widely used and studied in an effort to prove its validity for a wider range of materials. However, further studies are still needed to assure that the errors encountered by the first proposed model of this equation are completely eliminated by the introduction of the modified version.

2.4.9 Review of the Hyperbolic-Tangent Methodology

This technique has been developed by Rolls-Royce plc in the 1990s for the purpose of creep lifing predictions. It implies that the highest stress that can be applied on a specified material at a certain creep temperature is the ultimate tensile strength of that material, σ_{TS}. The stress rupture behaviour is described by hyperbolic tangent curves over a wide range of temperatures, such that [62, 63, 64]:

$$\sigma = \sigma_{TS} / 2 \{1 - \tanh [k \ln (t / t_i)]\} \quad \text{..... (2.22)}$$

where k and t_i are fitting parameters that can be obtained by regression analysis using the actual experimental data at each temperature. Once the values of k and t_i are obtained, they can be inserted into equation (2.22) to produce the stress rupture predictive curves.

Alternatively, using the creep strain values, another hyperbolic function is used to predict the rupture behaviour, such that [62, 63, 64]:

$$\sigma = S_i \{1 + \tanh [S_L \ln (\varepsilon / \varepsilon_i)]\} \quad \text{..... (2.23)}$$

where in this equation, the ($\sigma_{TS}/2$) term of equation (2.22) has been eliminated and replaced by the parameter S_i whereas k, t and t_i have been replaced by S_L, ε and ε_i, respectively. Again, the values of these parameters can be obtained by regression analysis using the actual experimental data at each temperature.

This method differs from the θ-projection method in that it does not try to fit the actual creep curves and then find an expression that relates the fitting constants with stress and temperature, but it represents the creep data at any temperature as a 3-D surface that combines stress, strain and time [63, 64]. This method provided a very good fit for the stress rupture and creep strain behaviour based on the time to fracture and creep strain measurements of many alloys. The only limitation is that inflection points were found in these predictive curves with no theoretical explanation [64]. Interestingly, in the stress rupture curves, these inflection points took place at around $0.5\sigma_{TS}$ at each temperature as a result of changing the pattern of stress rupture behaviour, which might be expected above and below σ_y (or σ_{TS}). Moreover, in the strain dependent rupture curves, this inflection point was found at around ε_i which has a physical significance as the strain value at the minimum creep rate point of a creep curve [64].

2.4.10 Review of the Minimum Commitment (MC) Methodology

This method was proposed by Manson and Ensign [65] in an effort to give a larger flexibility to the parametric analysis of creep data. In addition, it was invented in order to combine all the conflicting approaches into a single equation that will have a sufficient generality. This method is given by [65, 66]:

$$\log t + A\,P \log t + P = G \qquad \text{..... (2.24)}$$

where t is the time, A is a constant dependent on the metallurgical stability of the alloy, P is a variable equal to: $R_1 (T - T_{mid}) + R_2 (1/T - 1/T_{mid})$, G is a variable equal to: $(B + C \log \sigma + D\,\sigma + E\,\sigma^2)$, and B, C, D, E, R_1 and R_2 are regression coefficients and T_{mid} is the mid-value of the temperature range for which the data are to be analysed. In this equation, it is apparent that there are seven constants that need to be determined by regression analysis. It was also found that the more unstable the material, the higher the negative value of A required to fit the data [67]. As the constant A defines the metallurgical stability of the material, a negative value means that the material has the tendency to precipitate embrittling phases whereas a zero value would mean that the material is stable [68]. Unfortunately, the use of any value of A other than zero led to non-linear multiple regressions [68].

Among those who studied this methodology was Jow-Lian Ding et al [69] who found that the results of the regression analyses indicated that the Minimum Commitment model fit the data slightly better than the

Larson-Miller model. The reason was that this model has five independent variables whereas the Larson-Miller model has only two. This method was also studied thoroughly by Goldhoff [70] in his attempts to find the optimum value of A. In this regard, he found that when formulating a model using this technique, the resulting equations were always non-linear since the values of A and P were unknown. It was also found that when fitting the short-term data, there was, relatively, insensitivity to the value of A which is not true for the long-term creep data predictions.

In order to establish a confidence in the use and, alternatively, to reflect problems of this procedure, it should be applied to an existing set of data as well as much sparser data and there should be immediate research into the development of stability factors to enhance the effectiveness of this extrapolation procedure [70].

2.4.11 Review of the Goldhoff-Sherby (GS) Methodology

This methodology pre-supposed the convergence of the iso-stress lines to the point $(1/T_a, t_a)$ located just below the region of the experimental data. The general equation of this technique is given by [71]:

$$P_{GS} = f(\sigma) = (\log t - \log t_a) / (1/T - 1/T_a) \quad \text{..... (2.25)}$$

where t_a and T_a are the time and temperature constants, respectively. For the purpose of examining this equation, it was used to analyse the results of the experiments carried out by Sobrinho and Bueno [32] on steels where it was found that the worst results were obtained when the Goldhoff-Sherby equation was used to fit the data in all cases. Therefore, due to the very narrow use of this methodology in creep data predictions in addition to the fact that only few studies were carried out to examine the validity of this technique, more research should be completed before generalising the use of this technique in predicting the creep properties for long-term purposes.

2.4.12 Review of the Soviet Methodology

This method can be described by two models, namely: Soviet model (1) and (2), given by [72]:

Soviet Model (1): $$\log t = a + b \log T + c \log \sigma + d / T + f \sigma / T \quad \text{..... (2.26)}$$

Soviet Model (2): $$\log t = a + b \log T + c \log \sigma / T + d \sigma / T + f / T \quad \text{..... (2.27)}$$

where a, b, c, d and f are constants to be determined. In studying these models, some observations were presented by Evans [72] who stated that Soviet model (1) was highly effective in modeling the rupture times presented to it for estimation purposes, but it was totally inadequate for predicting data points not used in its

estimation. However, this inability to generalise, or the tendency to overfit the interpolative data set, is a characteristic of all parametric techniques [72].

2.4.13 Review of Other Techniques and Methods

In addition to the previous proposed methodologies, many techniques were developed as alternatives to avoid the errors and flaws encountered when the old traditional methodologies were used. These alternative techniques were based on a relation between the same three variables involved, i.e. stress, σ, time, t, and temperature, T. For instance, Clauss model [73] was based on a time-temperature parameter. In his equation, it was found that in some cases, the rate of change of rupture life with temperature at a constant stress value, i.e. the curve spacing in the stress-rupture plots, was a function of stress as well as temperature. If the curves were equally spaced or were in parallel, then this means that the change in rupture life will be only a function of temperature. But, since the change in rupture life was a function of temperature and stress, then this means that the curves in the stress-rupture plots were unequally spaced, i.e. nonparallel.

Murry [29], who studied a lot of the parametric formulae, assumed that the parameter P and the constant C in both the Larson-Miller and Orr-Sherby-Dorn equations are functions of stress from which he set his first model, Murry model (I). The same observation was found when he studied the Manson-Haferd equation and set his second model, Murry model (II). Another parameter was suggested by Rabotnov [74] in order to correlate creep strain data. He found that the strain-time curves could be re-plotted as strain-stress curves which can then be normalised to a single master curve that represents a time-compensated-stress correlating parameter. This new model was also studied by Goldhoff [70] who found it promising. In an effort to overcome some of the shortcomings of the time-temperature parameters involved in the traditional methods, algebraic methods were found to achieve this aim. For instance, the Conrad equation [75] was one of the algebraic methods that were proposed. In this model, a temperature-compensated-stress parameter was introduced to help in finding more rational methods of extrapolation.

Eventually, graphical methods were invented to find another way of correlating parameters together. For this purpose, the Grant and Bucklin method [76] was suggested to identify the metallurgical changes and their influence on rupture. In addition, the Glen method [77], which studied the same effects involved in Grant and Bucklin method, was developed in order to extrapolate the entire creep curve up to rupture. However, when these models were studied, it was deduced that the Grant and Bucklin method had no systematic procedure of extrapolation since it was dependent on the analyst's ability and his knowledge of the material involved.

However, the Glen method received little attention due to its subjective nature and the very detailed information required from a systematic creep testing program.

2.5 Discussion and Conclusions of the Extrapolation Methods

So far, many extrapolation methods have been discussed and critically reviewed so as to find a reliable method for extrapolation purposes but unfortunately, no such method exists [2]. However, until a better procedure is developed, they must be considered as mathematical tools without any preferences selecting whichever best fits the data. Any method should provide a numerical accuracy in extrapolation since these methods are considered and used as 'practical devices'. Furthermore, a method should give a physical feasibility and reflect the actual behaviour of a material instead of being only empirical so that the results of extrapolation can be trusted. These two criteria depend on the data required to establish the extrapolation where there should be a minimum number of data points and a certain degree of scatter [2].

Concerning the power law equation, for instance, there had been an increasing realisation that the secondary creep is unlikely to be a separate stage of the creep process. But instead, it was agreed that this stage is associated with a minimum in creep rate resulting from a balance between the primary and the tertiary creep processes [78]. It was also suggested that the high values of the minimum creep rate stress exponent, n, and the activation energy, Qc, in this law are a natural consequence of the combined effect of the primary and the tertiary processes [78]. Another study carried out by Evans et al [59] on the power law revealed that the values of the two 'constants' used in its equation were found to vary depending on the creep conditions imposed. This variation was explained on the basis that different mechanisms control the creep behaviour in different stress/temperature regimes. A similar interpretation was presented by Brown et al [20] and showed that the values of n and Qc also vary depending on the creep mechanism involved. In contrast to these explanations, Wilshire and Burt's experiments [79] showed that the variations in the value of n were not caused by creep mechanism transitions, because the microstructural studies and the curve shape analyses showed that the dominant deformation and damage processes were unchanged over the entire stress-temperature ranges studied. These disagreements about the power law behaviour prove that there are many problems will be encountered when such a law is used to predict the creep properties since no unique explanation has been presented for the variations in the values of these 'constants'.

The transition in the mode of deformation during creep tests was more obvious through the discontinuity in the plots of the time to fracture, t_f, versus stress, σ, at constant temperatures, according to Grant [80], which divided each curve into two different regimes, namely: the transcrystalline region (at the high temperature-

high stress portion) and the intergranular region (at the low temperature-low stress portion). This discontinuity is the primary cause of curvature in the plots of isostatic data versus the reciprocal of the absolute temperature [40]. Based on this, the parametric correlations must, thus, cover each regime individually instead of covering the whole set of data at once. Dealing with the data as a whole set is the main reason behind the failure of most parametric techniques which are applicable in one range leading to considerable errors if they are extended to include the other range of different conditions data [40].

Many of the traditional approaches ignore a considerable amount of information by reporting only a limited number of data such as the steady-state creep rate and the rupture life. These conventional approaches, therefore, should be replaced by procedures which quantify the whole creep curve shape and its dependence on test conditions [20]. The linear parametric methods vary in their ability to fit the data accurately and their simulation of the real physical behaviour. For example, the Larson-Miller equation is very convenient in comparing different materials directly but considered to be the least accurate even with good quality data [2]. Moreover, the Manson-Haferd technique provides a closer fit of the data because of the two independent constants used in its equation in contrast with the Larson-Miller and Orr-Sherby-Dorn equations which involve only a single constant. However, these methods might work properly with the 'industrial' data but their correlation of the 'research' data is significantly inferior due to the scatter found in these data. Therefore, they can not be reliable to predict the creep life at all times [2]. On the other hand, the complex methods, such as the non-linear Manson-Brown method and the graphical methods of Grant-Bucklin and Glen, were found to be more accurate than the linear extrapolation methods. Even though, the non-linear methods might be useless when dealing with information of large scatter bands. The graphical methods were able to provide accurate results in extrapolation only if accurate data were provided which disqualifies them from general use [2]. While short-term data up to several thousand hours indicate a linear relationship between the stress and the time to fracture, long-term studies have demonstrated that extrapolating the short duration tests can lead to serious overestimations of the rupture life as the stress rupture curves deviate from linearity at longer times [81]. The use of parametric extrapolation techniques, such as the Larson-Miller and Manson-Haferd methods, overestimates the long-term life. In addition, when data up to, say, 30,000 hours are available, the 100,000 hours predictions could be reasonably accurate which means that these extrapolation methods are just limited to three times the longest reliable test data available [81].

Due to the multiplicity of rate processes affecting the creep strength of complex alloys at high temperatures, it is impossible for a single parameter to describe accurately all the involved properties. These techniques provide only a semi-empirical approximation of the trend of data and thus, it is difficult to predict in advance

which technique will be the most suitable for a given alloy [37]. Based on their experiments, Larke and Inglis [28] added that whichever method of analysis is employed, errors between predicted and actual stress values must be anticipated. Moreover, they found that a significant difference between the observed fracture times and the predicted values was obvious from which they concluded that none of these methods are recommended for long-term extrapolations [28]. Further studies were carried out by Brozzo [40] in an effort to develop a better technique for processing the short-time test data. He found that each of the parametric techniques was based on particular simplifying assumptions whose validity had not been confirmed for all materials or on a wide range of the test variables. Therefore, he reached the conclusion that none of the available parametric techniques appeared to be fully satisfactory. In agreement with that, Goldhoff [70] deduced that the conditions imposed on the experimental data when using such techniques, e.g. to force the linearity of the iso-stress curves and the subsequent parallelism or convergence of these curves in a manner that is not descriptive of the actual behaviour, could induce large errors in extrapolation. This is because data do not always conform to these restrictions which might, in return, cause the large errors in extrapolation of the longer-time rupture [82].

In conclusion, the different evaluation procedures yielded significantly different results. These differences might be a result of the poor fitting ability of the parametric equations or due to the structural changes that might take place during the creep of a material. These differences might also be found even if the experimental findings agreed very well with the computed stress dependence of the times to fracture. For these reasons, there is no indication of how far the regression equation remains valid outside the boundaries of a given experiment [83].

CHAPTER 3

THE NEW EXTRAPOLATION TECHNIQUE

The previous chapter has established a strong background and a critical review to the most widely used extrapolation techniques for creep predictions. It was clear that the majority of these techniques were unable to predict the creep behaviour of many materials and that was clear from the significant errors obtained when such methods were used. For this reason, and in order to avoid such errors, a New Extrapolation Technique has been developed at Swansea University by Wilshire [21, 22] for such long-term creep predictions. Current programmes at Swansea University with partners in the UK power, aeroengine and automotive industries are ongoing to evaluate and assess the predictive capabilities of this methodology for steels and nickel-base superalloys, in addition to some aluminum and titanium alloys. The successful validation of this predictive technique would then minimise the durations and the costs of acquiring long-term creep data as well as simultaneously reducing the delay times between the development and the application of new creep-resistant alloys. The aim of the current work is to examine the ability of this newly invented methodology in predicting the creep behaviour of a chosen high temperature aerospace alloy. As a model material, Titanium IMI834, an aerospace high grade titanium alloy, has been employed to enable sensitivity studies using this new methodology.

3.1 BACKGROUND TO THE NEW METHODOLOGY

By using this new methodology, the values of the minimum creep rate, $\dot{\varepsilon}_m$, and the time to fracture, t_f, recorded at different temperatures can be superimposed onto 'Master Curves' by simply normalising the applied stress through the ultimate tensile strength, σ_{TS}, measured at various creep temperatures [21, 22]. Superimposition can also be achieved using the yield strength, σ_y, but the data fit is usually poorer since the value of σ_y is more difficult to be measured precisely than σ_{TS} [84]. Therefore, by selecting σ_{TS} values for such purposes, property comparisons for different metals and alloys can be significantly simplified [22].

Normalising the applied stress in the power law equation, $\dot{\varepsilon}_m = A\,\sigma^n \exp(-Qc/RT)$, and defining the minimum creep rate, $\dot{\varepsilon}_m$, as in the Monkman-Grant relationship, $\dot{\varepsilon}_m = M/t_f$, gives [21]:

$$\dot{\varepsilon}_m = M / t_f = A^* (\sigma/\sigma_{TS})^n \exp(- Qc^*/RT) \qquad \ldots\ldots\ldots\ldots\ldots\ldots (3.1)$$

where $A^* \neq A$ and $Qc^* \neq Qc$. In this case, Qc^* is determined from the temperature dependence of $\dot{\varepsilon}_m$ and/or t_f at constant (σ/σ_{TS}), in contrast to Qc which is normally calculated at constant σ. Although this equation still does not permit reliable extrapolation of the short-term measurements as a result of the unpredictable fall in n values as σ/σ_{TS} decreases, it reduces, at least, the scale and the number of the experimental tests undertaken to obtain long-term strength data, but not the maximum duration of these tests [21, 22].

The failure of the traditional procedures to give acceptable estimates of the 100,000 hours strengths by the analysis of the 30,000 hours data has frequently been attributed to different mechanisms of creep and/or creep fracture which become dominant in different stress and temperature regimes [21]. If the dominant mechanism changes, measurements made at high stresses would not allow prediction of the low-stress behaviour. For this reason, the new methodology has been introduced to examine and assess whether the change in the failure characteristics after prolonged creep exposure prevents accurate predictions of the long-term rupture strengths by extrapolating the short-term creep measurements [22]. In this regard, Wilshire [22] obtained very accurate estimation of the long-term creep rupture strength using this technique, irrespective of the transition from transgranular to intergranular fracture, by extrapolating the short-term creep data.

This technique is mainly based on the data rationalisation achieved through equation (3.1), where it is possible to rationalise the minimum creep rate, $\dot{\varepsilon}_m$, and the time to fracture, t_f, measurements by normalising σ through σ_{TS}. Since σ_{TS} represents the maximum stress that can be applied on a material at a specific creep temperature, the data sets can be described over the entire stress range from $(\sigma/\sigma_{TS} = 1)$ to $(\sigma/\sigma_{TS} = 0)$. In addition, it is evident that $(\dot{\varepsilon}_m \rightarrow \infty$ and $t_f \rightarrow 0)$ as $(\sigma/\sigma_{TS} \rightarrow 1)$, whereas $(\dot{\varepsilon}_m \rightarrow 0$ and $t_f \rightarrow \infty)$ when $(\sigma/\sigma_{TS} \rightarrow 0)$. These essential criteria are met by replacing equation (3.1), so that the stress and temperature dependences of the creep lives are described by [21, 22, 84]:

$$\sigma/\sigma_{TS} = \exp\left(- k_1 \left[t_f \exp\left(- Qc^*/RT\right)\right]^u\right) \qquad \ldots\ldots\ldots\ldots (3.2)$$

where the values of the coefficients k_1 and u can be easily evaluated from the plots of $\ln [t_f \exp(- Qc^*/RT)]$ against $\ln [- \ln (\sigma/\sigma_{TS})]$. The slope of these plots represents the value of u whereas the intercept with the y-axis represents the value of $\ln (k_1)$ from which k_1 can be calculated. The value of Qc^* can be evaluated at constant σ/σ_{TS} by plotting $\ln (t_f)$ against 1/T where the slope of these plots represents the value of Qc^*/R from which Qc^* can be obtained.

As with the representation of stress rupture properties through equation (3.2), the stress and temperature dependences of $\dot{\varepsilon}_m$ can be described using [21, 22, 84]:

$$\sigma/\sigma_{TS} = \exp\left(- k_2 \left[\dot{\varepsilon}_m \exp\left(Qc^*/RT\right)\right]^v\right) \qquad \ldots\ldots\ldots\ldots (3.3)$$

where the values of the coefficients k_2 and v can be obtained from the plots of ln [$\dot{\varepsilon}_m$ exp (Qc^*/RT)] against ln [- ln (σ/σ_{TS})]. The slope of these plots represents the value of v whereas the intercept with the y-axis represents the value of ln (k_2) from which k_2 can be calculated. The value of Qc^* can be evaluated at constant σ/σ_{TS} by plotting ln ($\dot{\varepsilon}_m$) against 1/T where the slope of these plots represents the value of - Qc^*/R from which Qc^* can be obtained.

In addition to equation (3.2) and (3.3), the planned operational life for some components must take into account the times required to reach certain limiting strains, t_ε. As with t_f in equation (3.2) and $\dot{\varepsilon}_m$ in equation (3.3), the stress and temperature dependences of t_ε can be quantified as [21, 22]:

$$\sigma/\sigma_{TS} = \exp (- k_3 [t_\varepsilon \exp (- Qc^*/RT)]^w) \quad \ldots\ldots\ldots\ldots\ldots\ldots (3.4)$$

where the values of the coefficients k_3 and w can be calculated from the plots of ln [t_ε exp (- Qc^*/RT)] against ln [-ln (σ/σ_{TS})]. The slope of these plots represents the value of w whereas the intercept with the y-axis represents the value of ln (k_3) from which k_3 can be calculated. The value of Qc^* can be evaluated at constant σ/σ_{TS} by either plotting ln (t_f) and/or ln ($\dot{\varepsilon}_m$) against 1/T where the value of Qc^* can be obtained from the slope of these plots (the slope will be either Qc^*/R or - Qc^*/R, respectively).

Studies by Wilshire and Scharning [21, 85] revealed that using equation (3.2) allowed extrapolation of the short-term creep life measurements and accurately predicted the 100,000 hours rupture strengths for several martensitic 9-12% chromium steels at different temperatures. Further studies by Wilshire and Scharning [22] also showed that equation (3.2), (3.3) and (3.4) permitted effective rationalisation and extended extrapolation of the time to fracture, t_f, the minimum creep rate, $\dot{\varepsilon}_m$, and the time to certain strains, t_ε, data for 1Cr-1Mo-0.25V steel, despite the tempering of the as received bainitic microstructure and the occurrence of a gradual transition from transgranular to intergranular fracture during creep exposure. In another study, Wilshire and Battenbough [84] proved that the stress and temperature dependences of $\dot{\varepsilon}_m$ and t_f were best described using equation (3.2) and (3.3) when they used this technique on polycrystalline copper.

Thus, using this new technique will certainly reduce the scale and duration of the test programmes currently undertaken to define the allowable creep strengths of power plants and aeroengines applications [85].

3.2 Objective of the New Methodology

The 'Wilshire equations', i.e. equation (3.2), (3.3) and (3.4), proved their precise and accurate capability of predicting the creep behaviour of different steels [21, 22, 85], copper [84] and aluminium alloys [86]. The long-term data obtained from these equations were, at least, as impressive as those obtained from the

parametric methods, but with the added advantage of that the empirical terms in the parametric expressions being replaced by physically-meaningful properties, i.e. the activation energy for matrix diffusion, Qc^*, and the relevant tensile strength, σ_{TS}, values. Moreover, these equations allowed not only data rationalisation and extrapolation, but also a straightforward interpretation of the behaviour patterns displayed by pure copper and aluminium alloys, as well as a range of power plant steels [21, 22, 84, 85, 86]. Therefore, the validation of this technique will provide a method by which the errors and flaws encountered by the other traditional parametric techniques can be, at least, reduced or even eliminated. This was proved, so far, by the reasonable predictions obtained using this technique on many different materials. For the same purpose, this capability of predicting the long-term creep data will be examined in this work on the Titanium IMI834 alloy using actual data obtained from creep tests completed under certain stresses and temperatures. This will, in return, provide an additional support to the predictive capability of this technique.

CHAPTER 4

PROCEDURES & PRACTICAL WORK

As a limited number of studies have been previously carried out on different materials using the new methodology, this research will thoroughly concentrate, for the first time, on using this new technique on Titanium IMI834. In addition, all the practical procedures followed, including all mechanical testing, along with the procedures adopted to prepare the samples for microstructural analyses will be discussed. The data obtained from these tests will be used to run the new model in order to prove the predictive capability of this technique using newly generated Titanium IMI834 data. Moreover, using the generated data, the Wilshire equations will be extended to re-construct full creep curves based on these actual measurements. After each creep test, the thickness of the alpha-case layer developed at the surfaces of the testpieces, as a result of oxidation, will be measured and used for further analysis. All images mentioned in this chapter are summarised in Appendix (A).

4.1 TITANIUM IMI834 ALLOY (TIMETAL 834)

Timetal 834 is a near alpha alloy which consists of 15% equiaxed primary alpha in a fine lamellar alpha/beta phase matrix [87, 88]. This unique microstructural composition of the alloy offers an increased tensile strength and creep resistance up to 873K [89]. Besides, the alloy derives its properties from the solid-solution strengthening and heat treatment in the alpha/beta phase field which makes it able to retain a good level of properties up to around 75cm diameter, with small reductions in strength in larger sections [89]. It is also reasonably forgeable and effectively weldable using all the established titanium welding techniques. This alloy is mainly used for the rings, compressor discs and blades of gas turbines and jet engines applications [89].

The chemical composition of this alloy consists primarily of: Ti-5.8Al-4.0Sn-3.5Zr-0.7Nb-0.5Mo-0.35Si [89]. The different elements which comprise this alloy provide, altogether, a stable composition and superior properties necessary for the high temperature applications. For instance, Aluminium (Al), Tin (Sn) and Zirconium (Zr) are considered as 'alpha stabilising elements' which act to stabilise the hexagonal alpha phase whereas Niobium (Nb) and Molybdenum (Mo) are 'beta stabilising elements' which act to stabilise the body centered cubic beta phase [90]. The addition of Silicon (Si) is to enhance the creep performance of the alloy [90]. The alpha stabilisers have the effect of increasing the transformation temperature between the alpha and

the beta phases in contrast to the beta stabilisers which tend to decrease this transformation temperature [90]. Another effect of the alpha stabilisers, Aluminium (Al) for instance, is that their atoms are slightly smaller and less dense than titanium atoms resulting in a lower density of this alloy in comparison with pure titanium [90]. Moreover, the hexagonal arrangement of atoms, i.e. the alpha phase, increases the hardness of the alloy in comparison to the body centered cubic arrangement, i.e. the beta phase, and thus, decreases the deformation under the effect of high stresses and temperatures [90].

This alloy has been developed for the high temperature applications of gas turbines and jet engines in order to replace the heavy nickel-base superalloys and increase the payload [91]. It has an added advantage of developing a wide variety of microstructures depending on the solution treatment and the subsequent cooling rate. Its bimodal microstructure that consists of 15% primary alpha in a matrix of a fine lamellar grained transformed beta provides a good combination of creep strength, low cycle fatigue and resistance against crack propagation properties [91]. The fact that the disks and blades of the compressor in a gas turbine are subjected to very high mechanical strain cycles accompanied by thermal transients during the start and the shut-down stages of modern gas turbines required materials that have fatigue, creep, tensile strength and fracture toughness capabilities which were specifically found in this alloy, Titanium IMI834 [90, 91].

4.2 Preparation and Microstructure of Titanium IMI834 Alloy

In order to obtain the as-received condition of the alloy, solution heat treatment was carried out at 1293K for 2 hours followed by oil-quenching [88]. The solution-treated sample was then thermally-aged at 973K for another 2 hours and subsequently air-cooled to improve the creep resistance of the alloy [88, 92]. The sample was then sectioned and mounted in epoxy mounts (Buehler Phenolic Resin Powder) using an automatic mounting press (Buehler Simplimet 3000), Figure A.1 (a), under a pressure of 290 bar for 1 minute heating time followed by 4 minutes cooling time. The mounting of the specimen was then followed by 4 stages of grinding which was carried out using SiC grinding sheets, Figure A.1 (b). At each successive stage of grinding, the sample was rotated 90° in order to get a better surface finish. The ground specimen was then polished using an automatic polishing wheel (Struers Polishing Machine), Figure A.1 (c), to achieve a mirror-like finish, and this was carried out in 3-successive steps, namely: (1) Polishing was first completed using the MD-Piano-220 disc and water as a lubricant and cooler, under a force of 25N for 1 minute at a speed of 300rpm. To keep the disc ready for another use, it should be water-rinsed and air-dried. (2) The specimen from the first polishing step was further polished using the MD-Plan disc lubricated by Diapro-Plan under a force of 30N for 5 Minutes at a speed of 150rpm. The disc was then air-dried. (3) Finally, the specimen was

polished using the MD-Chem disc and lubricated by OP-S Suspension (0.04 micron) diluted by water under a force of 20N for 8 minutes at 150rpm. The disc was then water-rinsed and air-dried. All the polishing discs used for polishing the sample are shown in Figure A.1 (d). Subsequently, etching was carried out using Kroll's reagent, Figure A.1 (e), which contains Hydrofluoric Acid (HF), for 40 seconds to highlight the grain structure and morphology. The study of the resulting microstructure under the optical microscope revealed the structure of the IMI834 in the as-received condition which consisted of 15% primary alpha colonies in a matrix of lamellar alpha and beta phases, Figure A.1 (f). However, this percentage has not been measured directly in this study, but the production routes and the heat treatment processes of this alloy has been referenced in the literature [87, 88] and was followed here which implies that the microstructural composition should be consistent.

4.3 Experimental Procedures (Mechanical Testing)

The Titanium IMI834 specimens investigated were supplied by Rolls-Royce plc as cylindrical tensile specimens, SC1-type, of a circular cross-section of 5.0 mm diameter and 12.0 mm gauge length in the as-received condition, Figure A.2 (a). The creep specimens, RLH 10259-type, were machined and prepared at Swansea University Workshop from the original tensile specimens by adding grips which were machined into them resulting in a 20.0 mm grip-to-grip distance and a diameter of 4.0 mm, Figure A.3 (a).

Five different types of tests were completed in order to obtain enough information about the behaviour of the Titanium IMI834 alloy under high temperatures, namely: Tensile and Stress Relaxation tests (using the SC1-type specimens), Creep, Creep-Step, or Cyclic-Creep, and Creep-Vacuum tests (using the RLH 10259-type specimens).

4.3.1 Tensile Tests

Tensile tests are necessary to select materials for engineering applications where the tensile properties obtained from these tests can be used to predict the behaviour of a material under different forms of loading other than only the uniaxial tension. These tests can be carried out by mounting a specimen in the tensile machine, gripping its ends and subjecting it to a tensile load. During the test, the load is recorded as a function of elongation. However, the load can be normalised by the initial cross-sectional area giving a stress value whereas the elongation can be normalised by the initial gauge length giving a strain value. A stress-strain curve is, thus, obtained having an identical shape to the force-elongation curve with the advantage that

it is independent of the specimen's dimensions [93]. It is worthwhile mentioning that the high-temperature tensile test is exactly the same as the normal tensile test with the only difference that in the former, the specimen is mounted and gripped in the tensile machine and heated up to a specific temperature prior to testing. The new gauge length as a result of the specimen's extension under the high temperature is, thus, recorded and used in calculating the strain of the specimen throughout the duration of the test. A typical stress-strain curve is illustrated in Figure (4.1). All the tensile tests were carried out under 'load' control.

The Titanium IMI834 specimens, Figure A.2 (a), were tested at three temperatures, namely: 823, 873 and 923K, where the stress-strain curve at each temperature was recorded. In each of these tests, the ends of the specimen were screwed into a threaded grip so that the specimen is held at the maximum load without slippage or failure in the grip section and then loaded into the tensile machine, Figure A.2 (b).

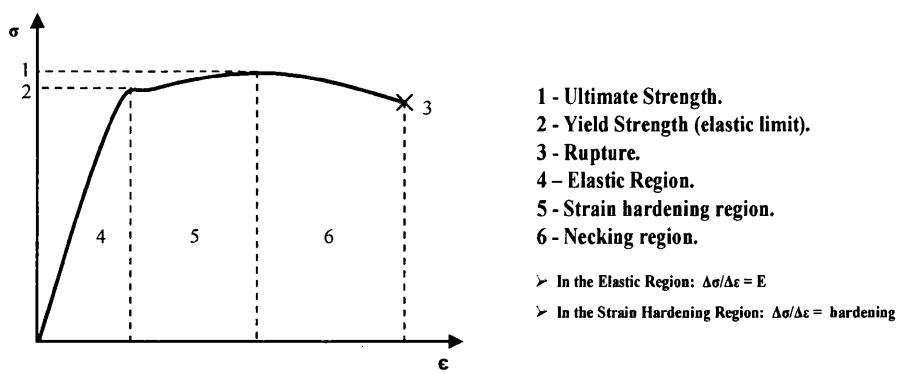

Figure (4.1): A sketch of the stress-strain curve showing the different regions of deformation during elongation.

Two type-N high-temperature thermocouples were located along the gauge length of the specimen to ensure that the temperature is uniform throughout the specimen's length, Figure A.2 (c). The temperature readings were displayed on a digital multi-meter by connecting the free ends of the thermocouples into the meter. The specimen's displacement was transmitted by heat-resistant rods, through a side aperture in the furnace wall, which were secured to the body of the strain-gauge extensometer that was located outside the furnace. The rods were attached precisely to the gauge length of the specimen using a spring system that screws to the furnace and uses struts to press the instrument in place, Figure A.2 (c). A small cooling fan was used to maintain the extensometer body temperature below 423K. The strain gauge was calibrated using a 12.0 mm setting bar so that the extensometer output is set to zero prior to the start of the test. Although this gauge length was used throughout the tensile test at different temperatures, it did not actually represent the 'total' gauge length when the specimen was heated up. In other words, after applying a high temperature, the specimen itself slightly deforms and, thus, extends before even applying any additional load. This extension

must be added to the original gauge length of 12.0 mm before the test starts. Therefore, the 'total' gauge length at elevated temperatures is calculated as:

Total gauge length = 12.0 mm + Extension after heating up the specimen (mm).

A Split Tube Furnace with optional side entry extensometer port was used to heat up the specimen prior to testing. The case of the furnace is constructed from stainless steel with aluminium and hardened insulation board end plates. The optional front cut-out allows the use of side-entry high-temperature extensometry. Adjustable stainless steel latches keep the furnace halves locked together during the test and can easily be opened once the test is complete. The specimen inside the furnace is heated through a combination of convection and radiation, dependent on the test temperature. The furnace's upper and lower sides should be securely insulated to reduce the level of heat loss using refractory ceramic-fiber insulation (KAO Wool) which consists of thermally efficient high temperature materials that combine the advantage of low heat storage with complete resistance to thermal shock.

During the test at 823K, the furnace was heated up to 843K with thermocouple readings of 824.5K and 822.3K giving an average specimen's temperature of ~ 823.4K. The furnace temperature was always higher than the specimen's temperature as a result of the heat loss from the furnace to the surroundings through the openings and unsecured places. Following heating up, a load of 0.5kN was applied to ensure that the specimen is kept in place without slippage. The specimen was kept for 2 hours in the furnace before the test took place to confirm that the desired temperature is attained, stable and uniform along the specimen's gauge length. The new 'total' length was calculated as 12.057 mm due to the specimen's extension under the high applied temperature. Eventually, the test started with a tensile rate of 1mm/min by increasing the tensile load and recording the corresponding elongation increment till the specimen fractured, Figure A.2 (d).

The same procedure was exactly followed at 873K where the furnace was heated up to 888K giving thermocouple readings of 874.5 and 872.7K and an average specimen's temperature of 873.6K. Before the test started, the initial tensile load on the specimen was 0.78kN and the new gauge length, following heating up, was 12.062 mm. The tensile rate of the test was 1mm/min, which is similar to the previous test.

Finally, the last test was carried out at 923K where the initial load was 0.68kN with a furnace temperature of 958K. The thermocouple readings were 924.4 and 923K which gave an average specimen's temperature of 923.7K. The total gauge length of the specimen was calculated as 12.068 mm. The tensile rate of the test was 2mm/min which is slightly faster than the previous tests.

Having completed these tests, the stress-strain curves were obtained at the applied temperatures. Besides, the fractured specimens, Figure A.2 (d), were then taken for further microstructural investigations using the Scanning Electron Microscope (SEM), for studying the fracture surfaces, and the Optical Microscope, for studying the grain structure, in order to compare the different modes of fracture under various test conditions.

4.3.2 Stress Relaxation Tests

The stress relaxation test can be considered as a special case of the tensile test with the only difference that after applying a certain amount of load, a sudden finite amount of constraint or 'constant strain,' is applied, Figure 4.2 (I), and kept constant for a certain duration of time during which the stress starts to drop or 'relax', Figure 4.2 (II), with time [94]. The value of the Elasticity Modulus, E, can be calculated in Figure 4.2 (I) from the slope of the stress-strain curve during the initial loading stage before reaching the yield point.

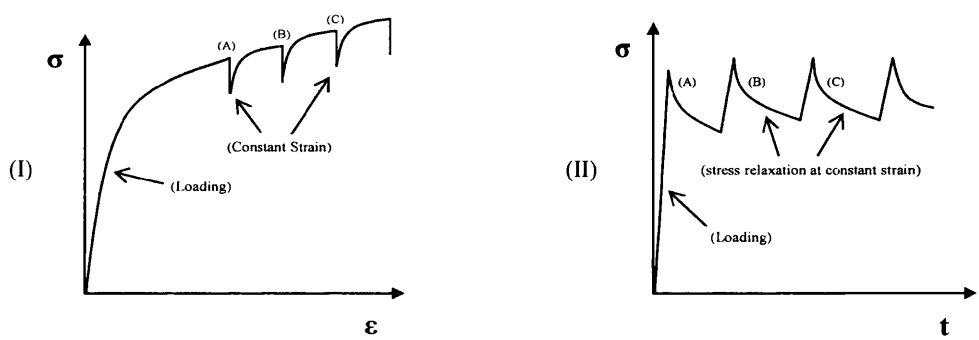

Figure (4.2): A sketch of the (I) stress-strain curve with a sudden applied constraint (constant strain) and (II) stress relaxation behaviour corresponding to the selected strain levels in (I).

Moreover, other values of the elasticity modulus can be obtained at point A, B and C, of the same curve, where other loadings are being applied after relaxation at each stage [94, 95]. On the other hand, at each stage of Figure 4.2 (II), it can be observed that the stress continues to decrease with time during relaxation from which the stress relaxation rate, $d\sigma/dt$, can be obtained [94, 95].

At any time during stress relaxation, the sum of the elastic strain, ε_e, and the inelastic strain (or plastic strain), ε_p, is given by [95]:

$$\varepsilon_{total} = \varepsilon_e + \varepsilon_p \quad \text{..... (4.1)}$$

In this equation, if ε_{total} is kept constant then: $d\varepsilon_{total}/dt = 0$, and $d\varepsilon_p/dt$, at any time after the beginning of the stress relaxation, is given by [94, 95]:

$$d\varepsilon_p/dt = - d\varepsilon_e/dt = - d(\sigma/E)/dt \quad \text{..... (4.2)}$$

where $\varepsilon_e = \sigma/E$, which is the elastic strain. This equation can be rearranged to give [94, 95]:

$$\dot{\varepsilon}_p = - (d\sigma/dt)/E \qquad \text{.....} \quad (4.3)$$

where $\dot{\varepsilon}_p$ is the plastic strain rate, $d\varepsilon_p/dt$. From this equation, calculating the plastic strain rate is a straight forward procedure where the value of E is obtained from Figure 4.2 (I) during the elastic loading whereas the value of the stress relaxation rate, $d\sigma/dt$, is calculated from Figure 4.2 (II). Plotting the values of ε_p against $1/\dot{\varepsilon}_p$ might be fitted using regression analysis such that: $1/\dot{\varepsilon}_p = f(\varepsilon_p)$, which can be rewritten as: $dt/d\varepsilon_p = f(\varepsilon_p)$, from which the time can be calculated according to [95]:

$$t = \int_{\varepsilon_{po}} f(\varepsilon_p)\, d\varepsilon_p \qquad \text{.....} \quad (4.4)$$

At each value of stress, the corresponding plastic strain, ε_p, and time, t, can be calculated using equation (4.1) and (4.4), respectively, from which creep curves might be re-constructed [95].

Another type of stress relaxation tests involves loading, stress relaxation and then complete unloading, in contrast to the previous type where the load is not removed completely after relaxation [94], as shown in Figure 4.3 (I). The behaviour of the material during the loading and the unloading stages is shown in Figure 4.3 (II), from which two values of the elasticity modulus, E, can be obtained and an average value can accordingly be calculated.

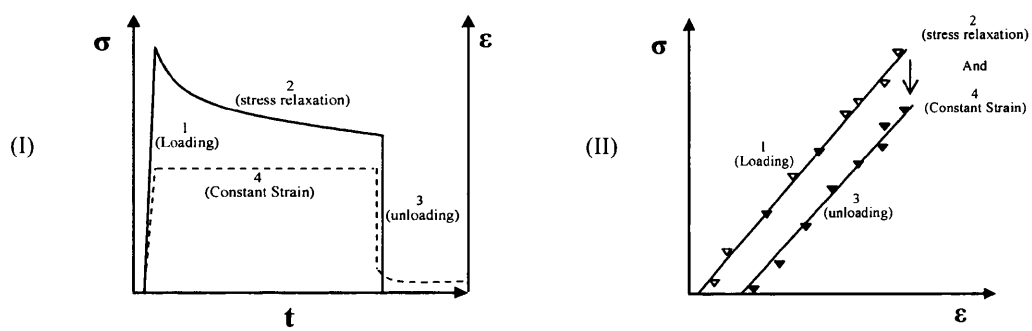

Figure (4.3): A sketch of the (I) stress-strain-time curve involving loading, relaxation and unloading, (II) stress-strain values obtained from Figure (I) during the loading and the unloading stages from which two values of the elasticity modulus, E, can be calculated.

All the stress relaxation tests were carried out under 'strain' control using the same batch of the Titanium IMI834 specimens, used in the previous tensile tests, of 5.0 mm diameter and 12.0 mm gauge length, Figure A.2 (a), and using the same tensile machine, Figure A.2 (b), but with changing the test conditions. The tests were completed at five selected temperatures, namely: 823, 848, 873, 898 and 923K. The machine was connected to the logging system via three channels: Channel 0 (Strain; 0.5mm/10volts), Channel 1 (Load; 50kN/10volts) and Channel 2 (Position; 10mm/10volts). The readings were taken at the order of (1 Reading/0.2 seconds) for the first 10 seconds, followed by (1 Reading/5 seconds) for the remaining duration

of the test. A hold period, in which the strain is held constant, of 30 minutes was used for each step followed by a specified increase in the value of strain which was again held constant for another 30 minutes and so on for the successive stages. Two type-N thermocouples, calibrated to a high precision of ± 2K, were used, Figure A.2 (c). A calibrated extensometer was used to measure the elongation of the specimen, Figure A.2 (c). The extensometer was accurately calibrated prior to the start of each test using a 12.0 mm setting bar to obtain accurate measurements.

The first test was carried out at 923K with a furnace temperature of 935K and thermocouple readings of 924.5 and 922K giving a specimen's average temperature of 923.25K. As with the previous tensile tests, before the test started, the new gauge length of the specimen, as a result of extension under the high temperature, was calculated as 12.053 mm. The same procedures of the previous tensile tests were followed by applying a certain amount of load and recording the stress against strain. After reaching a strain of, say, 0.5%, this value of strain was held constant for a period of time, 30 minutes in our test, during which the stress started to decrease, or relax. More successive stages were completed by increasing the strain value by 0.5% at each successive step up to 4% total strain, when the steps were increased by 1% up to 6% total strain. It is worthwhile mentioning that at this value of total strain, the specimen did not fracture and thus, the test was interrupted and the tested specimen was sectioned and sent to further metallurgical investigations.

At 873K, the furnace was heated up to 880K which gave thermocouple readings of 875 and 872.3K resulting in an average specimen's temperature of 873.65K. The new gauge length was recorded as 12.134 mm. The strain was held constant at an order of 0.5% up to 3% when the steps were increased by 1% up to 4% total strain. Again, the test was interrupted as the specimen did not fracture and the stress-strain curve was obtained. At 823K, the furnace was heated up to 833K, and the new gauge length of the specimen was 12.03 mm. The thermocouple readings were 824K and 823K with an average specimen's temperature of 823.5K. As with the 873K test, the strain was increased in an order of 0.5% up to 3% when it was changed to an order of 1% up to 4% total strain and then, interrupted. The tested specimens were then sectioned and examined under the Optical microscope.

The same procedures were repeated at the intermediate temperatures of 848 and 898K where the stress relaxation curves were also obtained. These intermediate tests were necessary to support the results of the previous tests such that if an interpolation was carried out between, say, 873 and 923K, the results of this interpolation must be consistent with the values obtained from the actual 898K test. The same outcome should be valid for the results of the 848K test which should lie between the 823 and the 873K tests results.

After completing these tests, similar curves as the ones in Figure (4.2) were obtained and many data points were recorded to run the analysis which involved the steps mentioned in equation (4.1), (4.2), (4.3) and (4.4) from which the creep curves might be re-produced. In addition, the values of the elasticity modulus, E, were calculated from the slopes of the stress-strain curves during the loading stage at the different temperatures which should be comparable with the values obtained from the former tensile tests at the same selected temperatures.

It is worthwhile mentioning that after each stress relaxation test, the machine's control should be changed from 'strain' into 'load' control to avoid the fracture of the specimen when the furnace is switched off. In an effort to understand this effect, the machine was left under 'strain' control after completing the first two tests at 923 and 873K. It was noticed that when the furnace was turned off and cooled down, the specimen fractured after shrinkage at room temperature. The reason was that when the machine is held under 'strain' control, the cross-head or the actuator of the machine is already fixed in a certain position regardless of any change in strain, i.e. the specimen will shrink while its ends are fixed, which then leads to fracture. The cooling process of the specimen means that the atoms' thermal energy is decreasing which results in bonding the atoms together leading to a decrease in the material's ductility. In this case, the material's toughness is decreasing and thus, if there were any surface cracks, this will facilitate the growth of these cracks into the material leading to fracture. On the other hand, when the machine was changed into 'load' control, the specimen did not fracture after shrinkage at room temperature. The explanation is that under 'load' control, the cross-head will move according to any shrinkage of the specimen's length to keep the 'load' constant. In other words, as the specimen was shrinking, its ends were moving with the cross-head and thus, no fracture took place after cooling down.

4.3.3 Creep Tests

Cylindrical Titanium IMI834 creep specimens of 25.0 mm gauge length and 4.0 mm diameter, Figure A.3 (a), were tested in tension using the high-precision constant-stress creep machines, Figure A.3 (b). Two type-R thermocouples located at several positions along the specimen's gauge length, Figure A.3 (c), established that temperatures were controlled to a very high precision. The upper and the lower parts of the specimen were tightly fixed in the grips of the creep machine, Figure A.3 (c), such that high stresses could be applied without causing slippage of the specimen at the grip position. These grips were attached to the extensometers which are responsible for recording the displacement of the specimen during the test. High-temperature paste was used to protect the threads of all components used in the harsh environments inside the furnace which

involved very high temperatures and stresses. The measurements of each specimen's elongation and temperature were continuously monitored during the test with a fluke data logger, Figure A.3 (b). The system can store a large number of readings from each machine for subsequent processing. The specimen was surrounded by a sliding tube furnace which was connected to the logger system, Figure A.3 (b).

Creep tests were carried out at temperatures 823, 848, 873, 898 and 923K under different stresses ranging from a minimum of 140MPa up to a maximum of 600MPa. Rupture times varied from 14.4 hours, as a minimum, at 873K and 550MPa, up to 5805.5 hours, as a maximum, at 873K and 200MPa. However, some of these creep tests were carried out at Swansea University in the past using the same batch of Titanium IMI834 used in this study and thus, the creep properties from these tests were available. For the purpose of having more creep data to fill the gaps between some creep data points, more creep tests were, thus, carried out recently on Titanium IMI834, as show in the test matrix in Appendix (C). The data logging rates were 1 reading/5 seconds at the start of each test followed by 1 reading/1 minute for the first hour or two and then 1 reading/2 hours throughout the remaining duration of the test, depending on the creep deformation rates. For each test, a total of 700 to 800 points were stored and then filtered down to 300 to 400 readings only. This number of points was considered sufficient to define well the shape of each creep curve. During each test, time was recorded against strain under a defined tensile stress up to fracture.

Many factors could significantly affect the creep life, during a test, if caution has not been taken in advance. The diameter of the specimen and thus, the cross sectional area, for instance, must be accurately measured. This was carried out by taking five measurements of the diameter all the way along the gauge length, and then taking the average of these measurements which represents the actual diameter. Based on this calculated diameter, the stress can then be calculated through dividing the applied load by the cross sectional area of the specimen. The applied load on the specimens was generated using suspended weights. A ratio of 10:1 was used to calculate the required stress where each 1kg of the suspended weights was multiplied by 10 to give the required stress value for the corresponding specimen's diameter. Another factor that could minimise the anticipated life of the specimen is the temperature throughout the test. For this purpose, two type-R thermocouples were used along the gauge length of the specimen. These thermocouples were calibrated to a high precision prior to the start of the test. During each test, the readings of the thermocouples were around ± 2K of the actual test temperature which gave a reasonable average value that represents the required specimen's temperature. Another very important factor is the surface finish of the specimen. This can significantly cause the specimen to fail in an unexpected earlier life time. The specimens were machined and polished to an excellent condition so as to eliminate any scratches or surface defects.

The crept specimens, Figure A.3 (d), were given a certain number related to the test carried out in order to differentiate each specimen from the others. The crept specimens were metallographically examined using the SEM, for the studying the fracture surfaces, and the Optical Microscope, for studying the morphology of the grains on the longitudinal polished sections.

4.3.4 Creep-Step Tests (Air)

This test can be considered as a special case of the normal creep test previously carried out with the only difference that it involves changing the test conditions while the test is still ongoing. In other words, the test starts with applying a certain stress at a specified temperature and the specimen is allowed to creep for a certain period of time when the test conditions, either the stress and/or temperature, are altered. As with the previous creep tests, cylindrical creep specimens of 20.0 mm gauge length and 4.0 mm diameter were used, Figure A.3 (a). The same procedures of the previous creep tests were followed by gripping the specimen in the creep machine, Figure A.3 (b), and attaching it to the extensometers. Two type-R thermocouples were used to measure the specimen's temperature, Figure A.3 (c). As the name of the test implies, the creep-time curves were recorded at each single step during which the stress and/or temperature were/was changed after a certain period of time, Δt. The crept specimens, Figure A.3 (d), were then sectioned and studied under the SEM and Optical microscope in order to compare the modes of fracture involved in the creep-step test fractured specimens with the ones obtained from the normal creep conditions.

This kind of step-tests can take any of the following three scenarios: (1) changing both the stress, $\Delta\sigma$, and temperature, ΔT, (2) changing the stress, $\Delta\sigma$, at a constant temperature, T, and (3) changing the temperature, ΔT, at a constant stress, σ. In all cases, a transition from one creep curve to another is expected to take place. However, this transition might not be very obvious due to the narrow change in stress, $\Delta\sigma \sim 220$MPa, and temperature, $\Delta T \sim 50$K, that were used in our tests. The conditions were selected upon a creep life of no more than 300 hours from the previously obtained creep curves. The main aim of these tests is to study the effect of changing the conditions in the actual gas turbines on the creep life during starting-up/shutting-down which involve loading/unloading and heating/cooling of all components and blades.

(1) Changing both the stress, $\Delta\sigma$, and temperature, ΔT, during creep:

This test started with ($\sigma_1 = 455$MPa/$T_1 = 848$K) and was changed to ($\sigma_2 = 280$MPa/$T_2 = 898$K) every 24 hours till the specimen fractured. These two conditions were selected from the previously completed creep tests based on a creep life of ~ 300 hours. The test started at step (1) when the furnace was heated up to 870K giving thermocouple readings of 851 and 845K resulting in an average specimen's temperature of ~ 848K.

The specimen was allowed to creep up to a certain level when the test condition was changed to step (2) after a period of $\Delta t = 24$ hours, which represents the duration of each step, as shown in Figure 4.4 (a) and (b). This change from one condition to another was first done by unloading to σ_2 at a constant temperature, T_1, followed by an increase in temperature to T_2, at the constant stress, σ_2. The reason behind this sequence in changing the test conditions is that if the temperature was increased to T_2 before unloading to σ_2, the specimen might have fractured as σ_1 could have been higher than the UTS at T_2.

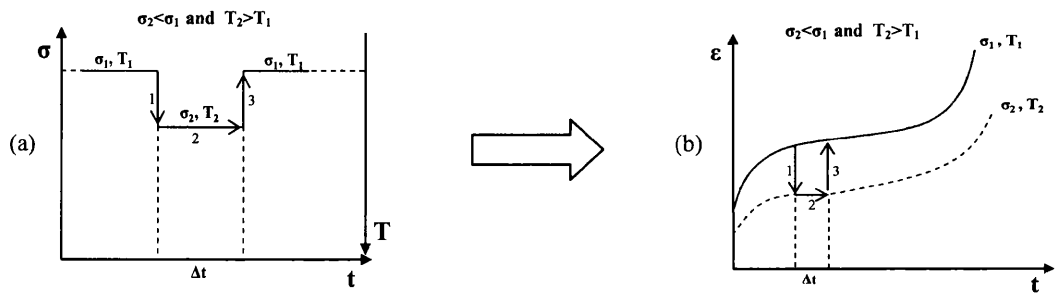

Figure (4.4): A sketch of a creep-step test by; (a) changing the stress and temperature, and (b) the expected creep curve.

After another period of $\Delta t = 24$ hours, the change in test conditions took place in a reverse order, i.e. by decreasing the temperature from T_2 to T_1 at a constant stress, σ_2, followed by reloading to σ_1 at a constant temperature, T_1. This sequence was necessary to avoid reaching the UTS at T_2 as σ_1 might have exceeded the value of the UTS at this temperature. To reduce the specimen's temperature, the furnace temperature was reduced and a cooling fan was used to speed up the cooling process. The furnace was cooled down to 918K giving thermocouple readings of 901 and 896K which gave an average specimen's temperature of 898.5K. Reloading the specimen was done by carefully adding more hanging weights to reach the anticipated stress, σ_1, with the least amount of scatter in the output data. The test continued with changing the conditions every 24 hours till the specimen fractured and the strain-time curve was obtained. It is worthwhile mentioning that this test has been repeated, under the same conditions, in order to confirm the results obtained from the first attempt.

The same steps were carried out for another test with different conditions of ($\sigma_1 = 560$MPa/$T_1 = 823$K) and ($\sigma_2 = 340$MPa/$T_2 = 873$K), where another strain-time curve was obtained for further analysis. These two conditions were based on a creep life of ~ 300 hours.

(2) Changing the stress, $\Delta\sigma$, at a constant temperature, T:

This test is less complicated than the former one as the temperature, T, is kept constant throughout the test while changing the stress from σ_1 to σ_2 , and vice versa, at each successive step. The specimen should be allowed to creep at σ_1 and T up to a certain point before the test conditions are altered, after a period of 24

hours, by reloading to σ_2, at the same T, as shown in Figure 4.5 (a) and (b). After another period of $\Delta t = 24$ hours, the specimen should be unloaded to σ_1 by removing some of the hanging weights. Caution must be always taken when reloading to σ_2 by checking that it is always less than the UTS at the specified temperature, by at least 10-15%. The loading/unloading process requires adding/removing certain weights while the test is still ongoing which requires an extra caution so as to reduce the amount of scatter in the output data.

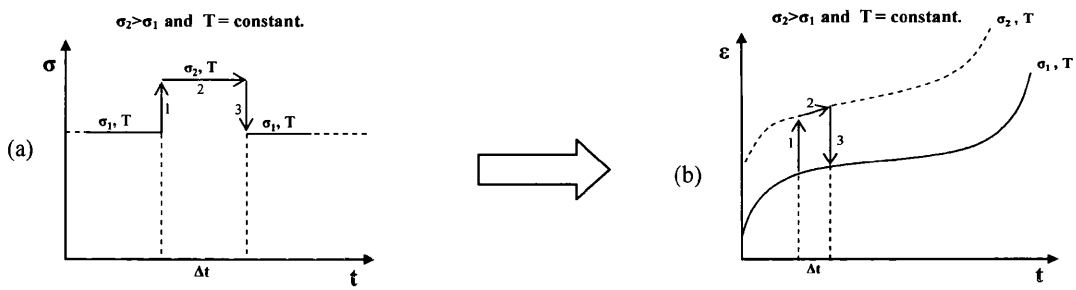

Figure (4.5): A sketch of a creep-step test by; (a) changing the stress at a constant T, and (b) the expected creep curve.

(3) Changing the temperature, ΔT, at a constant stress, σ:

This test is the least complicated test of all the previously mentioned step tests as the stress is kept constant at σ while only adjusting the furnace temperature to switch from T_1 to T_2 , and vice versa, every 24 hours. The specimen should be allowed to creep at a constant stress, σ, and temperature, T_1, up to a certain extent before the specimen's temperature is increased to T_2, as illustrated in Figure 4.6 (a) and (b).

After another period of $\Delta t = 24$ hours, the specimen's temperature should be decreased by reducing the furnace temperature and using a cooling fan to speed up the process. Caution must be always taken when selecting the amount of load that is being applied as it should be always lower than the UTS value.

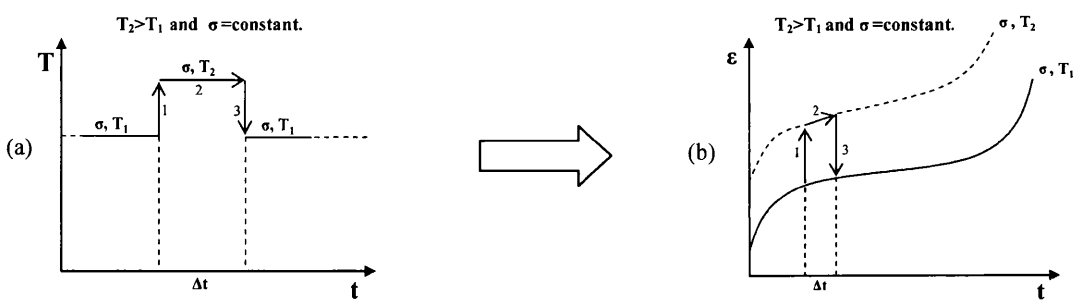

Figure (4.6): A sketch of a creep-step test by; (a) changing the temperature at constant σ, and (b) the expected creep curve.

In conclusion, many factors could affect the creep behaviour when changing the creep conditions while the test is still ongoing and might lead, in return, to an earlier fracture of the specimen. For instance, the

maximum load that is being applied to the specimen, at a certain temperature, must be always lower than the corresponding UTS at that temperature, by at least 10-15%. Moreover, unloading/reloading must be carried out slowly and carefully to avoid a sudden tension and thus, a sudden fracture of the specimen. In addition, output data of inferior quality could be obtained if the unloading/reloading process is carried out quickly, without caution, due to the larger amount of scatter that might result.

4.3.5 Creep-Step Tests (Vacuum)

Vacuum tests were carried out using a vacuum chamber that has been refurbished and reinstalled on the creep machines at Swansea University. The installation of such a chamber was a challenge since these vacuum chambers have not been used for more than 15 years. Therefore, collecting the vacuum kit parts, checking for any air leaks, obtaining the necessary pumps, assembling the apparatus together, installing the cooling water system and, finally, put it into operation took ~ 4 months of continuous work. These efforts made it possible to run, for the first time since 15 years, such vacuum creep tests for future studies at Swansea University.

The motivation behind carrying out such vacuum tests was that previous microstructural studies [87, 88, 96, 97] revealed that a brittle alpha-case layer was developed at the Titanium IMI834 specimen surfaces when tested in oxidising atmospheres, i.e. in air, and thus, modified the mechanical properties of the alloy. This layer was a consequence of the inward diffusion of oxygen, which is an alpha stabiliser, causing the beta-phase to destabilise and transform to an alpha-case layer on the surface [87, 88, 96, 97]. Extensive studies on the kinetics of this brittle layer were carried out by Gurappa [96] where the hardness measurements showed that an increase in hardness of this layer was observed when compared to the substrate material. Besides, models to predict the rate by which this alpha-case layer builds up were presented by Gurappa [97] under different test conditions. To eliminate the effect of this brittle layer on the mechanical properties, various coating techniques were proposed [96, 97].

However, in this research, in order to eliminate the effect of the alpha-case layer on the creep life and whether it actually affects the total life of a material, creep-step vacuum tests were carried out on the same creep machines, Figure A.4 (a), using the assembled vacuum chamber that can be fitted into the machine, Figure A.4 (b). This test was completed using exactly the same procedure described in Figure (4.4), by changing both the stress and temperature during the test, with the only difference that this test was done in a vacuum atmosphere. The vacuum chamber can be inserted inside the tube furnace of the machine to maintain a vacuum pressure of $\sim 4\times10^{-4}$ mbar throughout the test. This vacuum pressure was obtained by using two vacuum pumps in a series connection, namely: a roughing and a turbo pump, Figure A.4 (a). The main task

of the roughing pump, sometimes called the 'backing' pump, is to drop the atmospheric pressure inside the chamber to a 'rough' vacuum at which the high-vacuum pump, i.e. the turbo pump, takes over to reduce the pressure to a lower value. In the completed tests, the roughing pump provided a pressure of ~ 6×10^{-3} mbar which was further reduced to the required vacuum pressure of ~ 4×10^{-4} mbar by applying the turbo pump. The pressure was measured using a pressure gauge which was connected to a digital penning gauge, Figure A.4 (a), to display the pressure readings. Rubber O-rings, i.e. gaskets, were used at the top and the bottom interfaces of the vacuum chamber to provide the necessary seal which was improved by applying silicon grease to these gaskets to preserve them, as it is very tolerant at high temperatures, and to provide an additional seal to maintain the vacuum pressure. Cooling water was used at the upper and the lower parts of the chamber to preserve these gaskets and to cool the chamber around them, Figure A.4 (b). Two type-N thermocouples were inserted securely inside the chamber, through a sealed port, Figure A.4 (b), to measure the specimen's temperature which was displayed on a digital fluke meter. An illustration of the vacuum creep kit is shown in Figure (4.7).

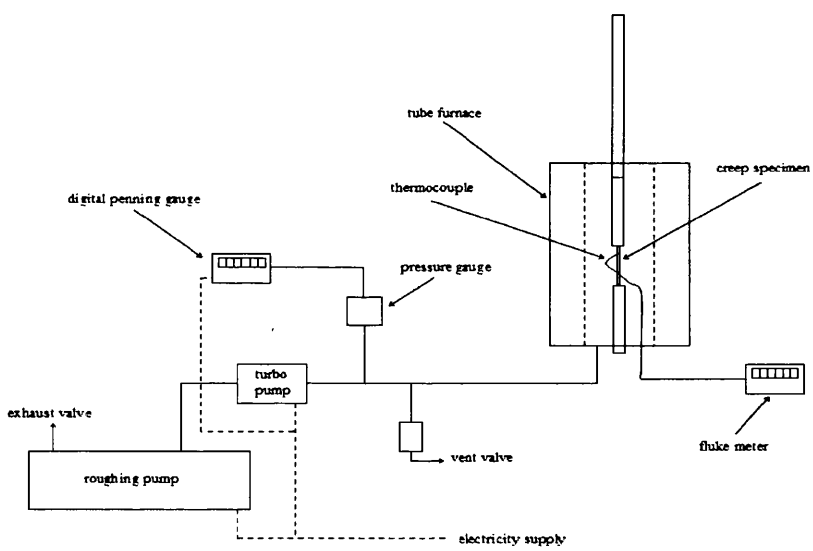

Figure (4.7): A schematic diagram of the vacuum creep kit showing the main components.

The sequence of the test started by turning the roughing pump on for ~ 10 minutes to get the required rough pressure followed by the turbo pump that provided the required high-vacuum pressure of ~ 4×10^{-4} mbar inside the chamber. At this stage, air leaks into the chamber can be detected by either monitoring the penning pressure gauge reading or the 4-speed indicating lights on the turbo pump control unit (all lights should be on: the red and the green ones). When no air leaks are detected, the cooling water and the furnace can then be switched on, respectively. This sequence, i.e. reaching the required vacuum before the furnace is turned on, is

necessary to ensure that no oxygen exists inside the chamber at the same time when the furnace is turned on so as to avoid the formation of the brittle alpha-case on the specimen's surface, which is the main aim of this test. The first test was a repeat, but in vacuum, of the test that was completed in air at (σ_1 = 560MPa/T_1 = 823K) and (σ_2 = 340MPa/T_2 = 873K). The same sequence as described in Figure (4.4) was followed after the required vacuum pressure was attained, which is: (1) rising the specimen's temperature up to 823K, applying a stress of 560MPa and then leaving the specimen to creep for a period of Δt = 24 hours. (2) unloading the specimen down to 340MPa before increasing the temperature up to 873K so as to avoid the UTS value at this temperature. (3) a reverse sequence was then followed in the successive step, i.e. cooling then reloading, and so on. Each step was then repeated every 24 hours till the specimen fractured and thus, the total life was recorded. At the end of each test, the furnace was first turned off while the vacuum pumps are still ongoing to ensure that a high-vacuum pressure is still available inside the chamber while the furnace is still hot to avoid any formation of the alpha-case at the end of the test. It is worthwhile mentioning that this test has been repeated, under the same conditions in order to confirm the results obtained from the first attempt. Moreover, two other tests were carried out at (σ_1 = 455MPa/T_1 = 848K) and (σ_2 = 280MPa/T_2 = 898K) in order to compare their results with the tests carried out in air under the same conditions.

Due to the vacuum chamber's design limitations, no creep curves were obtained as it was difficult to fit the extensometers inside the vacuum chamber. However, the full creep curves are not as necessary as the time to rupture of the specimen as the main goal of the test is to compare the life obtained from tests under vacuum with the life obtained, under the same test conditions, in an oxidising air atmosphere and thus, the effect of eliminating the alpha-case layer on the total creep life. Metallographic examinations of the crept specimens, Figure A.4 (c), using the SEM and the Optical Microscope were carried out in order to compare the results of the crept specimens under vacuum conditions with those previously obtained in air.

CHAPTER 5

RESULTS & DISCUSSION

The tests results that have been obtained from testing the Titanium IMI834 specimens will be used here to run the Wilshire new model in an effort to predict the creep life of this alloy based on some physically meaningful parameters. The plots of results and micro images, tables of all analysed data and the detailed analytical and mathematical procedures followed are summarised in Appendix (B), (C) and (D), respectively.

5.1 EXPERIMENTAL TESTS RESULTS

This part will discuss the details of all the mechanical tests results that have been obtained from the mechanical testing of the Titanium IMI834 specimens.

5.1.1 TENSILE TESTS RESULTS

The mechanical properties of Titanium IMI834 were determined through the tensile tests that were performed. From these tests, full stress-strain curves at 823, 873 and 923K were produced, Figure (B1.1-B1.3), respectively, from which the yield (or proof), ultimate and fracture strengths were obtained. At the beginning of each test, all tensile curves at the applied temperatures showed a linear-elastic behaviour, as described by Hooke's law: $\sigma = \varepsilon E$, from which the elasticity modulus, E, was evaluated, followed by a plastic deformation region. From the obtained tensile curves, Titanium IMI834 showed a ductile behaviour wherein elastic, strain hardening and necking regions were observed, in contrast to the brittle materials behaviour in which little or no plastic deformation takes place and thus, the material fractures near the end of the liner-elastic portion of the curve. At the end of the elastic region, the yield point was observed when the linear stress-strain line deviated from linearity as the strain increased rapidly relative to the applied stress. The ductility, i.e. the total elongation up to fracture, was found to be proportional to temperature. In other words, higher ductility was obtained as the temperature was increased from 823 to 923K. This is apparent from the higher strain values obtained at fracture as the temperature increased. In addition to the ductility results, another very important outcome of the tensile tests is the ultimate tensile strength, σ_{TS}, values that were obtained at all temperatures. In contrast to ductility, the ultimate tensile strength values were inversely

proportional to temperature. This is in agreement with the fact that as temperature increases, the ductility, or the malleability, of a material also increases and thus, a lower stress is required to deform the material. As the values of the elasticity modulus, E, yield strength, σ_{yield}, and the ultimate tensile strength, σ_{TS}, showed a linear trend when plotted against the temperature, Figure (B1.4), it was possible to obtain the values of these parameters at the intermediate temperatures, i.e. 848 and 898K, without the need to carry out tests at these intermediate temperatures.

The microstructural examination of the fractured specimens confirms that a ductile fracture took place at all temperatures. The Macro images of the fractured specimen at 823K, Figure (B1.1), shows almost a cup-and-cone ductile failure surface which can be seen more obviously in the SEM images from which microvoids coalescence among the grains can be observed. The images of the fractured specimen at 873K, Figure (B1.2), shows a different trend of the ductile fracture where the cup-and-cone is not as obvious as in the one obtained at 823K, but this fracture is still ductile as it can be seen more clearly in the SEM images. The fracture at 923K, Figure (B1.3), is also ductile but a sheared fracture surface is very obvious. The optical images show that no surface cracks were found at the surfaces, along the gauge length, of the fractured specimens at all temperatures, but some voids among the grains were observed. This confirms that the fracture started with necking, voids nucleation, coalescence and propagation and ended up with a ductile fracture.

5.1.2 Stress Relaxation Tests Results

Stress relaxation tests were carried out at 823, 848, 873, 898 and 923K. At each of these tests, three plots were necessary to be recorded, namely: the strain-time, stress-strain, and the stress-time (or relaxation) curve, Figure (B2.1-B2.5). The strain-time plots show the strain values that have been accumulated throughout the test as well as the time intervals between each successive re-loading stages. It is worthwhile mentioning that all tests were interrupted at a certain amount of accumulated strain before fracture and thus, no fracture surfaces or SEM images were taken for these testpieces. On the other hand, the stress-strain curves provided the value of the elasticity modulus, E, from the slope of the curve during the initial loading before reaching the yield point. These values of the elasticity modulus were consistent with those previously obtained from the tensile tests curves. Other values of the elasticity modulus, at each temperature, might also be obtained from the same curves during the re-loading stages every 30-minutes interval. However, the values of the elasticity modulus in the re-loading stages, after passing the yield point, are expected to be lower than the original value obtained during the initial loading. This can be explained based on the fact that when re-loading the specimen after the material has been plastically deformed, less stress is, thus, needed to deform

the material as an accumulated plastic strain still exists. This means that at each successive stage, a lower load is needed to deform the material as the resistance of the material to be deformed, which is the definition of the elasticity modulus, decreases and thus, a lower value of the modulus is obtained.

The stress-time, or the relaxation, curves show a trend according to which the stress decreases with time when the strain is held constant. From these plots, the rate by which the stress decreases with time can be calculated by dividing the change in stress, $\Delta\sigma$, by the change in time, Δt, using the '3-Secant' method. The analytical procedure described by equations (4.1 – 4.4) has been applied to the stress relaxation results but did not provide any precise description of the creep curve behaviour when compared to actual creep curves previously obtained at the same corresponding conditions, Figure (B2.6-B2.10). This might be a result of the scatter in the output data, the value of E that has been used in the analysis as this value was decreasing at each reloading stage throughout the duration of the test, the strain increment at each stage, the period at which the strain was held constant or the calculations involved in the integration function that has been used in equation (4.4). Any of these possible sources of errors would, in return, provide results which are inconsistent with the actual material's behaviour. In agreement with these outcomes, when this method was used to construct the creep curves based on the data of the nickel-base superalloys [95], it did not provide any precise description of the creep behaviour although: (1) shorter hold periods of 300 seconds were used in their experiments which should give more accurate results in comparison to 30 minutes hold period in our experiments, (2) the strain increment was 0.1% in their study in comparison to 0.5% in our work, (3) an overall average value of E was used in their calculations which should not be the case as more deviations are expected when the actual value of E at each successive stage is used, as in our calculations, (4) their predictions of the creep curve was only up to 4% and even though, it was not impressive since less accurate predictions would have been obtained if higher strain values have been used. Therefore, even when more simplifications are used [95] to predict the creep curves based on this technique, this method was unable to construct any full creep curves and thus, it was a motivation to find an alternative method for creep curves predictions.

The Optical images of the sectioned testpieces, Figure (B2.1-B2.5), showed neither surface cracks nor internal voids or cavities. In general, since voids nucleate and propagate after necking takes place, this means that the tests were interrupted before necking took place at all temperatures. This can be confirmed by projecting the stress-strain curves obtained from relaxation onto the tensile curves previously carried out and comparing the total ductilities at the end of each curve. It can be obviously seen that the ductilities in the tensile curves at fracture ranged from ~ 0.08, at 823K, to ~ 0.15, at 923K, in comparison with ductilities of

~ 0.04, at 823K, to ~ 0.06, at 923K, during relaxation at the point where the tests were interrupted. This confirms that the points at which the relaxation tests were interrupted are well below the point at which necking took place during the tensile tests.

5.1.3 Creep Tests Results

Creep tests were carried out at temperature 823, 848, 873, 898 and 923K under various stresses. Full creep curves were obtained from which the minimum creep rate, $\dot{\varepsilon}_m$, the time to predefined strains, t_ε, the time to fracture, t_f, and the creep ductility, ε_f, values were calculated. The slope at any point of the creep curve represents the strain rate, $\dot{\varepsilon} = d\varepsilon/dt$, at that point which can be easily calculated, using the '3-Secant Method', by dividing the change in strain, $\Delta\varepsilon$, by the change in time, Δt.

In order to study the effect of stress and temperature on the shape of the creep curve, these curves were normalised (by dividing the time and strain values by the total creep life, t_f, and ductility, ε_f, respectively) and then plotted at constant temperatures, Figure (B3.1). From these plots, it can be observed that the curves become more tertiary dominated with increasing the stress value, at a constant temperature. This implies that the strain rate increases as a result of increasing the stress, at a constant temperature, which, in return, affects the total creep life, t_f, and ductility, ε_f. This effect can be more obviously seen when plotting the actual creep curves, at constant temperatures, without normalising them, Figure (B3.2). Here, it is very clear that as the stress increases, the creep rate increases and thus, the total creep life and ductility decrease. When comparing all the plots at the different temperatures together, it is also true that as the temperature increases, the strain rate increases and thus, the total life and ductility decrease. This creep behaviour agrees very well with the Monkman-Grant relation, equation (2.1), and the power law, equation (2.8).

Each creep curve was then studied individually in order to understand the creep mechanism more closely. For this purpose, the creep curves were plotted at each stress and temperature, separately, along with their corresponding strain rate plots and micrographs, Figure (B4.1-B4.28). All creep curves showed a normal creep behaviour which consisted of a primary, secondary and a tertiary stage, respectively. In order to confirm the existence of these stages during creep, the strain rate was plotted against the strain for all test conditions. These plots showed a decreasing, steady-state and an increasing strain rate which corresponds with the occurrence of primary, secondary and tertiary creep, respectively. The microstructural examination, i.e. the Optical images in Figure (B4.1-B4.28), of all testpieces revealed that different creep mechanisms were involved in the creep process and led, eventually, to a different mode of fracture as the stress and temperature were altered. This can be summarised as follows:

- A brittle alpha-case was found in the testpieces crept at higher temperatures, typically at 898 and 923K. This layer was found to be temperature and time dependent regardless of the applied stress. In other words, as the temperature is higher, the low stresses allow a longer creep life and thus, a longer exposure of the specimen's surface to the oxidising atmosphere which leads, eventually, to more oxygen diffusion through the surface causing the formation of this brittle layer along the gauge length of the fractured specimen. Detailed analysis on the alpha-case and the surface cracks measurements and predictions will follow in the remaining part of this chapter and also in Figure (B23.1-B23.6) and Table (C11-C14).

- Large surface cracks were found along the gauge length of the crept specimens at the lower stresses in comparison to smaller cracks found in those crept at the higher stresses at the same test temperature. This is in agreement with the fracture toughness (K_{IC}) phenomenon: $K_{IC} = \sigma \sqrt{\pi}\, c$, where c is the surface crack depth. For a specific temperature, the value of K_{IC} is constant and thus, an inverse relationship between the crack depth, c, and stress, σ, can be obtained at the corresponding temperature.

Based on this understanding between the surface cracks depth and stress, at the lower stresses, these cracks penetrated well beyond the surface through the central regions of the specimen and led, eventually, to a transgranular fracture. This can be explained based on the following: (1) under low stresses, test durations were sufficiently long to allow an alpha-case layer to develop on the surface within which surface cracks were initiated and propagated through the substrate material, (2) the propagation of cracks within this brittle layer was fast enough to cause deep and more penetrating cracks (3) as creep continues, these cracks develop their own alpha-case layer on the sides and ahead of the crack, (4) the deformation of the central regions caused more voids to nucleate at the grain boundaries, link-up and propagate through the material, (5) the ductile deformation of the central regions also caused fracture of the alpha zones ahead of the crack tips which facilitated the growth and the penetration of these cracks through the central regions resulting in very deep cracks and leading to transgranular fracture. Whereas at the higher stresses, (1) the test durations were insufficient to allow the formation of thick alpha-case layers on the surface, (2) the surface cracks started to appear, even before the appearance of the alpha-case, but their growth was inhibited by the ductile substrate, (3) the stress intensities at the cracks tips were not high enough to allow the propagation of these surface cracks, (4) this led to that the central portions of the testpieces were fractured in a ductile intergranular manner by creep void nucleation and link up at the grain boundaries.

5.1.4 Creep-Step Tests Results (Air)

Full creep curves were obtained from these tests which showed the same creep behaviour obtained previously during normal creep, i.e. a primary, steady-state followed by a tertiary creep. However, the results obtained from the first test, Figure (B5.1), that was carried out at σ_1 = 455MPa/ T_1 = 848K and changed to σ_2 = 280MPa/T_2 = 898K, were expected to give a total life of 300 hours (as these two conditions of stress and temperature were selected on this basis) but unexpectedly, it gave only ~ 80 hours total life which is less than one-third of the anticipated life of 300 hours. In order to confirm these results, a repeat test at the same conditions was carried out and gave a total life of ~ 100 hours, Figure (B5.2). In order to understand and generalise this trend of the unexpected shorter life, a third test was carried out at (σ_1 = 560MPa/T_1 = 823K) and (σ_2 = 340MPa/T_2 = 873K) from which almost the same creep life was obtained, i.e. ~ 115 hours, instead of 300 hours, Figure (B5.3). The first and the repeat tests showed a ductility of 0.28 which is higher than the one obtained from the third test which was ~ 0.16. This might be explained on the basis that a higher ductility is expected at higher temperatures where in the first and the repeat tests, the change was between 848 and 898K whereas in the third test, it was between 823 and 873K. Besides, the applied stresses in the first two tests were lower than those of the last test which allowed more creep to take place and hence, a higher strain or ductility at fracture. On the other hand, comparing these results with the actual creep curves at the same conditions, showed a lower ductility in addition to the lower creep life. This might be a result of that lowering the temperatures, while changing from one step to another, makes the parent material less ductile and cause a sudden fracture.

In an effort to explain the shorter life obtained from these tests, microscopic analysis was carried out on the fractured specimens. The Macro, SEM and the Optical images of the investigated testpieces, Figure (B5.1, B5.2 and B5.3), showed large surface cracks that penetrated from the surface through the material, a huge reduction in the cross sectional area as a result of necking, a large number of voids among the grains and a brittle surface layer of the alpha-case. The alpha-case layer was expected to build up at these high temperatures in the oxidising air atmosphere. The large number of voids can be explained based on the fact that as necking took place before fracture, a lot of voids, in return, will nucleate, link up and propagate speeding up the fracture of the material. The occurrence of necking confirms that the fracture of the specimen was purely ductile. The shorter total life obtained might be explained as follows: (1) when applying high temperatures, the brittle alpha-case layer starts to build up and surface cracks start to develop while the test is ongoing. (2) when switching to a lower temperature, the alpha-case layer becomes more brittle and thus,

easier to break. (3) when applying a higher stress, these surface cracks penetrate more through the surface and get wider and the brittle alpha-case at the tips of the cracks breaks easily. (4) When switching to a lower stress, the surface cracks tend to 'close' and push the oxidised layer outside the cracks as 'flakes', as can be seen in the SEM images. (5) as necking took place, voids start to nucleate at the grain boundaries and link up with the tip of the cracks which speeds up the process with which the specimen fractures. However, these results do not contradict the fact that this alloy, i.e. Titanium IMI834, is a high temperature creep resistant alloy, but the issues of oxidation in this alloy are the main reasons behind this premature failure under these cyclic conditions. In order to confirm these outcomes, ongoing programs at Swansea University are examining the effect of this cyclic creep on Titanium Ti-6Al-4V at lower temperatures, i.e. no alpha-case layer is developed, and lower stresses. The results revealed that the testpieces lasted for more than 300 hours which confirms that when the effect of oxidation is eliminated, longer creep life can be obtained. Therefore, to eliminate the effect of the alpha-case layer, the test temperatures should be lower to avoid oxidation. However, since Titanium IMI834 is used in applications which involve high temperatures between 550 and 650 °C, in contrast to Titanium Ti-6Al-4V which is used at lower temperatures, this alloy should be always evaluated at high temperatures. One way of testing that combines both high temperatures and the elimination of the alpha-case is the vacuum test. For these purposes, the previous tests were repeated, but in vacuum.

5.1.5 Creep-Step Tests Results (Vacuum)

In comparison to the third previously carried out creep-step test in air, Figure (B5.3), the vacuum test that was carried out at the same conditions did improve the creep life of the material. For this test at the same conditions, i.e. between (σ_1 = 560MPa/T_1 = 823K) and (σ_2 = 340MPa/T_2 = 873K), the total creep life was improved by 48% of the life obtained in air at the same conditions, i.e. increased from 115 hours (in air) to 170 hours (in vacuum). The same test was then repeated at a higher vacuum of ~ 8×10^{-5} mbar where the creep life was improved by 160% of the life obtained in air at the same test conditions, i.e. from 115 hours (in air) to 300 hours (in vacuum). Interestingly, these new results are very impressive as the 300 hours creep life of the vacuum step-test is consistent with the creep life of the 'normal' creep tests, without stepping, carried out in air at these conditions of stress and temperature. Moreover, the vacuum tests that were carried out between σ_1 = 455MPa/T_1 = 848K and σ_2 = 280MPa/T_2 = 898K lasted for more than 300 hours, when the test was interrupted. These results confirm that the creep life was improved by ~ 275% of the life obtained in air under the same conditions. These improvements of the creep life in vacuum are consistent with the results obtained elsewhere [33] where the improvements ranged from ~ 150 - 320% of the creep life obtained in air

when tests were carried out on steels. The SEM pictures taken for the failed testpieces from these vacuum tests, Figure (B6.1 and B6.2), revealed that failure by transgranular surface cracks propagation took place in comparison to the ductile intergranular fracture obtained for the test carried out in air, Figure (B5.3). Necking of the failed testepieces in air is obvious in comparison to the flat fracture surface obtained under vacuum. This can be explained based on the results of the optical images where in vacuum, less voids among the grains and much deeper and more penetrating surface cracks were found which led to the flat surface fracture in comparison to the larger number of voids in the testepieces failed in air which led to necking and thus, an intergranular ductile fracture. It can be observed that although more surface cracks were obtained in air, they did not penetrate enough, as in vacuum, and thus, necking due to voids nucleation and linking-up took place under air conditions. The alpha-case layer was thinner under vacuum which improved the total life of the material.

5.2 Analytical and Modeling Results

This part of the research will discuss all the analytical work that has been carried out using the experimental Titanium IMI834 data obtained from the previously completed mechanical tests.

5.2.1 The Power Law Results

From the obtained creep curves, it was proved that the creep life decreased with increasing either the stress or temperature, Figure (B3.1) and (B3.2), which is in agreement with the power law and the Monkman-Grant relations [1, 2]. For the same purpose, the stress, σ, was plotted, at constant temperatures, against the time to fracture, t_f, obtained from each creep test at the corresponding stress and temperature, Figure (B7). From this plot, at any constant value of stress, the creep life decreases with increasing the temperature, T. In the same manner, at any constant temperature, the creep life decreases with increasing the stress. In both cases, as the creep life decreases, this implies that the creep process is faster, i.e. a higher strain rate, and thus, fracture takes place earlier. This trend of the time to fracture and the strain rate suggests that the former is inversely proportional to the stress and temperature in contrast to the latter which is directly proportional to them, which agrees well with equation (2.1) and (2.8). These two equations were studied thoroughly in order to find the value of n and Qc for Titanium IMI834. Plotting ln (σ) against ln (t_f), Figure (B7), reveals the inverse proportionality between the stress and the time to fracture, where the slope of these plots represents the value

of - n, where n is the stress exponent used in equation (2.8), whereas plotting ln (σ) against ln ($\dot{\varepsilon}_m$), Figure (B7), shows the direct proportionality between the stress and the minimum creep rate and gives almost similar values of the stress exponent n, where the slope of these plots is n. It is obvious from these plots that the value of n is not constant and depends on the stress and temperature, which violates the power law which assumes that the value of n is 'constant'. However, the power law provides a direct mean to measure the activation energy, Qc, required for the initiation of creep in a material. This can be obtained by either plotting, at constant stresses, ln (t_f) against 1/T, where the slope of these plots is the value of Qc/R, where R is the gas constant ~ 8.314 J/K mol, or ln ($\dot{\varepsilon}_m$) against 1/T, where the slope of these plots is the value of -Qc/R, Figure (B7). From these plots, it is also clear that the value of Qc is not constant and is dependent on the stress and temperature which, again, does not agree with the power law. These outcomes are consistent with previous studies [20, 21, 22, 59, 79] which also confirmed that the value of n and Qc was depending on the test conditions. Despite this variation in the value of Qc and n, the minimum creep rate analysis provided an average value of Qc and n for Titanium IMI834 of ~ 344kJ/mol and ~ 5.74, respectively, whereas the time to fracture analysis gave an average value of Qc and n of ~ 327kJ/mol and ~ 5.44, respectively. However, these average values and thus, the power law equation, can not be reliable in predicting the long-term properties and will, thus, lead to considerable errors and overestimations. All the calculated results using the power law are tabulated in Table (C1) and a detailed mathematical analysis using the power law is provided in Section (D.1).

5.2.2 The Monkman-Grant Technique Results

On the other hand, applying the Monkman-Grant equation to the creep data provided reasonable values as it was anticipated. A linear relationship between the time to fracture and the minimum creep rate can be obtained using the general form of the Monkman-Grant technique, equation (2.1), by plotting $\dot{\varepsilon}_m$ against $1/t_f$, Figure (B8), where the slope of this plot is the value of the Monkman-Grant constant, M, which was ~ 0.074. This is consistent with studies previously carried out on Titanium IMI834 [87] where the value of this constant was ~ 0.09. Plotting $\dot{\varepsilon}_m$ against t_f, according to equation (2.17), gave a power function behaviour, Figure (B8), in which the time to fracture is raised to the power m = 1.0631 with a Monkman-Grant constant of ~ 0.1925. Alternatively, by changing the axes, i.e. plotting t_f against $\dot{\varepsilon}_m$ according to equation (2.18), another power function behaviour is obtained, Figure (B8), wherein the minimum creep rate is raised to the power m = 0.9533 with a Monkman-Grant constant of ~ 0.1669. These three expressions were used to

calculate the time to fracture based on the minimum creep rate measurements from which the predicted life was obtained and plotted against the actual life values, Figure (B8). From this plot, overestimations of ~ 25 to 35 hours of the actual time values were resulted when equation (2.17) and (2.18) were used, respectively, in comparison to less than ~ 7 hours underestimation time resulted when equation (2.1) was used. In this case, underestimation is more preferable since it keeps, at least, the component within the planned operational life. However, these errors limit the use of the Monkman-Grant relation to predict the long-term creep behaviour since they might lead to considerable errors from the long-term perspective. All the calculated results using the Monkman-Grant equations are tabulated in Table (C2) and a detailed mathematical analysis using these equations is provided in Section (D.2).

5.2.3 The Larson-Miller Technique Results

This technique has been investigated in order to find out whether the value of the constant, C_{LM}, used in its equation is actually a 'constant' or dependent on the test conditions. For this purpose, at constant stresses, log (t_f) was plotted against 1/T, Figure (B9), which gave straight lines of a slope equals to P_{LM} (the Larson-Miller Parameter) and an intercept of - C_{LM} (the Larson-Miller Constant). The first observation that is in agreement with earlier studies [28, 29] was that even when these lines were extrapolated, they did not intersect at a certain point, which was assumed to represent the value of C_{LM}, as some studies [24] suggested. Besides, it is obvious from these plots that the value of C_{LM} is not constant (varied from ~ 14 to ~ 17). This analysis, therefore, suggests that the value of C_{LM} varies according to the test conditions, which agrees with previous studies [21, 25, 29] and thus, disagrees with the assumption of the Larson-Miller technique [23]. However, as a first trial, an average value between 14 and 17 was used in order to obtain the stress rupture curves based on the Larson-Miller relation, equation (2.9), but unfortunately, these curves did not fit the actual measurements accurately. The next attempt was to force all the creep data to collapse onto a single master curve by plotting the stress, σ, against the parameter P_{LM}, Figure (B9), at randomly selected values of C_{LM}. The value of C_{LM} was considered only when it fitted the raw data perfectly based on the trial and error method. It was found that the best fit of the data was obtained when the value of C_{LM} was 20. From this plot, a relationship between the stress, time and temperature was obtained from which the stress-time predictive curves were constructed, Figure (B9). The obtained curves were linear, equidistant and parallel. This implies that the relation between the stress and the time is, simply, linear which could lead, in return, to considerable errors as these curves did not fit the creep data accurately, especially at the higher stresses of each temperature, which agrees well with

previous studies carried out on steels [27]. Actually, if fitting the creep data was that simple using a linear line, there would not have been any need to develop complex relations to fit the data. But since the creep behaviour requires more complicated fitting equations to describe the actual creep behaviour, due to changes in creep mechanisms, linear relations will eventually lead to wrong estimations. All the calculations are tabulated in Table (C3) in addition to a detailed mathematical analysis in Section (D.3).

5.2.4 The Manson-Haferd Technique Results

As with all techniques, a relationship between the stress and the creep life at various temperatures is required. To start with the Manson-Haferd method, log (t_f) was plotted against T, at constant stresses, which gave straight linear lines of slope - P_{MH}, the Manson-Haferd Parameter, Figure (B10). When these lines were extrapolated, they did not meet at an intersection point of (T_a, t_a), as some studies [30] previously suggested. For this reason, another procedure was followed in order to calculate the values of these constants from the intersection point of the lines with the y and x-axes. The intercept of these linear lines represents the value of (P_{MH} T_a + log t_a) from which the value of T_a and t_a can be calculated, sequentially. The average calculated values of T_a and log t_a for Titanium IMI834 were ~ 1061 and 29.713, respectively, which differ from the values suggested by Manson and Haferd and agree with other literature studies [31, 32, 33]. These values were then inserted into the Manson-Haferd equation and plotted against the stress, σ, at constant temperatures, Figure (B10), from which a relation between the stress and the Manson-Haferd parameter was obtained. This plot disagrees with some studies [30] which assumed that plotting this parameter against the stress superimposes all the data points into a single master curve. However, the predictive stress-time curves were obtained and plotted along with the actual creep results, Figure (B10). The curves showed a better capability of fitting the actual data points when compared with the Larson-Miller technique. This proves that the more complex the technique the better its capability in predicting the creep properties. All calculations and analytical procedures are summarized in Table (C4) and Section (D.4), respectively.

5.2.5 The Orr-Sherby-Dorn Technique Results

The starting point of using this technique is similar to the Larson-Miller's analysis in which log (t_f) was plotted against 1/T, at constant stresses, Figure (B11). These plots gave straight lines of a slope which represents the value of C_{OSD}, the Orr-Sherby-Dorn constant, and an intercept with the y-axis equals to - P_{OSD}, the Orr-Sherby-Dorn parameter. The first result that can be drawn from these plots is that the value of C_{OSD} is

not constant as the slope was changing from ~ 16,244 to ~ 20,053 with changing the stress and temperature. This outcome disagrees with the assumption of Orr, Sherby and Dorn [35] who assumed that the value of C_{OSD} is constant. As with the Larson-Miller technique, the same method employed there was used here to force all the data points to collapse onto a master curve by plotting the stress, σ, against the Orr-Sherby-Dorn parameter, P_{OSD}, with randomly selected values of C_{OSD}. The best fit of data was obtained when the value of C_{OSD} was ~ 20,000, Figure (B11). This is consistent with the fact that this value lies in the range between 16,244 and 20,053, i.e. the values of the slopes of the constant stress lines previously discussed, Figure (B11). From this master curve, a relationship between the stress, time and temperature can be obtained from which the predictive stress-time curves can be constructed, Figure (B11), at all temperatures. The curves fitted the actual creep data quite well where the curvature of these curves improved the fit. When compared with the Larson-Miller curves, Figure (B9), it showed much better fit of the data at all temperatures and stresses. However, the Manson-Haferd curves, Figure (B10), showed better consistency of the predictive curves with the actual data than the Orr-Sherby-Dorn curves, Figure (B11), as a higher degree of curvature was involved in the Manson-Haferd's curves as a result of the more complex function used in its equation. Useful calculations and analyses using the Orr-Sherby-Dorn technique are summarised in Table (C5) and Section (D.5), respectively.

5.2.6 The Manson-Succop Technique Results

The analysis using this technique started with plotting the values of log (t_f) against T, at constant stresses, which gave straight lines of slope equals to - C_{MS}, the Manson-Succop constant, and an intercept with the y-axis equals to P_{MS}, the Manson-Succop constant, according to equation (2.14). These plots, Figure (B12), revealed that the slope, and hence the value of C_{MS}, varied between ~ 0.024 and 0.028 with varying the test conditions. This variation is relatively small but it could become more obvious if the tests conditions varied within a larger range of stresses and temperatures which might lead to a disagreement with the assumption of Manson and Succop [41] who confirmed that the value of C_{MS}, should be constant regardless of stress and temperature. However, an average value for C_{MS} was chosen, ~ 0.025, to superimpose all the data points onto a single curve by plotting the stress, σ, against the parameter, P_{MS}, from which a relation between the stress, time and temperature was obtained, Figure (B12). This relation was then used to construct the stress-time curves on which the actual data points were projected, Figure (B12). The stress-time curves were almost linear, equidistant and parallel (similar to the ones obtained using the Larson-Miller analysis). However, at

the high temperatures (898 and 923K), the fits were quite good in the high stress regime in comparison to the poor fits obtained in the low stress regime. In contrast, the fits were quite good in the low stress regime of the lower temperatures (823, 848 and 873K), in comparison to the inferior fits obtained in high stress regime at these temperatures. Generally speaking, the fits were much better than those obtained from the Larson-Miller's analysis, but slightly less accurate than those obtained using the Manson-Haferd and Orr-Sherby-Dorn techniques. All the calculations and analyses used to construct these predictive curves are summarised in Table (C6) and Section (D.6).

5.2.7 The Hyperbolic-Tangent Technique Results

For the purpose of finding the fitting parameters of equation (2.22), plotting $\tanh^{-1}(1 - 2(\sigma/\sigma_{TS}))$ against ln (t_f), at constant temperatures, gave straight lines of a slope which represents the value of k and an intercept point with the y-axis equals to $(k \ln t_i)$, Figure (B13). From these plots, the values of the constant k and t_i were calculated at each corresponding temperature. These values were then inserted into equation (2.22) from which the predictive stress-time curves were obtained, Figure (B13). These curves showed an impressive fit of the actual creep data as a result of the complex functions used in this technique and thus, the smooth curvature which improved the fit. It can also be observed that there is an inflection point at around 50% σ_{TS}, at each corresponding temperature, which agrees with other studies [62, 63, 64] and implies that the creep mechanism is dependent on the applied stress level. Another observation is that at the intermediate temperatures, i.e. 848 and 873K, the curves slightly deviated from the actual creep data trend at the stresses between ~ 300 and 500MPa. Even though, this technique can be considered as an easy and a straightforward method which directly relates the stress to the time and temperature without the need to superimpose the data onto a master curve to obtain the stress as a function of these two parameters, as with the previous techniques. Moreover, the predictions are much better and more reliable than all of the previously obtained results of the other methods, as can be seen from the constructed plots. Detailed calculations and mathematical analyses are summarised in Table (C7) and Section (D.7), respectively.

5.2.8 The Goldhoff-Sherby Technique Results

This technique is very similar to the Manson-Haferd methodology concerning the procedure of analysing the Titanium IMI834 data with the only difference that log (t_f) is plotted against the reciprocal of T at constant stresses, as shown in Figure (B.14), where the slope of the lines represents the value of the Goldhoff-Sherby

parameter, P_{GS}. Moreover, this plot provides the value of the constants log t_a and $1/T_a$ from which a relationship between the stress and the Goldhoff-Sherby parameter, P_{GS}, can be obtained. For this purpose, an average value of log t_a and $1/T_a$ were taken as 15.824 and 0.0008, respectively. These relations between the stress and the parameter P_{GS} were then used in order to construct the stress rupture curves which showed a very good description of the actual creep results. The curves are very similar to those obtained by the Manson-Haferd technique which explains the similarity between these two methodologies in analysing the creep data. This again proves that the more complex the technique the better its capability in predicting the long-term creep properties when compared to the simpler techniques. All calculations and analytical procedures are summarised in Table (C8) and Section (D.8), respectively.

5.2.9 The θ-Projection Technique Results

Unlike the previously discussed models, this method was intended to fit the actual creep curves at various conditions and then express the fitting constants as functions of stress and temperature. The first version of this technique, the 4-θ (equation 2.20), was slightly able to fit the actual creep curves of Titanium IMI834. However, it did not give a very accurate description of the primary creep as many previous studies [57, 61] concluded and as can be seen in the obtained results, Figure (B15.1-B15.32). For this reason, the other version of this technique, the 6-θ (equation 2.21), was used to fit the actual creep curves. Surprisingly, this equation provided a much better description of the primary creep behaviour as can be seen in the obtained results, Figure (B15.1-B15.32), which agreed very well with previous studies [57, 58, 61]. This improvement in accurately fitting the primary creep confirms that the added two parameters, i.e. θ_5 and θ_6, to the first version of this equation took into account the effect of grain boundary relaxation during the primary creep [58]. For both versions of the θ-method, the fitting procedure was possible by finding the values of the θ-parameters involved in their equation. The values of these parameters were obtained by non-linear least square curve fitting routines (using SOLVER in Excel). Having obtained these parameters, many points and regions along the creep curve can then be defined, such as the primary and tertiary points, the minimum creep rate point, and the creep fracture, or the total ductility, point, Figure (B16). In these plots, the variation of each θ-term was plotted against stress at each individual temperature. The 4-θ results did not provide a systematic variation of the θ-parameters with stress for the primary creep region whereas the variation with the stress for the tertiary stage was slightly better, as it was found before [57]. This might be a result of the poor fit capability of this equation for the primary creep region. On the other hand, the 6-θ results provided a

better description of all regions along the creep curve which is evident from the smooth and the linear variation with the stress, Figure (B16). However, the trend of θ_3 and θ_5 was not purely linear, Figure (B16), as they were, respectively, increasing/decreasing up to a certain stress level where they started to decrease/increase again at higher values of stress above that point. This unexpected change in the slope of these two parameters made it difficult to express them as a function of stress. If the trend of all parameters was completely linear, the values of these parameters could have been derived for any stress within the ranges studied experimentally. This means that this trend could have allowed interpolation of the data although it might have also allowed reasonable extrapolation of creep properties. If the linear trends of the values of these parameters have been obtained, this means that they could have been expressed as functions of stresses and temperatures such that:

$$\theta = f(\sigma, T) \quad \text{..... (5.1)}$$

which means that equation (2.20) and (2.21) could have been re-written as:

$$\varepsilon = f(t, \sigma, T) \quad \text{..... (5.2)}$$

In conclusion, this method requires the availability of full creep curves prior to using it as a predictive tool. This technique can be considered as a 'fitting' technique rather than a 'predictive' model as the stress-time curves can not be derived from its equation. All calculations and mathematical analyses for the 4 and 6-θ methods are provided in Table (C9 and C10) and in Section (D.9), respectively.

5.2.10 The Wilshire Technique Results

In order to start the analysis using this technique, it was essential to find the value of the apparent activation energy, Qc^*, the tensile strength, σ_{TS}, at the applied temperatures and the values of the fitting parameters (k_1, k_2, k_3, u, v and w). Unlike the calculations of Qc, described in equation (2.8), at constant σ, the value of Qc^*, used in equation (3.1-3.4), was determined at constant σ/σ_{TS} using the power law principle. This was possible by either plotting ln (t_f) or ln ($\dot{\varepsilon}_m$) against 1/T at constant σ/σ_{TS}, Figure (B17), where the slope of these plots represents the value of Qc^*/R and - Qc^*/R, respectively. From the plot of ln (t_f) against 1/T, the value of Qc^* was ~ 305kJ/mol whereas it was ~ 332kJ/mol from the plots of ln ($\dot{\varepsilon}_m$) against 1/T. The difference in the value of Qc^* using either of these two procedures was not too large and thus, an overall average value of 320kJ/mol was used to run the analysis. It can be seen that this overall value of Qc^* is not far away from the value of Qc (~ 327-344kJ/mol) calculated at constant σ, Figure (B7). The values of the tensile strength, σ_{TS}, were obtained from the previously carried out tensile tests at various temperatures, Figure (B1.1-B1.3). However, although the tensile tests were only carried out at 823, 873 and 923K, the values of the tensile

strengths showed a linear trend, Figure (B1.4), from which it was possible to interpolate and find the values of the tensile strengths at the intermediate temperatures, i.e. 848 and 898K.

Using equation (3.1), the data of Titanium IMI834 were very well rationalised using Qc^* as 320kJ/mol, Figure (B17). This was possible by either plotting ($\dot{\varepsilon}_m$ exp (320,000/RT)) or (t_f exp (- 320,000/RT)) against σ/σ_{TS}, Figure (B17). However, the adoption of this equation did not eliminate the change in n values (where the slope of these plots, at any point, represents the value of n and - n, respectively), which was approaching $n \sim 1$ with decreasing the value of σ/σ_{TS}. This confirms that the change in n values is related to the change in stress level above and below the yield stress of the material which involves creation of more dislocations above the material's yield point. The calculated values at all test conditions in addition to a detailed mathematical analysis are summarised in Table (C11) and Section (D10).

The values of the constants k_1 and u were determined using equation (3.2) by plotting ln (-ln σ/σ_{TS}) against ln (t_f exp (- Qc^*/RT)), Figure (B18), where the slope of these plots provided the value of u whereas the intercept is the value of ln k_1. However, it was observed that the linear trend of these plots deviated at a certain point that separated the data into two linear regimes, namely: the high and the low stress regimes. Based on this fact, different values of u and k_1 were obtained from these two regimes. Equation (3.2) along with the calculated values of u and k_1 were used to force all the data points to collapse onto a sigmoidal 'master curve', by plotting (σ/σ_{TS}) against (t_f exp (- Qc^*/RT)), Figure (B18). This curve showed the general behaviour of the actual creep data at different stress levels and eliminated the temperature dependence of these points. This equation was also used to predict the long-term stress rupture behaviour over a wide stress range at the selected temperatures, Figure (B18). The predictive curves showed a superb fit of the actual measurements in both the high and the low stress regimes at all temperatures. It can be observed from these curves that there is a 'kink' point at which the trend of the creep data changed according to the stress level involved. This point exactly corresponds to the point found earlier in the plots of ln (-ln σ/σ_{TS}) against ln (t_f exp (- Qc^*/RT)) and this confirms that the dependence on stress level is more dominant than the temperature dependence, as the generated sigmoidal curve implied when the temperature dependence was eliminated. This predictability of the long-term creep behaviour using this equation proves that it is possible to extrapolate the short-term creep measurements at all test conditions. All the calculations are tabulated and summarised in Table (C11.1) and Section (D.10).

Similarly, the values of the constants k_2 and v were determined using equation (3.3) by plotting ln (-ln σ/σ_{TS}) against ln ($\dot{\varepsilon}_m$ exp (Qc^*/RT)), Figure (B19), where the slope of these plots is the value of v whereas the intercept point is the value of ln k_2. As with the previous plots of equation (3.2), it was observed that there is

a 'kink' point which separated the data into two linear high and low stress regimes and gave, thus, different values of v and k_2 for these two regimes. These values were then used to construct the sigmoidal 'master curve', by plotting (σ/σ_{TS}) against ($\dot{\varepsilon}_m$ exp (Qc^*/RT)), which forced all the data points to be fitted onto a single curve and thus, eliminated the dependence of these points on temperature, Figure (B19). This equation was also used to predict the minimum creep rate behaviour over a wide stress range at the selected temperatures, Figure (B19). The predictive curves showed a very impressive match with the actual minimum creep rate measurements at all temperatures. These curves also showed a 'kink' point which corresponds to the point at which the slope of the plots of ln (-ln σ/σ_{TS}) against ln ($\dot{\varepsilon}_m$ exp (Qc^*/RT)) changed. The calculations using this equation are summarised in Table (C11.1) and Section (D.10).

In an effort to explain the 'kink' points observed in these predictive curves, some investigations were carried out on the results obtained from the Titanium IMI834 tests:

(1) The stresses at these kink points, Table (C11.1.1.), were plotted against the corresponding temperatures, Figure (B20). The yield and the ultimate tensile stresses, Figure (B1.4), were projected on the same graph. These plots showed that the data can be fitted using a decreasing linear trendline. This behaviour of the 'kink' points confirmed the linearity between the stress and temperature wherein the former was decreasing with increasing the latter, which agrees with the tensile results. Interestingly, the lines of the Wilshire 'kink' points and the yield stress regression line were linear, equidistant and parallel (slope ~ 0.6). Besides, the ratio of the stresses at the kink points was ~ 85% of the yield stress at each corresponding temperature. This implies that the inflection points of the Wilshire curves are a result of the different deformation mechanisms above and below the material's yield point which play a key role in the creep behaviour. This physical explanation provides a possible reason for having two stress regimes and thus, the 'kink' in the predictive curves. It is worthwhile mentioning that the kink points were ~ 60% of the ultimate tensile strength, which is almost consistent with the Hyperbolic Tangent technique results, Figure (B13), where the inflection point of its curves was at ~ 50% of the ultimate tensile strength at each corresponding temperature.

(2) Moreover, the ductility measurements, Figure (B20), were used to explain the behaviour of Titanium IMI834 in the high and the low stress regimes, i.e. above and below the kink points in the predictive curves plots. It was observed that at each temperature, the ductility was increasing up to a certain point where it started to fall down with increasing the stress. Accurate measurements confirmed that for each temperature, the point at which the ductility started to decrease was exactly the point where the kink in the plots took place. The explanation for this variation in ductility can be attributed to that as the stress level increases above the kink points, it does not allow the bulk material to deform and extend for a long time and thus, low

ductility at fracture. Whereas when decreasing the stress level below the kink points, more alpha-case builds up and thus, more penetrating surface cracks propagate within the alpha-case in a rate which is faster than that of the central regions resulting in a low ductility at fracture.

(3) Microscopic studies revealed that in the low stress regime below the kink points, larger surface cracks, less voids, thicker alpha-case layer and transgranular fracture were observed in contrast to the high stress regime above the kink points where smaller surface cracks, more voids, thinner alpha-case layer and intergranular fracture took place. All these results are summarised in Figure (B20).

The same procedure was used to calculate the value of k_3 and w at times to pre-defined strain levels (from 0.1% up to 20% strain) by plotting ln (-ln σ/σ_{TS}) against ln (t_ε exp (-Qc^*/RT)), based on equation (3.4), which gave the value of w and ln k_3 from the slope and the intercept points of these plots, respectively, Figure (B21.1-B21.13). In these plots, the same trend was observed which involved a high and a low stress regime separated by a 'kink' point. These values of w and k_3 were then inserted into equation (3.4) from which the predictive curve at each strain level was obtained, Figure (B21.1-B21.13). The curves fitted the actual measurements very well which implies that this equation can be used to predict the creep behaviour at any selected level of strain. For comparison purposes, all the curves of ln (-ln σ/σ_{TS}) against ln (t_ε exp (-Qc^*/RT)) were plotted on the same graph, Figure (B22.1), so as to study the influence of changing the strain level on the position of this kink point. It can be observed that the kink points are almost fixed in a certain position (which corresponds to 85% of the yield stress) regardless of changing the strain level. Moreover, it can be seen that the slope, which represents the value of w, of these lines looks almost the same in both the low and the high stress regimes whereas the value of ln k_3, which is the intercept point with the y-axis, was decreasing with increasing the strain level. These outcomes are the basis on which full creep curves can be constructed based on the Wilshire equations. All calculations are summarised in Table (C11.2-C11.14) and Section (D.10).

5.2.11 Construction of the Full Creep Curves Based on the Wilshire Technique

From Figure (B22.1) along with Figure (B21.1-B21.13), it can be observed that the average value of w in the low and the high stress regimes was ~ 0.21 and ~ 0.8, respectively, at all strain levels. These two values were considered at all strain levels and were inserted into equation (3.4) from which the corresponding values of k_3 at each strain level were calculated, Figure (B22.2 and B22.3). The decreasing trend of k_3 is logical since it represents the intercept with the y-axis of Figure (B22.1) which was decreasing with increasing the strain level in both the low and the high stress regimes. This agrees very well with that the intercept point of the

curves in Figure (B22.1) was decreasing with increasing the strain level. Besides, based on the fact that the kink points occur at ~ 85% of the yield stress, as previously discussed, these kink points have to be in the same location for each curve regardless of any values of w and k_3 that are being used. Therefore, if w is kept constant, the value of k_3 has to decrease, as obtained experimentally, to keep the position of the kink points in place at all strain levels.

Since the value of w and k_3 is independent of stress and temperature at any selected strain level, Figure (B22.2 and B22.3), they can, thus, be expressed over a range of selected strains, such that:

$$w = f_1(\varepsilon) \quad \text{..... (5.3)}$$

and

$$k_3 = f_2(\varepsilon) \quad \text{..... (5.4)}$$

Inserting these two expressions into equation (3.4) gives:

$$\sigma/\sigma_{TS} = \exp\left(-f_2(\varepsilon)\left[t_\varepsilon \exp\left(-Qc^*/RT\right)\right]^{f_1(\varepsilon)}\right) \quad \text{..... (5.5)}$$

Re-arranging this equation will provide an equation that relates the strain, ε, to stress, σ, and temperature, T, with time, t, such that:

$$\varepsilon = f(t, \sigma, T) \quad \text{..... (5.6)}$$

Obtaining equation (5.6) means that full creep curves at various stresses and temperatures can be re-produced based on the Wilshire equation (3.4). This was confirmed by the re-constructed creep curves obtained from the Titanium IMI834 data, Figure (B23.1-B23.34). These plots provided a full description of the creep curves at various conditions in addition to the very impressive description of the primary creep. The primary creep was described very well in most cases, except at some high stresses. This exception might be a result of the poor curve fitting of k_3 values in the high stress regime, Figure (B22.3), as their values were massively larger than those obtained for the low stress regime, Figure (B22.2). In other cases, the tertiary creep was not described very well. However, the fracture point of any creep curve can be obtained accurately using equation (3.2) which describes the fracture point quite well instead of using equation (3.4).

The advantage of equation (3.4) can be summarised in that when the time required to reach a certain strain level is obtained from a creep curve, the stress-time curves for that strain level can be constructed based on this equation. Moreover, expressing w and k_3 as functions of strain can provide a description of the creep curves at any stress and temperature. Similarly, equation (3.2) presents a way to define the end point of the creep curve. In other words, when the time to fracture is obtained from any creep curve, it can be used to construct the stress rupture curves based on this equation. Another way of predicting the long-term behaviour can be based on equation (3.3) wherein the minimum creep rates are required to run the analysis. Once these

values are obtained from the actual creep curves and entered into this equation, the stress versus the minimum creep rate curves can then be constructed at any stress and temperature. Therefore, equation (3.2) defines the end point of a creep curve whereas equation (3.4) defines any point along the creep curve and equation (3.3) defines the point where the minimum creep rate takes place during creep.

In conclusion, in aerospace applications where the time to reach pre-defined strain levels is the main concern, typically ~ 1% strain level, then equation (3.4) provides an impressive description of the low strain levels required for such applications from the constructed creep curves. As an alternative for power generation applications, since the constructed creep curves showed some deviations from the actual behaviour at the fracture point, equation (3.2) which defines the fracture point can, thus, be used.

5.2.12 The Alpha-Case Measurements Results

The micrographs showed that an alpha-case layer was found in the crept specimens of Titanium IMI834 at all temperatures from 823 to 923K. However, this layer can be seen most clearly and most deeply penetrated at the extreme temperatures, i.e. at 898 and 923K. The depth of this alpha-case was measured at all temperatures, Table (C12), and plotted against the total life, t_f, at each corresponding temperature, Figure (B24.1). This plot shows a parabolic trend which agrees with the trend obtained from other studies [87, 88, 97] where at each temperature, the depth of this alpha-case increases with increasing the exposure time. Interestingly, the rate by which the alpha-case depth was building up, which is the slope at any point along these curves, was much faster at the higher temperatures in comparison with the lower temperatures. This temperature dependence of the alpha-case layer can also be obtained from the micrographs included in Figure (B24.1). Therefore, the thickness of the alpha-case layer is, thus, purely time and temperature dependent. In order to confirm these outcomes, measurements of the alpha-case layer developed in temperature-exposed un-stressed samples, carried out by Brown [98] on Titanium IMI834, were virtually identical to those obtained from the crept specimens, as shown in Figure (B24.2). This plot demonstrates that the thickness of the alpha-case, under the same temperature exposure, was the same in both the tested and the un-tested specimens. Moreover, Brown's model [98] predicts very accurately the thickness of the alpha-case, Figure (B24.2) and Table (C13), where the predicted measurements also confirmed that the alpha-case layer is purely time and temperature dependent as can be seen from the impressive consistency of the predicted values and the actual measurements. However, at 873K, the predicted values of the alpha-case thickness were slightly higher than the measured values. The same outcome was observed by Gurappa [97] where the predicted values were slightly higher than those actually measured under the same conditions. The

explanation was that in the actual situation, the oxygen absorbed by the alloy is used up for forming both an alpha-case layer (diffused into the material) and an oxide-scale (not diffused, but on the outer surface) whereas the predictive model assumes that the entire oxygen is used up in forming a diffused alpha-case.

The depth of the penetrating cracks and the alpha-case thicknesses at the surfaces of each penetrating crack were measured at three points down the crack depth, Table (C12), and plotted at each stress and temperature, Figure (B24.3). From these plots, it is apparent that with decreasing the stress value at a constant temperature, the test duration, t_f, is longer and thus, there is enough time for the surface cracks to penetrate more and get deeper through the material. The time required for an alpha-case thickness to be attained can be obtained from Figure (B24.1). As each crack penetrates prior to the formation of the alpha-case on its surfaces, this means that at a certain crack depth, an alpha-case layer starts to develop at its exposed surfaces. Thus, the time at which the alpha-case starts to build up is the same as the time at which that surface crack was initiated. Therefore, any thickness of the alpha-case on the exposed surfaces of the penetrating cracks can be measured and the time for that thickness to be reached, $t_{\alpha\text{-case}}$, can be read from Figure (B24.1) which is a fraction of the total life, t_f, of the specimen. Thus, subtracting the time spent in developing the alpha-case from the total life should give the starting point at which that crack was initiated according to:

$$\text{Initiation time for a surface crack, } t_{crack} = t_f - t_{\alpha\text{-case}} \quad \ldots\ldots\ldots\ldots\ldots\ldots \quad (5.7)$$

This equation was applied to all the plots in Figure (B24.3) to obtain the plots in Figure (B24.4) which relates the crack depth to the time, t_{crack}, at which each crack was initiated. All calculations are included in Table (C14). From these plots, a linear relation between the time, t_{crack}, and the corresponding crack depth can be obtained by regression analysis. At each stress level, these linear lines can be extrapolated backwards to intersect the x-axis where the intersection point represents the critical time at which the first crack along the surface appeared. Projecting these critical time values on the actual creep curves at the corresponding test conditions will provide the strain values at which these cracks were initiated, ε_{crack}. This procedure of relating the alpha-case and surface cracks to the critical time and strain (based on the actual creep curves) provides a technique which defines the stage of creep at which these cracks appeared. These values are summarised in Table (C15). Plotting the critical time and strain values against stress gives Figure (B24.5) and (B24.6), respectively. From these plots, along with Figure (B24.4), the following outcomes can be observed:

- At the lower stresses, the initiation of cracks is late during creep, the alpha-case layer is thick, the time to fracture is long, the ductility and the critical strain decrease with decreasing the stress level, at a constant

temperature, and the cracks depth at fracture is large. The possible explanation for these outcomes is that at the lower stresses, a thick alpha-case layer was developed after long time exposures prior to the formation of the surface cracks. Hence, the surface cracks were initiated later in the alpha-case and penetrated more at fracture through this brittle layer. As the critical time and strain values are fractions of the total time to fracture and ductility, respectively, they, thus, follow the same trends. The reason behind the drop in ductility and thus, the critical strain, as the stress decreases can be attributed to the formation of a thick alpha-case which causes the bulk material to become less ductile and thus, less strain is required to cause the cracking of the alpha-case layer. This trend of the decreasing ductility with increasing the alpha-case thickness was also confirmed in previous studies [87] carried out on Titanium IMI834. In other words, the lower the stress, the thicker the alpha-case developed on the surface and thus, the lower the strain required to cause cracking of the alpha-case layer. This explains the decreasing trends, to the left of the kink points, in Figure (B24.6). The penetration through the brittle alpha-case was easy and led, therefore, to deeper cracks at fracture. For this reason, the fracture in the low stress regime was controlled by surface cracks penetration through the material rather than purely creep fracture characterised by voids nucleation at grain boundaries.

- At the higher stresses, the initiation of cracks is early, the alpha-case layer is thin, the time to fracture is short, the ductility and the critical strain increase with decreasing stress level, at a constant temperature, and the cracks penetration at fracture is small. The possible reason behind these outcomes is that surface cracks were initiated early prior to the development of the alpha-case layer. The alpha-case layer was, generally, thinner due to the short times of exposure. Although the surface cracks were initiated early, they did not penetrate fast enough as the thin alpha-case did not have any effect on the total ductility of the material which made it difficult for these cracks to penetrate through the ductile substrate. For this reason, the absence of a thick alpha-case caused the material to behave in a normal manner expected under creep conditions characterised by an increasing ductility with decreasing the stress level. The increasing trend, to the right of the kink points, in Figure (B24.6) with decreasing the stress can, thus, be explained based on the fact that as the ductility increases with decreasing the stress, more strain is required to cause cracking of the substrate. This resulted in a purely intergranular creep fracture at these higher stresses due to voids nucleation, propagation and link-up along grain boundaries which confirms the normal creep behaviour discussed earlier under these stress levels.

In conclusion, an alpha-case of 150μm thickness, for instance, will have a volume fraction of ~ 15% of a specimen with 4.0mm diameter and 20.0mm gauge length (as with the specimens used in this study). This

volume fraction will have a considerable effect on the overall performance and ductility of the alloy, especially in thin sections, i.e. when the diameter is relatively small. Whereas in large sections, this effect might be negligible as the oxidised layer could be very small when compared to the overall diameter of the component. However, as we are studying the effect of this alpha-case on the compressor blades of the gas turbine which have thin sections, this is, therefore, considered as a very limiting factor of the life of these components.

5.2.13 The Strong Predictive Capability of the Wilshire Equations

The Wilshire equations were successfully able to predict the long-term behaviour of Titanium IMI834. As previously shown in this study and many other studies [87, 88], especially at high temperatures, the oxidation problems had a major influence on the mechanical properties and the ductility of this alloy. This oxidation and the formation of the alpha-case can be considered as phase changes within the alloy. In general, as titanium alloys are produced very precisely to give a specific microstructural composition via heat treatment, this means that any changes in this composition by oxidation could drastically change the capabilities of the alloy. In real applications, this could be the case and thus, a comprehensive model is needed to predict the life of components in both oxidation-free and oxidising atmospheres.

This section is aimed to examine the Wilshire technique's ability to predict the life of the Titanium IMI834 alloy with real-life problems where surface oxidation is an issue. For this purpose, the previously generated creep data have been divided into two categories according to the thickness of the alpha-case found in the fractured specimens, namely: specimens with (< 35μm) alpha-case thicknesses where the alpha-case has a very limited, or negligible, influence on the mechanical properties and others with (> 35μm) where the effect of the alpha-case is severe and able to drastically affect the mechanical properties of the alloy. The Wilshire technique was then used to produce the long-term creep predictive curves based on the data of the specimens with the thin, or negligible, alpha-case on their surfaces (i.e. < 35μm), as shown in Figure (B25.1). It can be seen from this figure that the Wilshire technique provided a precise description of the creep behaviour of the alloy under these conditions. In order to prove the ability of this technique to predict the behaviour of the alloy under the severe conditions where the alpha-case thickness is > 35 μm, the predictive curves of Figure (B25.1) were used on which the data of the thick alpha-case were then projected, as shown in Figure (B25.2). From this plot, it can be seen that the Wilshire's predictive curves slightly under-predicted the data points of the heavily oxidised data (i.e. the lower stresses/higher temperatures and longer-lives). This behaviour was

perhaps unexpected as the oxidation of Titanium IMI834 can drastically change the long-term life of this alloy and it would, thus, be anticipated that the oxidation would lead to life reduction. However, under-prediction of the long-term behaviour is still better than over-prediction as it keeps the component's life within the safe operational life conditions in all cases. Moreover, it should be acknowledged that this under-prediction may be due to the limitations of a relatively small data set.

In conclusion, the ability of the Wilshire technique to adequately describe the long-term creep behaviour based on short-term measurements shows the promise of this technique. This capability was shown using the three different possible scenarios, namely: in the case when all the data points are treated as a bulk, Figure (B.18), in the case where the alpha-case had a limited effect (< 35μm thickness), Figure (B25.1), and in the worst case when the alpha-case effect is considerable (> 35μm thickness), Figure (B25.2). The ability of this technique of predicting the long-term creep behaviour under all conditions is a consequence of using physically meaningful parameters in its equations which seemingly makes it more reliable for long-term predictions than other parametric methods which mostly used only 'fitting parameters' which did not necessarily have any physical explanations.

CHAPTER 6

CONCLUSIONS AND FUTURE WORK

6.1 MAIN CONCLUSIONS

(1) As a milestone of this project, the Wilshire Technique has been extended to re-construct, for the first time, full creep curves under different test conditions. This aim of creating full creep curves has been an extensive topic for study and a challenge for many researchers using other techniques but fortunately, it has been achieved in this study.

(2) Titanium IMI834 creep data have been used, for the first time, to examine the ability of the Wilshire technique to predict the long-term creep behaviour. It was proved that the Wilshire equations were able to accurately predict the long-term creep properties of Titanium IMI834 under different creep conditions. This ability of the Wilshire technique in precisely predicting the creep behaviour was a direct result of using physically meaningful parameters in its equations, i.e. the material's tensile strength, σ_{TS}, and the apparent activation energy, Qc^*.

(3) The Wilshire technique was able to predict and fit the creep data in the three possible scenarios, namely: when treating the whole set of data as a bulk, when studying the specimens with the thin, or ignorable, alpha-case thickness (< 35μm) and in the worst case where the thickness of the alpha-case is extremely detrimental (> 35μm). This ability in fitting the creep data under different test environments shows the strength of this technique.

(4) Unlike other prediction techniques, the 'kink' points which appeared in the predictive curves of the Wilshire technique were a real-effect of the material's behaviour above and below the material's yield point, σ_{yield}, where it was found at ~ 85% of the yield stress values at all test temperatures. This was experimentally confirmed in this study which makes this technique superior when compared to the other parametric techniques which tried to ignore such inflection in their predictive curves and only attempted to fit the creep data using continuous non-intermittent curves.

(5) In order to make this study as comprehensive as possible, the Titanium IMI834 creep data have been used to examine ten other widely used parametric techniques from which it was proved that the Wilshire methodology was on the top of all other techniques in its ability to predict the creep behaviour and also in re-constructing full creep curves under various test conditions.

(6) Oxidation of Titanium IMI834 is a very detrimental effect of oxygen diffusion that appears and quickly builds up when using this alloy at temperatures higher than 600°C. However, in this study, the oxidised layer, or the alpha-case, of the crept specimens has been measured and intelligently used in predicting the initiation time of the surface cracks under the different test conditions.

(7) Surprisingly, the surface cracks were dependent on the stress level and test temperature where it was proved that they appeared during the late stages of the creep life and penetrated more at fracture under the effect of low stresses, at a constant temperature. Whereas at the higher stresses, they were initiated early during the creep life but penetrated less at fracture, at a constant test temperature. The critical time values, t_c, at which these cracks were initiated were projected on the actual creep curves at the corresponding conditions from which critical strain values, ε_c, were obtained.

(8) The mechanical properties of Titanium IMI834 can be drastically affected by the oxidised layer. This was confirmed by the drop in the ductility of the specimens with a thick alpha-case layer. The appearance of this oxidised layer can be considered as a phase change in the material's exposed/oxidised surface. This effect can be extremely severe in thin sections where an alpha-case thickness of 150μm was ~ 15% of the volume fraction of the specimens used in this study (which has 20.0mm gauge length and 4.0mm diameter). Therefore, since this alloy is being used in the compressor blades which are relatively thin, this effect should be more seriously considered in any future studies.

6.2 FUTURE WORK

(1) To examine the Wilshire equations using more materials in order to generalise its use for long-term creep predictions. This could include not only metals, but also other materials such as ceramics and composites. Its ability to predict both the long-term creep behaviour along with re-constructing full creep curves might become an alternative of carrying out actual creep tests which, in return, will save time and cost for such actual tests.

(2) In future studies, the Wilshire technique could be based on other mechanical properties rather than only the ultimate tensile strength. In other words, as this technique was able to predict the time required to reach a certain strain level based on the ultimate tensile strength, the data could be fit using a stress value from the tensile curve that corresponds to that certain strain level (i.e. using σ_ε from the tensile curve instead of σ_{TS}).

(3) The Wilshire technique fitted the actual creep properties which were obtained from creep tests carried out in air. Besides, it used the ultimate tensile strength values obtained from tensile tests carried out in air. This technique could be able to fit vacuum creep tests data using an ultimate tensile strength value that could be obtained from vacuum tensile tests.

(4) When using the Wilshire equations on new materials, the predictive curves of these materials will be monitored and compared to the Titanium IMI834 plots concerning the appearance of 'kink' points. If there are any kink points, they could be physically explained using other techniques, such as:

- **Transmission Electron Microscopy (TEM):** in order to study the density of dislocations above and below the 'kink' points.
- **Optical Microscopy (OP):** in order to see whether there is any elongation of the individual grains, above and below the 'kink' points, especially at the regions where fracture took place.
- **Scanning Electron Microscopy (SEM):** in order to study the mode of fracture above and below the 'kink' points and whether it is intergranular, transgranular or a mixed mode.

(5) The behaviour of the new materials in oxidising atmospheres should be thoroughly investigated. If there are any oxidised surface layers, the effect of these layers should be studied through:

- **Vacuum creep tests:** these tests will eliminate the oxdising atmospheres. If the life is improved in comparison to tests carried out in air under the same conditions, then these brittle surface layers might be the reason behind the shorter creep life obtained in air.

- **Testing two testpieces; exposed and unexposed**. The exposed one might have developed a brittle oxidised surface layer prior to testing. If these test pieces were tested under the same conditions, then any difference in the total life can be linked to this brittle surface layer.

- **Testing two testpieces; both exposed to high temperatures prior to testing,** but the surface layer of one of them is removed off the surface by a very precise polishing. This polishing must be carried out accurately and should only go few microns through the material's surface so that the cross sectional area does not change. If the total life of this surface-free testpiece is improved in comparison to the oxidised one then this implies that the surface cracks nucleated in the surface layer might have affected and shortened the creep life of the oxidised testpiece.

(6) Determining the elasticity modulus value of the alpha-case layer, E_{α}. This could be carried out by exposing a very thin specimen (diameter ~ 1mm) to high temperatures and allow an alpha-case layer to develop on the surface and penetrate through the whole substrate material. Afterwards, tensile tests can be carried out from which the elasticity modulus of the exposed material can be obtained.

(7) Studying the effect of the alpha-case layer on both thin and large sections. The effect of the alpha-case layer on the mechanical properties might be dependent on the volume fraction of the alpha-case relative to the bulk material where the fraction might be significant in small sections whereas it could be negligible in large sections.

(8) Studying the effect of the alpha-case not only under creep conditions, but also under tensile and fatigue conditions and its effect on the total life and ductility. This can be done by exposing testpieces to high temperatures to allow a certain thickness of the alpha case to develop prior to testing. Tests of the exposed and the non-exposed testpieces can then be evaluated.

REFERENCES

[1] B.Wilshire, R.W.Evans
Introduction to Creep, 1993. London: The Institute of Materials.

[2] R.K.Penny, D.L.Marriott
Design for Creep. Second edition, 1995. London: Chapman & Hall.

[3] R.J.Arsenault
Treatise on Material Science & Technology: Plastic Deformation of Materials, Volume 6, 1975. New York: Academic Press.

[4] G.E.Dieter
Mechanical Metallurgy, 1988. London: McGraw Hill.

[5] T.H.Courtney
Mechanical Behaviour of Materials, 1999. New York: McGraw Hill.

[6] F.R.Nabarro, H.L. De Villiers
The Physics of Creep: Creep and Creep-Resistant Alloys, 1995. London: Taylor and Francis.

[7] J.G.Harper, J.E.Dorn
Viscous Creep of Aluminium Near its Melting Temperature: Theory of Steady-State Creep Based on Dislocation Climb. Acta Metallurgica, 1957. Volume 5: p. 654-665.

[8] J.Weertman
Steady-State Creep of Crystals. Journal of Applied Physics, 1957. Volume 28: p. 1185-1191.

[9] T.G.Nieh, J.Wadsworth, O.D.Sherby
Superplasticity in Metals and Ceramics, 1997. Cambridge: Cambridge University Press.

[10] J.Weertman
Dislocation Climb Theory of Steady-State Creep, Trans. ASM, 1968. Volume 61: p. 681-694.

[11] M.F.Ashby
Mechanisms of Deformation and Fracture, in *Advances in Applied Mechanics*, 1983. Edited by J.W.Hutchinson and T.Y.Wu, Volume 23: p. 118-172.

[12] T.G.Langdon
Identifying Creep Mechanisms at Low Stresses. Materials Science and Engineering A, 2000. Volume 283: p. 266-273.

[13] R.C.Gifkins
Grain Boundary Sliding and its Accommodation During Creep and Superplasticity. Metall. Trans., 7A. 1976, p. 1225-1232.

[14] P.W.Davies, B.Wilshire
An Interpretation of the Relationship Between Creep and Fracture. Structural Processes in Creep / The Iron and Steel Institute, 1960: p. 34-43.

[15] R.I.Todd
Critical Review of Mechanism of Superplastic Deformation in Fine Grained Metallic Materials. Materials Science and Technology, 2000.Volume 16: p. 1287-1294.

[16] B.Wilshire, J.P.Dennison, I.C.Elliot
Fracture Processes During Creep of Conventionally Cast and Directionally Solidified Mar M002. Materials Science and Engineering 1982. Volume 53: p. 291-293.

[17] H.Burt, J.P.Dennison, I.C.Elliott, B.Wilshire
The Effect of Hot Isostatic Pressing on the Creep and Fracture Behaviour of the Cast Superalloy Mar M002. Materials Science and Engineering 1982. Volume 53: p. 245-250.

[18] D.A.Woodford, D.Stiles
High-Temperature Performance Evaluation of a Directionally Solidified Nickel-Base Superalloy, Journal of Materials Science and Engineering 1997. Volume 6 (No. 4): p. 521-533.

[19] B.J.Cane, P.F.Aplin
Creep Life Assessment Methods. The Journal of Strain Analysis for Engineering Design, 1994. Volume 29 (No. 3): p. 225-232.

[20] S.G.Brown, R.W.Evans, B.Wilshire
Creep Strain and Creep Life Prediction for the Cast Nickel-Based Superalloy IN-100. Materials Science and Engineering, 1986. Volume 84: p. 147-156.

[21] B.Wilshire, P.J.Scharning
A New Methodology for Analysis of Creep and Creep Fracture Data for 9-12% Chromium Steels. International Materials Reviews, 2008. Volume 53 (No. 2): p. 91-104.

[22] B.Wilshire, P.J.Scharning
Prediction of Long-Term Creep Data for Forged 1Cr-1Mo-0.25V Steel. Materials Science and Technology, 2008. Volume 24 (No.1): p. 1-9.

[23] F.R.Larson, J.Miller
A Time-Temperature Relationship for Rupture and Creep Stresses. Trans. ASME, 1952. Volume 74: p. 765-775.

[24] K.Grote, E.Antonsson
Springer Handbook of Mechanical Engineering. Volume 10*: Mechanical properties,* page 114-117. New York: Springer Science & Business Media.

[25] V.Krivenyuk, I.Mamuzic
Correlation of Creep-Rupture Data for Complex Alloys at Elevated Temperatures. Metalurgija, 2007. Volume 46 (No. 2): p. 79-85.

[26] J.Gilbert, Z.Long, S.Ningileri
Application of Time-Temperature-Stress Parameters to High Temperature Performance of Aluminium Alloys. The Minerals, Metals & Materials Society, 2007.

[27] L.Cipolla, J.Gabrel
New Creep Rupture Assessment of Grade 91. Published at: University of Cambridge, Department of Materials Science and Metallurgy, Phase Transformations & Complex Properties Research Group, 2005. [Available at: www.msm.cam.ac.uk/phase-trans/2005/LINK/162.pdf].

[28] E.C.Larke, N.P.Inglis
A Critical Examination of Some Methods of Analysing and Extrapolating Stress-Rupture Data, in *Proceedings of the Institution of Mechanical Engineers.* Conference Proceedings 1963. Volume 178 (No. 3A): p. 33-47.

[29] G.Murry
Extrapolation of the Results of Creep Tests by Means of Parametric Formulae, in *Proceedings of the Institution of Mechanical Engineers.* Conference Proceedings 1963. Volume 178 (No. 3A): p. 87-203.

[30] S.Manson, A.Haferd
A Linear Time-Temperature Relation for Extrapolation of Creep and Stress-Rupture Data. NACA Technical Note 2890, 1953.

[31] J.D.Murray, R.J.Truman
The High Temperature Properties of Cr-Ni-Nb and Cr-Ni-Mo Austenitic Steels, in Proceedings of the Institution of Mechanical Engineers. Conference Proceedings 1963. Volume 178 (No. 3A): p. 55-67.

[32] J.Sobrinho, L.Bueno
Correlation Between Creep and Hot Tensile Behaviour for 2.25 Cr-1Mo Steel from 500℃ to 700℃. Part 2: An Assessment According to Different Parameterization Methodologies. 2005. p. 463-471. [Available at: http: www.materia.coppe.ufrj.br/sarra/artigos/artigo10684].

[33] L.Bueno, V.Sordi, L.Marino
Constant Load Creep Data in Air and Vacuum on 2.25Cr-1Mo Steel from 600 °C to 700 °C. Materials Research, 2005. Volume 8 (No. 4): p. 401-408.

[34] E.Pink
Physical Significance and Reliability of Larson-Miller and Manson- Haferd Parameters. Materials Science and Technology, 1994. Volume 10 (No. 4): p. 340-344.

[35] R.Orr, O.Sherby, J.Dorn
Correlation of Rupture Data for Metals at Elevated Temperatures. Trans. ASM, 1954. Volume 46: p. 113-118.

[36] R.Carreker
Plastic Flow of Platinum Wires. Journal of Applied Physics, 1950. Volume 21: p. 1289-1296.

[37] A.Mullendore, J.Dhosi, R.Widmer, N.Grant
Study of Parameter Techniques for the Extrapolation of Creep Rupture Properties, in *Proceedings of the Institution of Mechanical Engineers,* Conference Proceedings 1963. Volume 178 (No. 3A): p. 15-20.

[38] F.Garofalo, G.Smith, B.Royle
Validity of Time Compensated Temperature Parameters for Correlating Creep and Creep Rupture Data. Trans. Amer. Soc. Mech. Engs. , 1956. (Included in Reference [29]: G.Murry).

[39] N.P.Allen
The Extrapolation of Creep Tests, A Review of Recent Opinion. Institute of Metals, 1960. (Included in Reference [29]: G.Murry).

[40] P.Brozzo
A Method for the Extrapolation of Creep and Stress-Rupture Data of Complex Alloys, in *Proceedings of the Institution of Mechanical Engineers.* Conference Proceedings 1963. Volume 178 (No. 3A): p. 77-85.

[41] S.Manson, G.Succop
Stress-Rupture Properties of Inconel 700 and Correlation on the Basis of Several Time-Temperature Parameters, 1956. ASTM Special Technical Publication (No. 174): p. 40.

[42] N.Zharkova, L.Botvina
Estimate of the Life of a Material Under Creep Conditions in the Phase Transition Theory. Doklady Physics, 2003. Volume 48 (No. 7): p. 379-381. (Translated from Doklady Akademii Nauk, 2003. Volume: 391 (No. 3): p. 334-336. Original Russian Text Copyright © 2003 by Zharkova, Botvina).

[43] S.Manson, W.Brown
Time-Temperature-Stress Relaxations for the Correlation and Extrapolation of Stress-Rupture Data. Proc. ASTM, 1953. Volume 53: p. 683-719.

[44] R.Viswanathan
Damage Mechanisms and Life Assessment of High-Temperature Components. Second edition, 1993. Ohio, USA: ASM International.

[45] S.Manson
Design Consideration for Long Life at Elevated Temperatures, in *Proceedings of the Institution of Mechanical Engineers.* Conference Proceedings 1963. Volume 178 (No. 3A): p. D29-D55.

[46] F.Monkman, N.Grant
An Empirical Relationship Between Rupture Life and Minimum Creep Rate in Creep Rupture Tests. Proc.ASTM, 1956. Volume 56: p. 593-620.

[47] C.Lin, D.Chu
Creep Rupture of Lead-Free Sn-3.5Ag and Sn-3.5Ag-0.5Cu Solders. Journal of Materials Science: Materials in Electronics, 2005. Volume 16: p. 355-365.

[48] V.Borisenko, V.Bukhanovskii, I.Mamuzic
Correlation Dependences Between Short-Term/Long-Term Static Strength Characteristics and Creep Resistance of Tungsten at High Temperatures. Strength of Materials, 2005. Volume 37 (No. 6): p. 584.

[49] A.Baldan, H.Kaftelen
Comparative Creep Damage Assessments Using the Various Models . Journal of Materials Science, 2004. Volume 39 (No. 13): p. 4199-4210.

[50] F.Dobes, K.Milicka
The Relation Between Minimum Creep Rate and Time to Fracture. Metal Science, 1976. Volume 10 (No. 11): p. 382-384.

[51] A.Dlouhy, K.Kucharova, A.Orlova
Long-Term Creep and Creep Rupture Characteristics of TiAl-Base Intermetallics. Materials Science and Engineering A, Structural Materials: properties, microstructure and processing, 2009. Volume 510-11: p. 350-355.

[52] K. Davanas, A. Solomon
Theory of Intergranular Creep Cavity Nucleation, Growth and Interaction. Acta Metallurgica, 1990. Volume 38 (No.10): p. 1905-1916.

[53] A.Baldan
Effects of Carbides and Cavitation on the Monkman-Grant Ductility of a Nickel-Base Superalloy. Journal of Materials Science Letters, 1992. Volume 11 (No. 19): p. 1315-1318.

[54] M.Menon, H.Fang, D.Wu1, M.Jenkins, M.Ferber
Creep and Stress Rupture Behaviour of an Advanced Silicon Nitride: Part III, Stress Rupture and the Monkman-Grant Relationship. Journal of the American Ceramic Society, 1994. Volume 77 (No. 5): p. 1235-1241.

[55] M.Evans
A Generalised Monkman-Grant Relation for Creep Life Prediction: An Application to 1CrMoV Rotor Steel. Journal of Materials Science, 2006. Volume 41 (No. 12): p. 3907-3915.

[56] F.Tancret, T.Sourmail, M.Yescas, R.W.Evans, et al
Design of a Creep Resistant Nickel-Base Superalloy for Power Plant Applications: Part 3 (experimental results). Materials Science and Technology, 2003. Volume 19: p. 296-302.

[57] M.Evans
Sensitivity of the Theta Projection Technique to the Functional Form of the Theta Interpolation/Extrapolation Function. Journal of Materials Science, 2002. Volume 37 (No.14): p. 2871-2884.

[58] R.W.Evans, P.J.Scharning
The Theta Projection Method Applied to Small Strain Creep of Commercial Aluminum Alloy. Materials Science and Technology, 2001. Volume 17 (No. 5): p. 487-493.

[59] R.W.Evans, E.A.Little, J.A.Preston, B.Wilshire
Rationalisation of the Creep Behaviour of Oxide-Dispersion-Strengthened Alloys, in *the Fifth International Conference on Creep and Fracture of Engineering Materials and Structures, 1993.* The Institute of Materials: p. 812.

[60] R.W.Evans, B.Wilshire
The Role of Grain Boundary Cavities During Tertiary Creep. Department of Metallurgy & Materials Technology-Swansea University-UK: p. 303-314.

[61] R.W.Evans
The Theta Projection Method and Low Creep Ductility Materials. Materials Science and Technology, 2000. Volume 16 (No. 1): p. 6-8.

[62] S.J.Williams
An Automatic Technique for the Analysis of Stress Rupture Data. Report MFR30017, Rolls-Royce plc, Derby, UK, 1993.

[63] S.J.Williams
The Implementation of Creep Data in Component FE Analyse. Compass 1999 (Proceedings of the 1st International Conference on Component Optimisation), University of Wales, Swansea, United Kingdom, 1999: p. 139-146.

[64] S.J.Williams, M.R.Bache, B.Wilshire
Recent Developments in the Analysis of High Temperature Creep and Creep Fracture Behaviour. Submitted to Materials Science & Technology, 2009 and has been accepted, April 2010. Volume 0 (No. 0): p. 1-6.

[65] S.Manson, C.Ensign
A Specialised Model for Analysis of Creep-Rupture Data by the Minimum Commitment, Station-Function Approach. NASA TM-X-52999, 1971.

[66] W.White, I.May, T.Silviera
Design Parameters for High Temperature Creep and the Minimum-Commitment Method. Journal of Materials for Energy Systems, 1980. Volume 2 (No. 2): p. 51-59.

[67] S.Manson, C.Ensign
Interpolation and Extrapolation of Creep Rupture Data by the Minimum Commitment Method, Part 1: Focal-point convergence. NASA TM-78881, 1978.

[68] J.Park, S.Manson
A New Approach for the Characterisation of Creep Rupture Properties for a Newly Fabricated Material, in the *Sixth International Conference on Creep and Fatigue Design and Life Assessment at High Temperatures.* 1996: p. 71-80.

[69] J.Ding, C.Kenneth, C.Brinkman
A Comparative Study of Existing and Newly Proposed Models for Creep Deformation and Life Prediction of Si3N4, in 'Life Prediction Methodologies and Data for Ceramic Materials', by C.R.Brinkman and S.F.Duffy, 1994: p. 62-83.

[70] R.Goldhoff
Towards the Standardisation of Time-Temperature Parameter Usage in Elevated Temperature Data Analysis. Journal of Testing and Evaluation, JTEVA 2 (1974). Volume 5: p. 387-424.

[71] R.Goldhoff, G.Hahn
Correlation and Extrapolation of Creep-Rupture Data of Several Steels and Superalloys Using Time-Temperature Parameters. ASM Publication D-8-100, American Society for Metals, Cleveland, 1968: p. 199-247.

[72] M.Evans
Method for Improving Parametric Creep Rupture Life of 2·25Cr-1Mo Steel Using Artificial Neural Networks. Materials Science and Technology, 1999. Volume 15: p. 647-658.

[73] F.J.Clauss
An Examination of High-Temperature Stress Rupture Correlating Parameters. Proc. ASTM, 1960. Volume 60: p. 905-927.

[74] Y.N.Rabotnov
Some Problems on the Theory of Creep. NACA-TM-1353, 1953.

[75] H.Conrad
Correlation of High Temperature Creep and Rupture Data. Journal of Basic Engineering D, 1959. Trans. ASME, Volume 81 (No. 2): p. 617-628.

[76] N.Grant, A.Bucklin
On the Extrapolation of Short Time Stress Rupture Data, in 'Deformation and Fracture at Elevated Temperatures', edited by: A.W.Mullendore and N.J.Grant. 1950, Boston: MIT Press. (Included in Reference [40]: P.Brozzo).

[77] J.Glen
A New Approach to the Problem of Creep. The Journal of the Iron and Steel Institute, 1958. (Included in Reference [40]: P.Brozzo).

[78] J.Brear, P.Aplin
Rationalisation of High Minimum Creep Rate Stress Exponents and Activation Energies in the Norton Creep Law Through Incorporation of Primary and Tertiary Creep Effects, in the *Fifth International Conference on Creep and Fracture of Engineering Materials and Structures*, 1993. UK: The Institute of Materials.

[79] B.Wilshire, H.Burt
Long-Term Creep Design Data for Forged 1Cr-1Mo-0.25V Steel. Journal of Strength, Fracture and Complexity, 2006. Volume 4 (No. 2): p. 65-73.

[80] N.J.Grant
Creep and Fracture of Metals at High Temperatures. (H.M.S.O., London), 1956.

[81] R.Johnson, J.Glen
In *Proceedings of the Conference on the Creep Strength of Steels and High Temperature Alloys*, 1973. Metals Society, London: p. 37.

[82] W.Kim, et al
Creep-Life Prediction of Type 316LN Stainless Steel by Minimum Commitment Method. Key Engineering Materials Journal, 2006. Volume 326-328: p. 1313-1316.

[83] V.Foldyna, A.Jakobova, V.Kupka
The Assessment of Creep Rupture Strength of Modified Chromium Steels, in the *Fifth International Conference on Creep and Fracture of Engineering Materials and Structures*, 1993: p. 573-582.

[84] B.Wilshire, A.Battenbough
Creep and Creep Fracture of Polycrystalline Copper, Materials Science and Engineering A, 2007. Volume 443: p.156 -166.

[85] B.Wilshire, P.J.Scharning
Long-Term Creep Life Prediction for a High Chromium Steel. Scripta Materialia, 2007. Volume 56: p.701-704.

[86] B.Wilshire, H.Burt, N.Lavery
Prediction of Long-Term Stress Rupture Data for 2124. Materials Science Forum, 2006.Volume 519-521: p. 1041-1046.

[87] R.W.Evans, R.Hull, B.Wilshire
The Effects of Alpha-Case Formation on the Creep Fracture Properties of the High-Temperature Titanium Alloy IMI834. Journal of Materials Processing Technology, 1996. Volume 56: p. 492-501.

[88] R.W.Evans, R.Hull, B.Wilshire
Creep Fracture Behaviour of the Near-Alpha Titanium Alloy IMI834, in the *8th International Conference on Fracture(ICF8)*, '*Advances in Fracture Resistance and structural Integrity*', Kiev, Ukraine, 1993. Pergamon Press, Oxford: p. 521-528.

[89] Titanium Metals Corporation
Timetal834: High Strength, High Temperature, Creep Resistant Alloy, 2010. (Available at: http://www.timet.com/834main.html).

[90] W.J.Evans
Aerospace Materials Engineering, 2007. Swansea, UK: Materials Research Centre (School of Engineering)-Swansea University.

[91] N.Singh, V.Singh
Effect of Temperature on Tensile Properties of Near-Alpha Alloy Timetal 834. Materials Science and Engineering A, 2007. Volume 485: p. 130-139.

[92] M.Es-Souni
Creep Behaviour and Creep Microstructures of a High-Temperature Titanium Alloy Ti-5.8Al-4.0Sn-3.5Zr-0.7Nb-0.35Si-0.06C (Timetal834): Part I. Primary and Steady-State Creep. Materials Characterisation, 2001. Volume 46: p.365-379.

[93] J.R.Davis
Tensile Testing. Second Edition, 2004. Ohio, USA: ASM International (The Materials Information Society).

[94] K.Sinha, S.Sinha
Stress Relaxation at High Temperatures and the Role of Delayed Elasticity. Materials Science and Engineering A, 2005. Volume 393: p.179-190.

[95] Z.Zhan, J.Tong
Determination of Creep Curves from Multiple Hardening-Relaxation Testing. The Journal of Strain Analysis for Engineering Design, 2003. Volume 38 (No.3): p. 277-280.

[96] I. Gurappa
Effect of Aluminising on the Oxidation Behaviour of the Titanium Alloy, IMI834. Oxidation of Metals, 2001. Volume 56 (No. 1/2): p. 73-87.

[97] I. Gurappa
Prediction of Titanium Alloy Component Life by Developing an Oxidation Model. Journal of Materials Science Letters, 2003. Voulme 22: p. 771-774.

[98] S.Brown
Swansea, UK: Materials Research Centre (School of Engineering) - Swansea University.

APPENDIX (A)

MACRO IMAGES OF TESTING MACHINES AND SPECIMENS

APPENDIX (A): CONTENTS

A.1 Metallographic Equipment

(a) Mounting Machine:

(b) Grinding Equipment:

(c) Polishing Machine:

(d) Polishing Discs:

(e) <u>Fume Cupboard and Kroll's Etchant</u>:

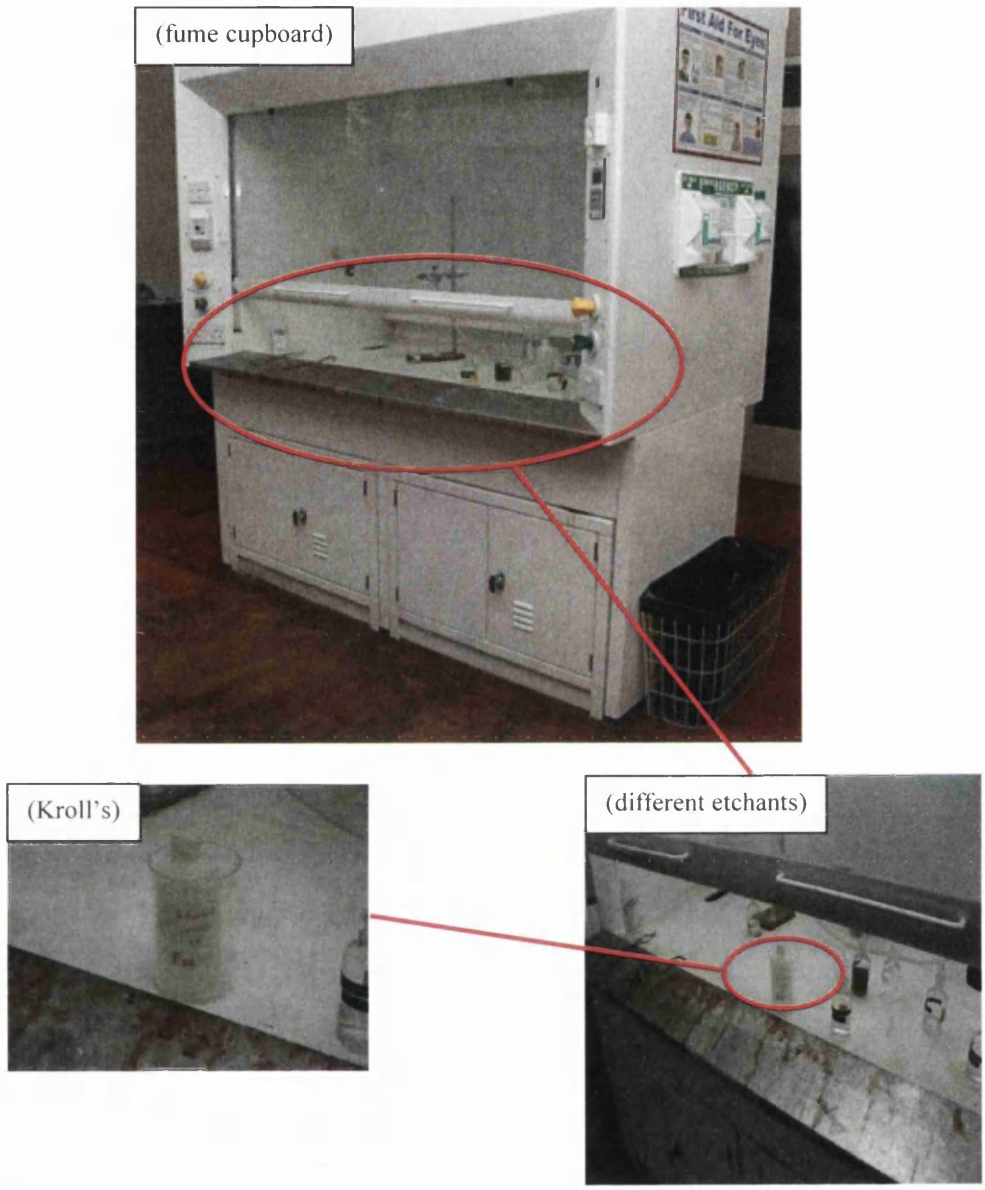

(f) <u>Titanium IMI834 Microstructure</u>:

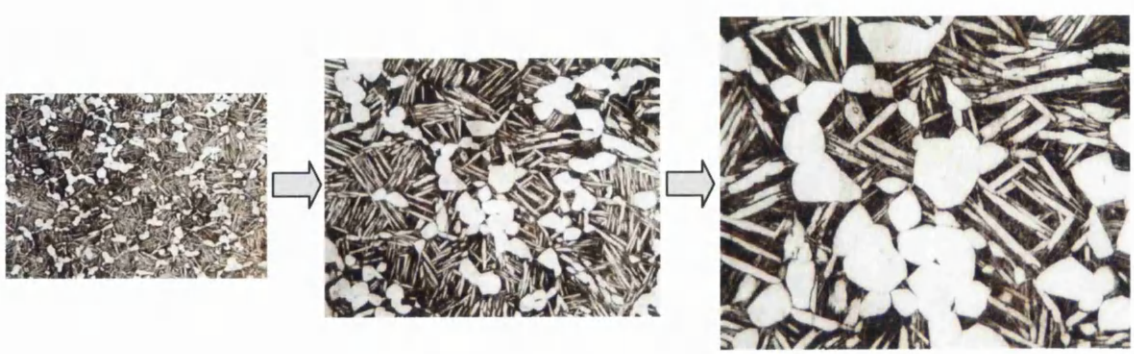

A.2 Tensile & Stress Relaxation Machines & Specimens

(a) Tensile and Stress Relaxation Specimen (SC1-Type):

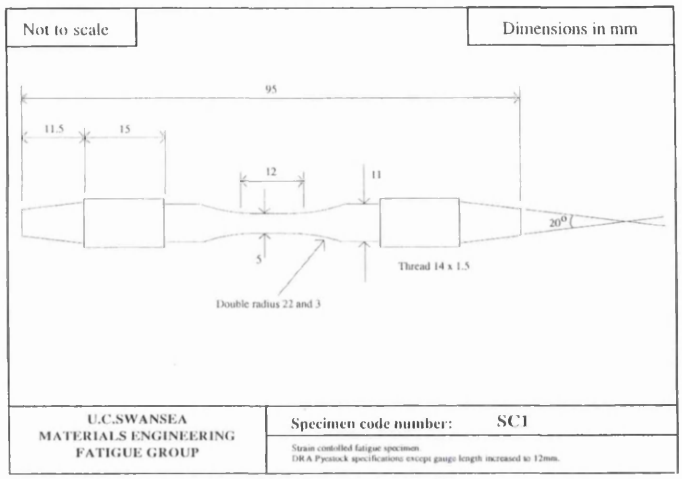

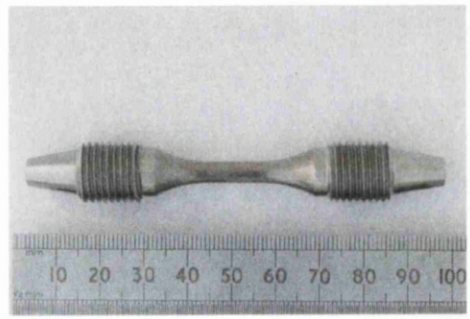

(b) Tensile and Stress Relaxation Machine:

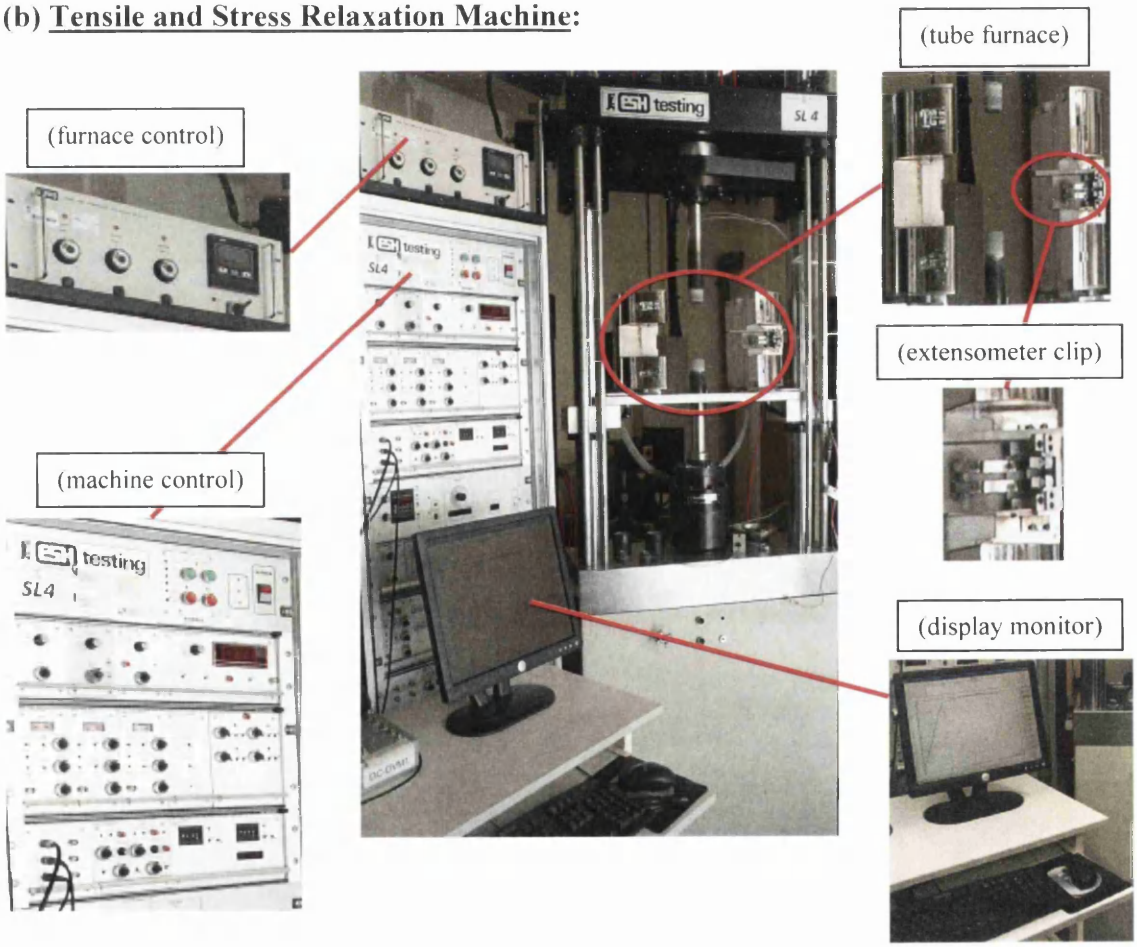

(c) <u>Loading the specimen into the Tensile Machine</u>:

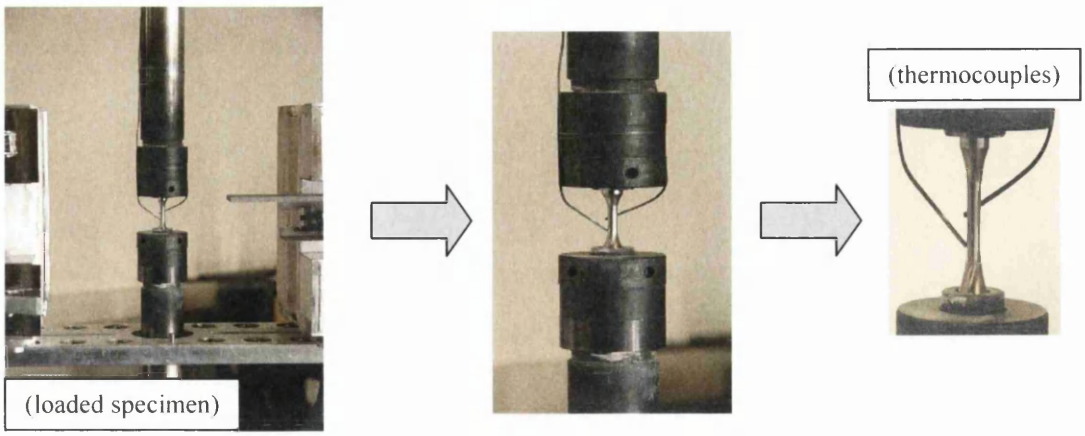

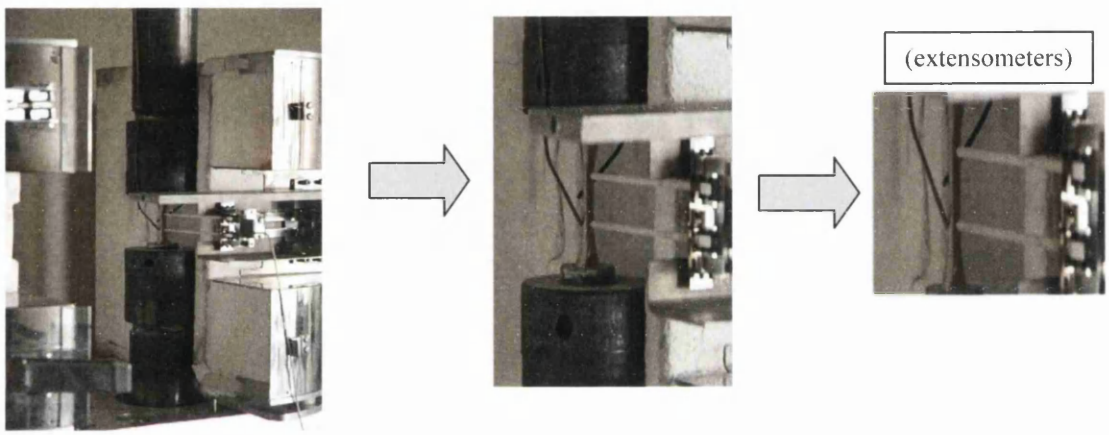

(d) <u>Fractured specimen</u>:

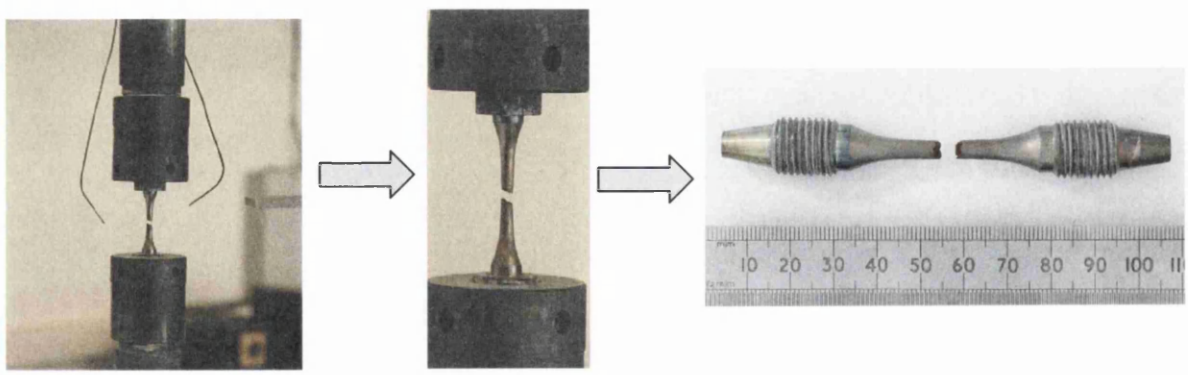

A.3 Creep & Creep-Step Machines & Specimens

(a) Creep and Creep-Step specimen (RLH 10259-Type):

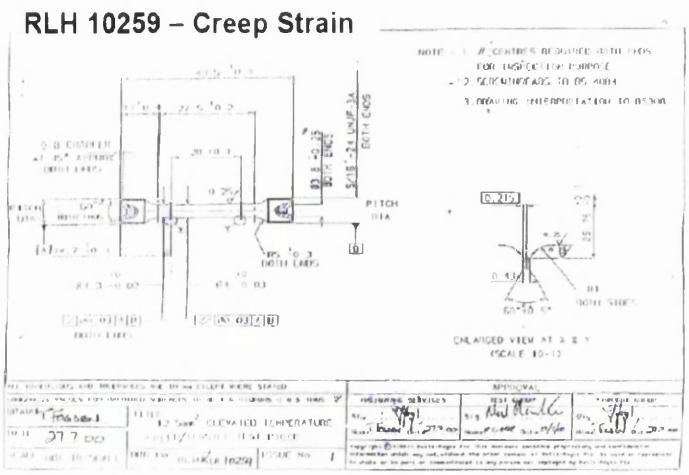

(b) Creep and Creep-Step Machine:

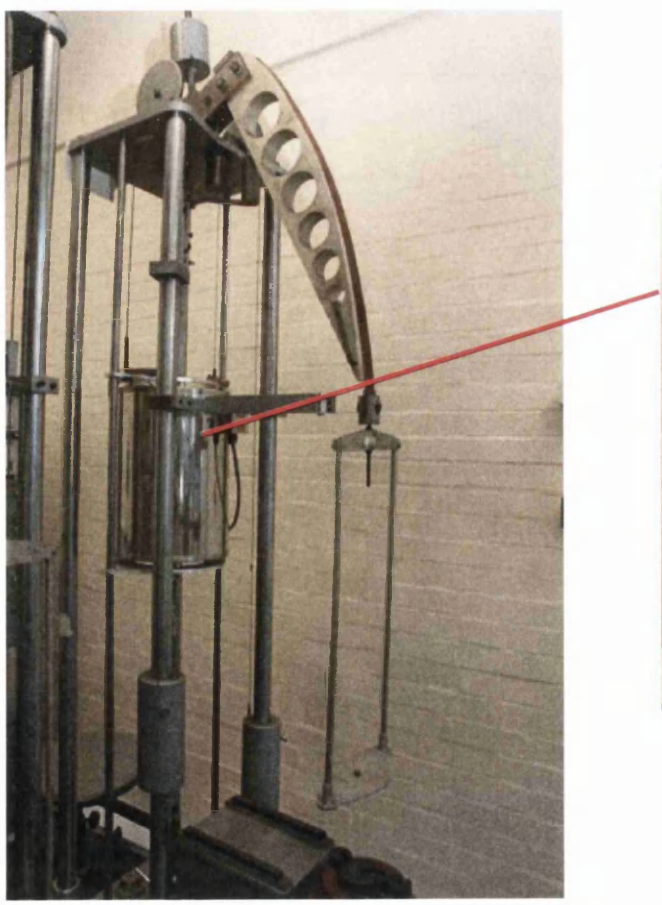

(tube furnace)

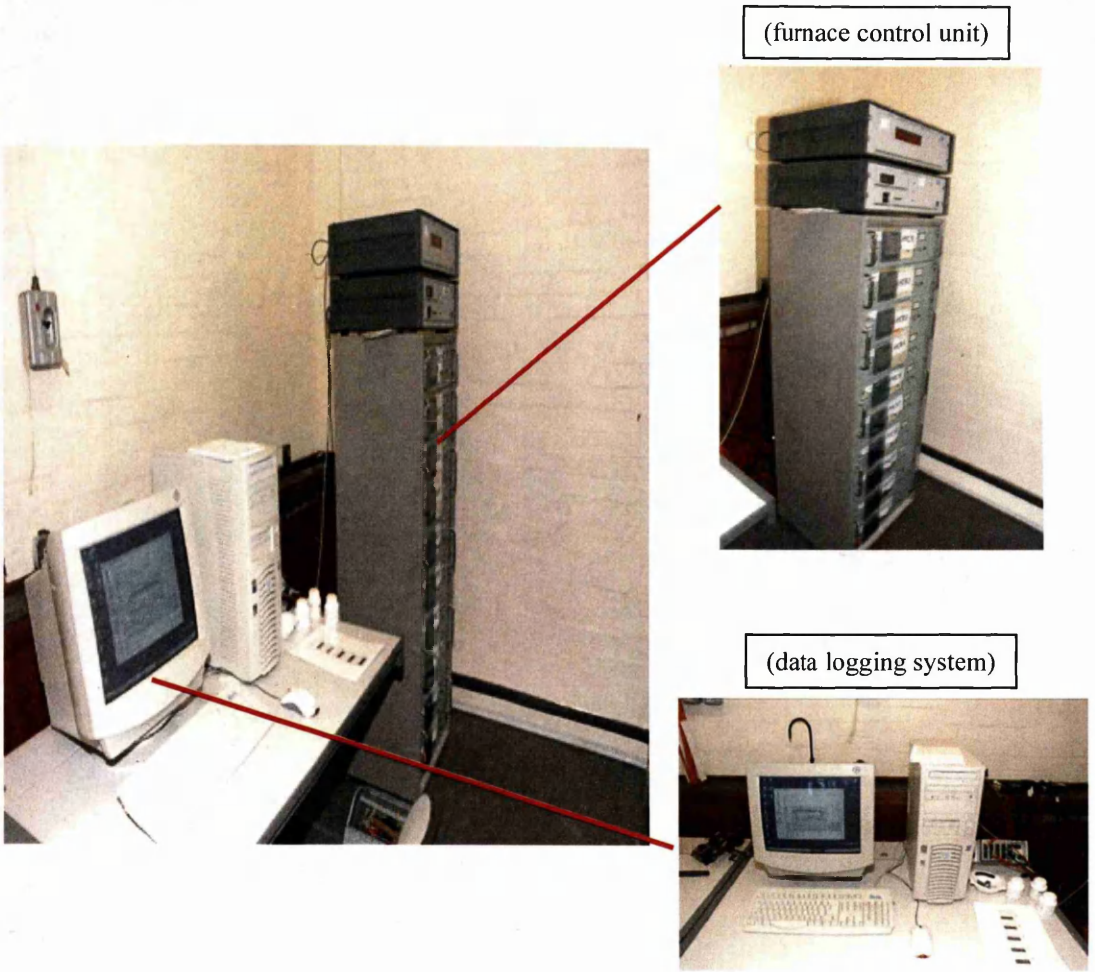

(c) <u>Loading the specimen into the Creep Machine</u>:

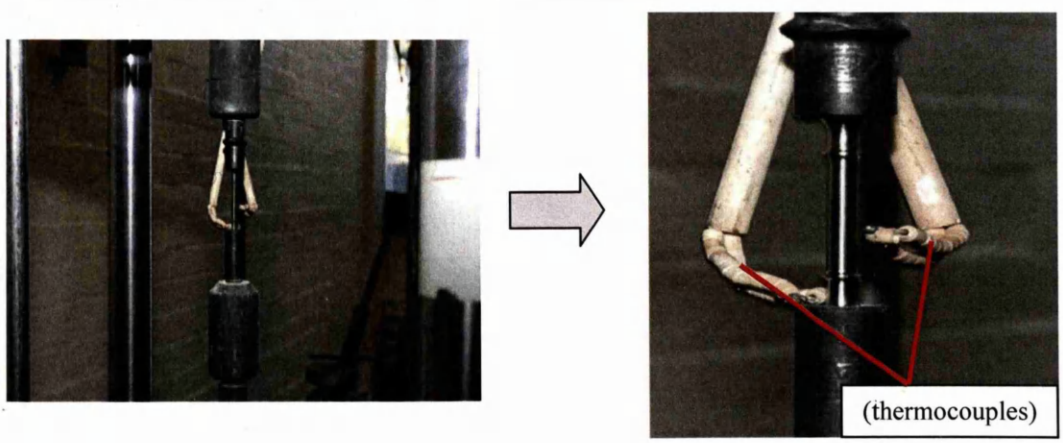

(d) <u>Crept specimen</u>:

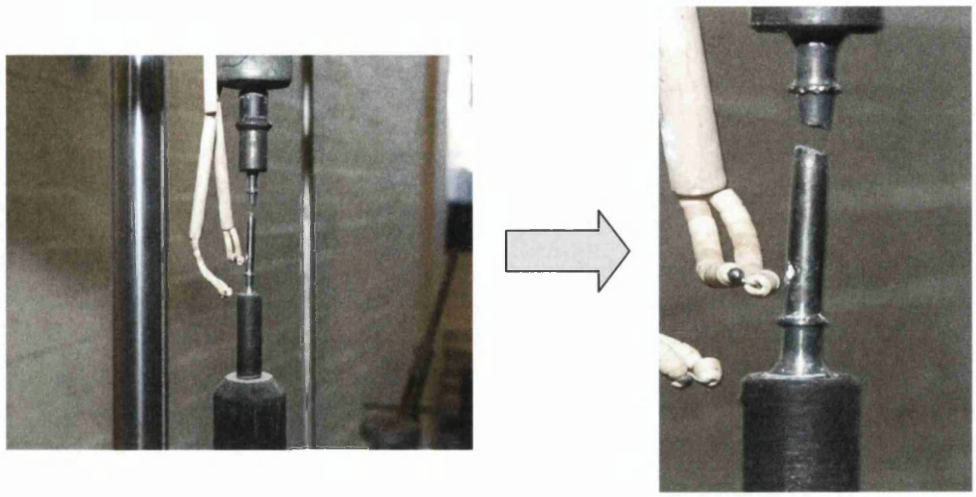

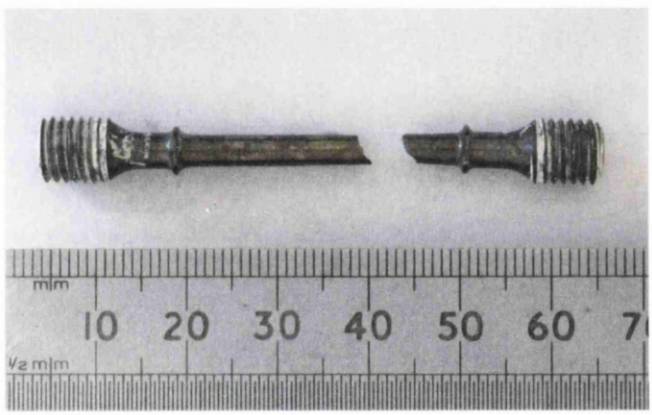

A.4 Vacuum Kit & Pumps

(a) <u>Vacuum Pumps and control</u>:

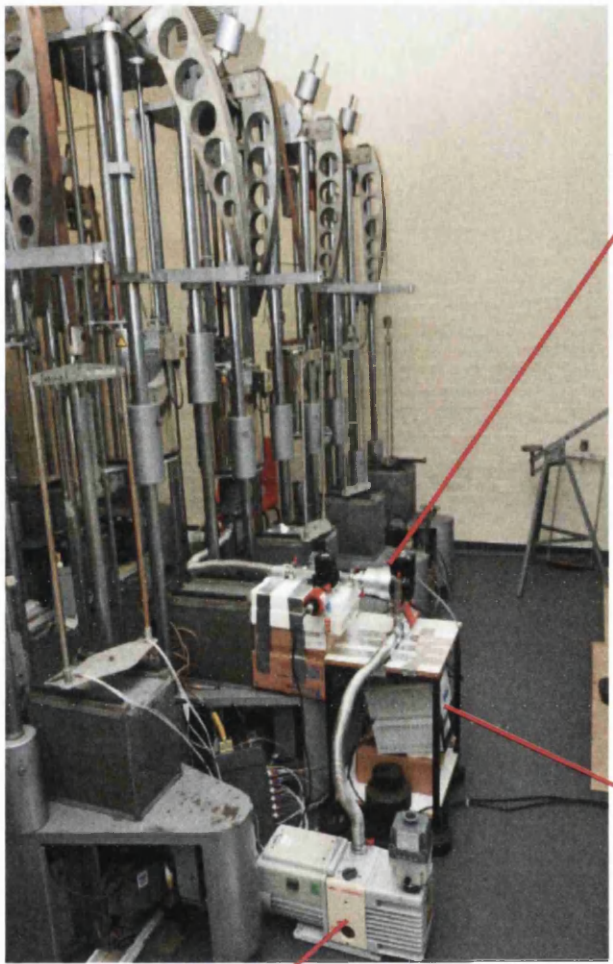

(turbo pump)

(turbo pump control & penning gauge)

(roughing pump)

(b) Vacuum Chamber:

(upper-part cooling water)

(lower-part cooling water)

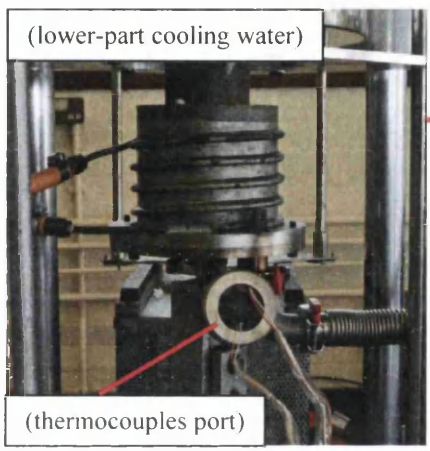

(thermocouples port)

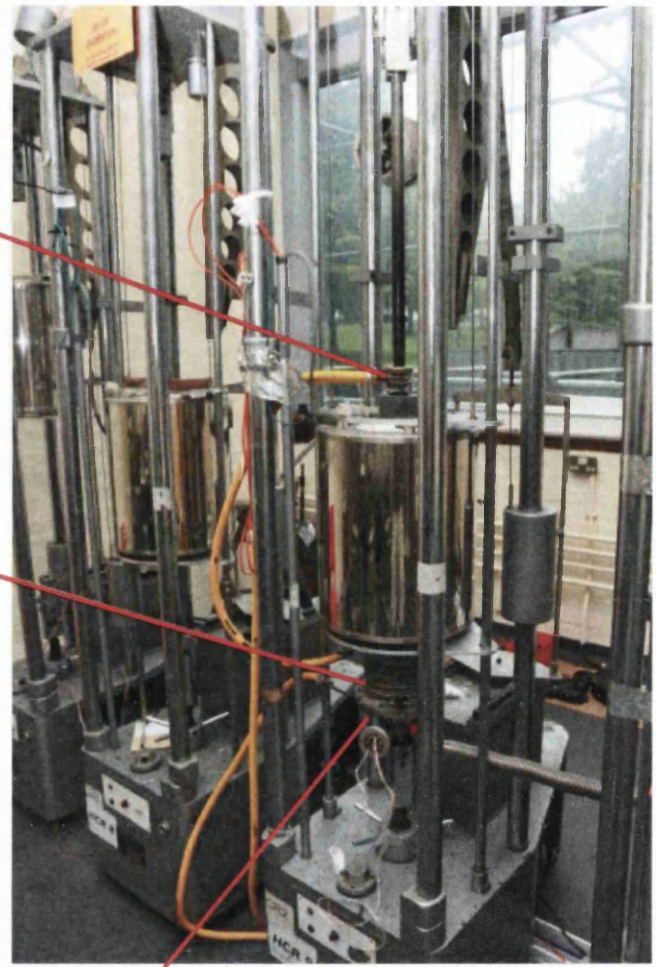

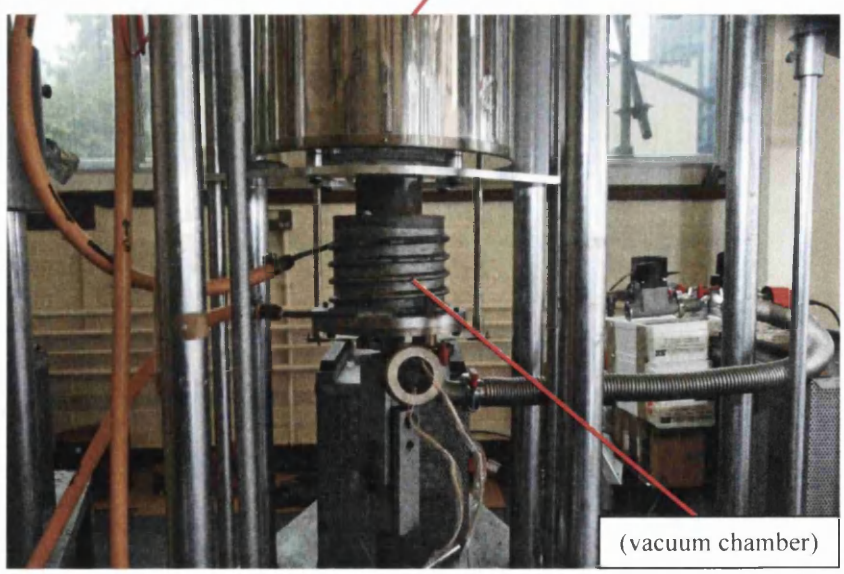

(vacuum chamber)

(c) Fractured specimen:

APPENDIX (B)

PLOTS OF RESULTS AND MICRO IMAGES

APPENDIX (B): CONTENTS

B.1 Tensile Tests Results

(B1.1): 823K

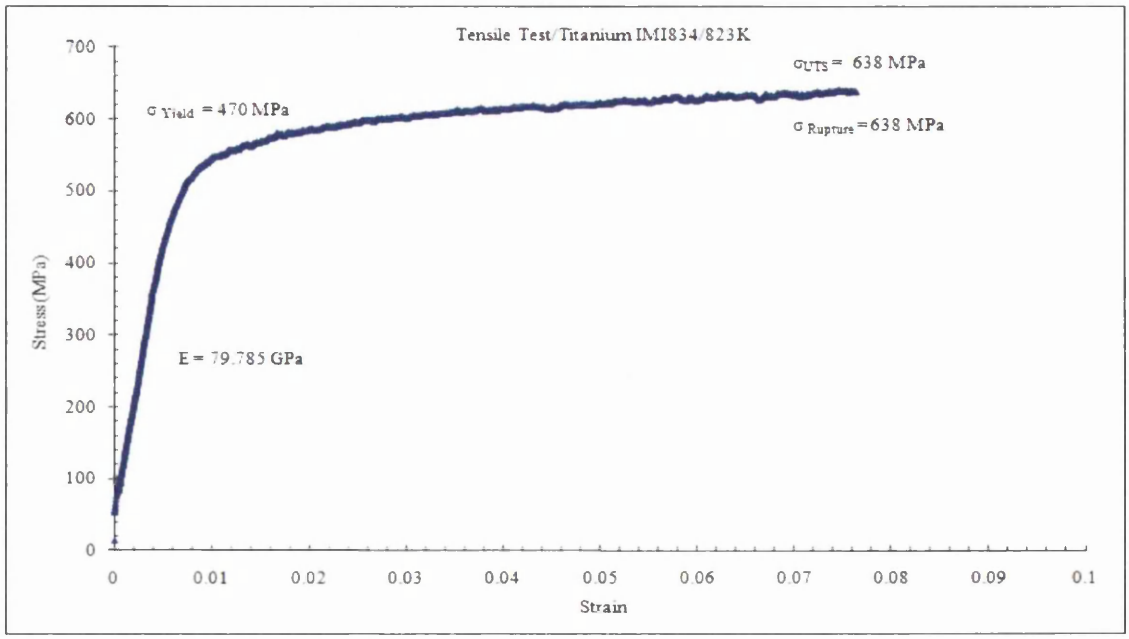

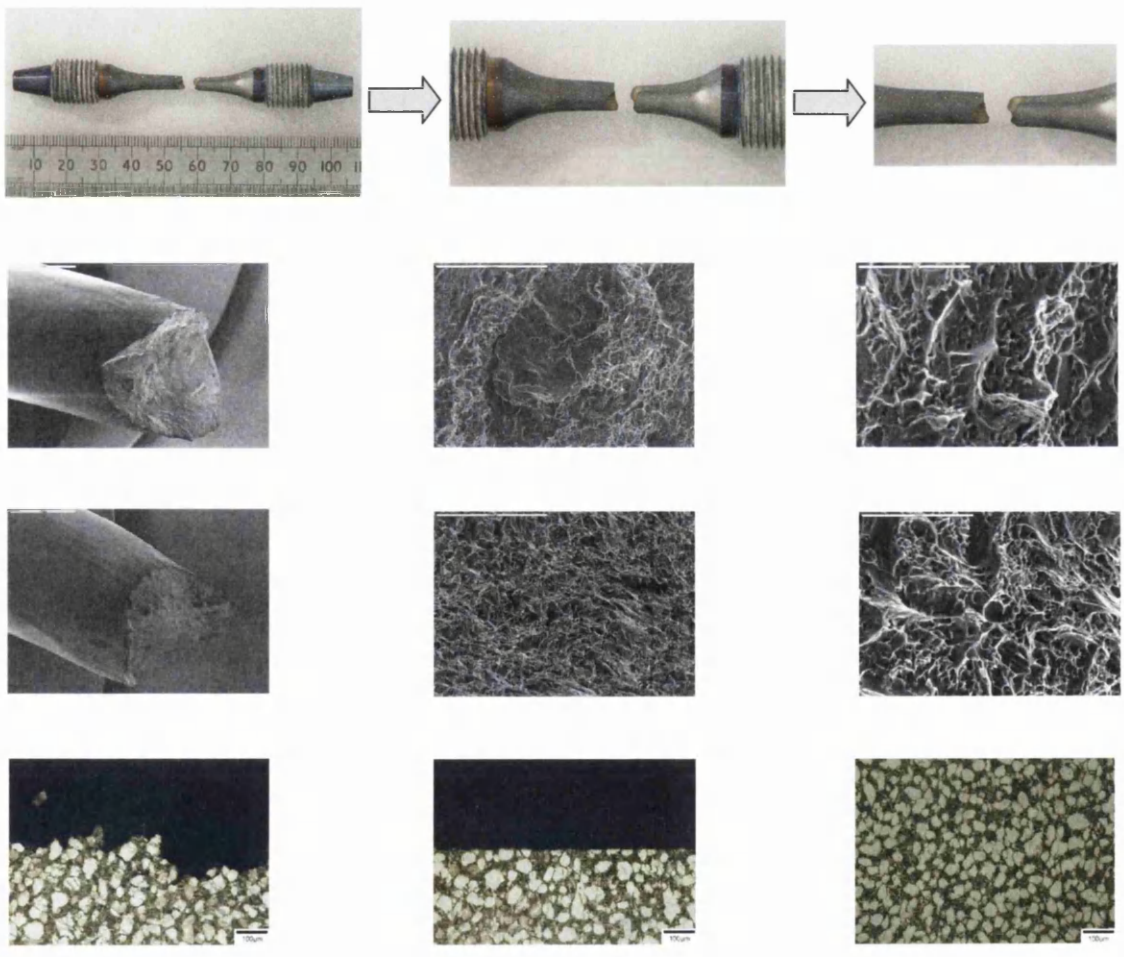

(B1.2): 873K

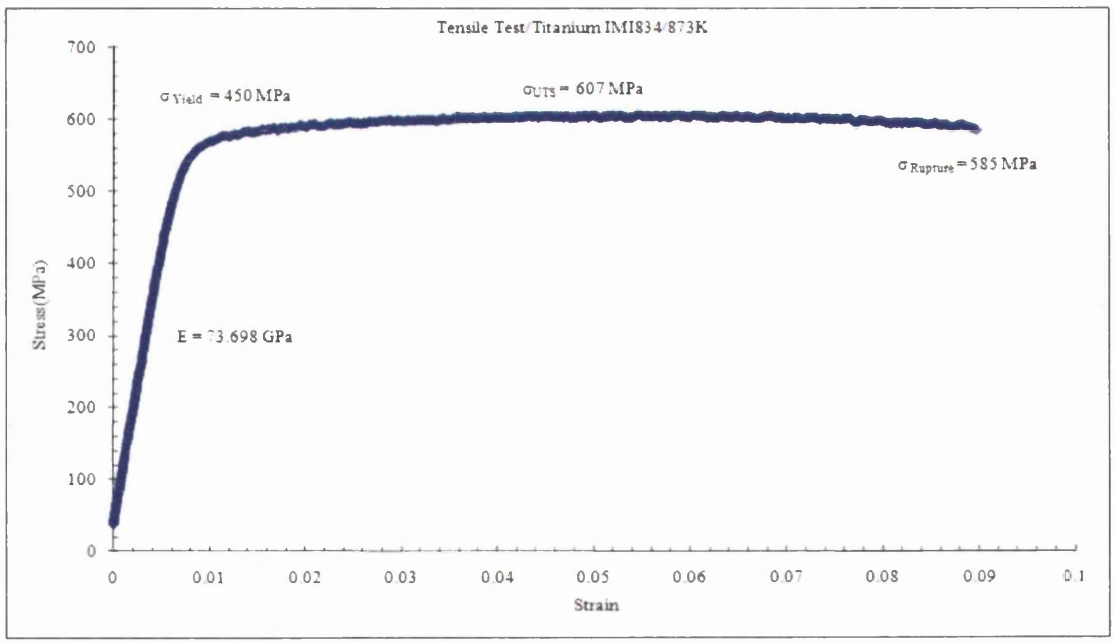
Tensile Test/Titanium IMI834/873K
σYield = 450 MPa
σUTS = 607 MPa
σRupture = 585 MPa
E = 73.698 GPa
Stress(MPa)
Strain
0
100
200
300
400
500
600
700
0
0.01
0.02
0.03
0.04
0.05
0.06
0.07
0.08
0.09
0.1

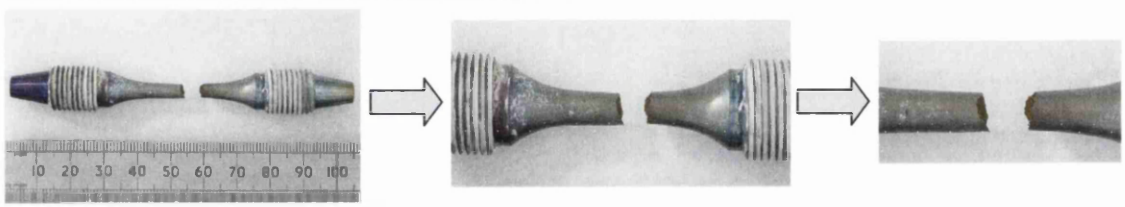
10 20 30 40 50 60 70 80 90 100

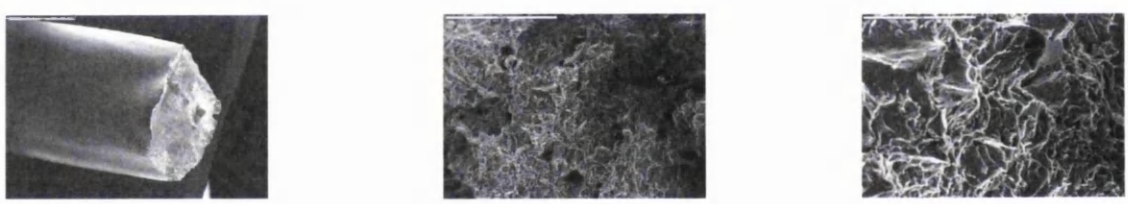

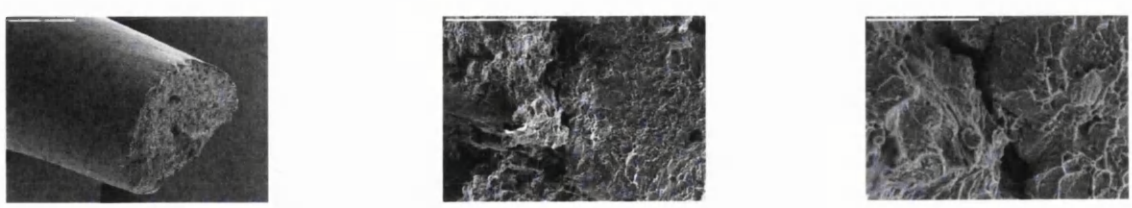

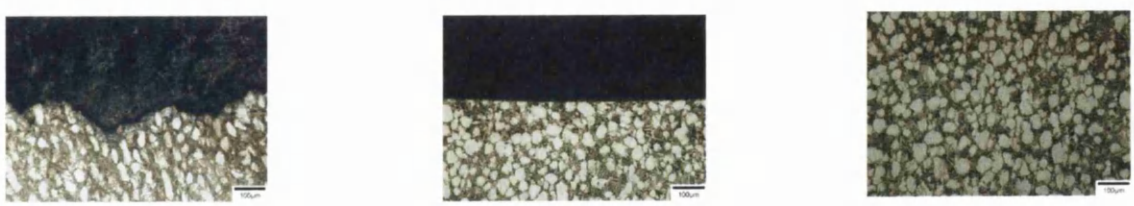

(B1.3): 923K

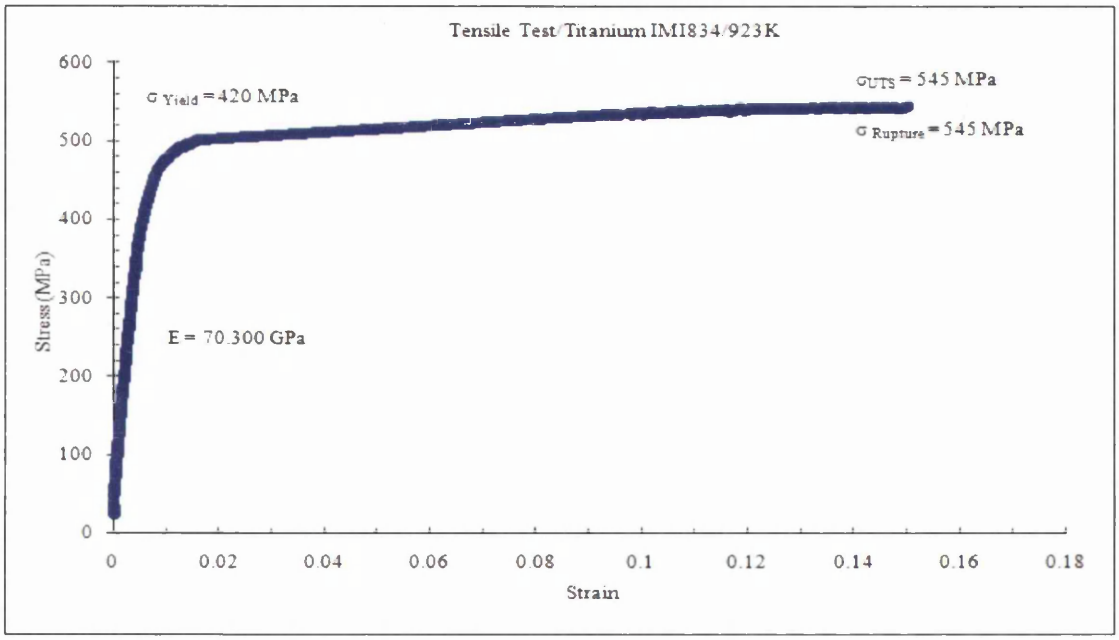
Tensile Test/ Titanium IMI834/923K
σ Yield = 420 MPa
σUTS = 545 MPa
σ Rupture = 545 MPa
E = 70.300 GPa
Stress (MPa)
Strain
600
500
400
300
200
100
0
0
0.02
0.04
0.06
0.08
0.1
0.12
0.14
0.16
0.18

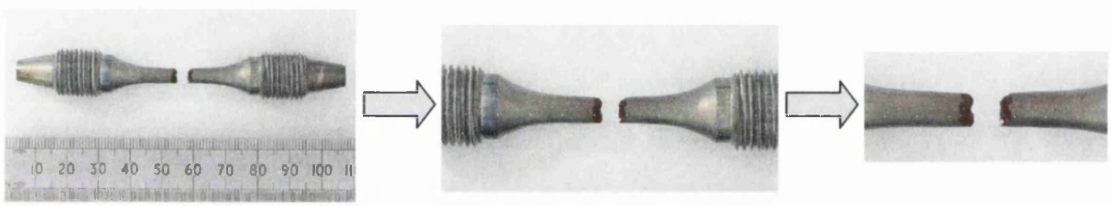

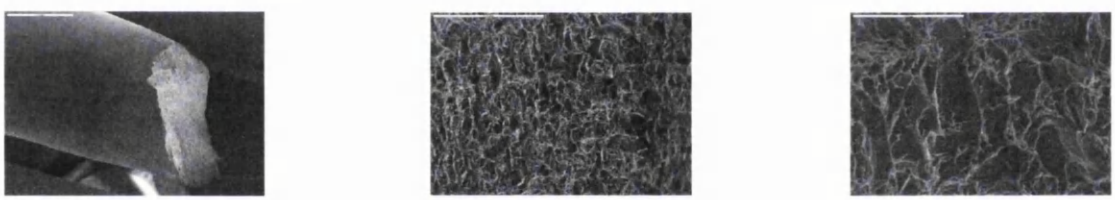

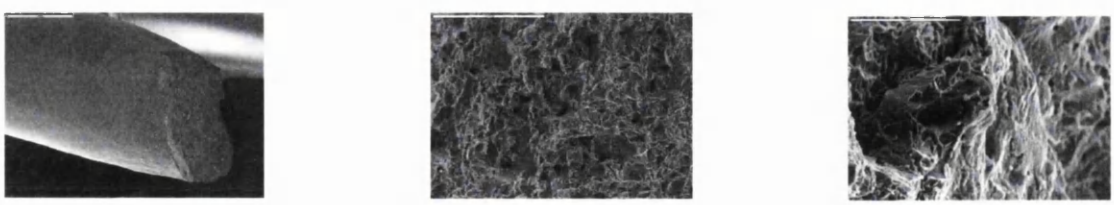

(B1.4): Actual and Interpolated values

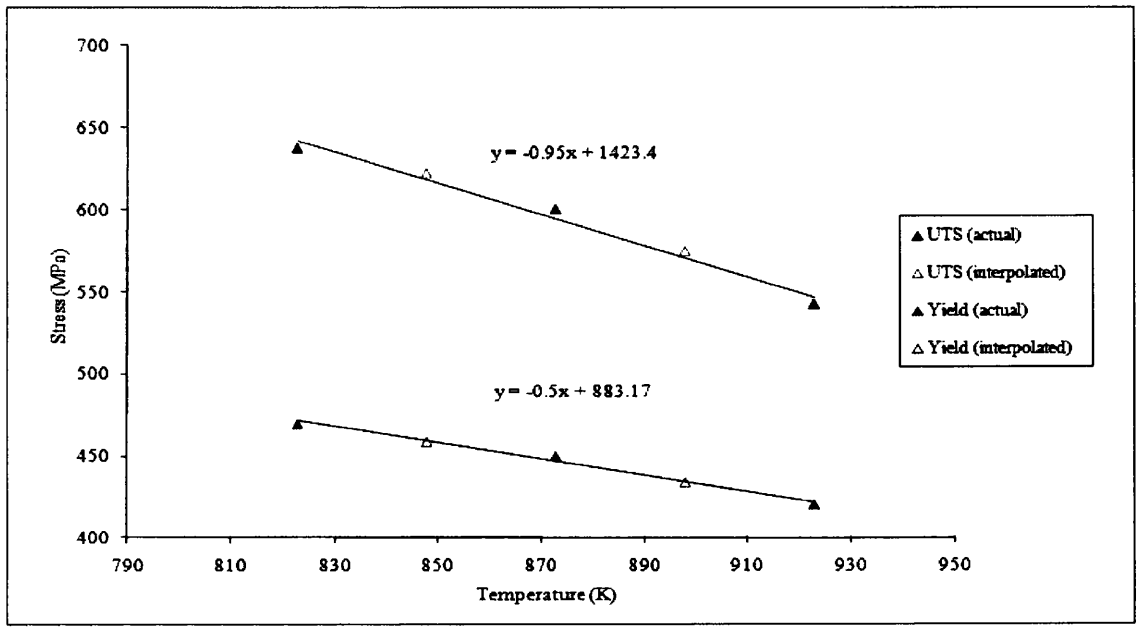

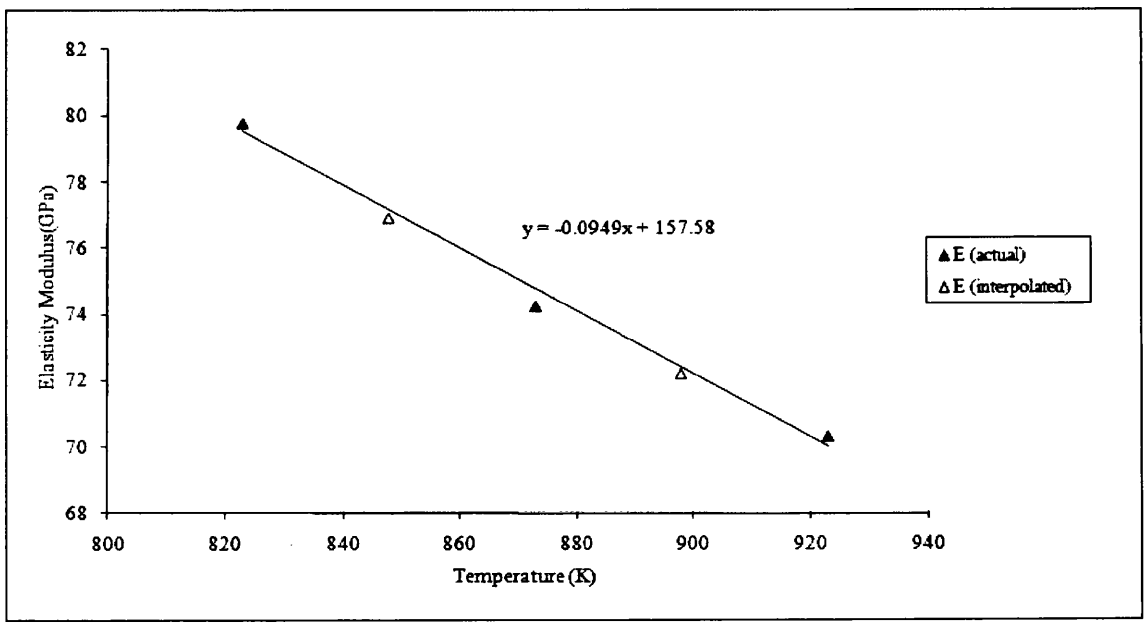

B.2 Stress Relaxation Tests Results

(B2.1): 823K

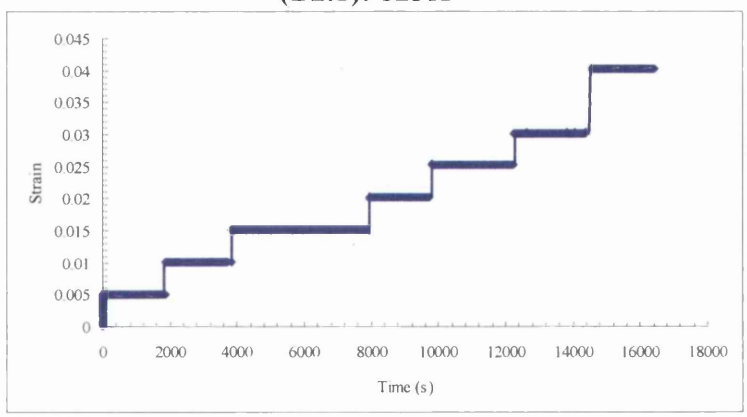

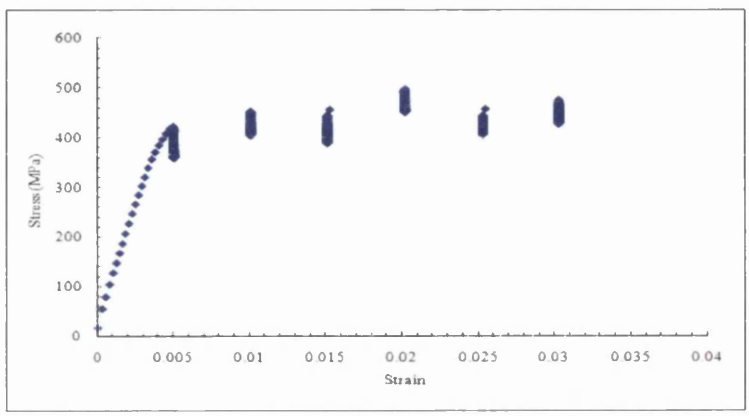

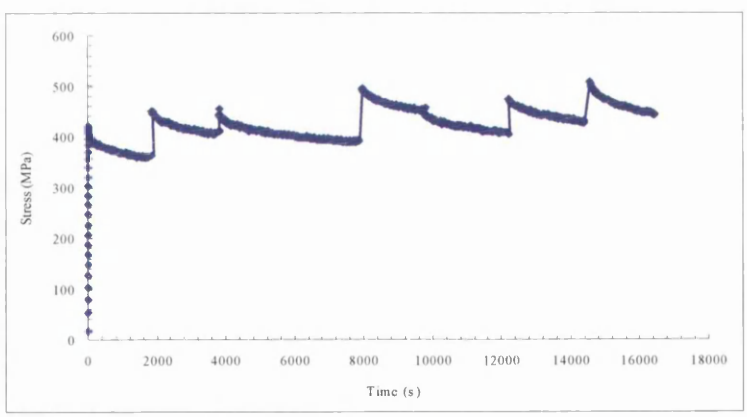

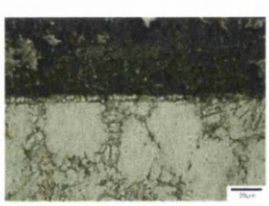

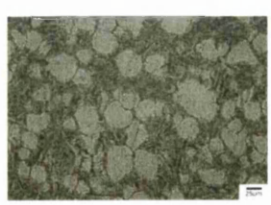

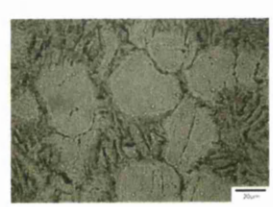

(B2.2): 848K

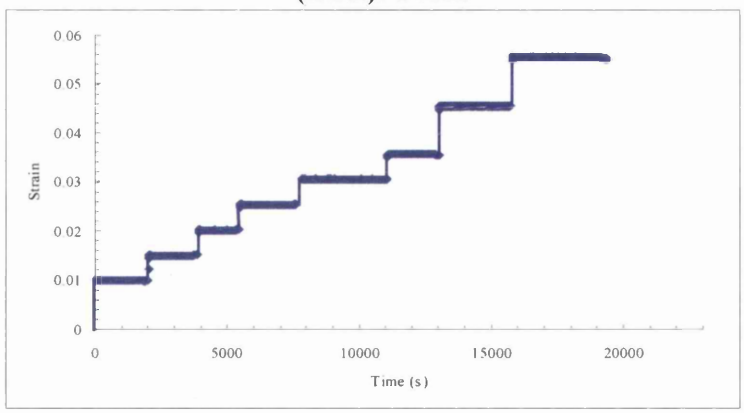
0.06
0.05
0.04
0.03
0.02
0.01
0
Strain
0
5000
10000
15000
20000
Time (s)

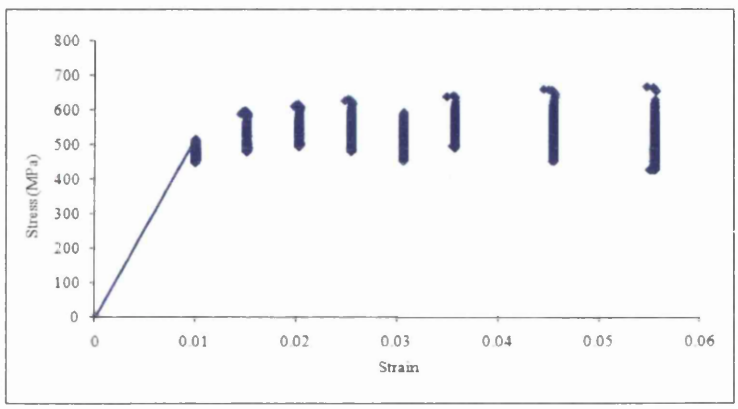
800
700
600
500
400
300
200
100
0
Stress (MPa)
0
0.01
0.02
0.03
0.04
0.05
0.06
Strain

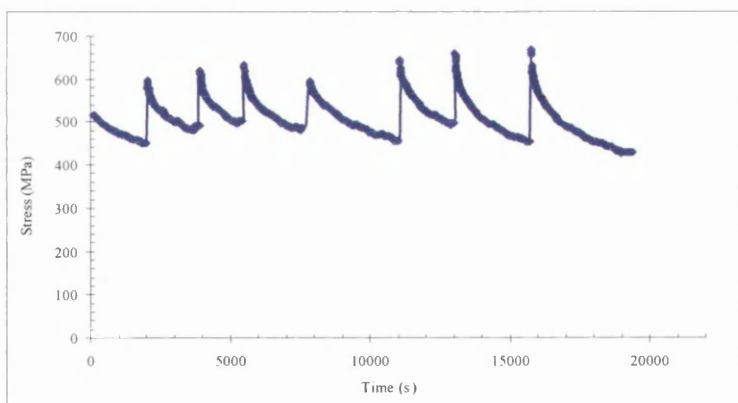
700
600
500
400
300
200
100
0
Stress (MPa)
0
5000
10000
15000
20000
Time (s)

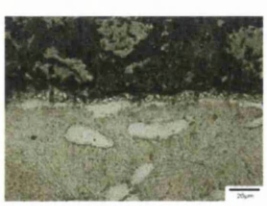

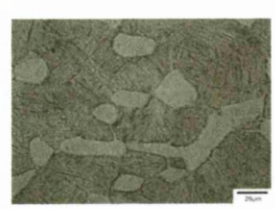

(B2.3): 873K

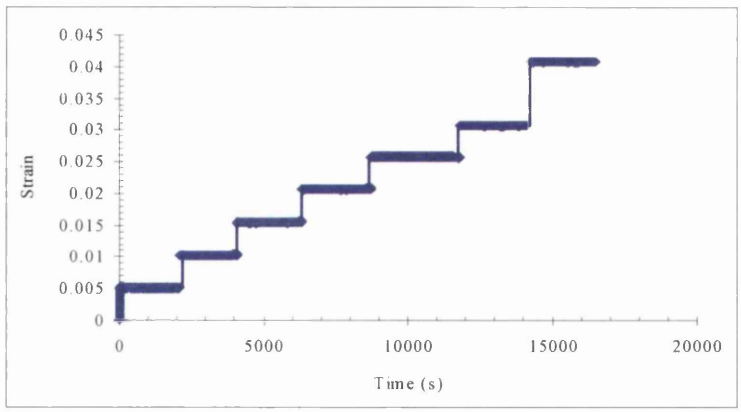
Strain
0.045
0.04
0.035
0.03
0.025
0.02
0.015
0.01
0.005
0
0
5000
10000
15000
20000
Time (s)

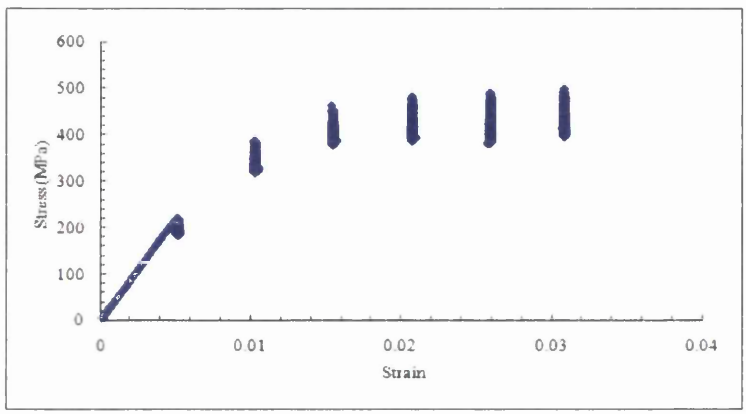
Stress (MPa)
600
500
400
300
200
100
0
0
0.01
0.02
0.03
0.04
Strain

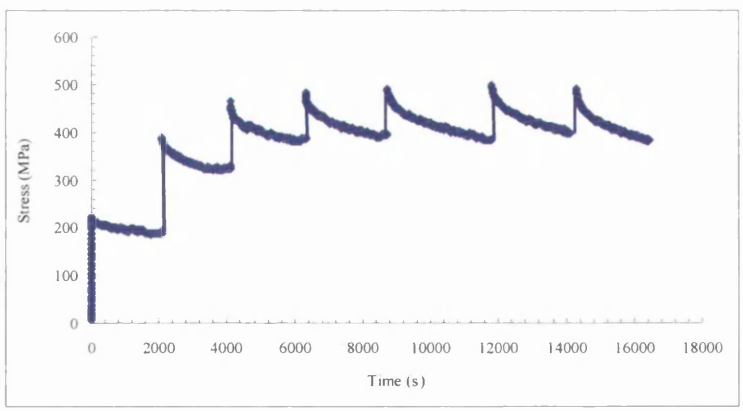
Stress (MPa)
600
500
400
300
200
100
0
0
2000
4000
6000
8000
10000
12000
14000
16000
18000
Time (s)

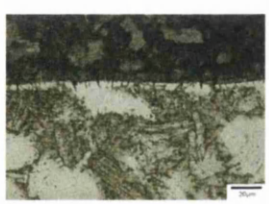

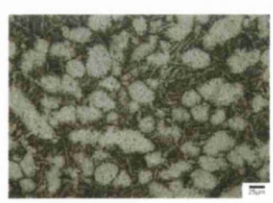

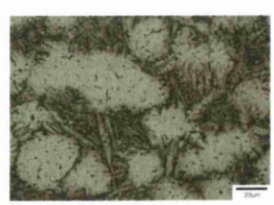

(B2.4): 898K

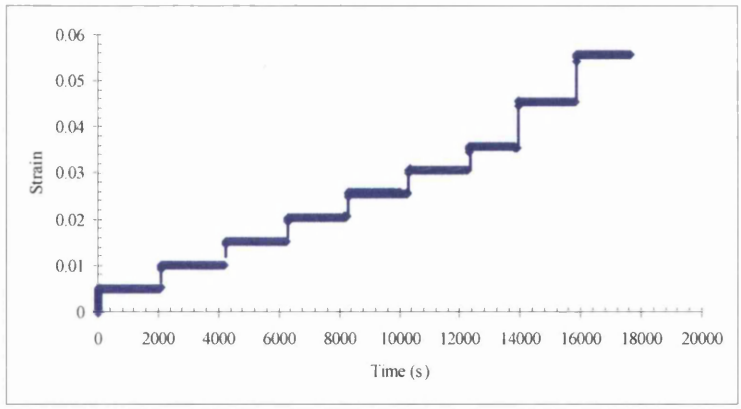
Strain
0.06
0.05
0.04
0.03
0.02
0.01
0
0 2000 4000 6000 8000 10000 12000 14000 16000 18000 20000
Time (s)

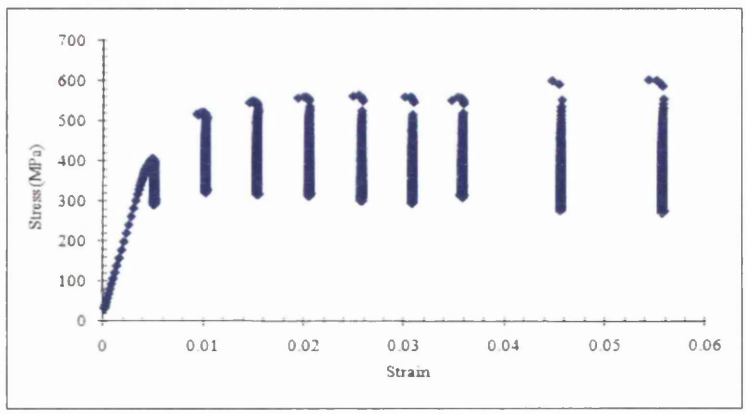
Stress (MPa)
700
600
500
400
300
200
100
0
0 0.01 0.02 0.03 0.04 0.05 0.06
Strain

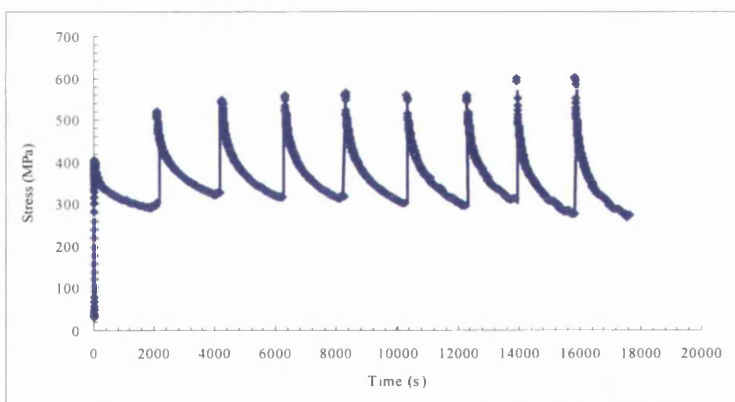
Stress (MPa)
700
600
500
400
300
200
100
0
0 2000 4000 6000 8000 10000 12000 14000 16000 18000 20000
Time (s)

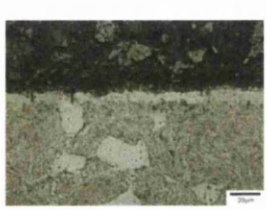

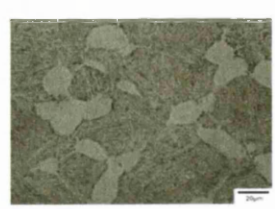

(B2.5): 923K

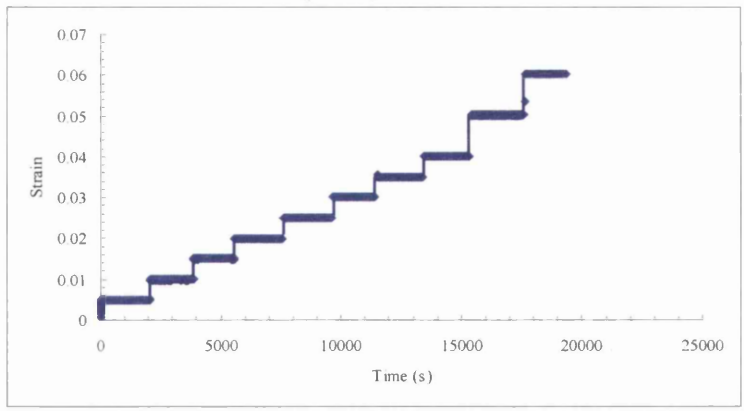
0.07
0.06
0.05
0.04
0.03
0.02
0.01
0
Strain
0
5000
10000
15000
20000
25000
Time (s)

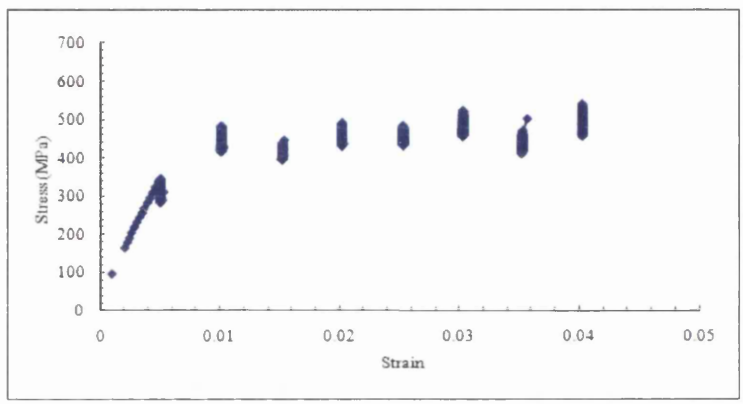
700
600
500
400
300
200
100
0
Stress (MPa)
0
0.01
0.02
0.03
0.04
0.05
Strain

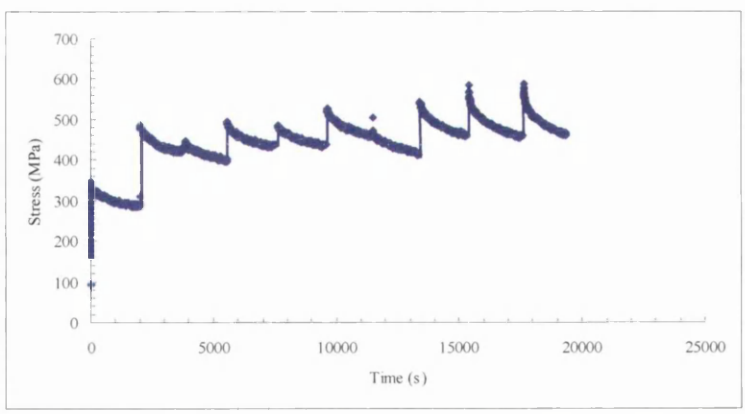
700
600
500
400
300
200
100
0
Stress (MPa)
0
5000
10000
15000
20000
25000
Time (s)

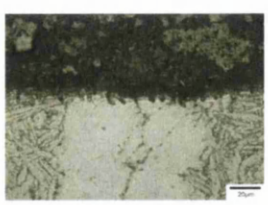

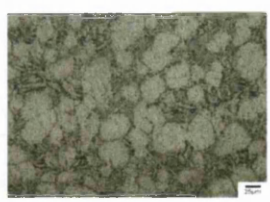

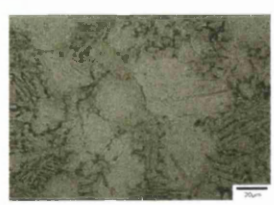

(B2.6): 823K/450MPa

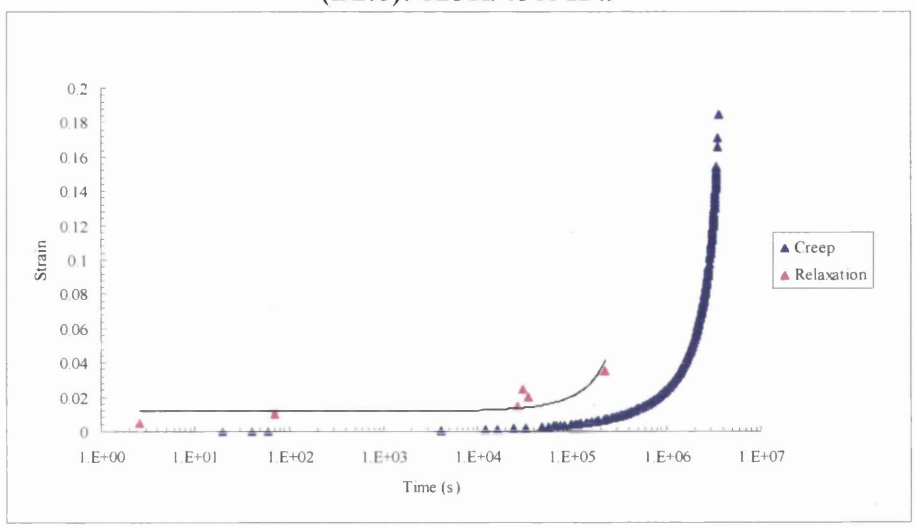

(B2.7): 848K/570MPa

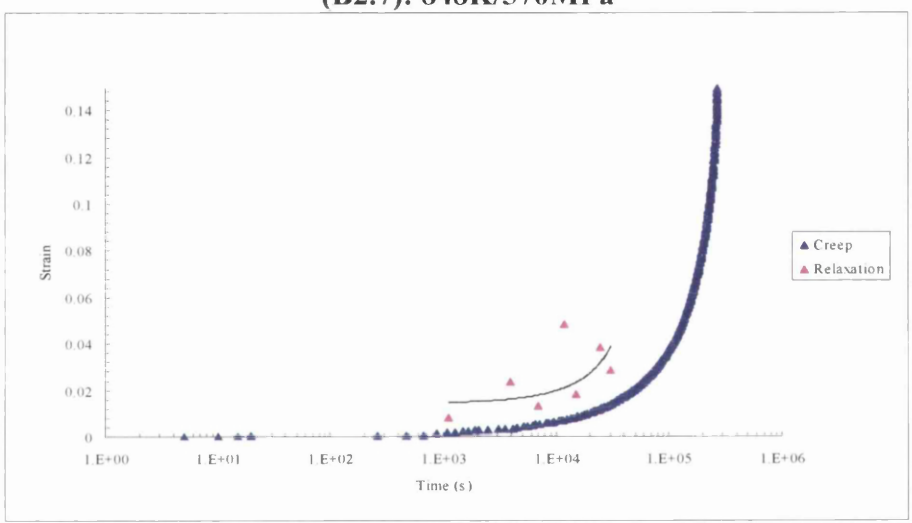

(B2.8): 873K/390MPa

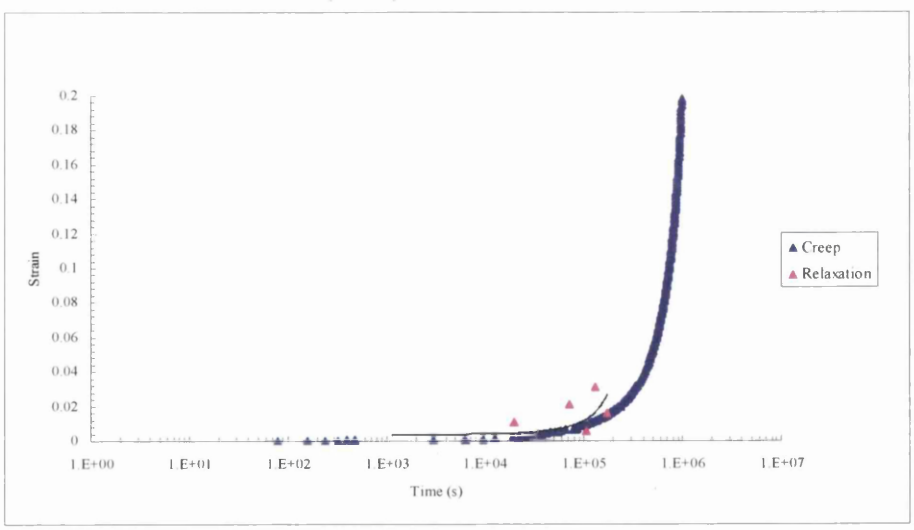

(B2.9): 898K/400MPa

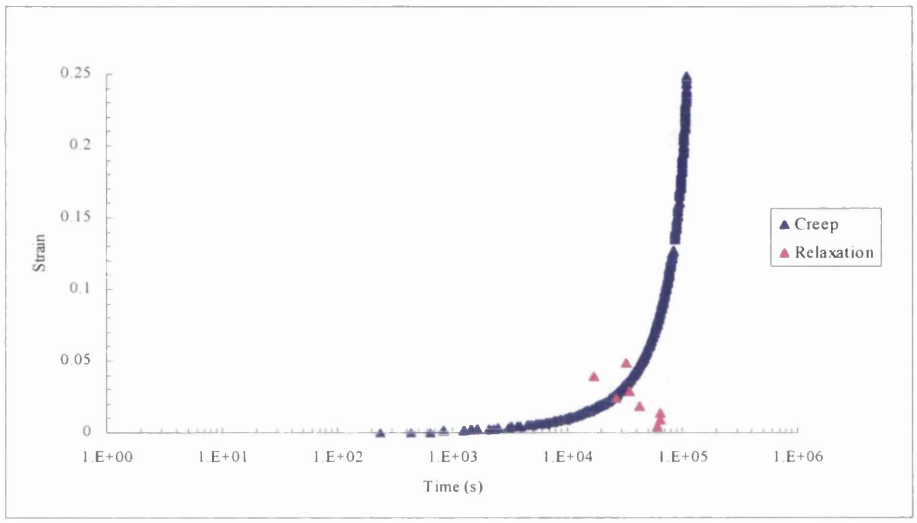

(B2.10): 923K/450MPa

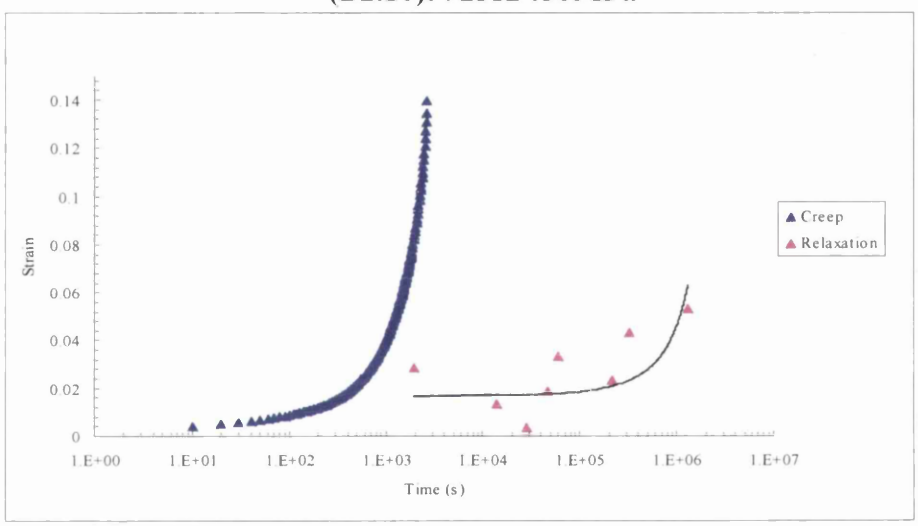

B.3 Creep Tests Results (combined creep curves)

(B3.1): normalized creep curves

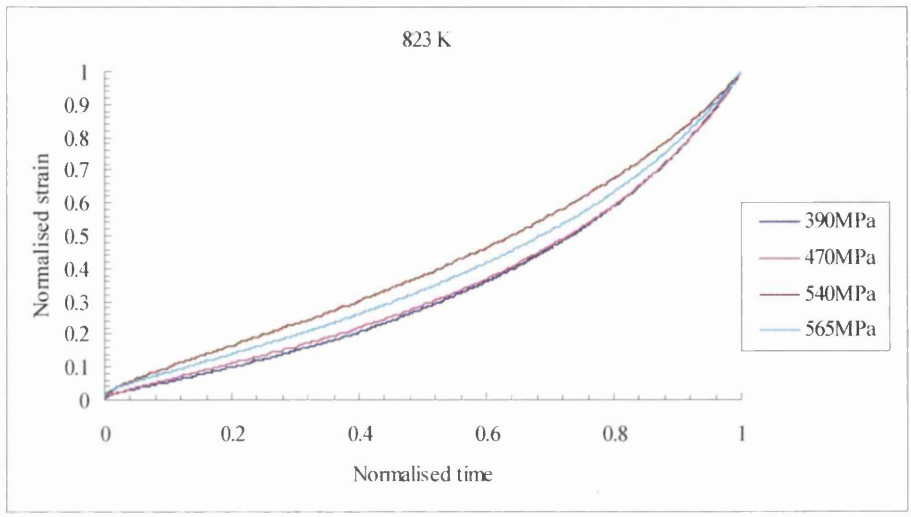

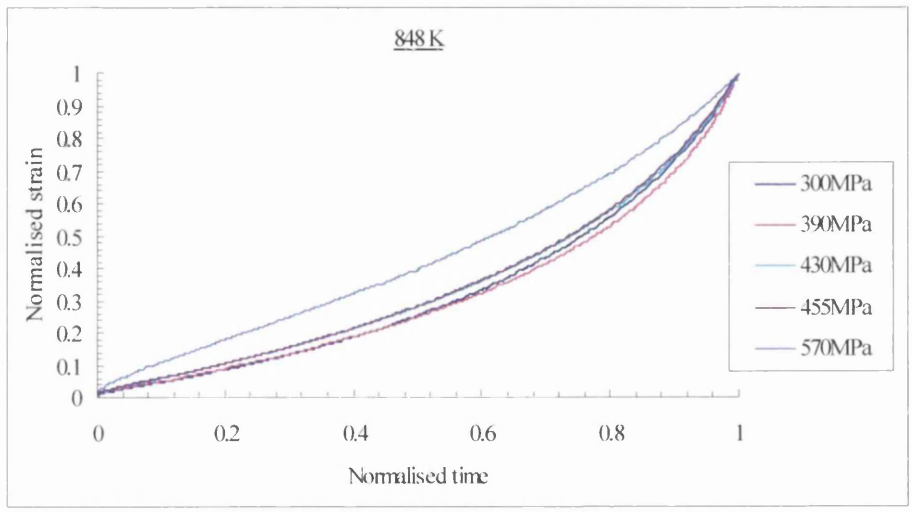

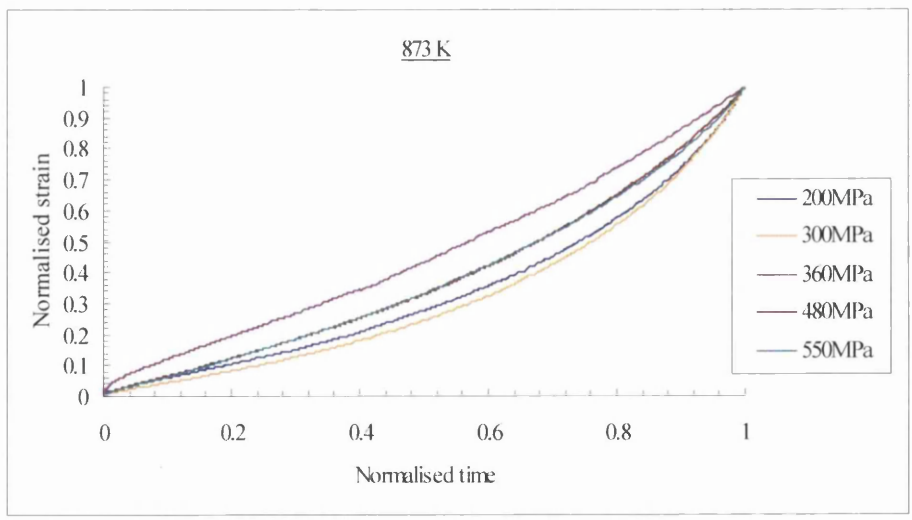

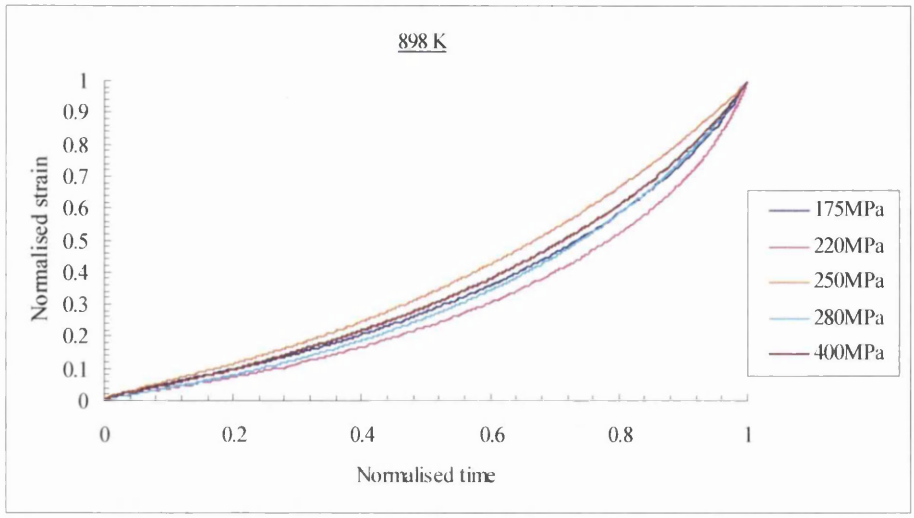
898 K
Normalised strain
Normalised time
0
0.1
0.2
0.3
0.4
0.5
0.6
0.7
0.8
0.9
1
0.2
0.4
0.6
0.8
175MPa
220MPa
250MPa
280MPa
400MPa

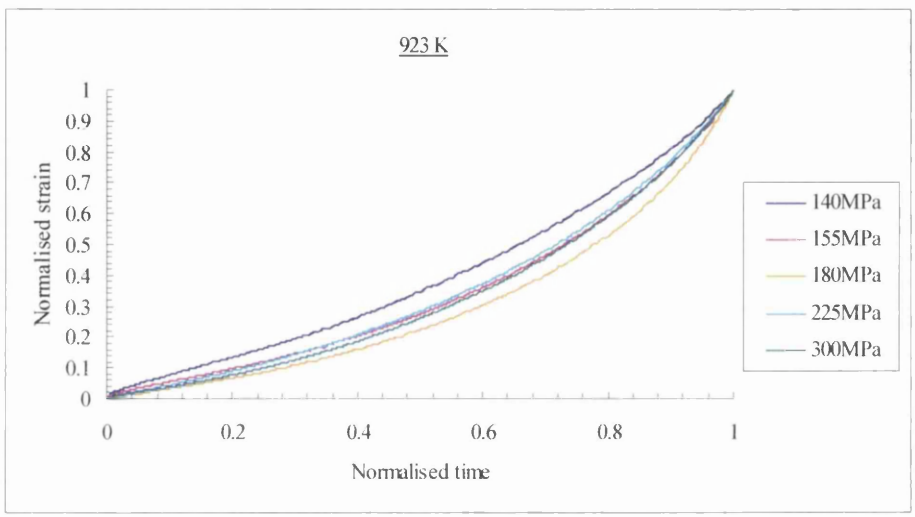
923 K
Normalised strain
Normalised time
0
0.1
0.2
0.3
0.4
0.5
0.6
0.7
0.8
0.9
1
0.2
0.4
0.6
0.8
140MPa
155MPa
180MPa
225MPa
300MPa

(B3.2): normal creep curves

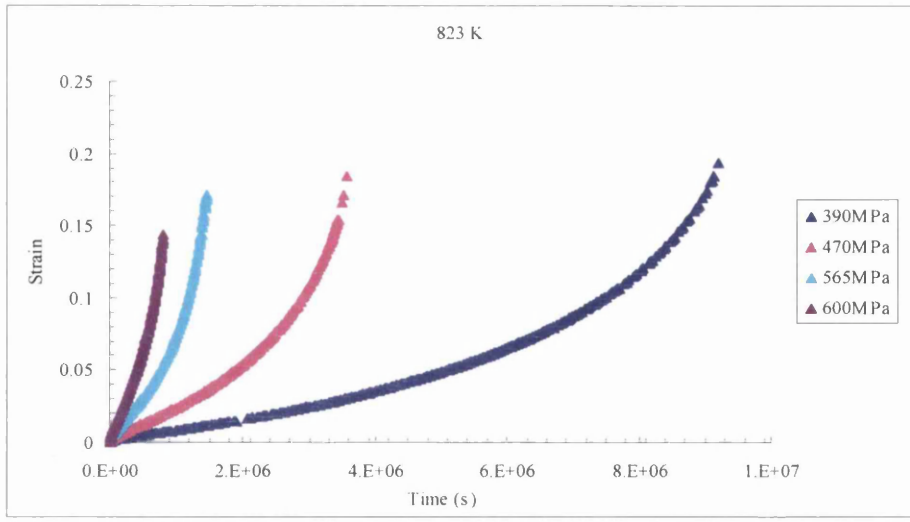

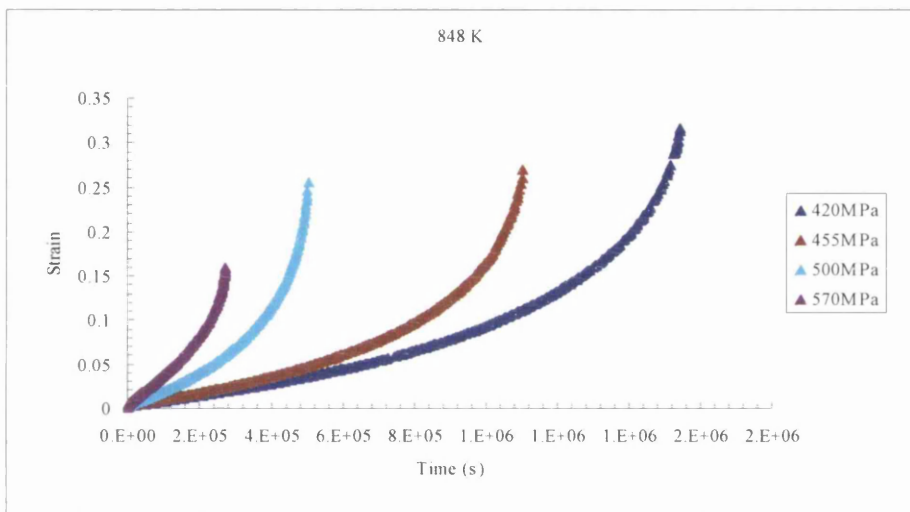

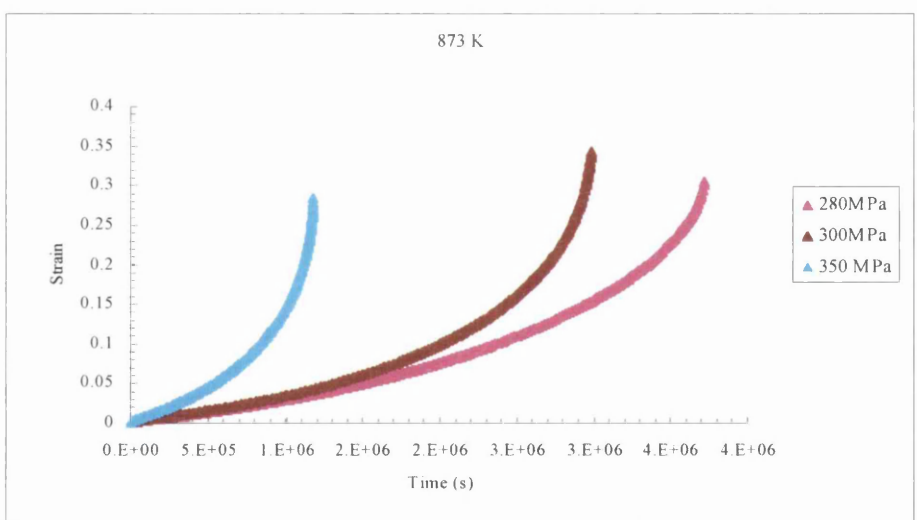

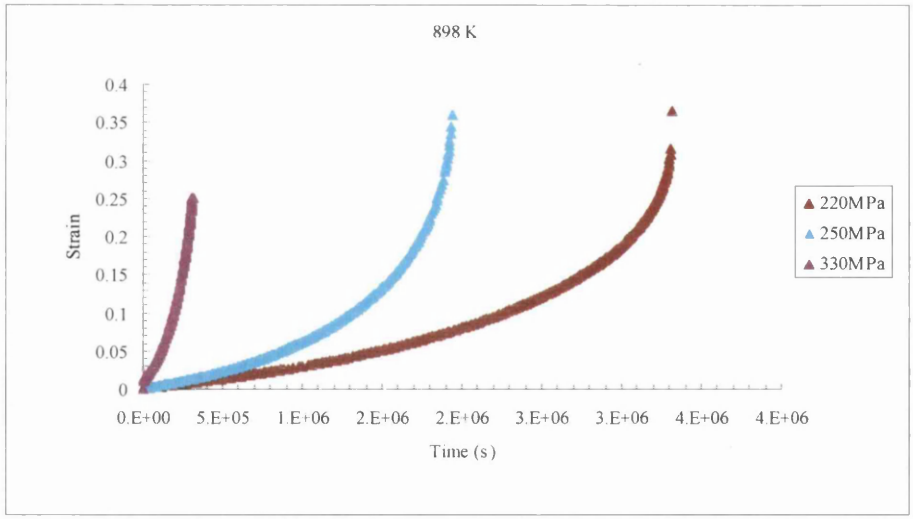
898 K
Strain
0.4
0.35
0.3
0.25
0.2
0.15
0.1
0.05
0
0.E+00
5.E+05
1.E+06
2.E+06
2.E+06
3.E+06
3.E+06
4.E+06
4.E+06
Time (s)
220MPa
250MPa
330MPa

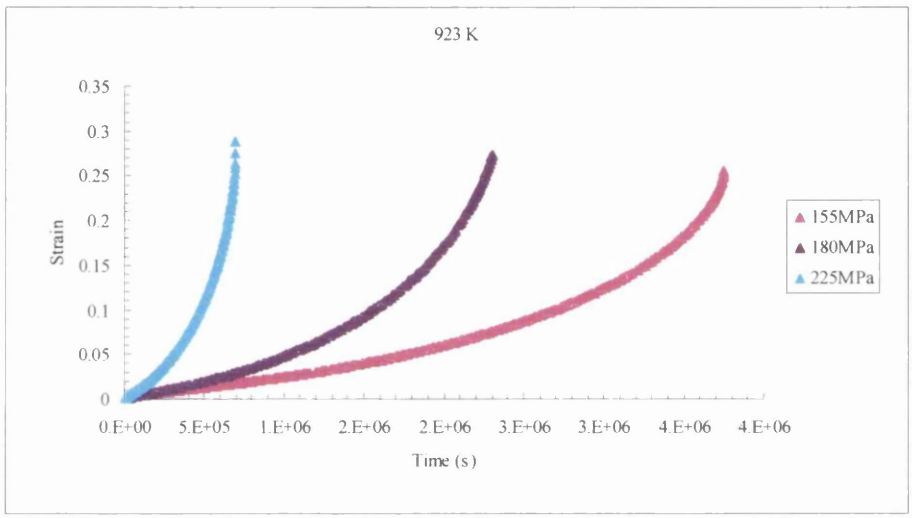
923 K
Strain
0.35
0.3
0.25
0.2
0.15
0.1
0.05
0
0.E+00
5.E+05
1.E+06
2.E+06
2.E+06
3.E+06
3.E+06
4.E+06
4.E+06
Time (s)
155MPa
180MPa
225MPa

B.4 Creep Tests Results (individual creep curves)

(B4.1): 823K/390MPa

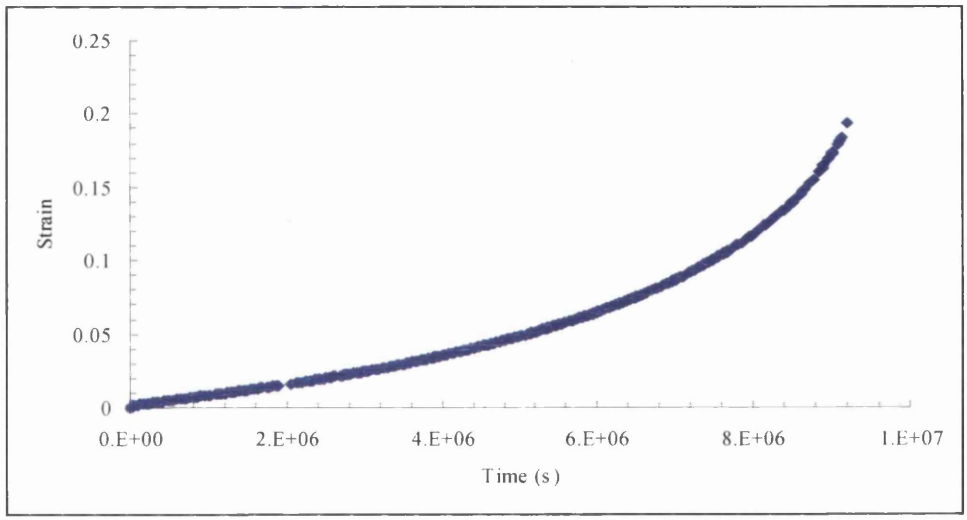

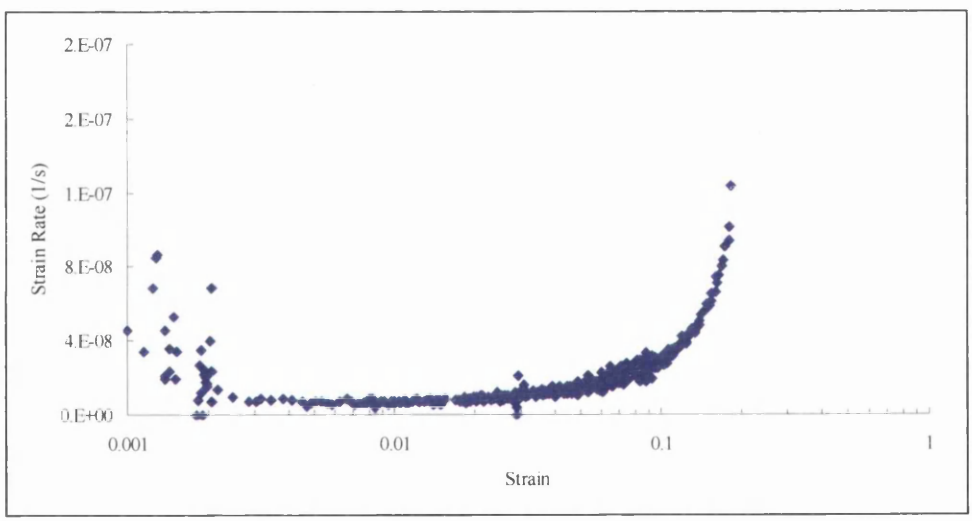

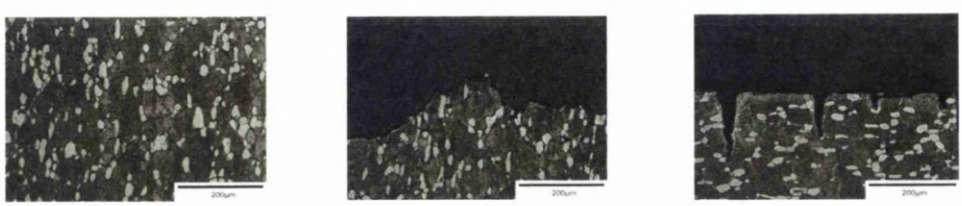

(B4.2): 823K/565MPa

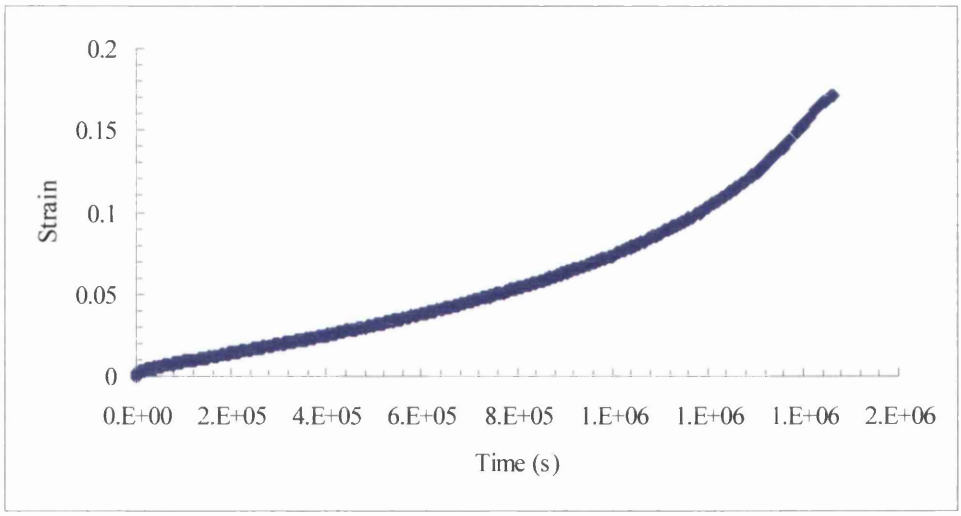

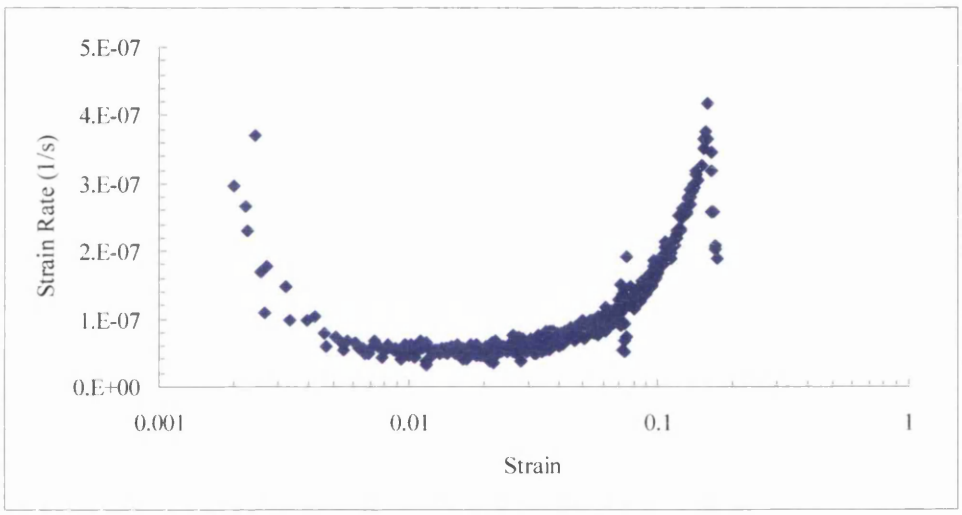

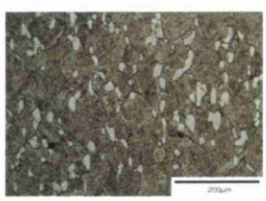

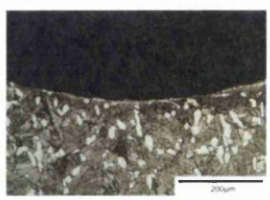

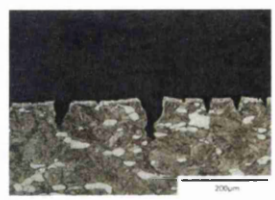

(B4.3): 823K/600MPa

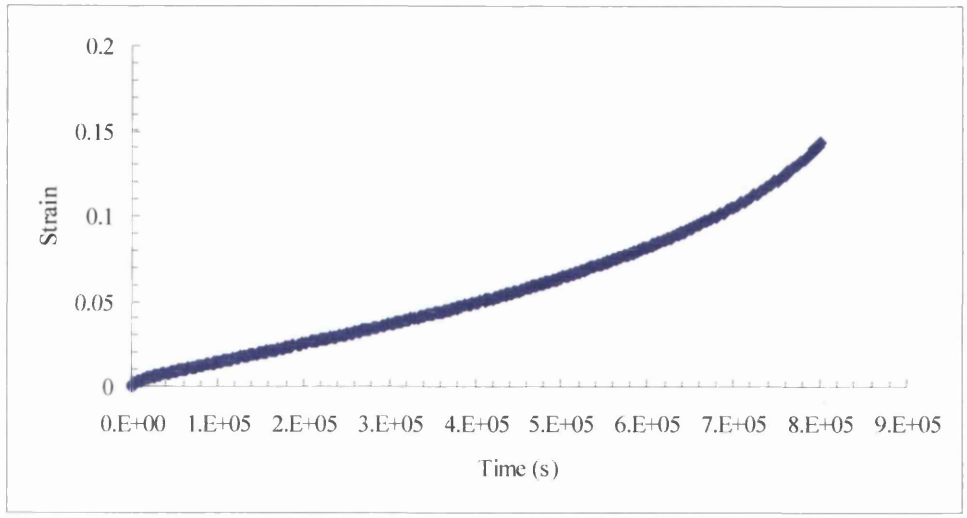

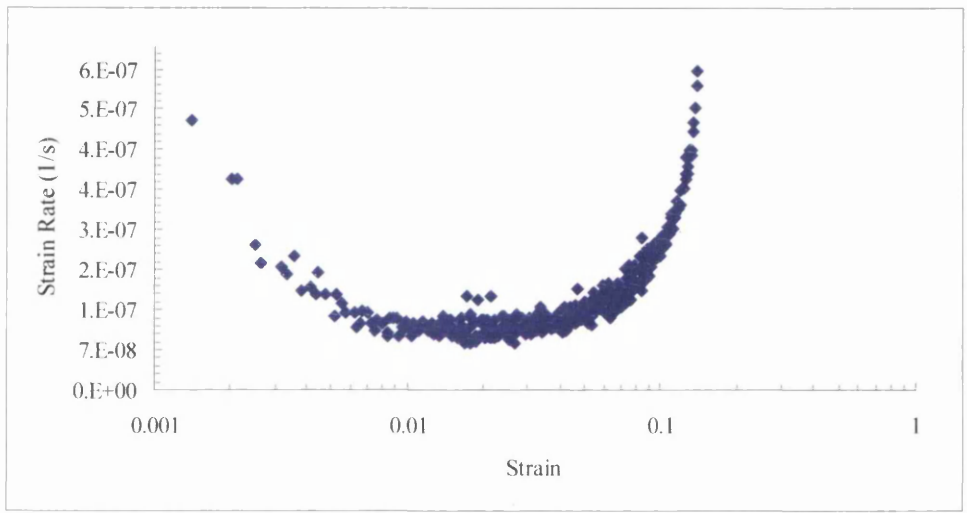

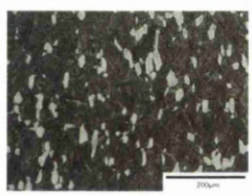

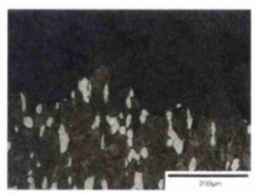

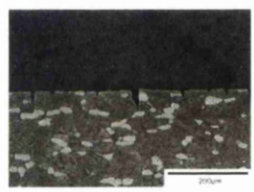

(B4.4): 848K/300MPa

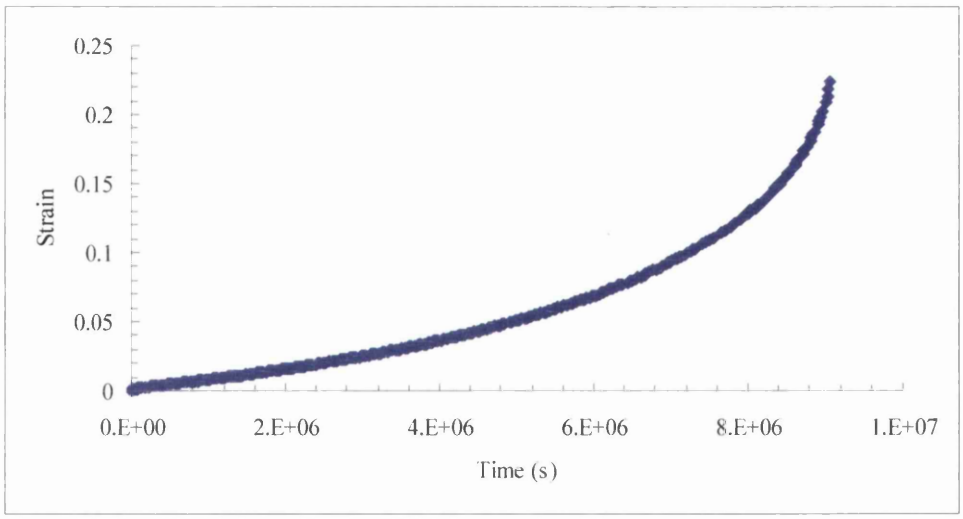

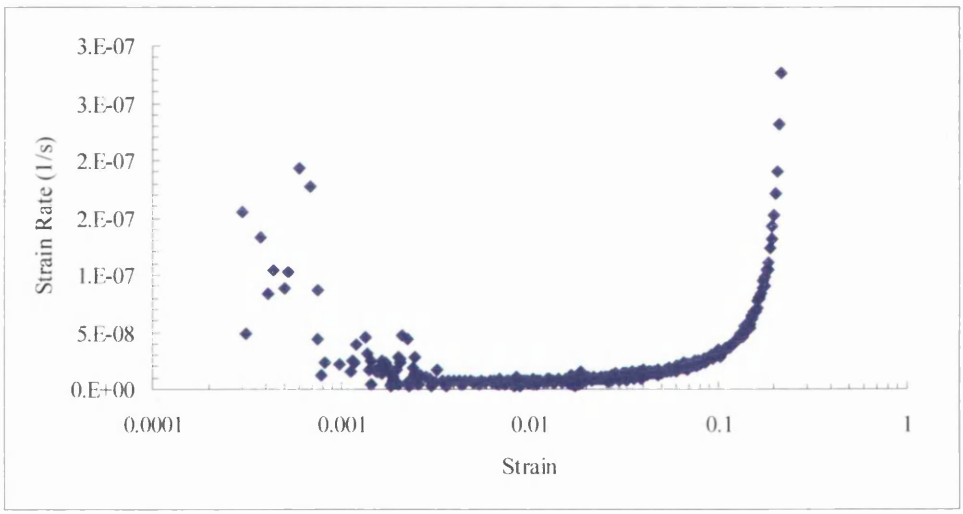

(B4.5): 848K/390MPa

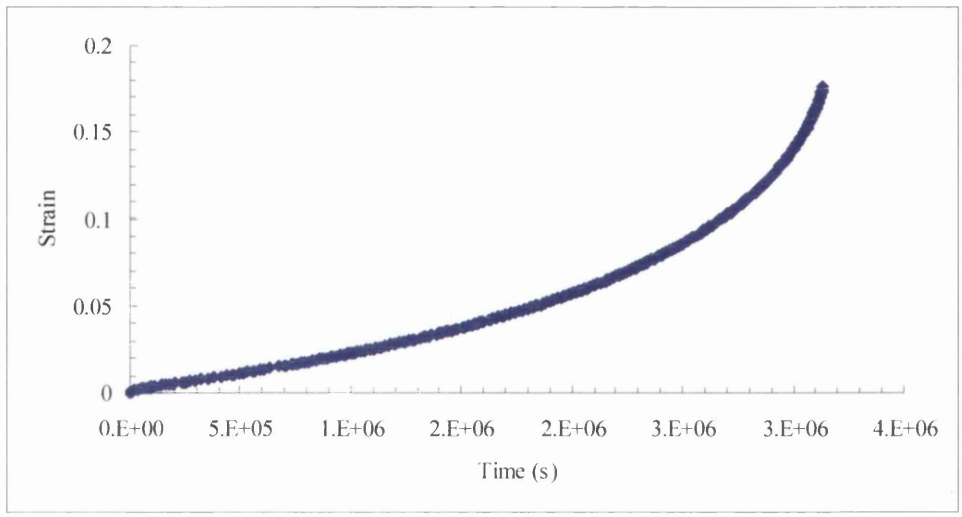

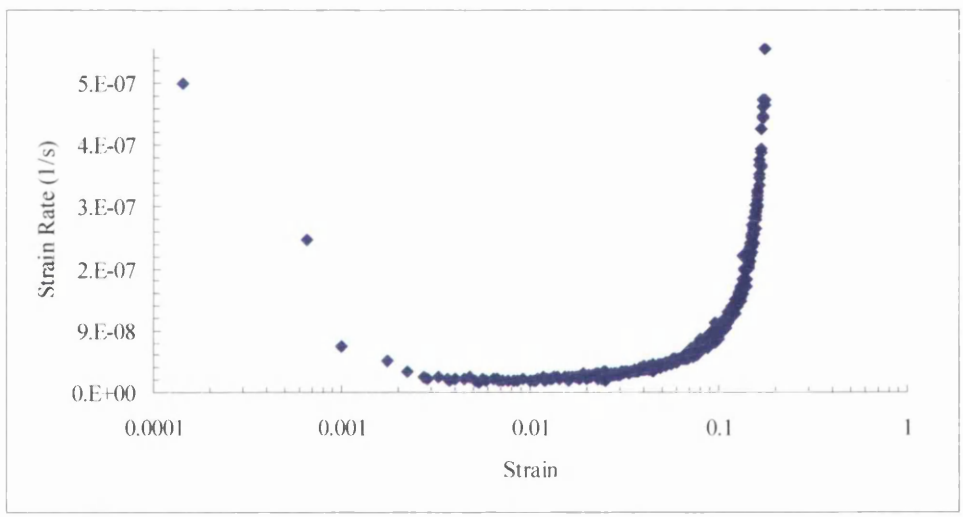

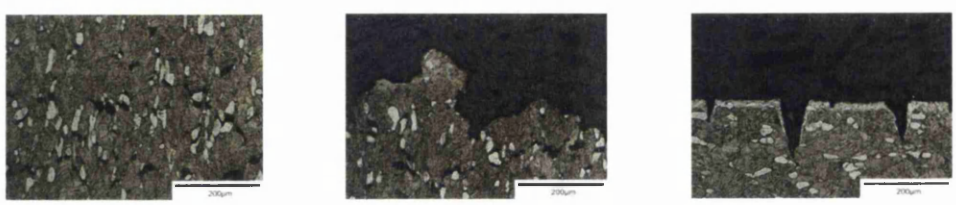

(B4.6): 848K/500MPa

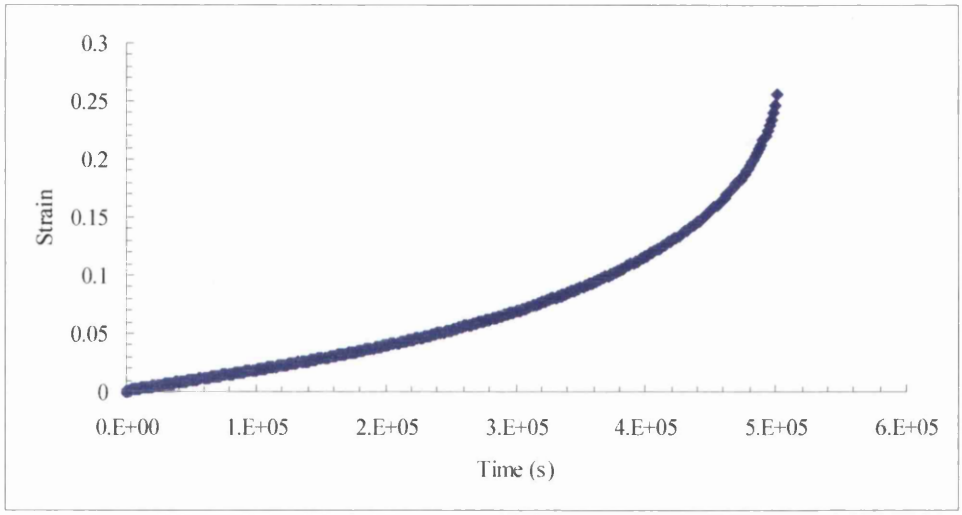

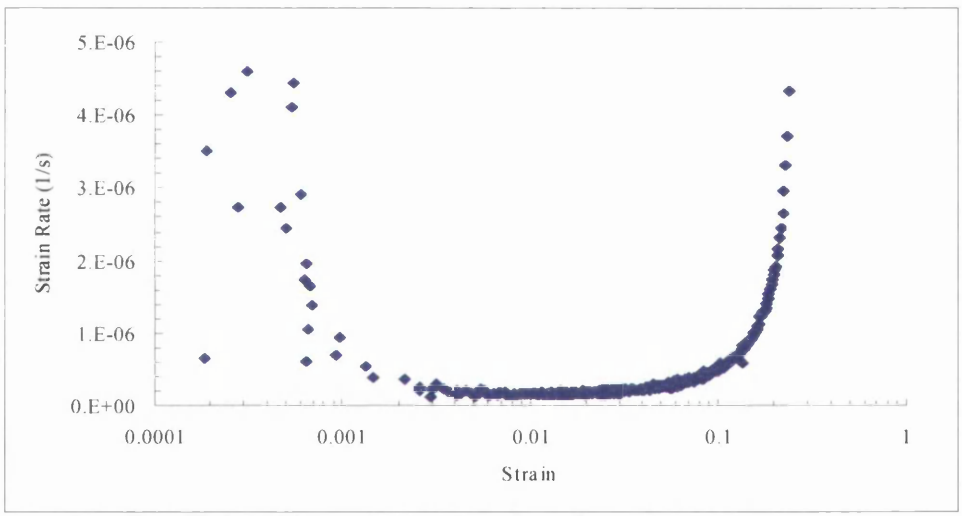

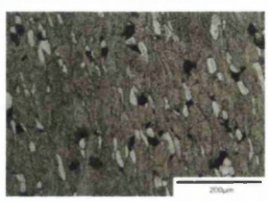

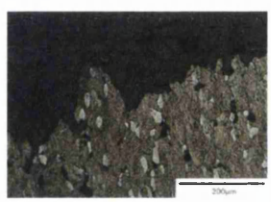

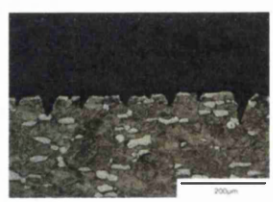

(B4.7): 848K/570MPa

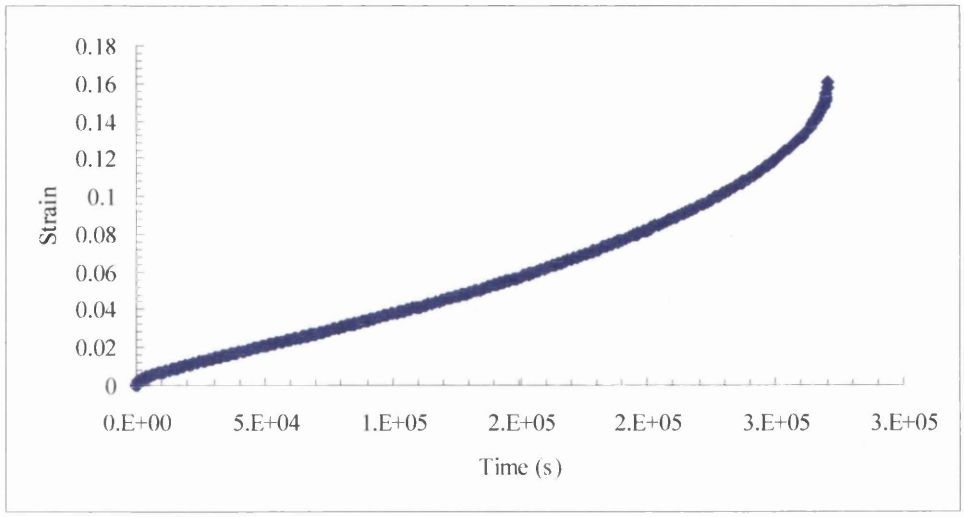

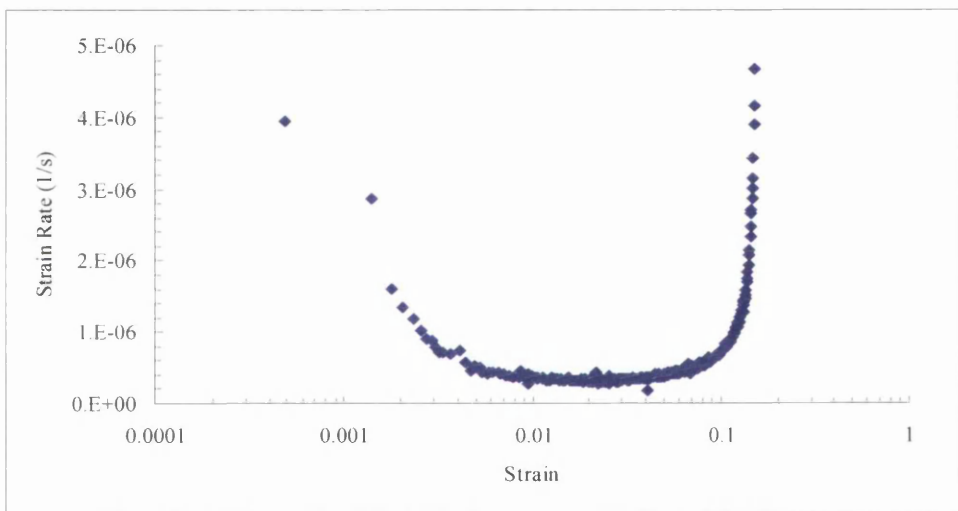

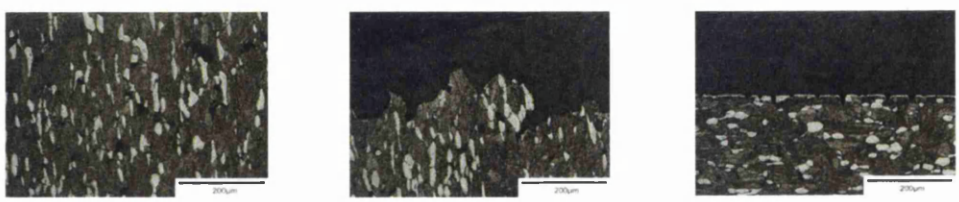

(B4.8): 873K/200MPa

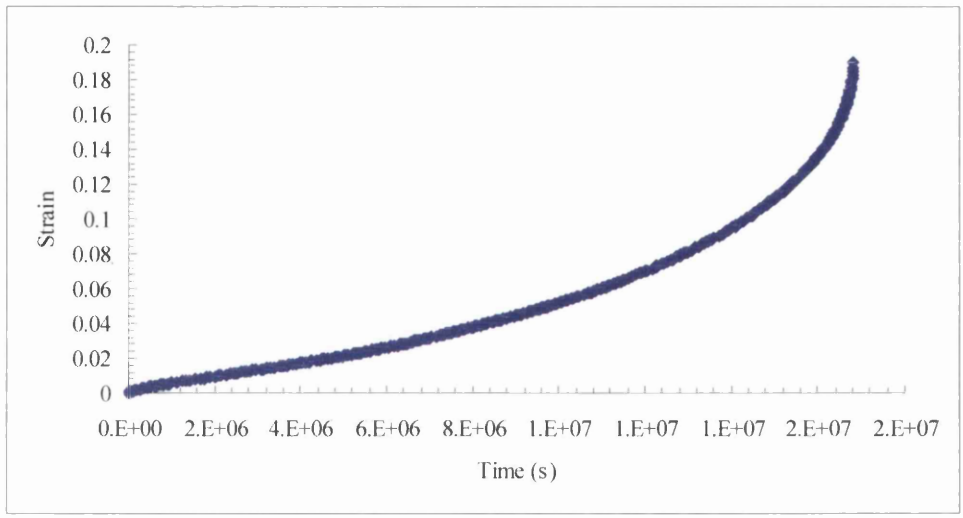

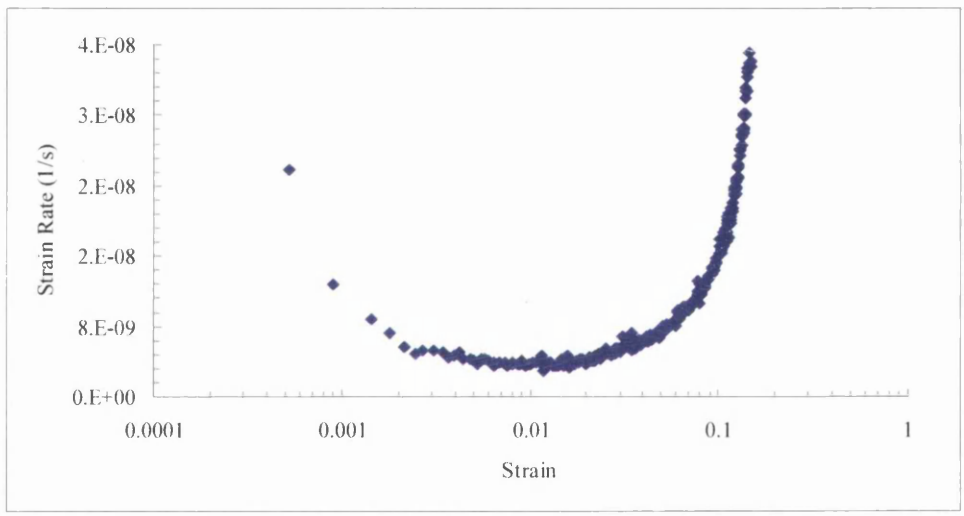

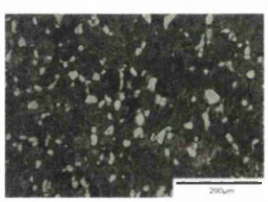

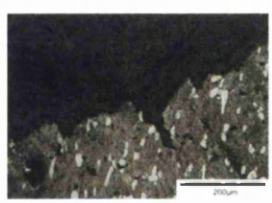

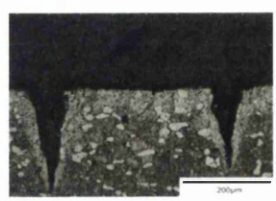

(B4.9): 873K/280MPa

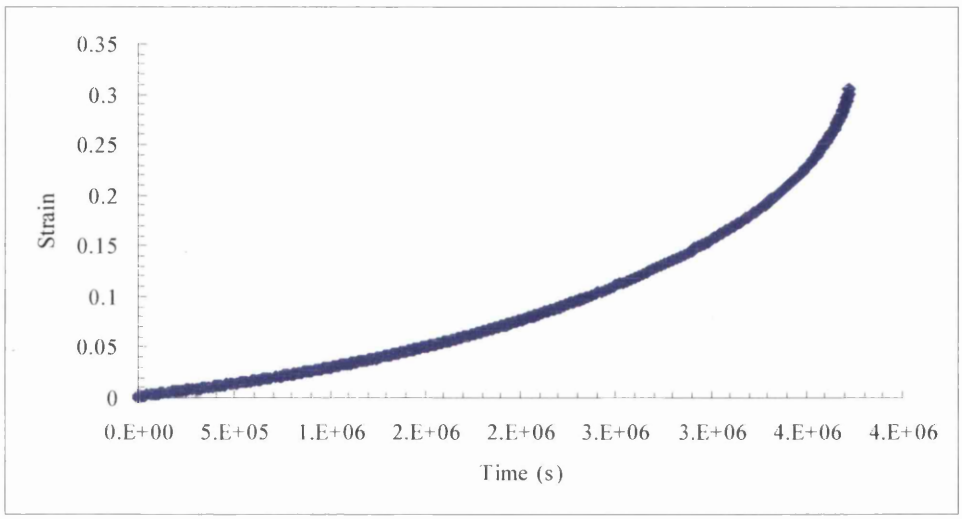

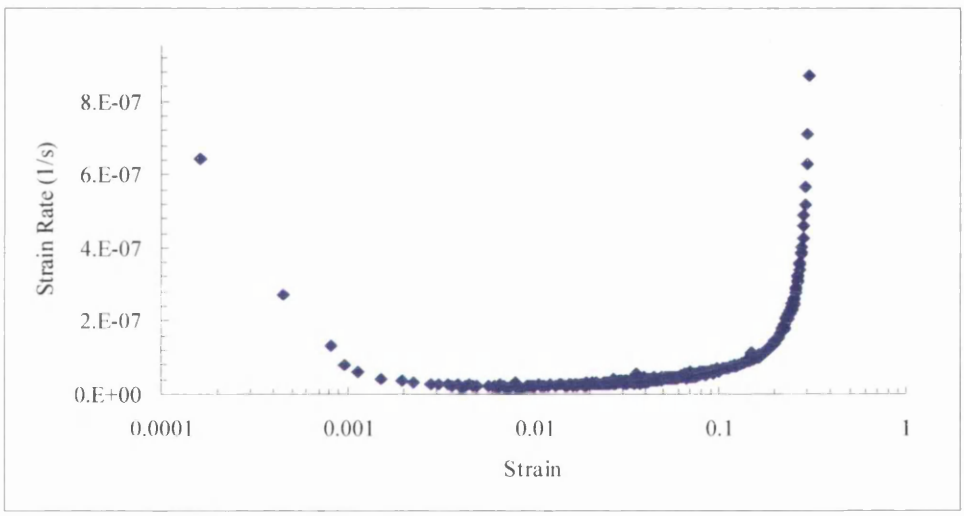

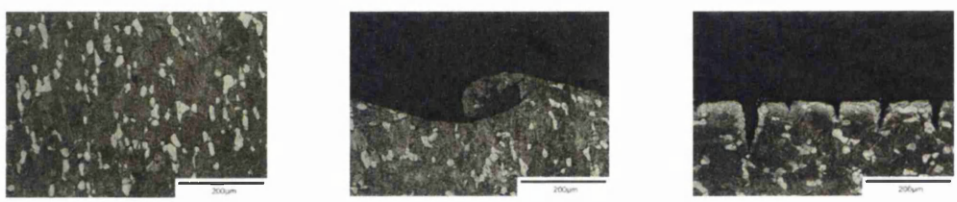

(B4.10): 873K/300MPa

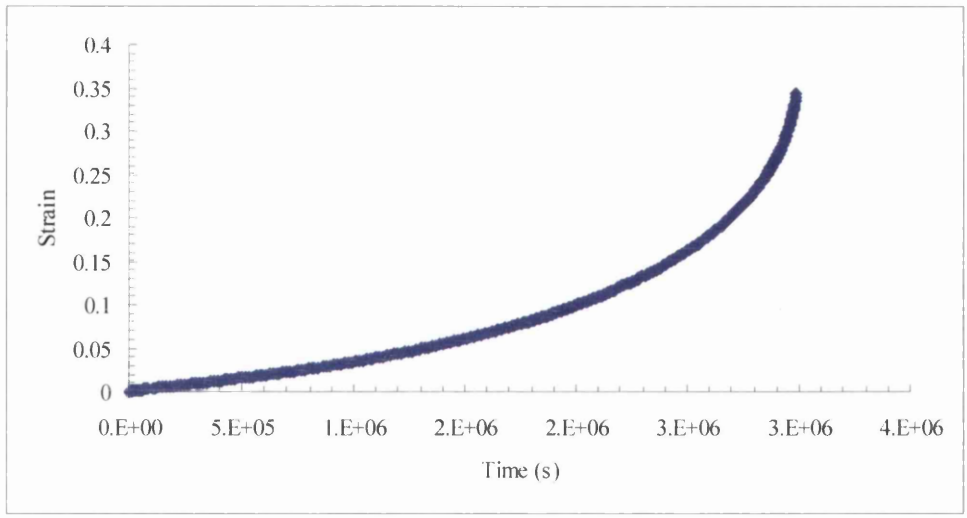

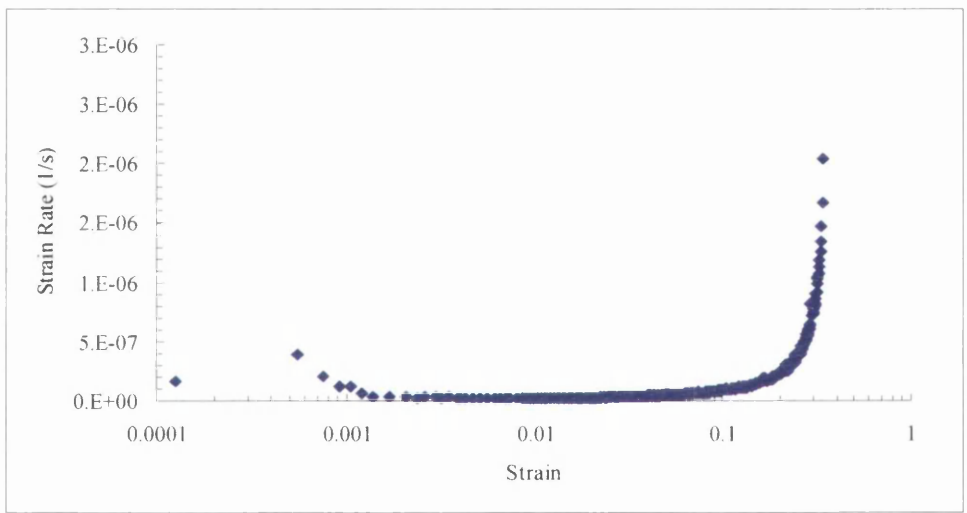

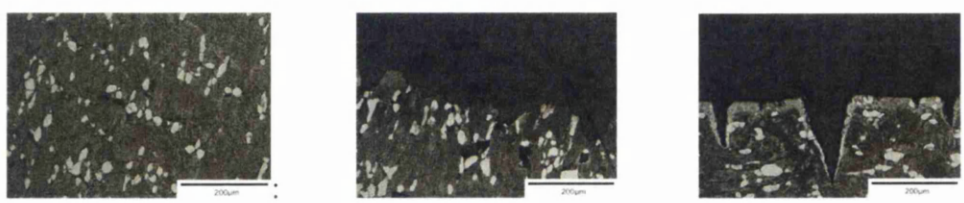

(B4.11): 873K/350MPa

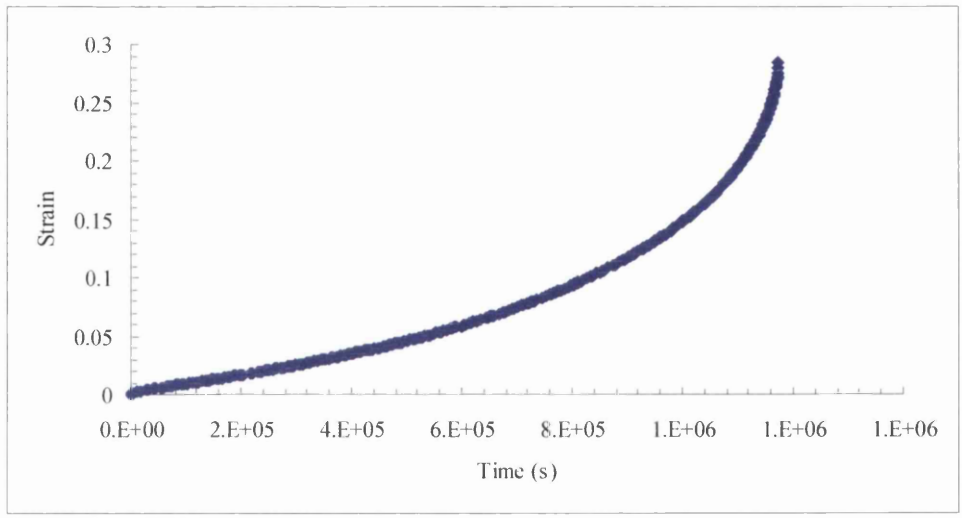

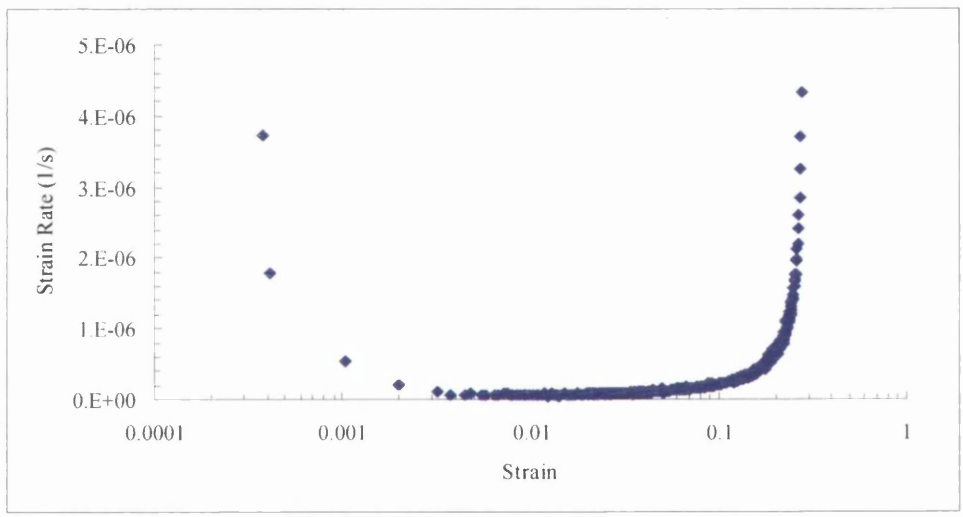

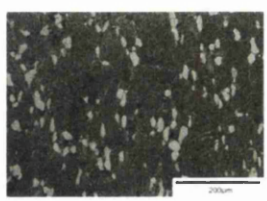

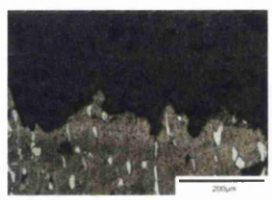

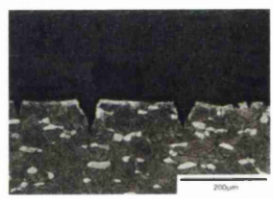

(B4.12): 873K/360MPa

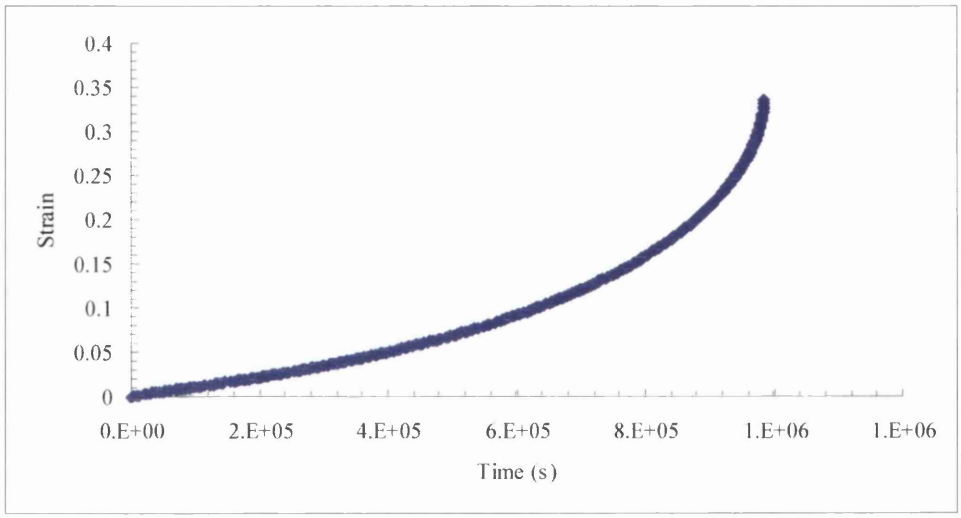

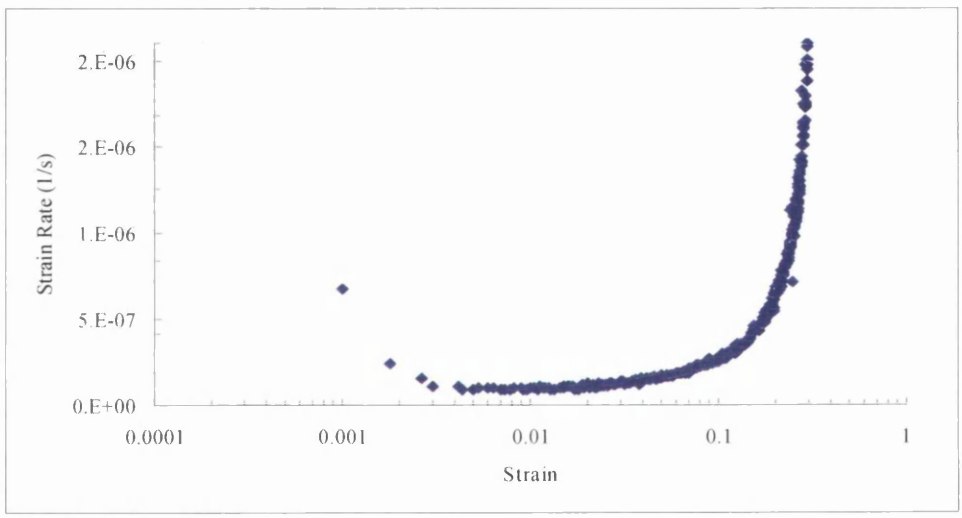

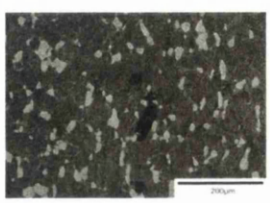

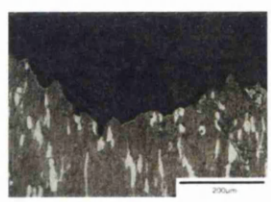

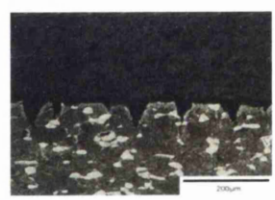

(B4.13): 873K/390MPa

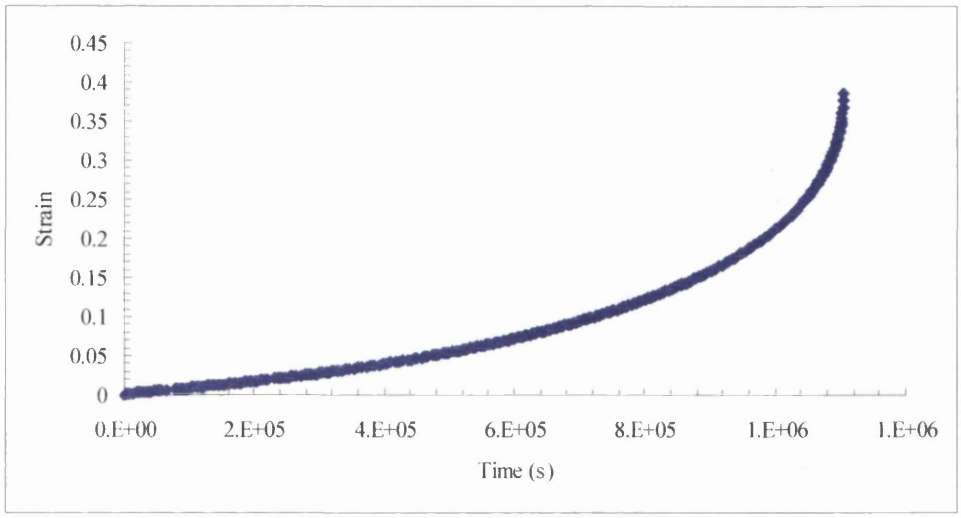

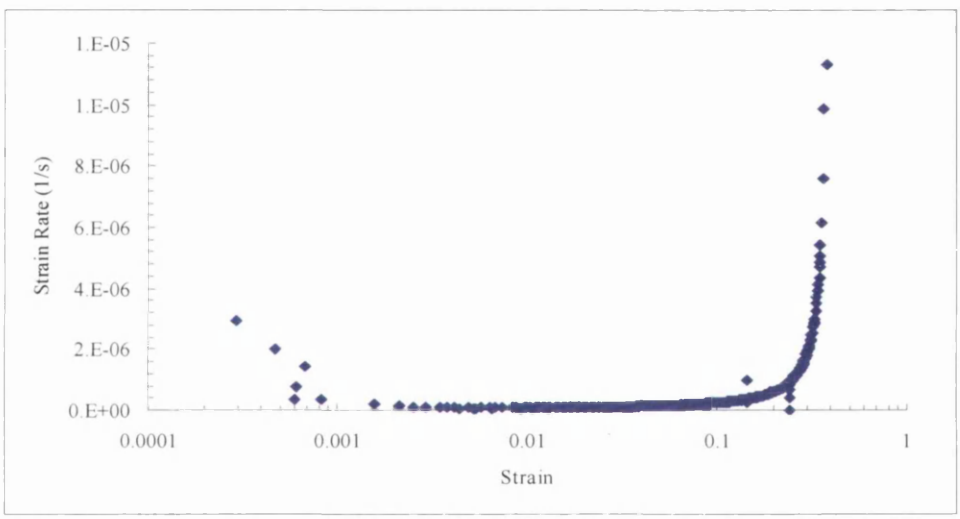

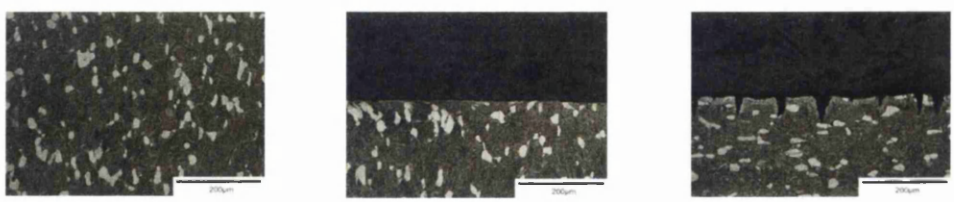

(B4.14): 873K/480MPa

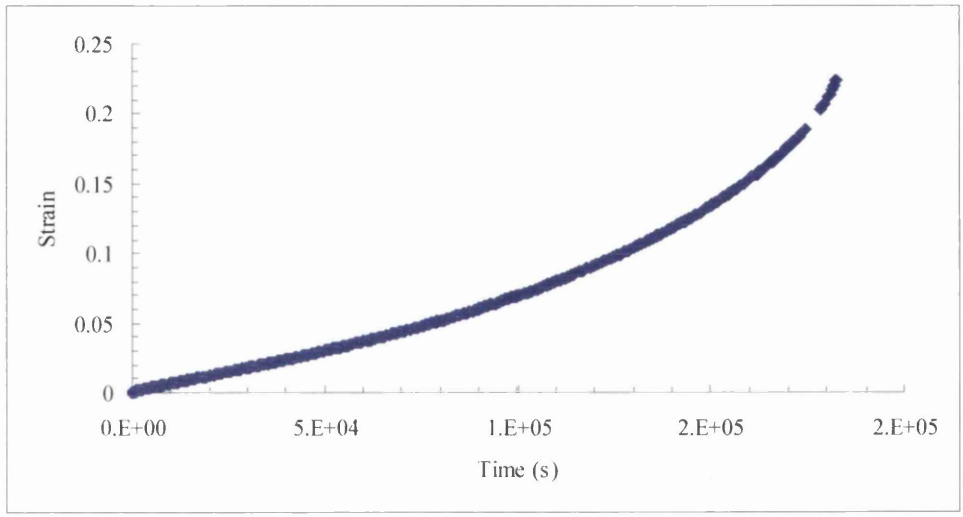

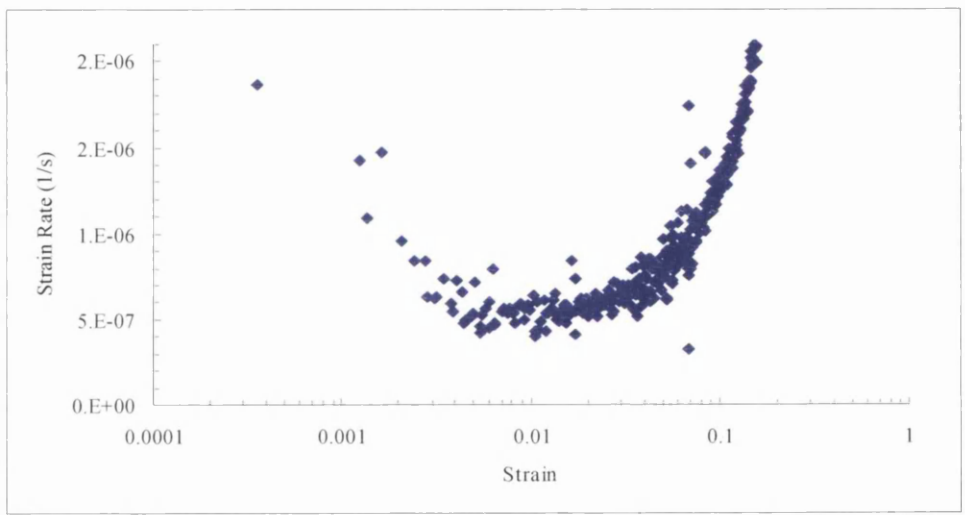

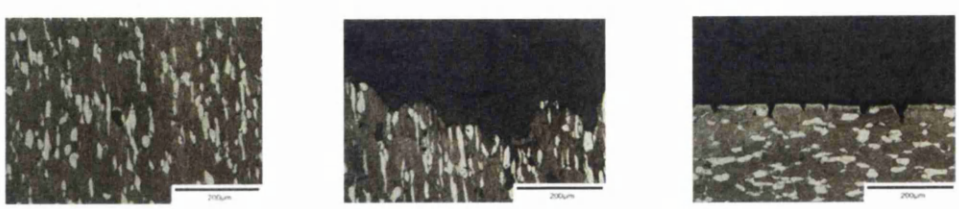

(B4.15): 873K/550MPa

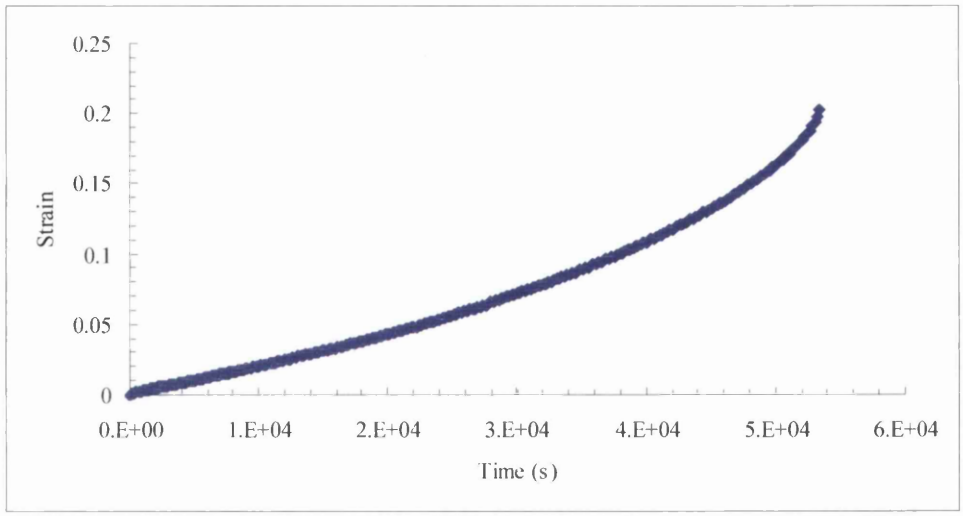

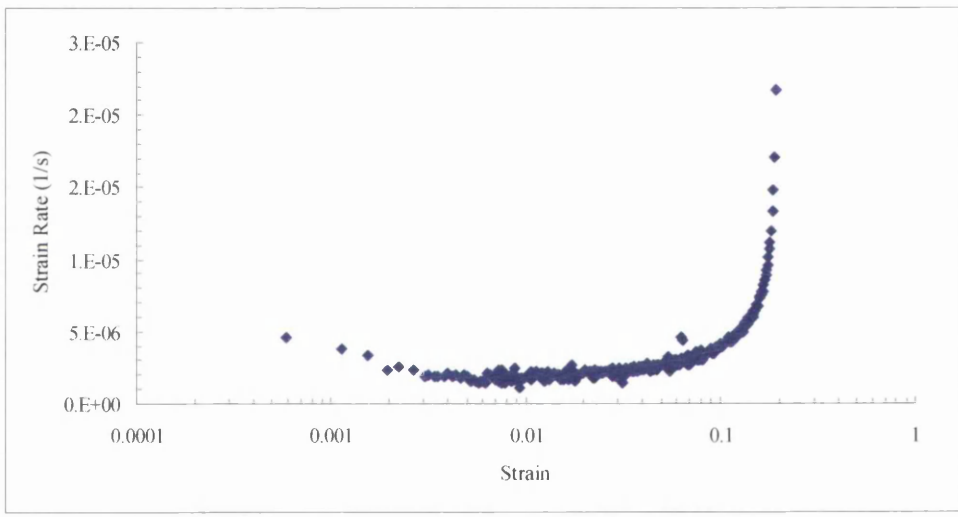

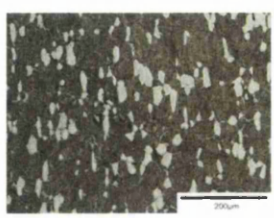

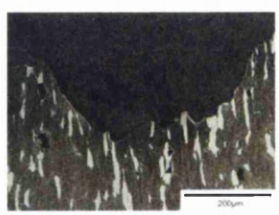

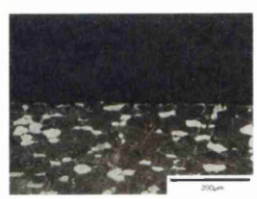

(B4.16): 898K/175MPa

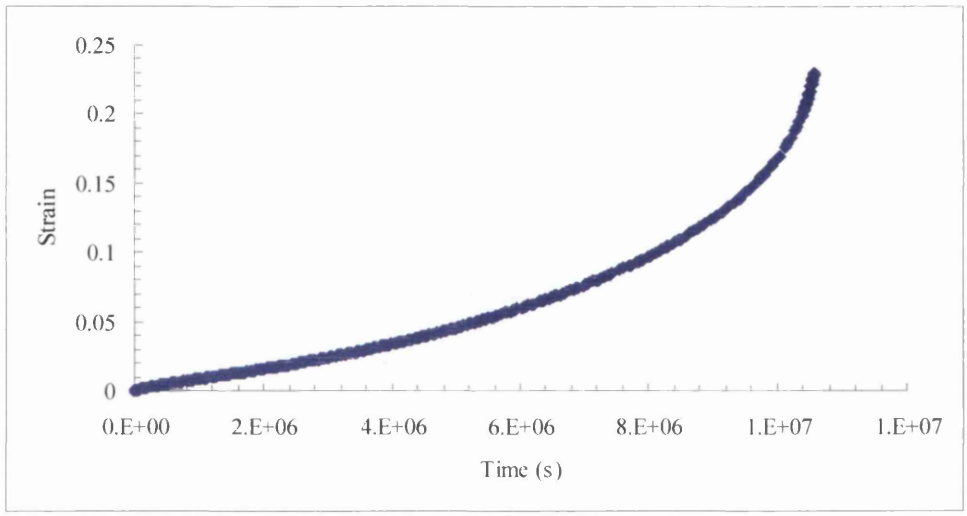

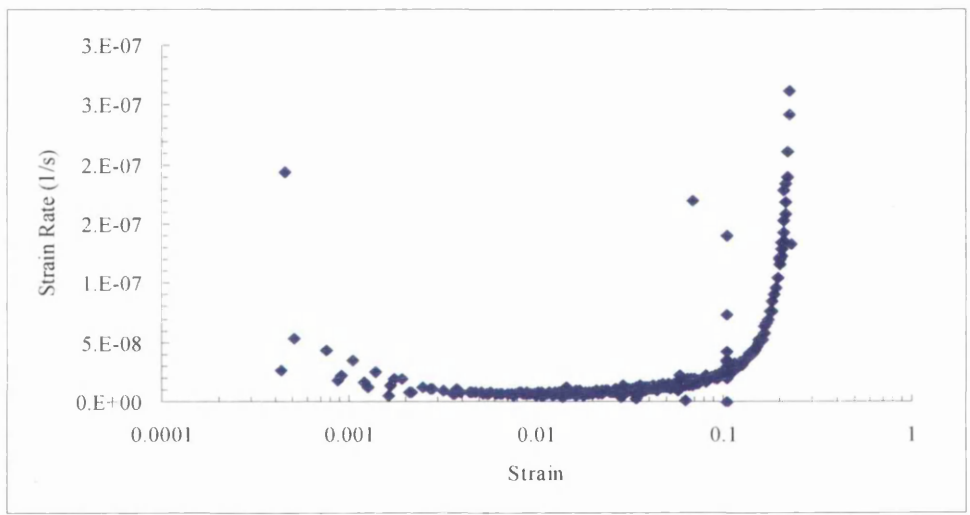

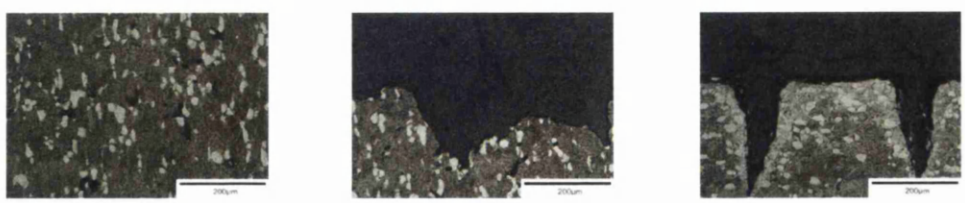

(B4.17): 898K/220MPa

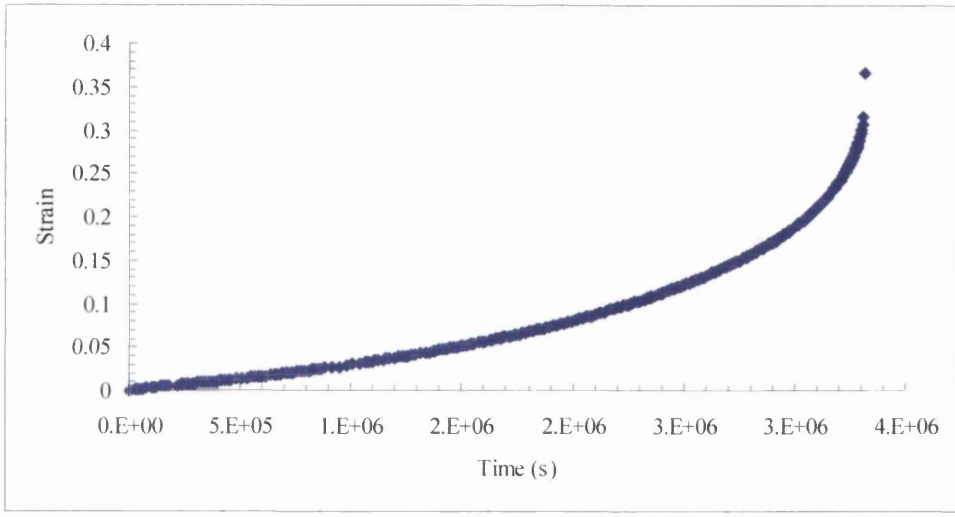

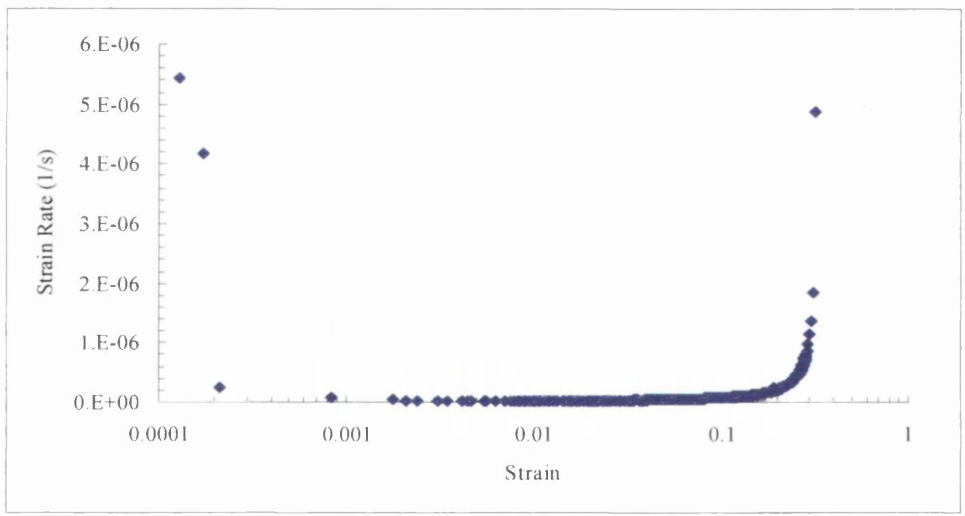

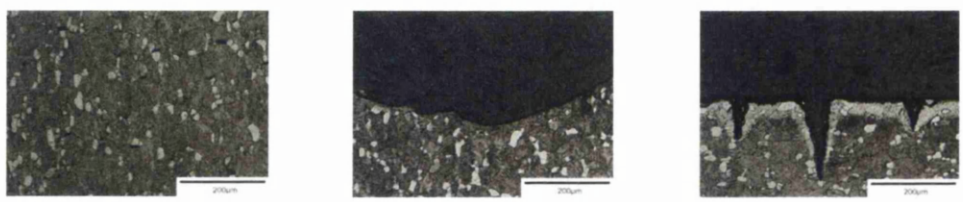

(B4.18): 898K/250MPa

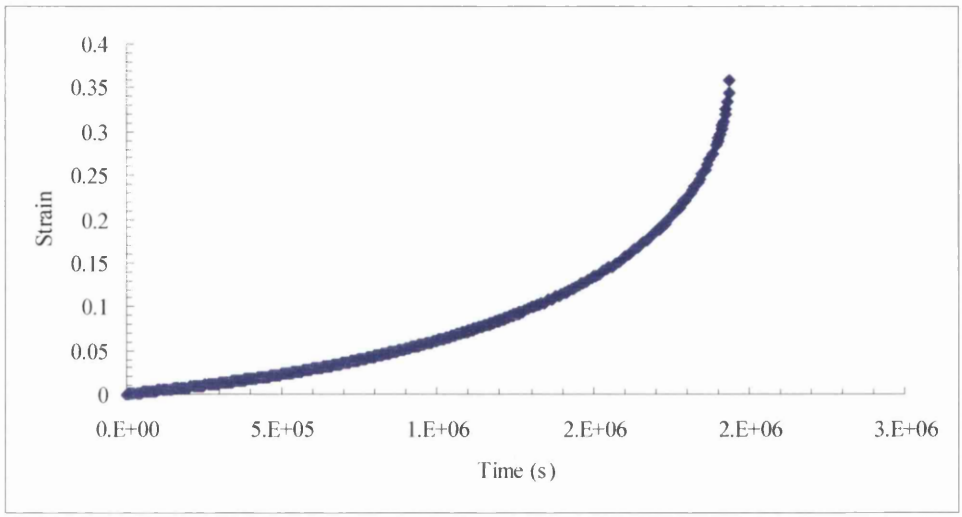

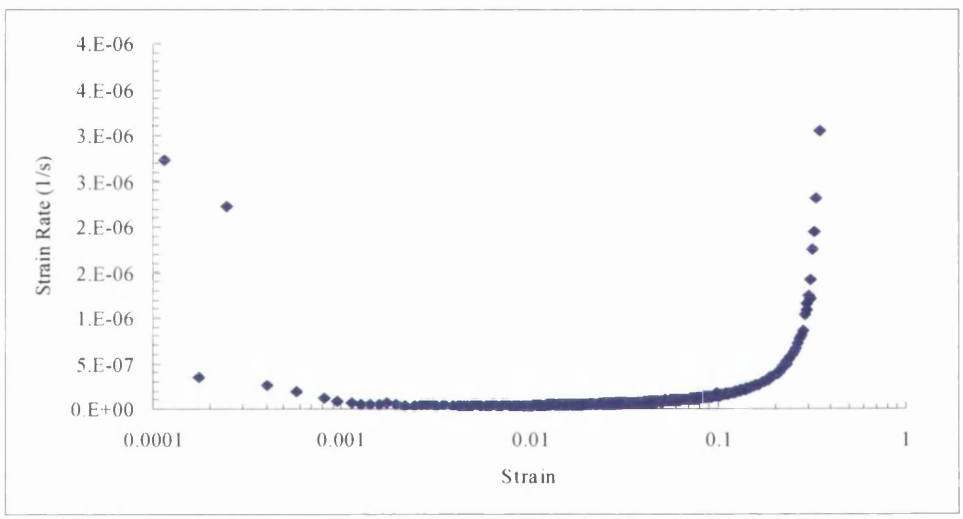

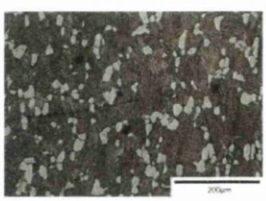

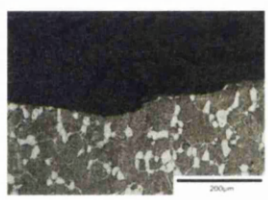

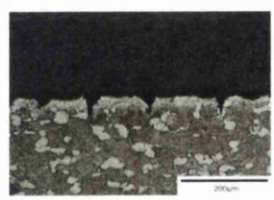

(B4.19): 898K/280MPa

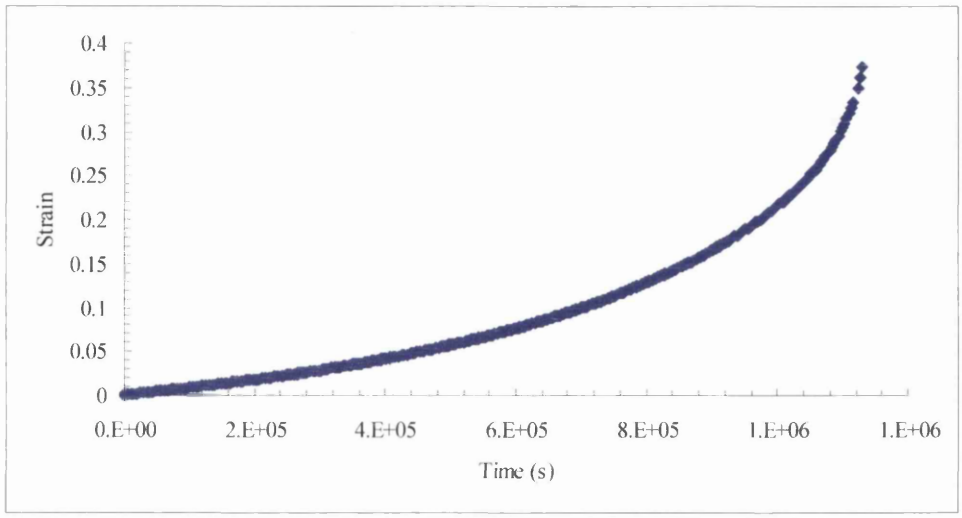

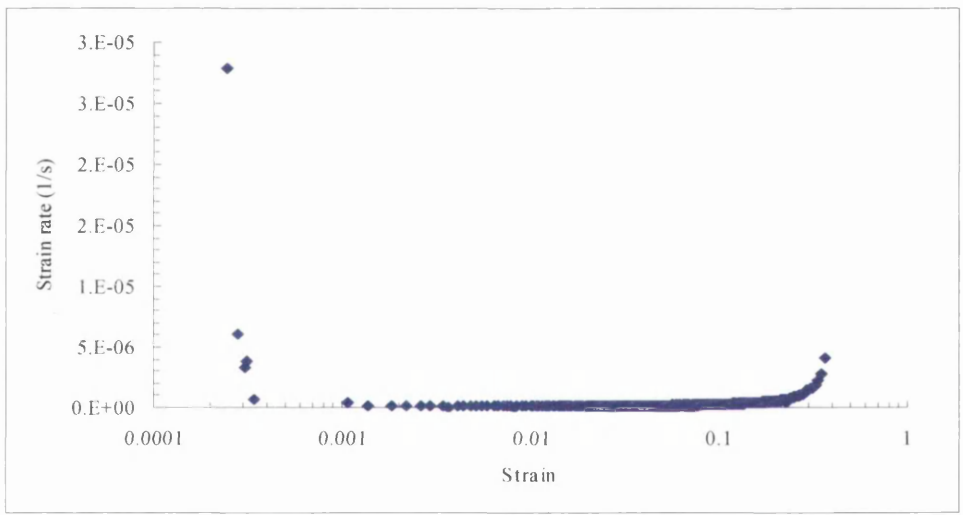

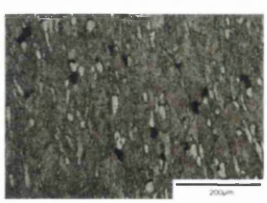

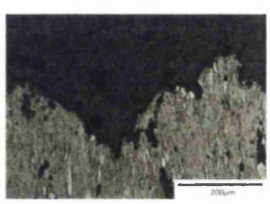

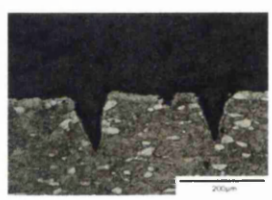

(B4.20): 898K/300MPa

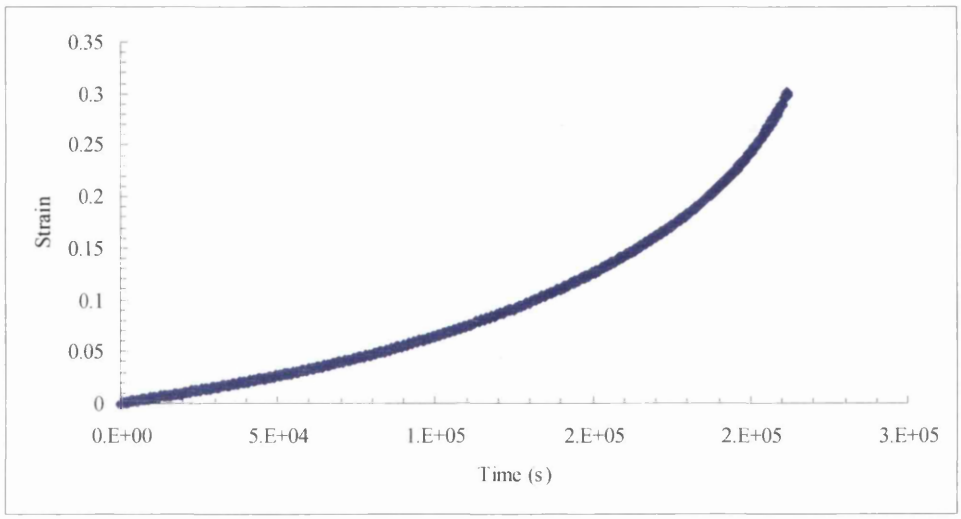

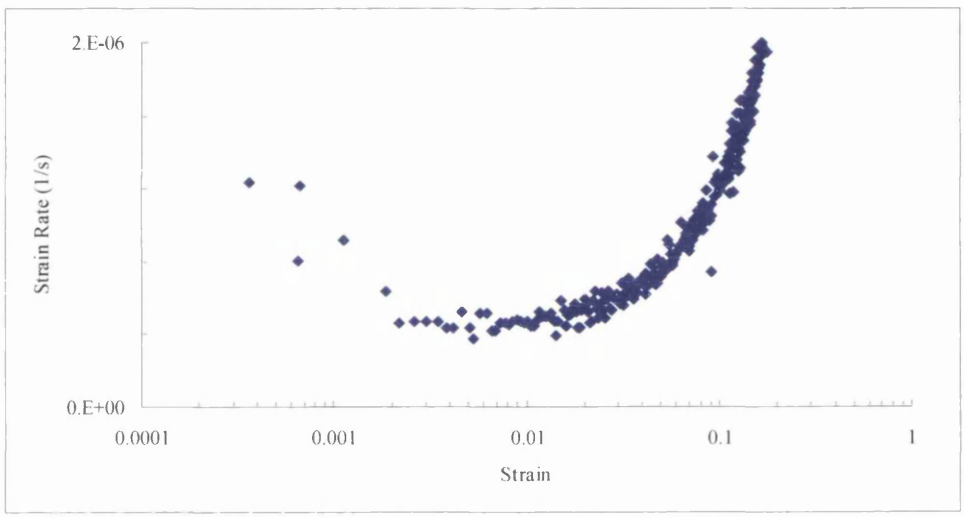

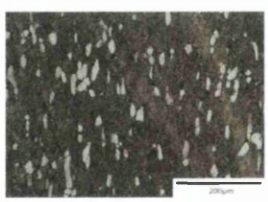

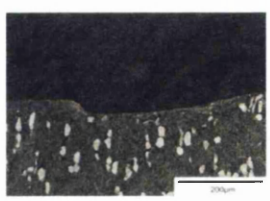

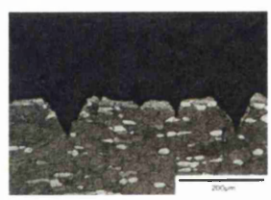

(B4.21): 898K/330MPa

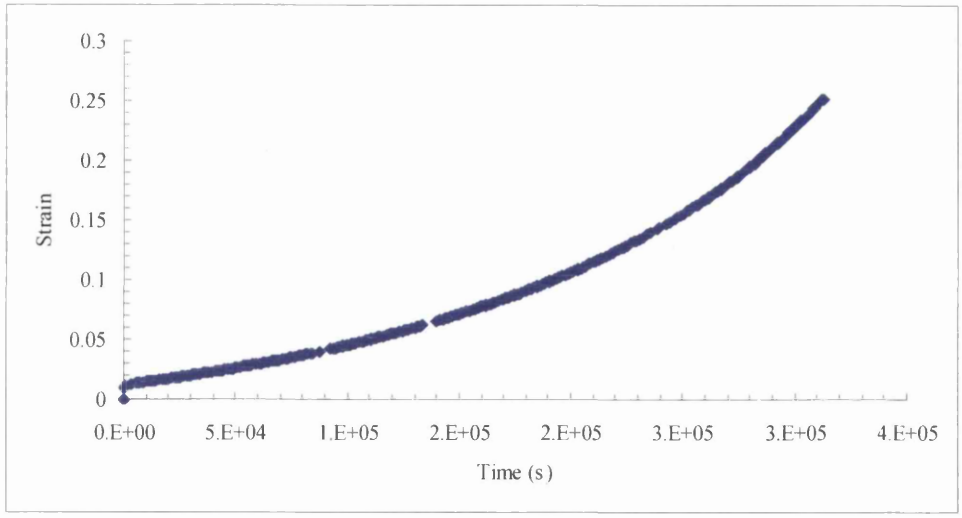

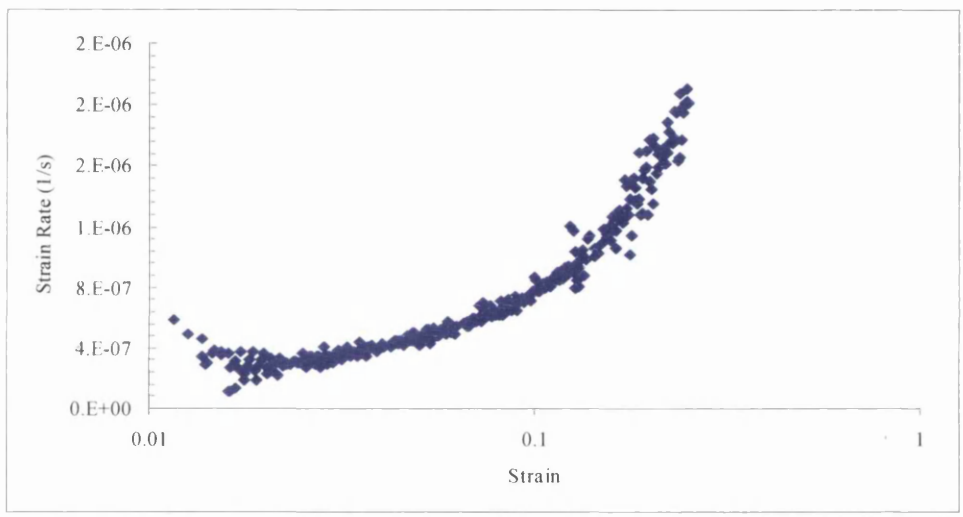

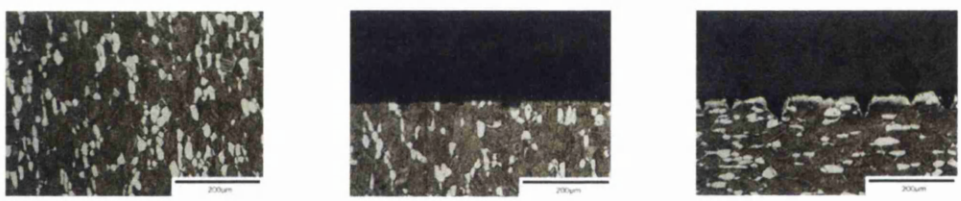

(B4.22): 898K/400MPa

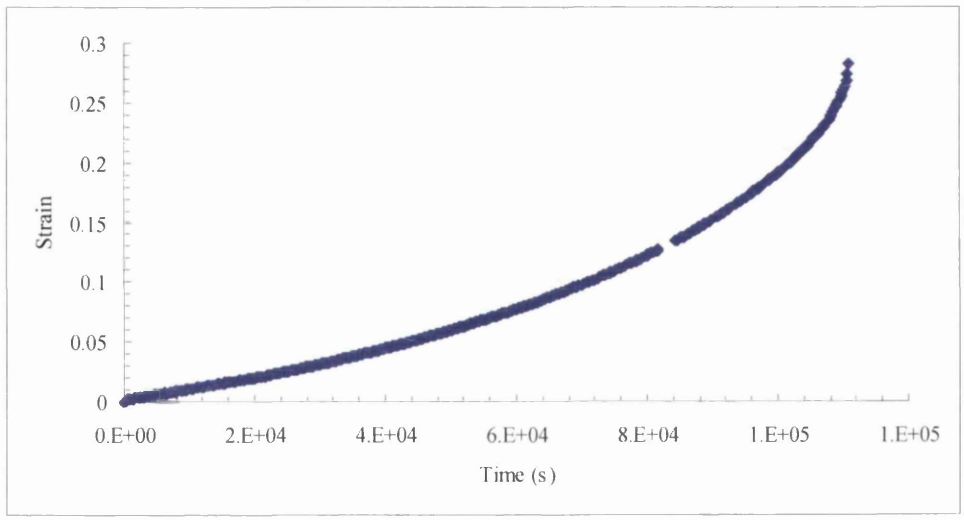

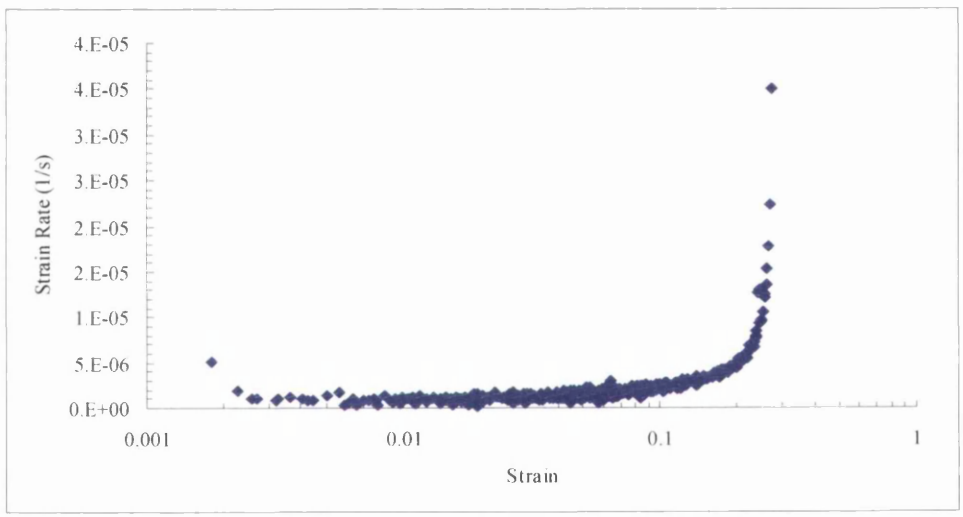

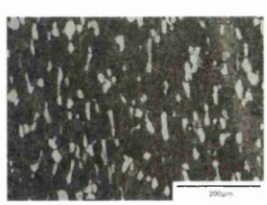

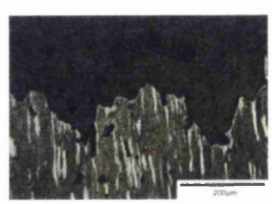

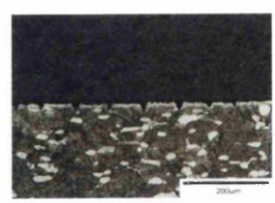

(B4.23): 923K/140MPa

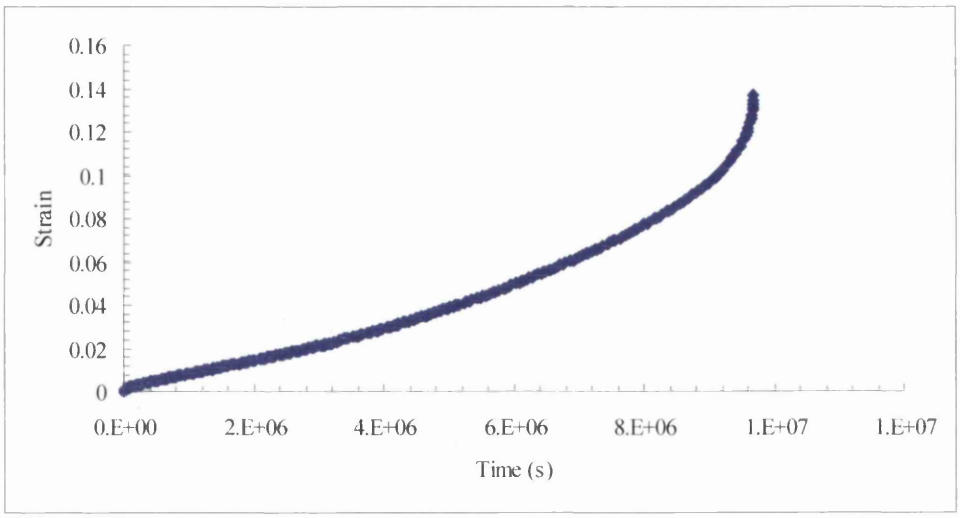

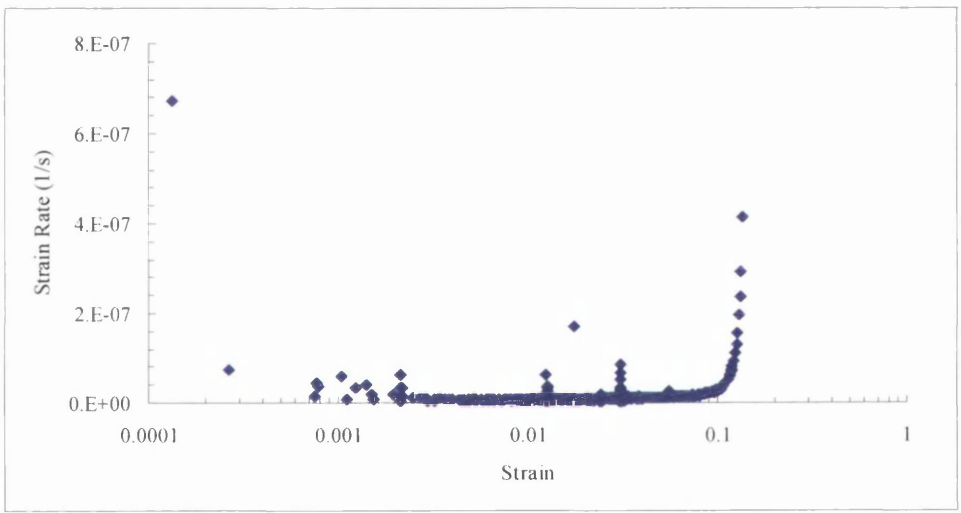

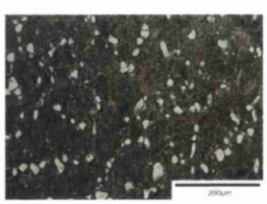

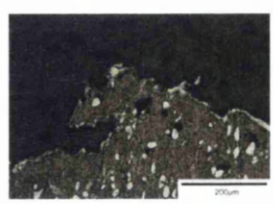

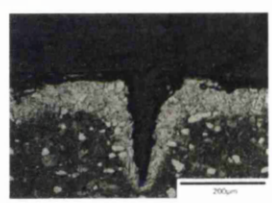

(B4.24): 923K/155MPa

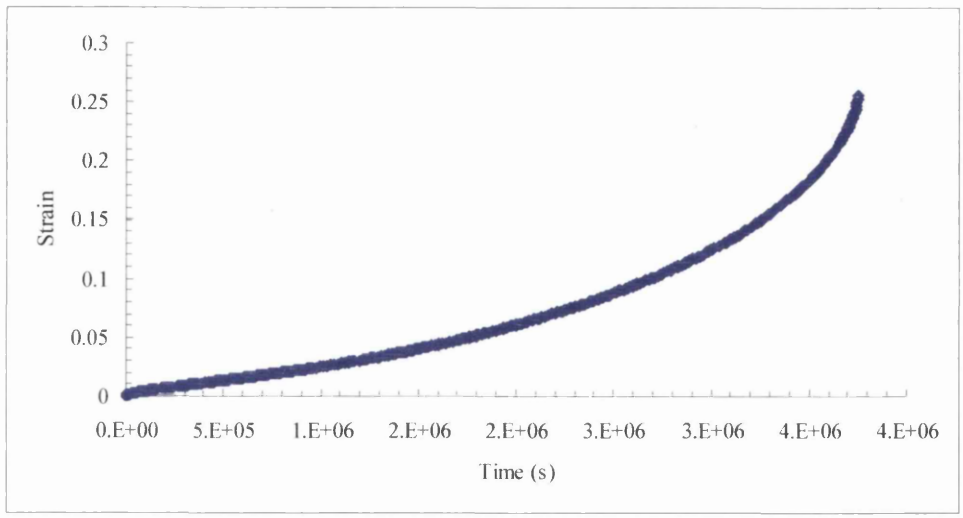

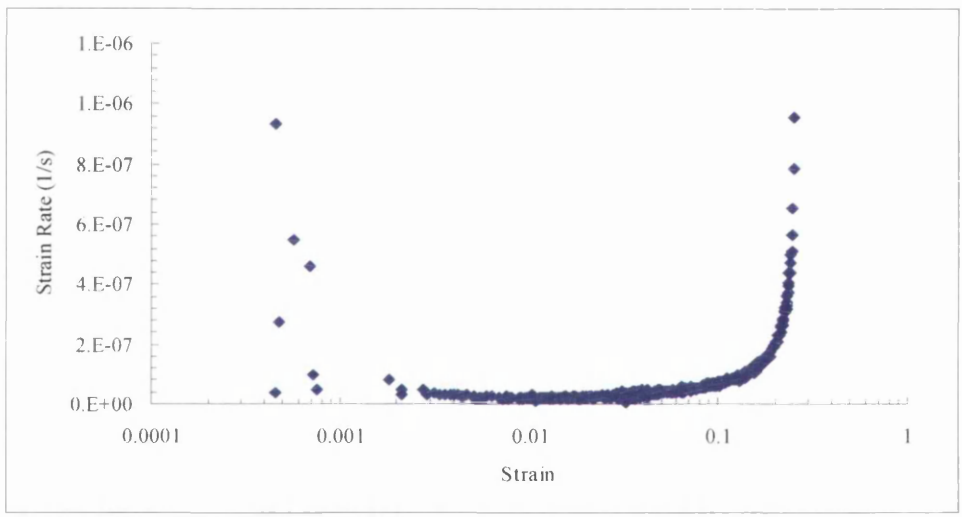

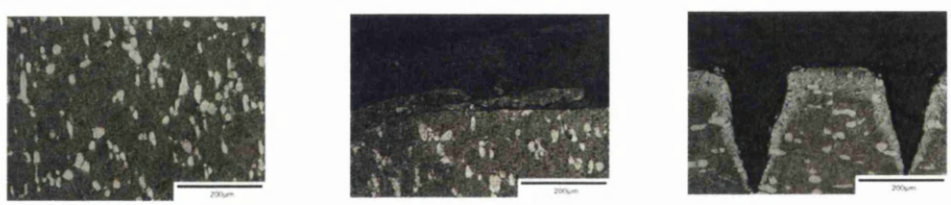

(B4.25): 923K/180MPa

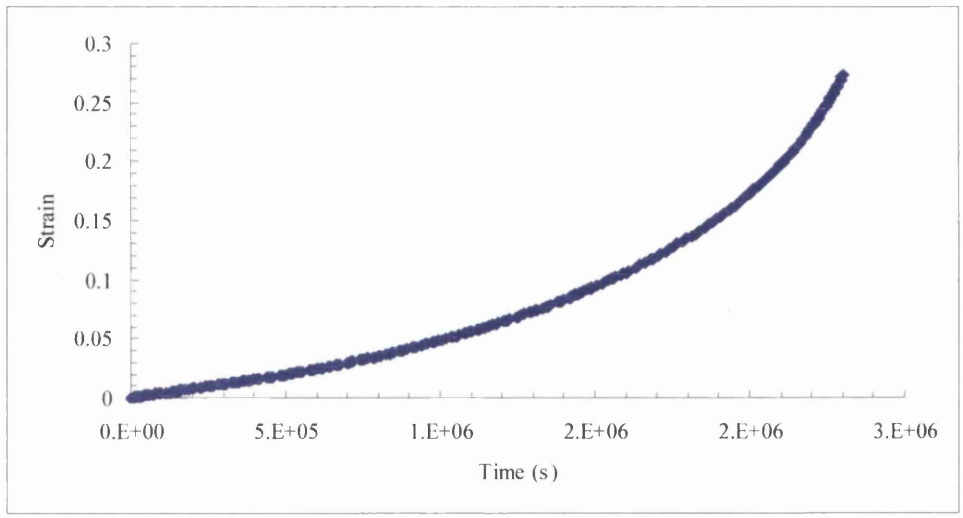

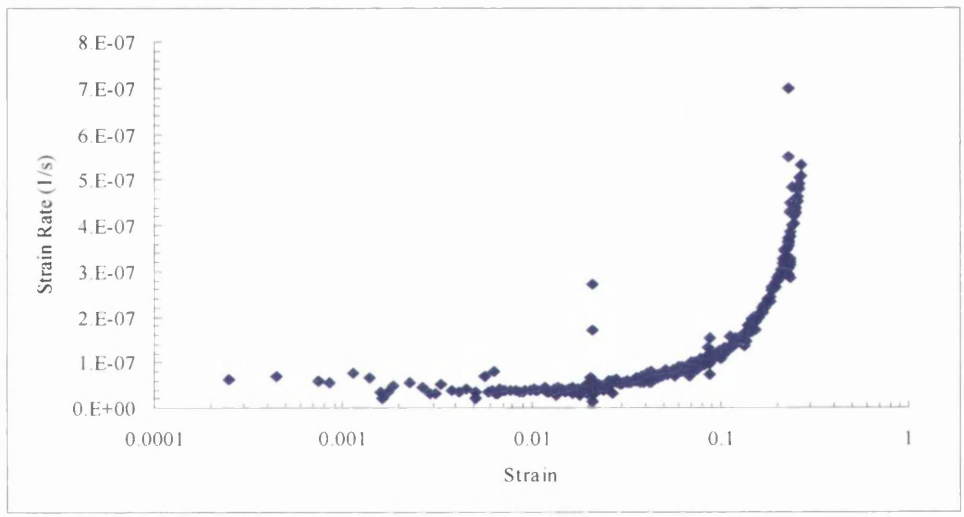

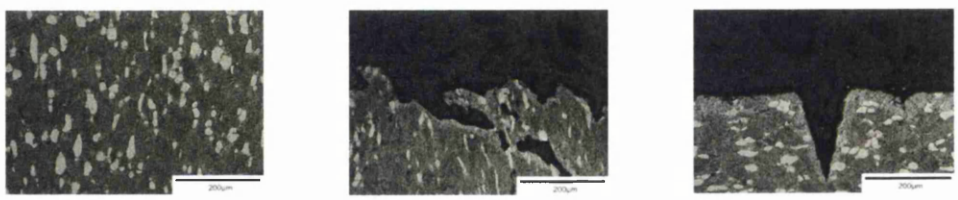

(B4.26): 923K/225MPa

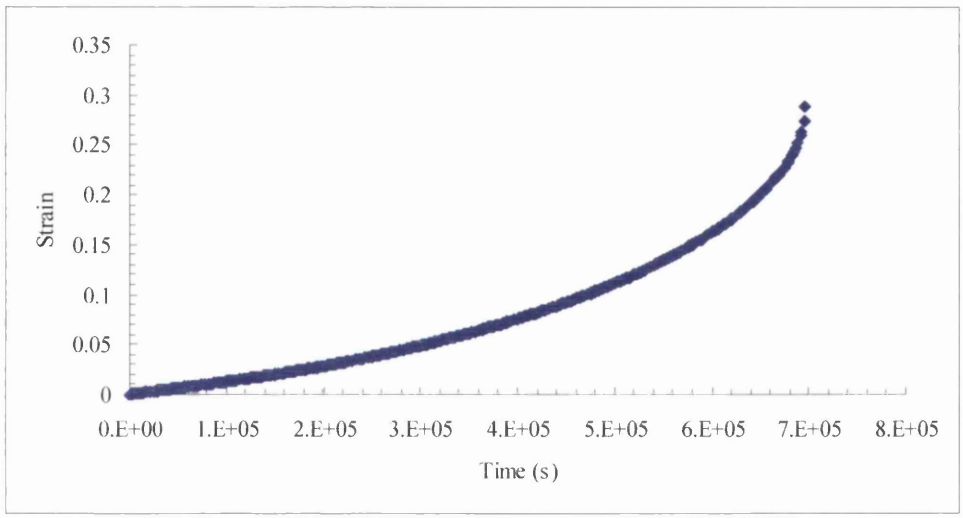

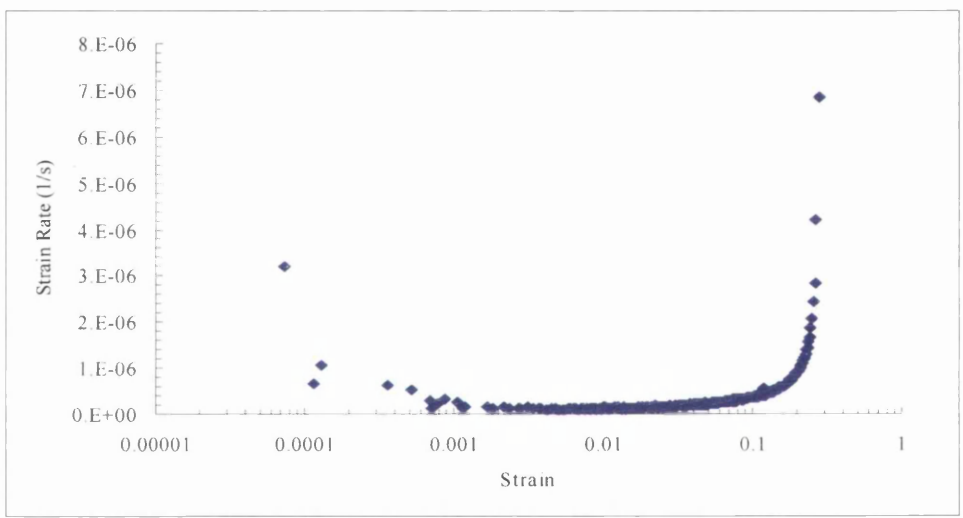

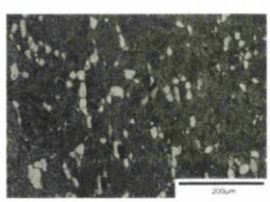

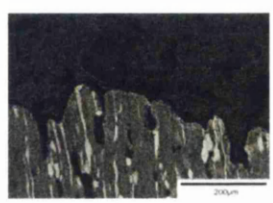

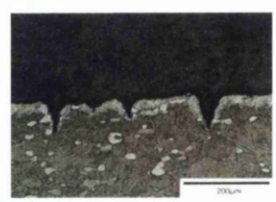

(B4.27): 923K/260MPa

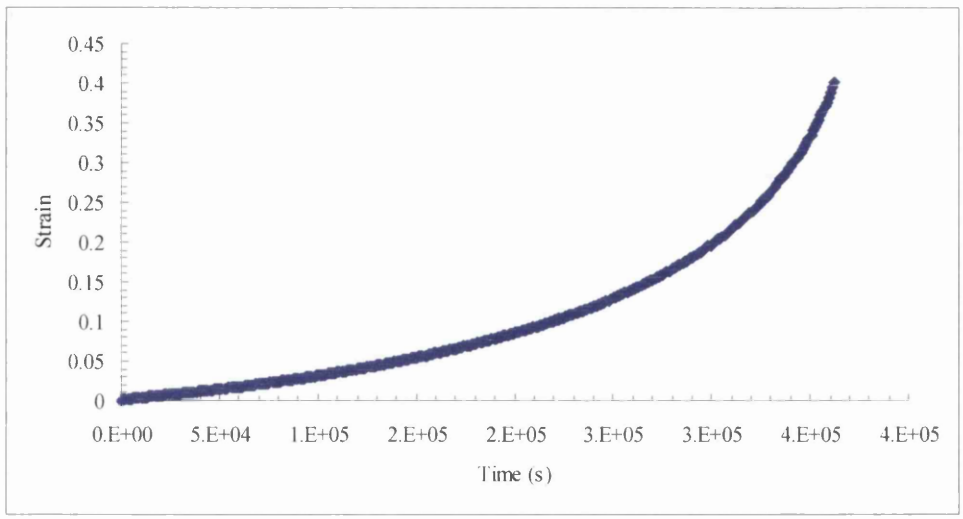

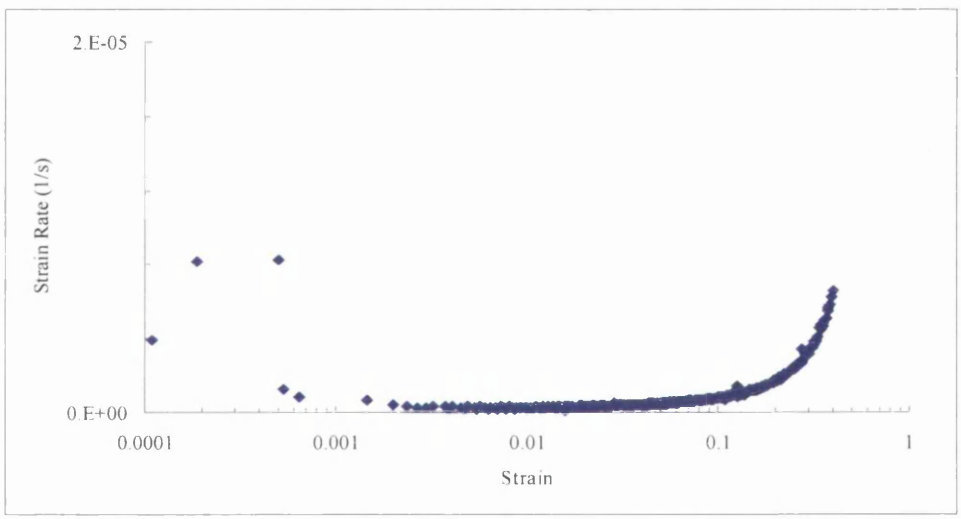

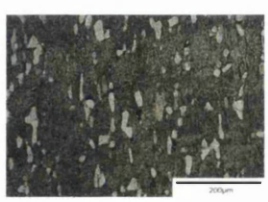

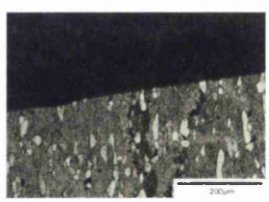

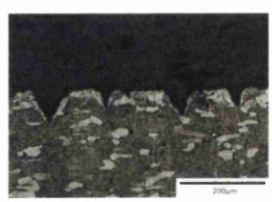

(B4.28): 923K/300MPa

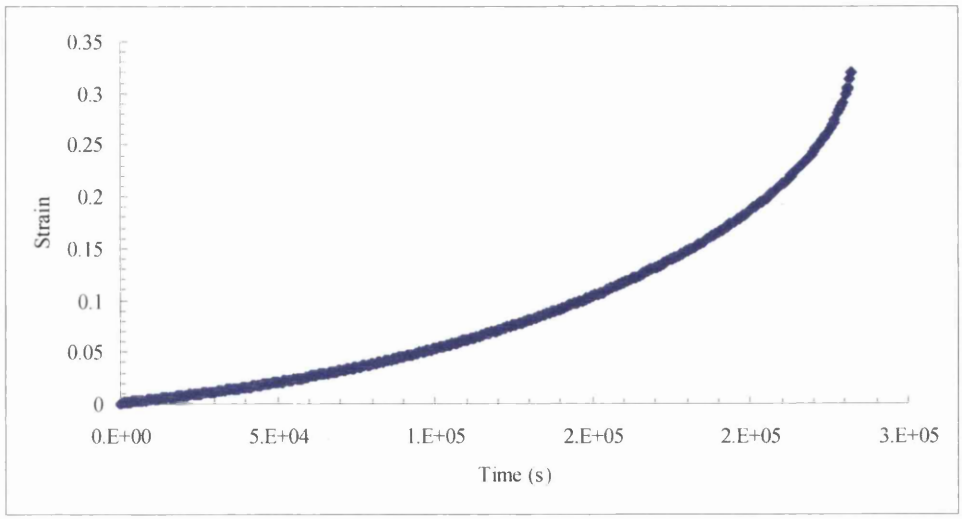

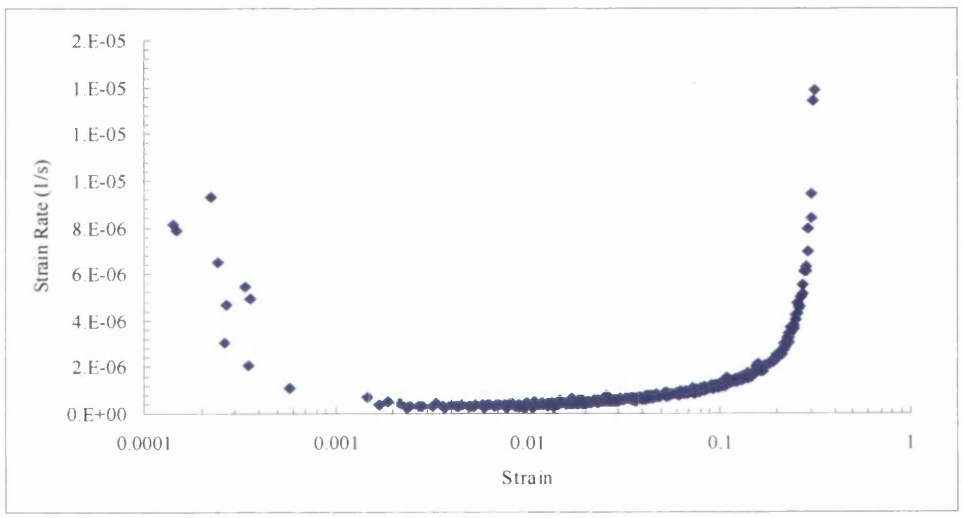

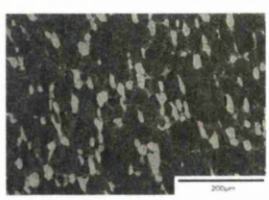

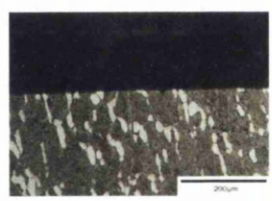

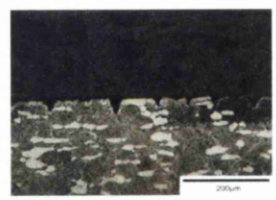

B.5 Creep-Step Tests Results (air)

(B5.1): Step between 848K/455MPa and 898K/280MPa

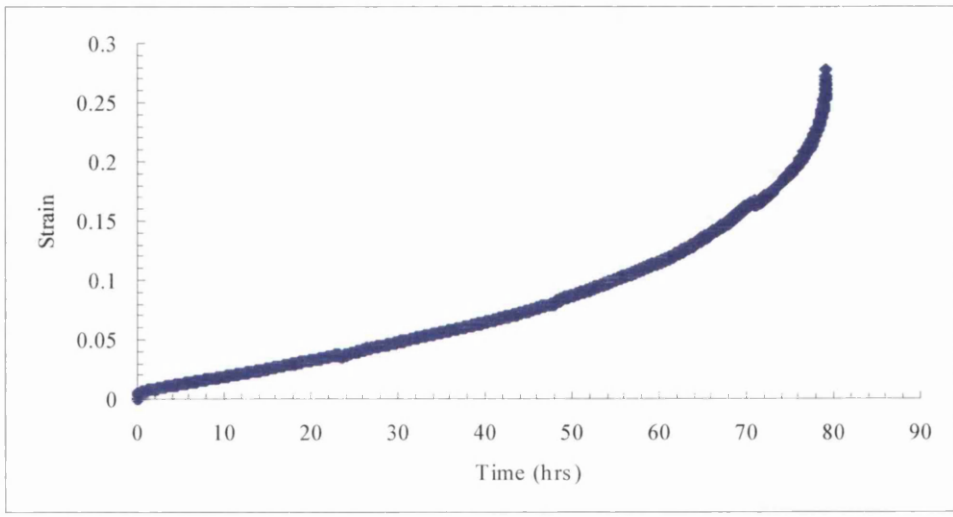

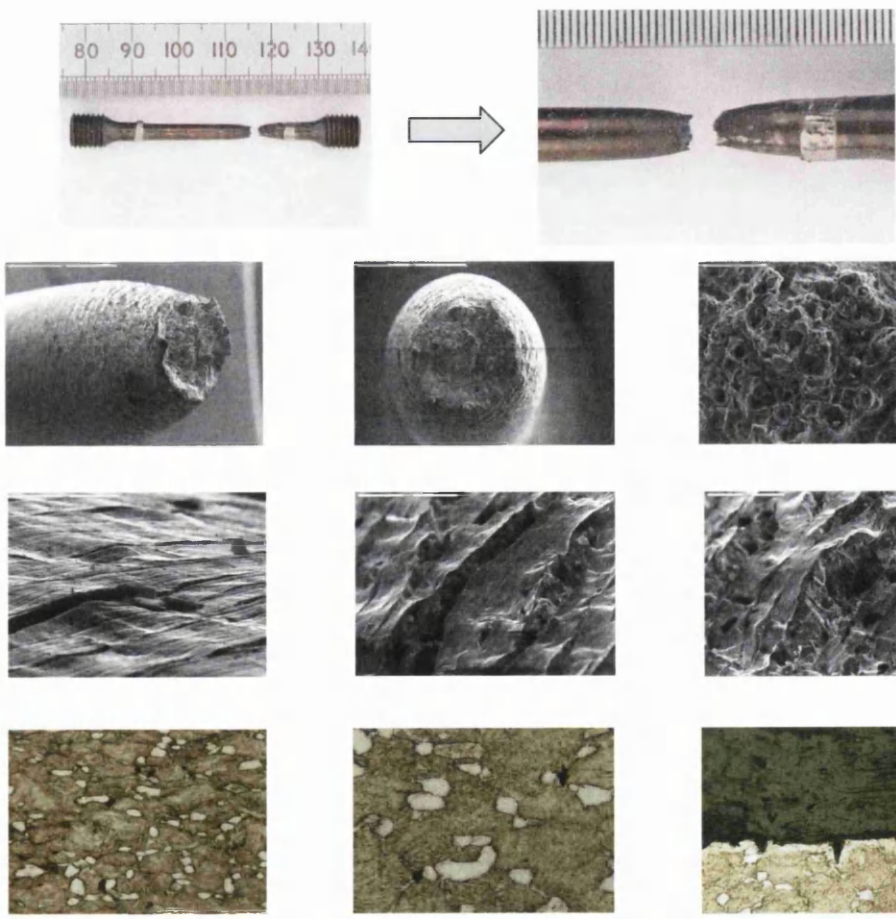

(B5.2): Step between 848K/455MPa and 898K/280MPa (repeat test)

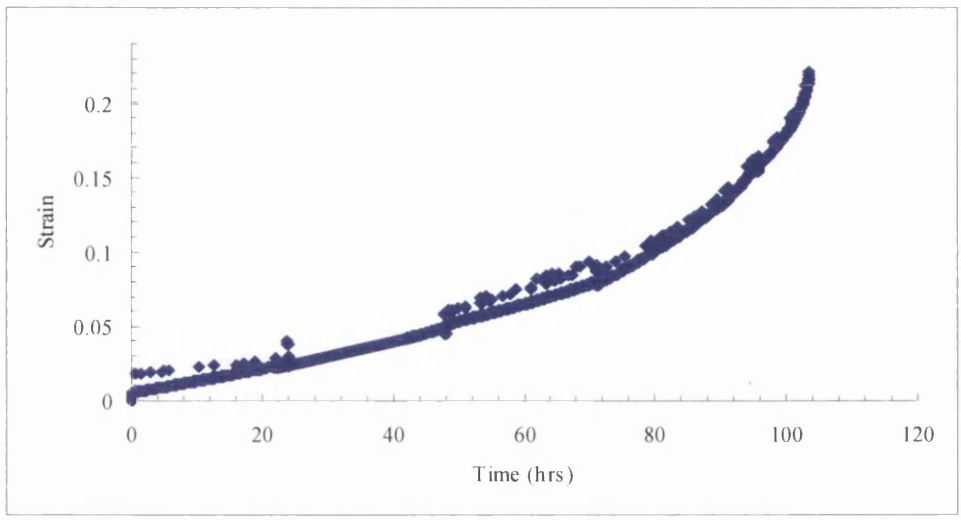

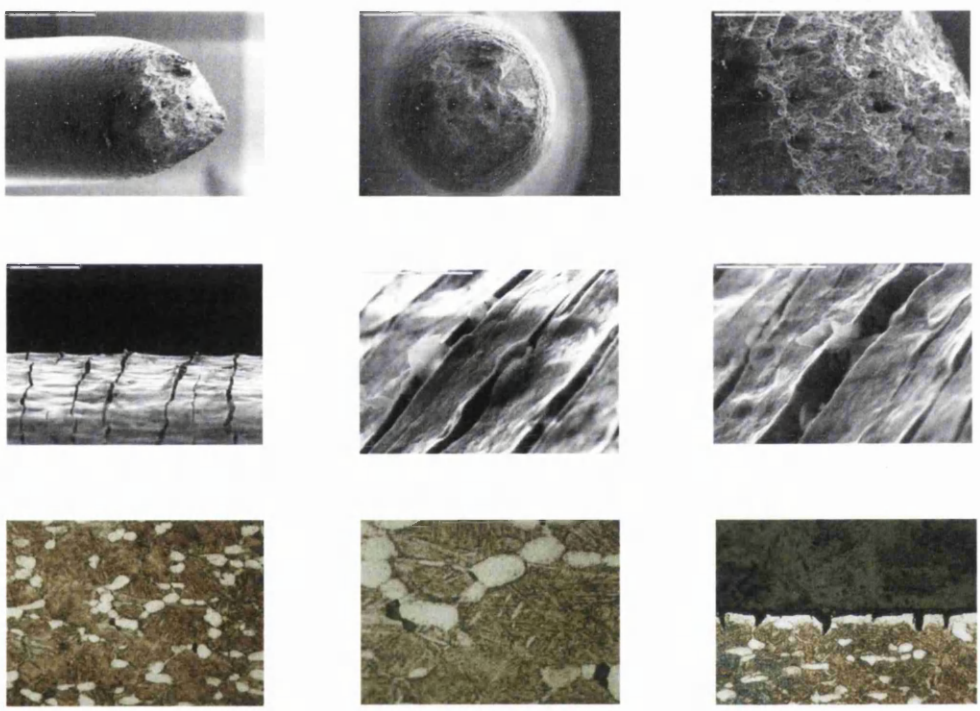

(B5.3): Step between 823K/560MPa and 873K/340MPa

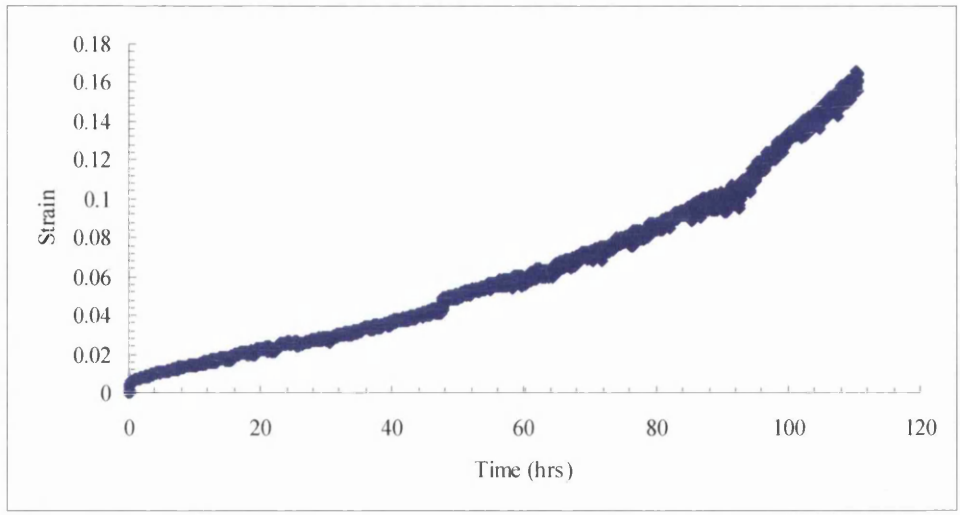

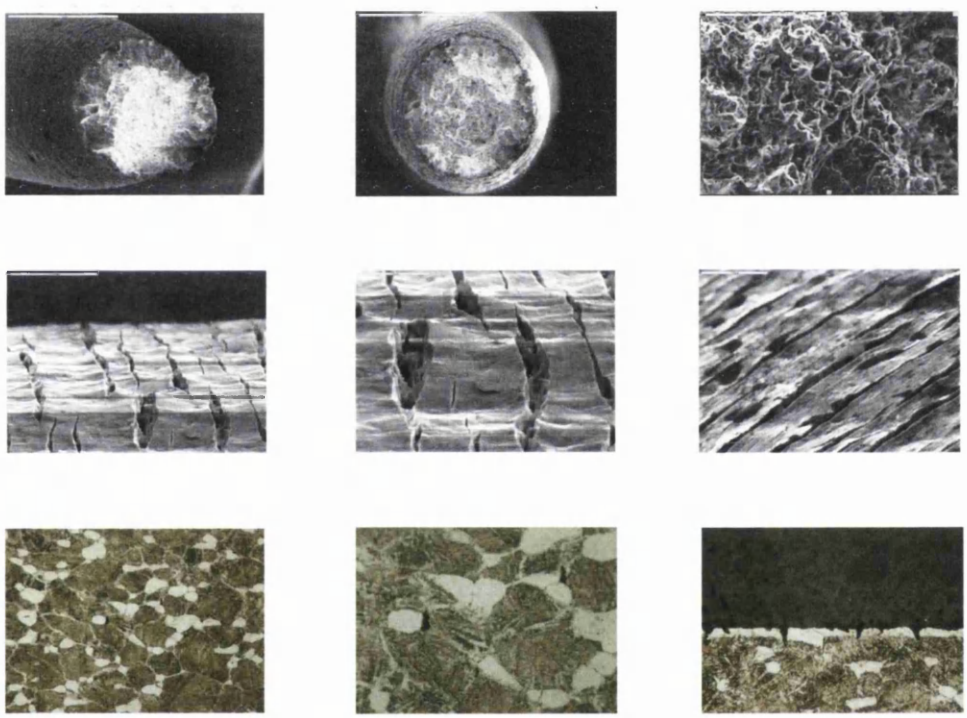

B.6 Creep-Step Tests Results (Vacuum)

(B6.1): Step between 823K/560MPa and 873K/340MPa

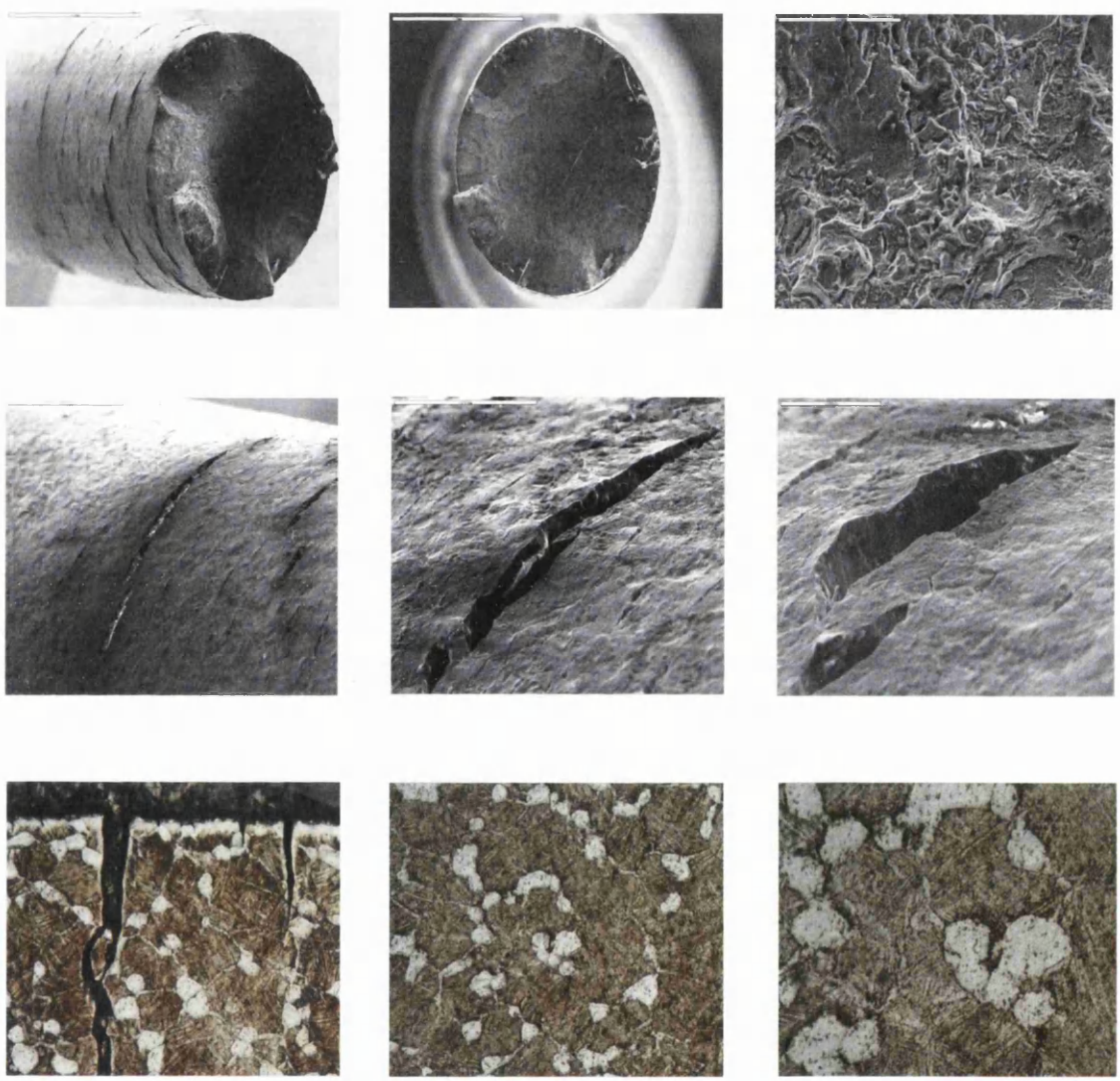

(Total creep life recorded at these conditions was ~ 170 hours)

(B6.2): Step between 823K/560MPa and 873K/340MPa (repeat test)

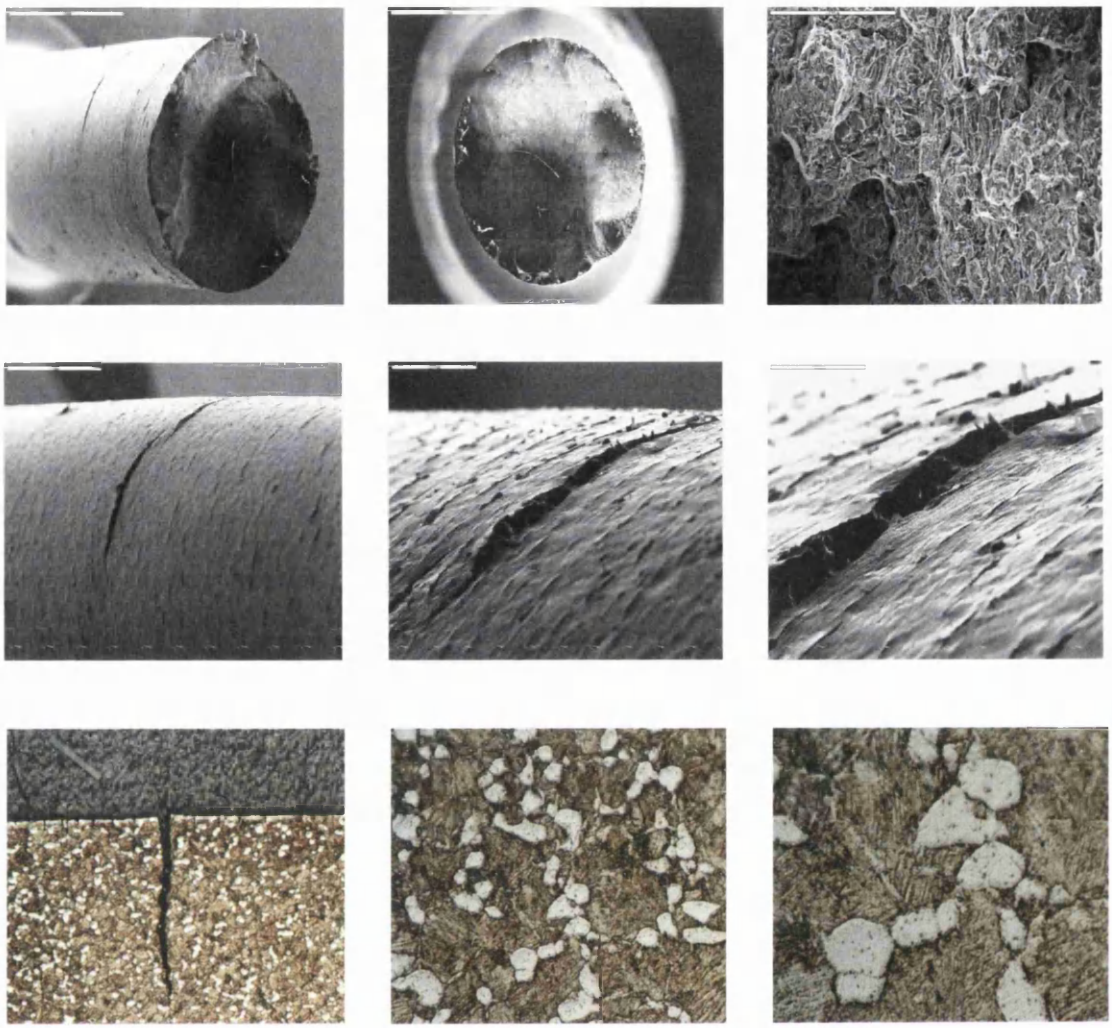

(Total creep life recorded at these conditions was ~ 300 hours)

B.7 The Power Law Results

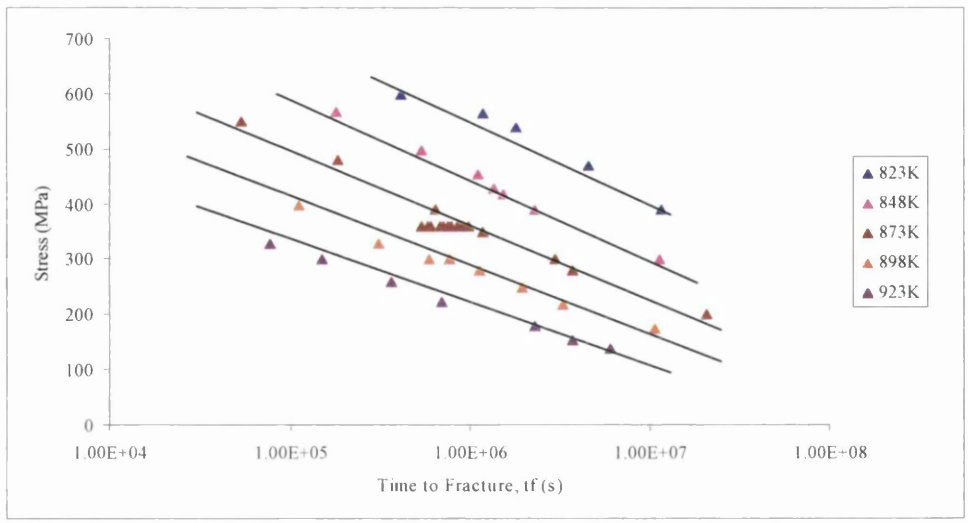

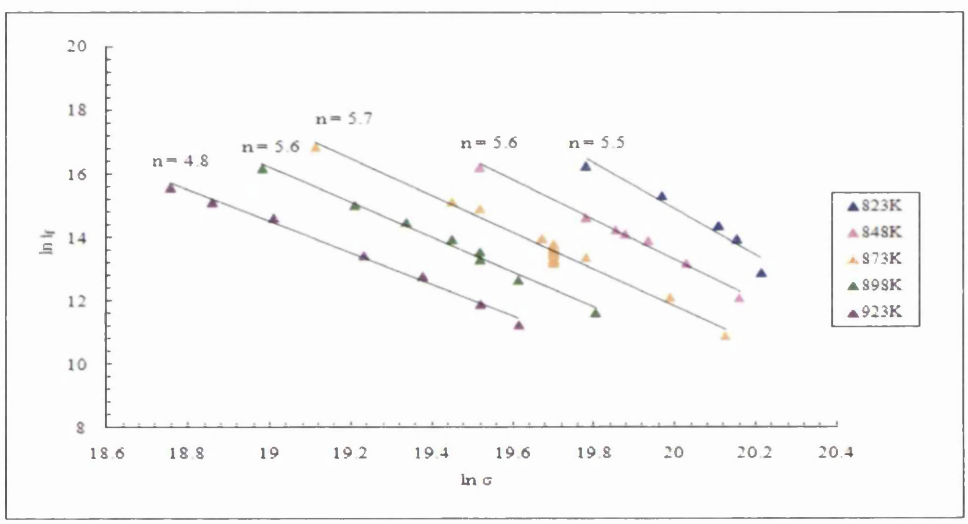

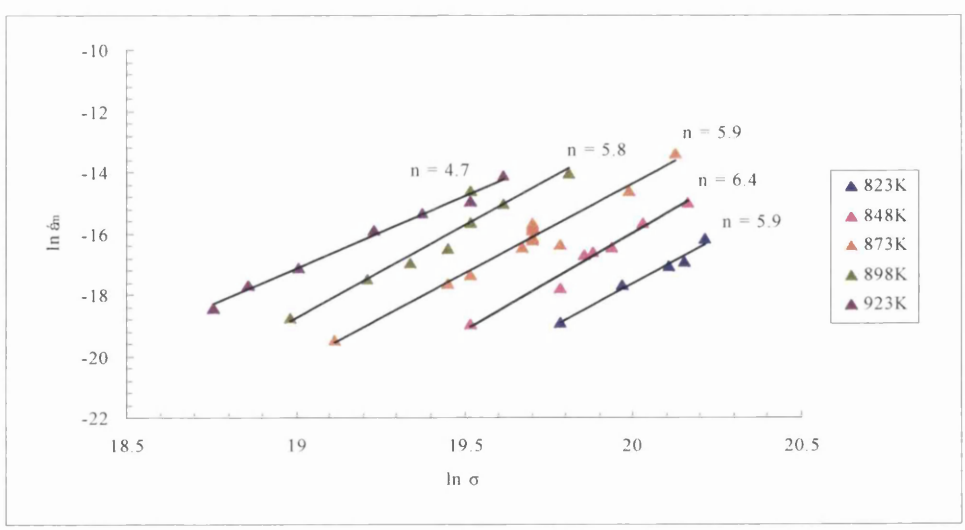

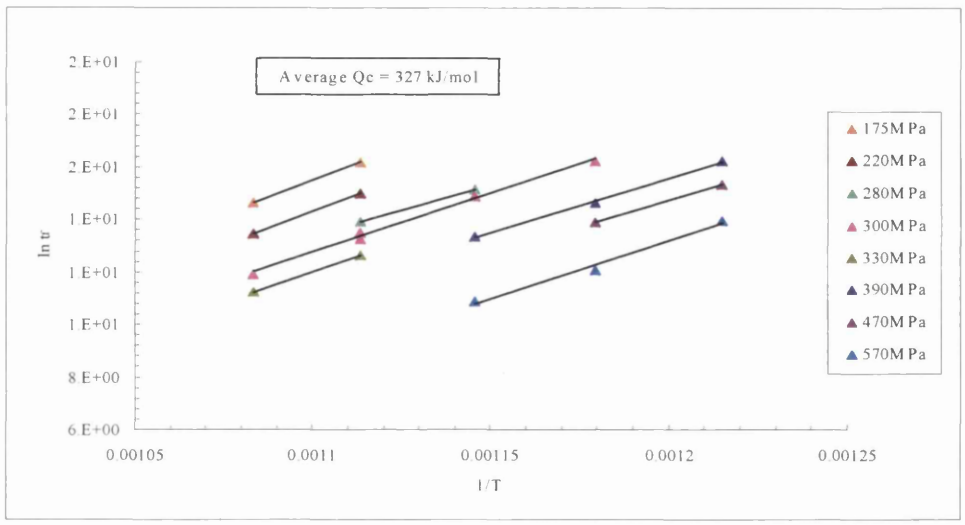
Average Qc = 327 kJ/mol
2.E+01
2.E+01
2.E+01
1.E+01
1.E+01
1.E+01
8.E+00
6.E+00
ln tr
0.00105
0.0011
0.00115
0.0012
0.00125
1/T
175M Pa
220M Pa
280M Pa
300M Pa
330M Pa
390M Pa
470M Pa
570M Pa

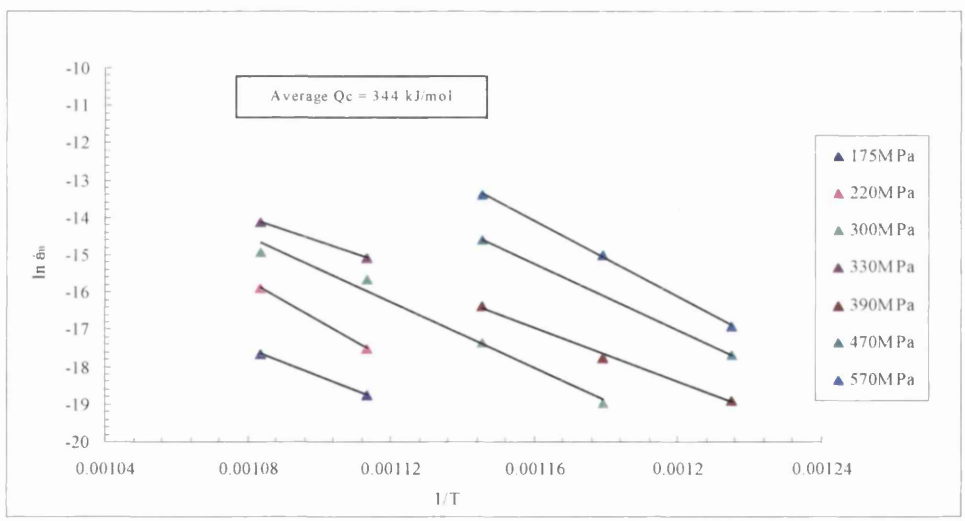
Average Qc = 344 kJ/mol
-10
-11
-12
-13
-14
-15
-16
-17
-18
-19
-20
ln ε̇ₕ
0.00104
0.00108
0.00112
0.00116
0.0012
0.00124
1/T
175M Pa
220M Pa
300M Pa
330M Pa
390M Pa
470M Pa
570M Pa

B.8 The Monkman-Grant Analysis Results

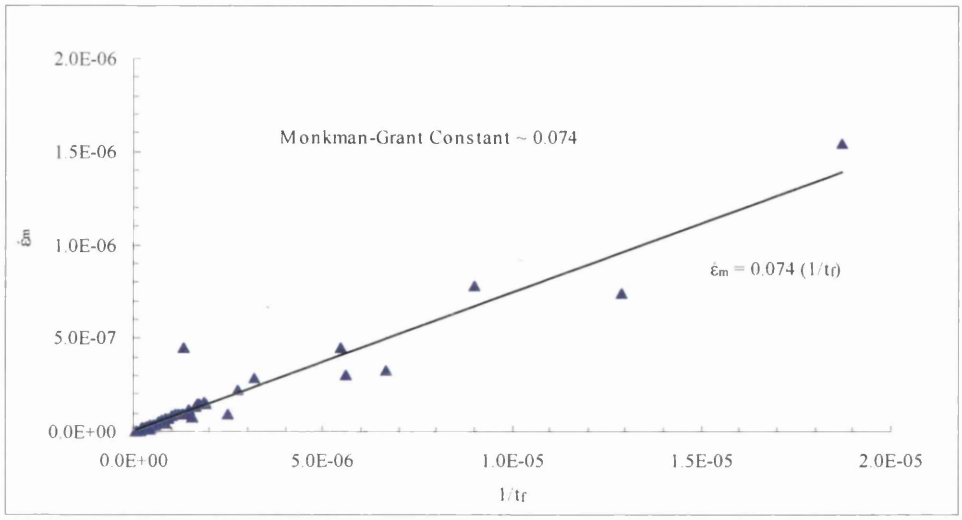

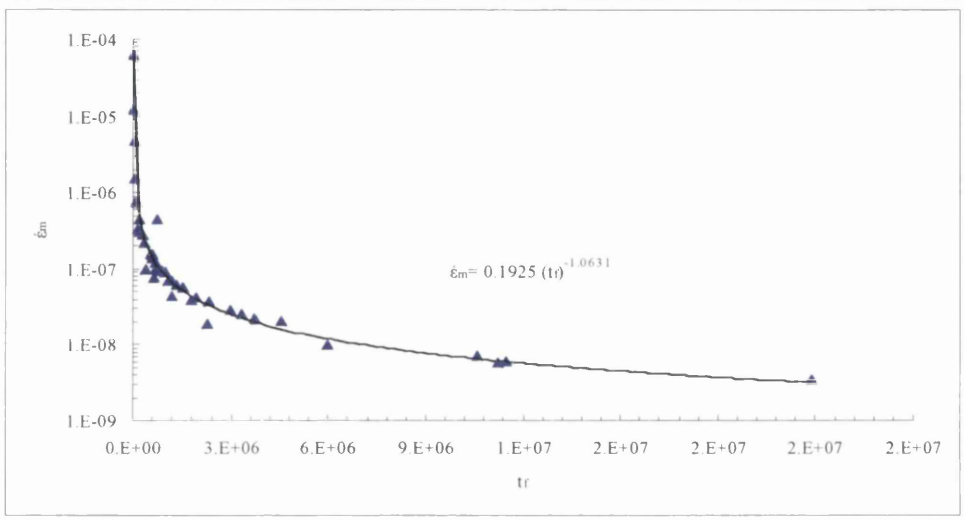

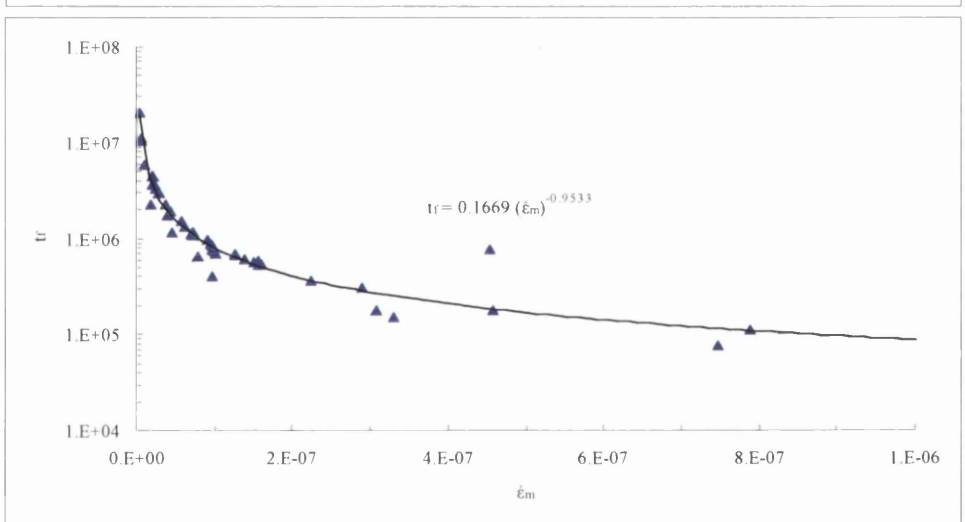

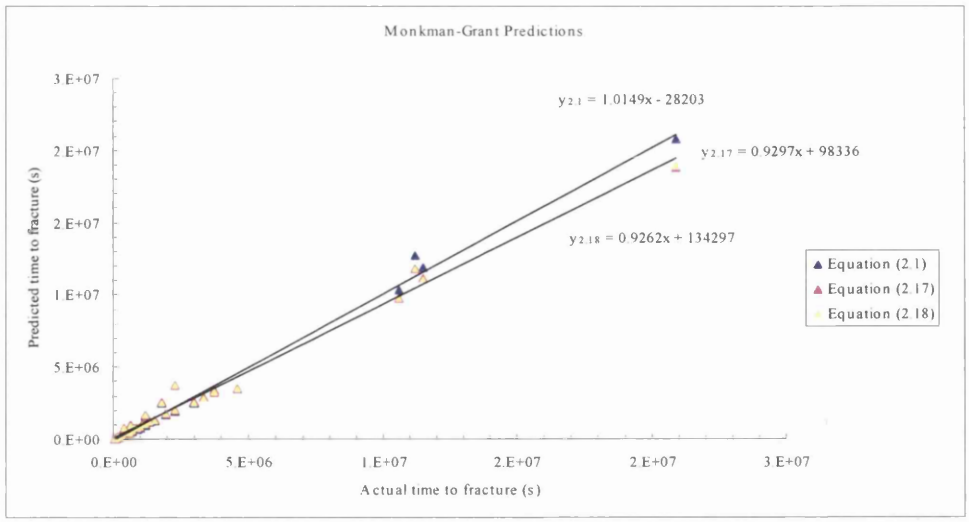
Monkman-Grant Predictions
y2.1 = 1.0149x - 28203
y2.17 = 0.9297x + 98336
y2.18 = 0.9262x + 134297
Equation (2.1)
Equation (2.17)
Equation (2.18)
Predicted time to fracture (s)
Actual time to fracture (s)
3 E+07
2 E+07
2 E+07
1 E+07
5 E+06
0 E+00
0 E+00
5 E+06
1 E+07
2 E+07
2 E+07
3 E+07

B.9 The Larson-Miller Analysis Results

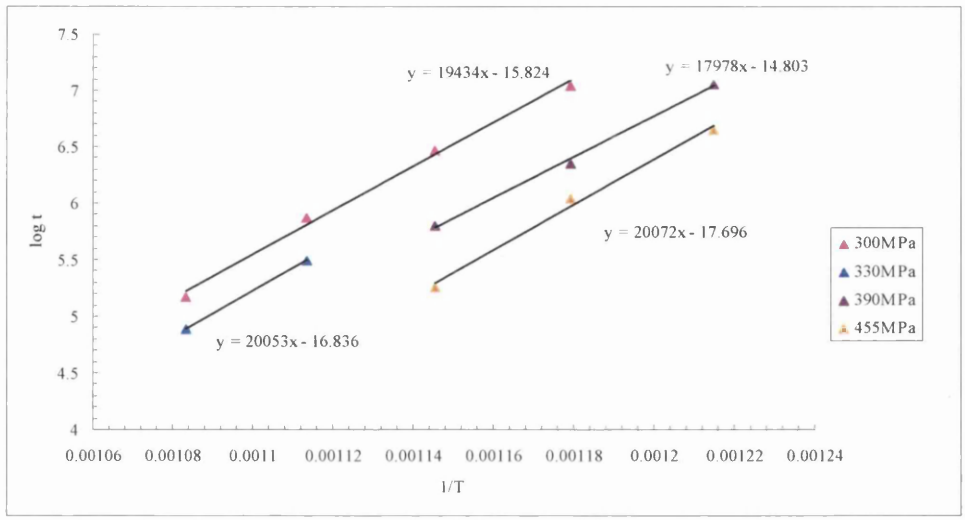

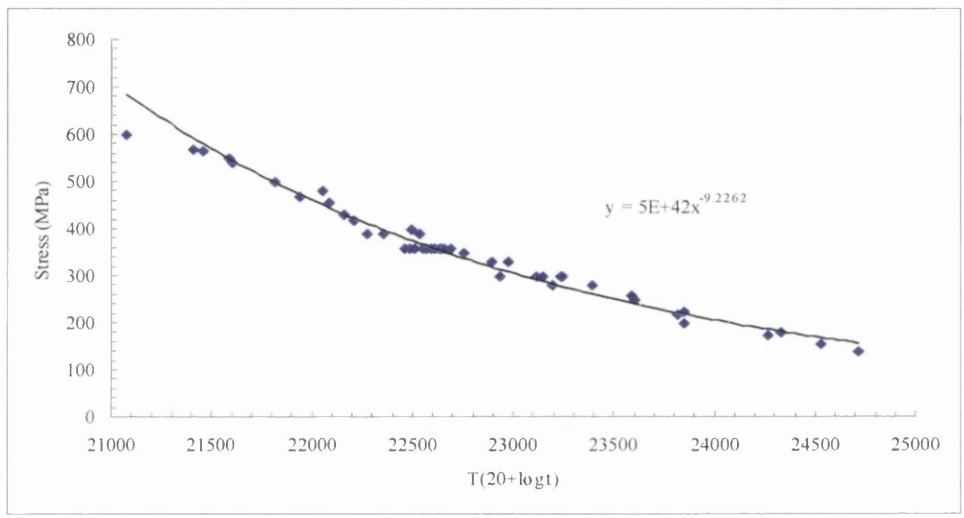

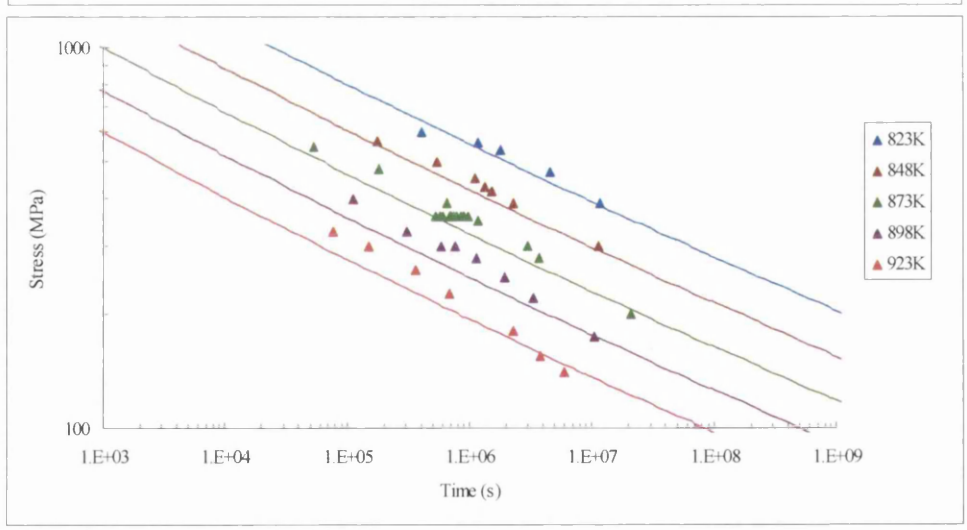

B.10 The Manson-Haferd Analysis Results

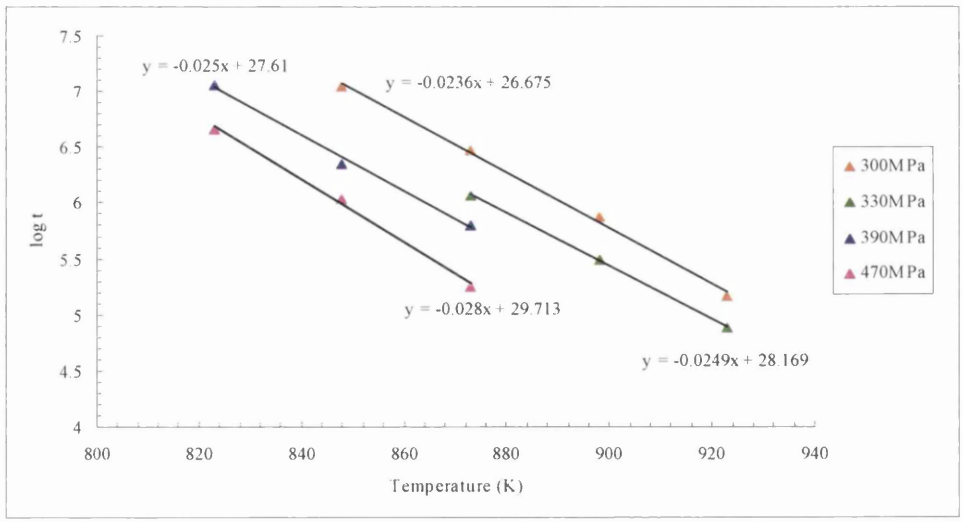

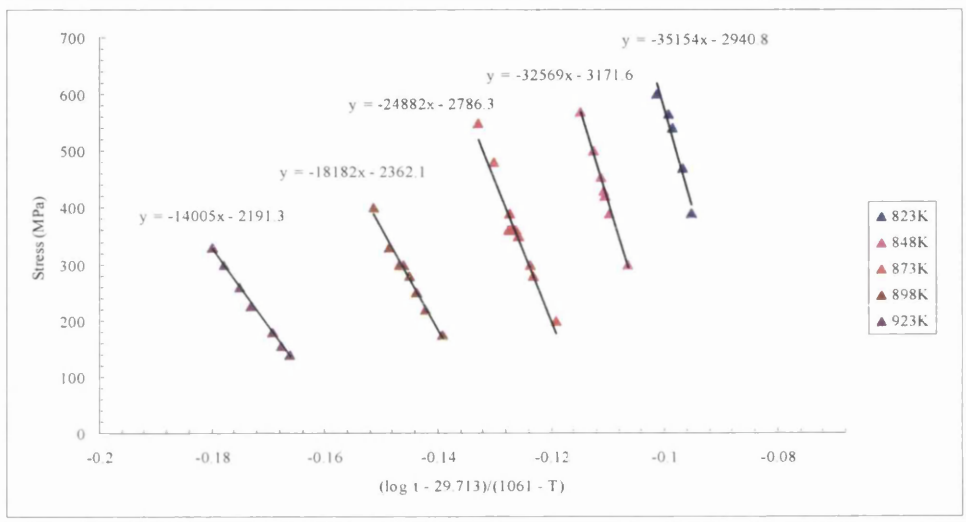

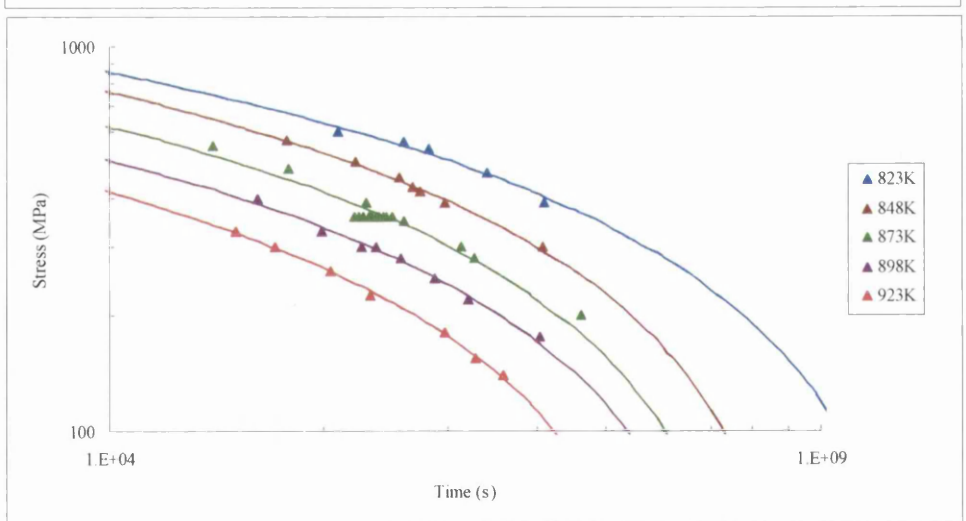

B.11 Orr-Sherby-Dorn Analysis Results

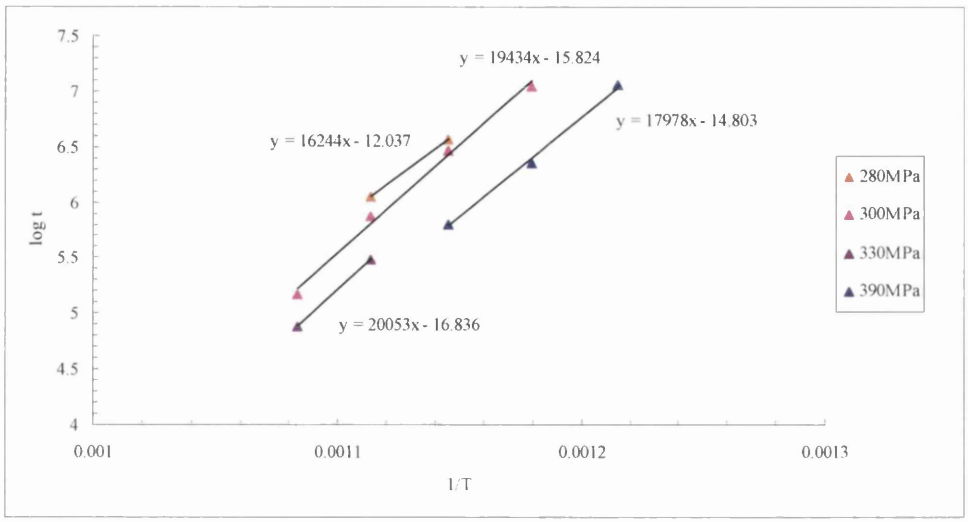

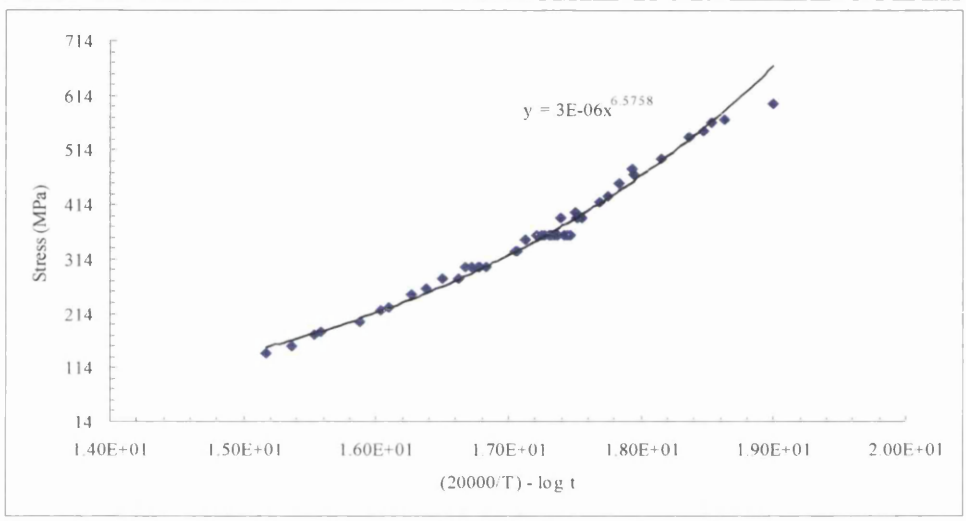

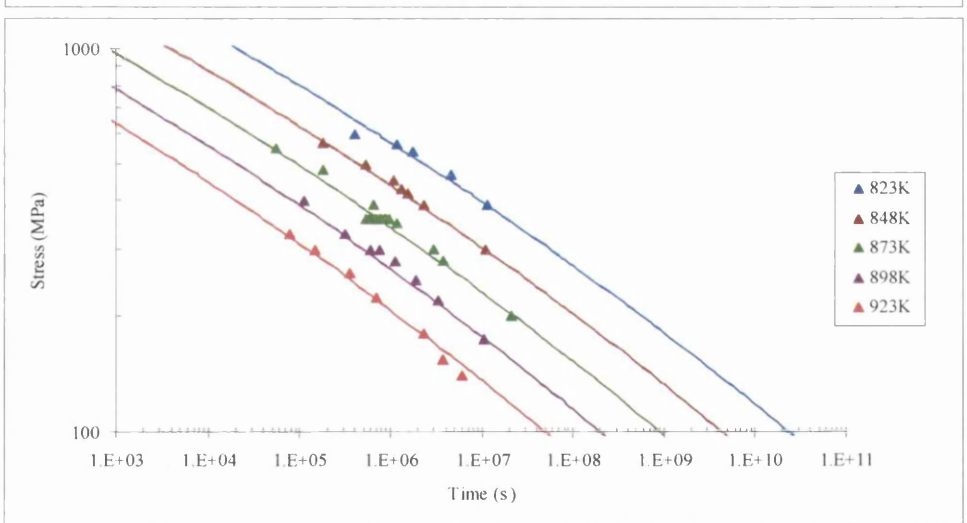

B.12 The Manson-Succop Analysis Results

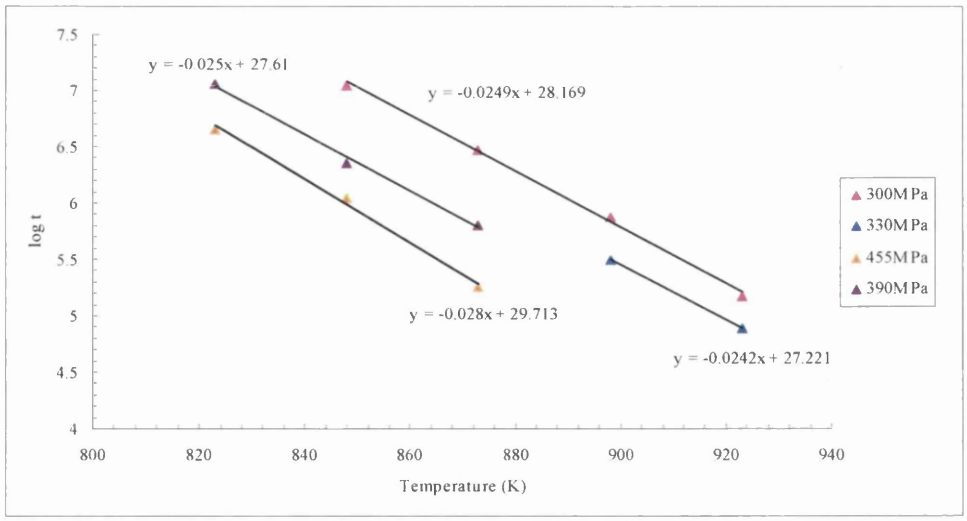

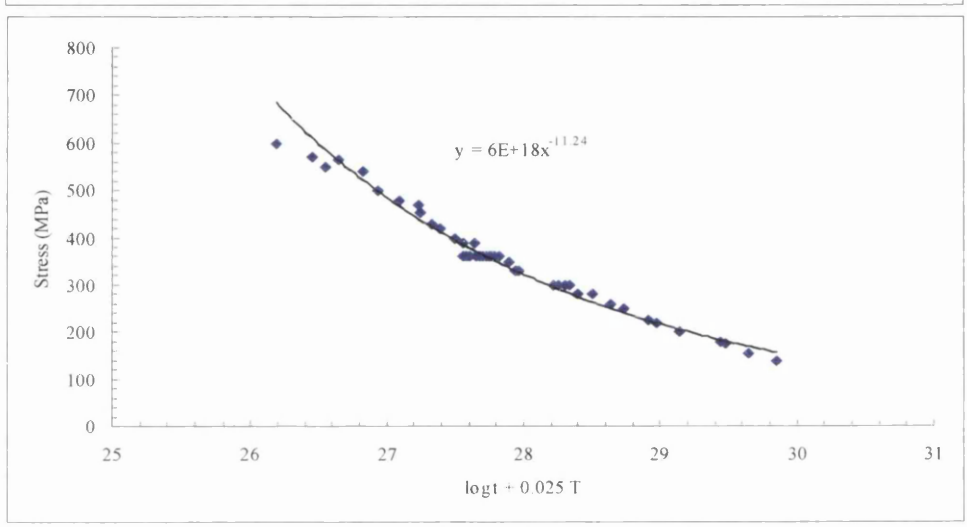

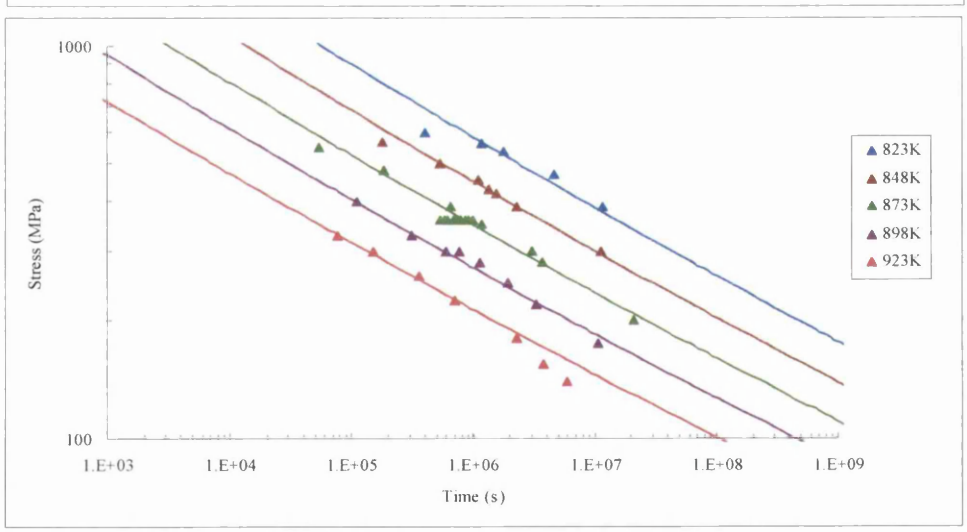

B.13 THE HYPERBOLIC-TANGENT ANALYSIS RESULTS

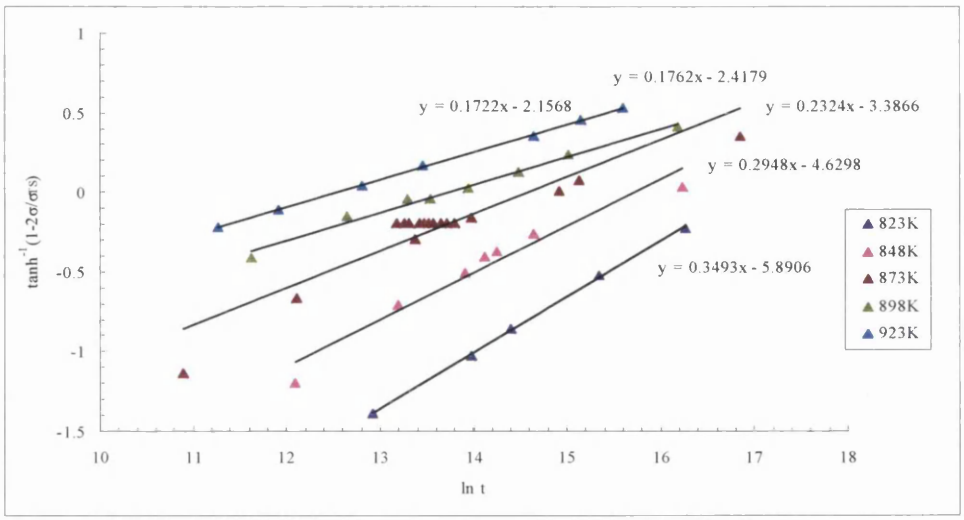

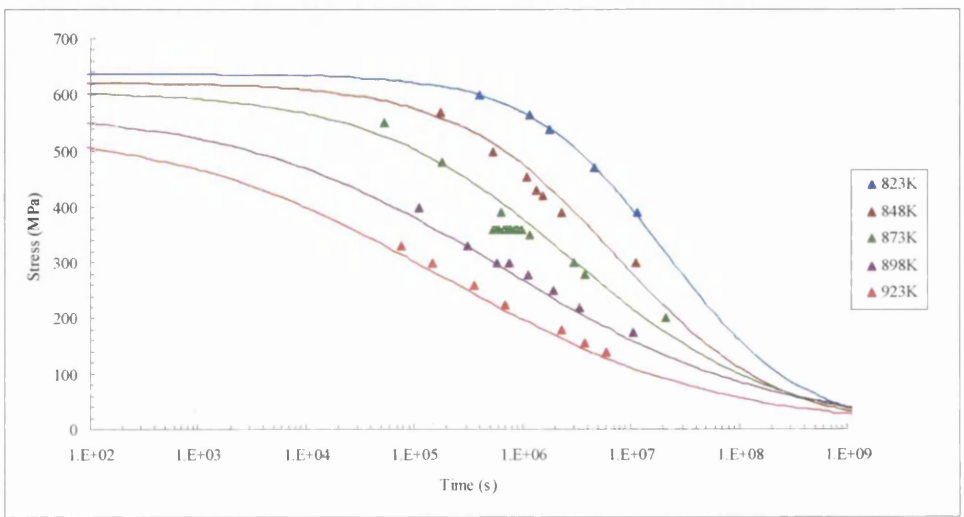

B.14 The Goldhoff-Sherby Analysis Results

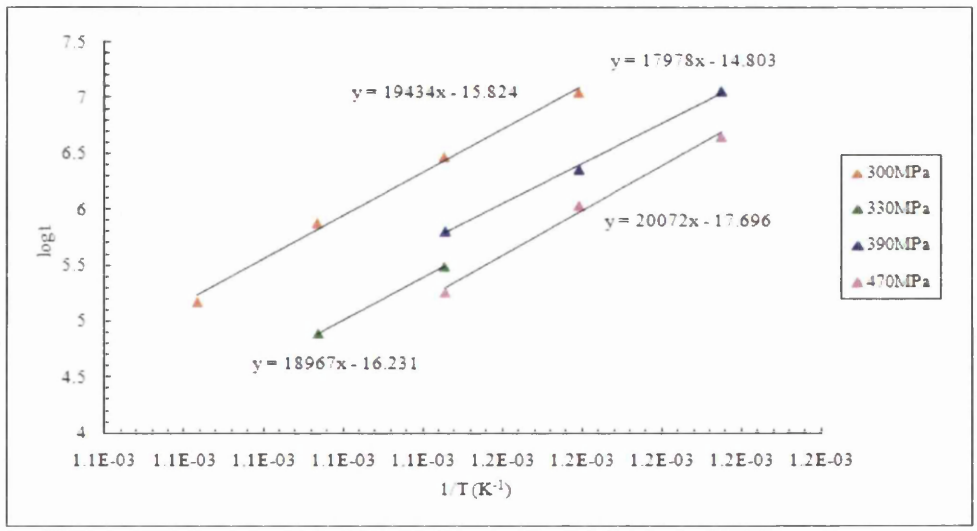

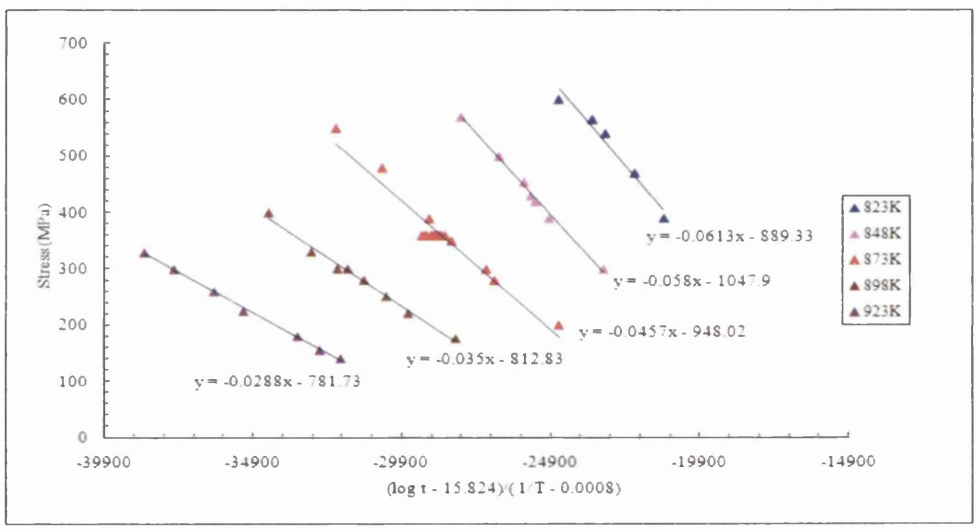

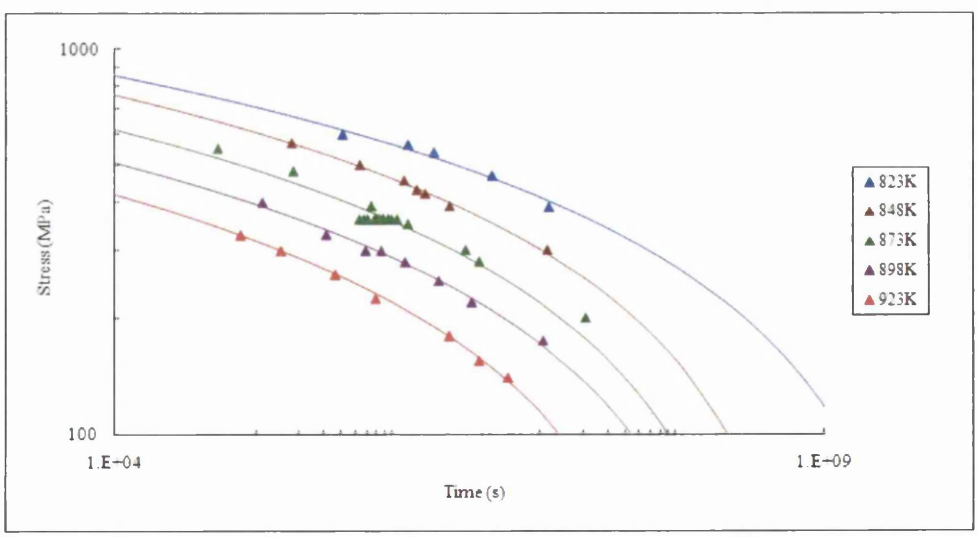

B.15 The θ-Method Analysis Results

(B15.1): 823K/390MPa

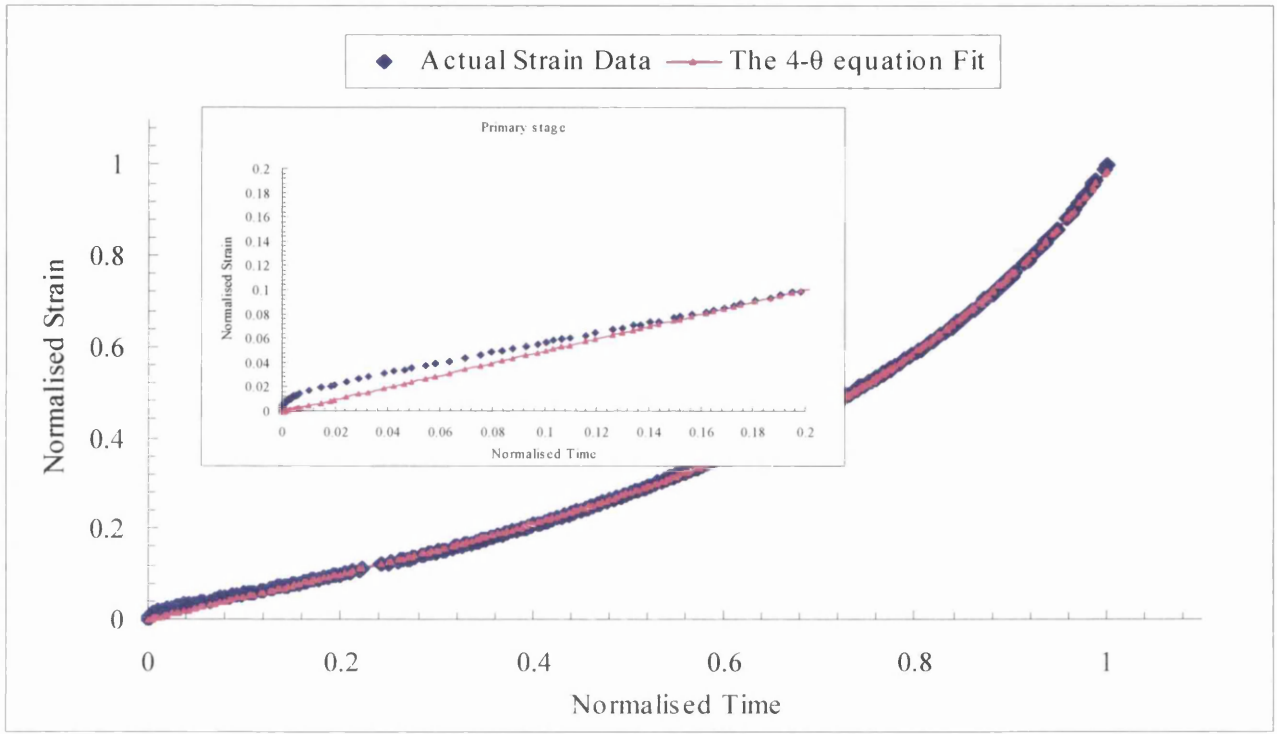

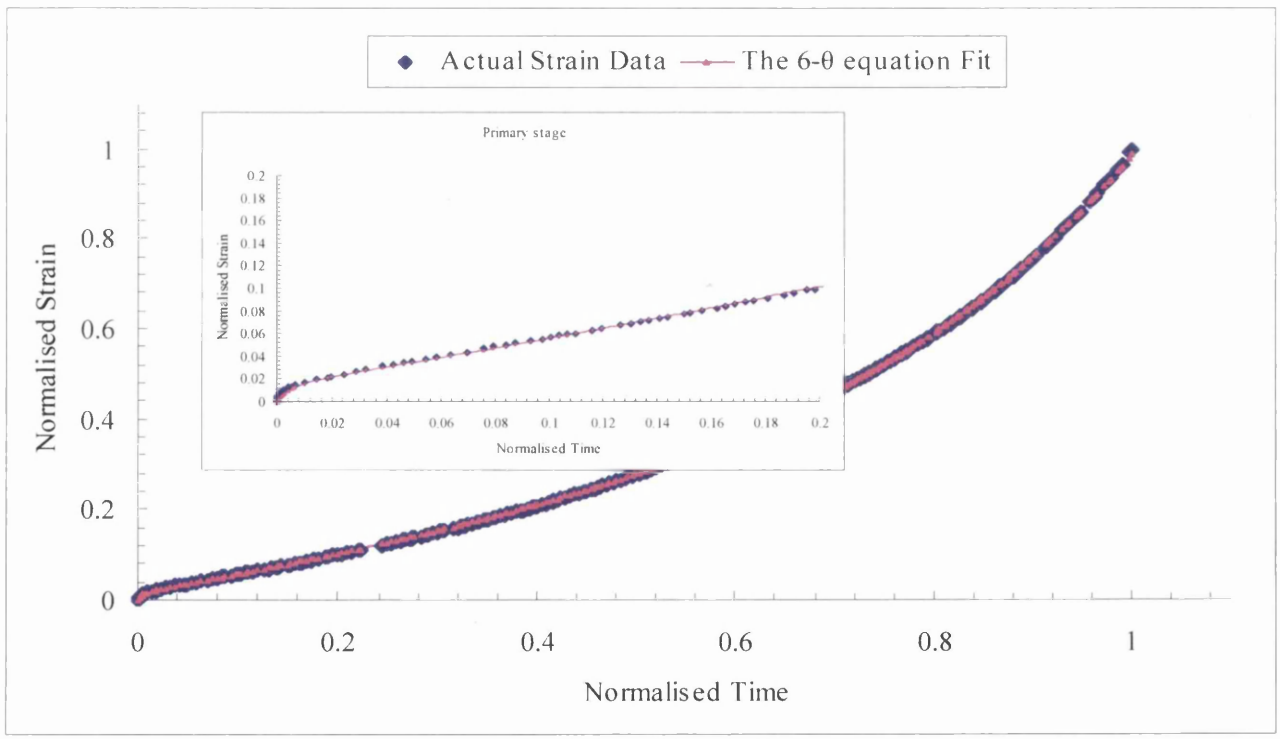

(B15.2): 823K/470MPa

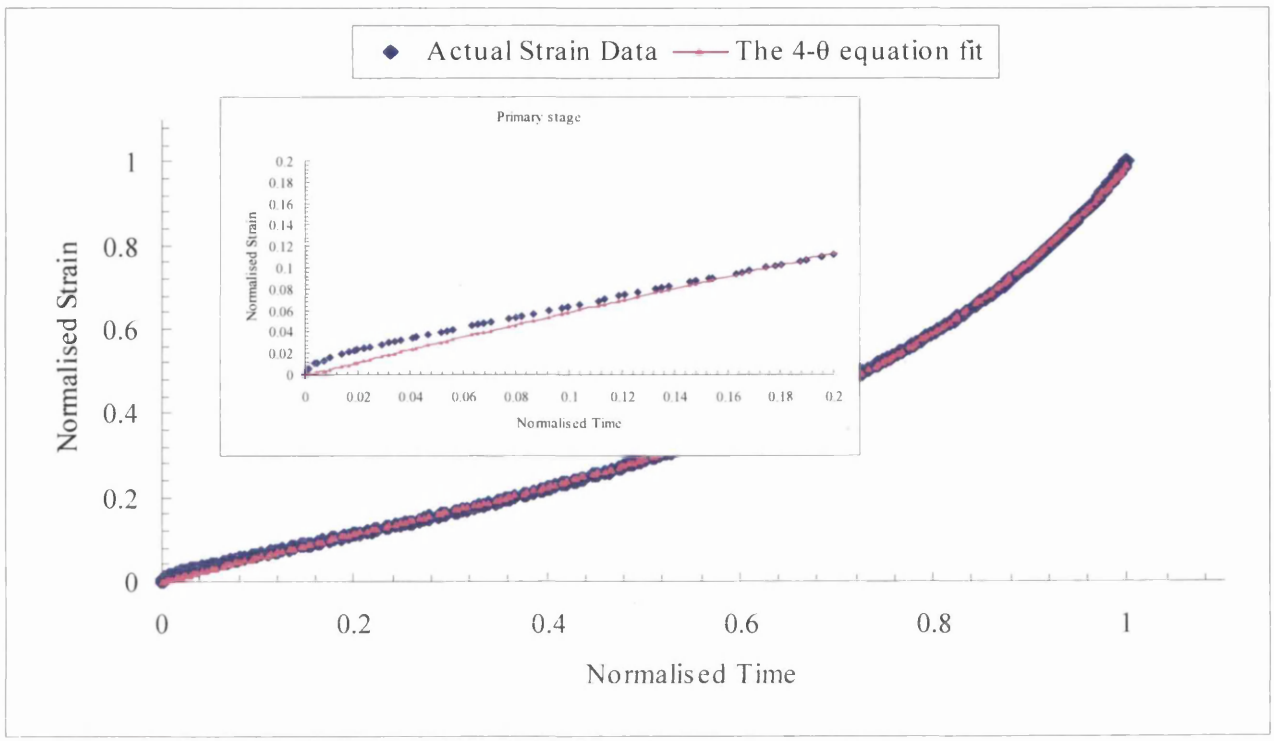

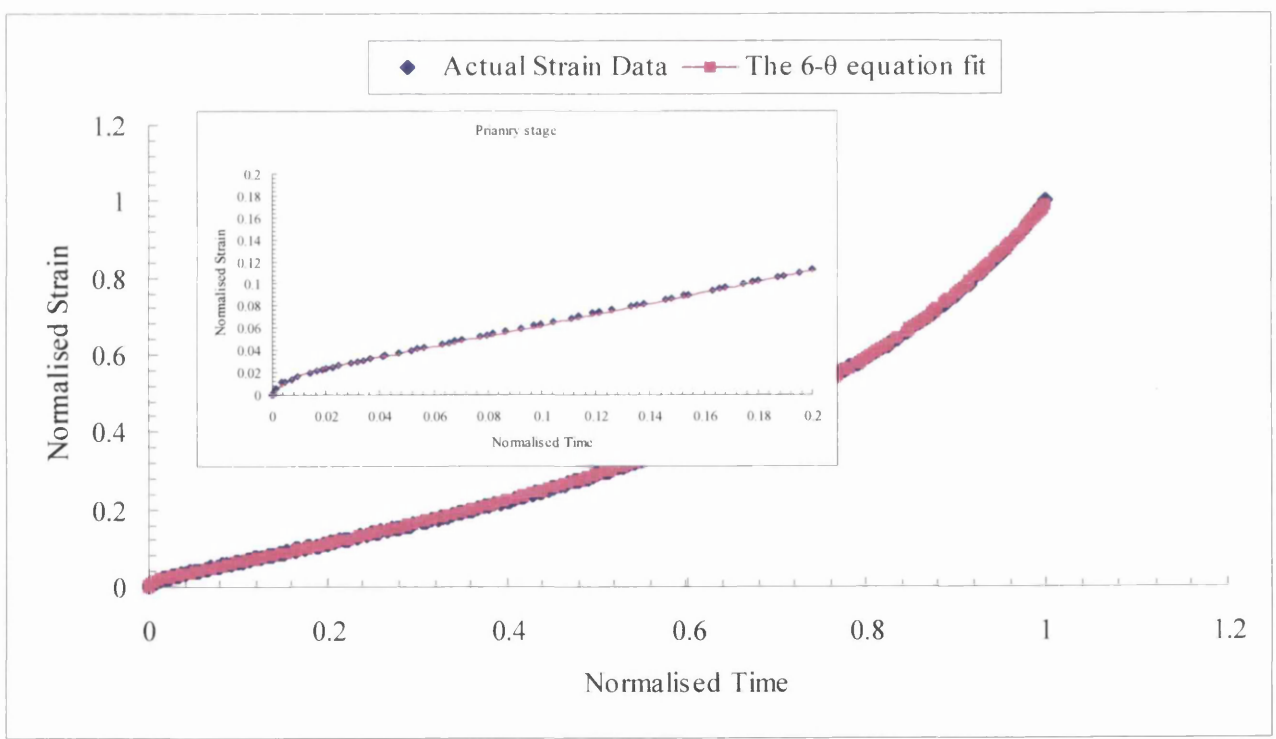

(B15.3): 823K/540MPa

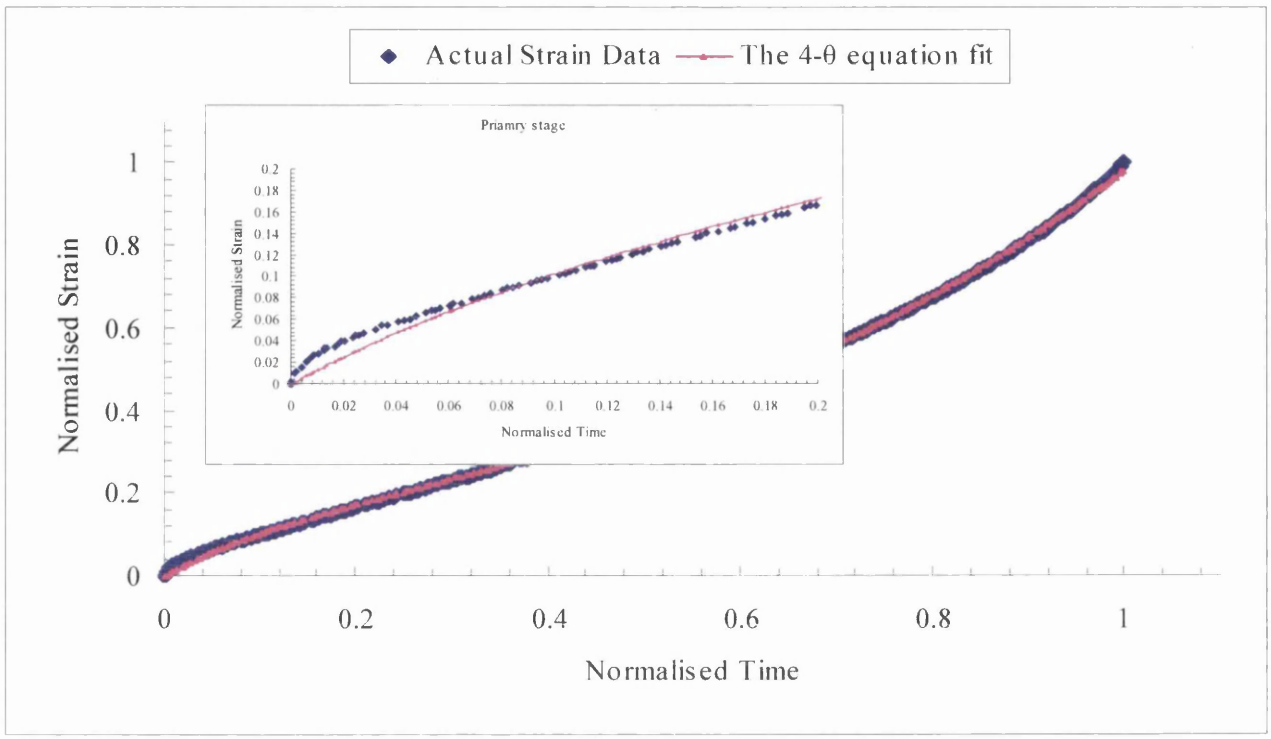

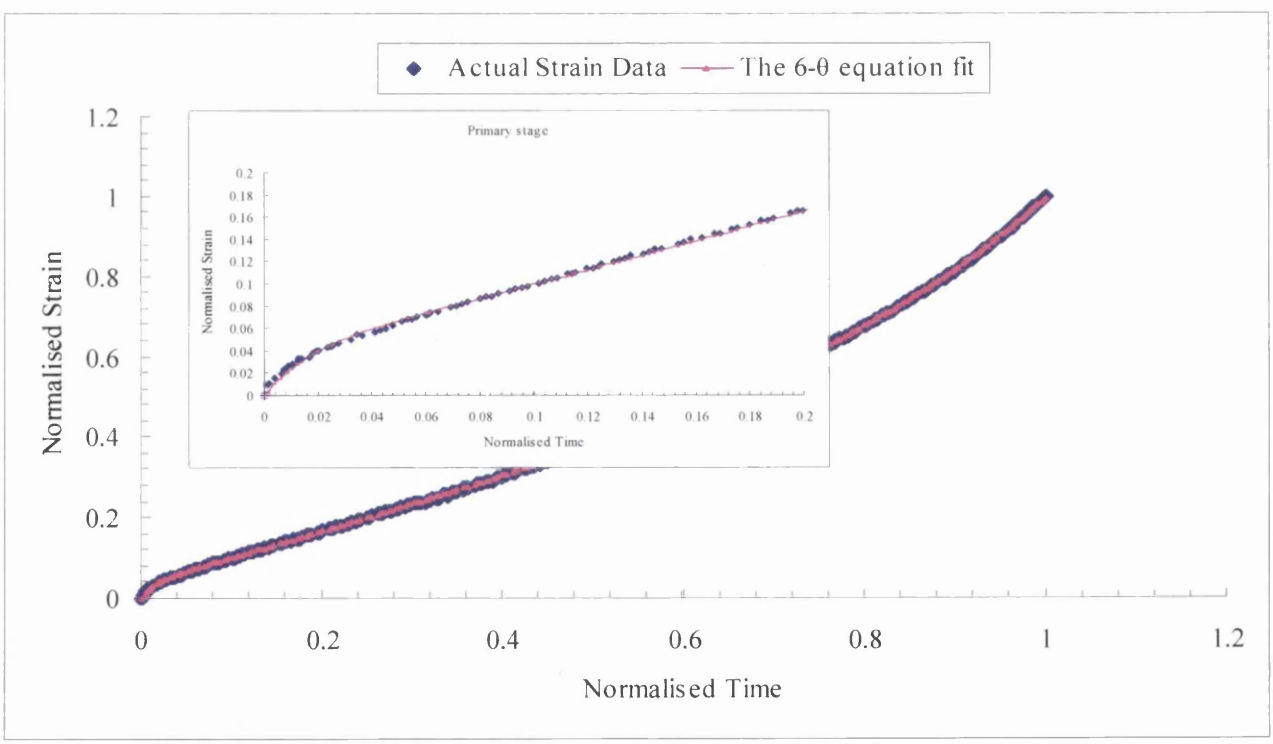

(B15.4): 823K/565MPa

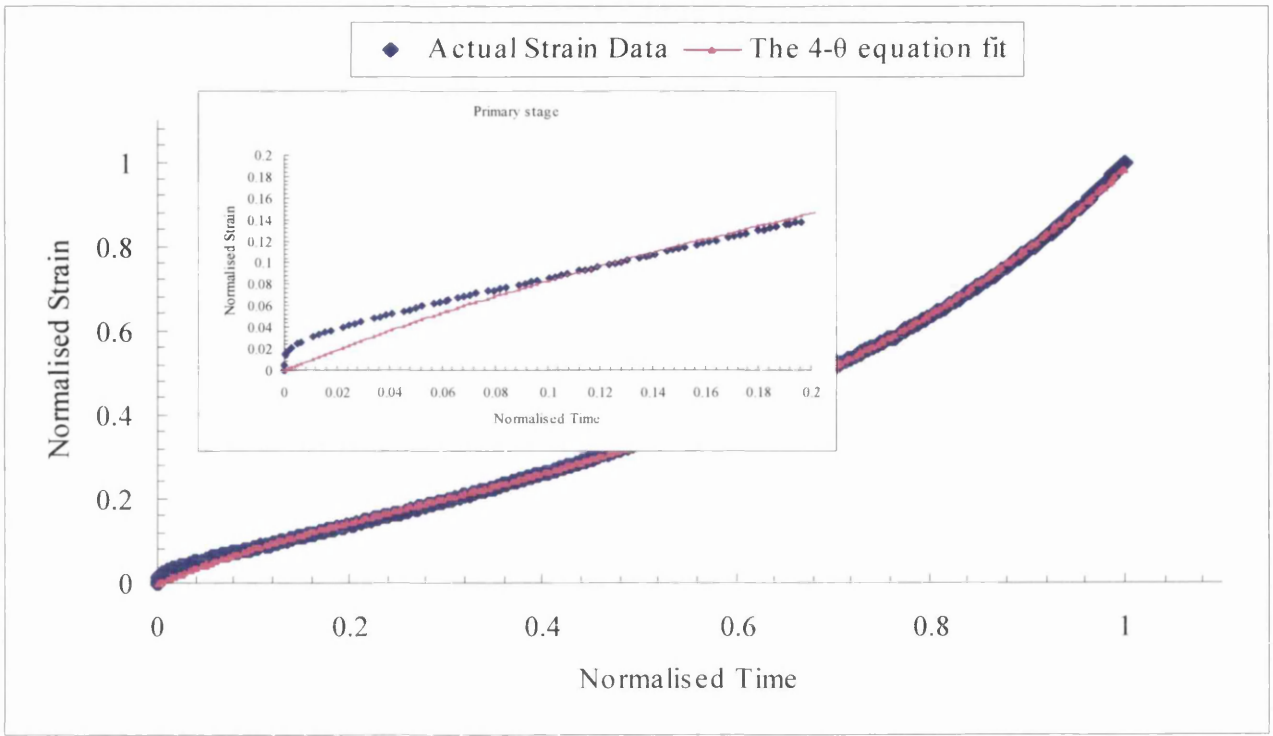

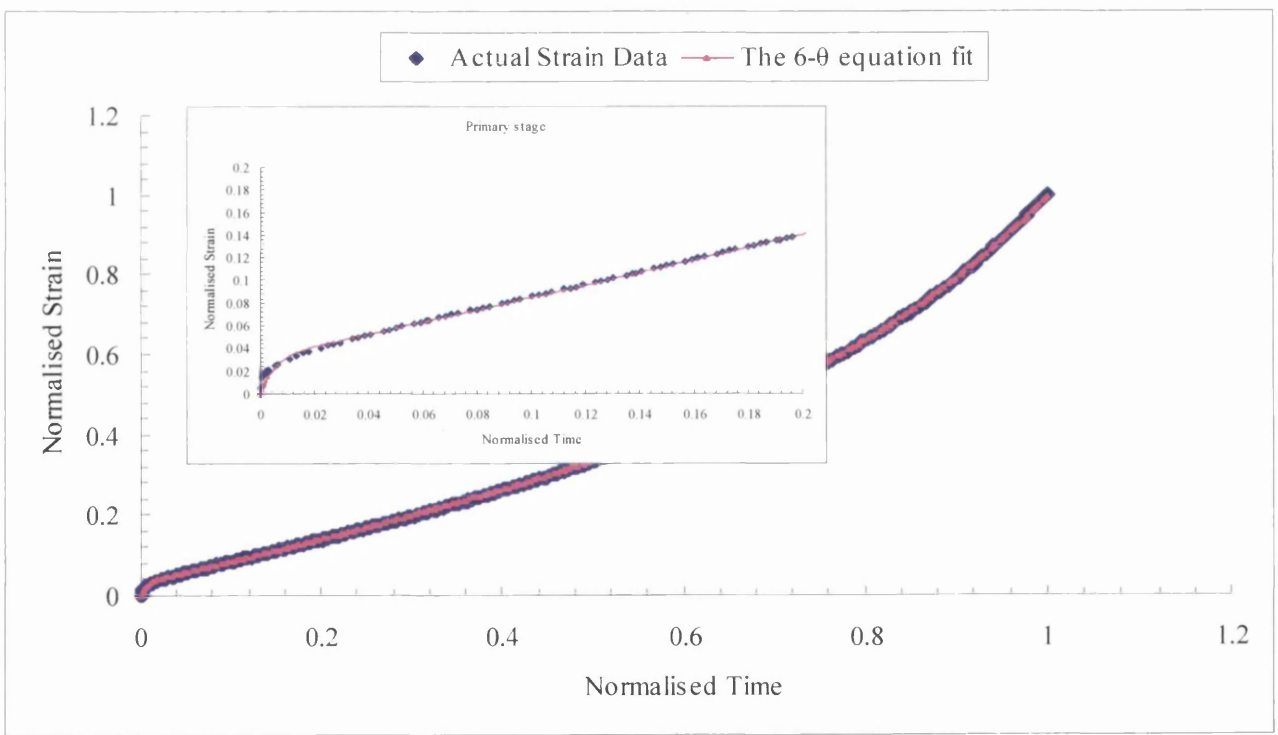

(B15.5): 823K/600MPa

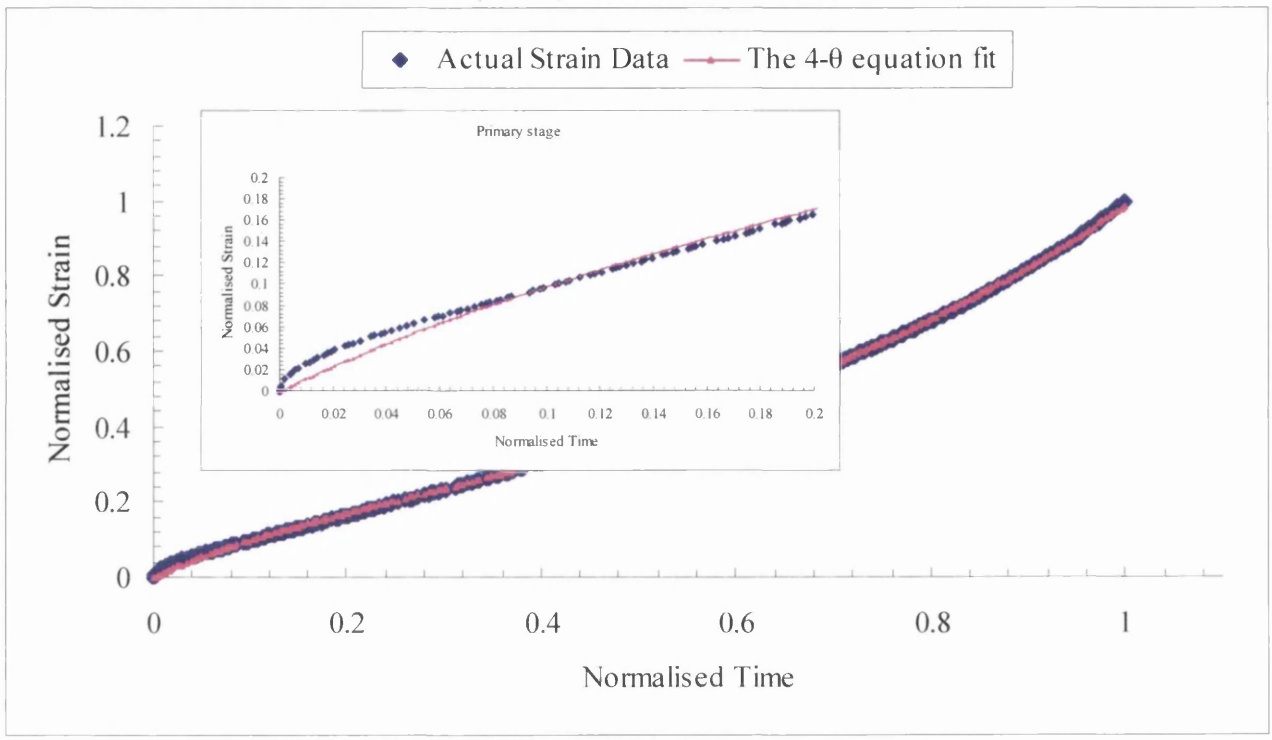

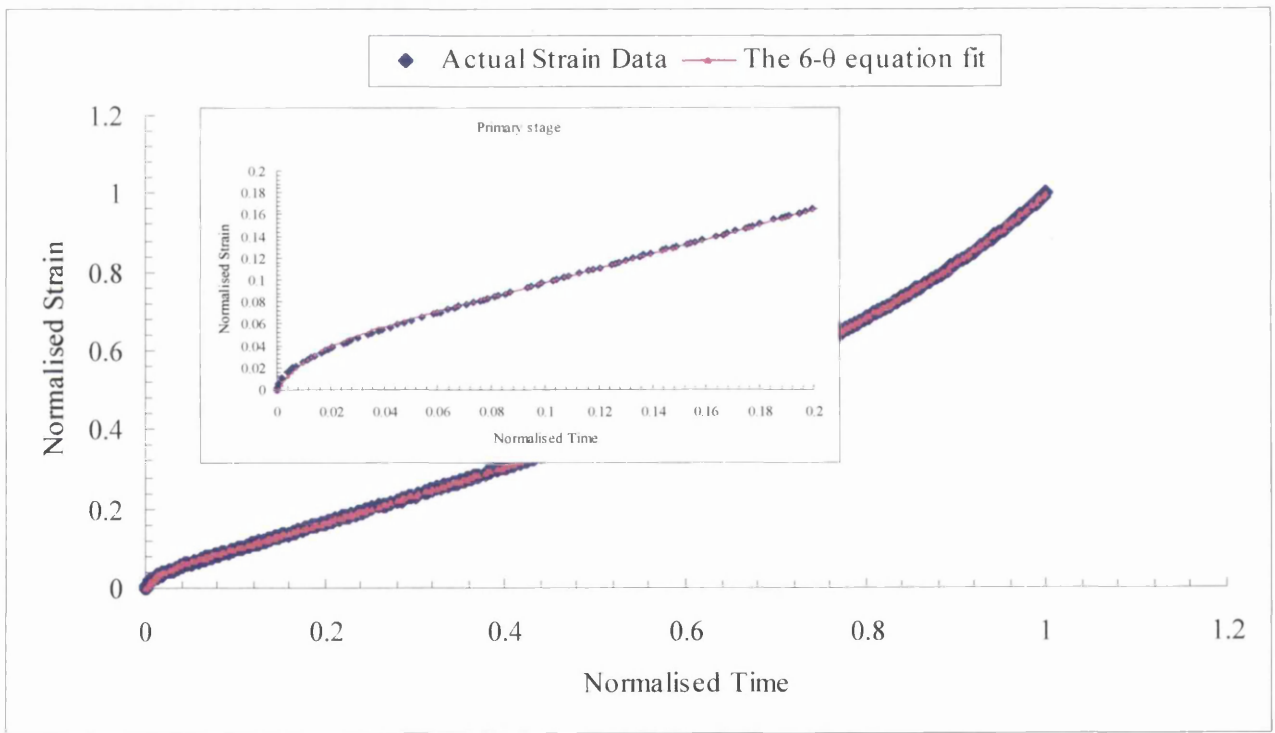

(B15.6): 848K/300MPa

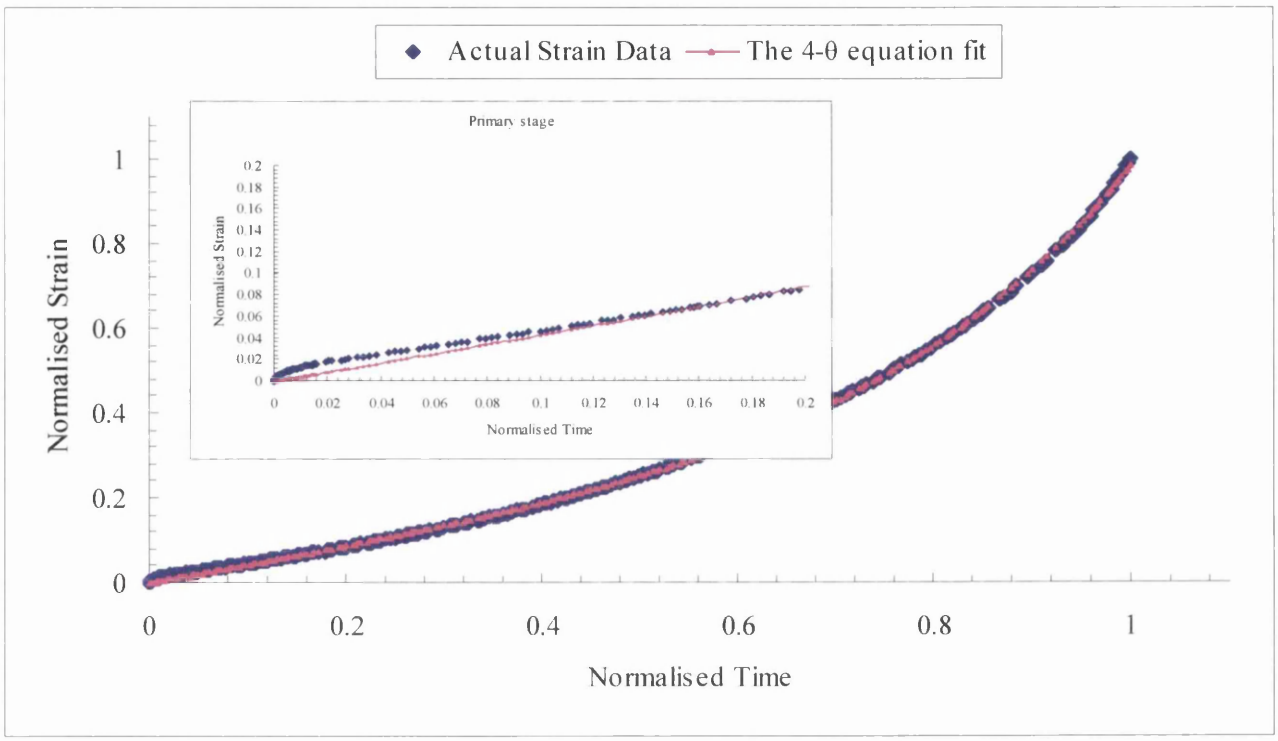

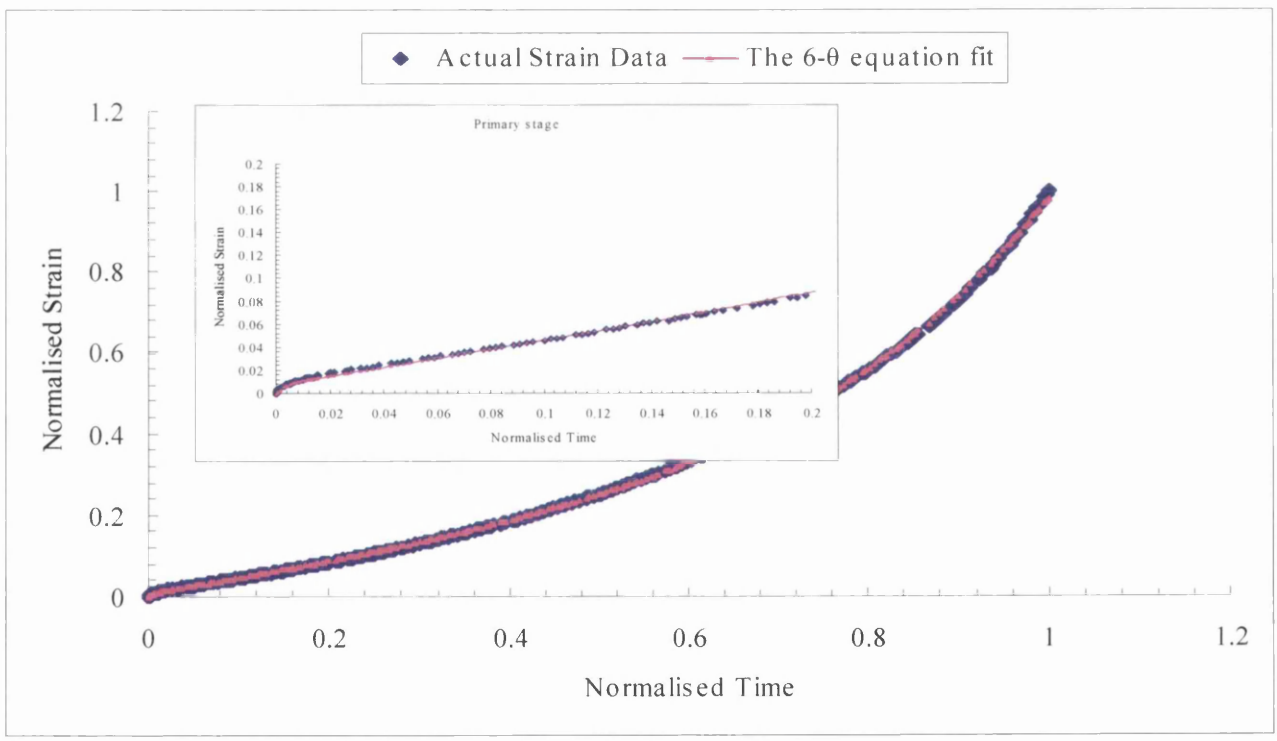

(B15.7): 848K/390MPa

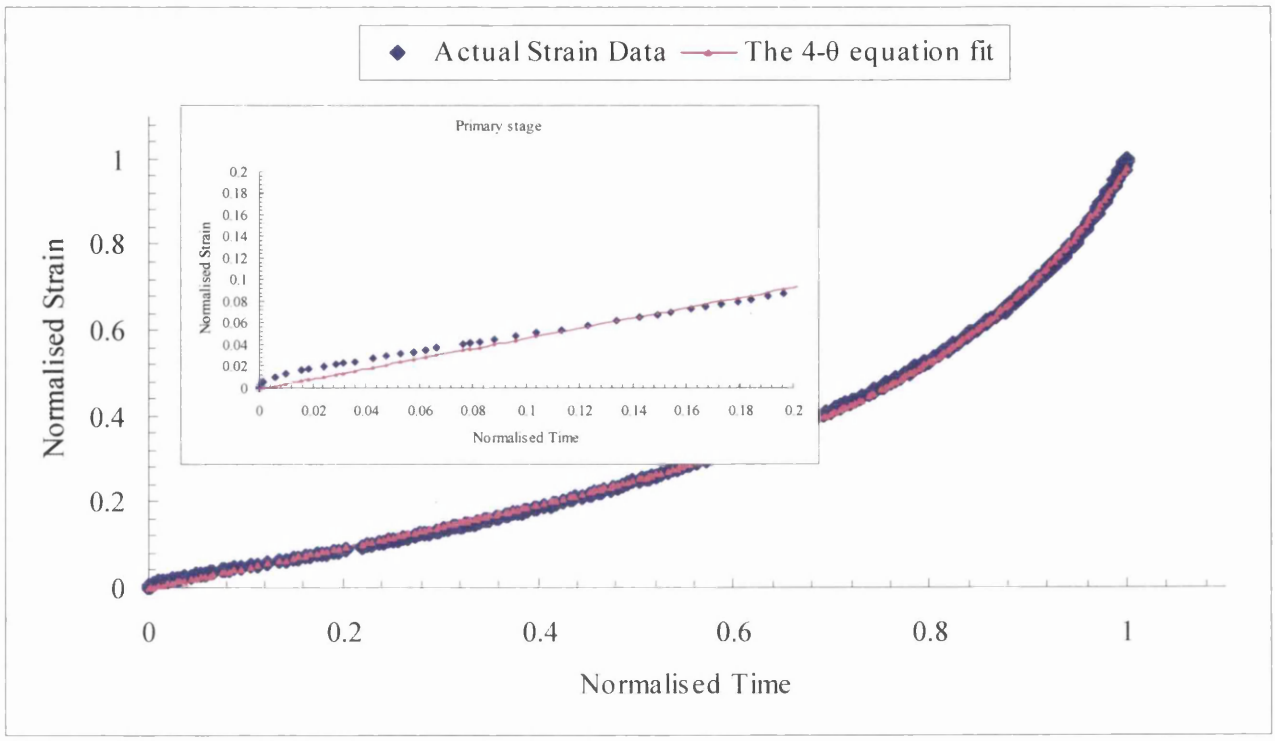

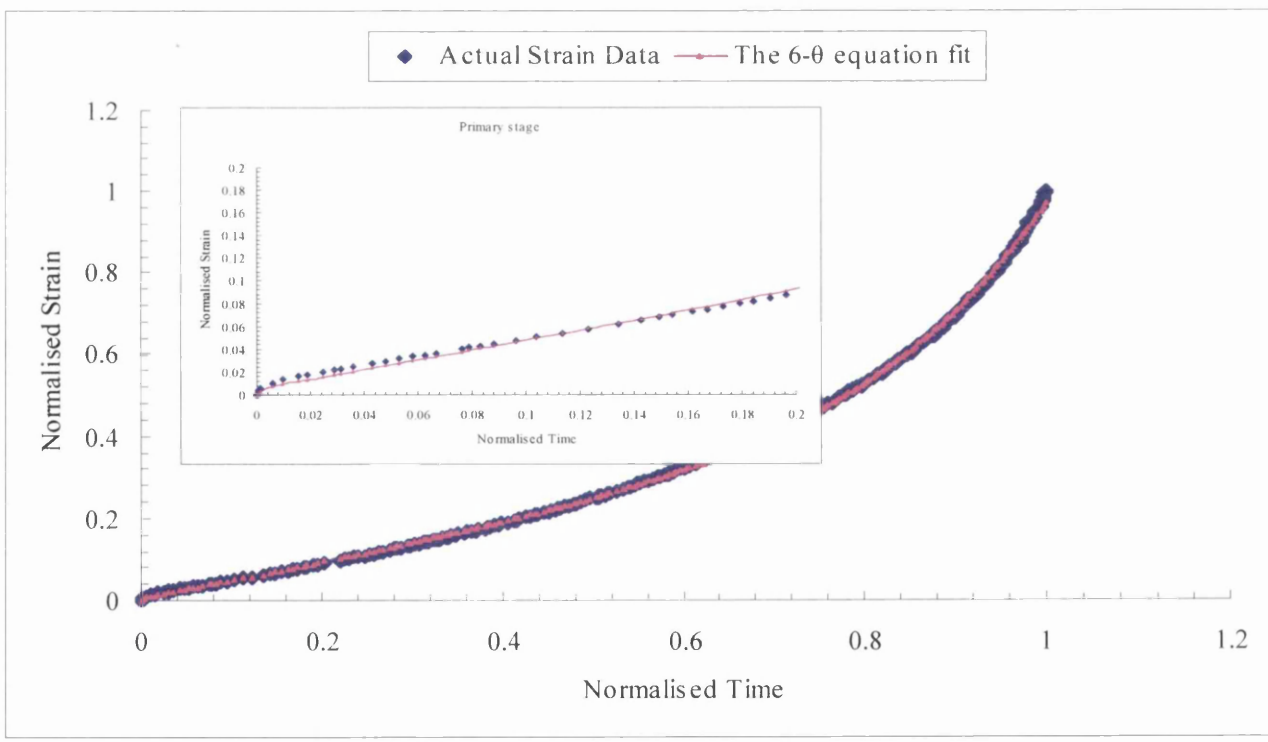

(B15.8): 848K/420MPa

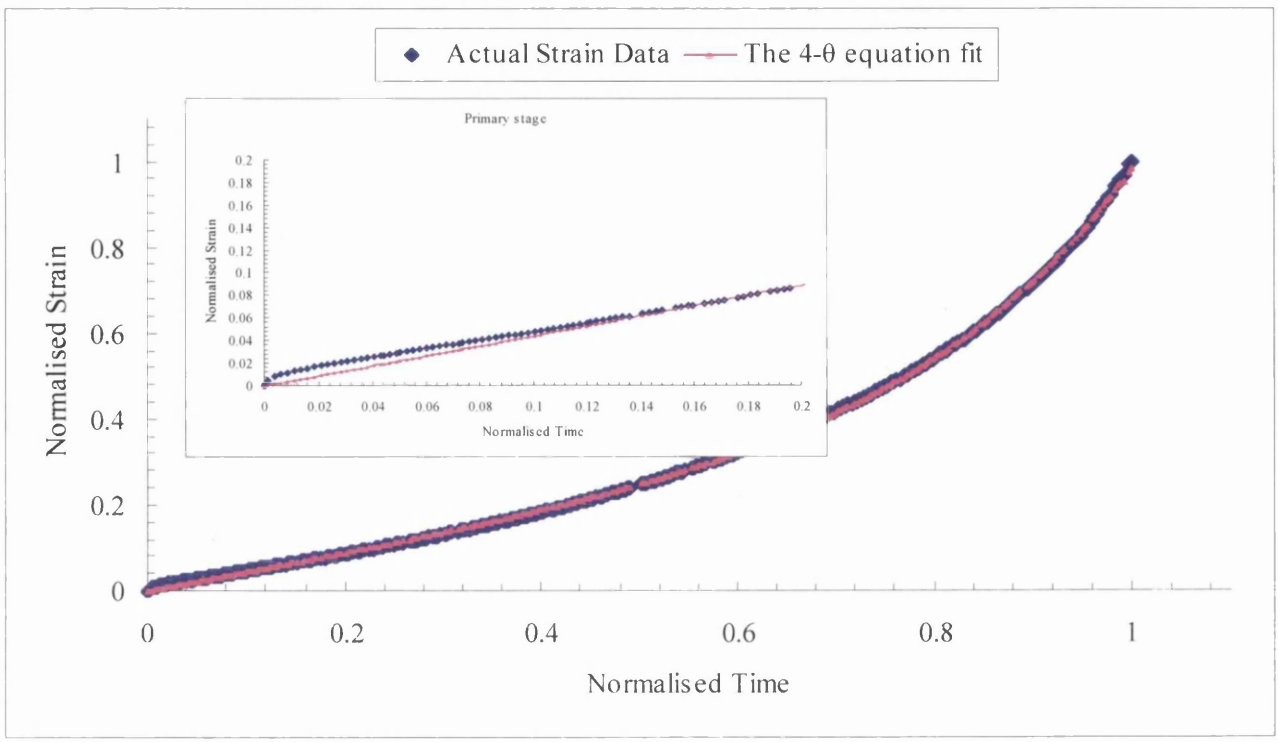

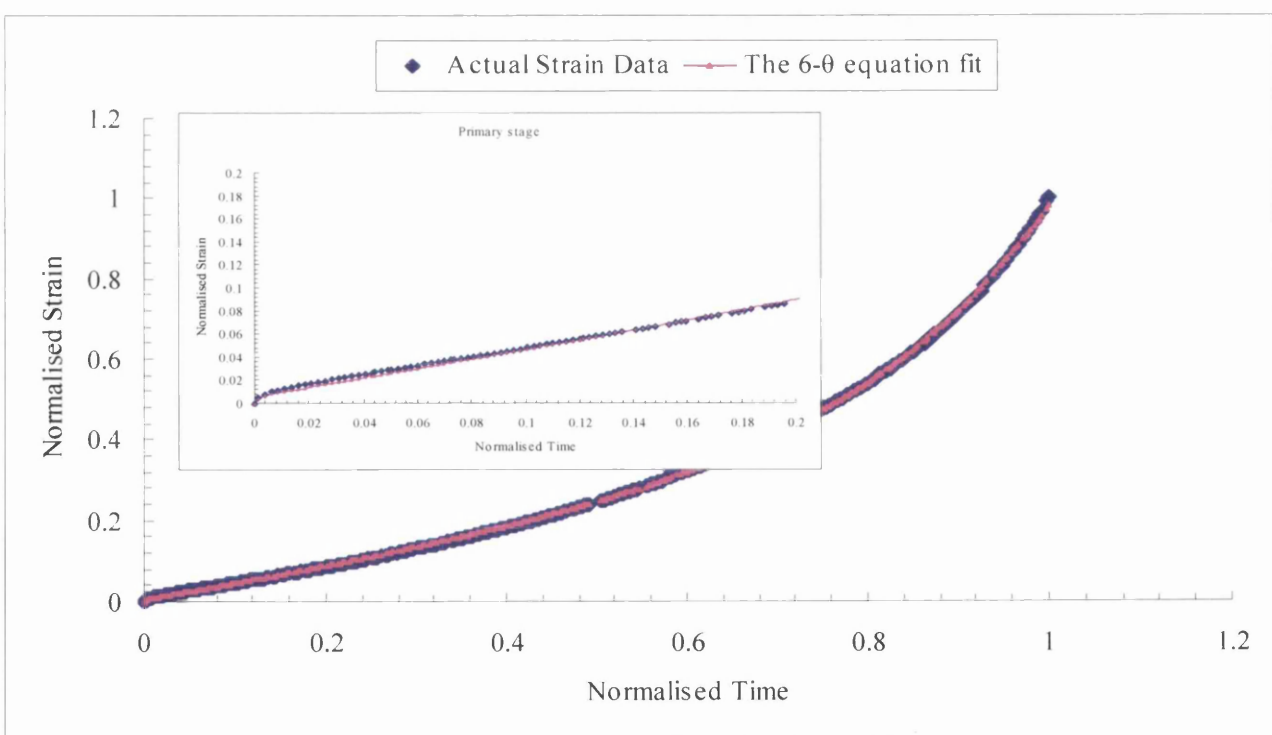

(B15.9): 848K/430MPa

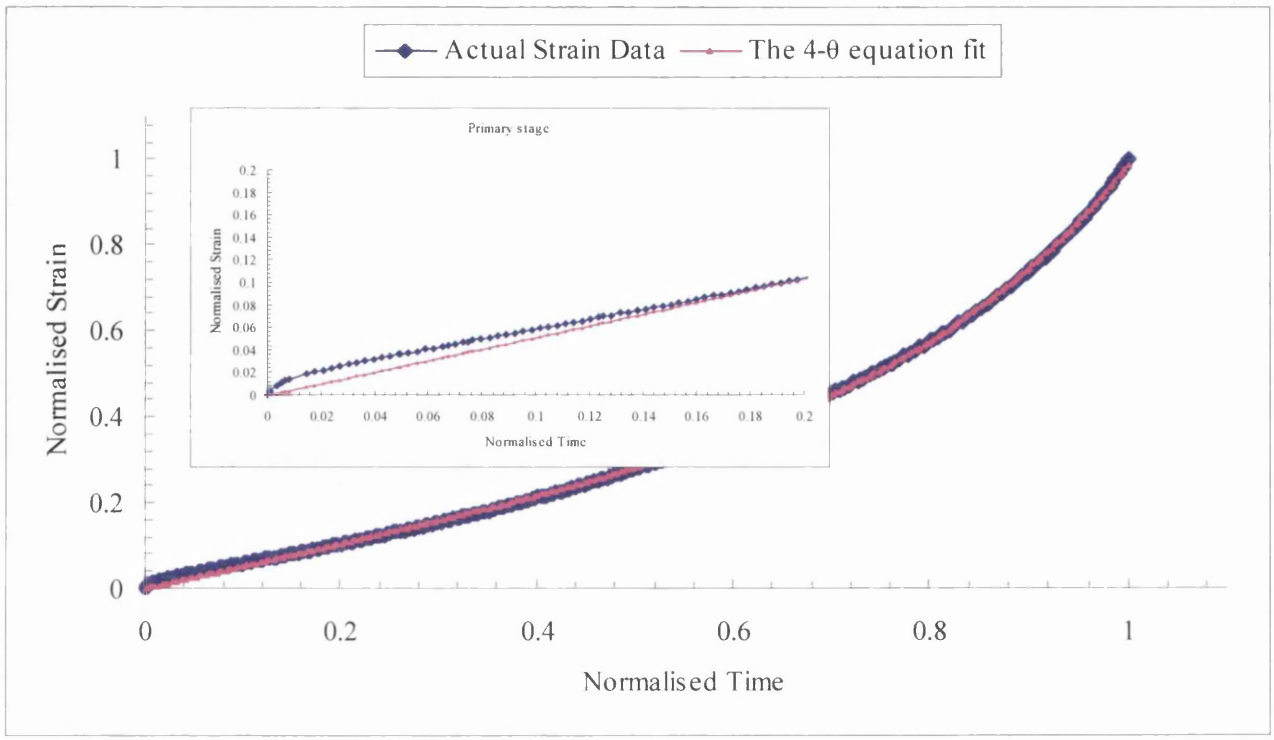

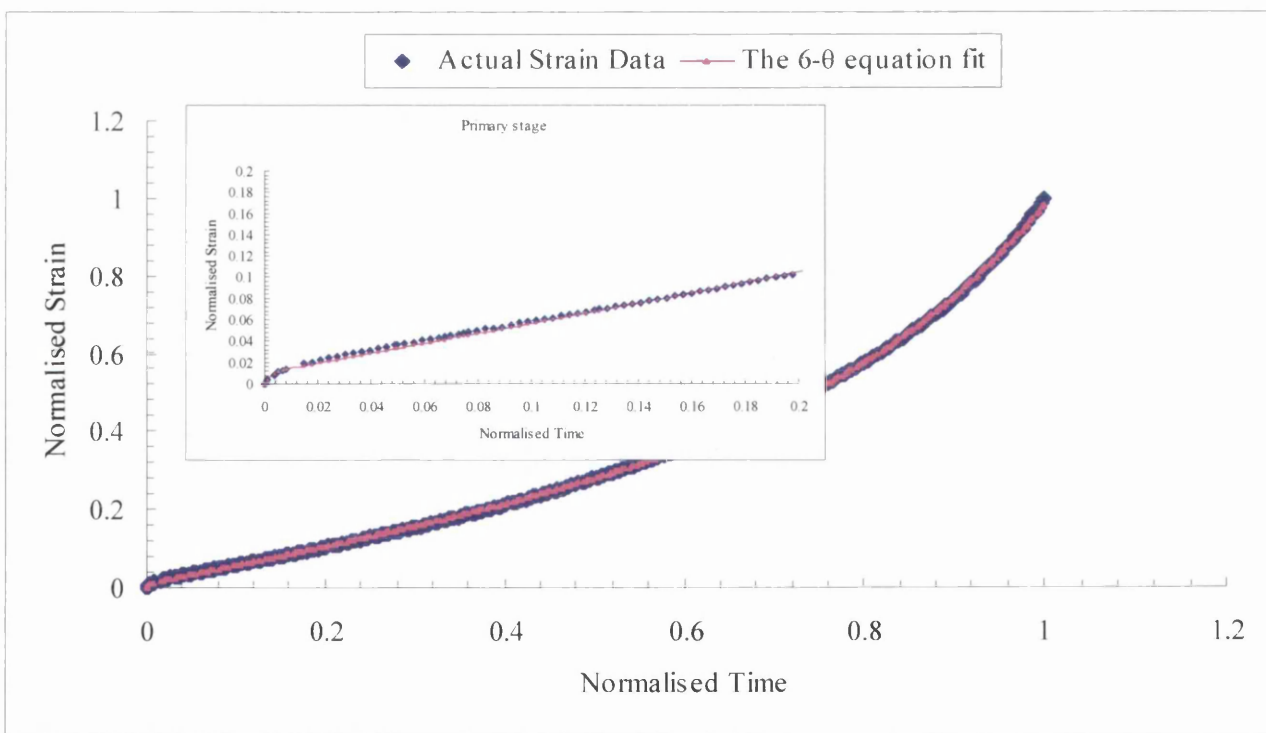

(B15.10): 848K/455MPa

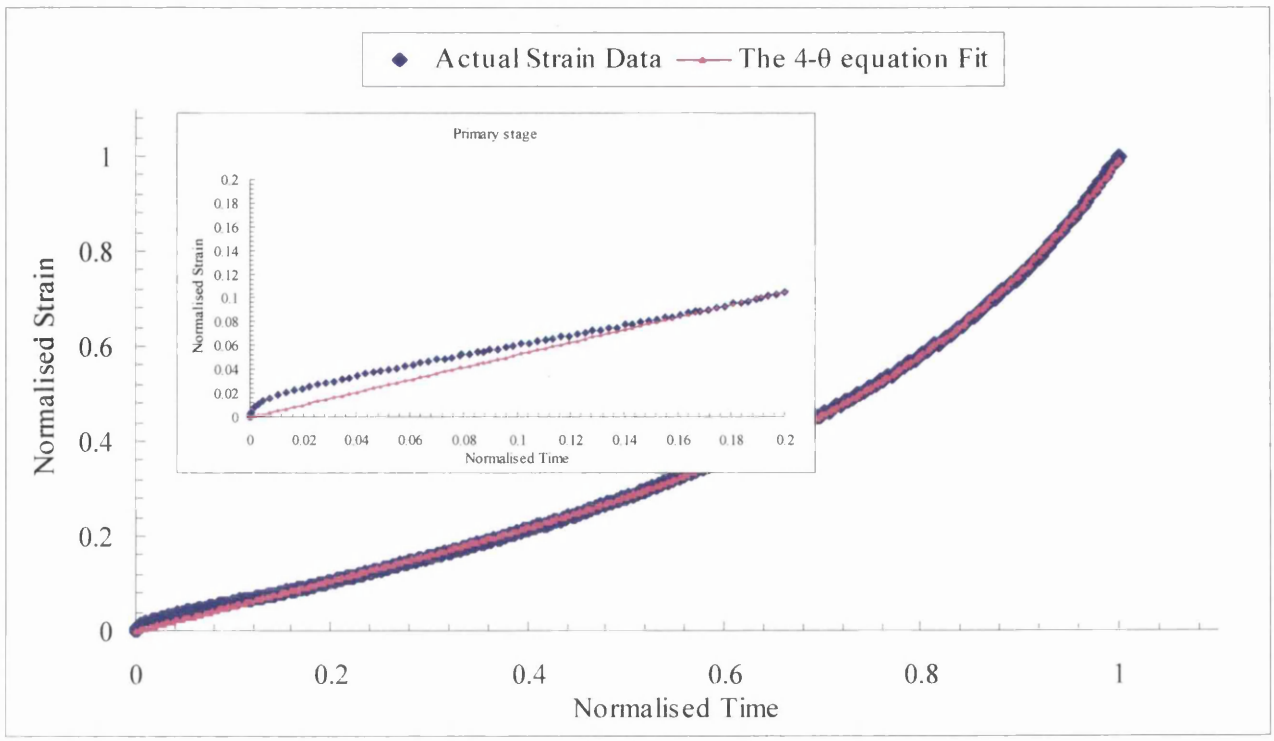

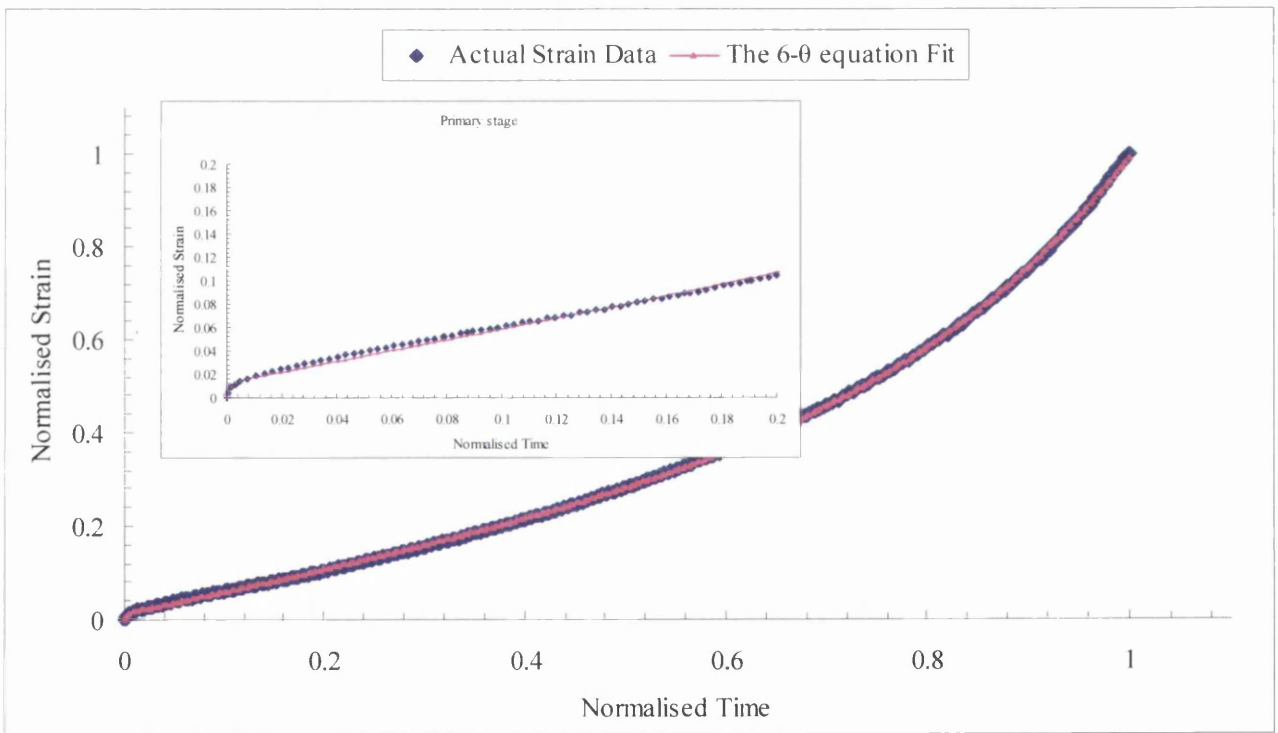

(B15.11): 848K/500MPa

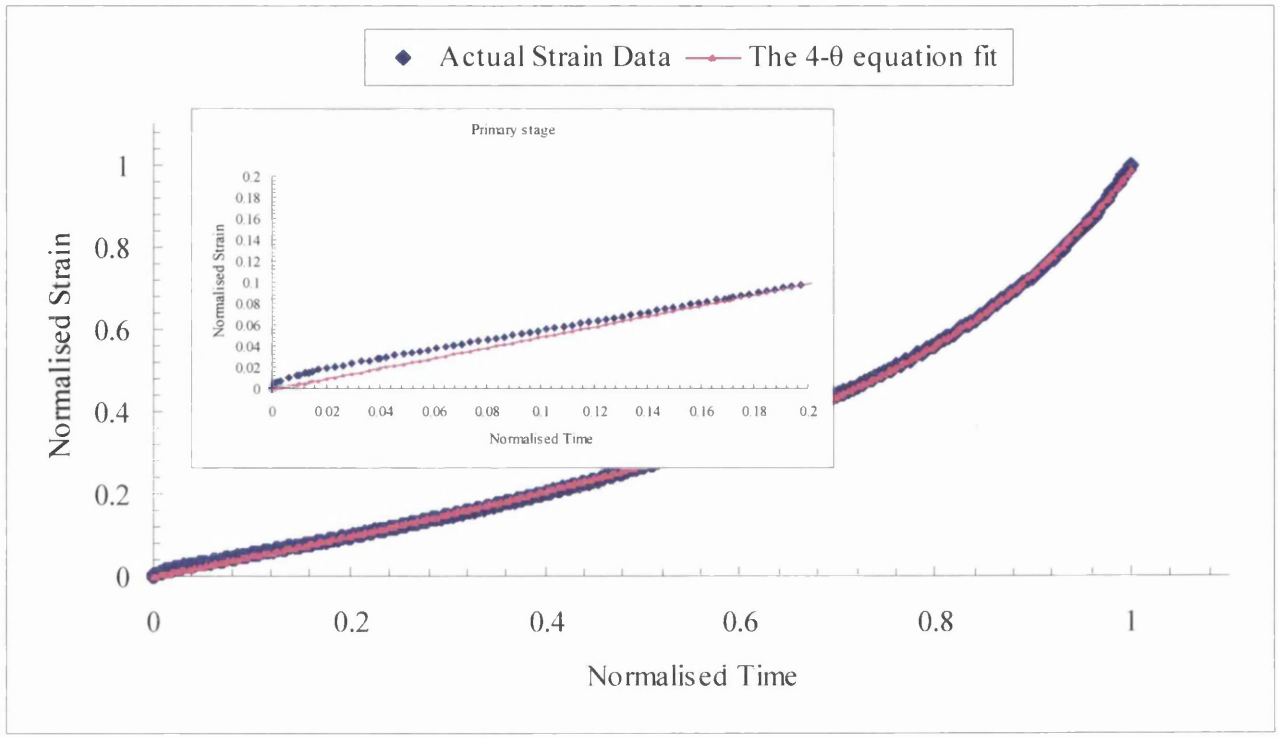

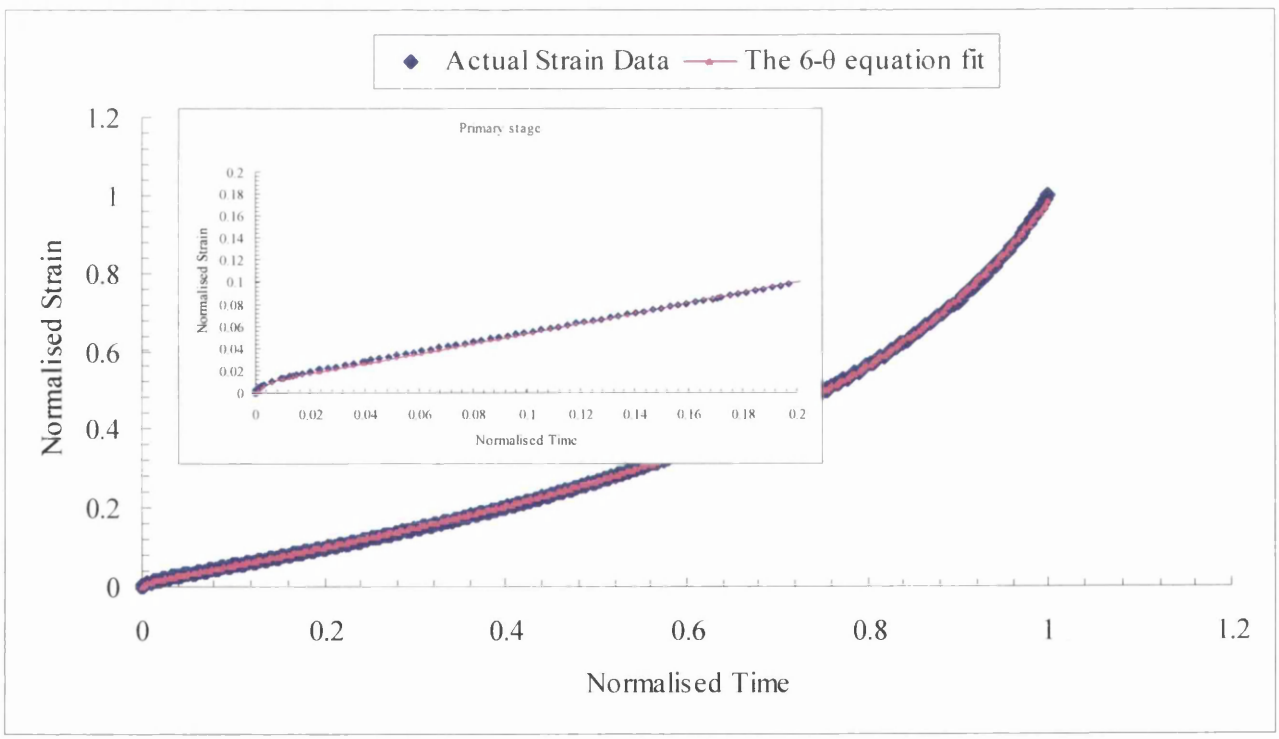

(B15.12): 848K/570MPa

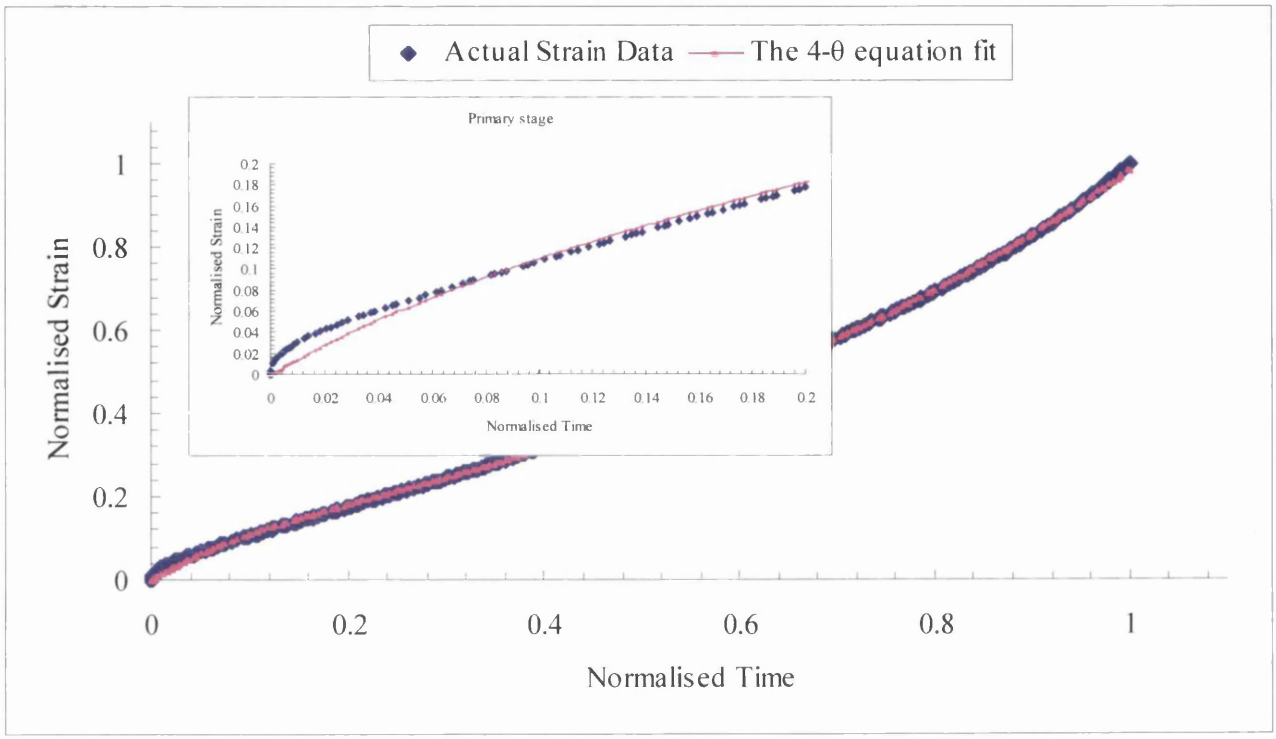

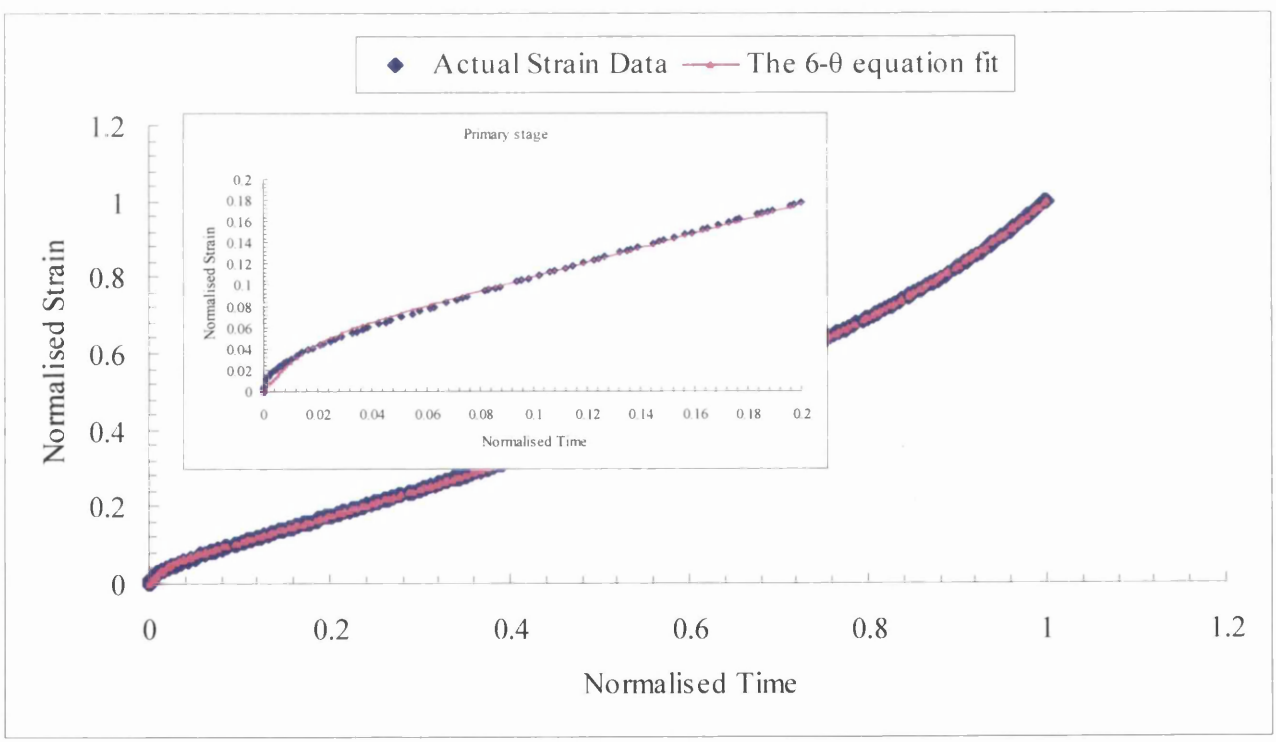

(B15.13): 873K/200MPa

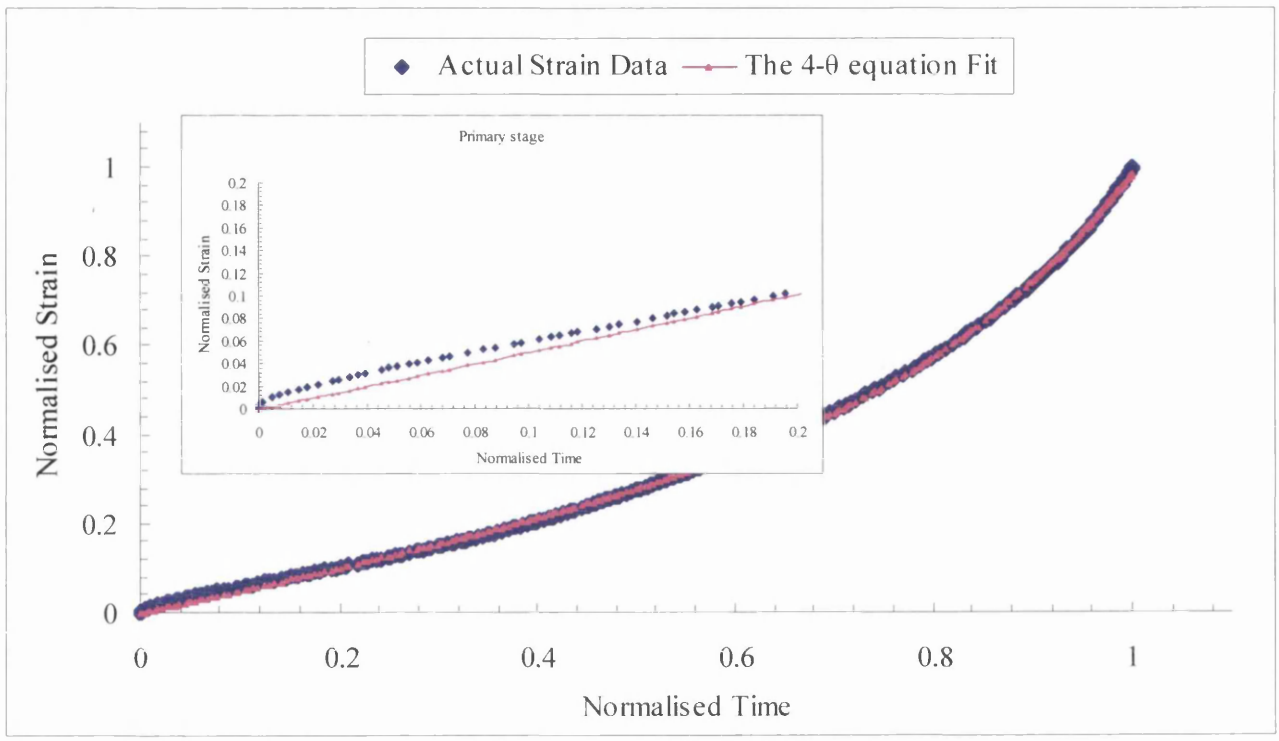

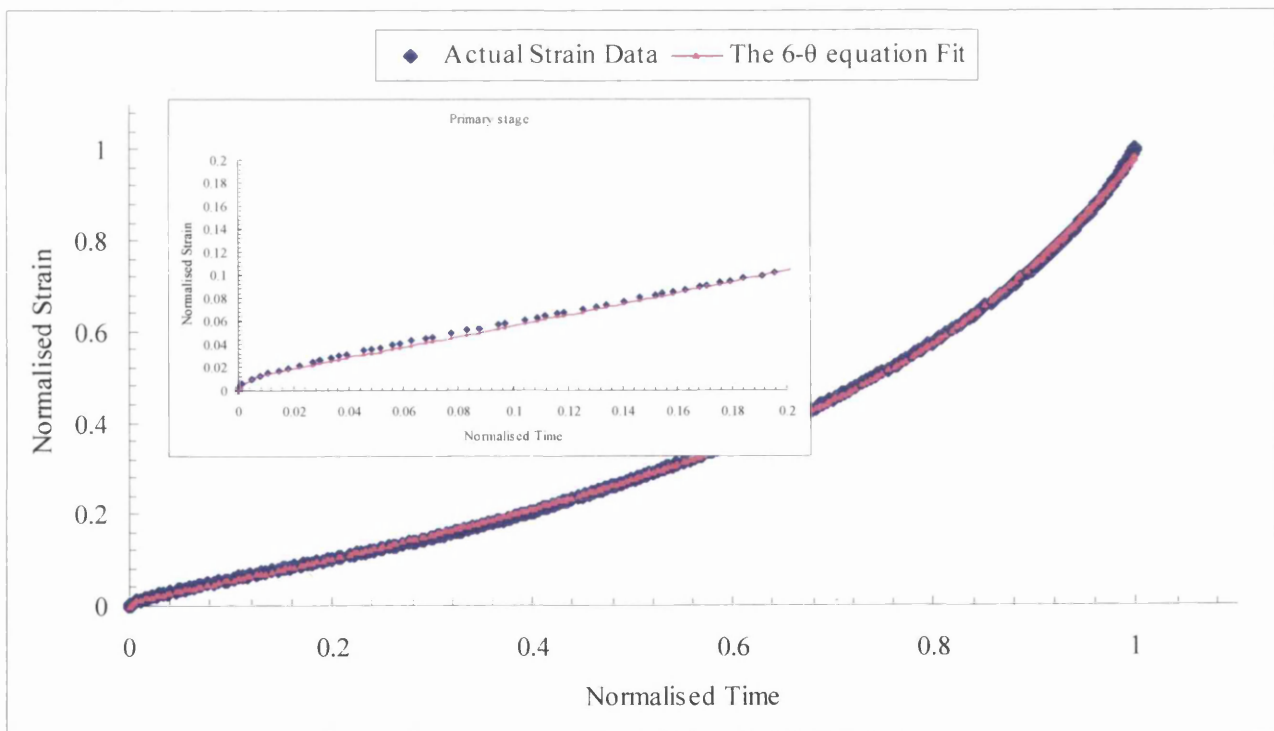

(B15.14): 873K/280MPa

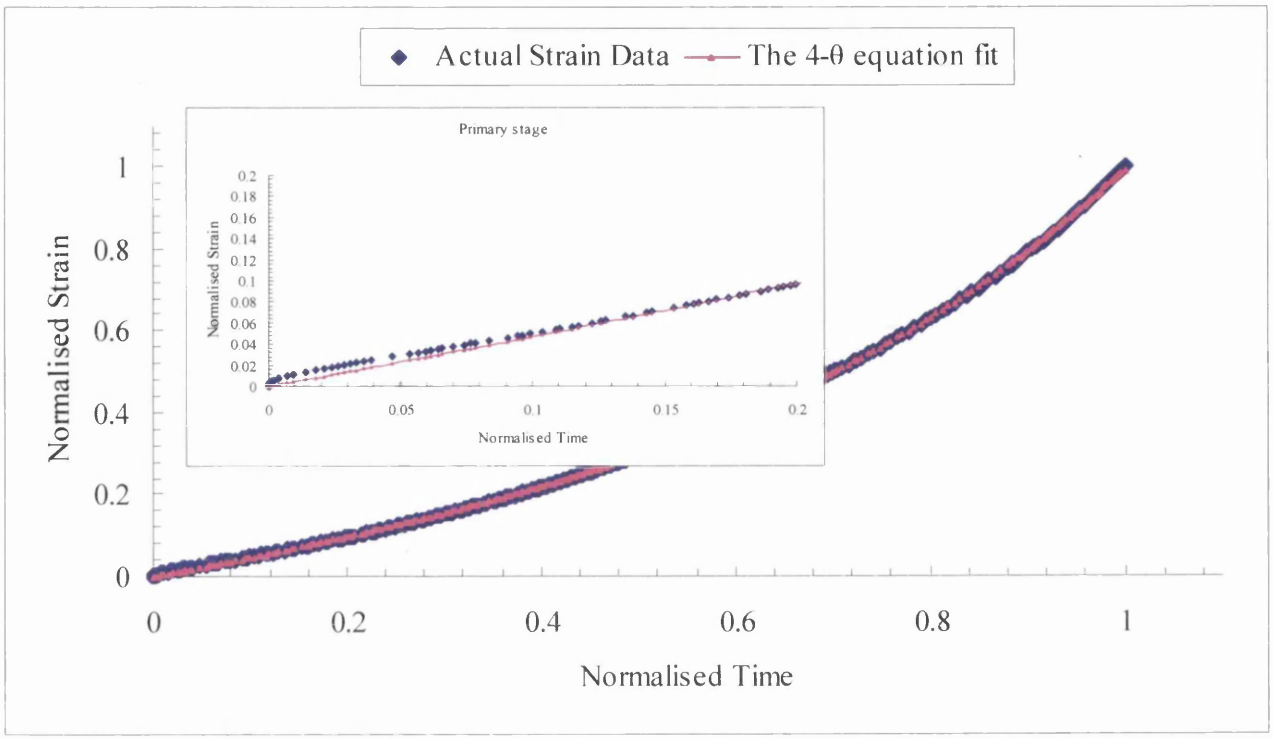

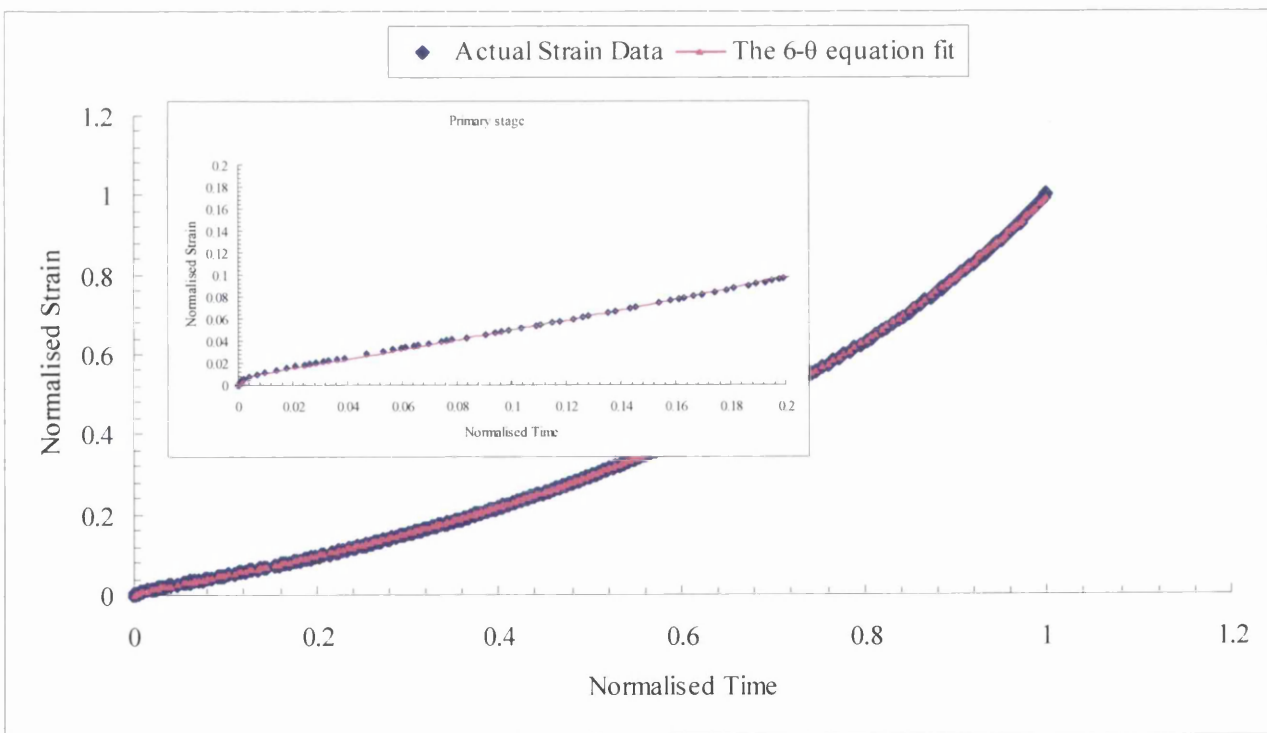

(B15.15): 873K/300MPa

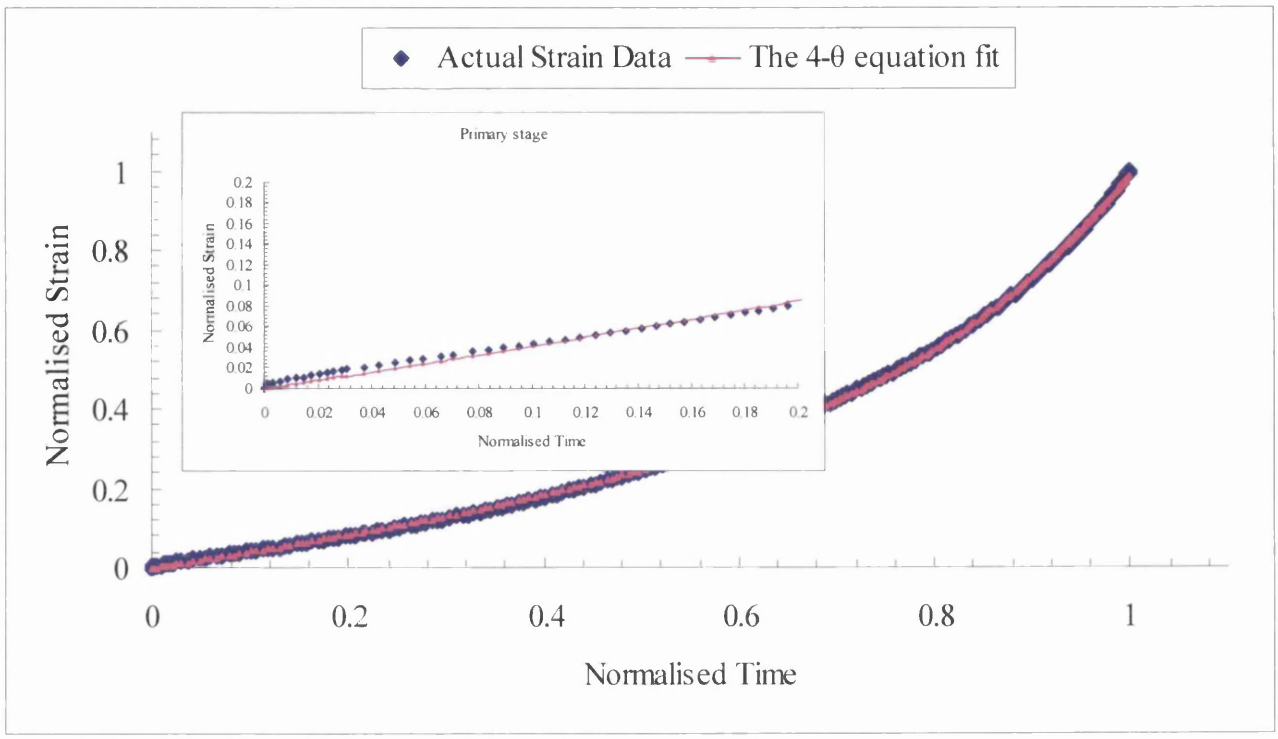

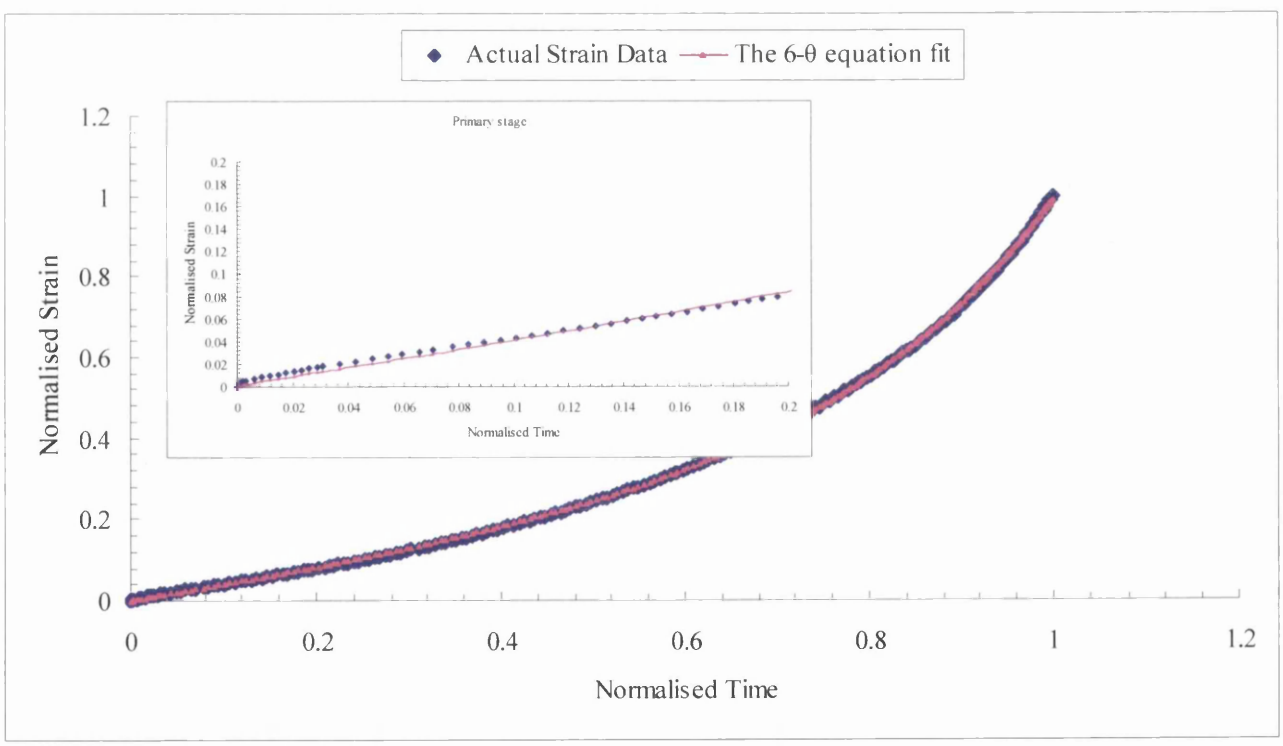

(B15.16): 873K/350MPa

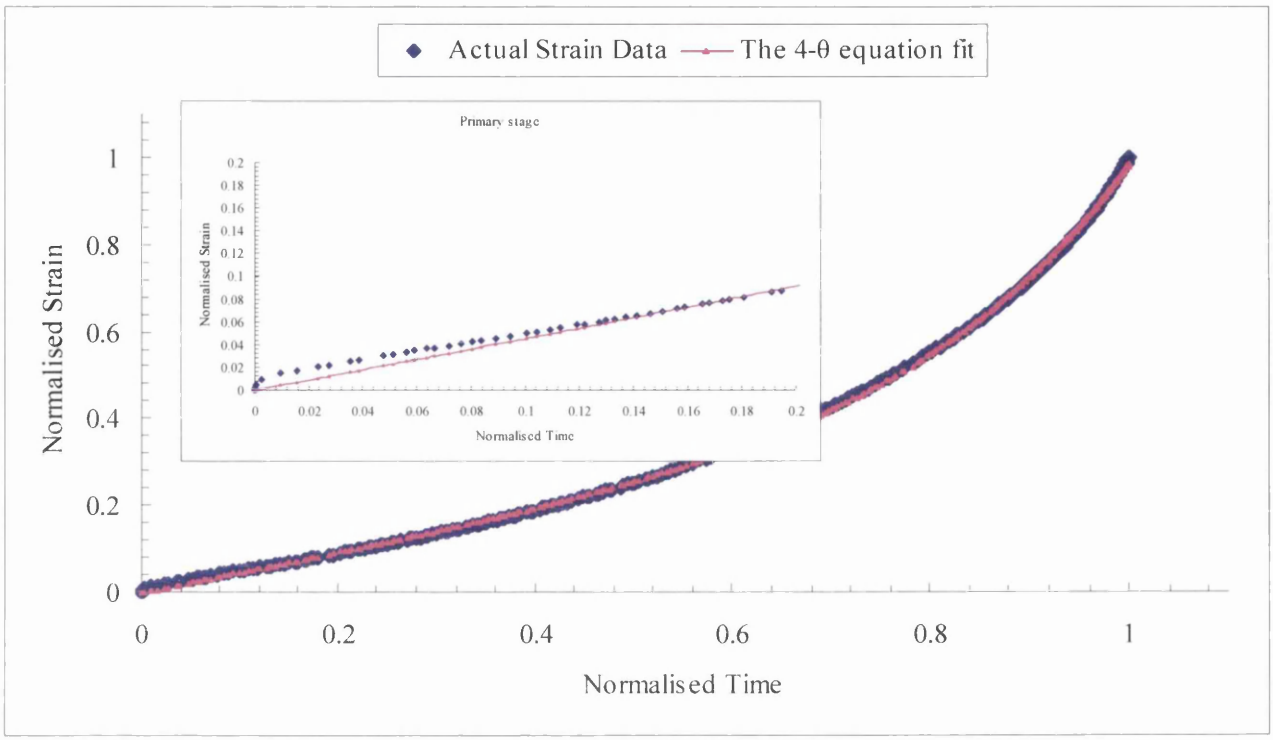

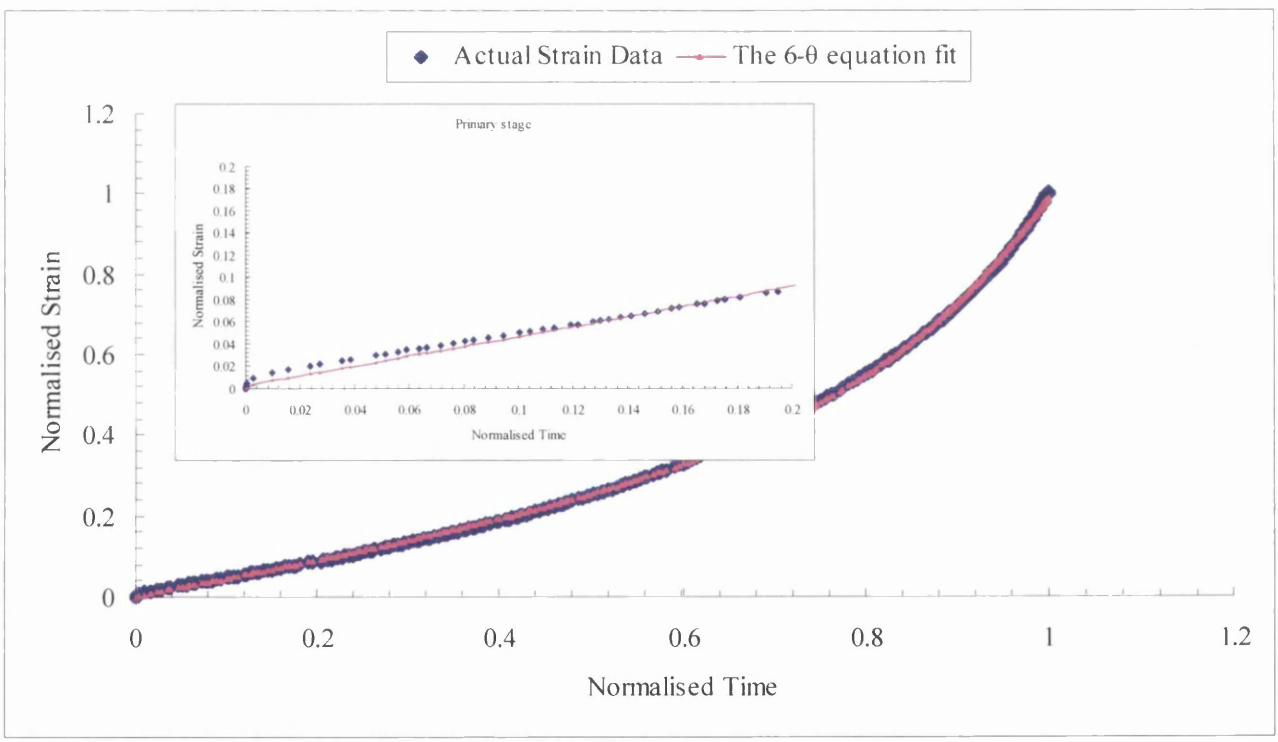

(B15.17): 873K/360MPa

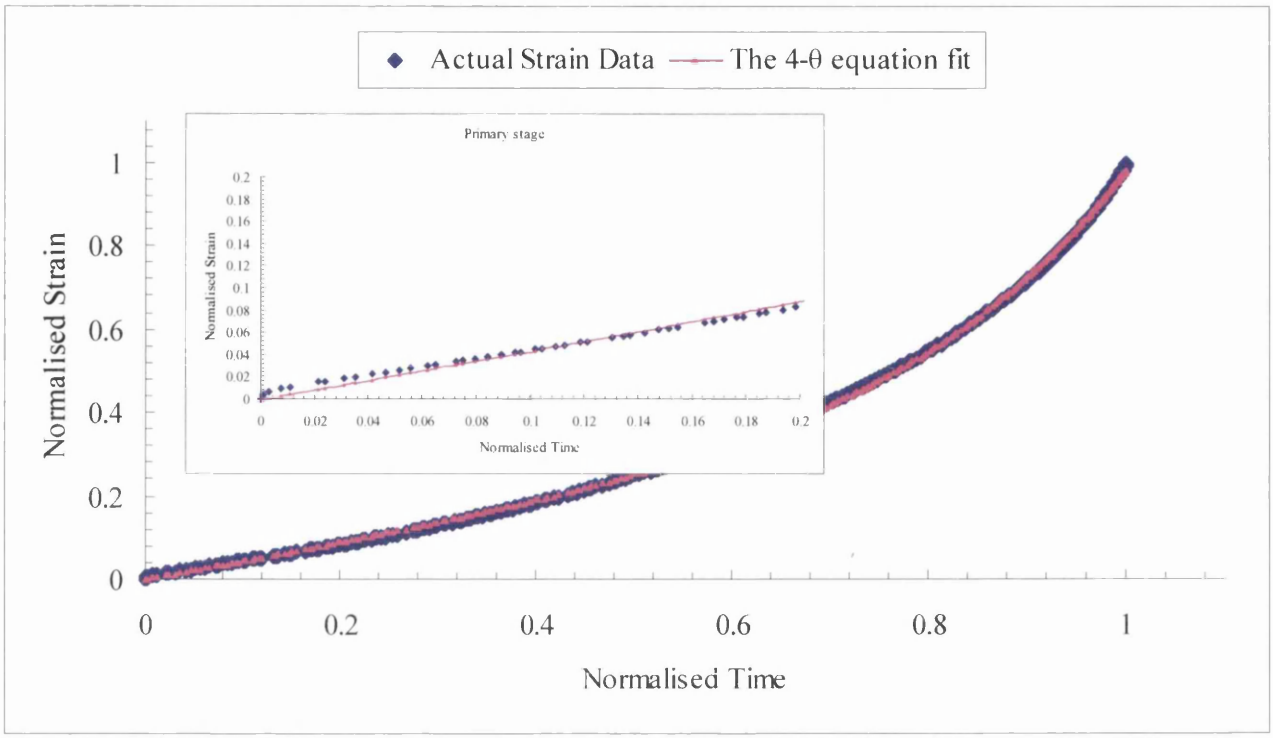

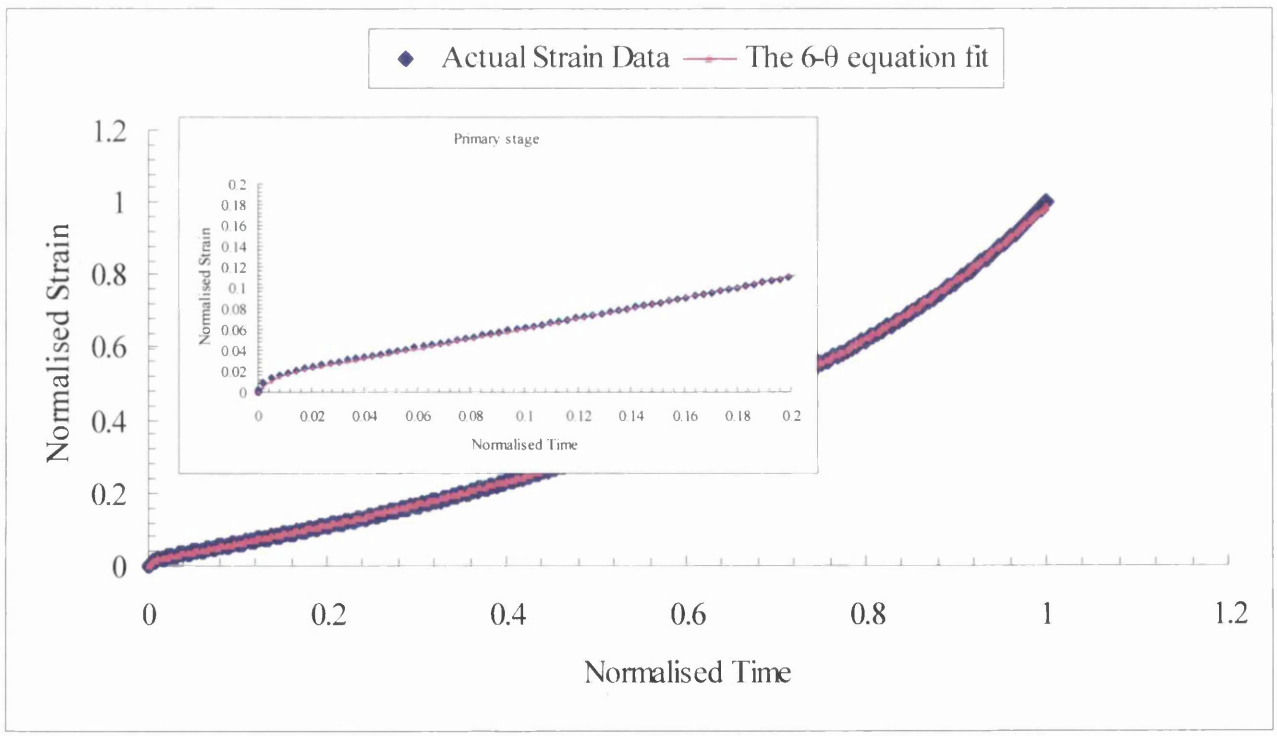

(B15.18): 873K/480MPa

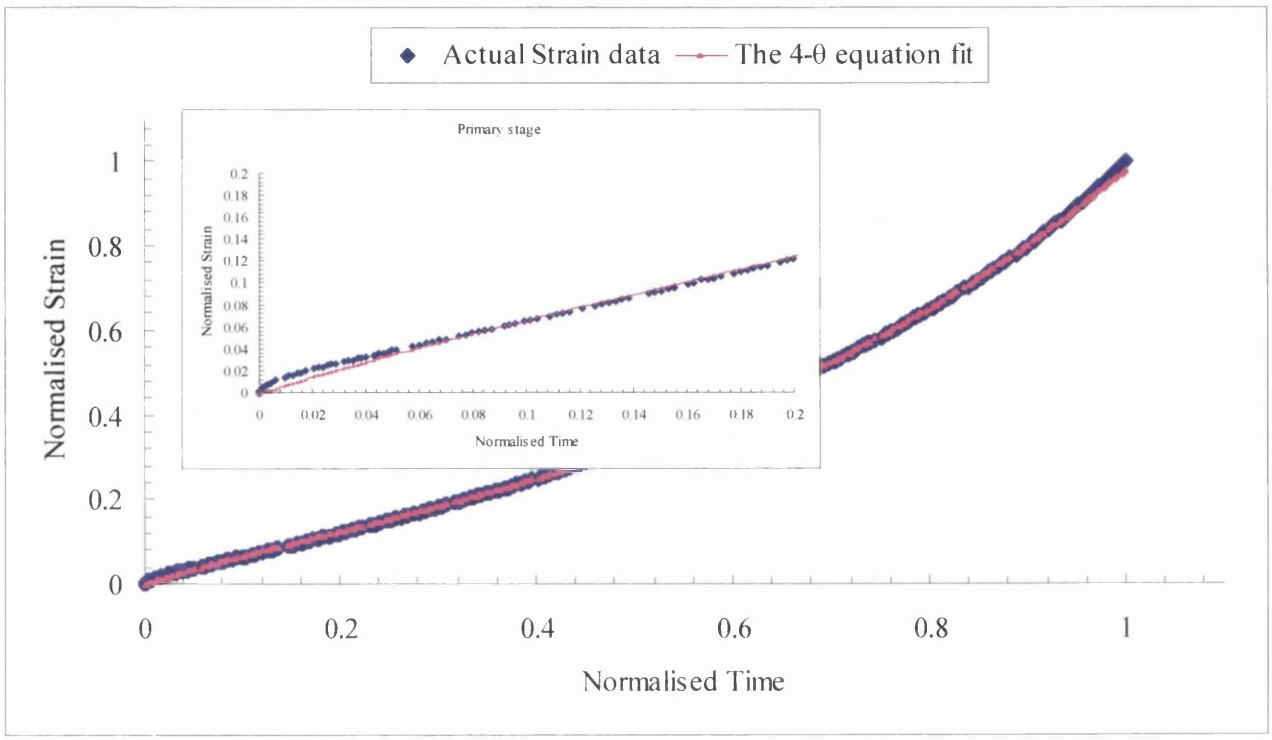

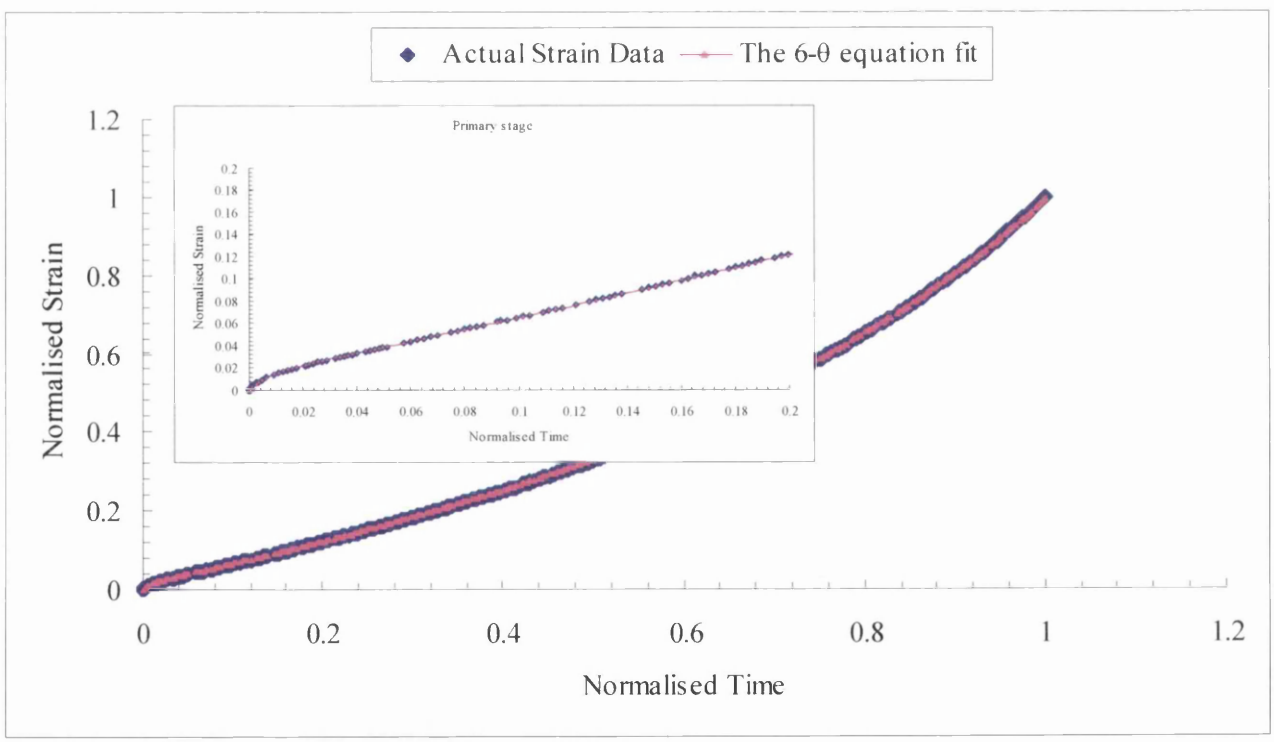

(B15.19): 873K/550MPa

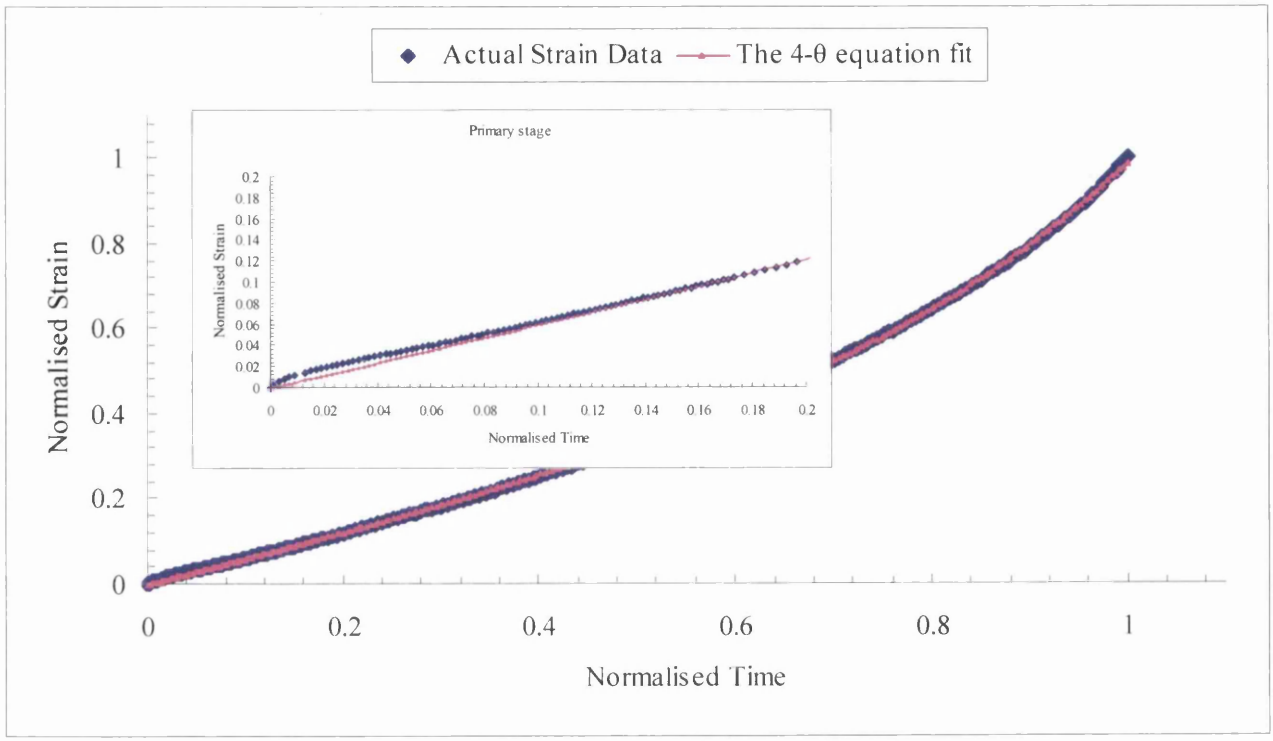

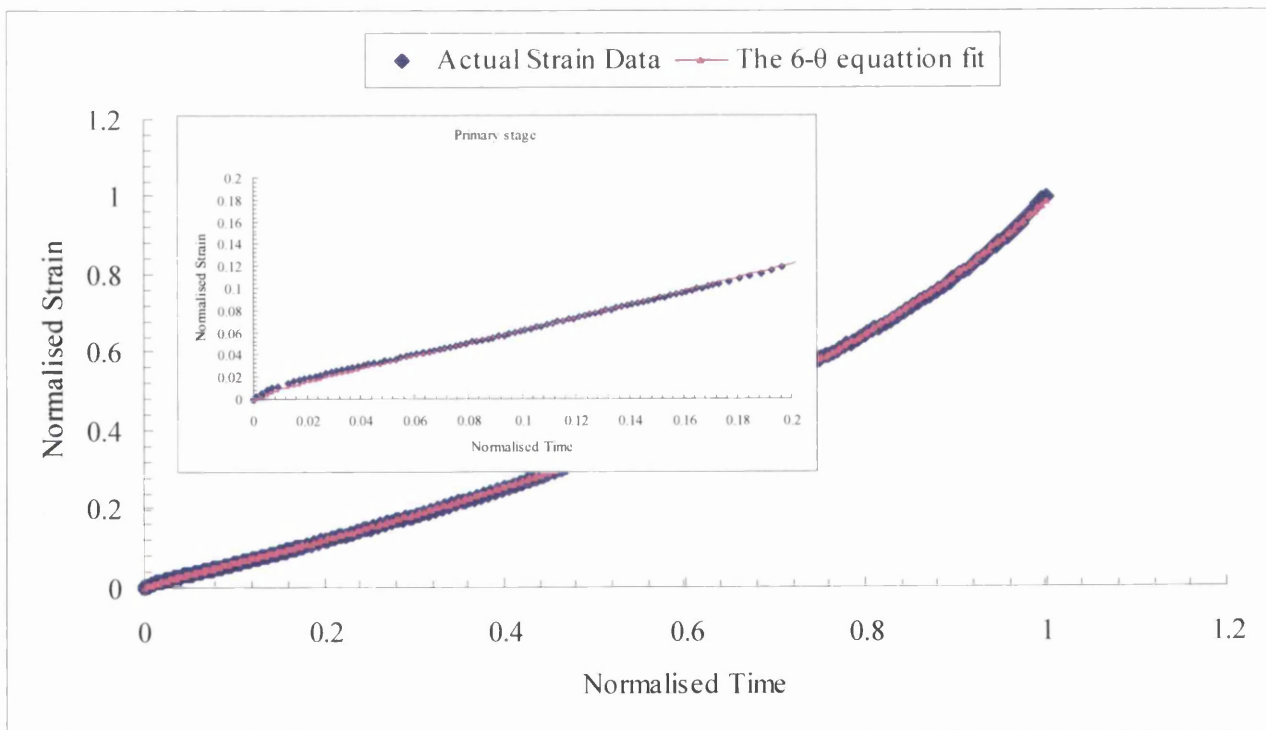

(B15.20): 898K/175MPa

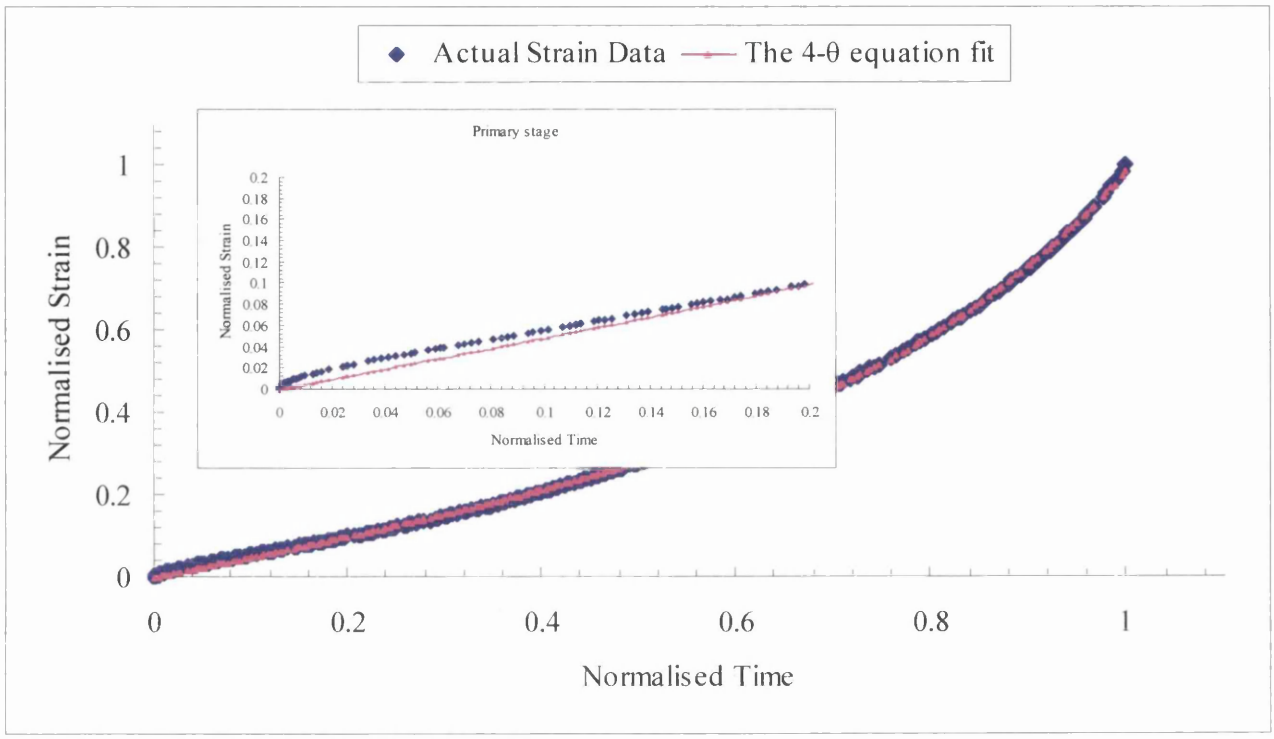

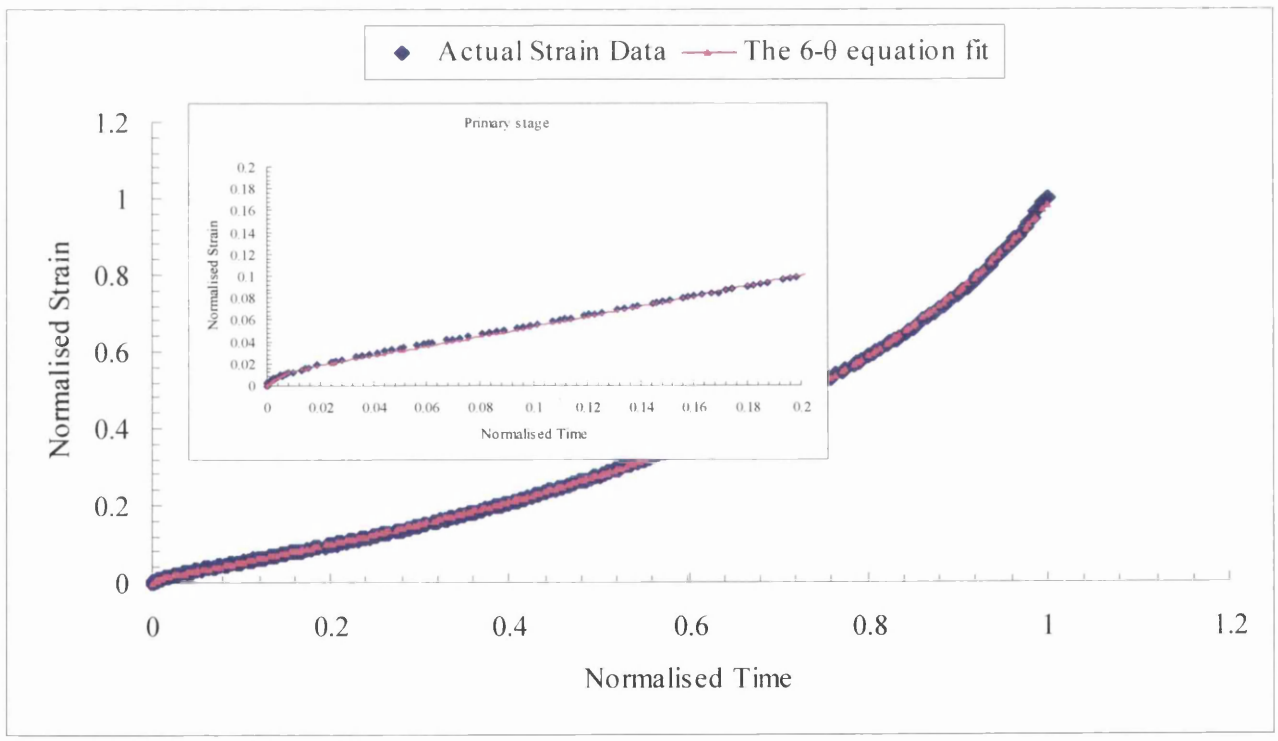

(B15.21): 898K/220MPa

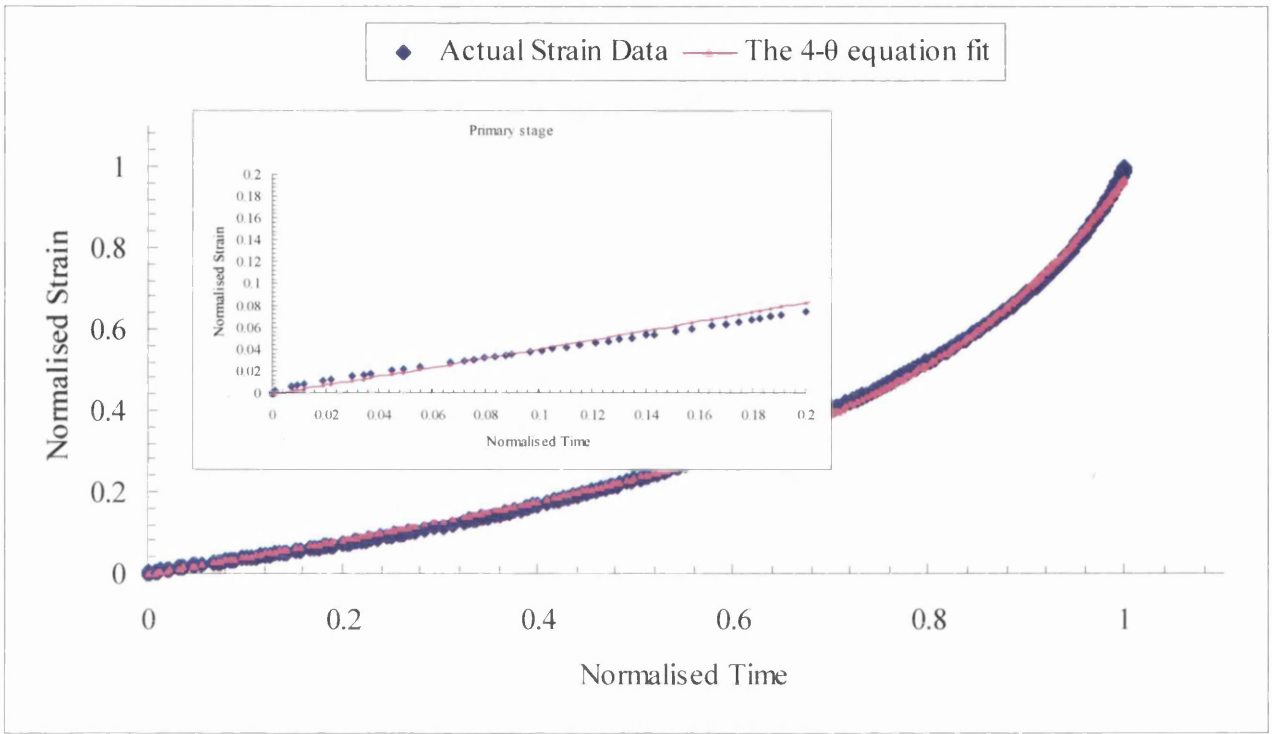

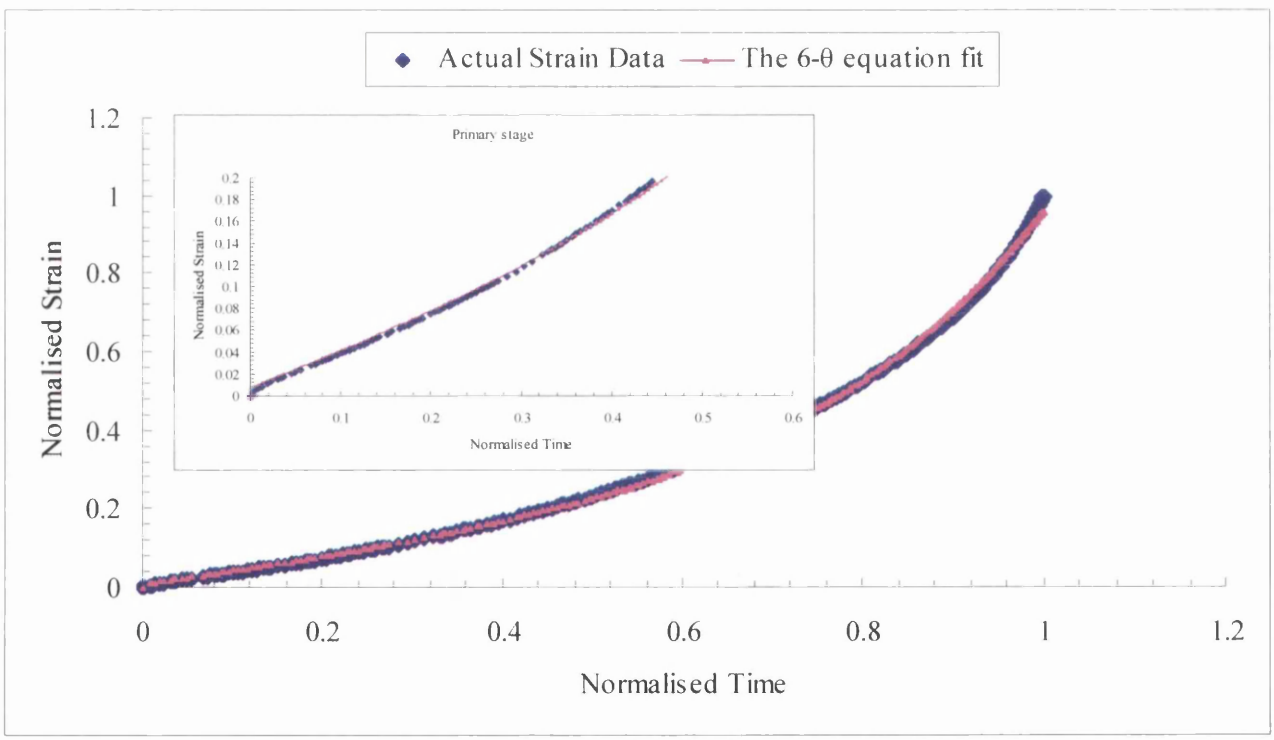

(B15.22): 898K/250MPa

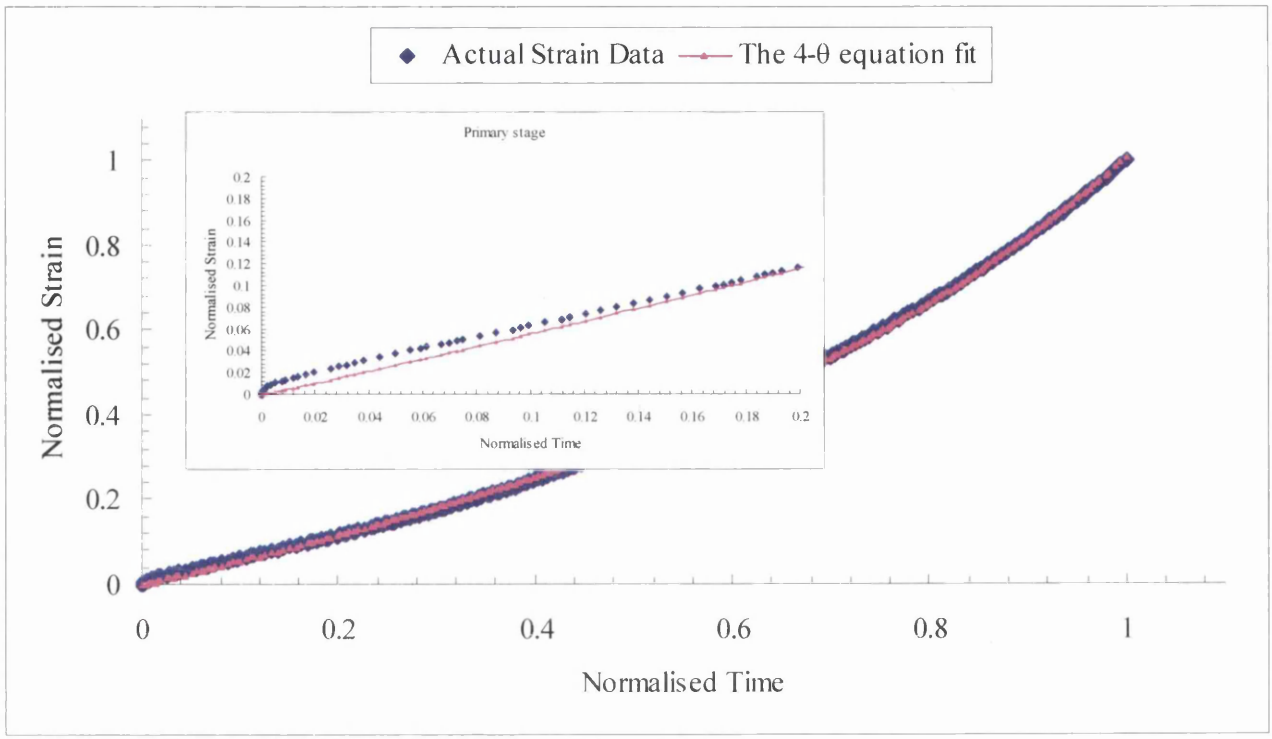

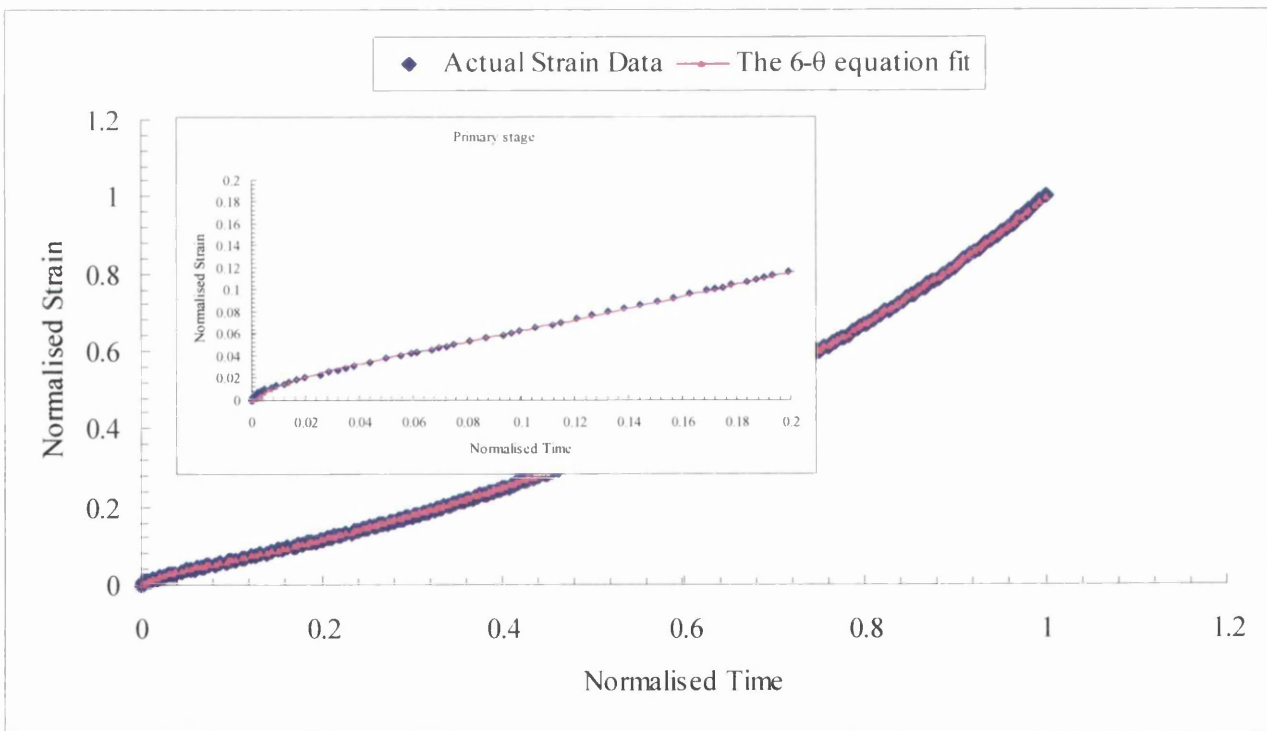

(B15.23): 898K/280MPa

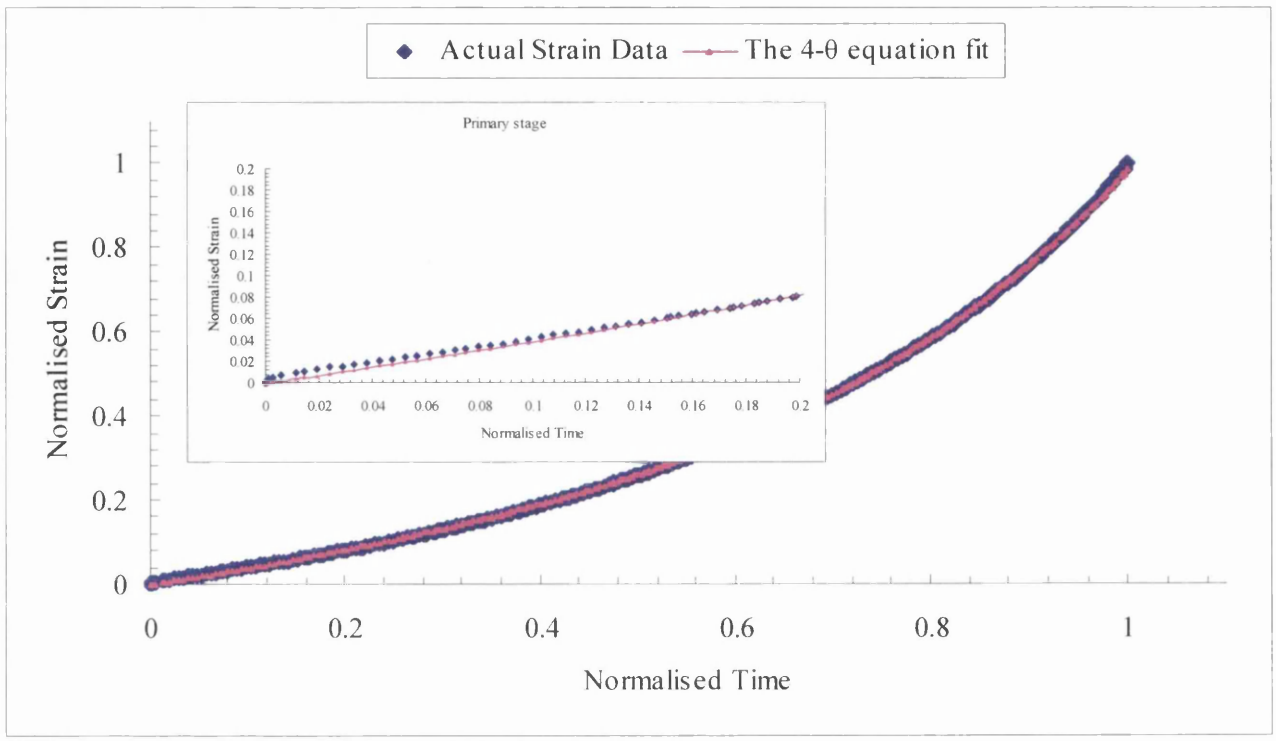

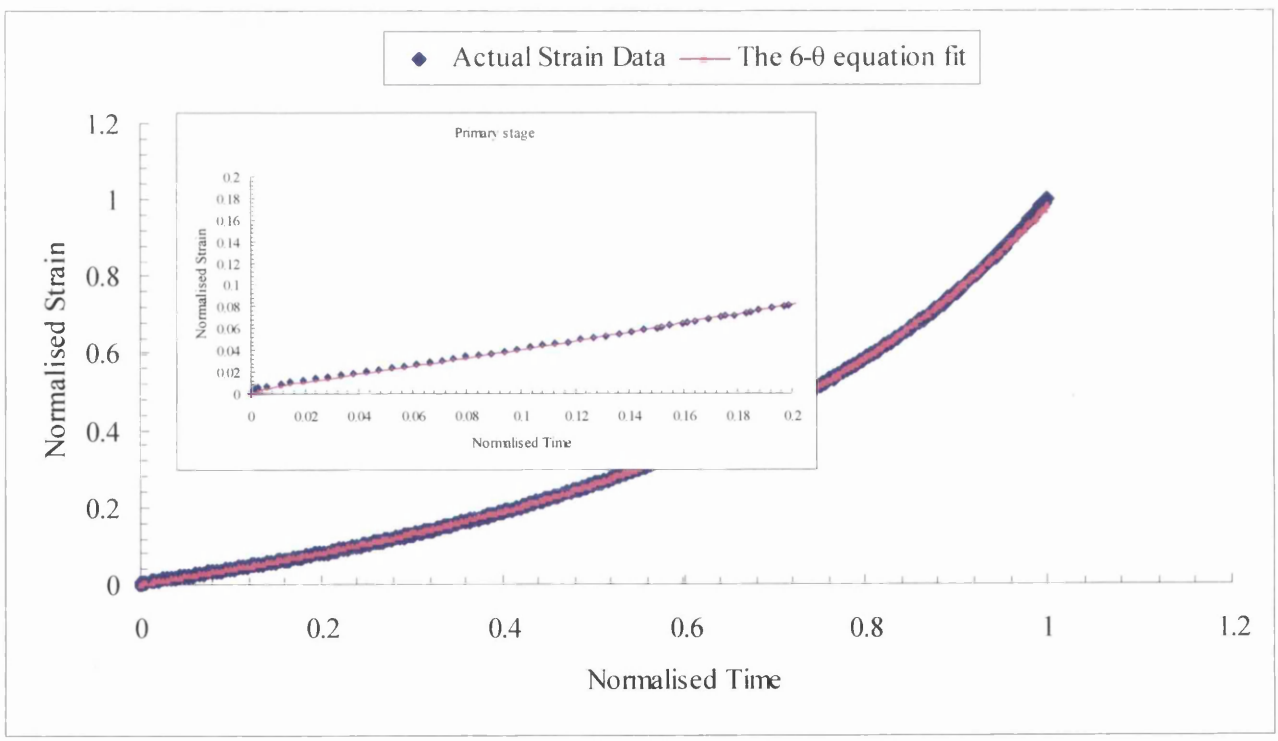

(B15.24): 898K/300MPa

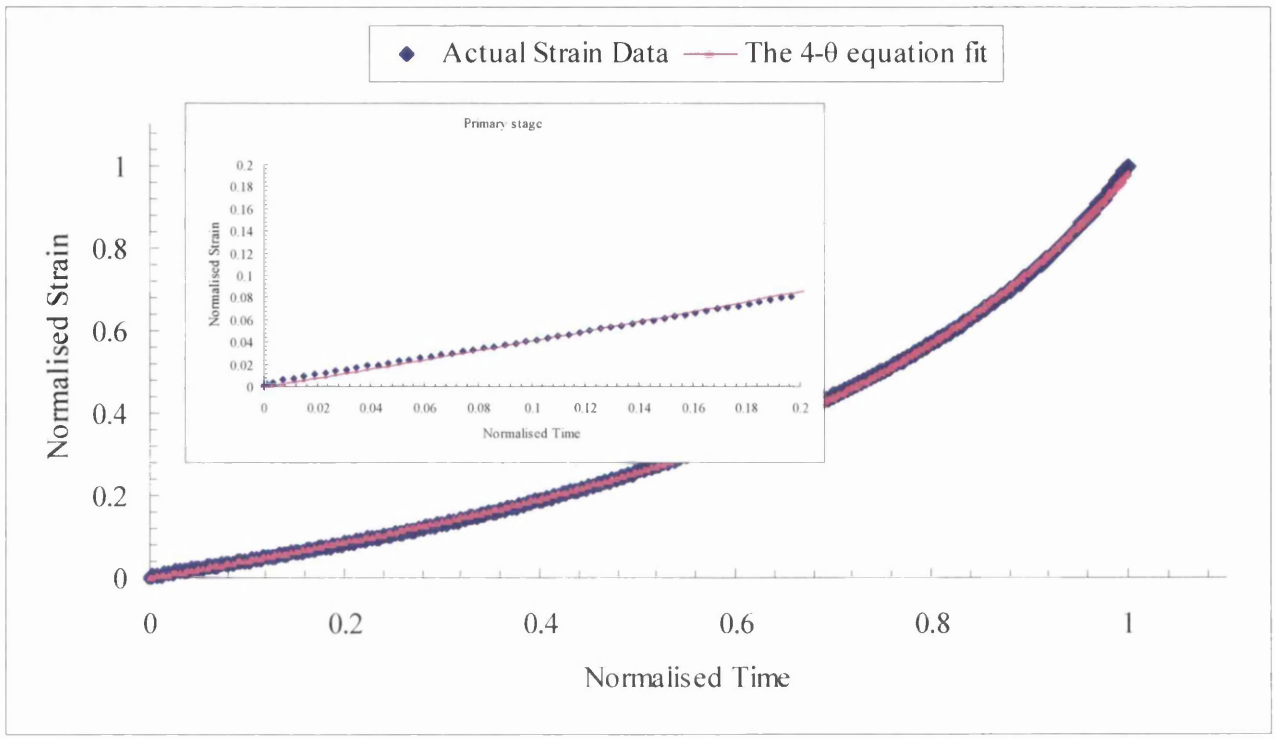

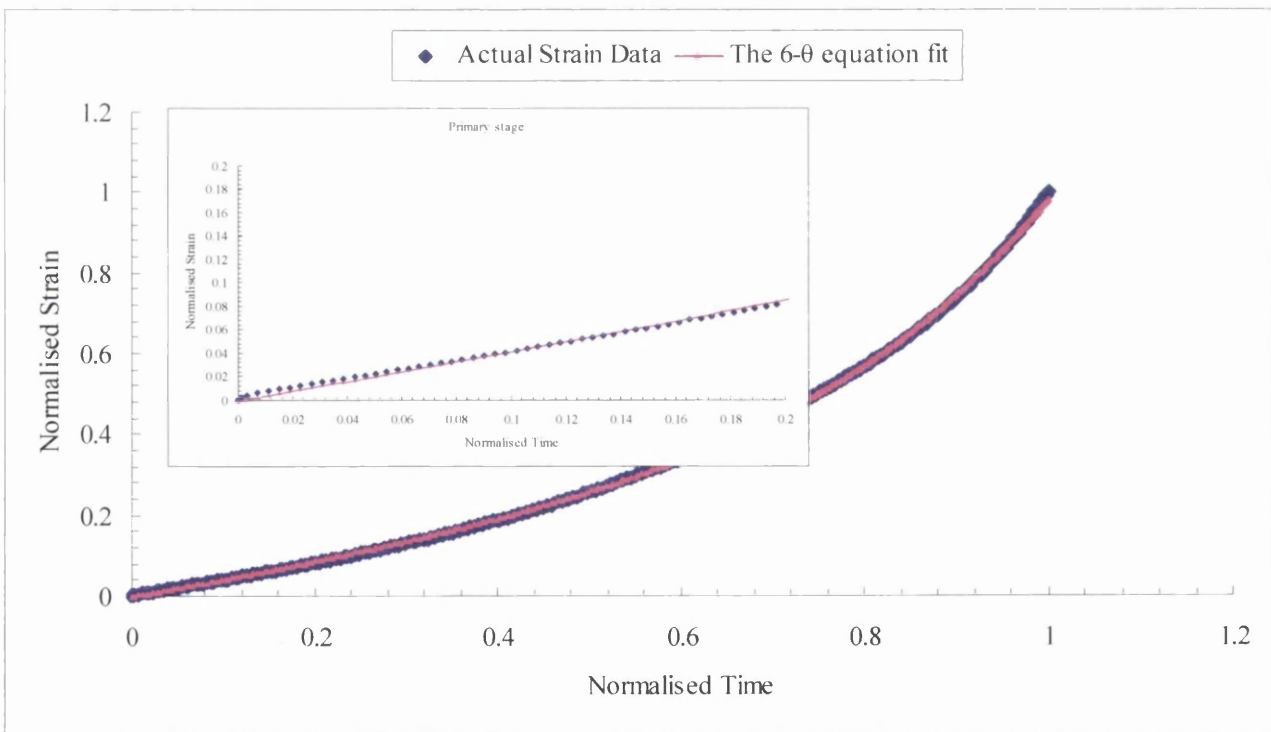

(B15.25): 898K/400MPa

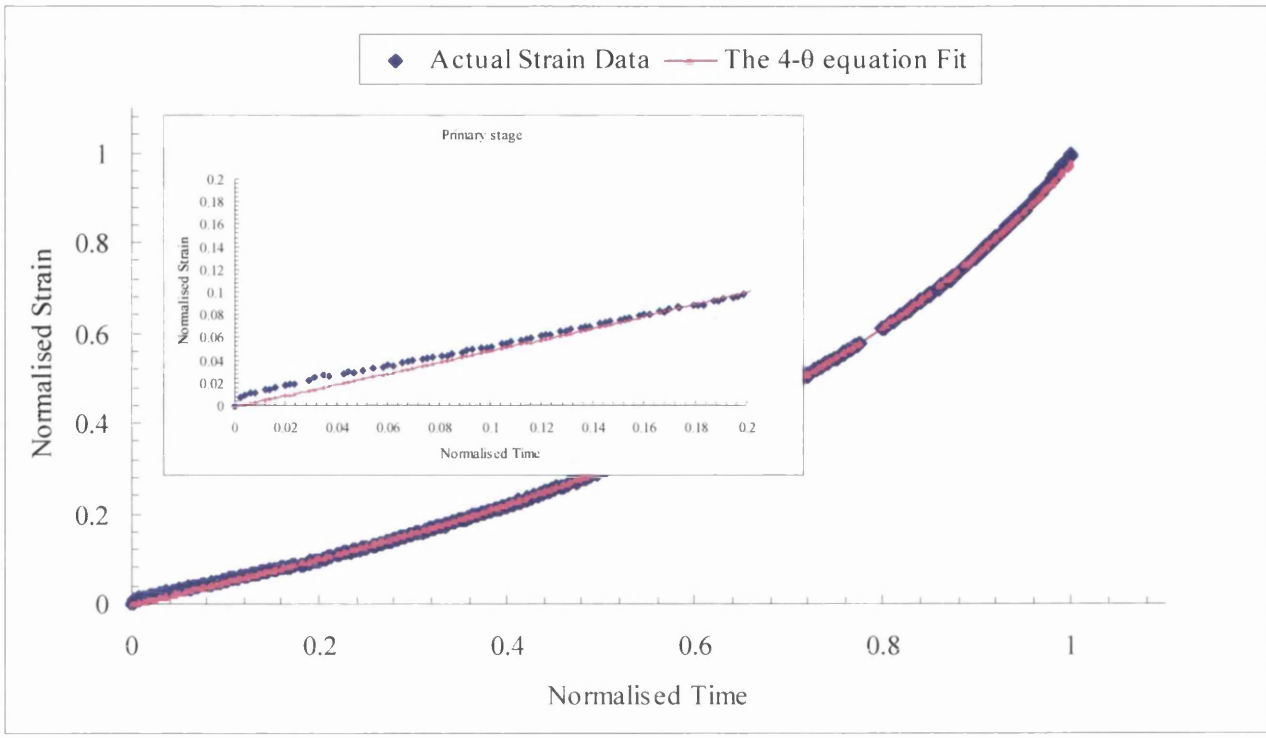

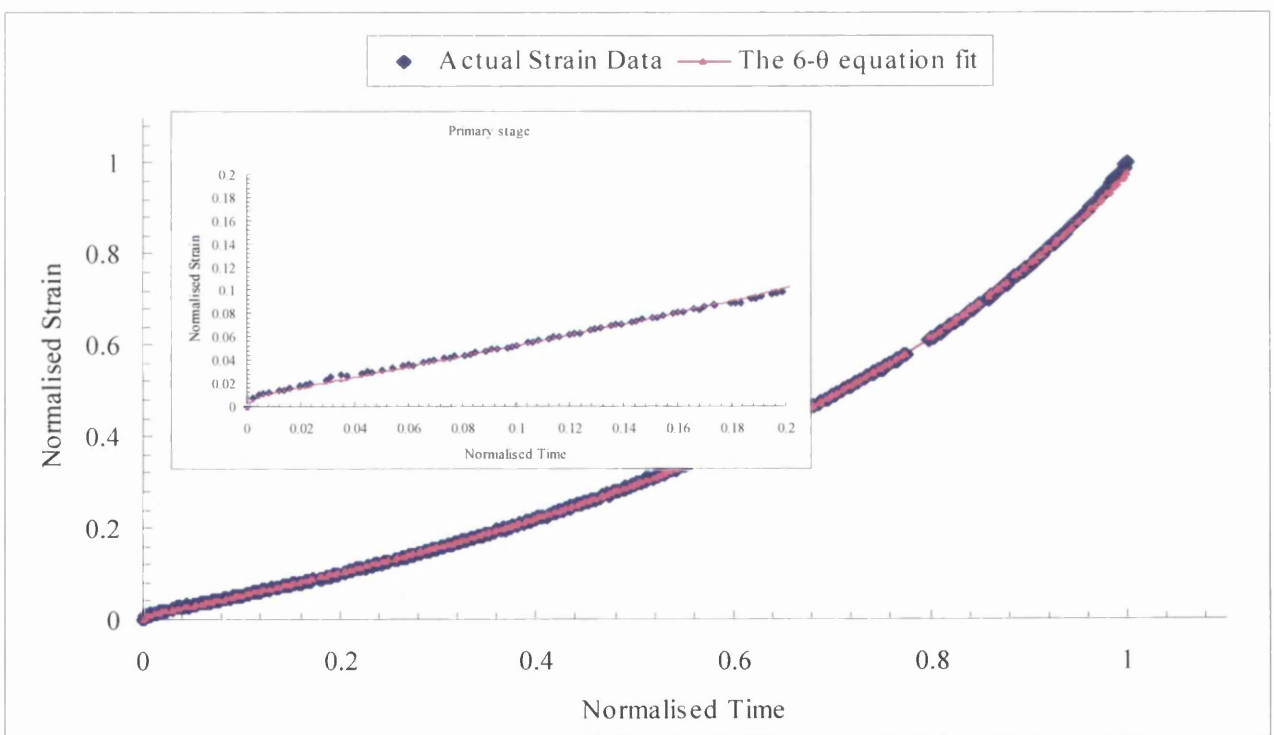

(B15.26): 923K/140MPa

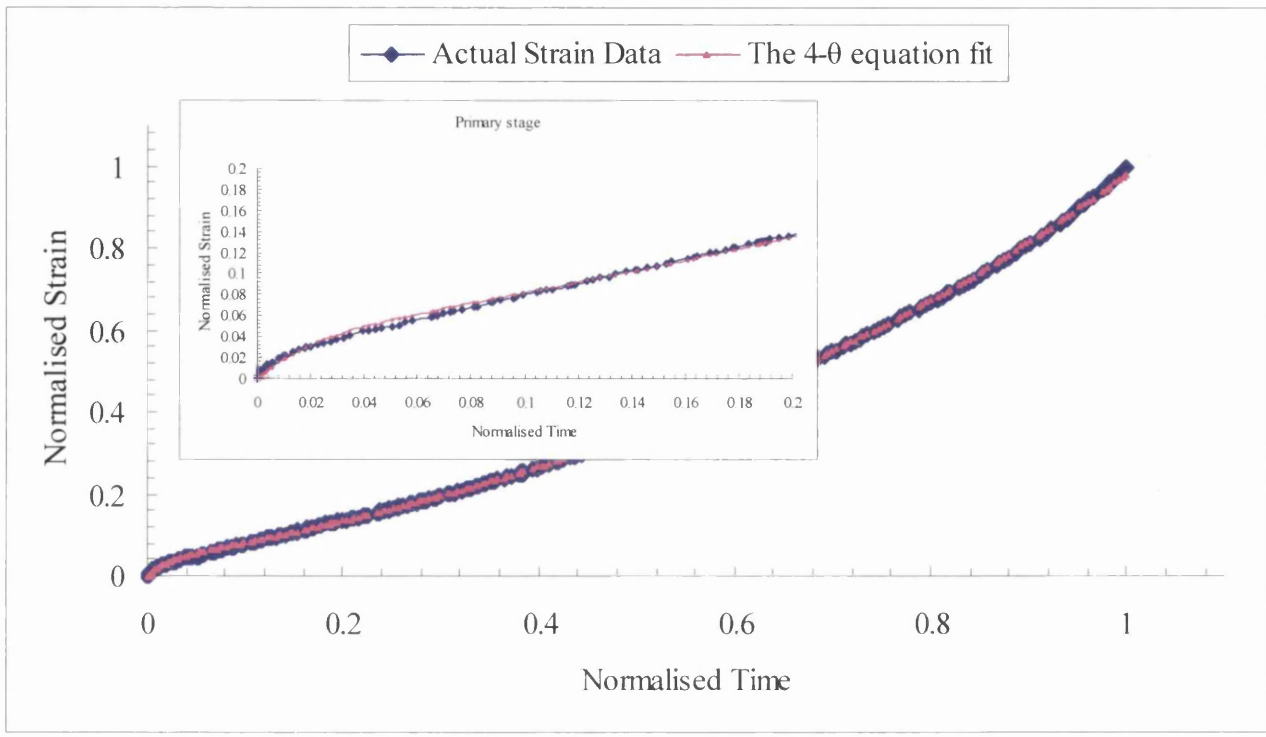

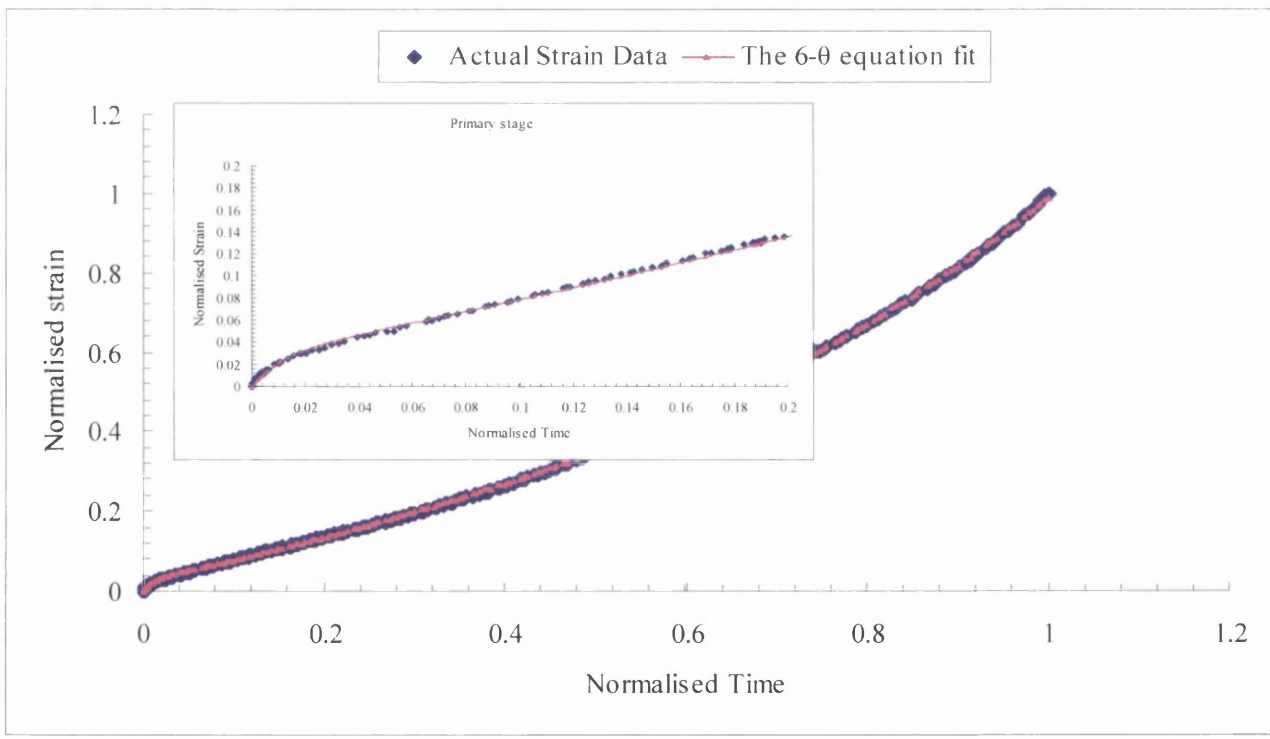

(B15.27): 923K/155MPa

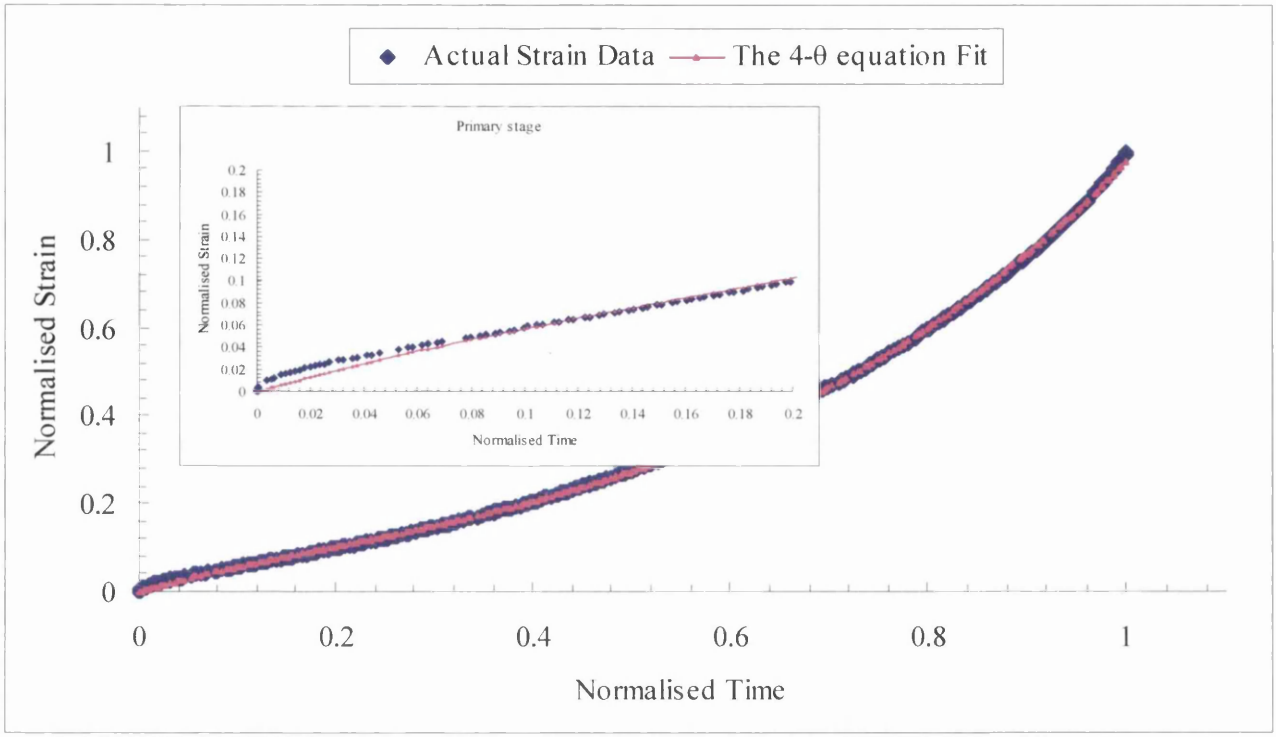

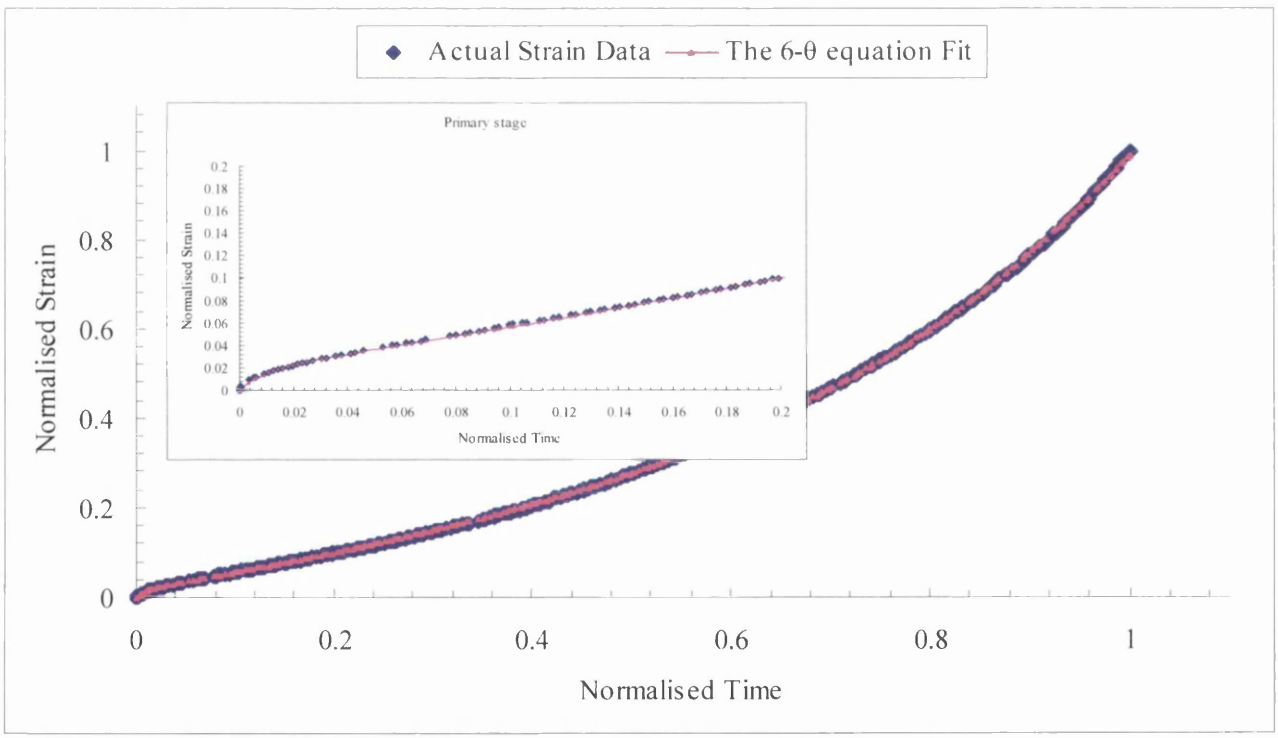

(B15.28): 923K/180MPa

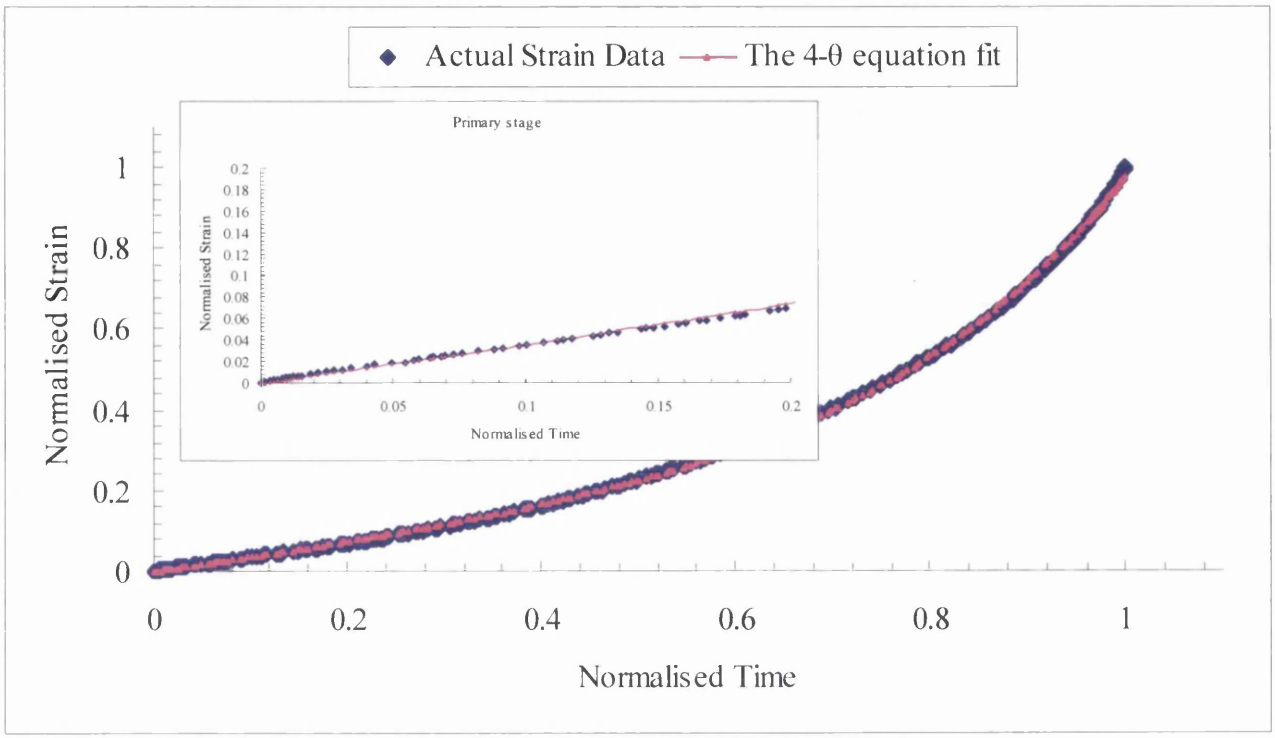

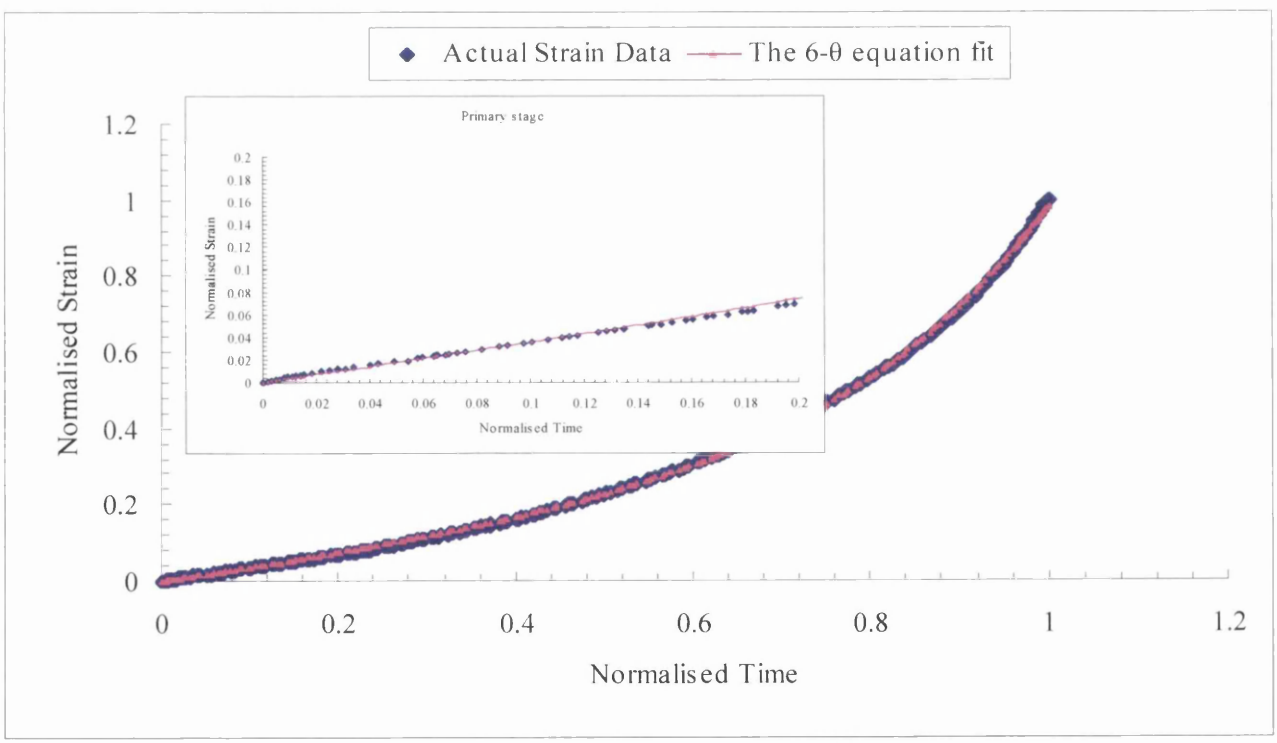

(B15.29): 923K/225MPa

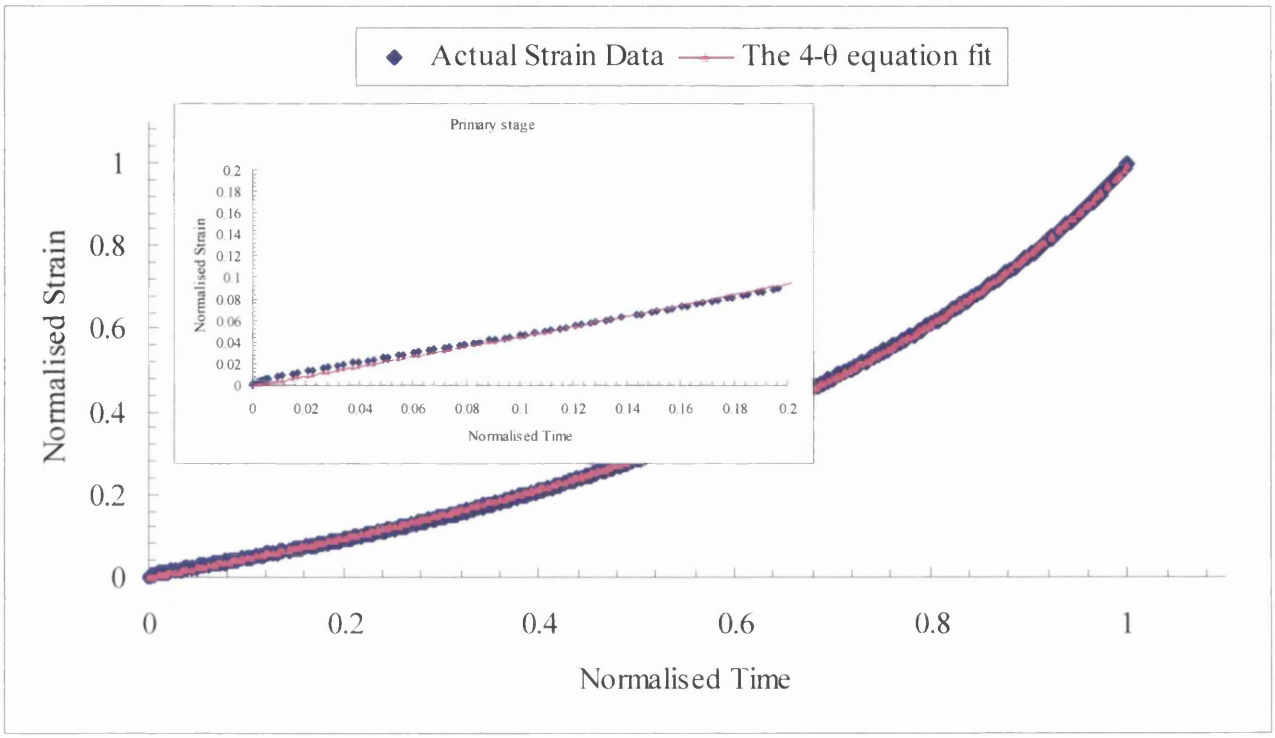

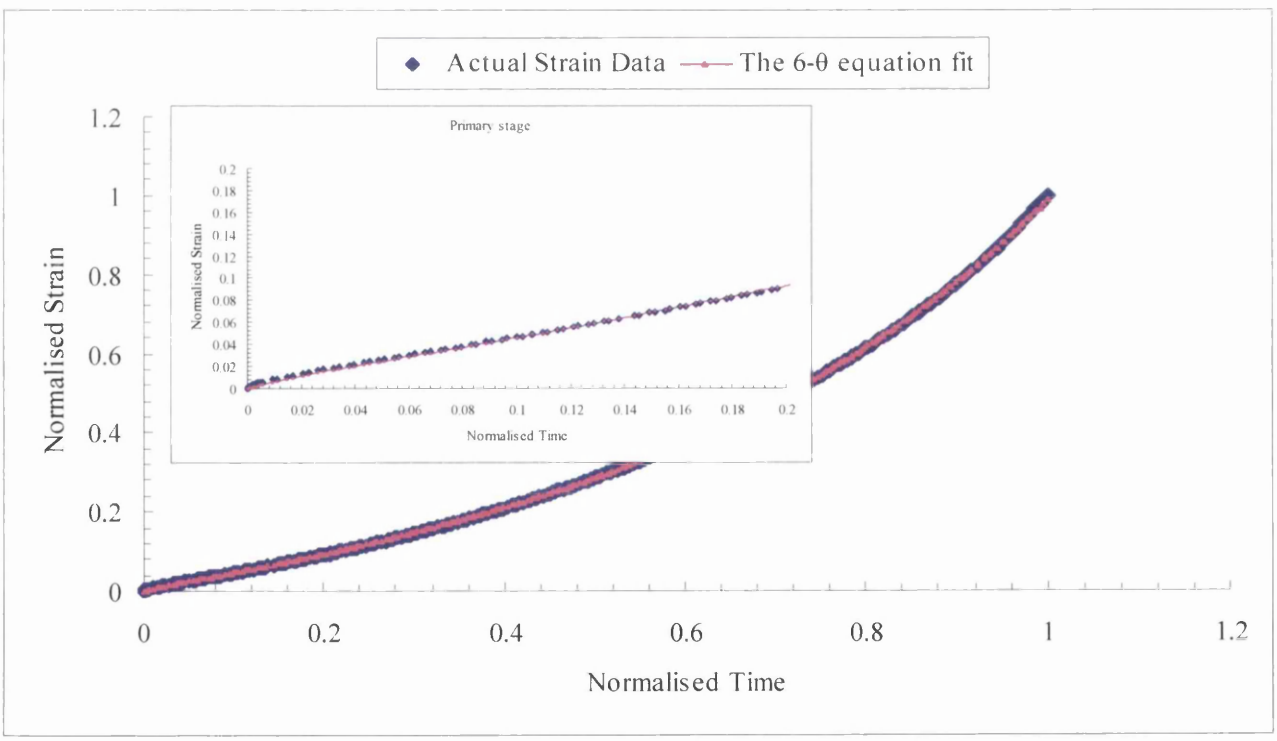

(B15.30): 923K/260MPa

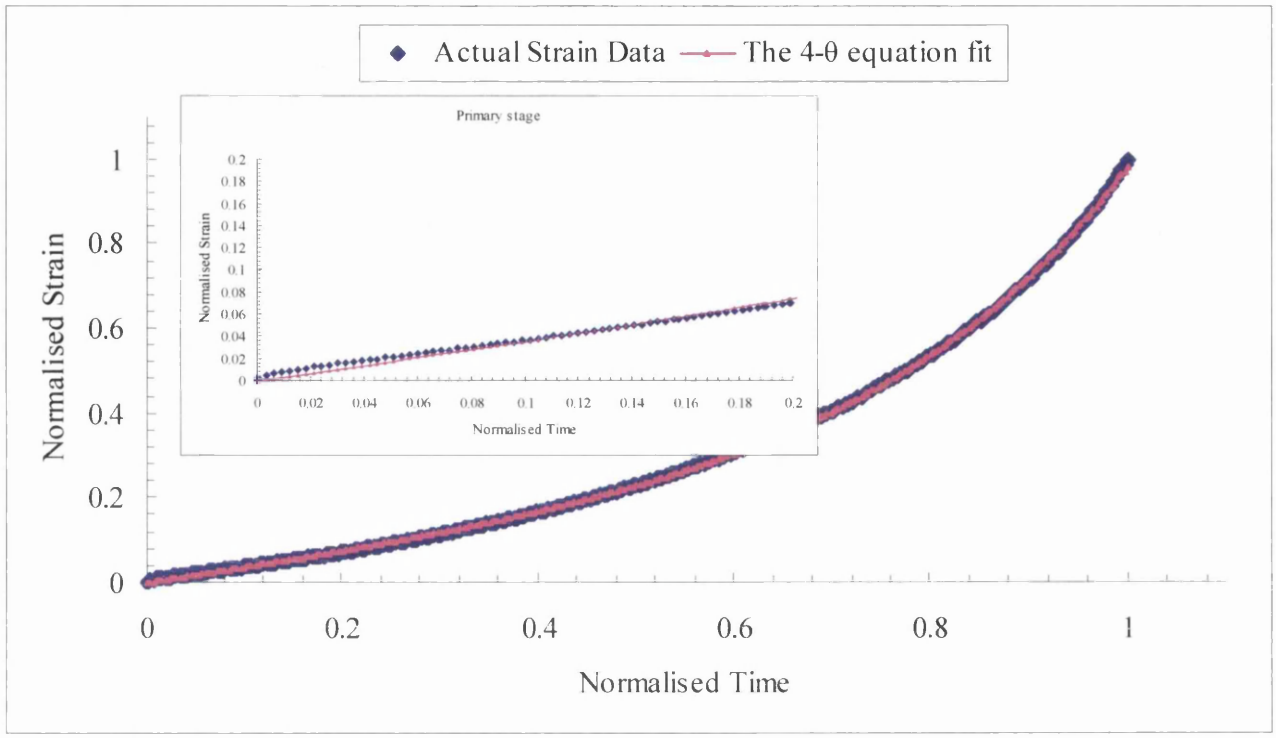

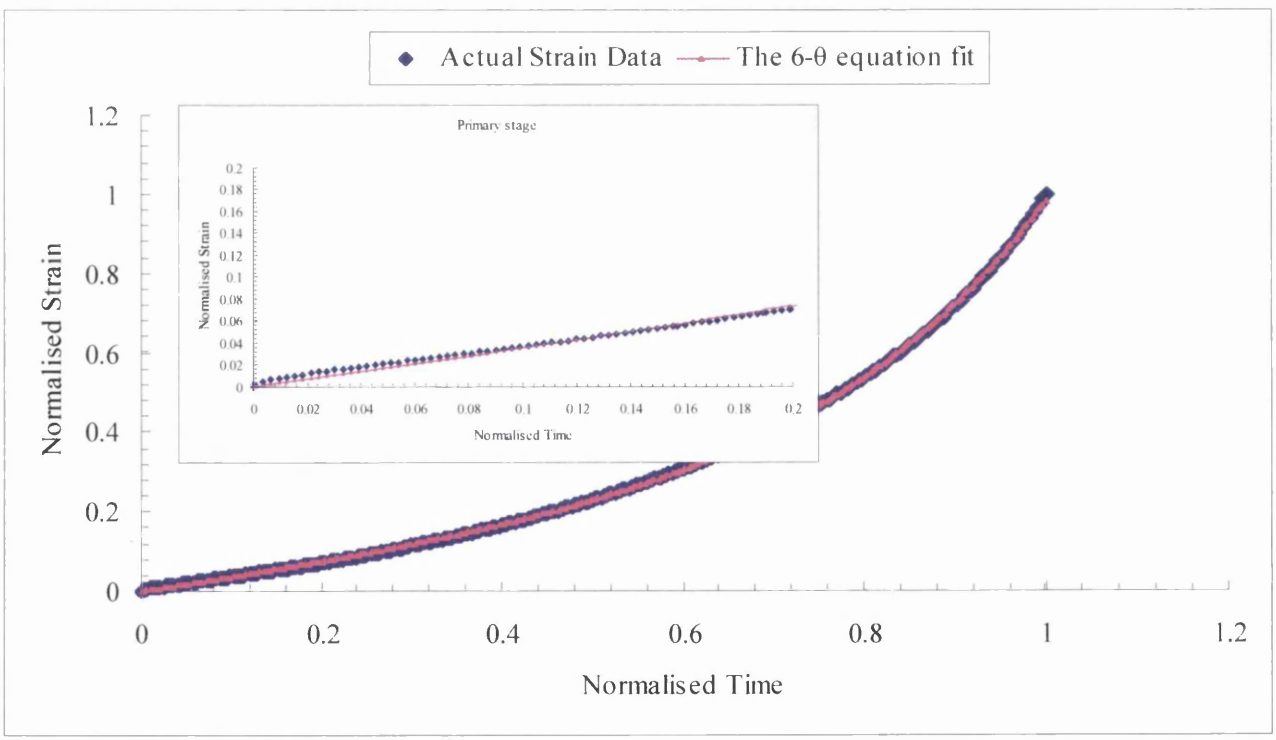

(B15.31): 923K/300MPa

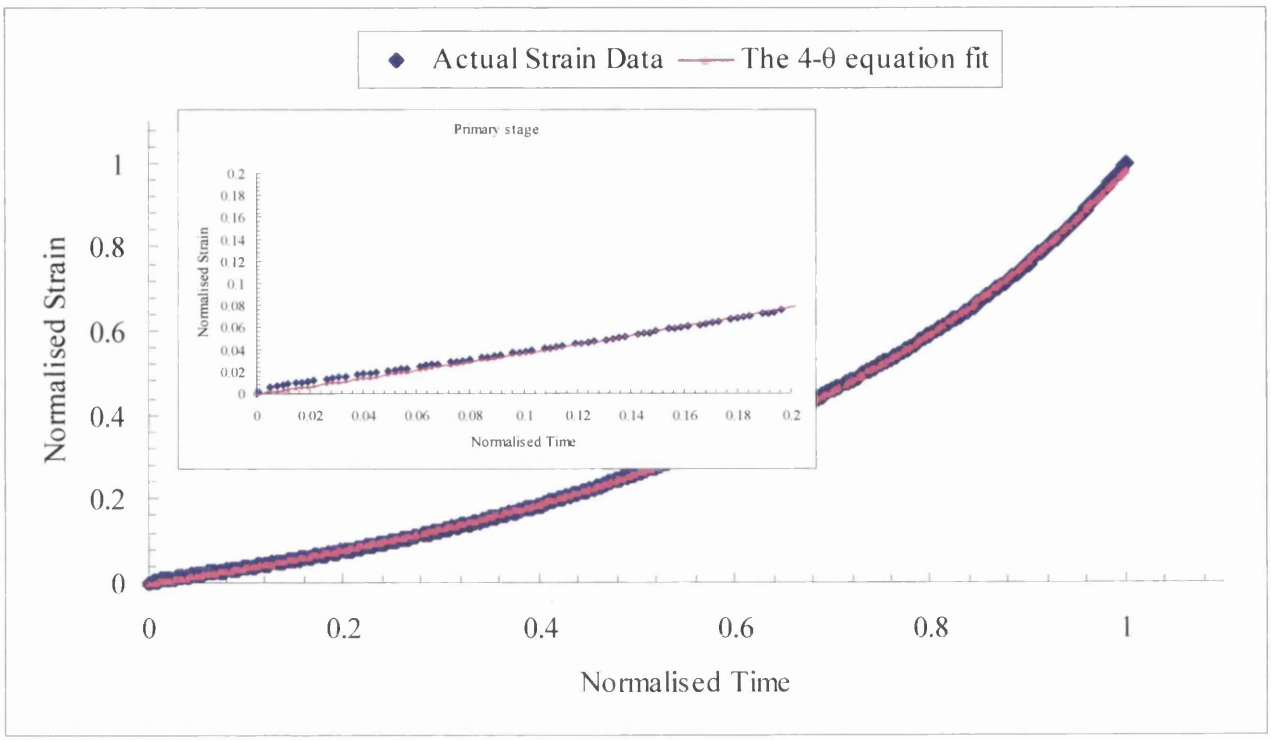

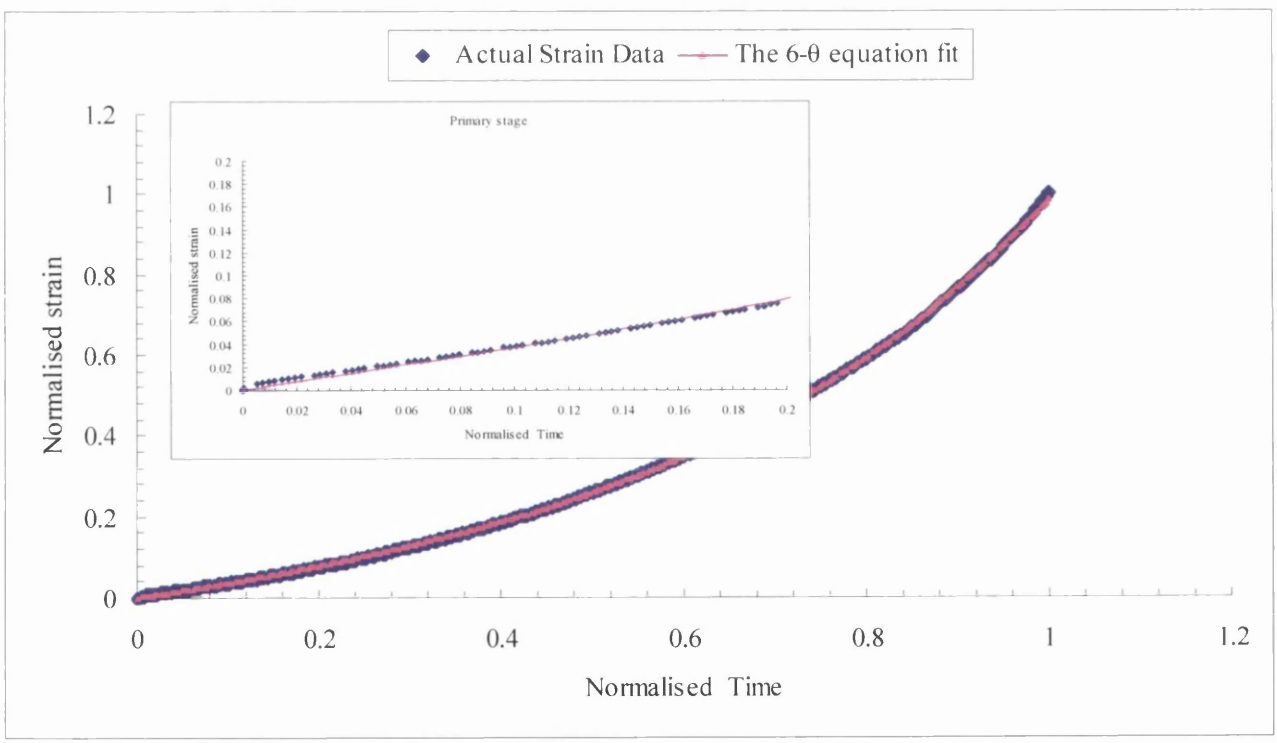

(B15.32): 923K/330MPa

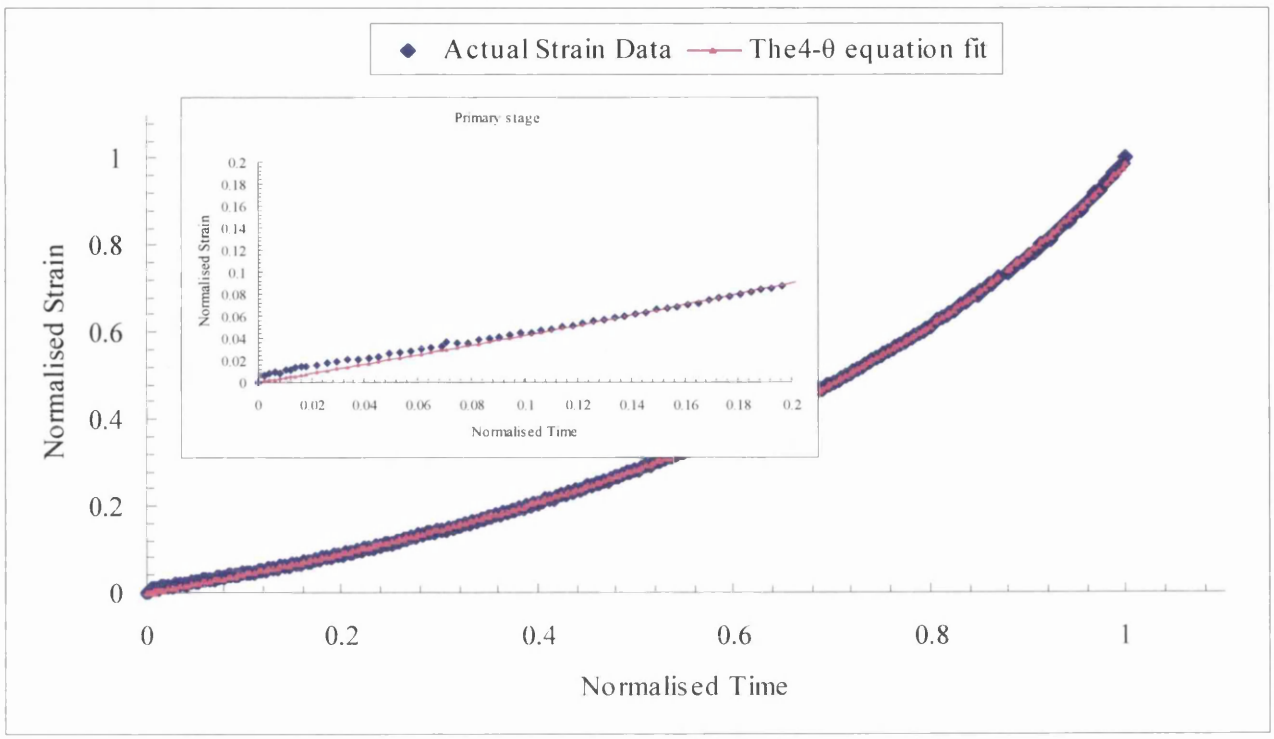

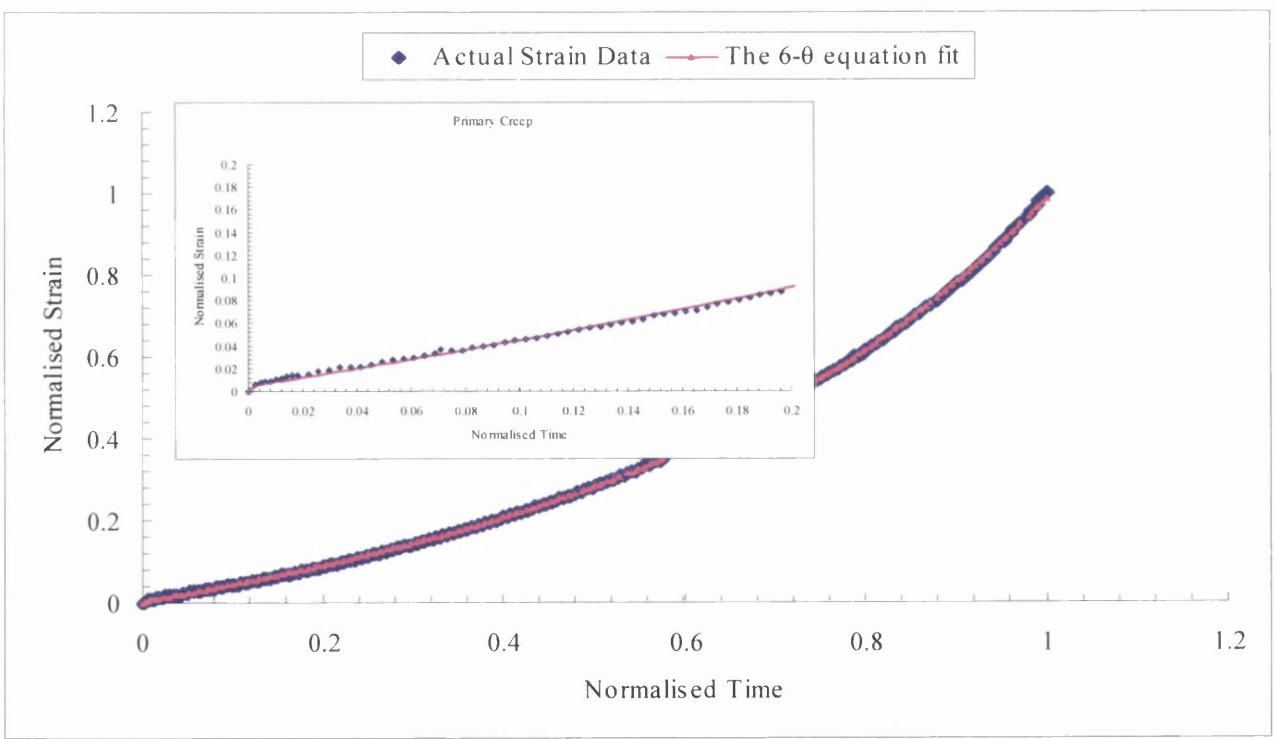

B.16 THE 6-θ PARAMETERS

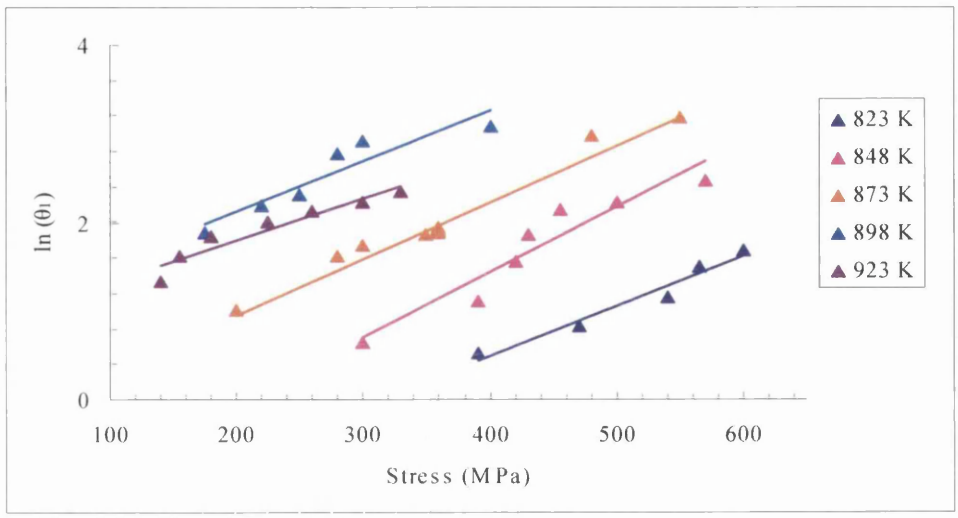

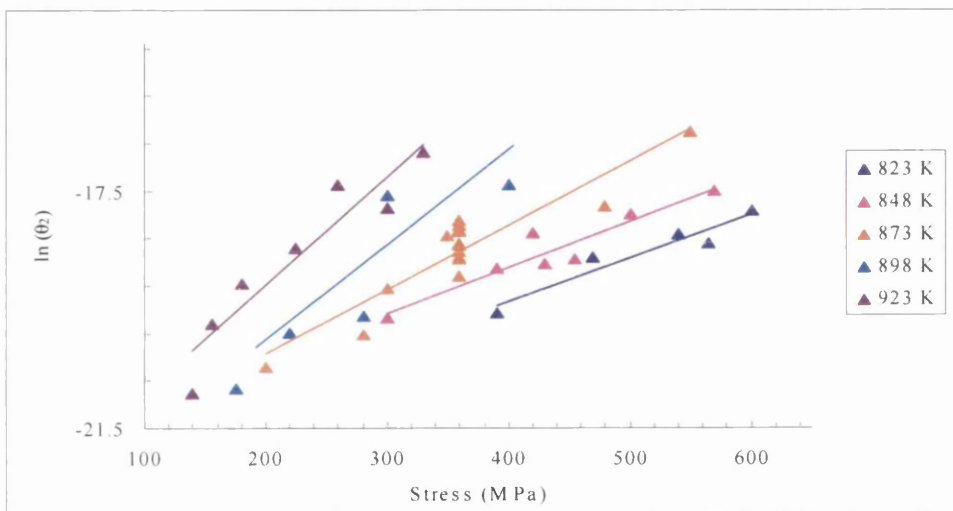

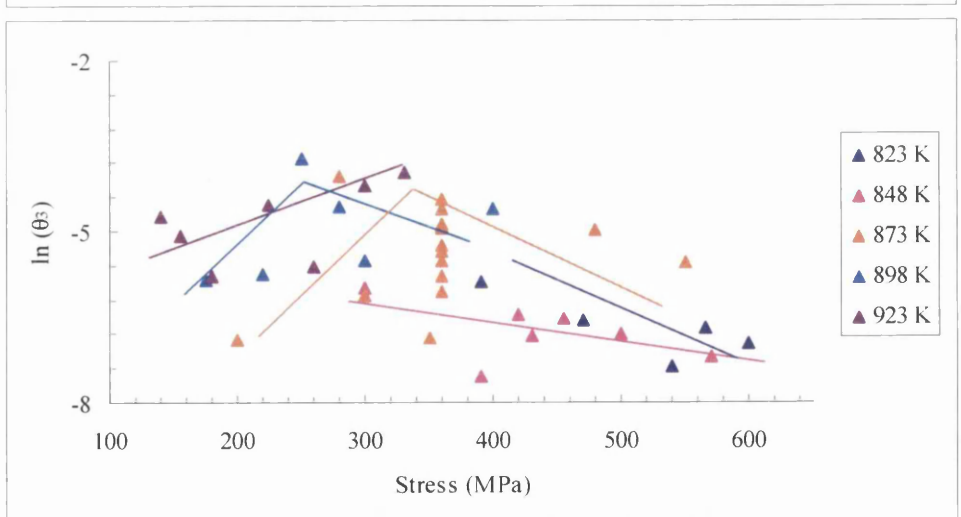

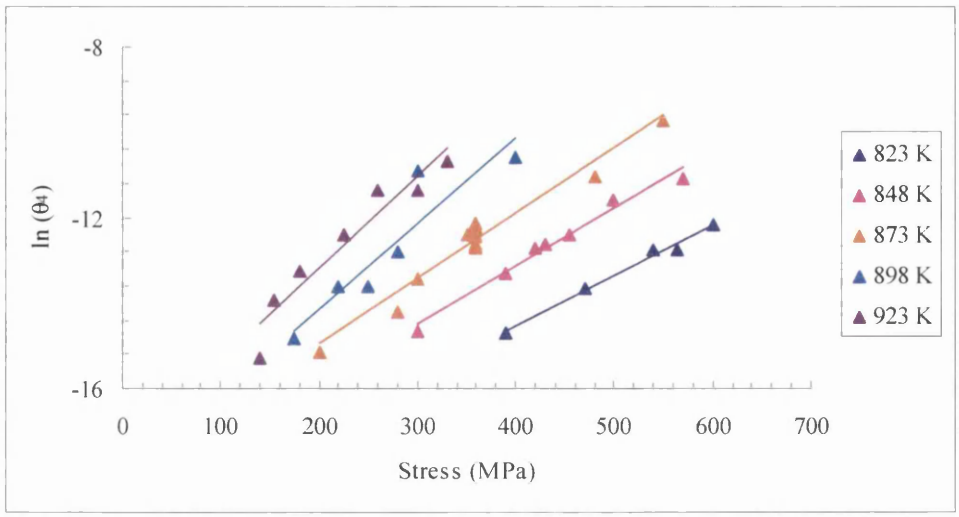
-8
-12
-16
ln (θ4)
0
100
200
300
400
500
600
700
Stress (MPa)
823 K
848 K
873 K
898 K
923 K

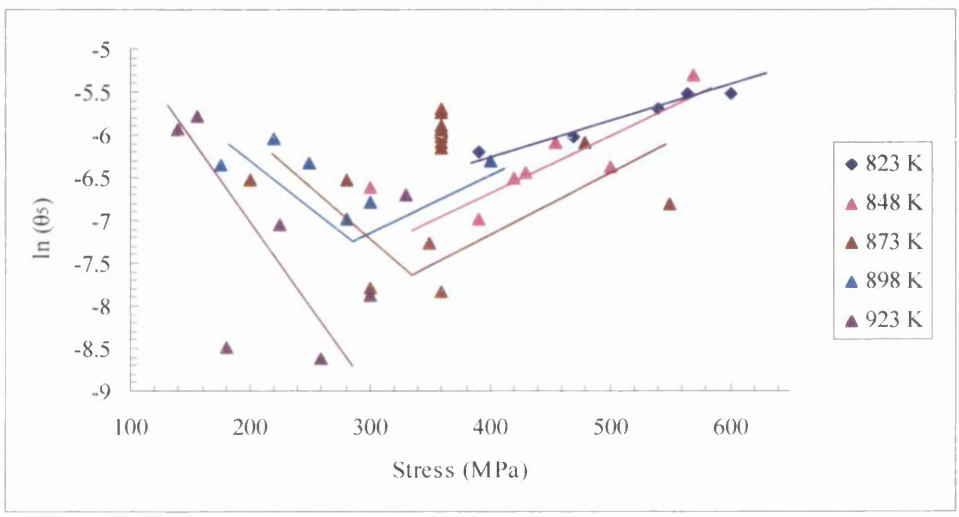
-5
-5.5
-6
-6.5
-7
-7.5
-8
-8.5
-9
ln (θ5)
100
200
300
400
500
600
Stress (MPa)
823 K
848 K
873 K
898 K
923 K

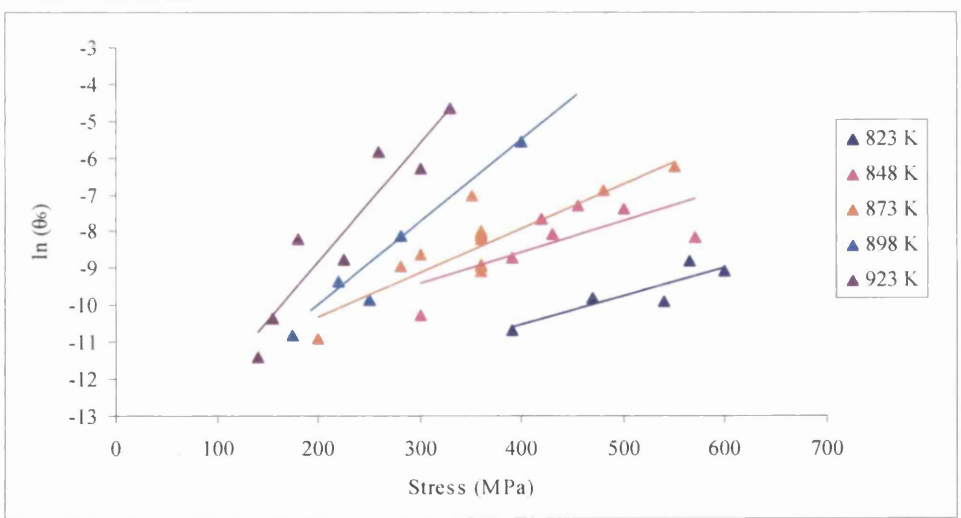
-3
-4
-5
-6
-7
-8
-9
-10
-11
-12
-13
ln (θ6)
0
100
200
300
400
500
600
700
Stress (MPa)
823 K
848 K
873 K
898 K
923 K

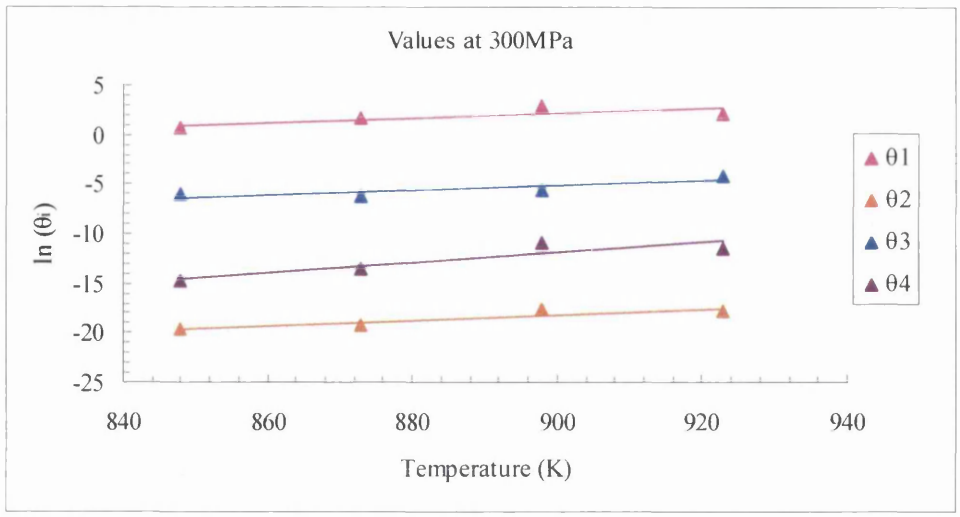
Values at 300MPa
ln (θi)
5
0
-5
-10
-15
-20
-25
840
860
880
900
920
940
Temperature (K)
θ1
θ2
θ3
θ4

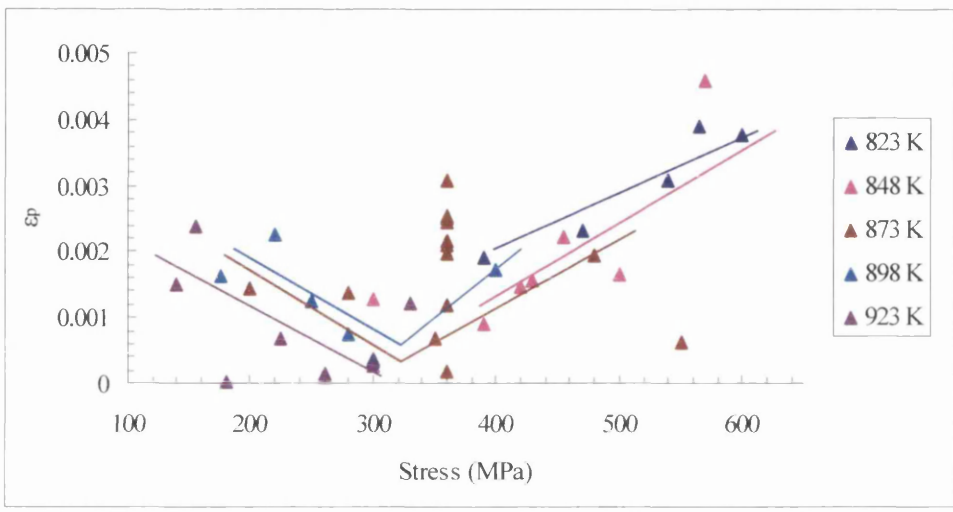
εp
0.005
0.004
0.003
0.002
0.001
0
100
200
300
400
500
600
Stress (MPa)
823 K
848 K
873 K
898 K
923 K

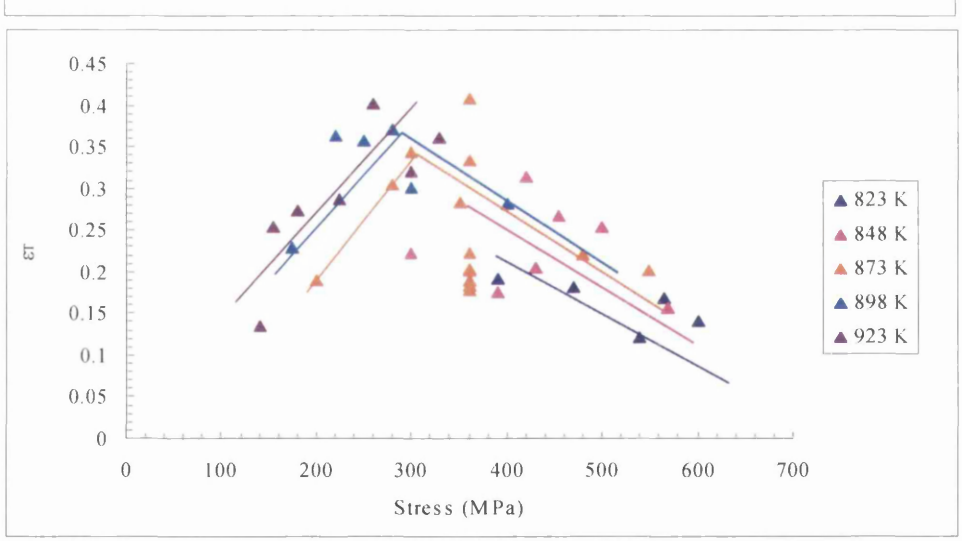
εT
0.45
0.4
0.35
0.3
0.25
0.2
0.15
0.1
0.05
0
0
100
200
300
400
500
600
700
Stress (MPa)
823 K
848 K
873 K
898 K
923 K

B.17 The Wilshire Technique Analysis Results (general)

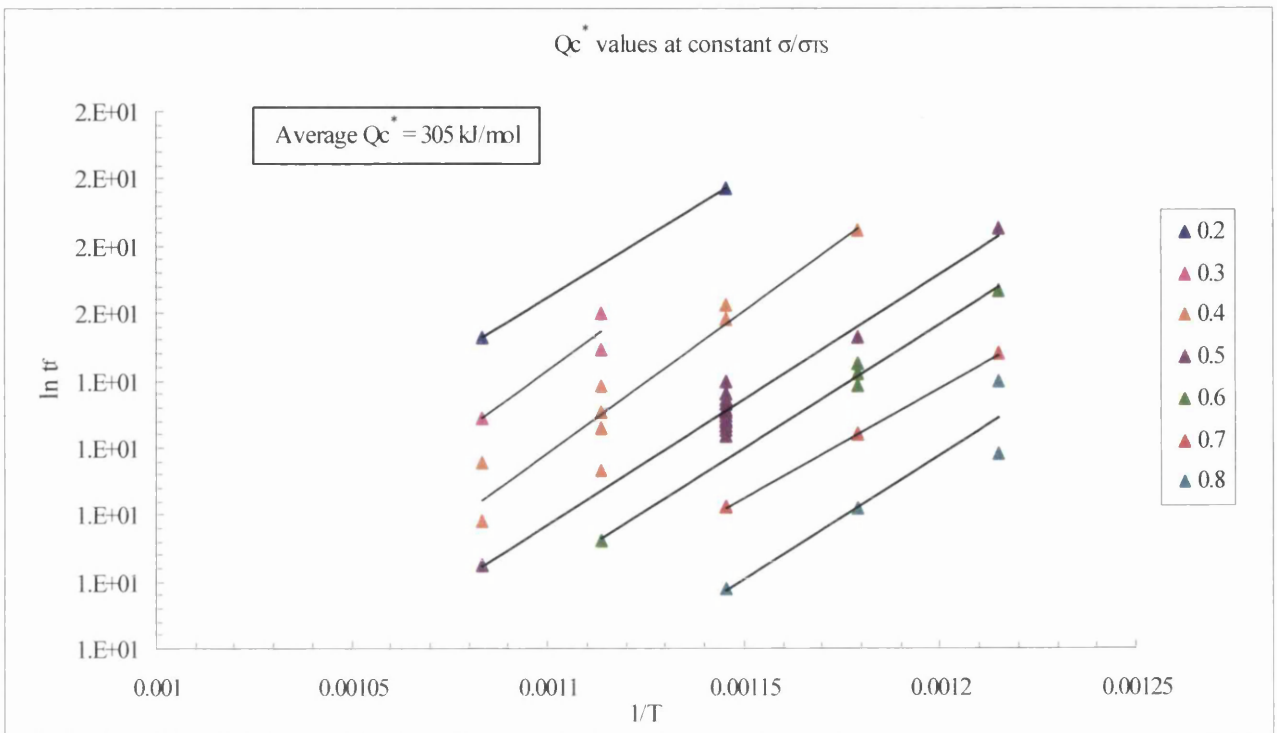

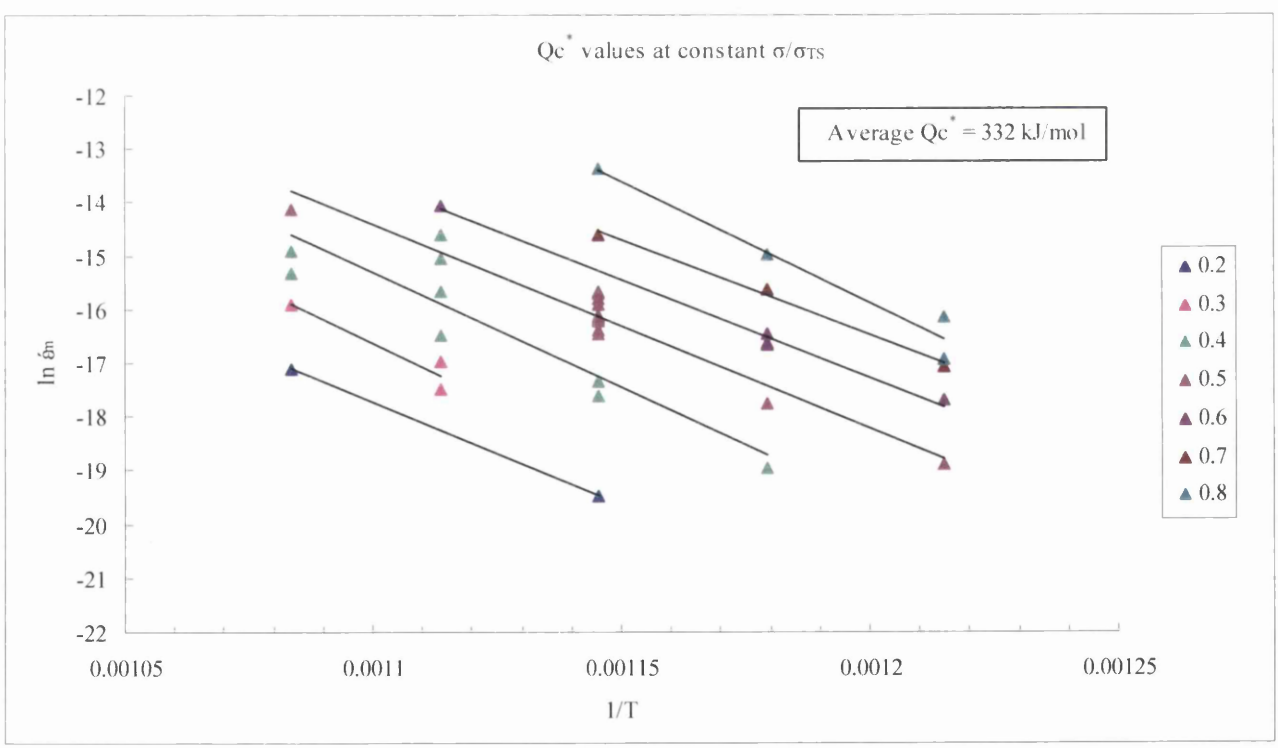

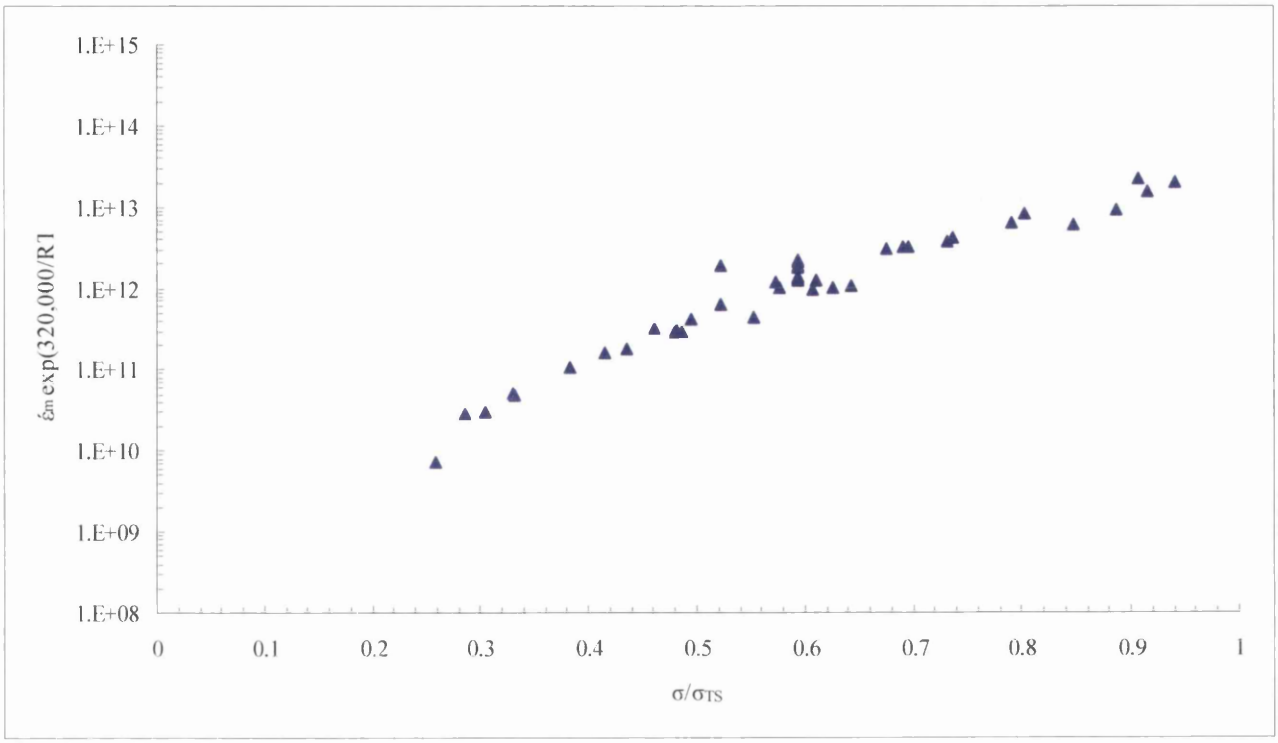
1.E+15
1.E+14
1.E+13
1.E+12
1.E+11
1.E+10
1.E+09
1.E+08
$\dot{\varepsilon}_{ss}$ exp(320,000/R1
0
0.1
0.2
0.3
0.4
0.5
0.6
0.7
0.8
0.9
1
σ/σ_{TS}

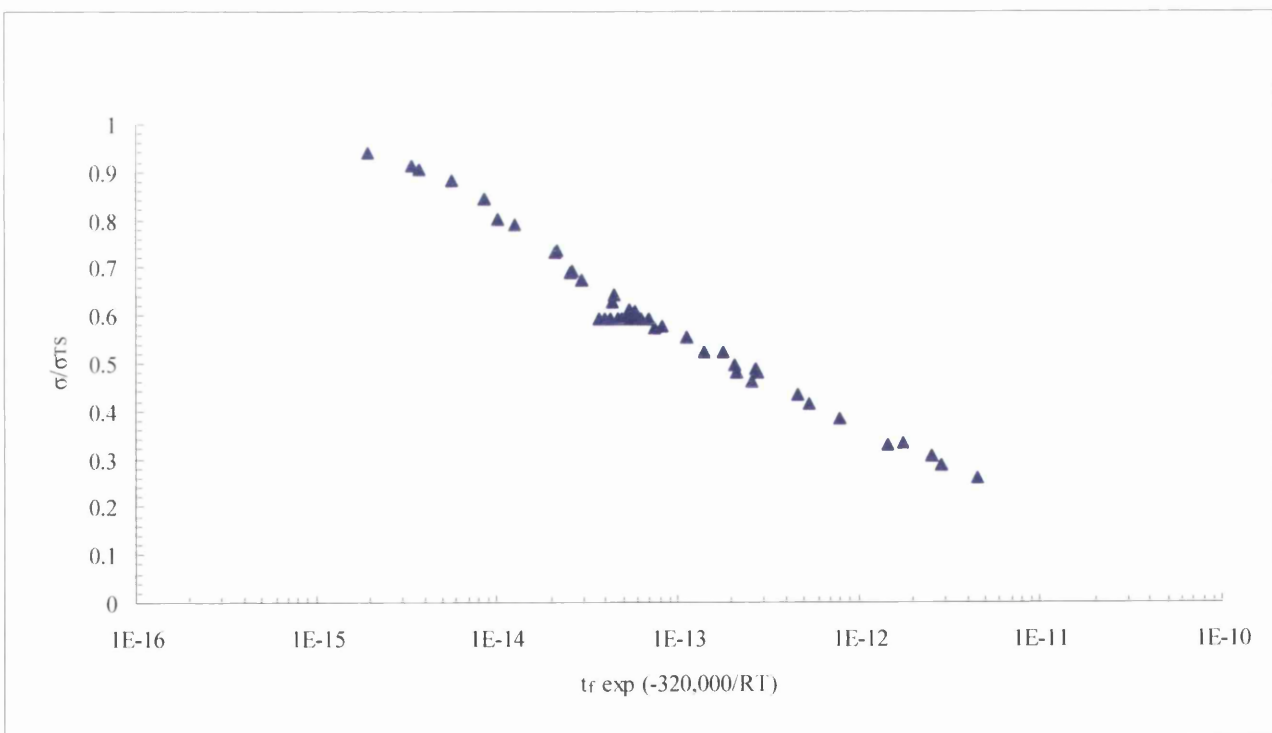
1
0.9
0.8
0.7
0.6
0.5
0.4
0.3
0.2
0.1
0
σ/σ_{TS}
1E-16
1E-15
1E-14
1E-13
1E-12
1E-11
1E-10
t_f exp (-320,000/RT)

B.18 THE WILSHIRE TECHNIQUE RESULTS (time to fracture)

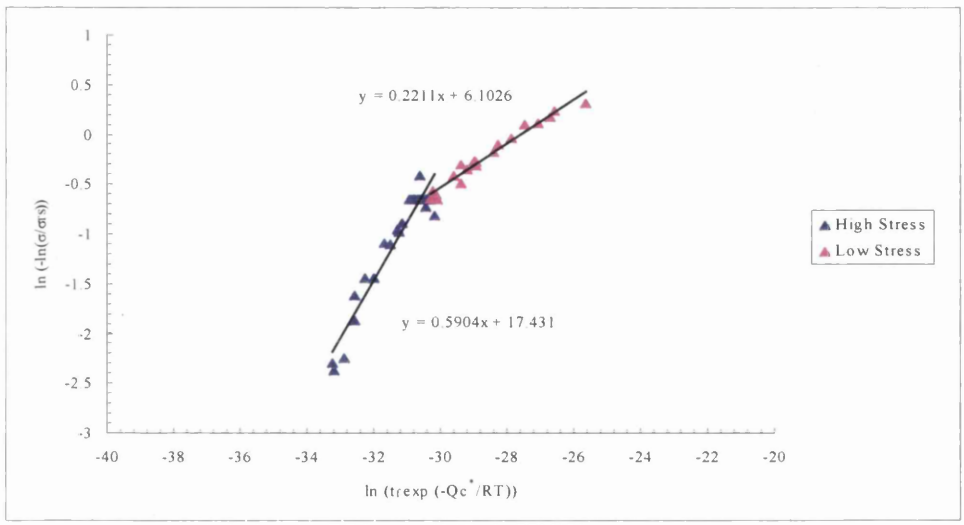

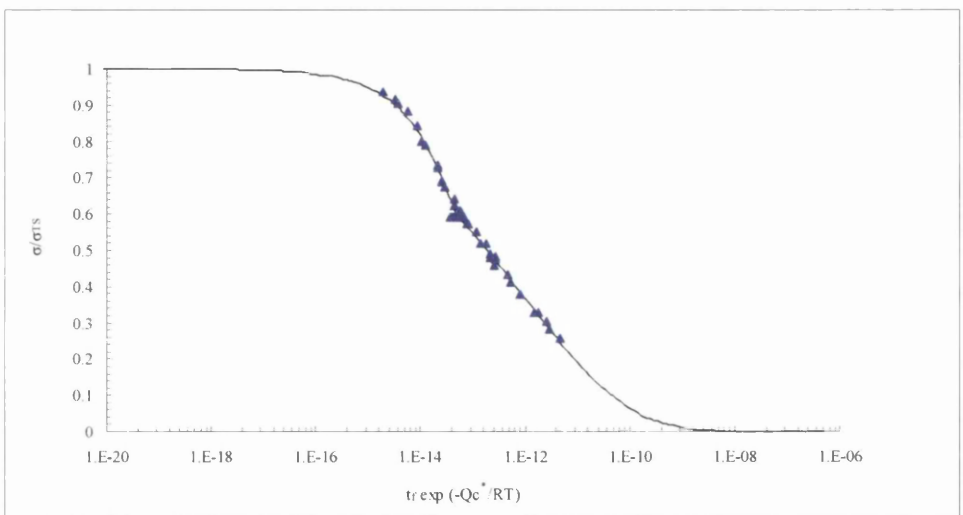

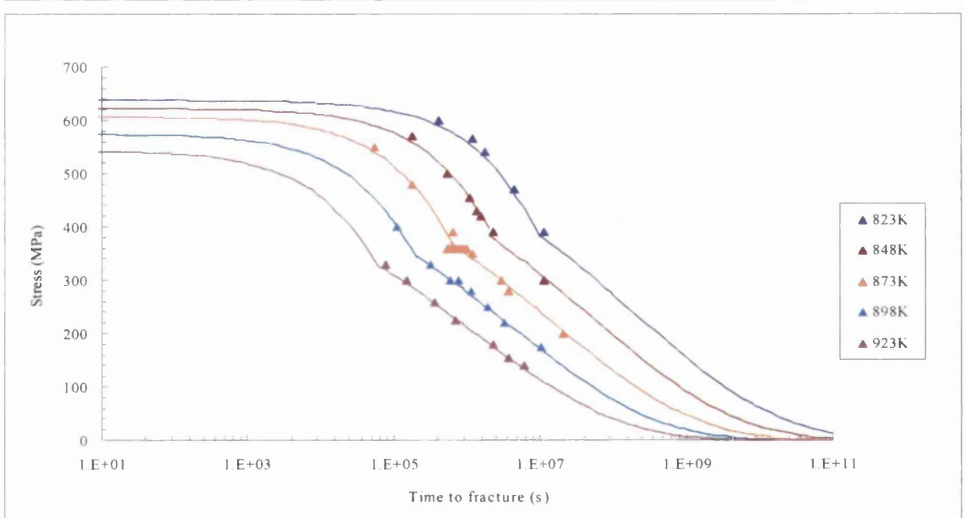

B.19 THE WILSHIRE TECHNIQUE RESULTS (minimum creep rate)

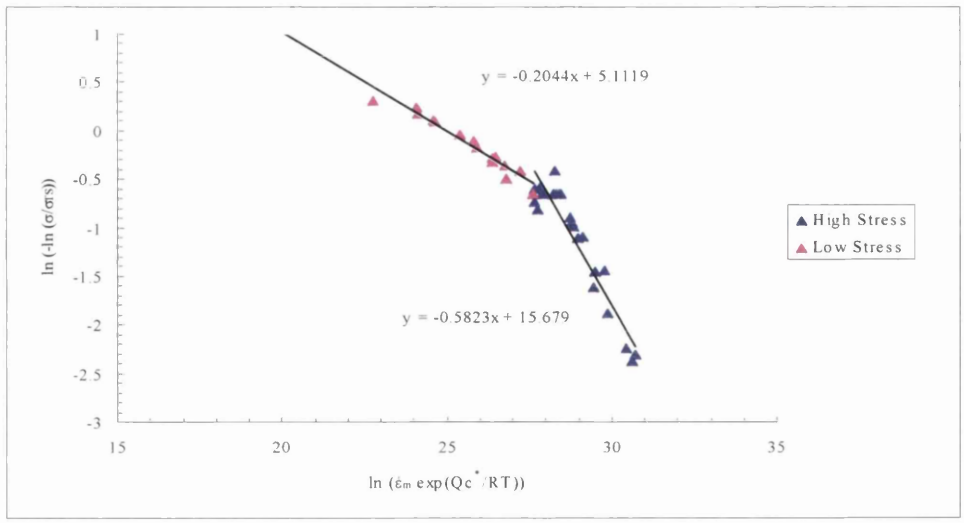

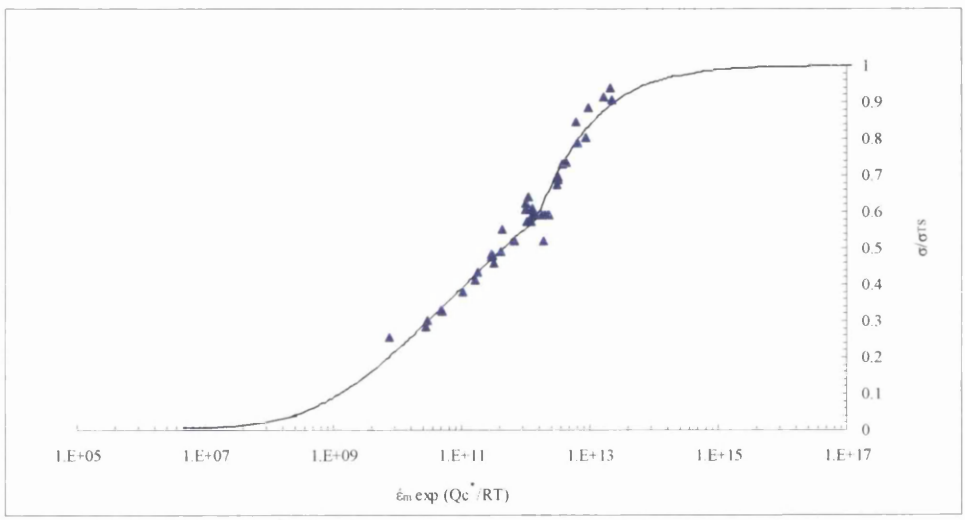

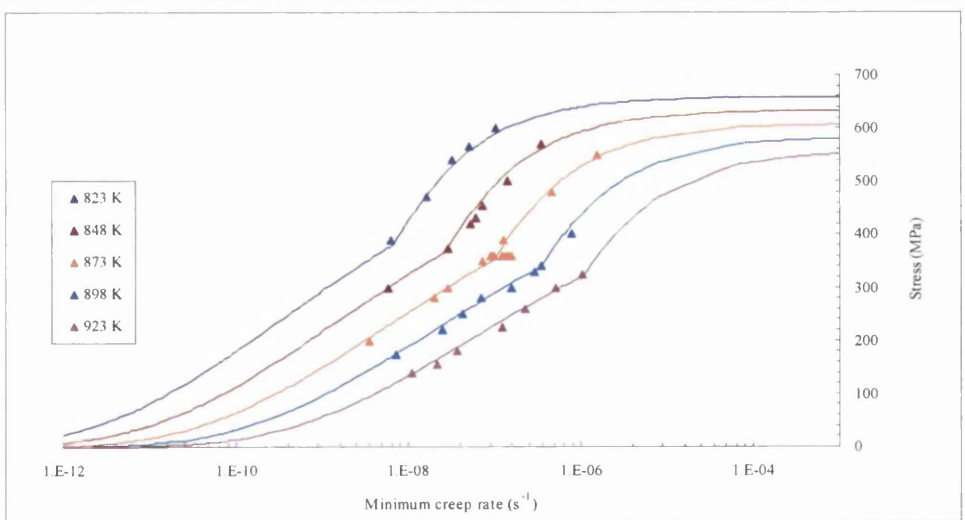

B.20 THE WILSHIRE KINK POINTS

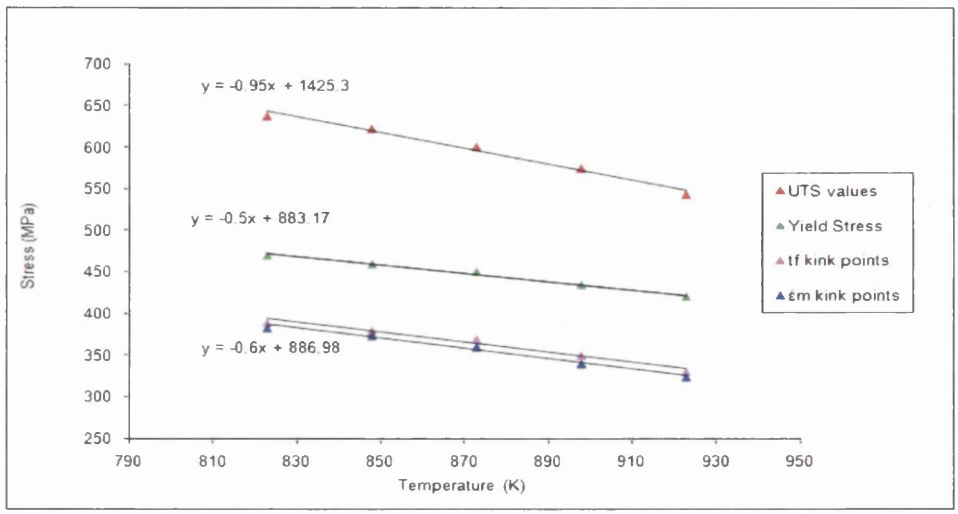

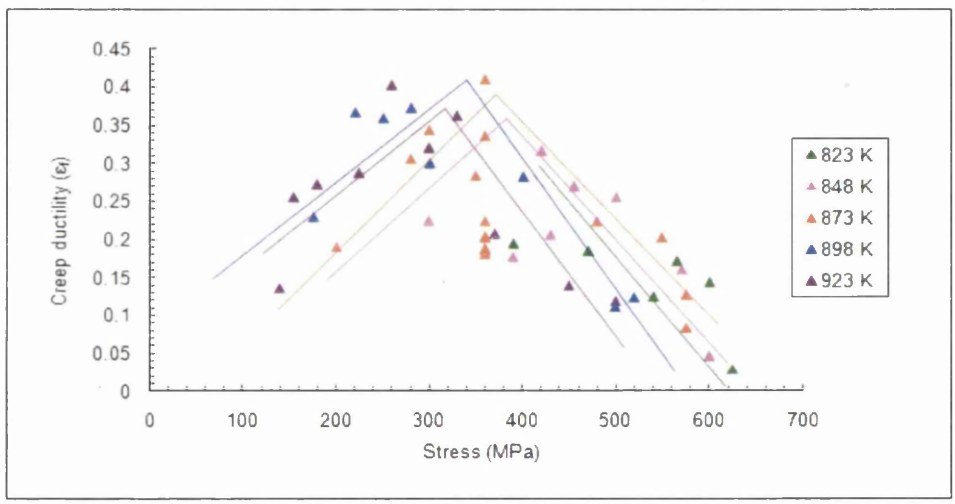

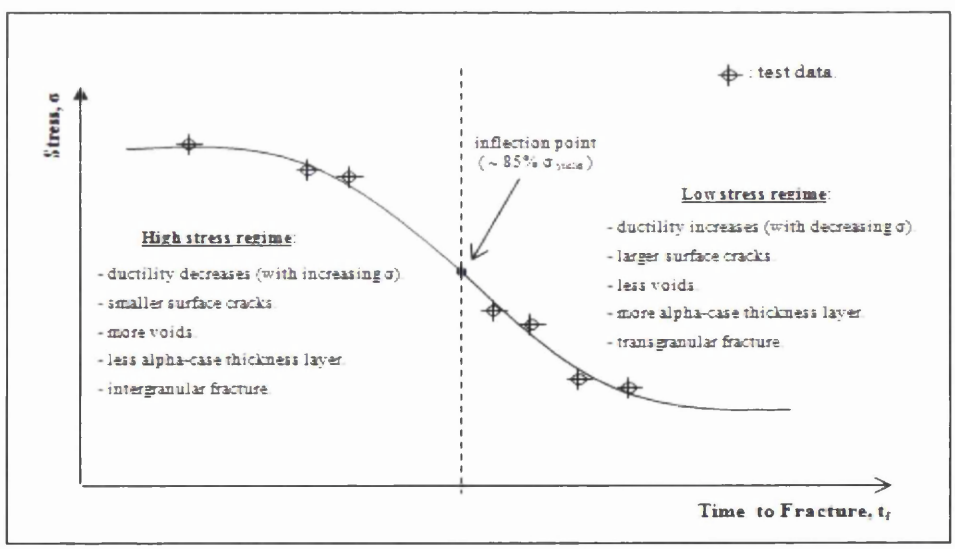

B.21 THE WILSHIRE TECHNIQUE RESULTS (time to pre-defined strains)

(B21.1): 0.1% strain

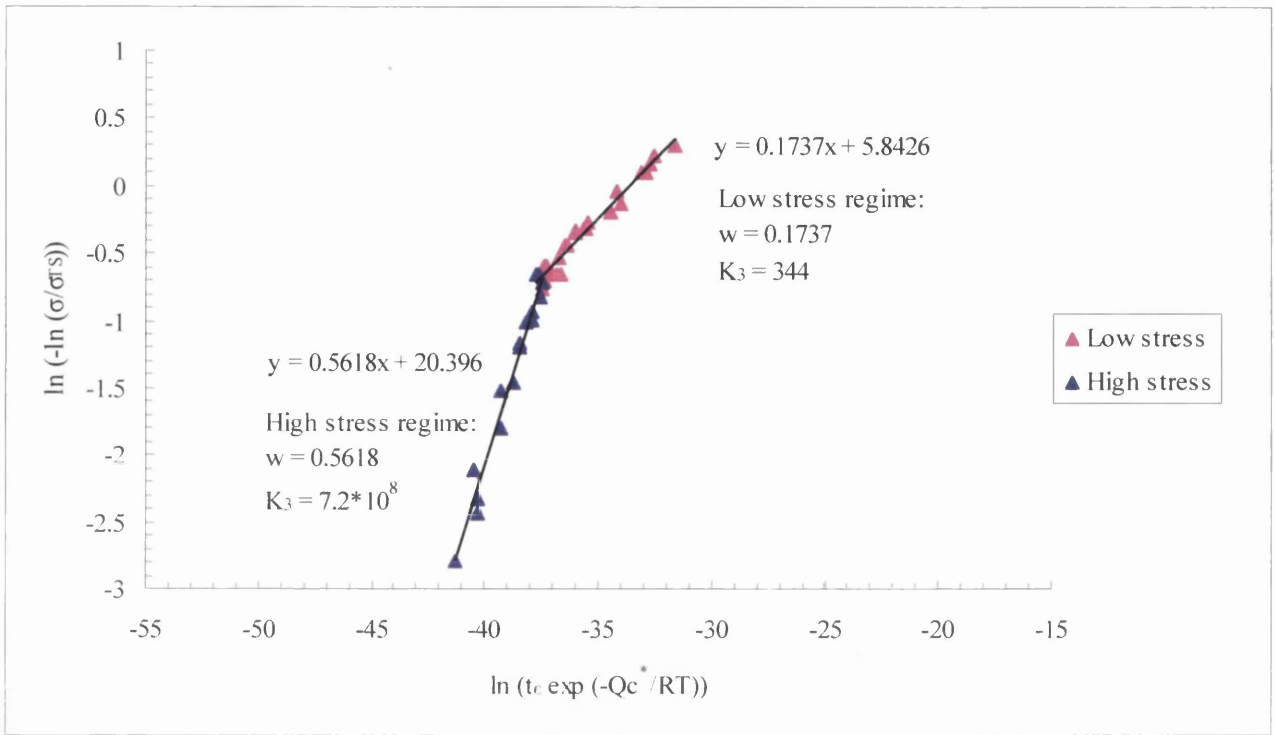

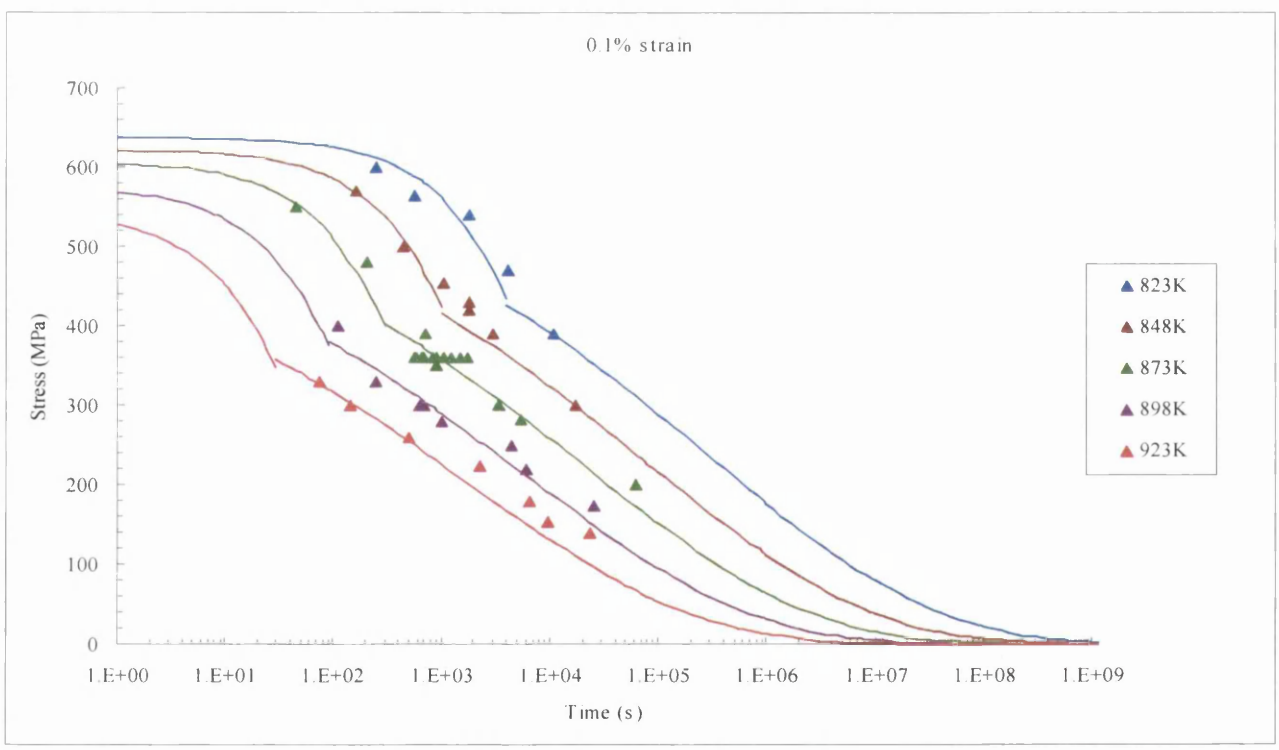

(B21.2): 0.15% strain

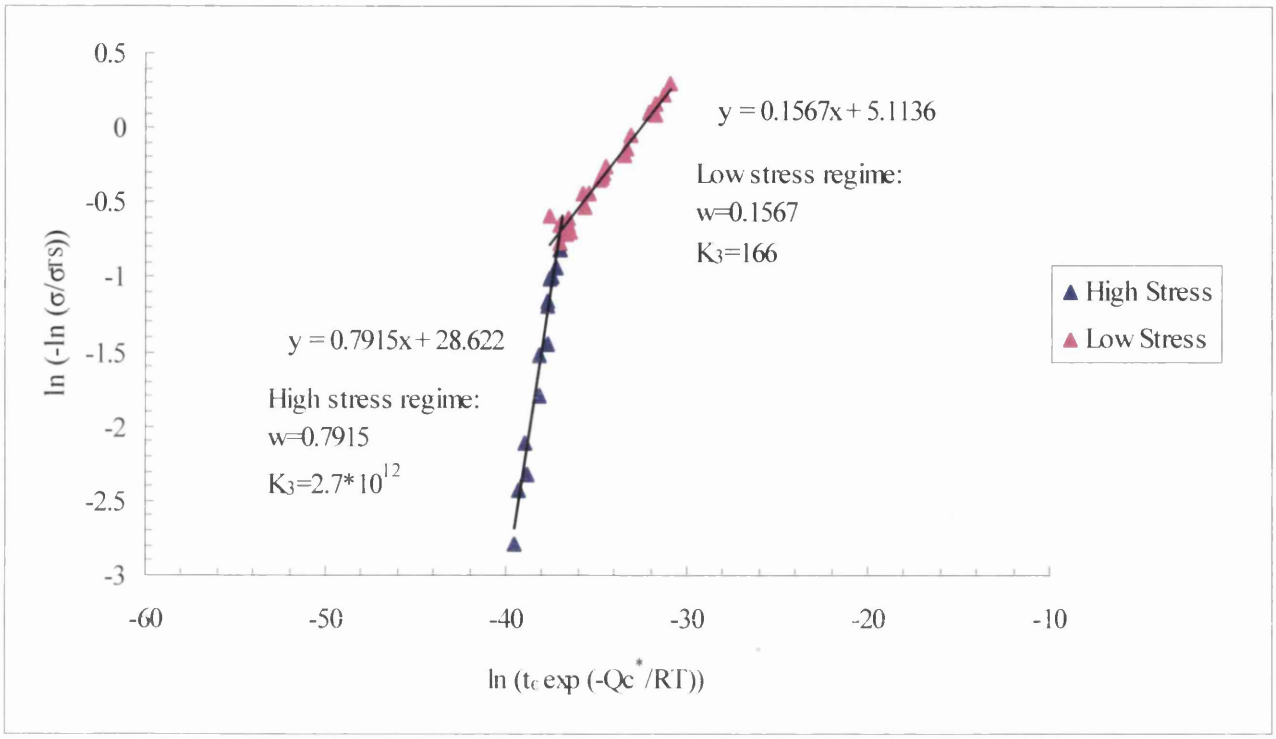

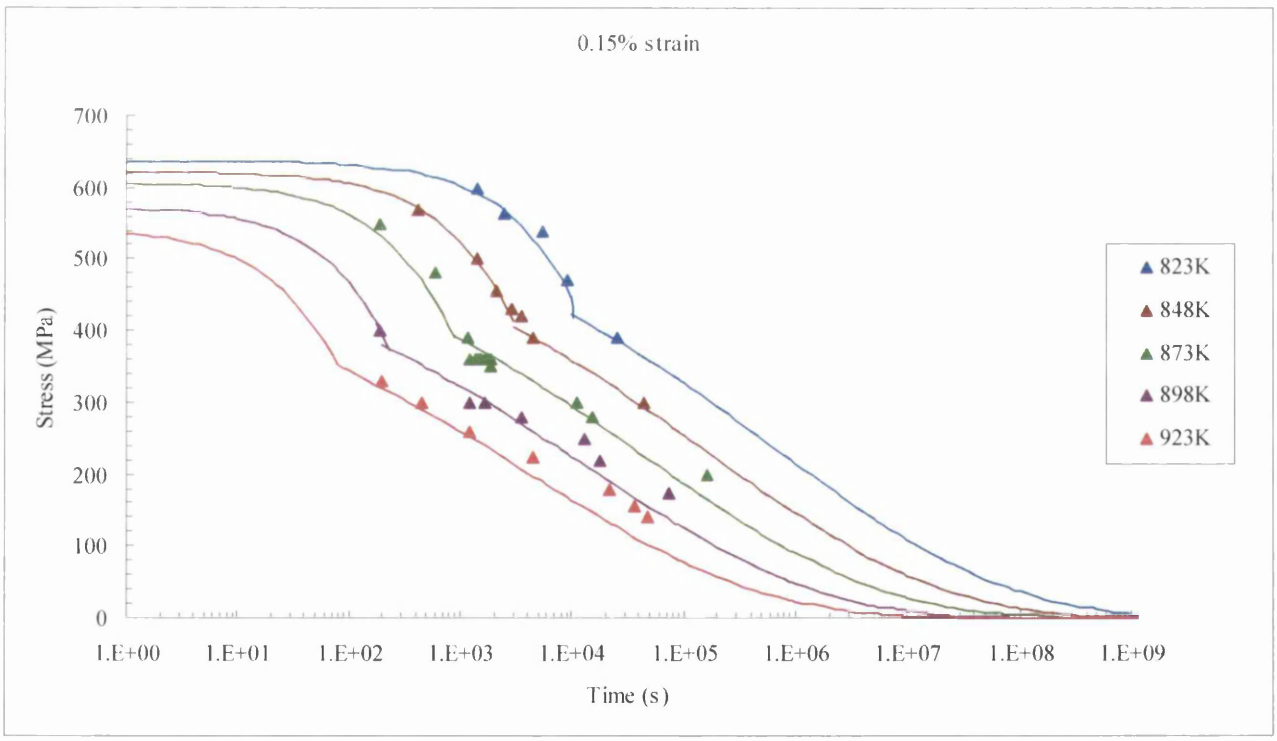

(B21.3): 0.2% strain

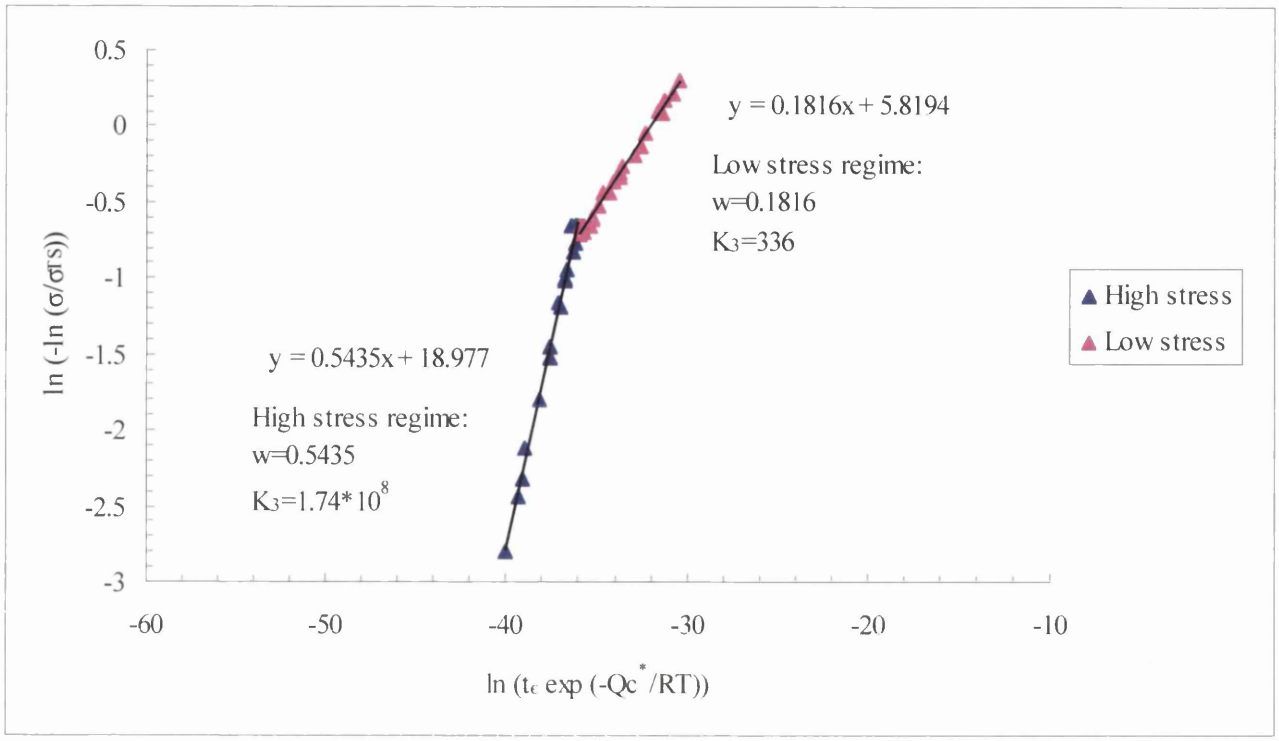

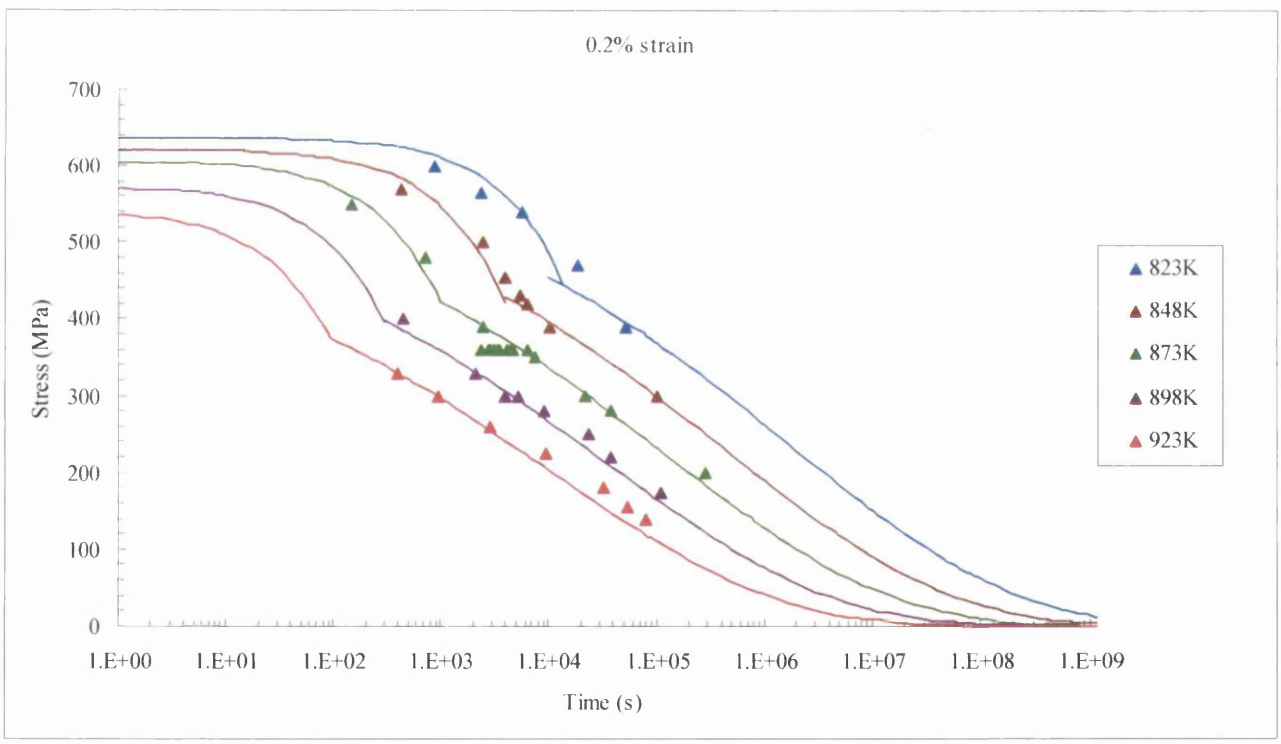

(B21.4): 0.5% strain

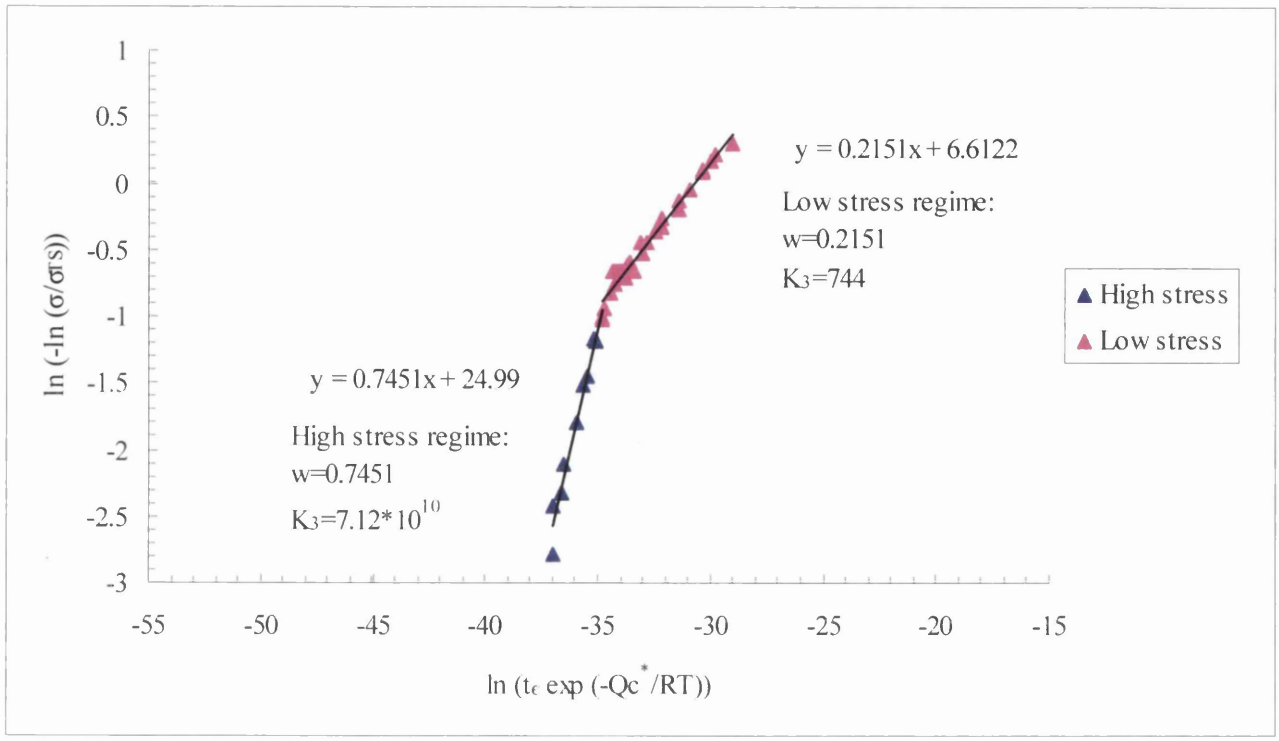

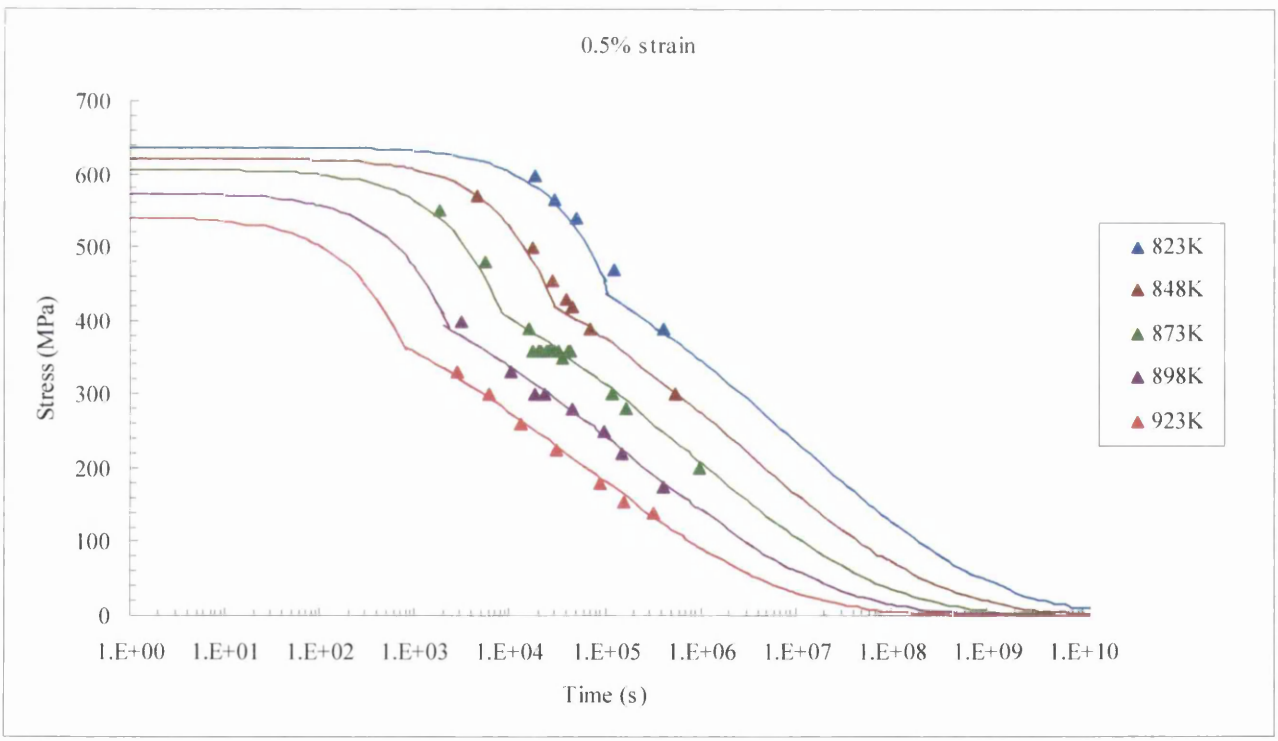

(B21.5): 0.7% strain

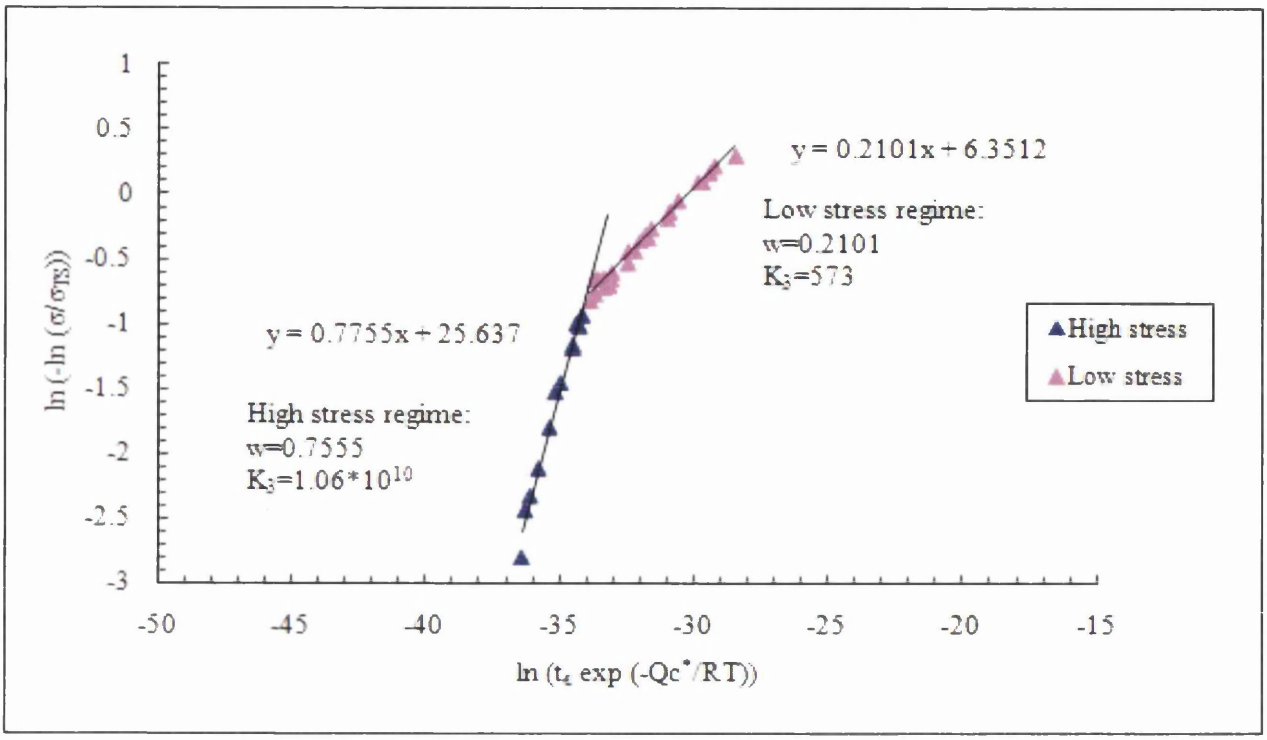

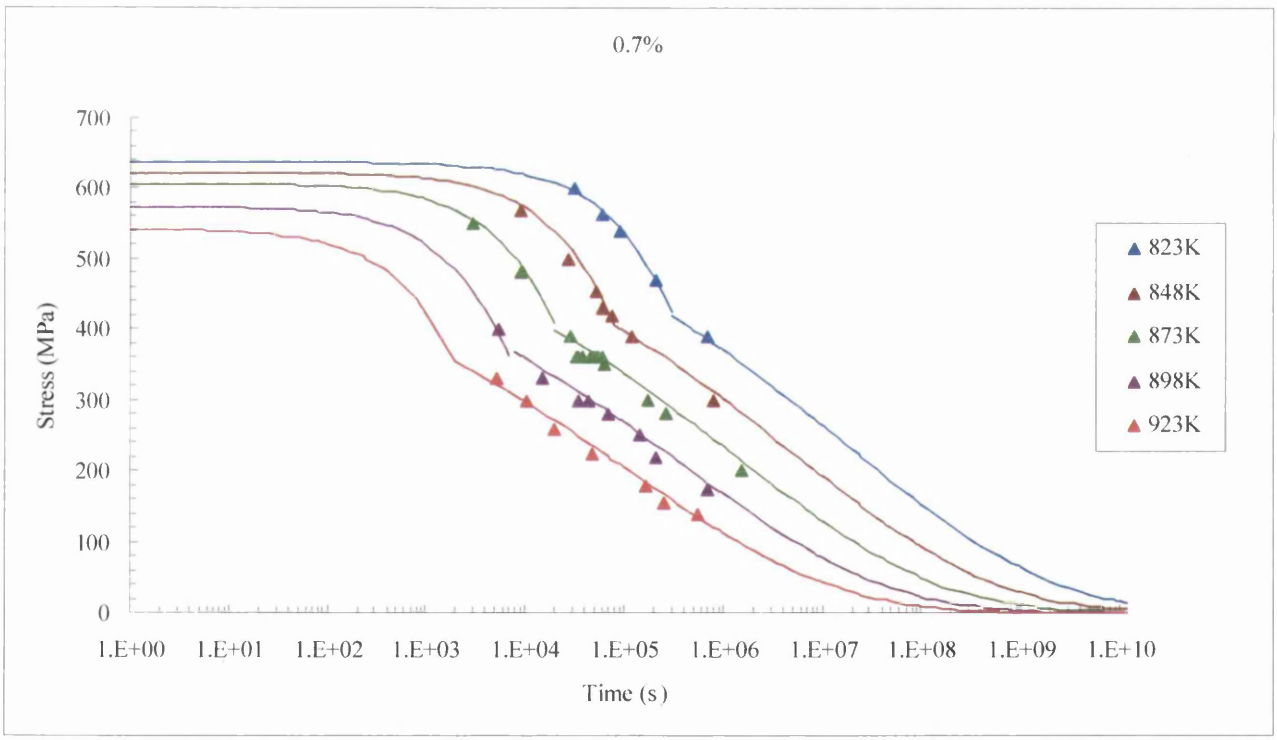

(B21.6): 1% strain

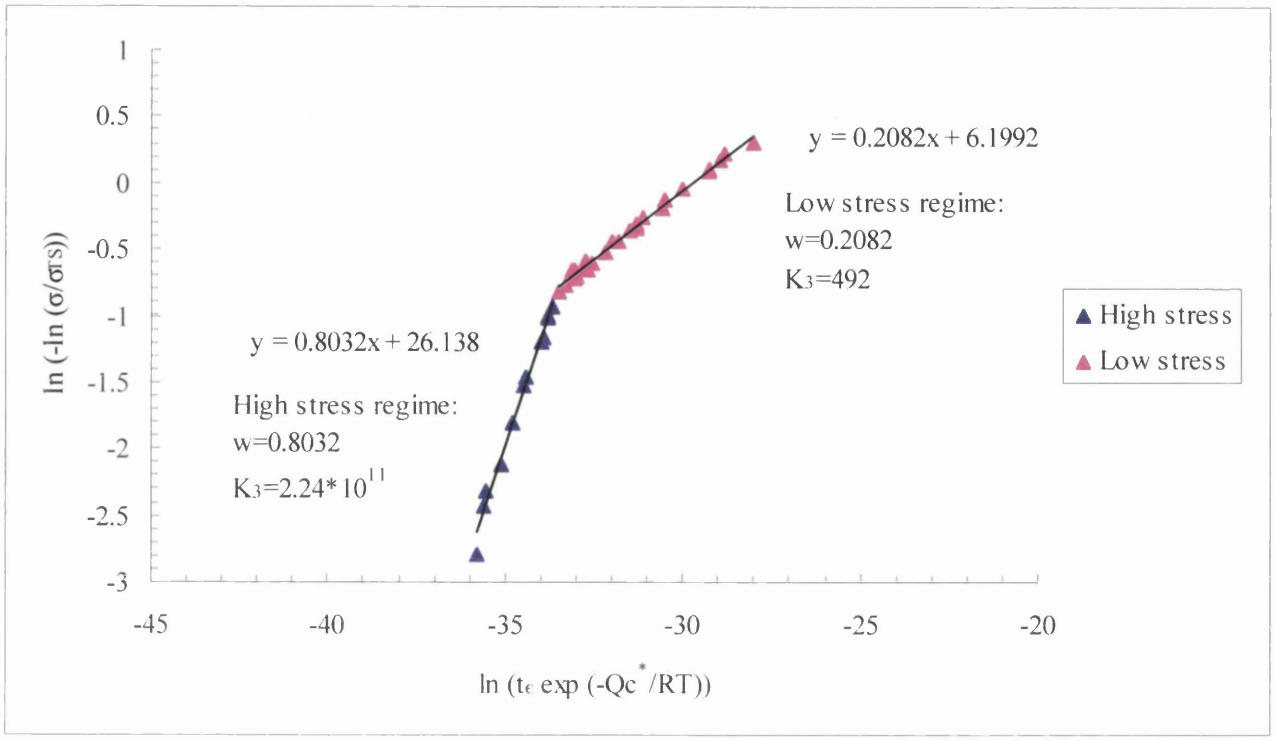

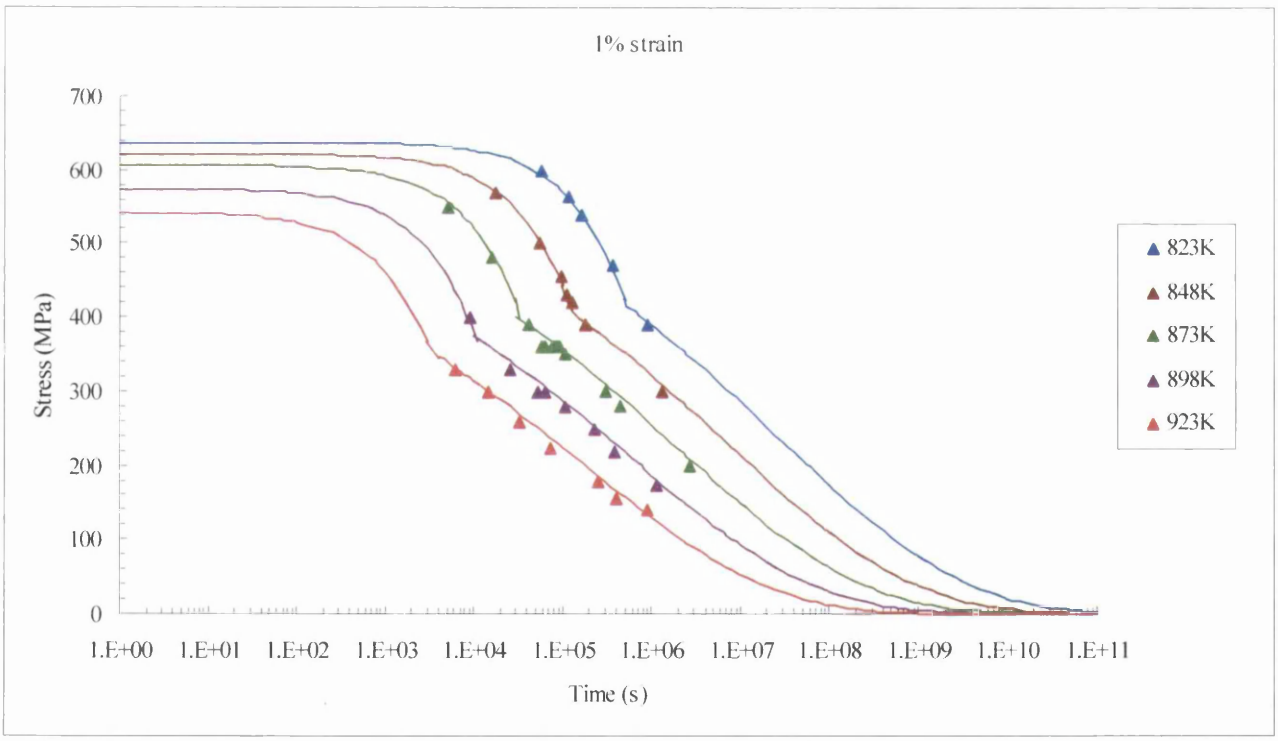

(B21.7): 2% strain

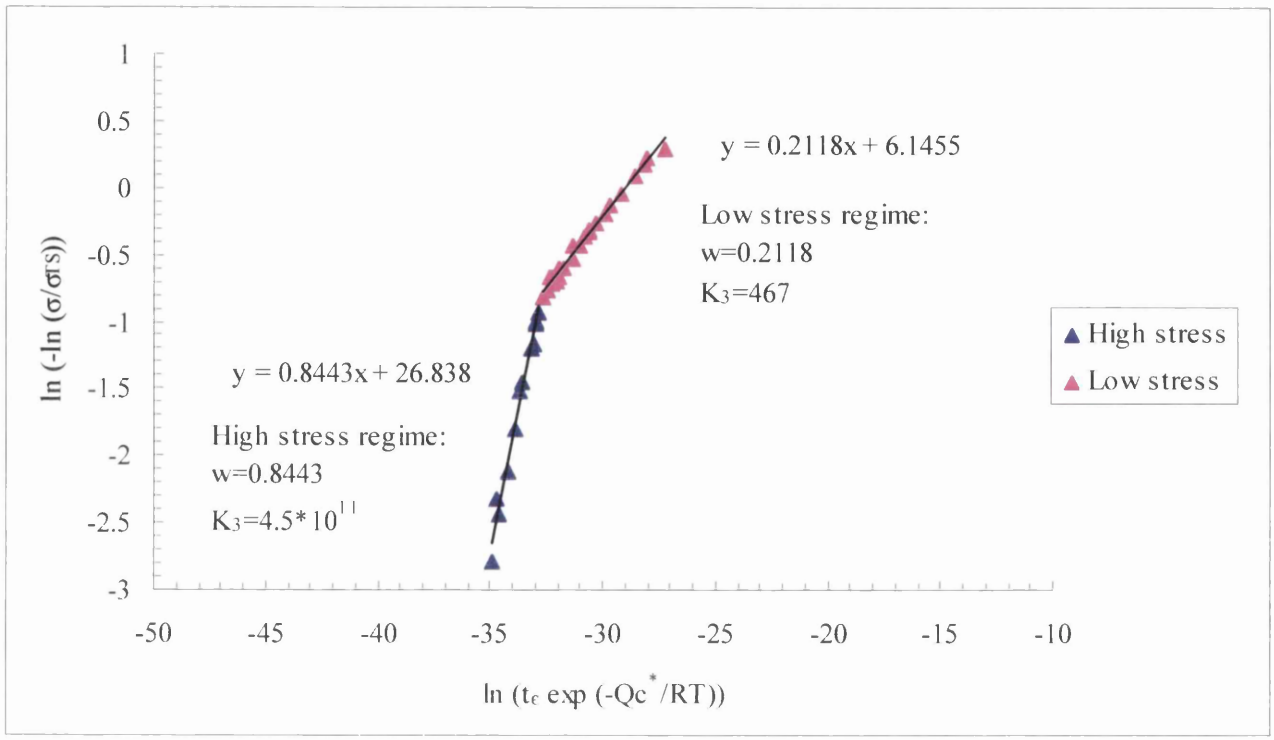

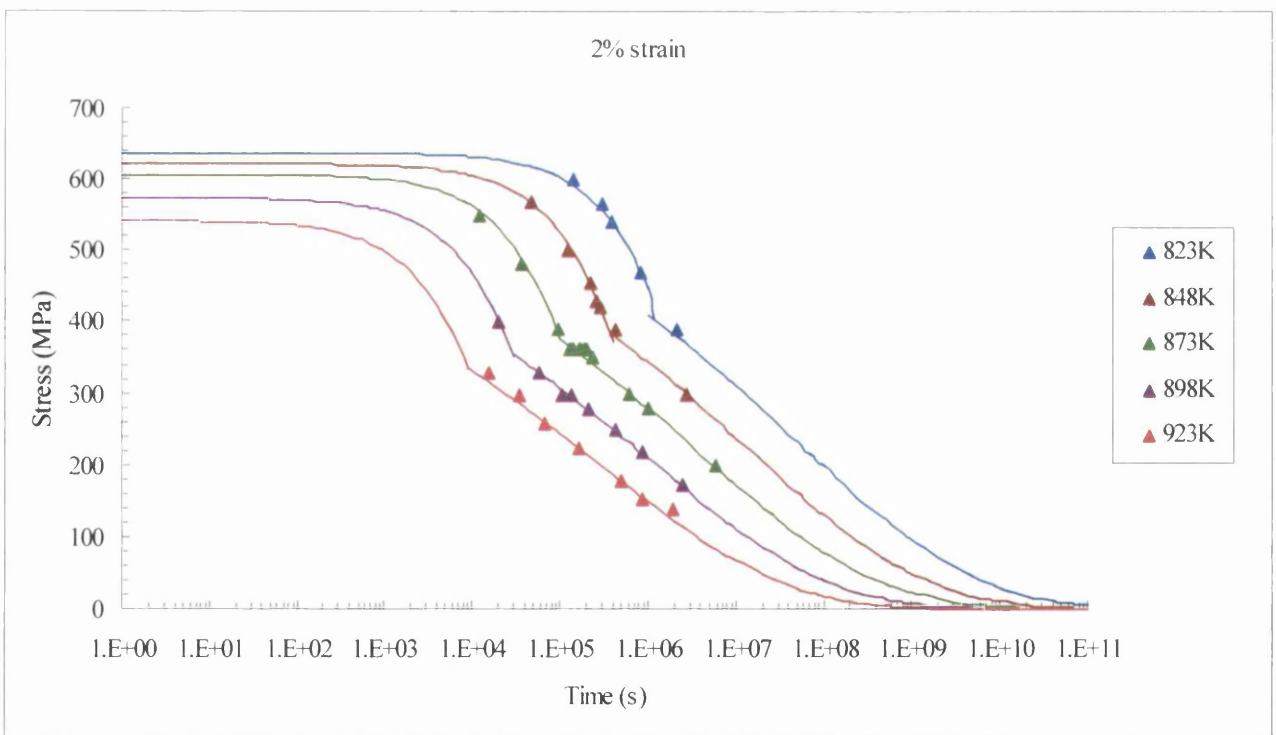

(B21.8): 5% strain

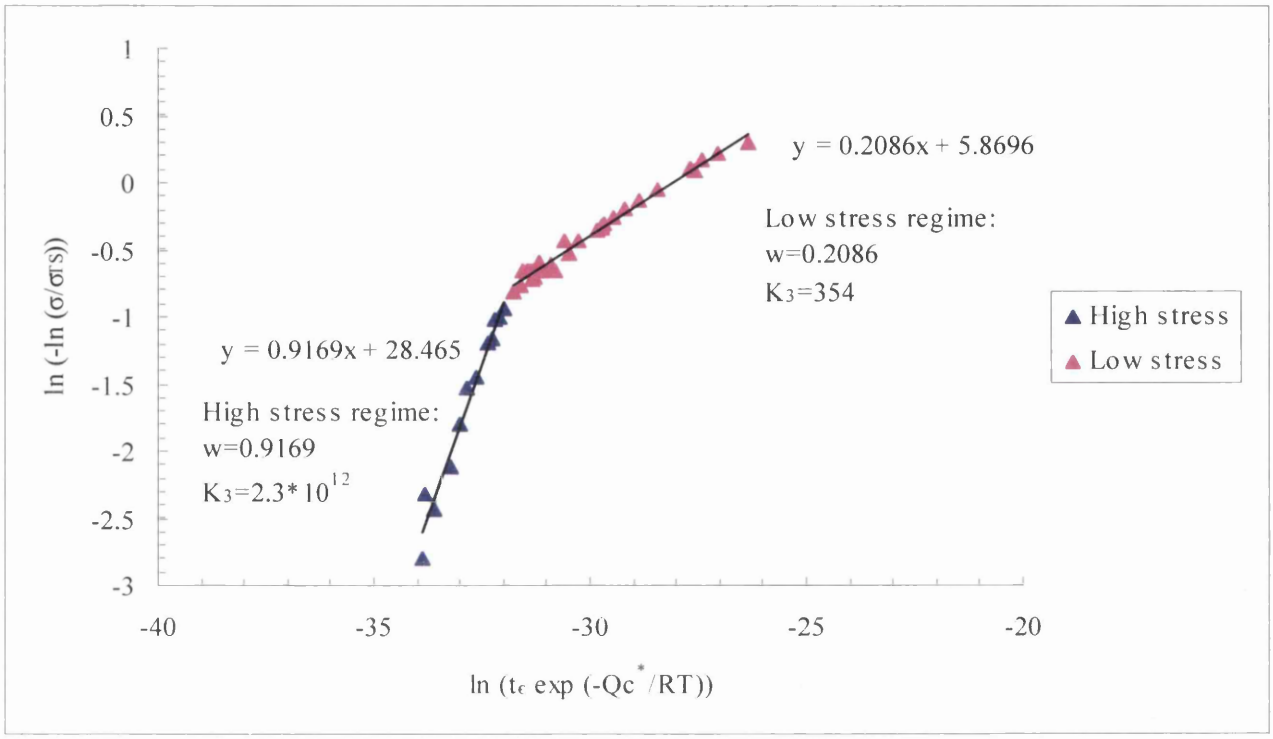

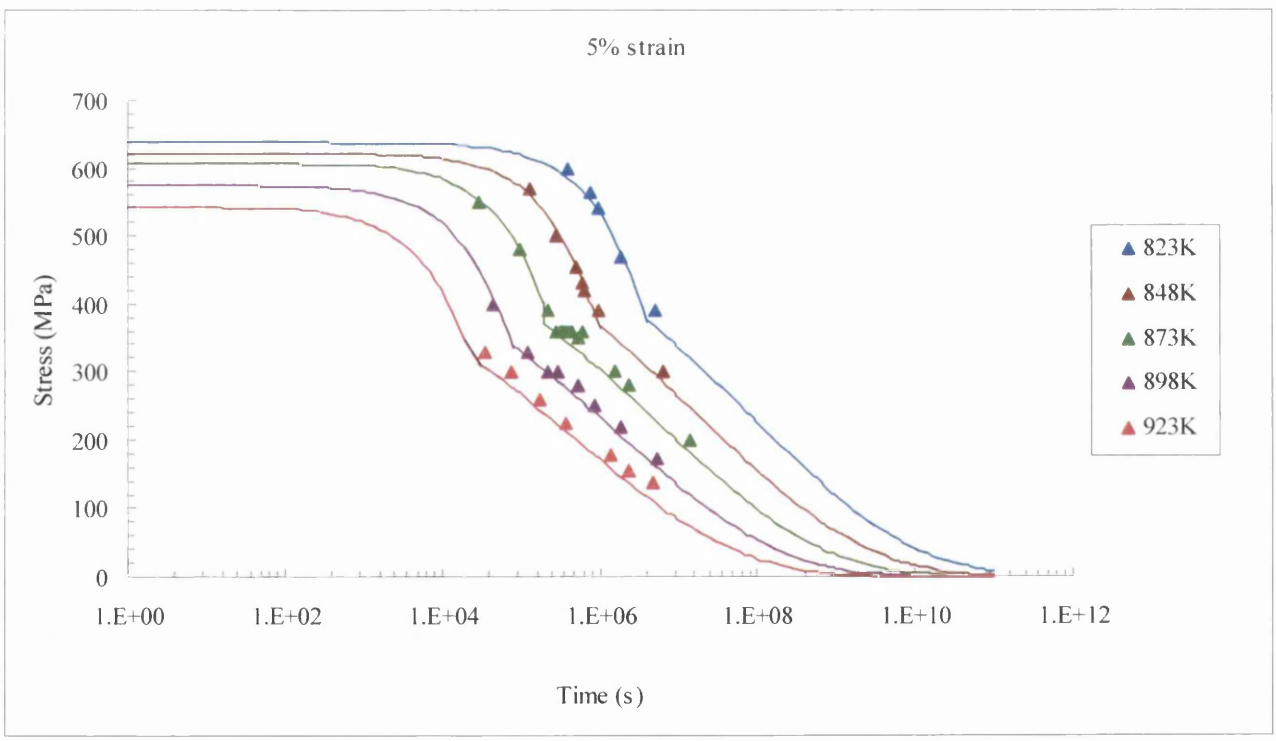

(B21.9): 7% strain

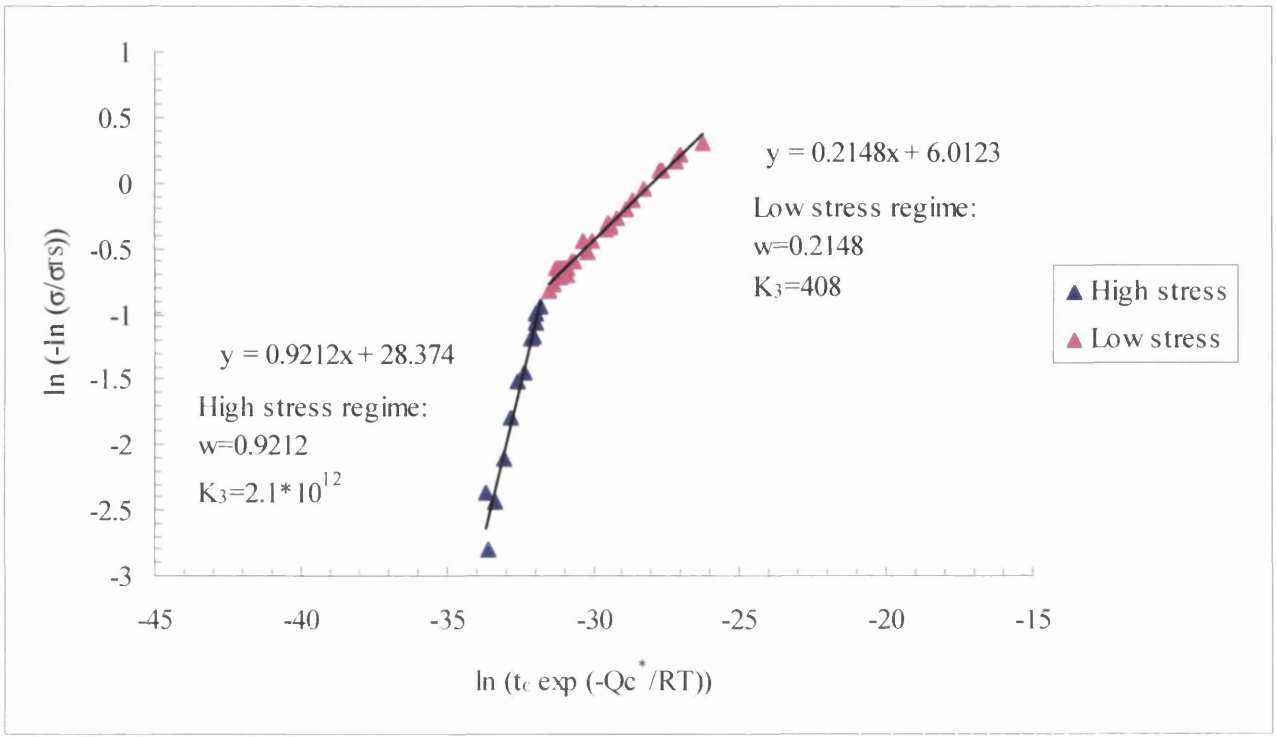

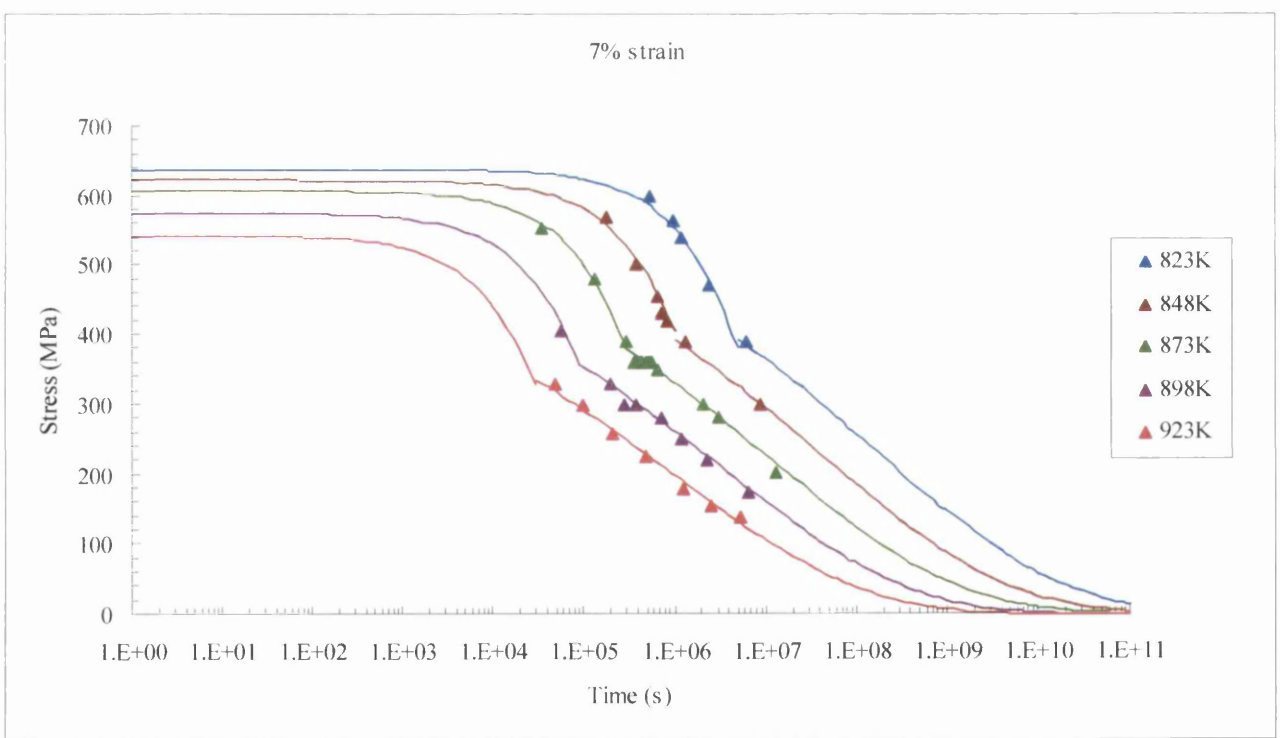

(B21.10): 10% strain

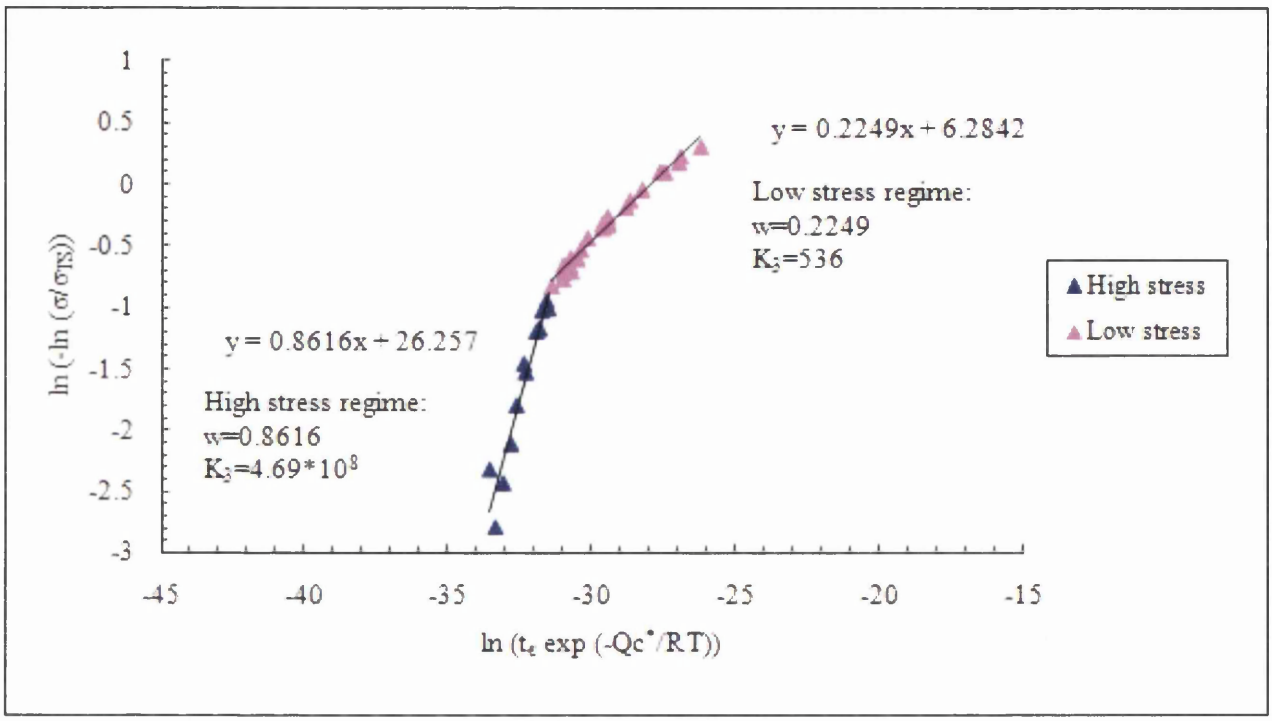

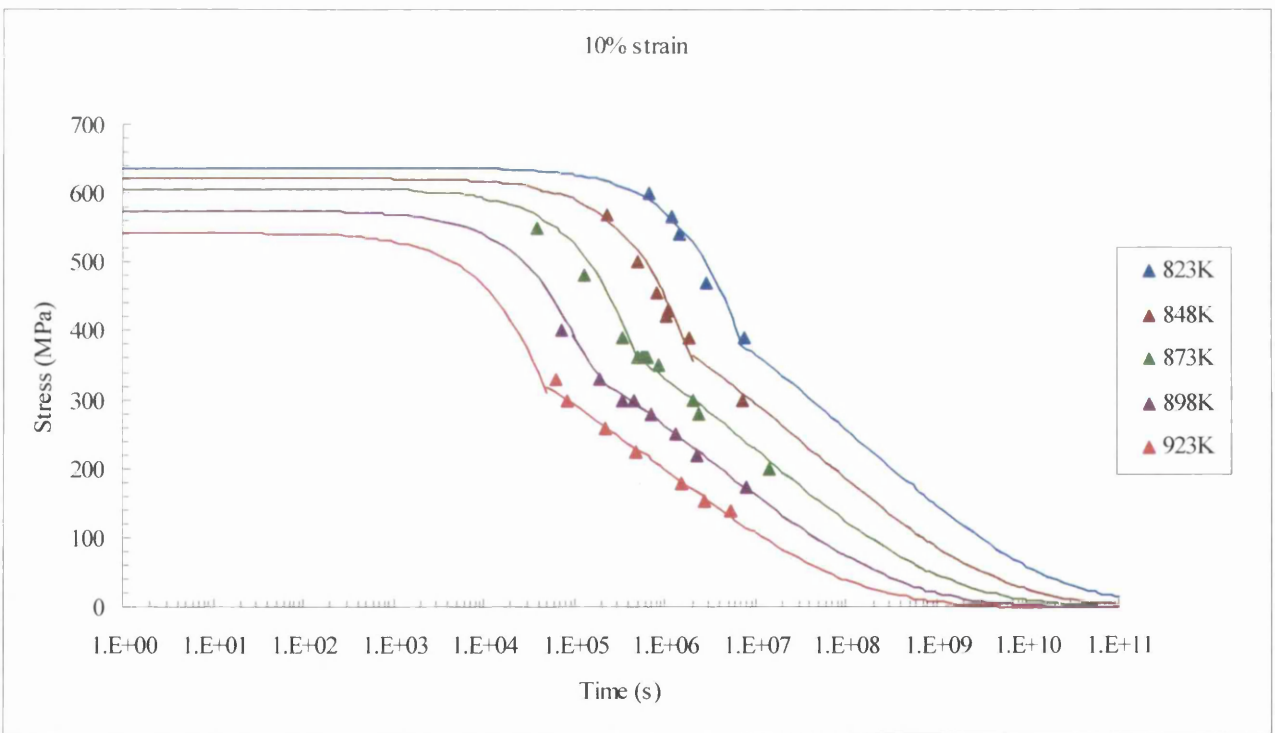

(B21.11): 13% strain

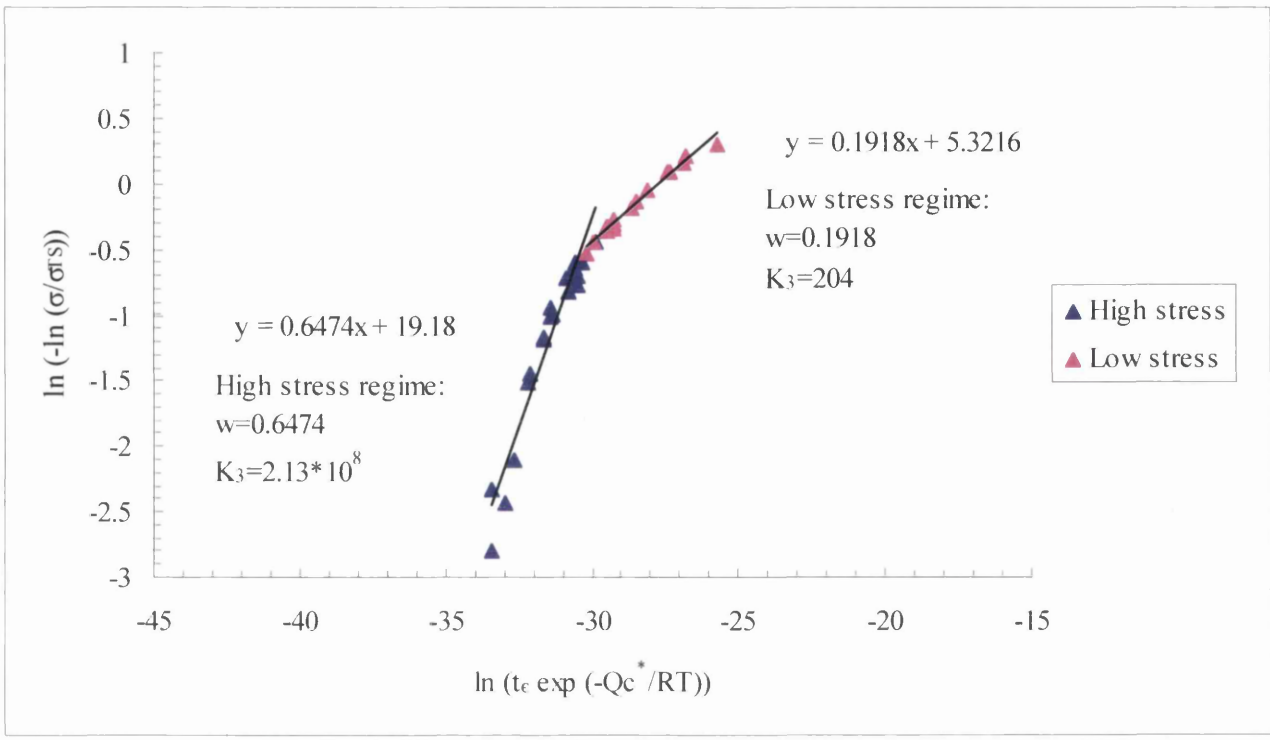

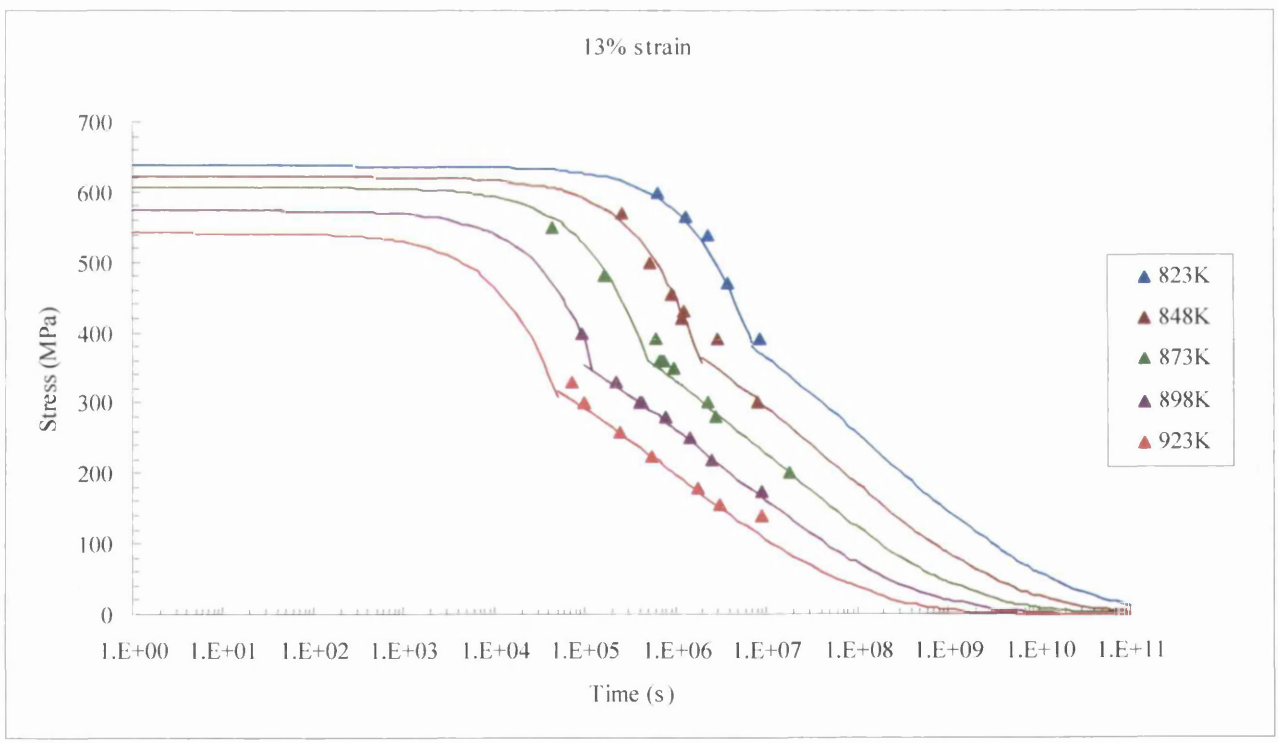

(B21.12): 15% strain

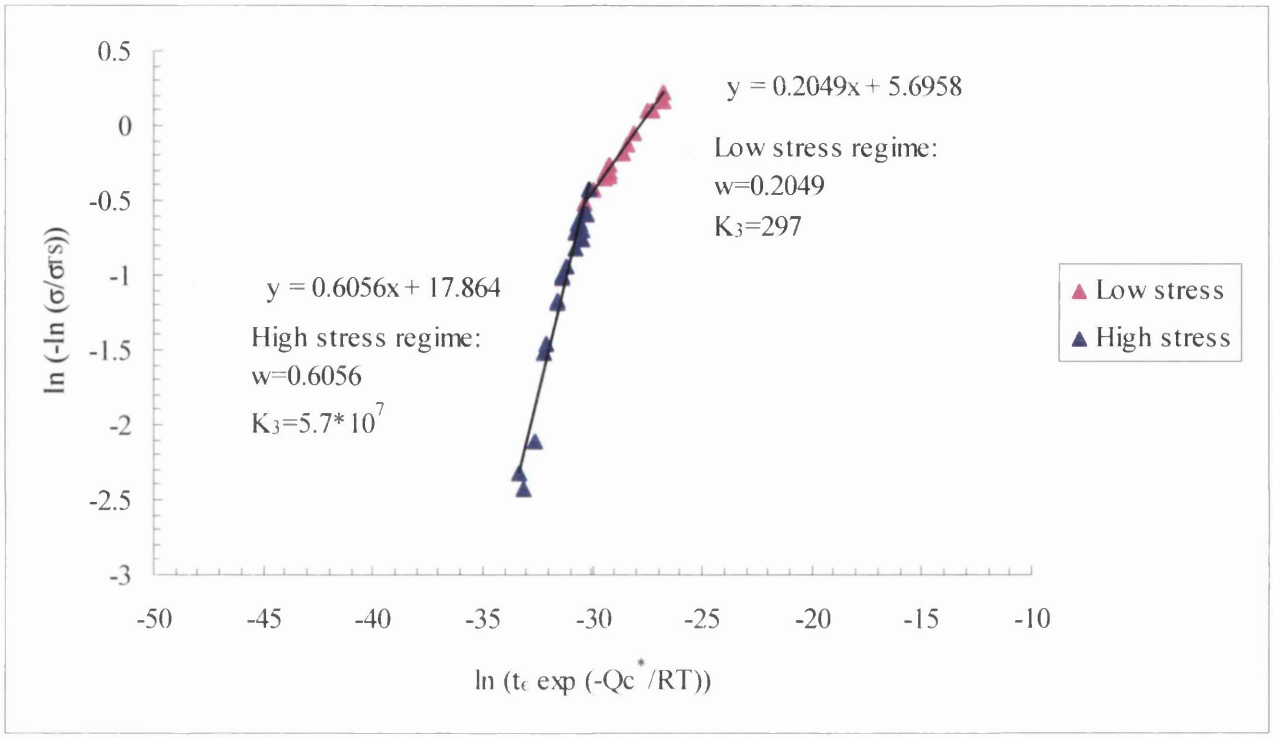

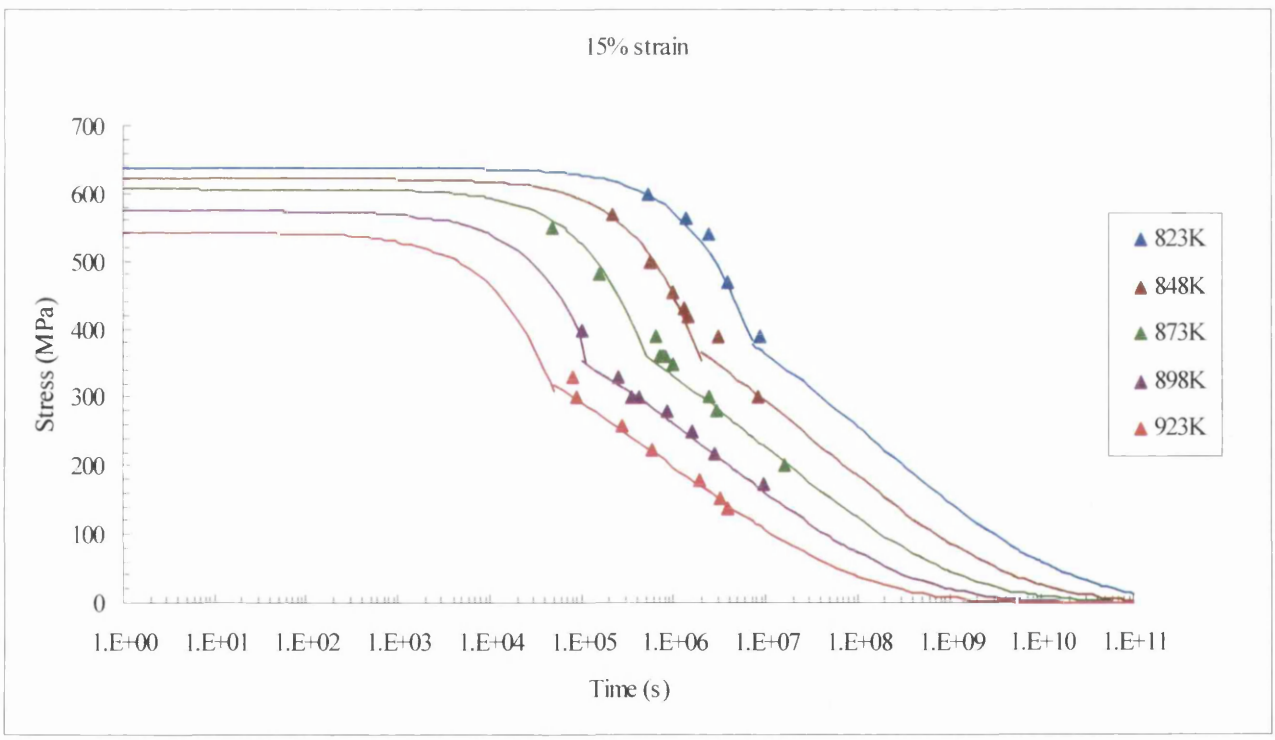

(B21.13): 20% strain

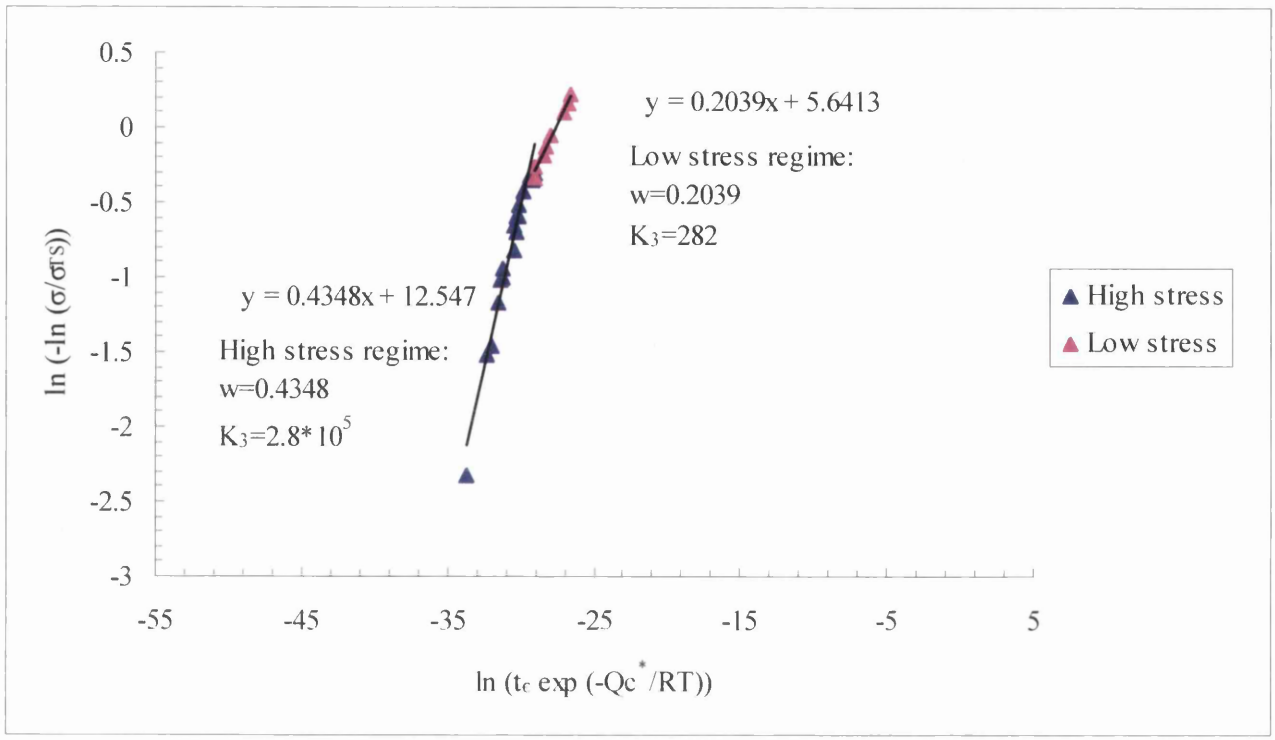

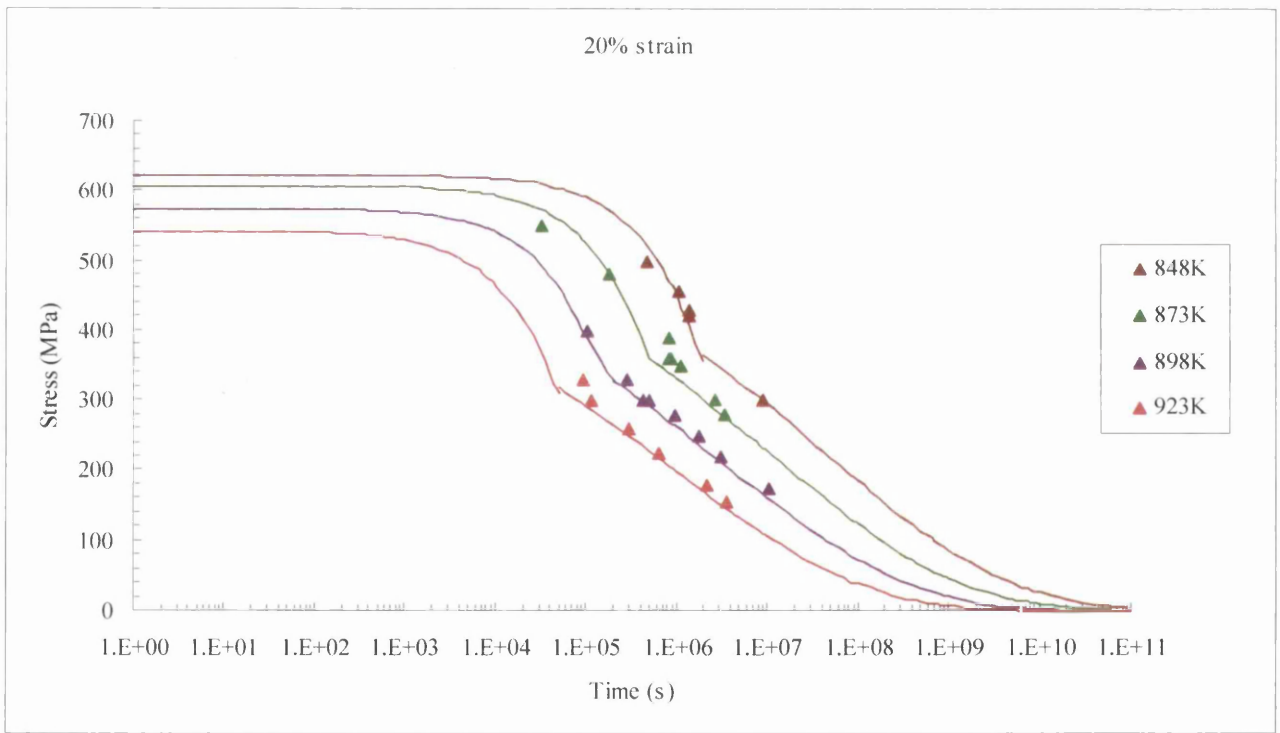

B.22 THE WILSHIRE TECHNIQUE RESULTS (w and k_3 curve fits)

(B22.1): w and k_3 for all strain levels

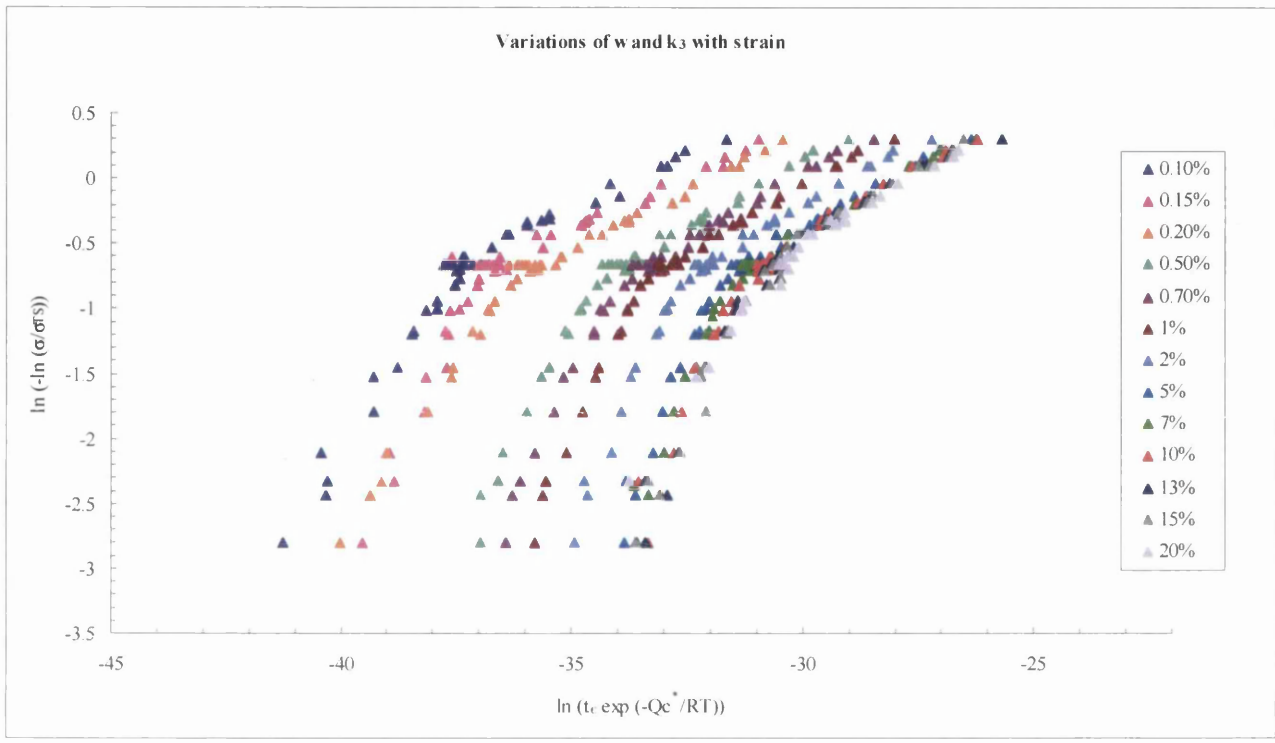

(B22.2): w and k_3 (low stress regime)

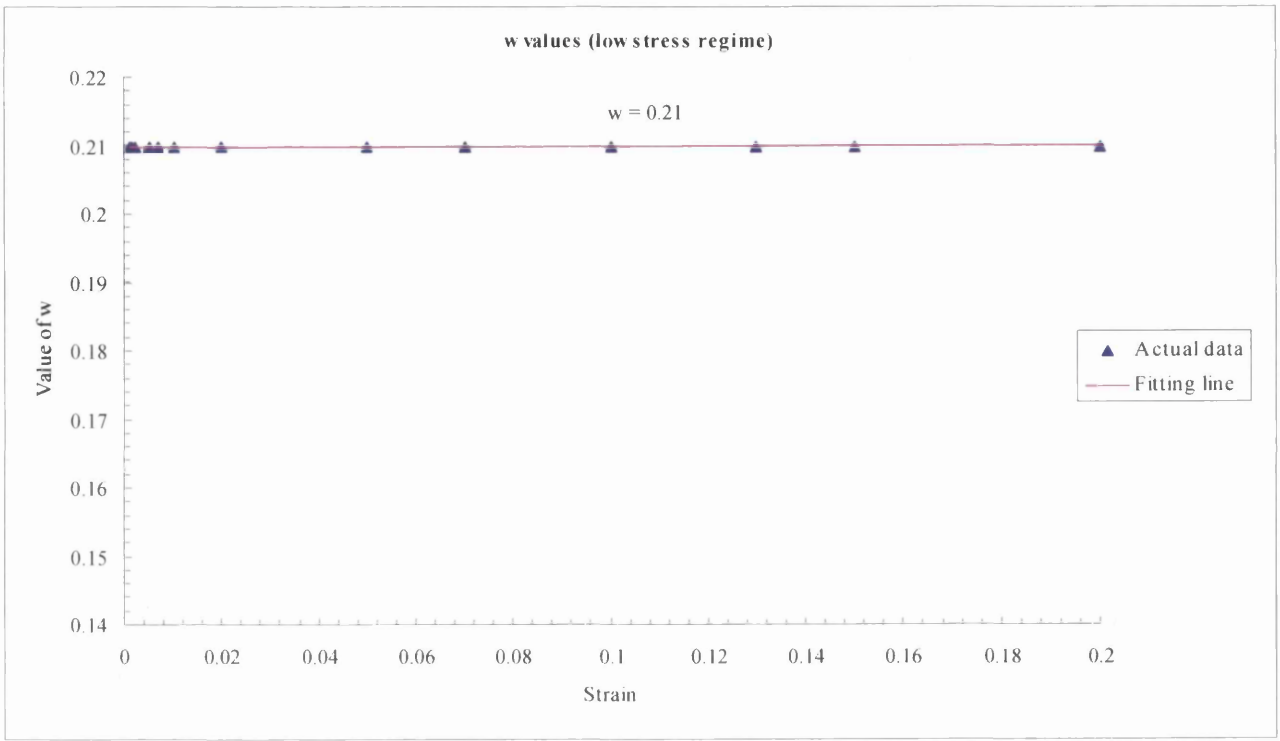

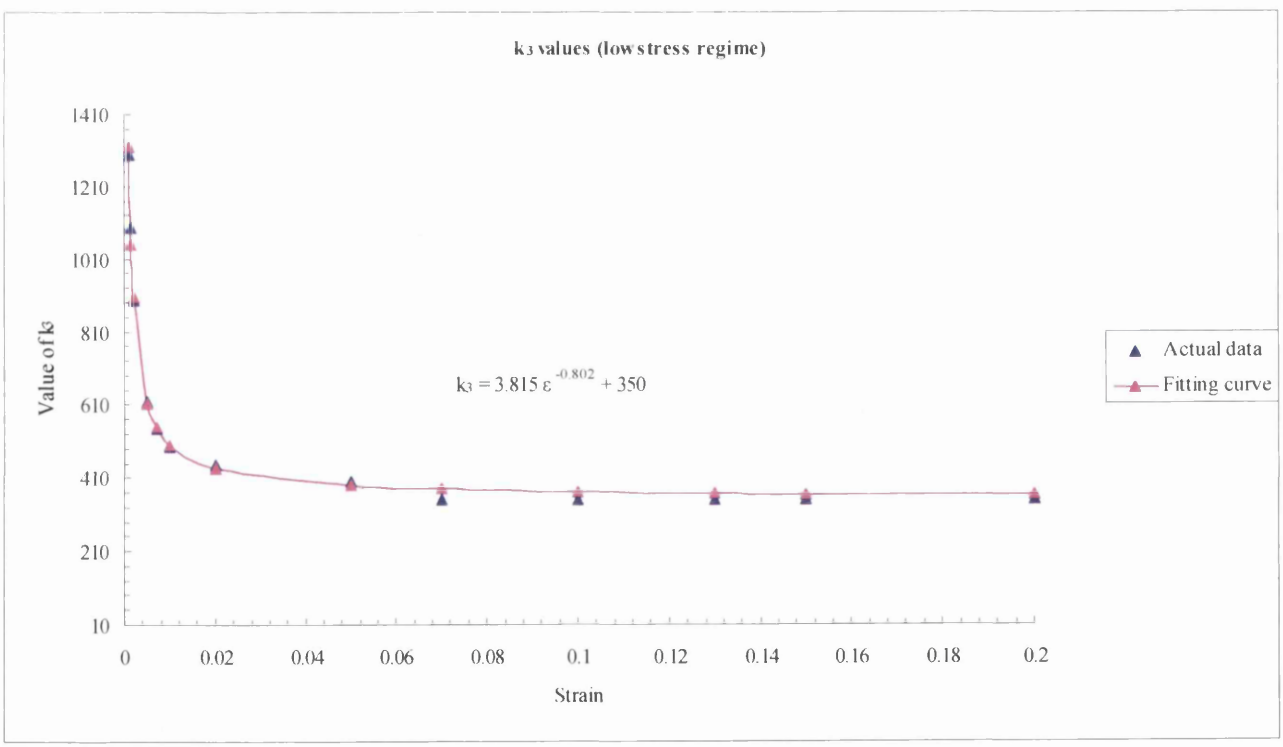

(B22.3): w and k_3 (high stress regime)

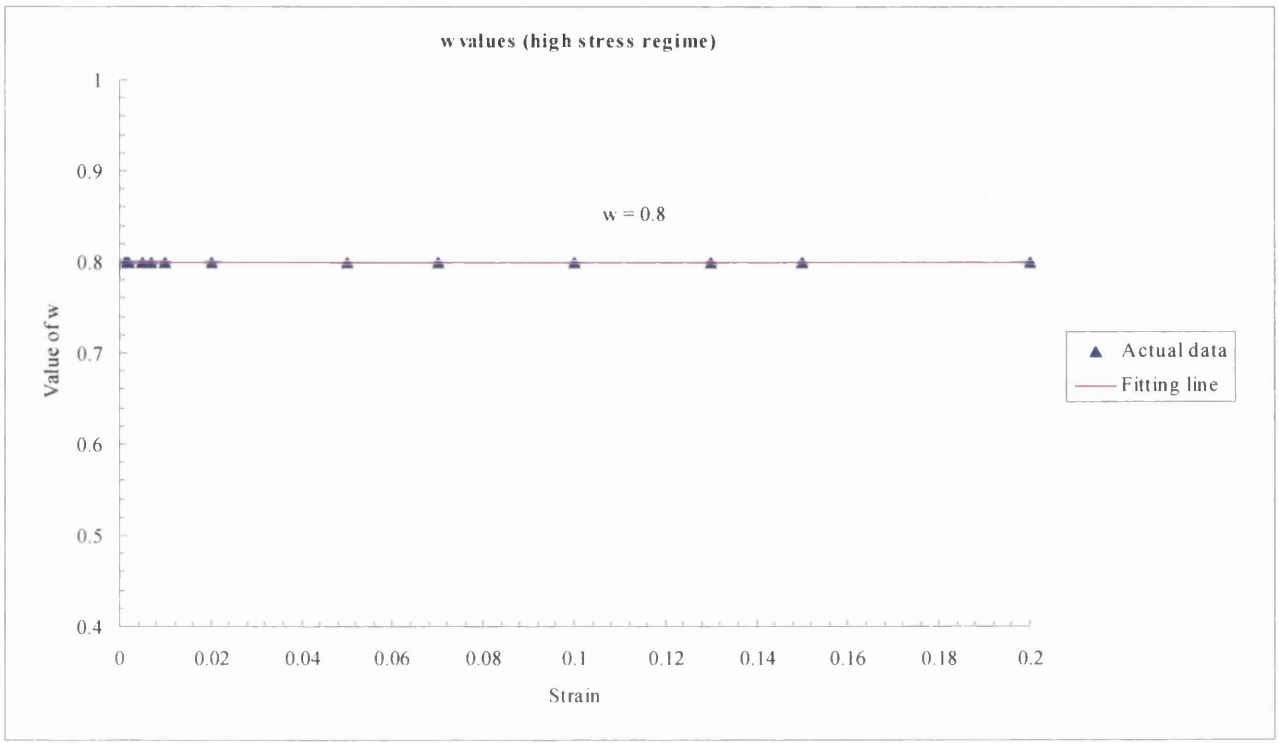

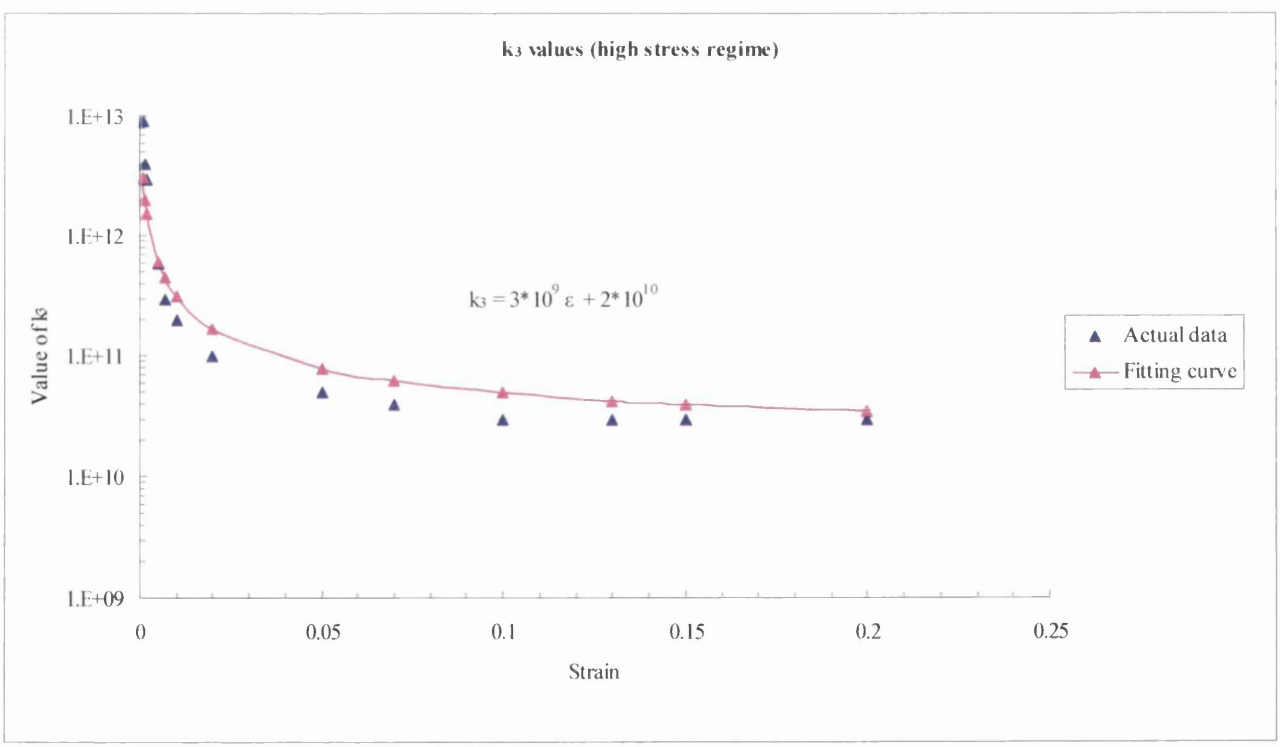

B.23 THE RE-PRODUCED CREEP CURVES

(B23.1): 823K/390MPa

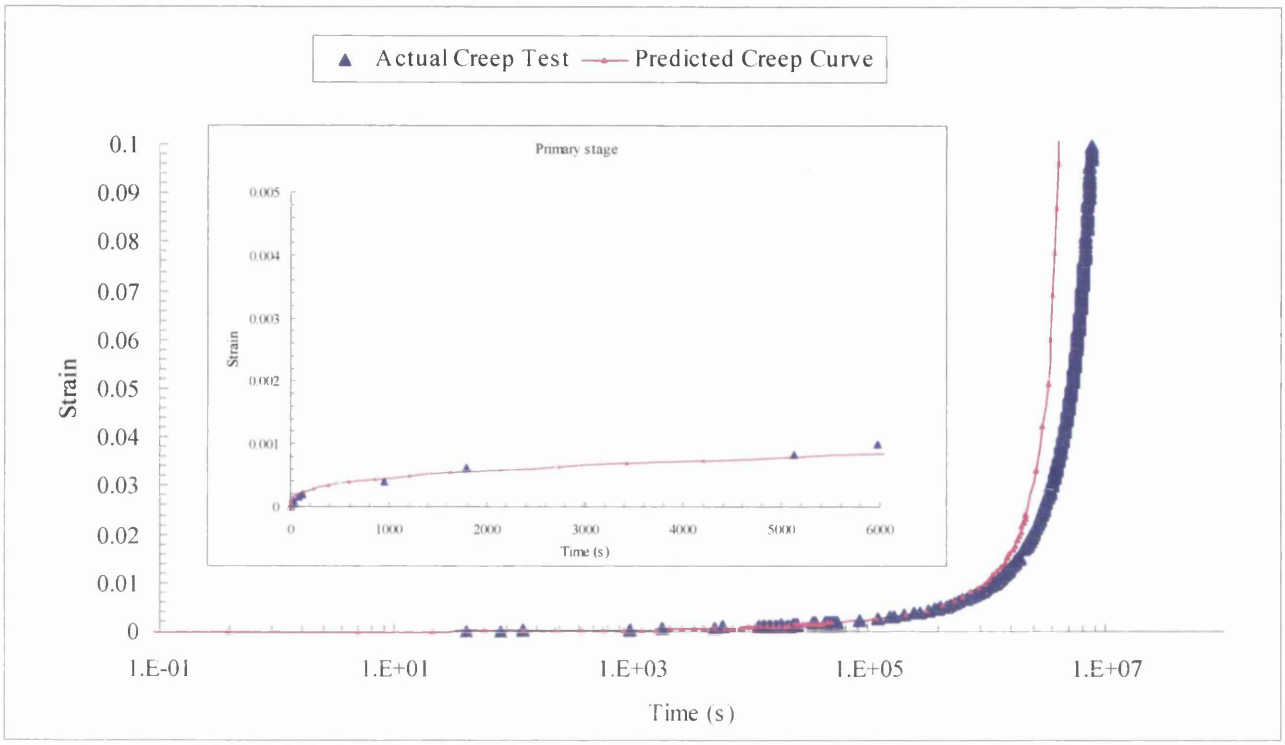

(B23.2): 823K/470MPa

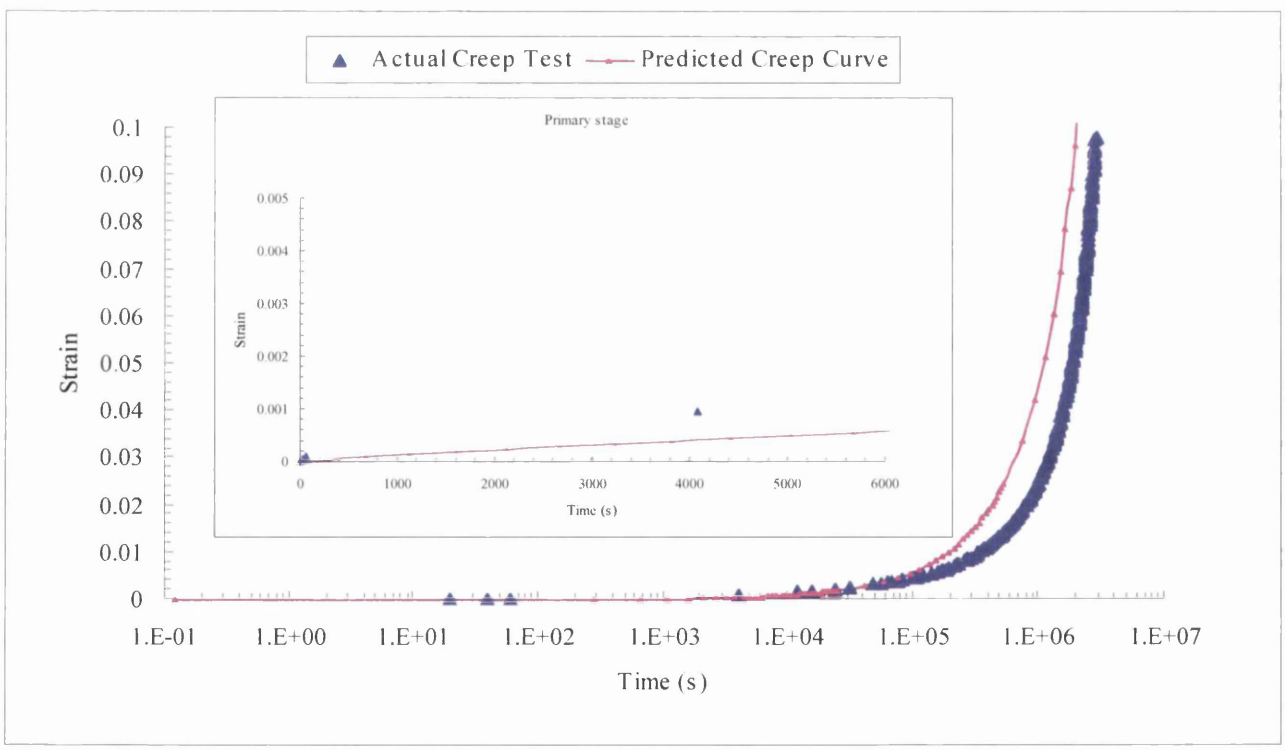

(B23.3): 823K/540MPa

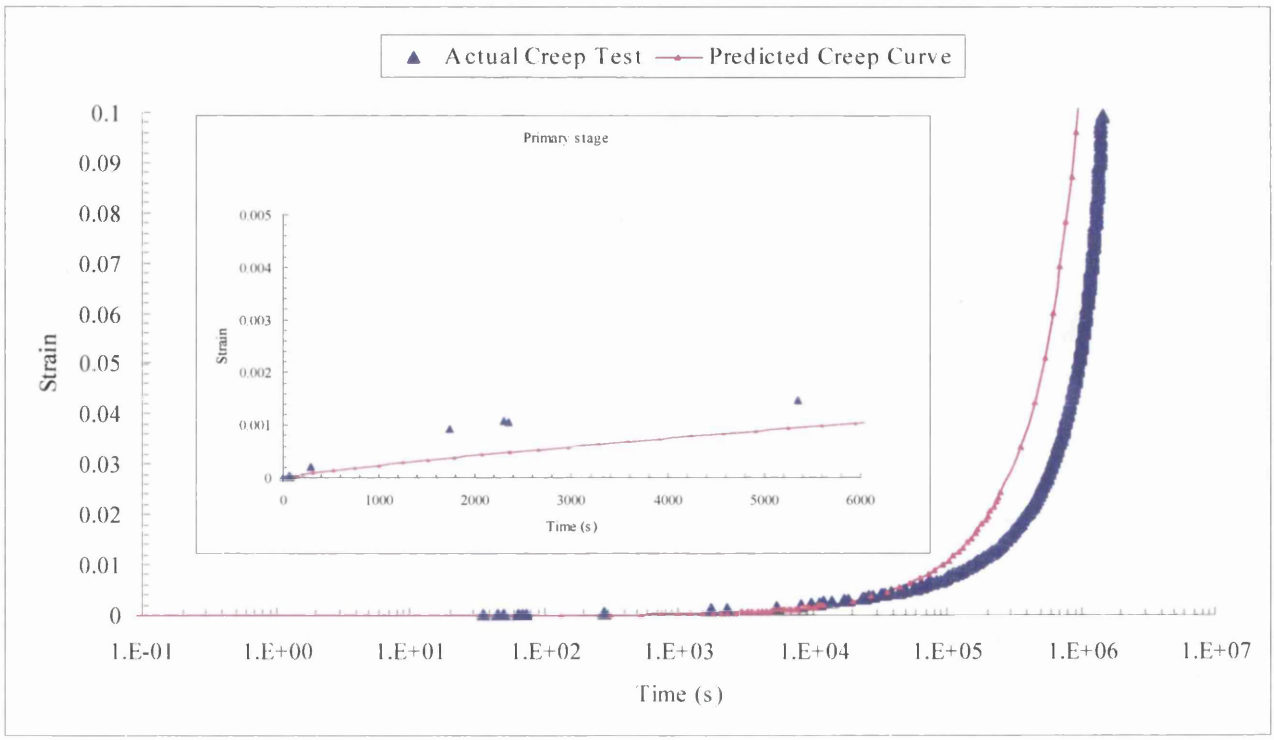

(B23.4): 823K/565MPa

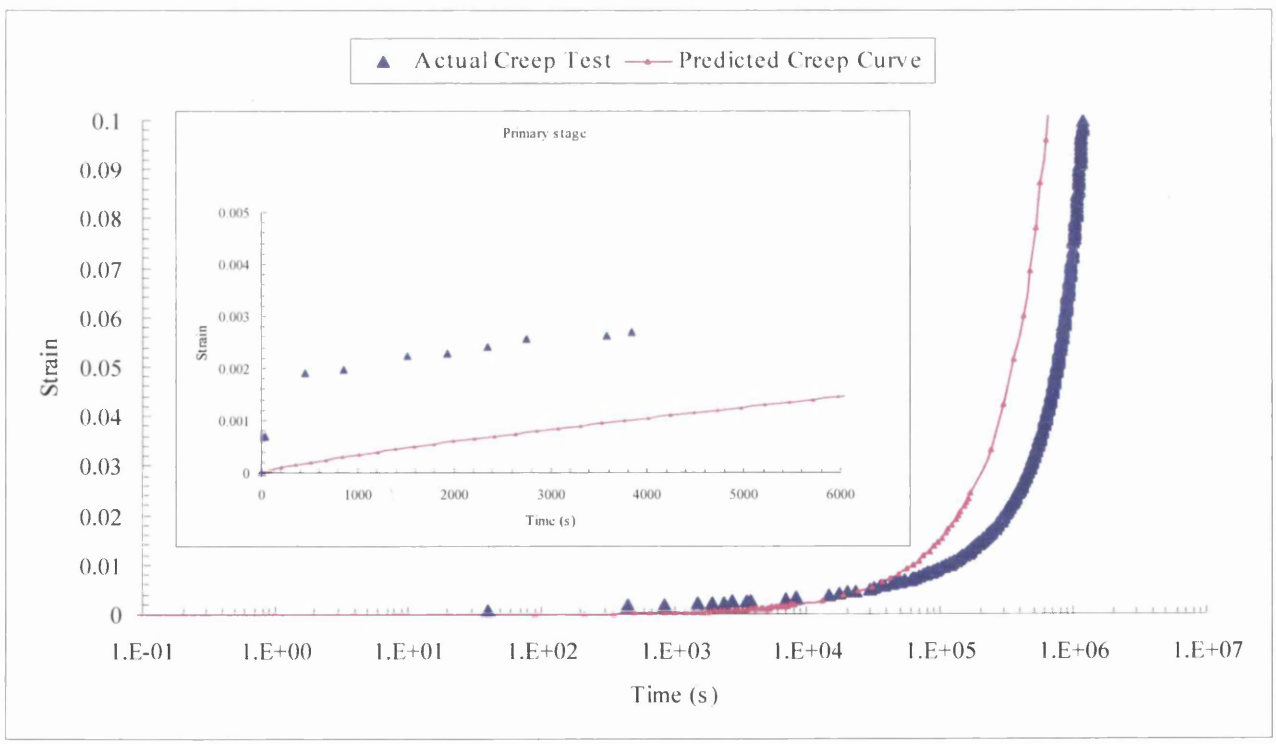

(B23.5): 823K/600MPa

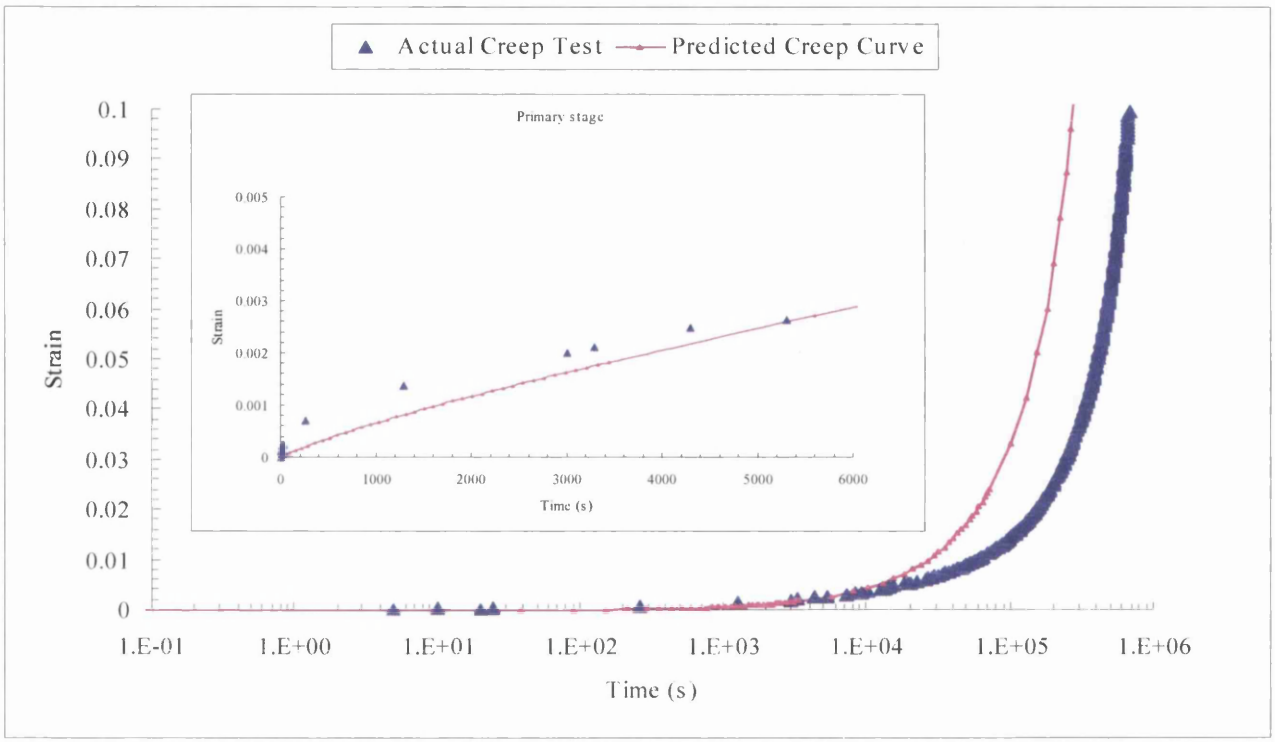

(B23.6): 848K/300MPa

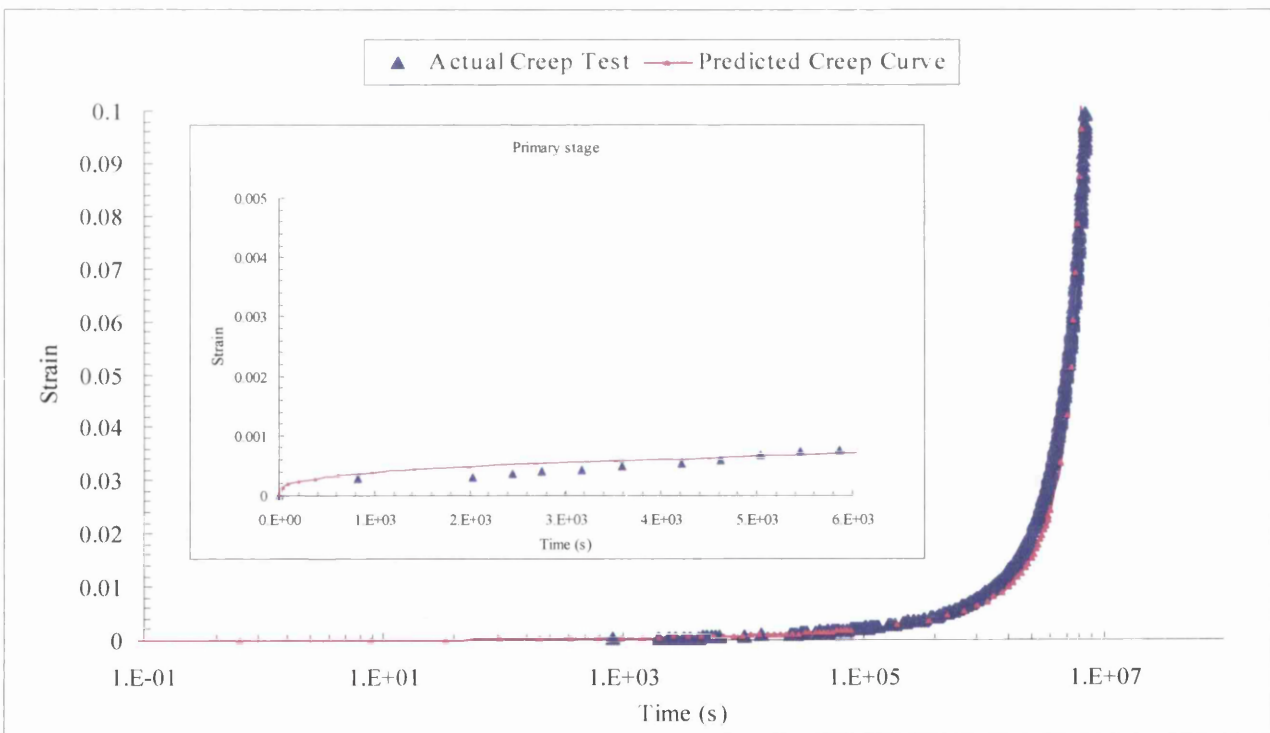

(B23.7): 848K/390MPa

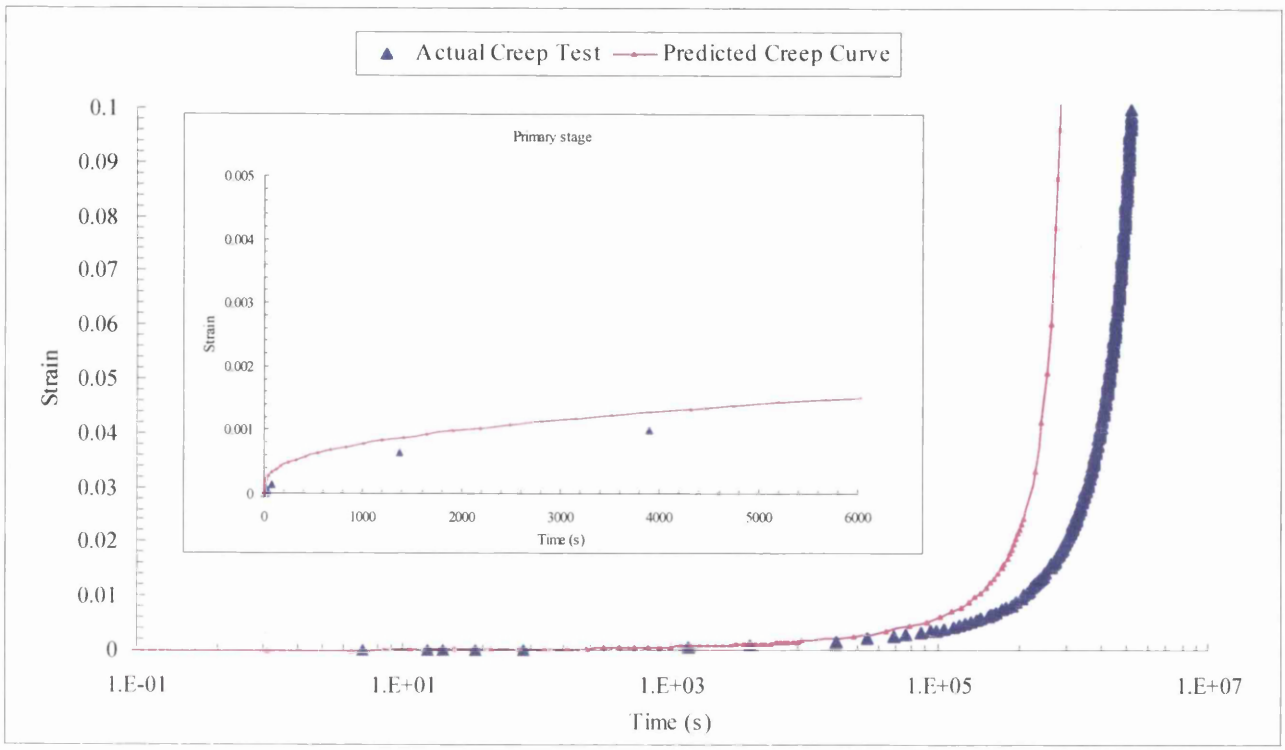

(B23.8): 848K/420MPa

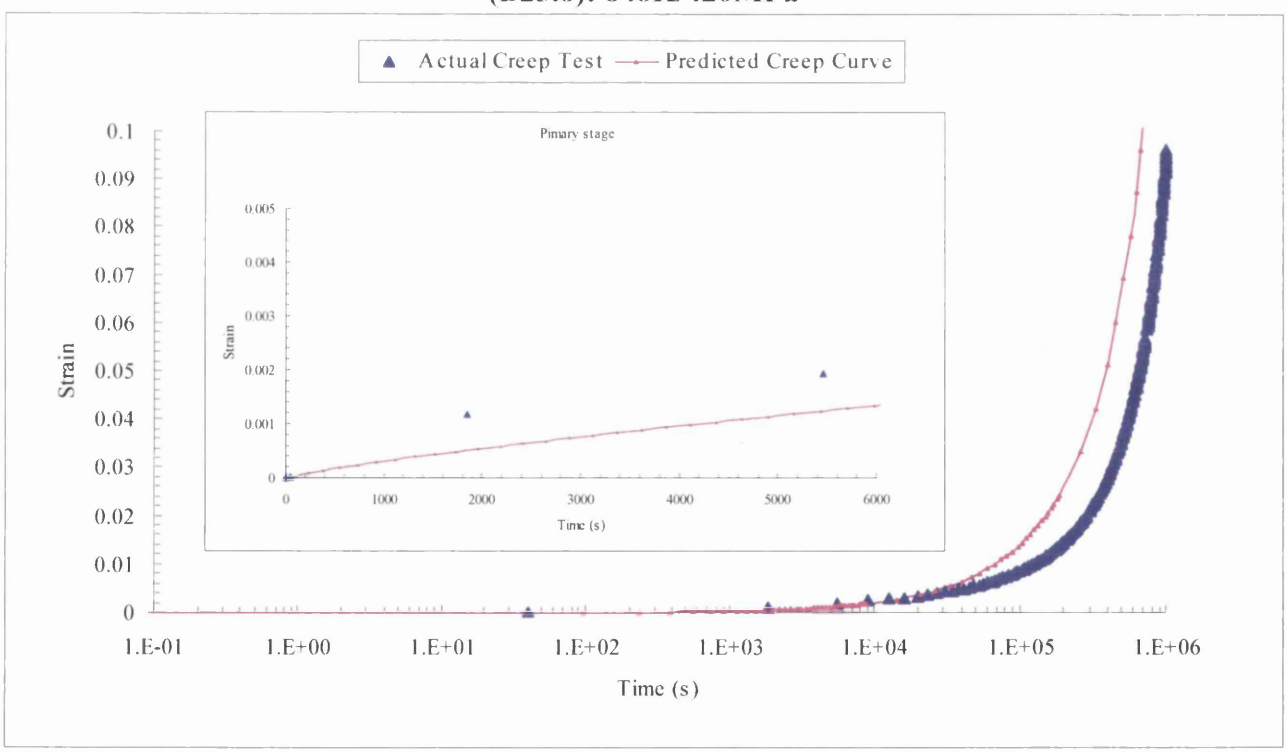

(B23.9): 848K/430MPa

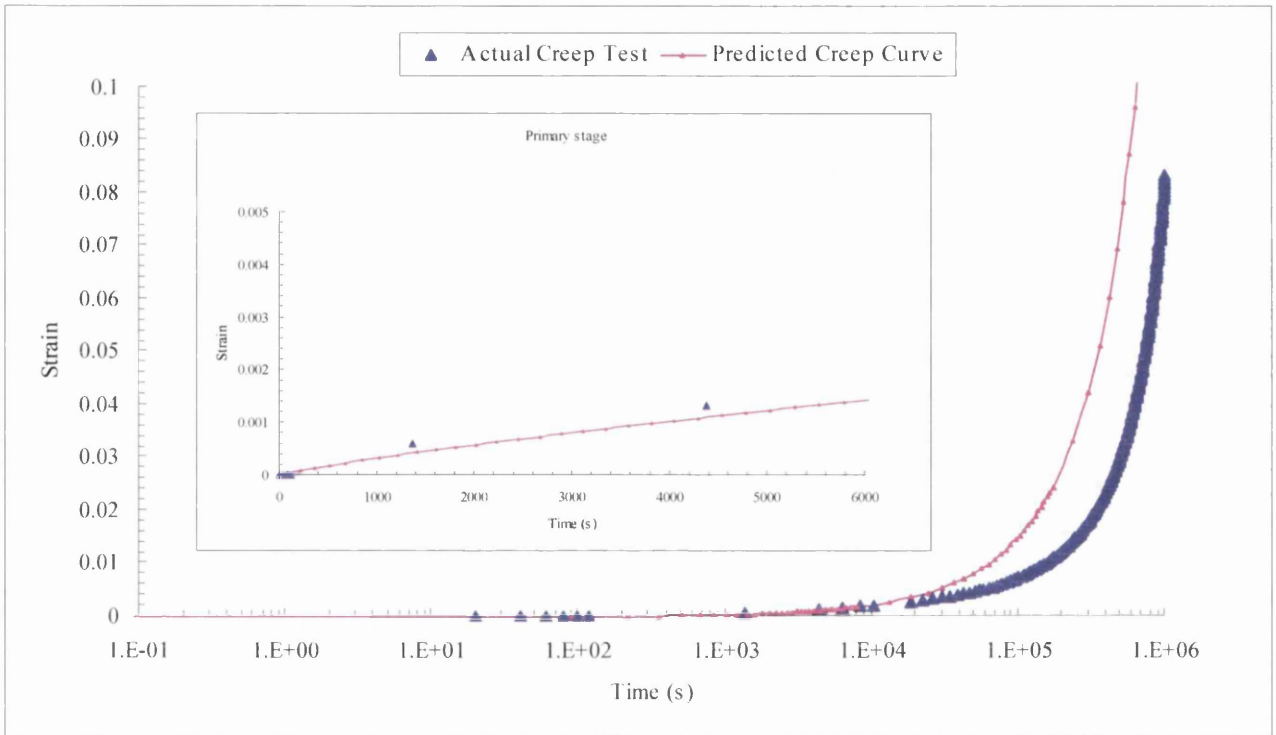

(B23.10): 848K/455MPa

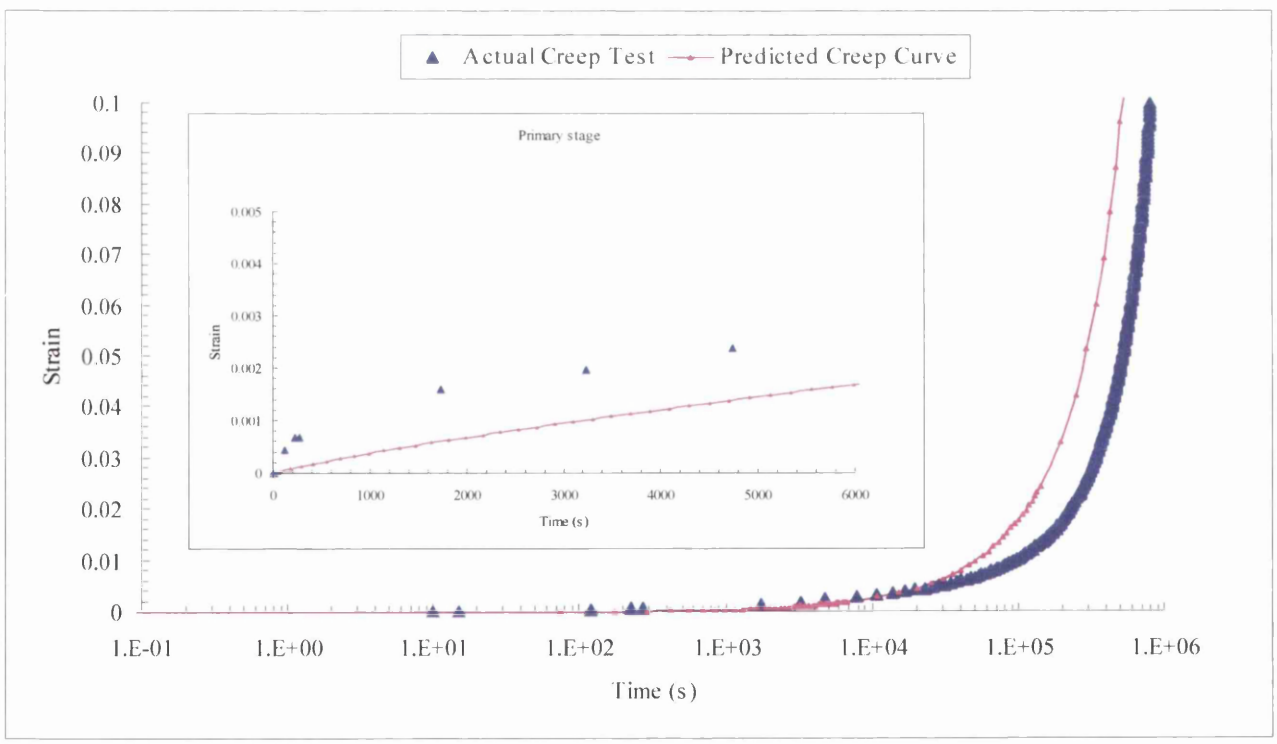

(B23.11): 848K/500MPa

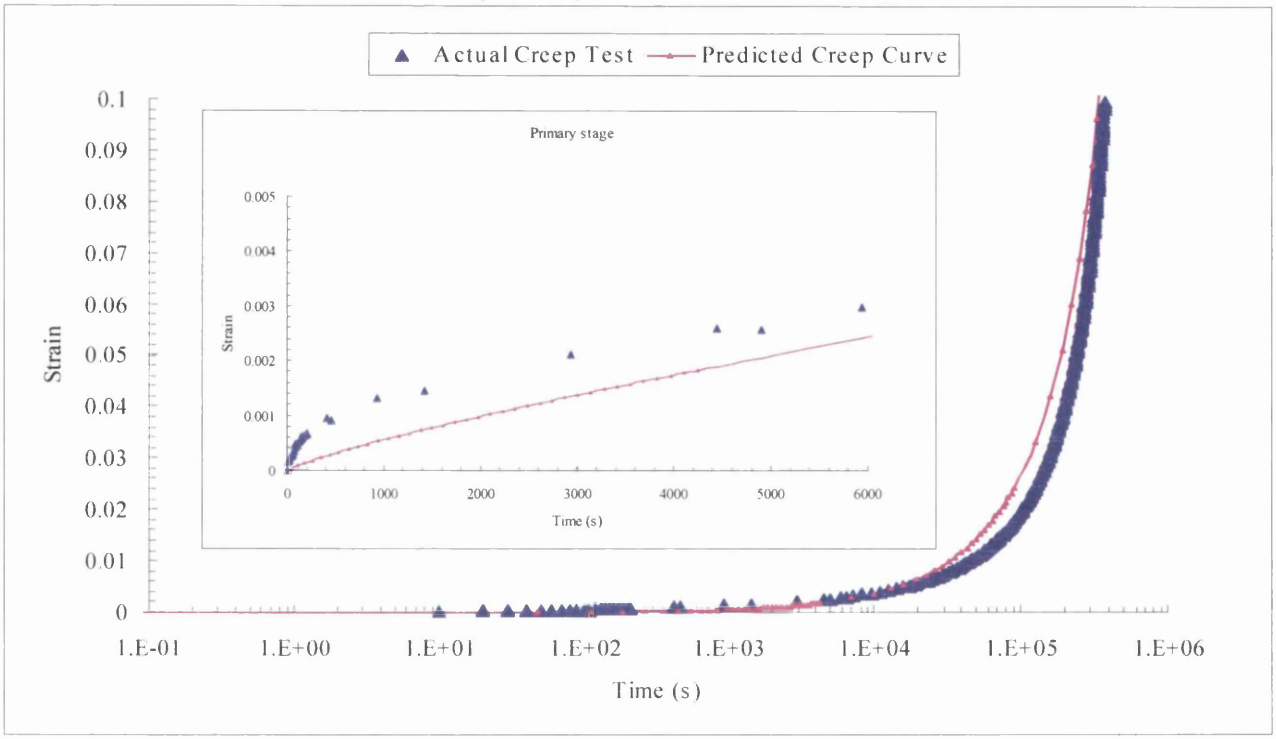

(B23.12): 848K/570MPa

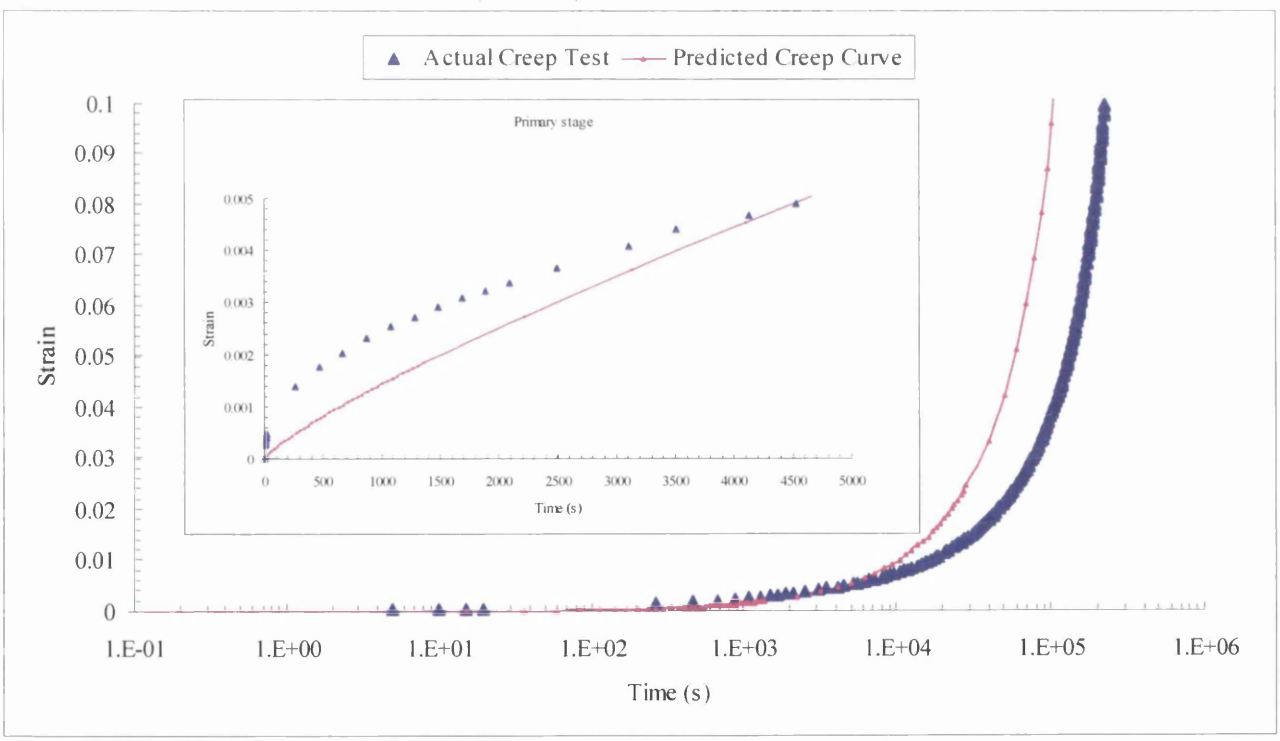

(B23.13): 873K/200MPa

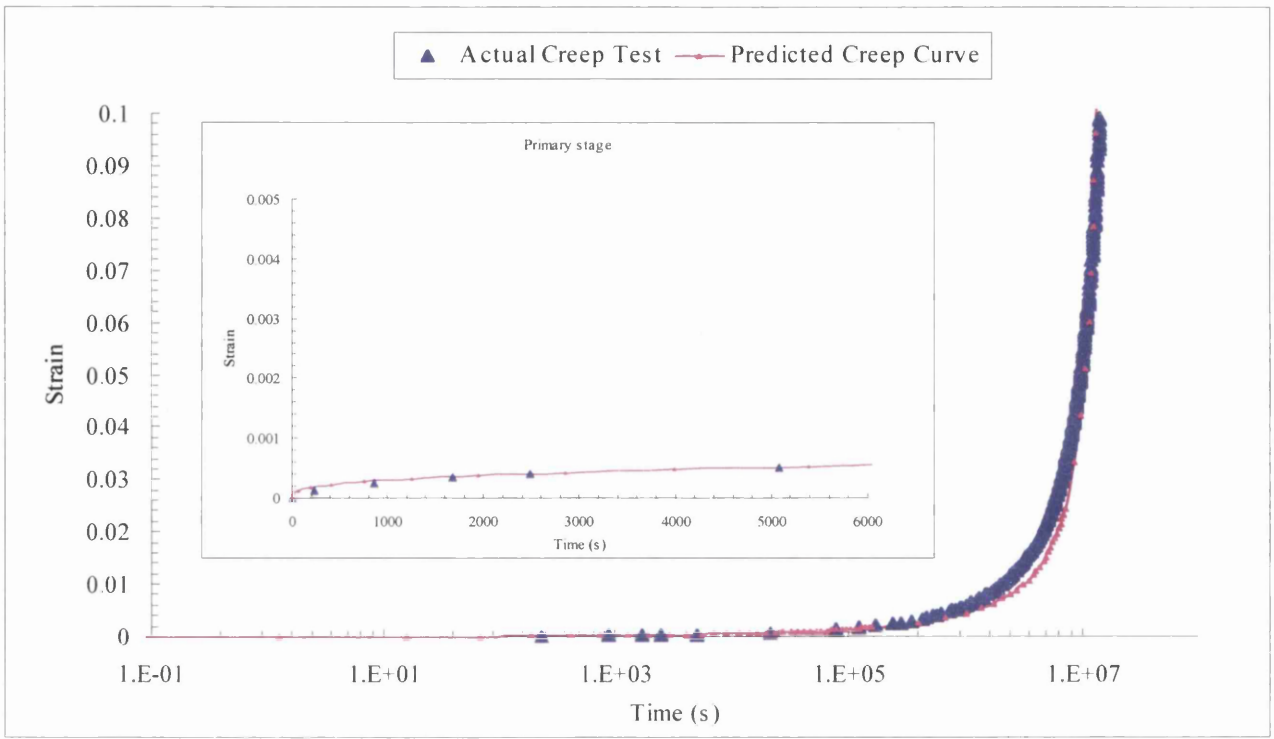

(B23.14): 873K/280MPa

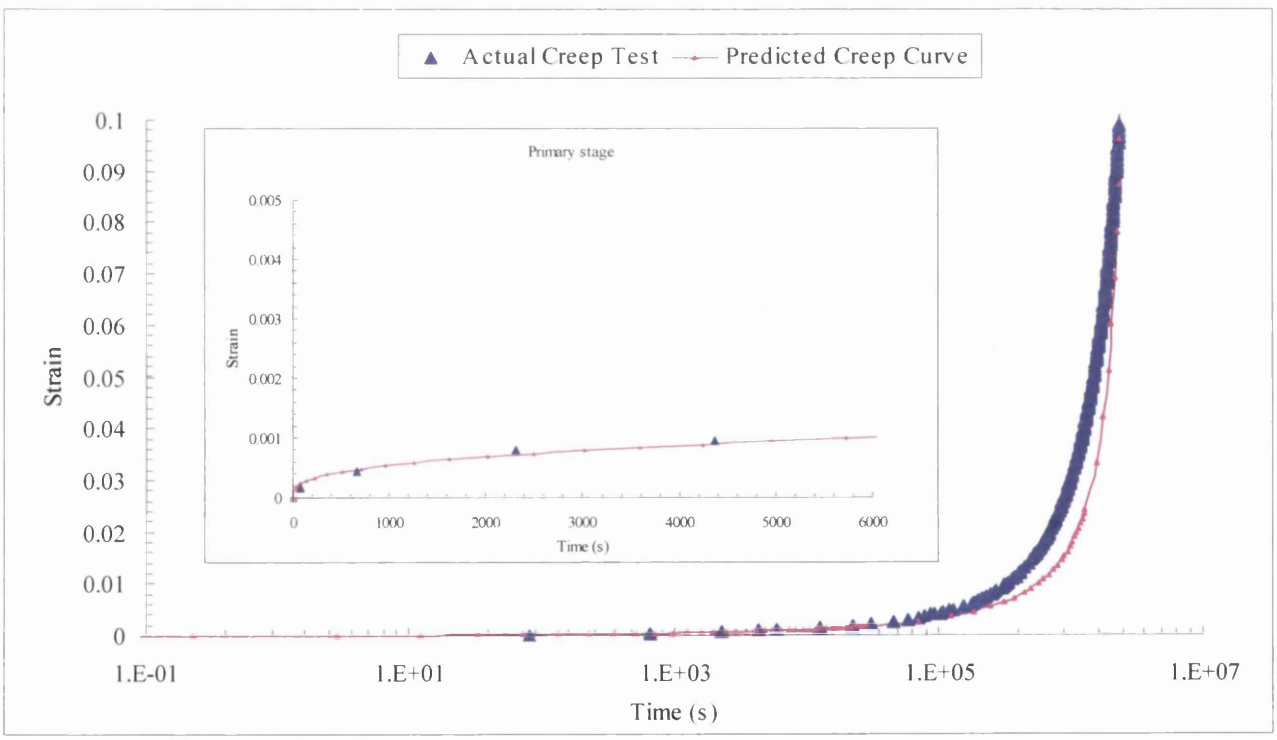

(B23.15): 873K/300MPa

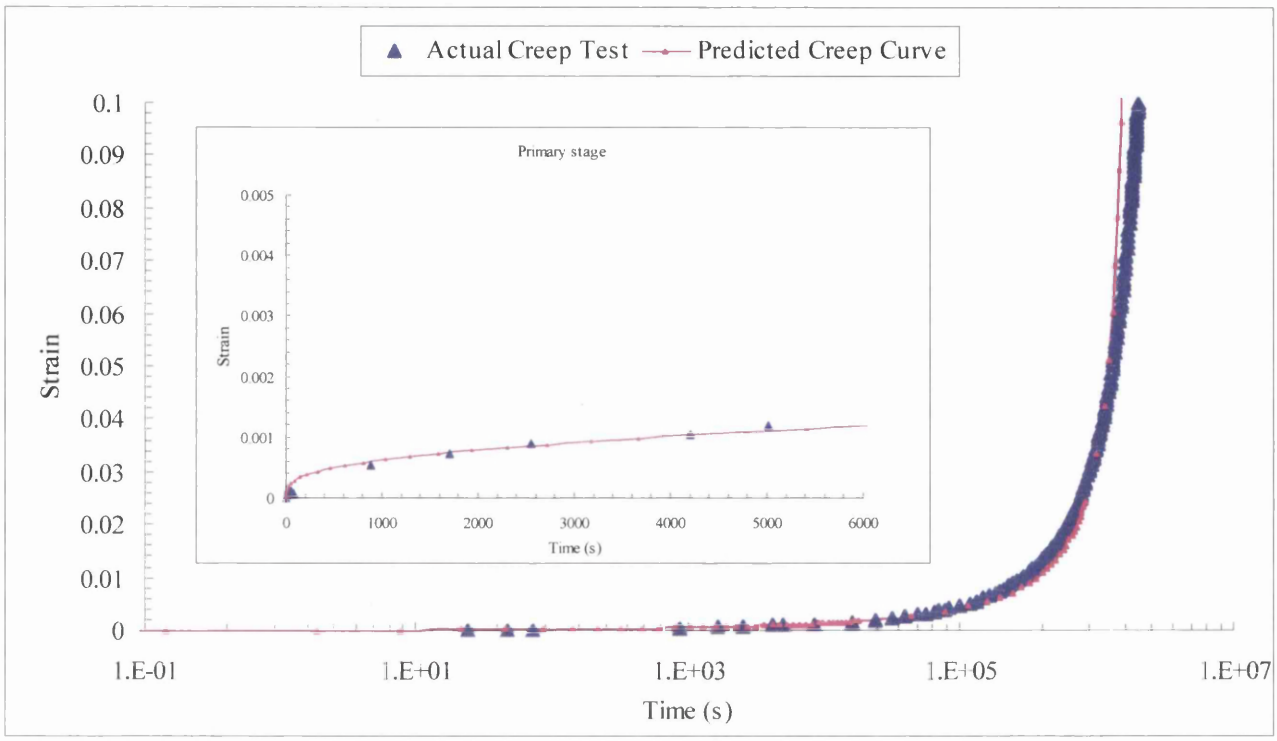

(B23.16): 873K/350MPa

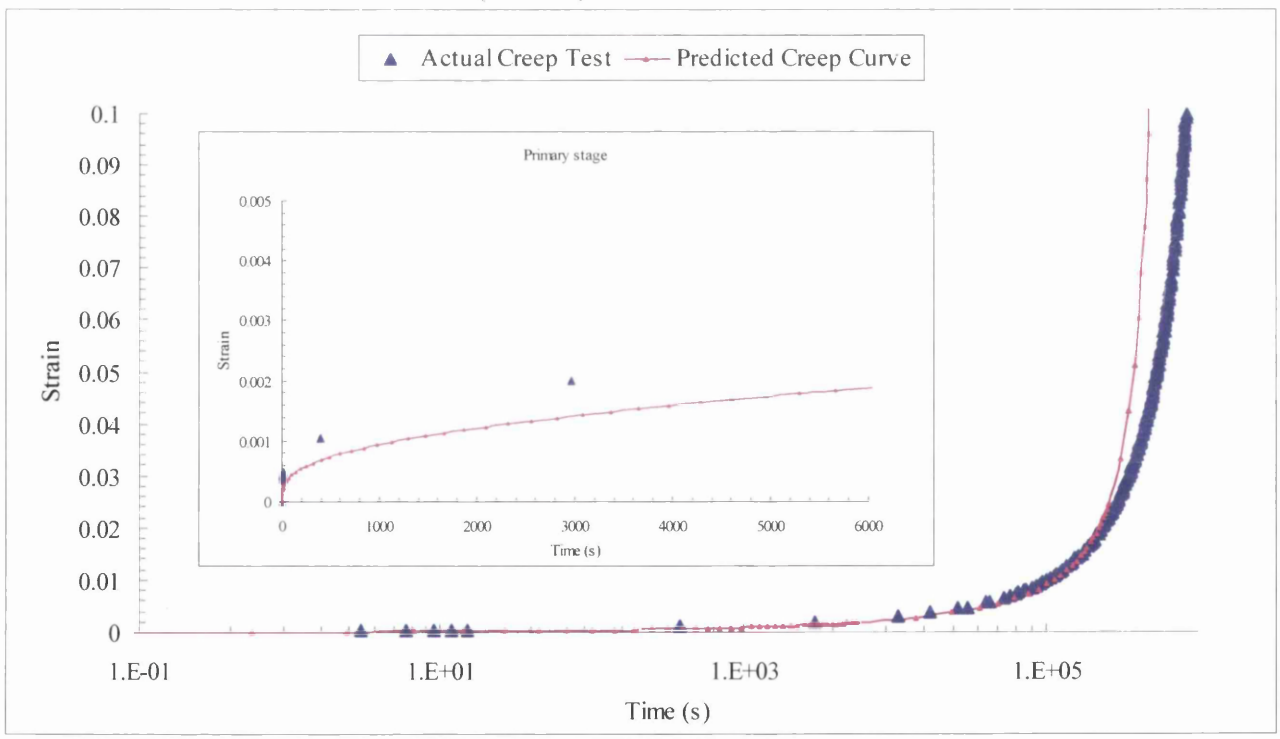

(B23.17): 873K/360MPa

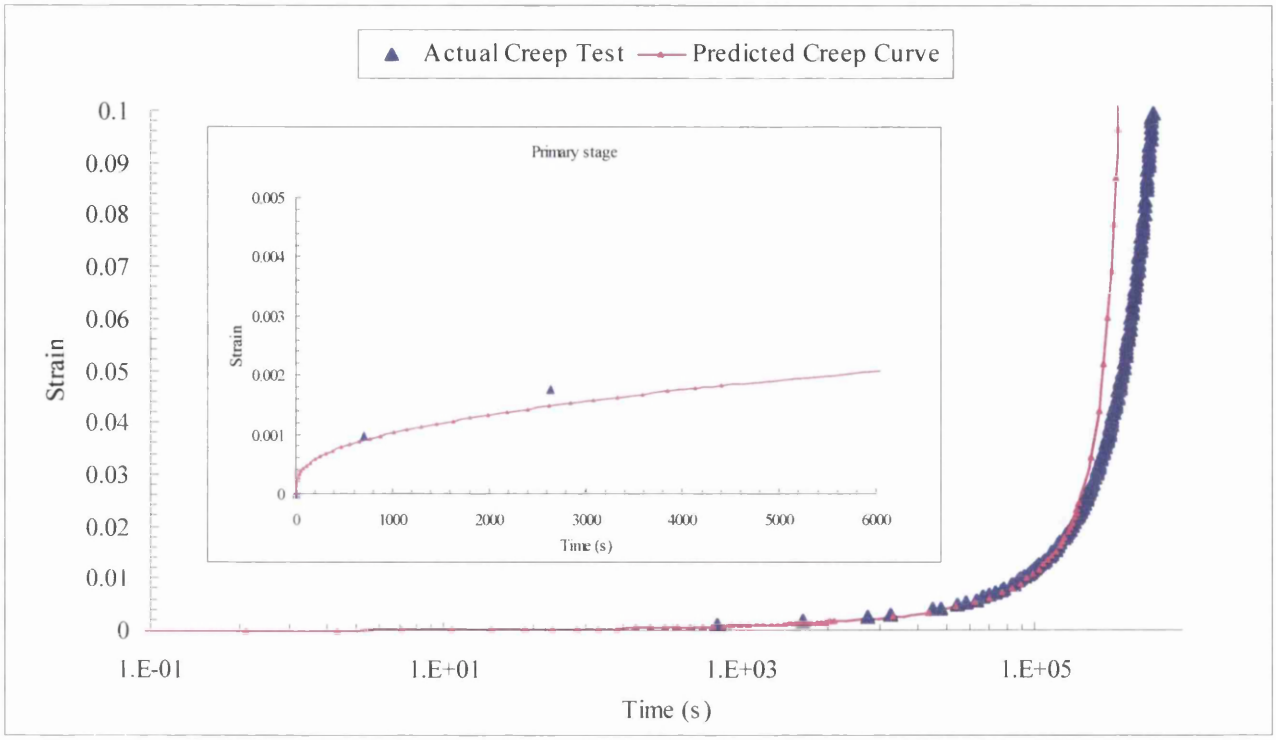

(B23.18): 873K/390MPa

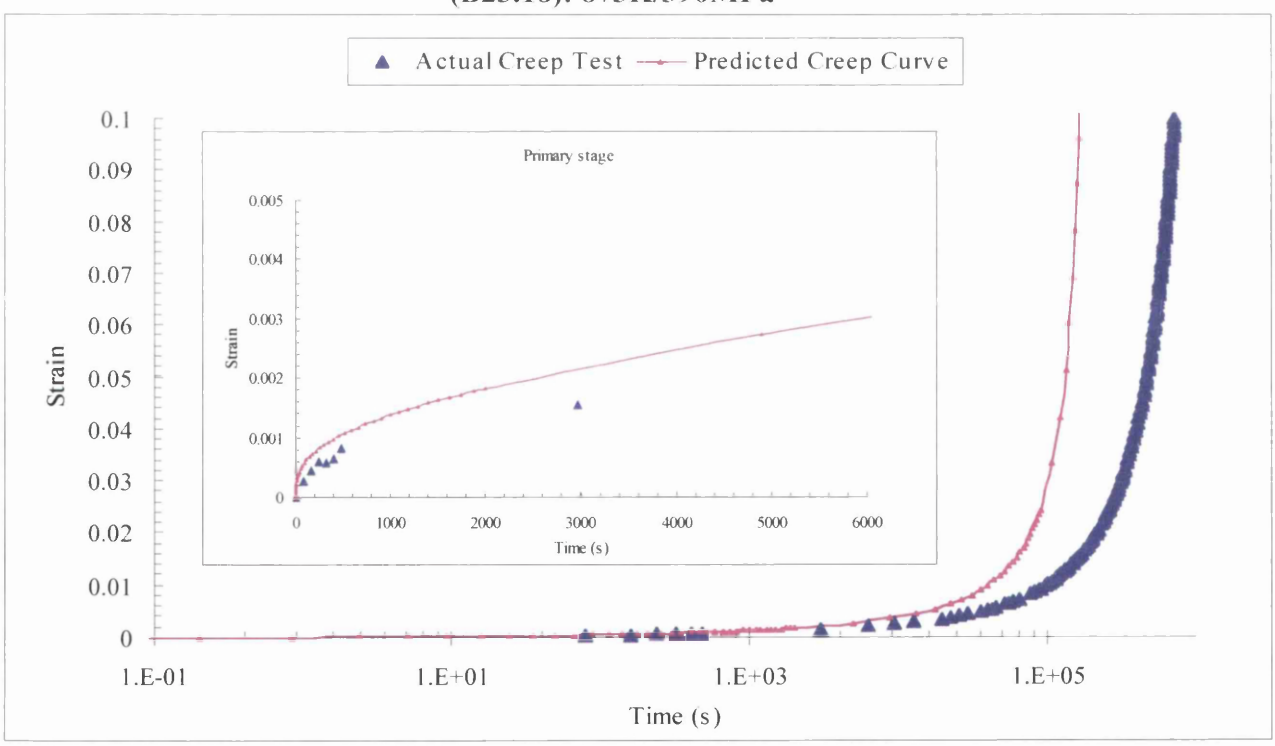

(B23.19): 873K/480MPa

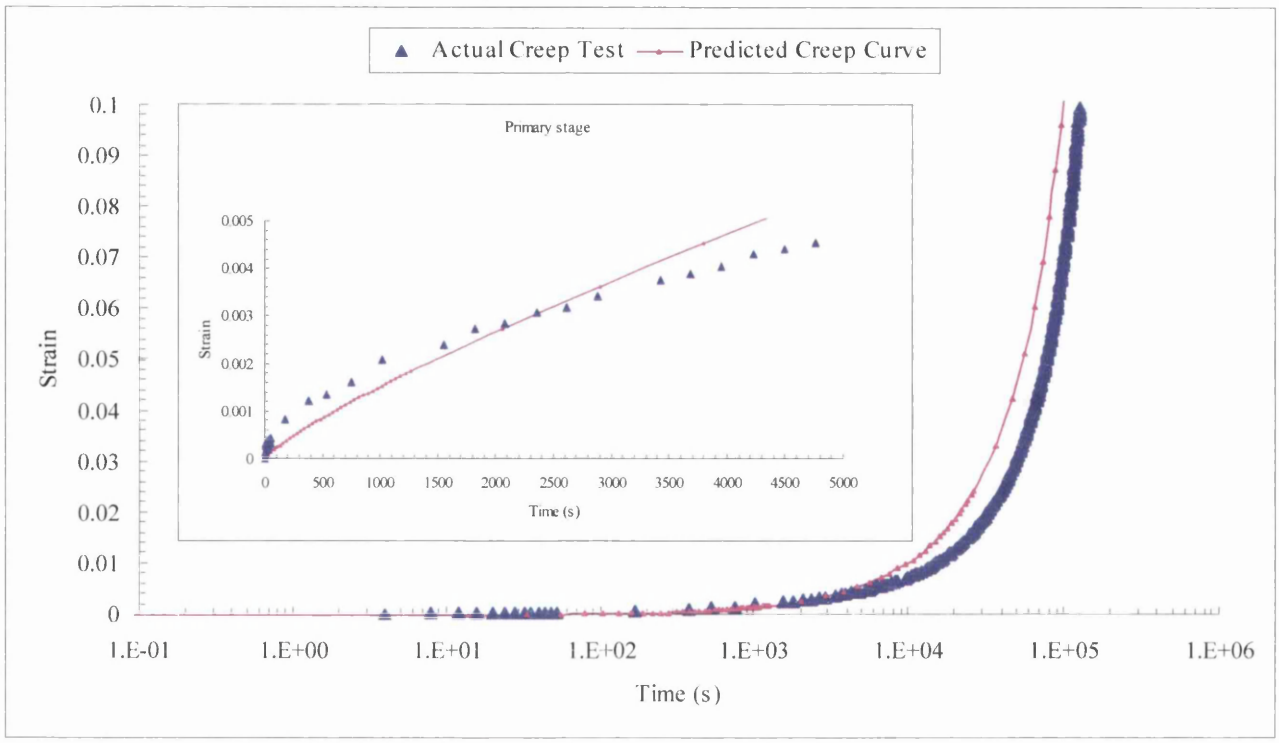

(B23.20): 873K/550MPa

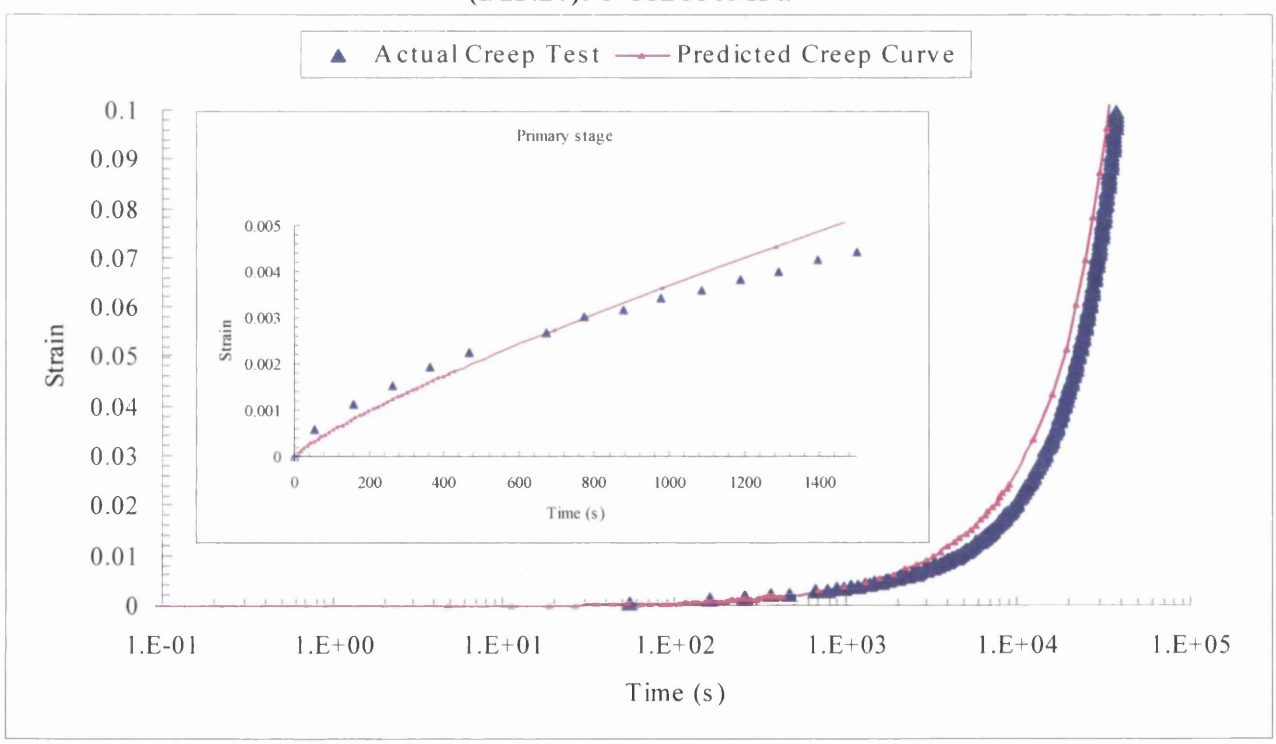

(B23.21): 898K/175MPa

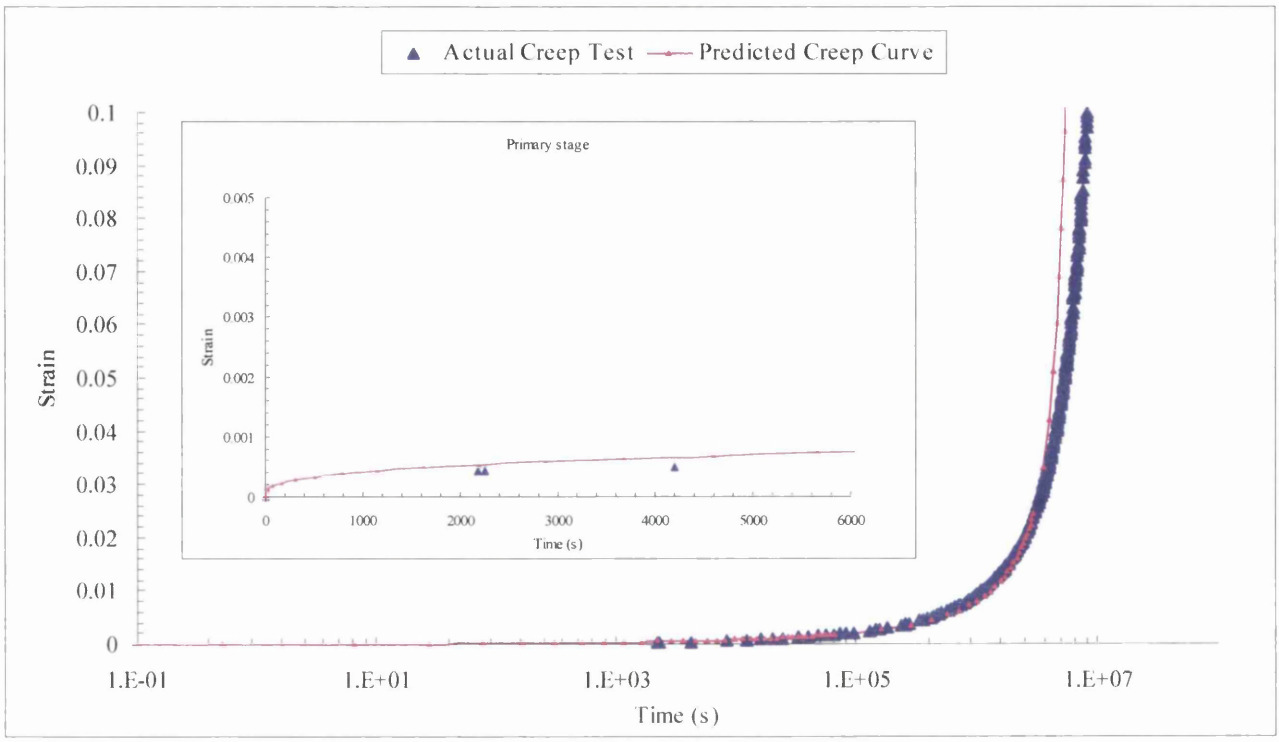

(B23.22): 898K/220MPa

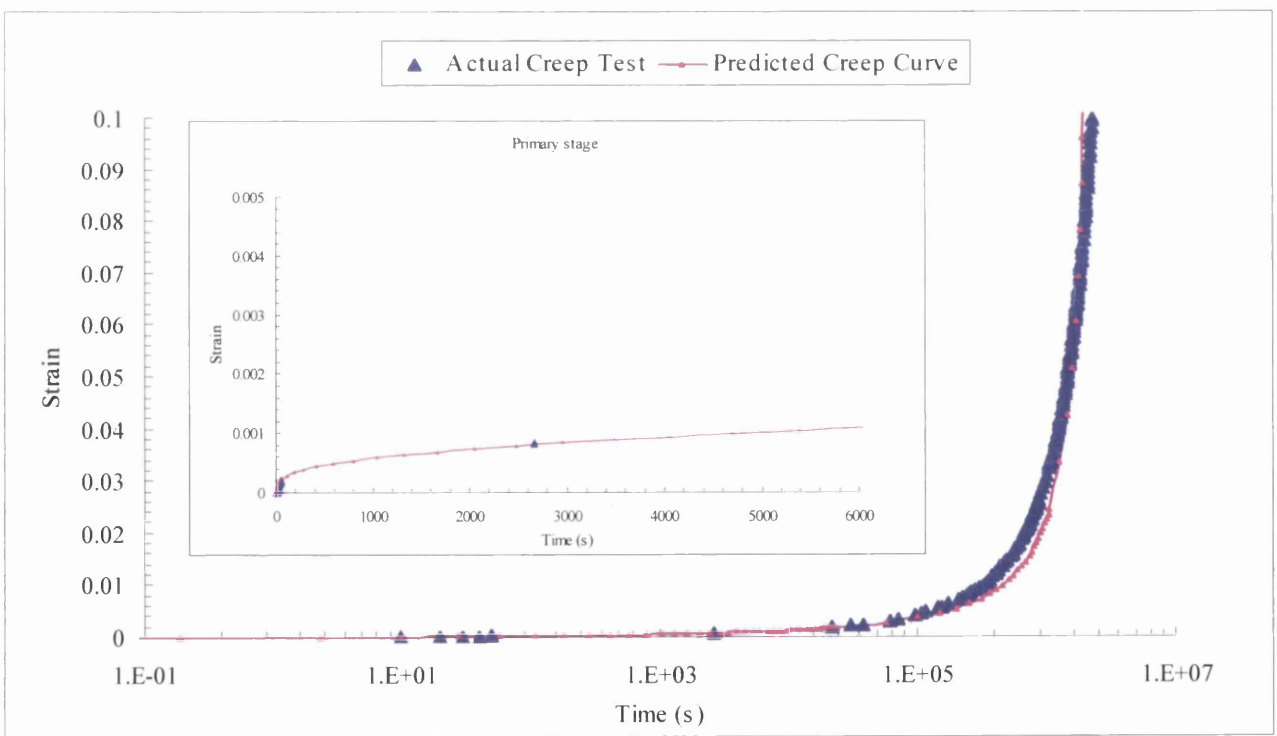

(B23.23): 898K/250MPa

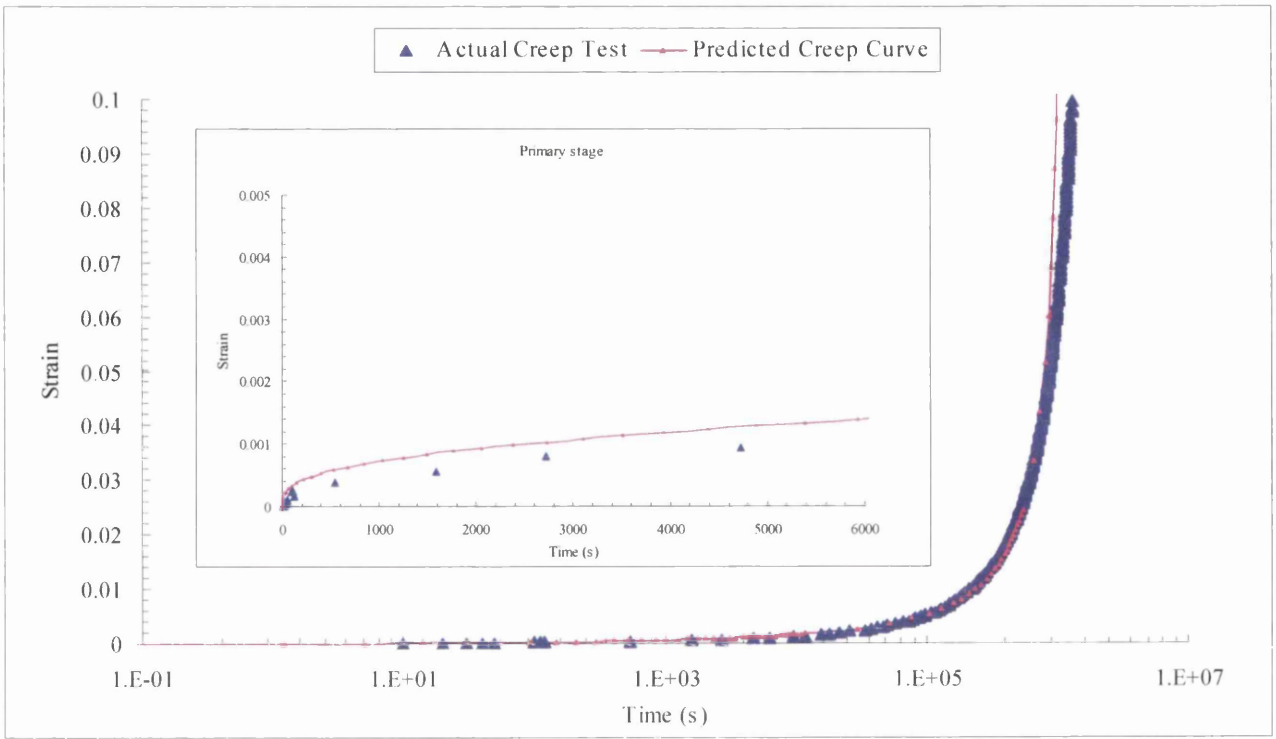

(B23.24): 898K/280MPa

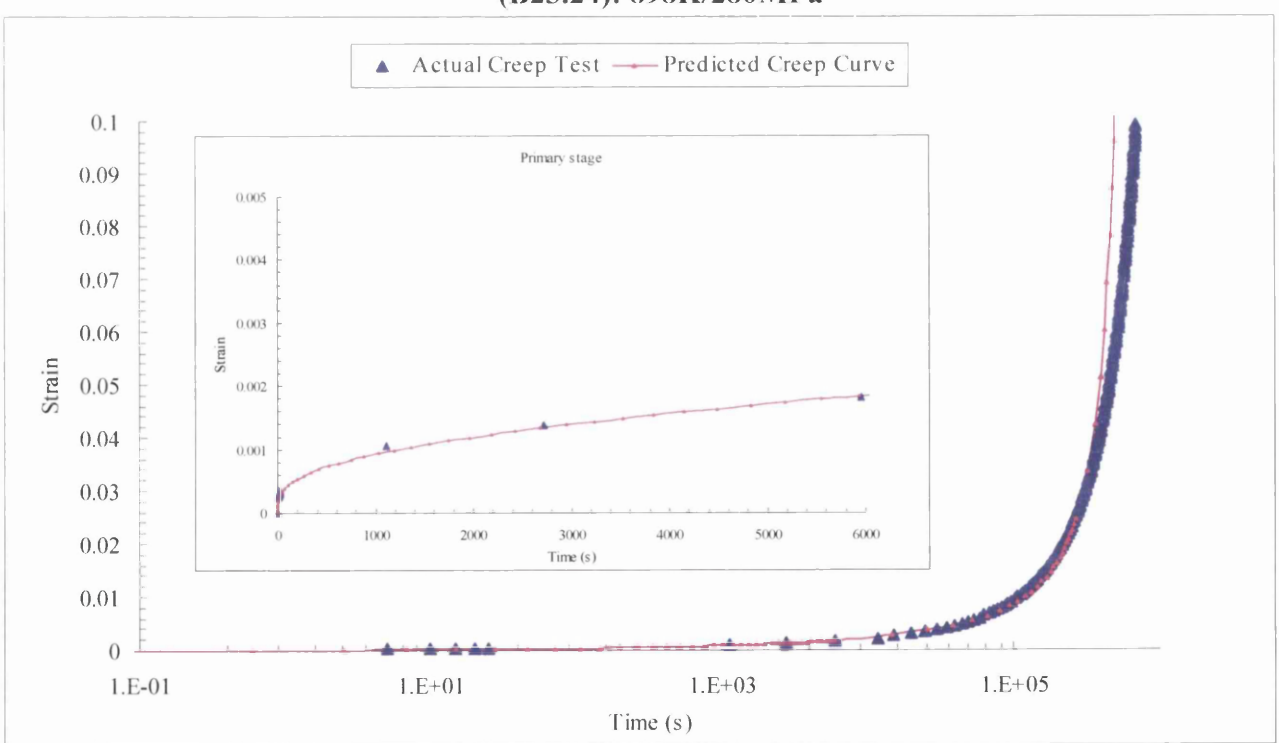

(B23.25): 898K/300MPa

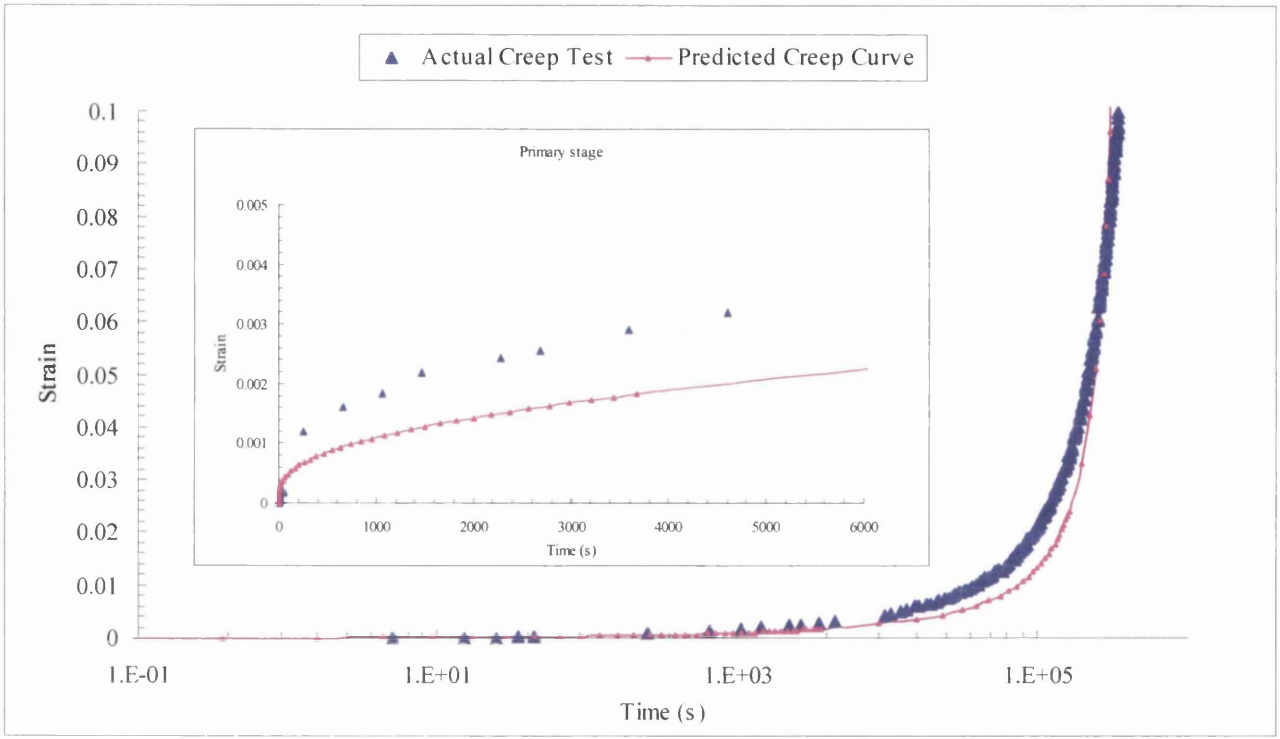

(B23.26): 898K/330MPa

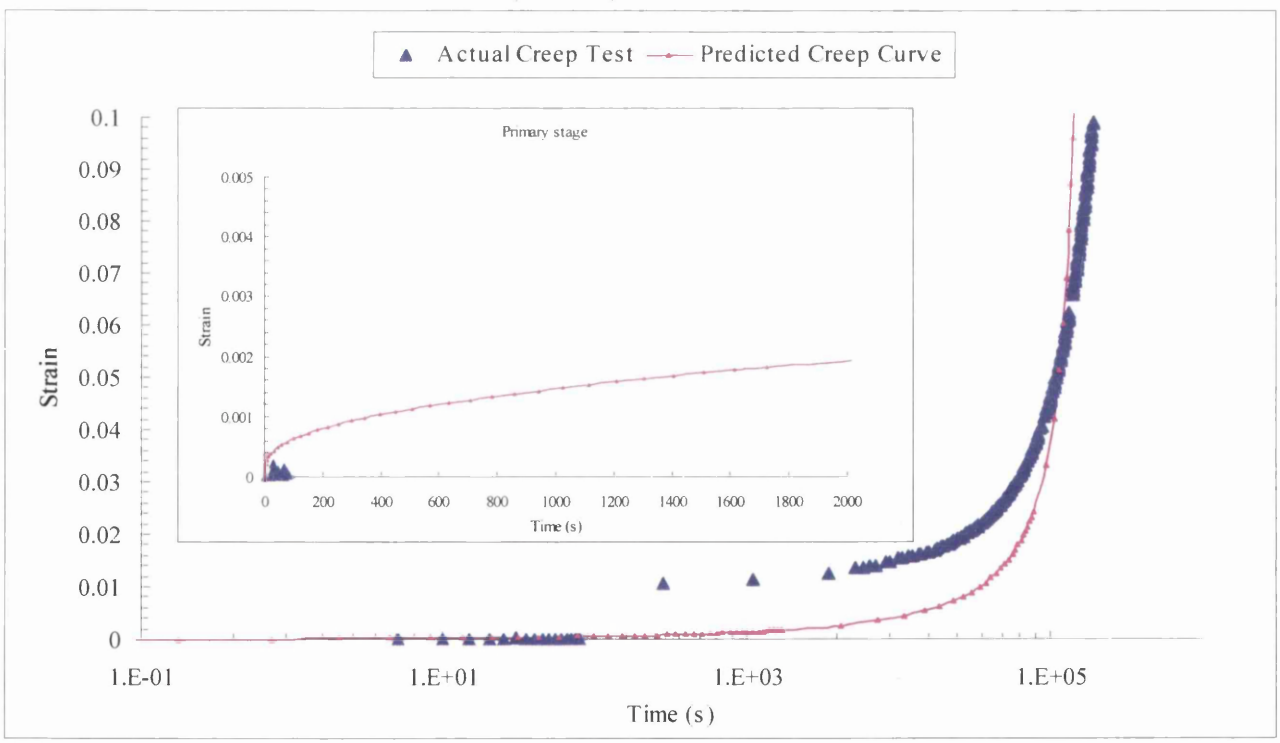

(B23.27): 898K/400MPa

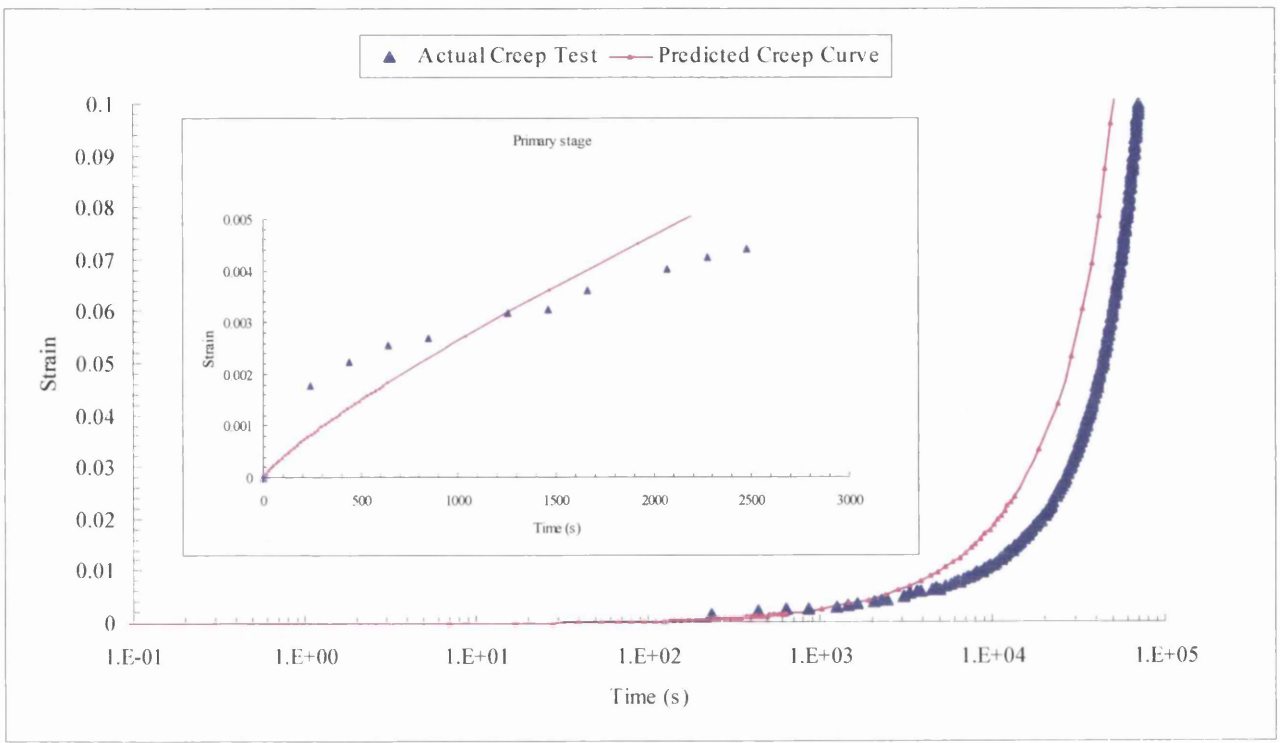

(B23.28): 923K/140MPa

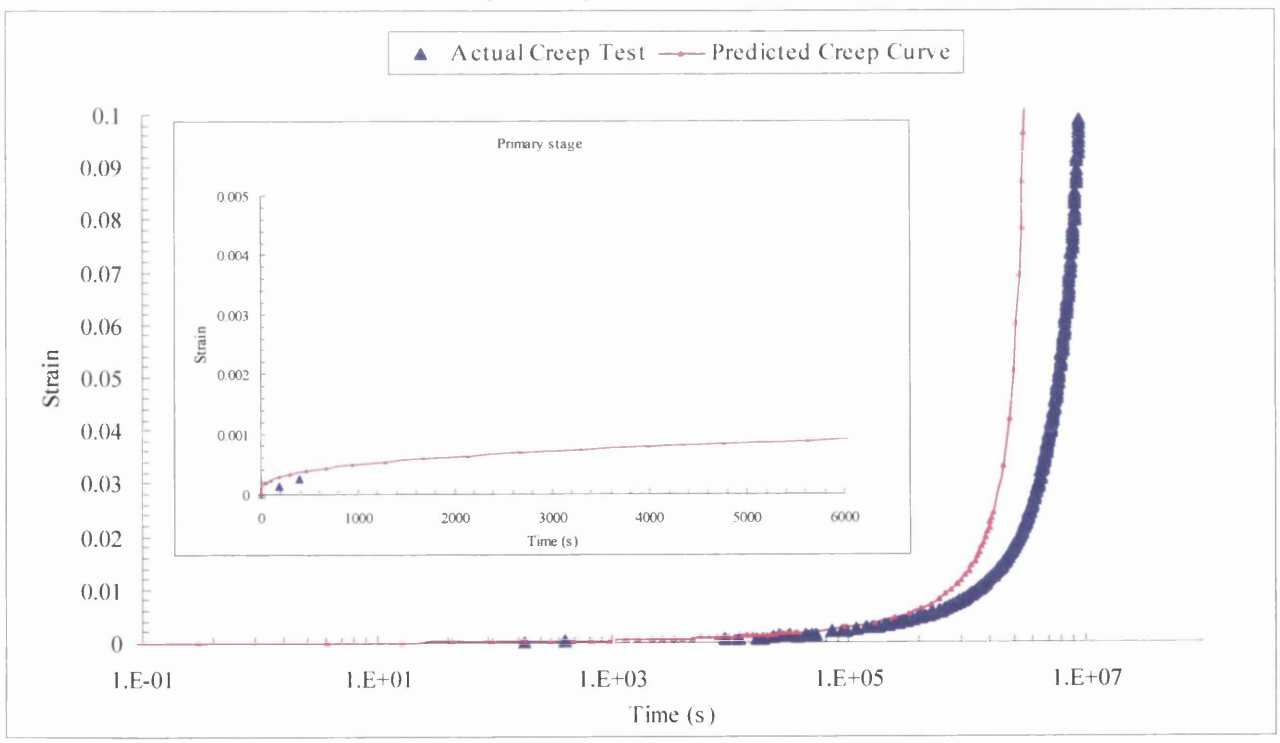

(B23.29): 923K/155MPa

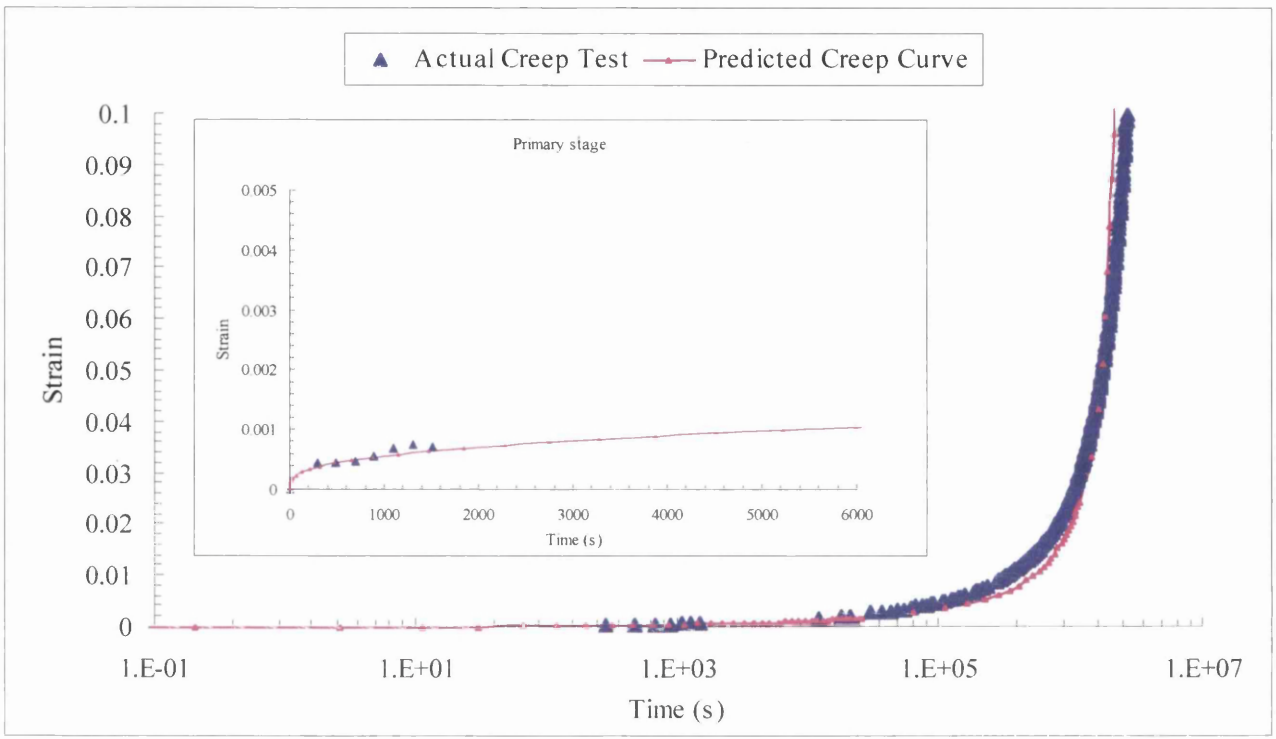

(B23.30): 923K/180MPa

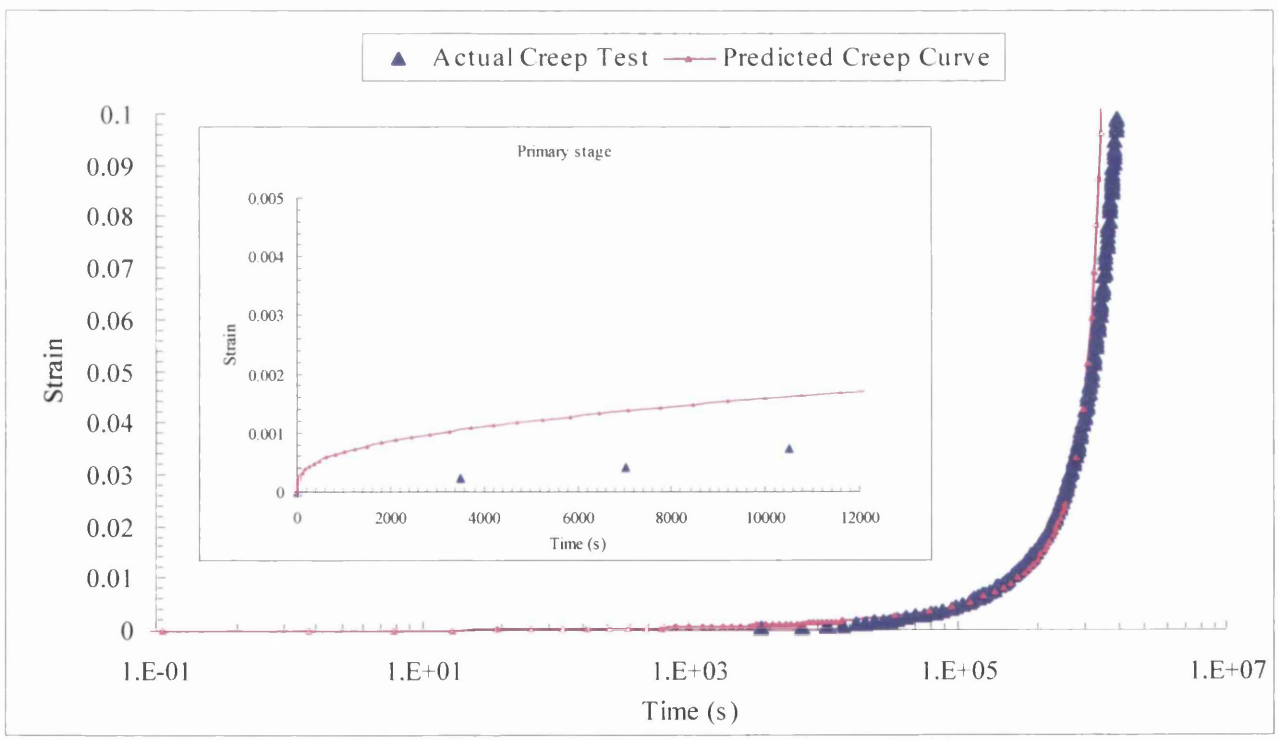

(B23.31): 923K/225MPa

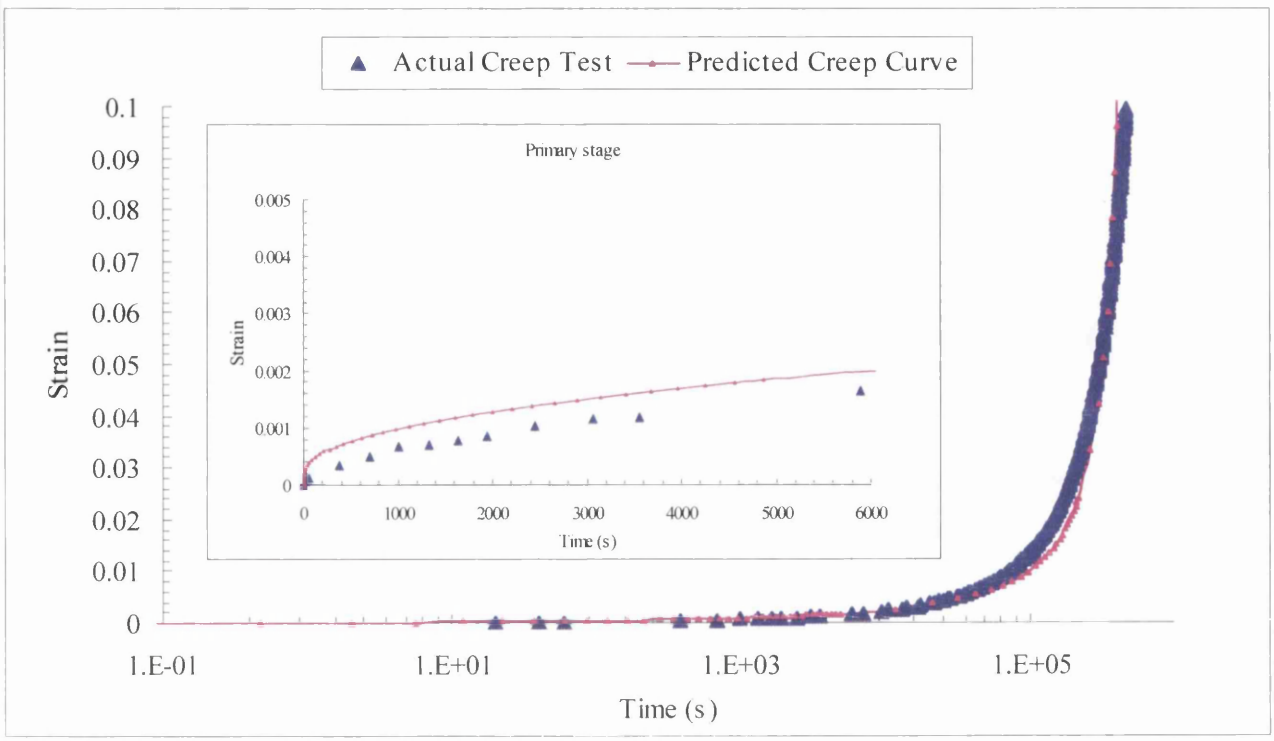

(B23.32): 923K/260MPa

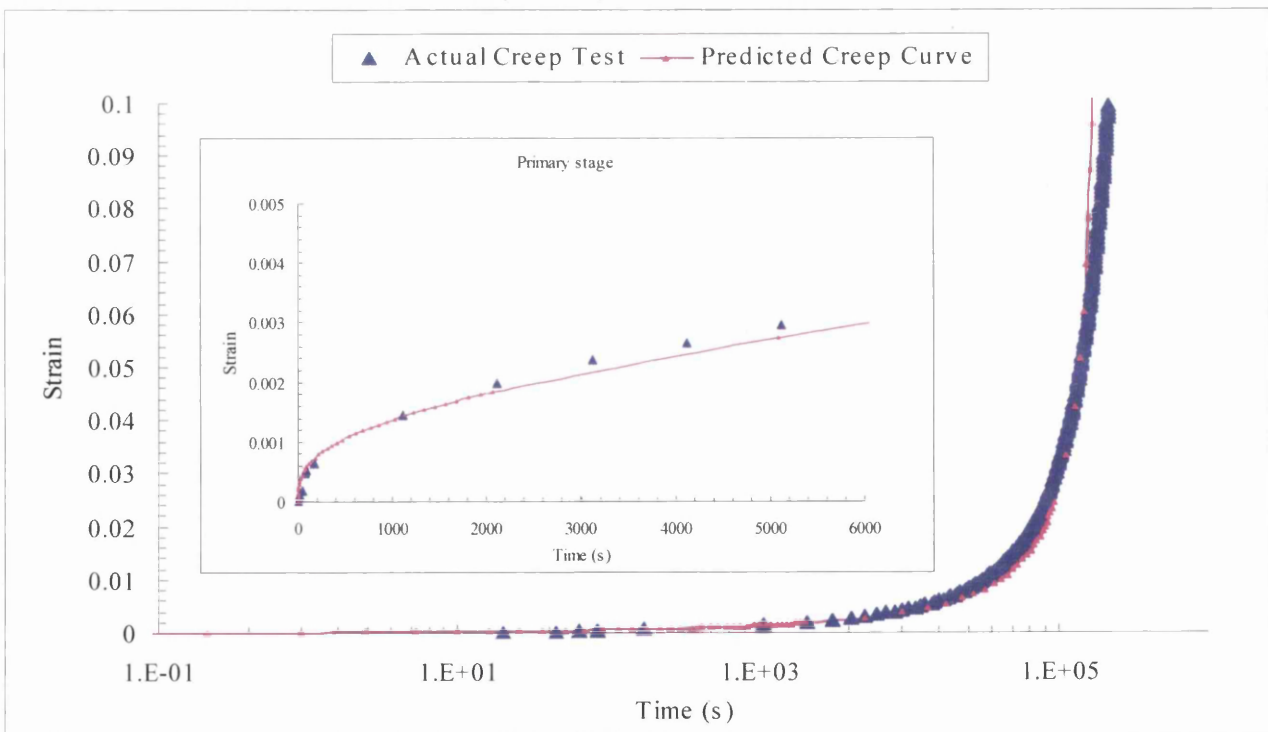

(B23.33): 923K/300MPa

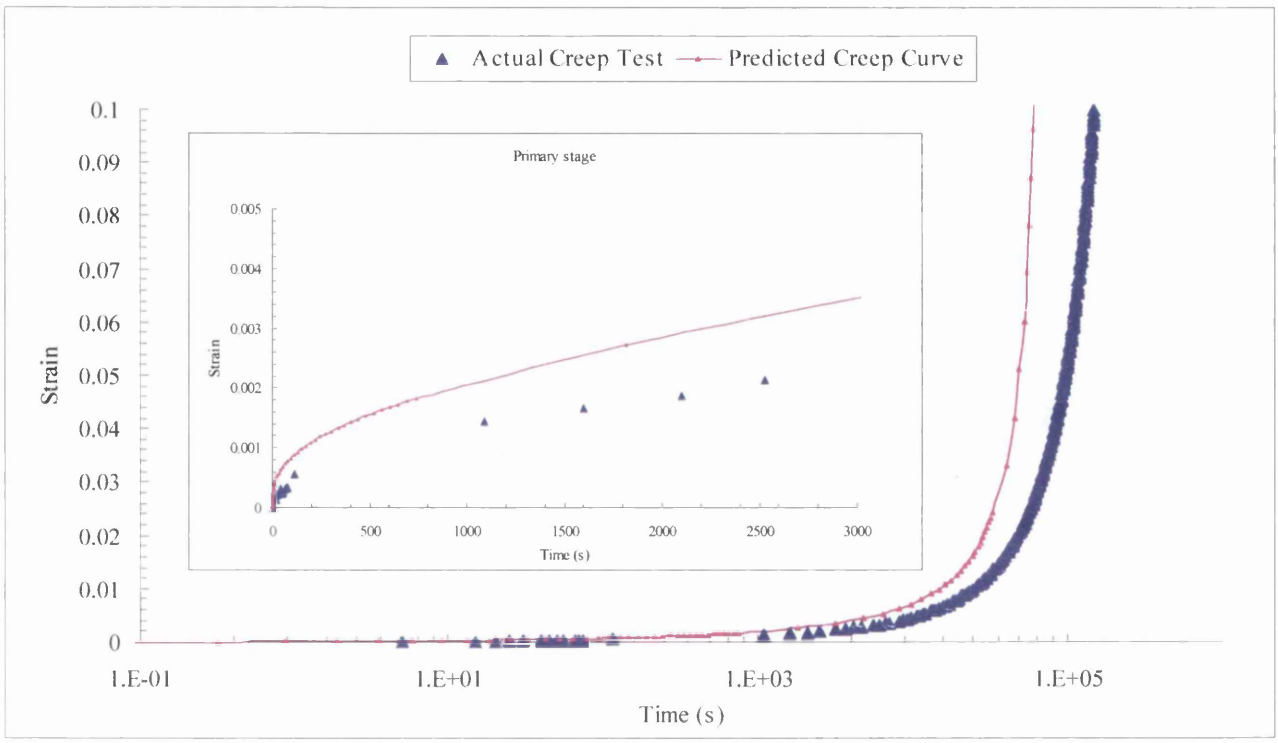

(B23.34): 923K/330MPa

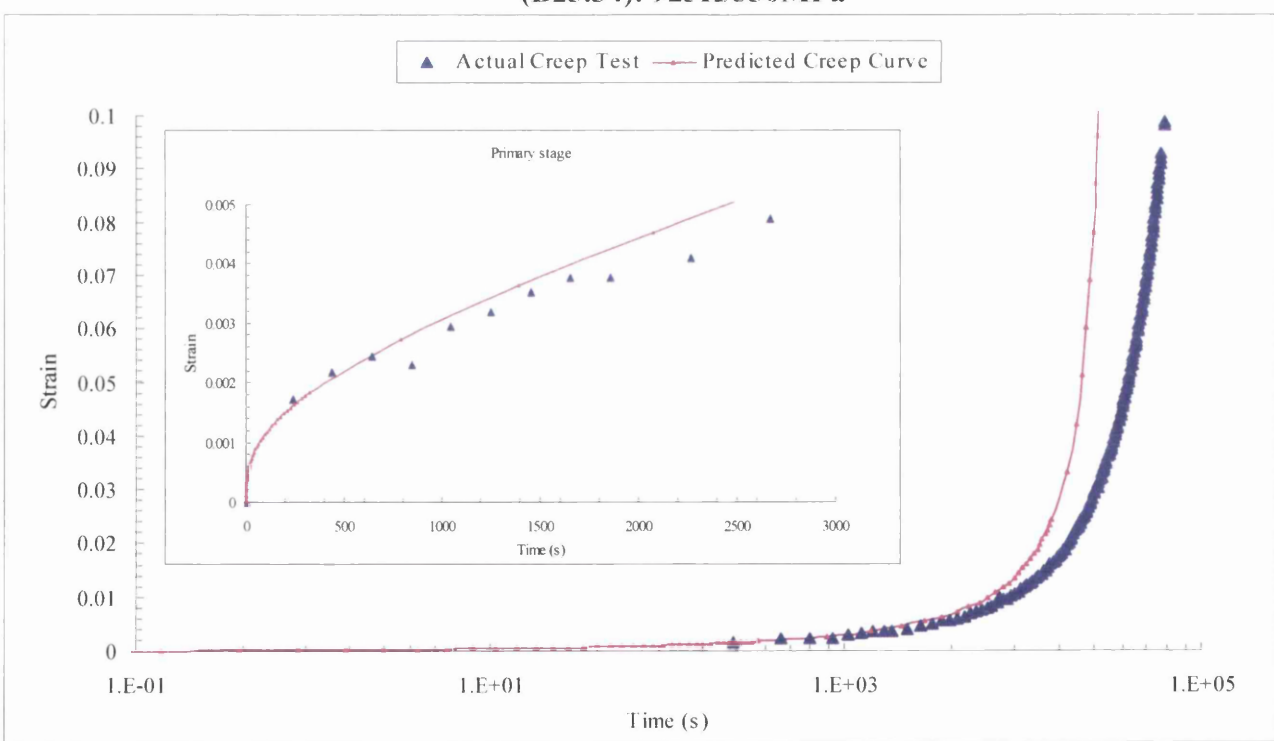

B.24 The Alpha-Case Analysis

(B24.1): Alpha-case thickness (measured data)

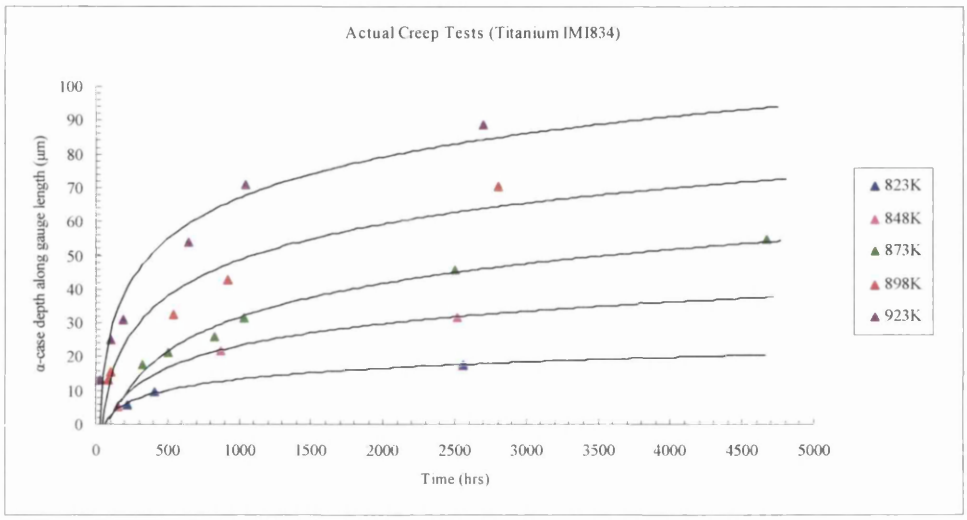

823K:

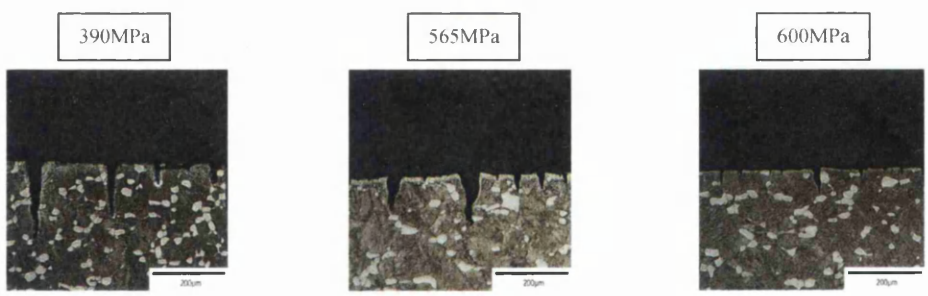

848K:

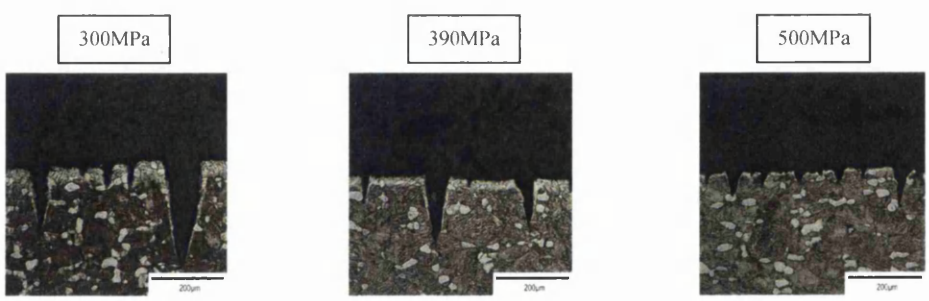

873K:

200MPa

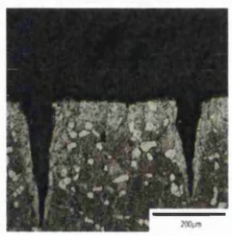

269MPa

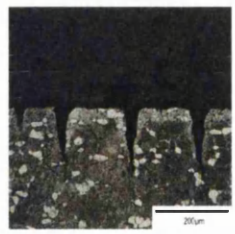

280MPa

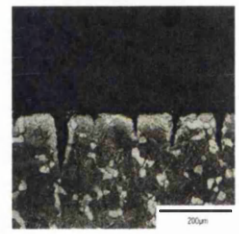

300MPa

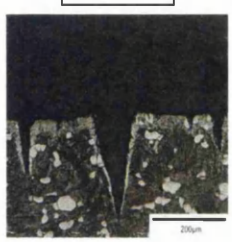

338MPa

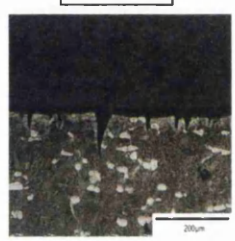

350MPa

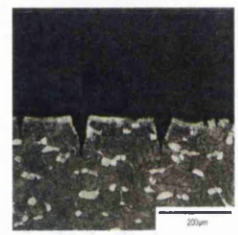

390MPa

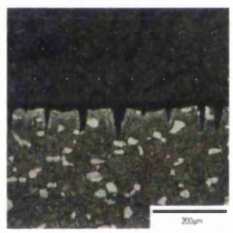

480MPa

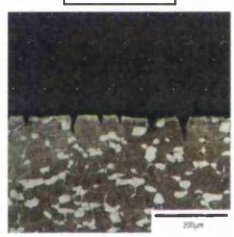

550MPa

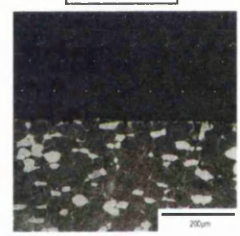

898K:

175MPa

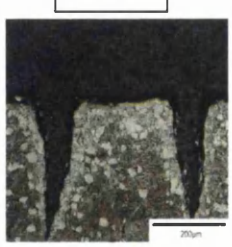

220MPa

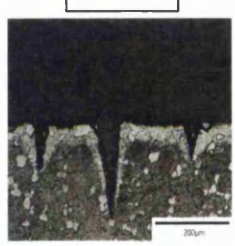

250MPa

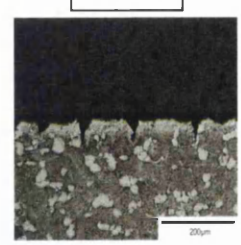

280MPa

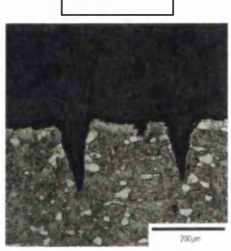

330MPa

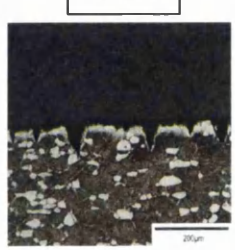

400MPa

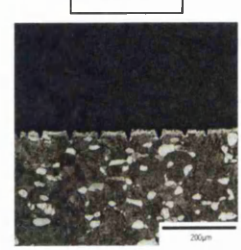

923K:

140MPa

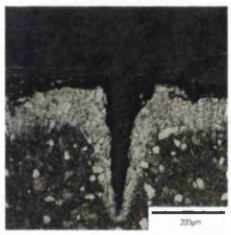

155MPa

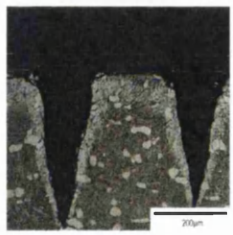

180MPa

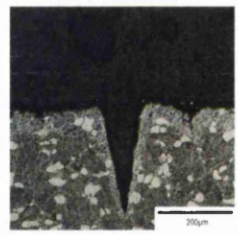

225MPa

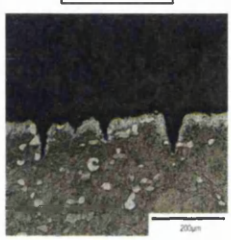

260MPa

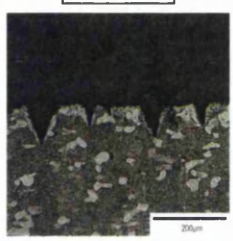

330MPa

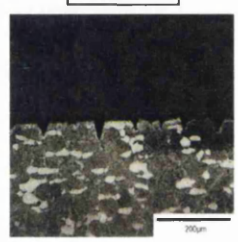

(B24.2): Steve-Brown's 'Alpha-Case Thickness' Model (measured and predicted)

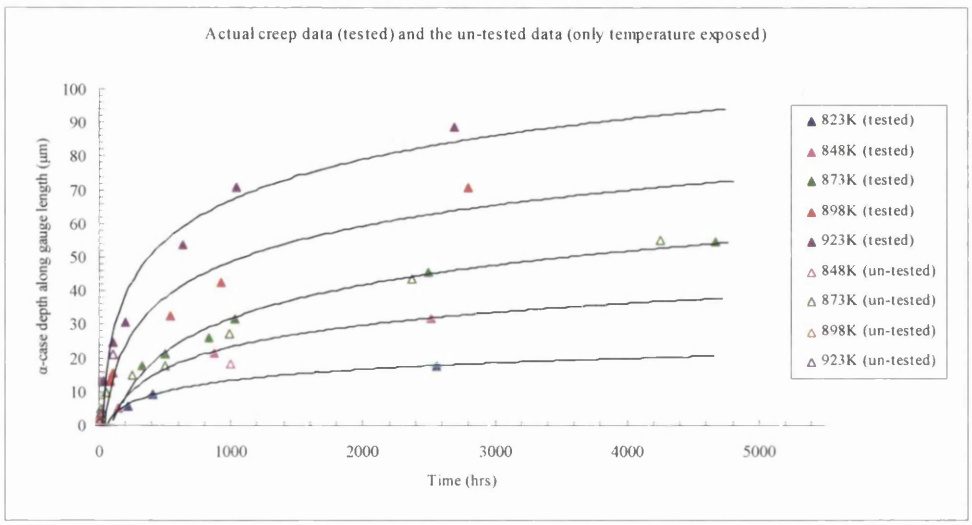

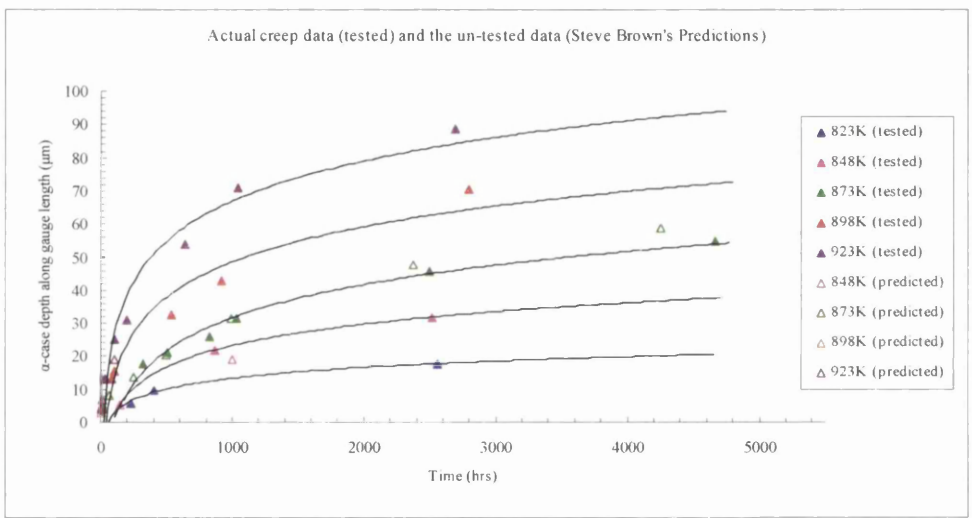

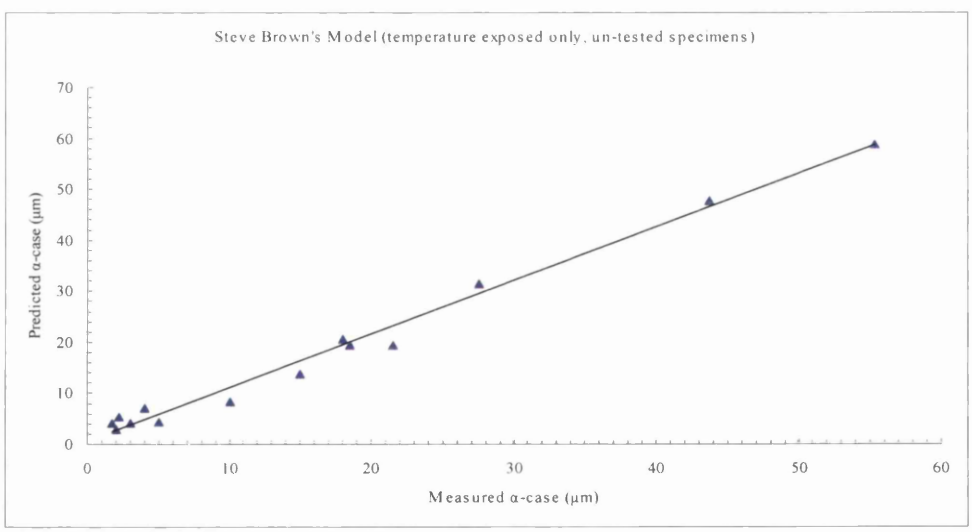

(B24.3): Alpha-case thickness at the surface of the penetrating cracks against the crack depth (measured)

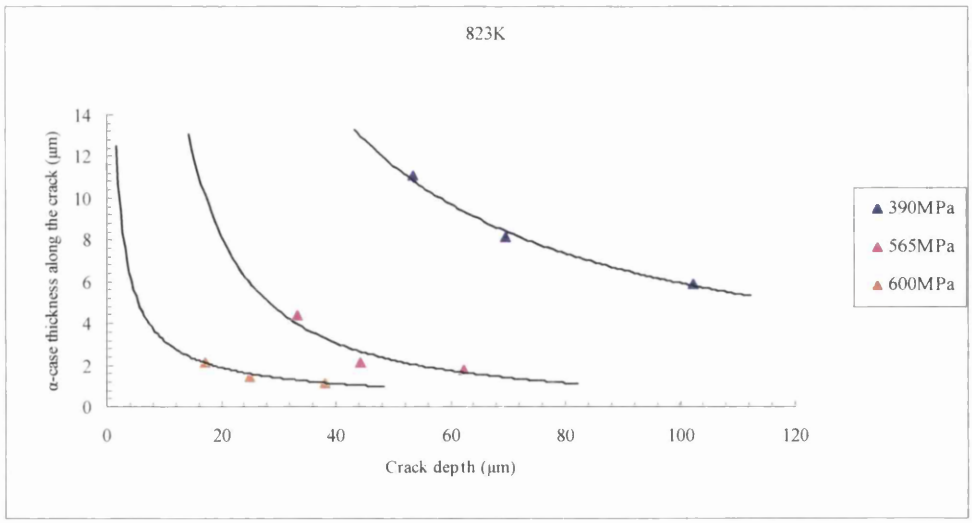

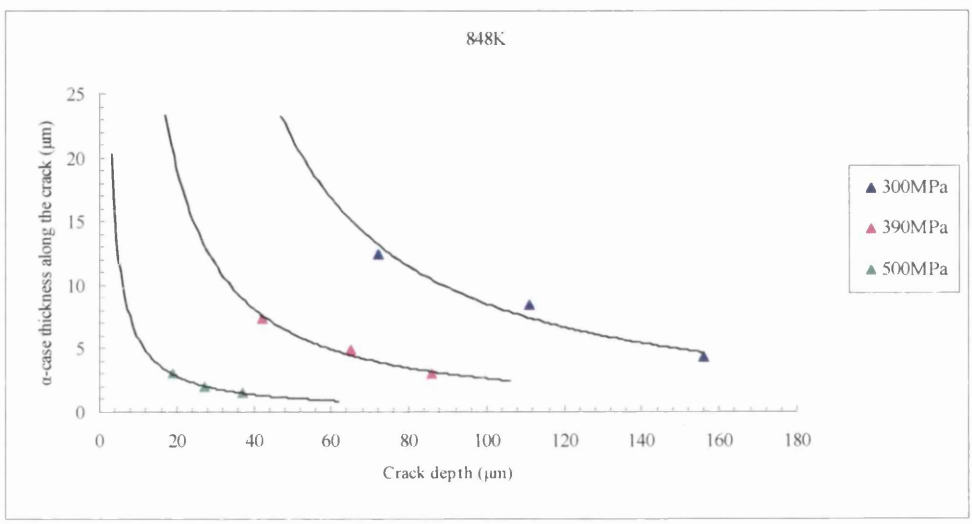

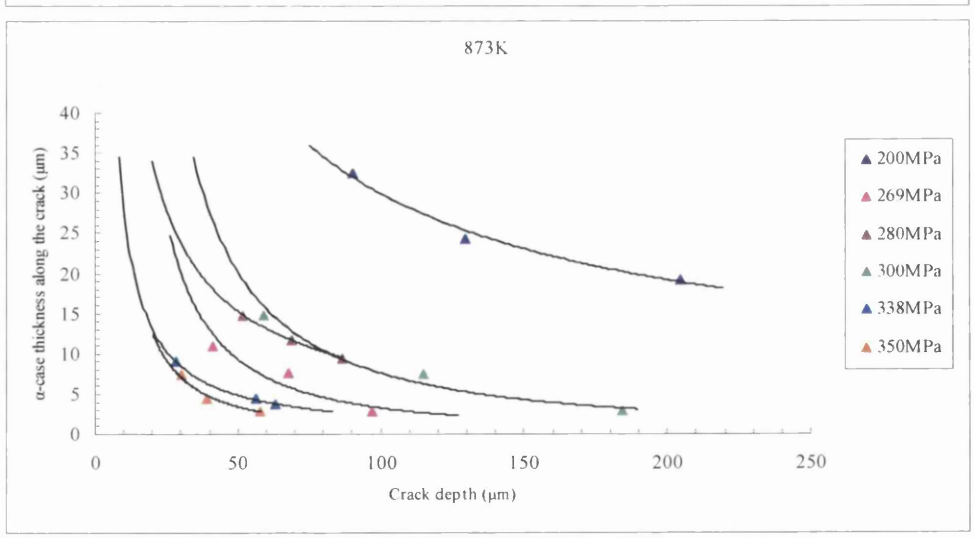

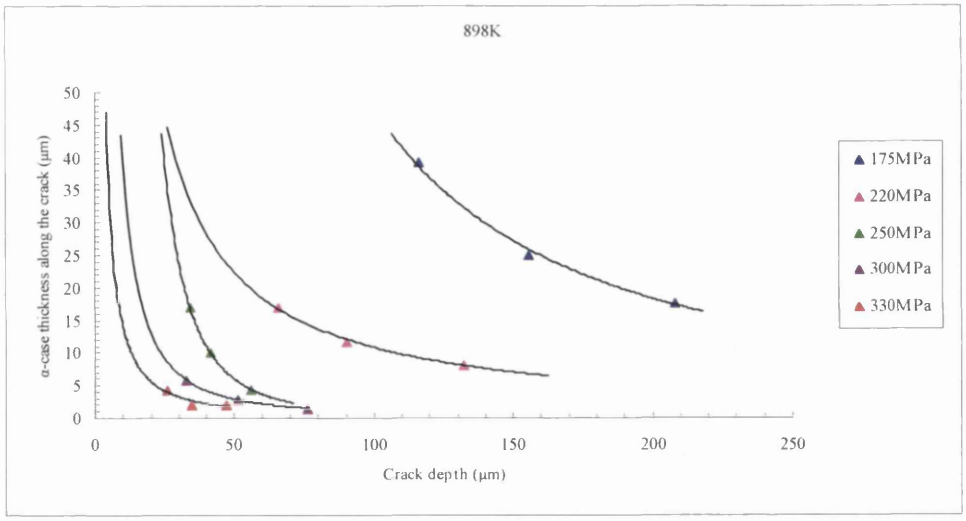
898K
α-case thickness along the crack (μm)
Crack depth (μm)
175MPa
220MPa
250MPa
300MPa
330MPa

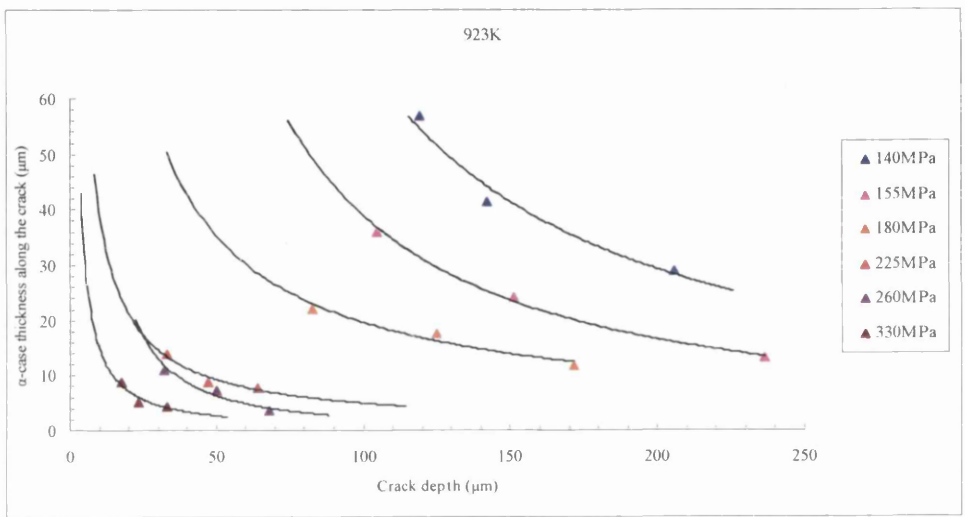
923K
α-case thickness along the crack (μm)
Crack depth (μm)
140MPa
155MPa
180MPa
225MPa
260MPa
330MPa

(B24.4): Crack initiation predictions (based on Figure B23.1)

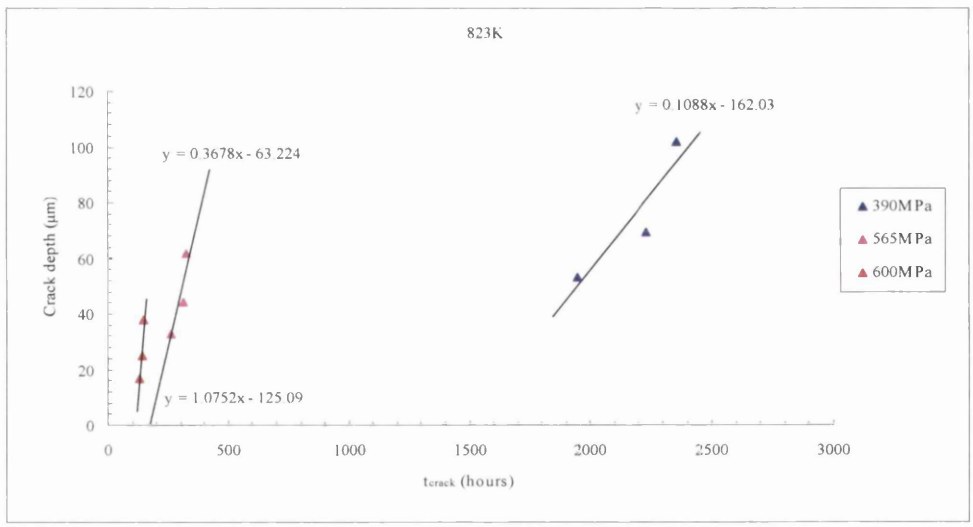

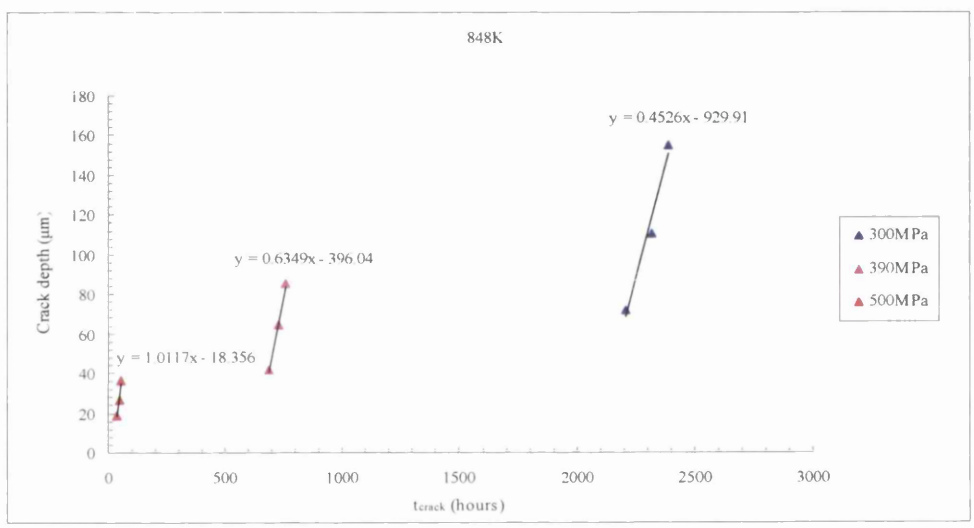

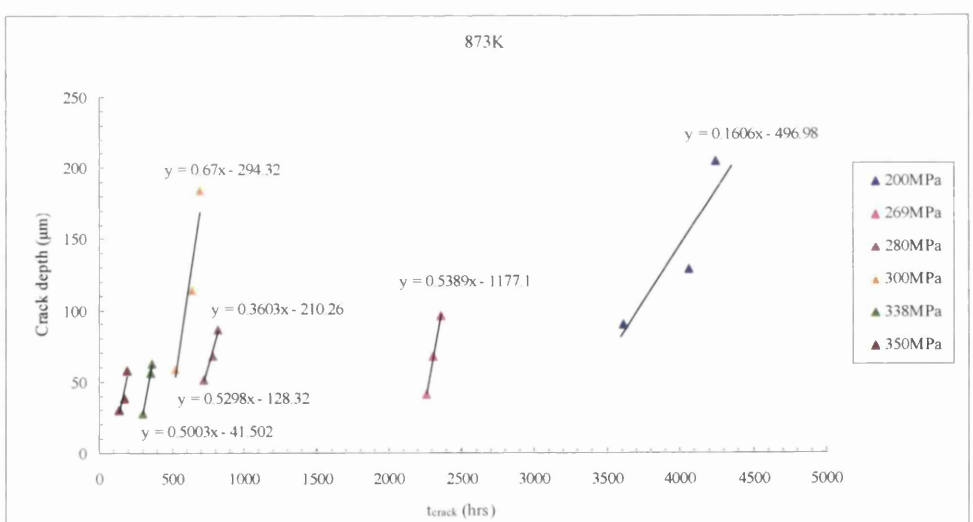

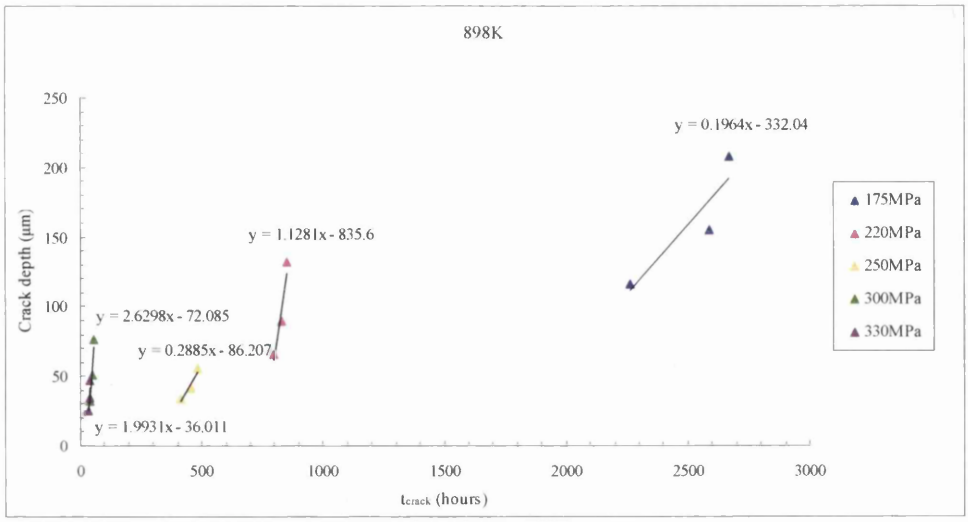
898K
Crack depth (μm)
tcrack (hours)
y = 0.1964x - 332.04
y = 1.1281x - 835.6
y = 2.6298x - 72.085
y = 0.2885x - 86.207
y = 1.9931x - 36.011
175MPa
220MPa
250MPa
300MPa
330MPa

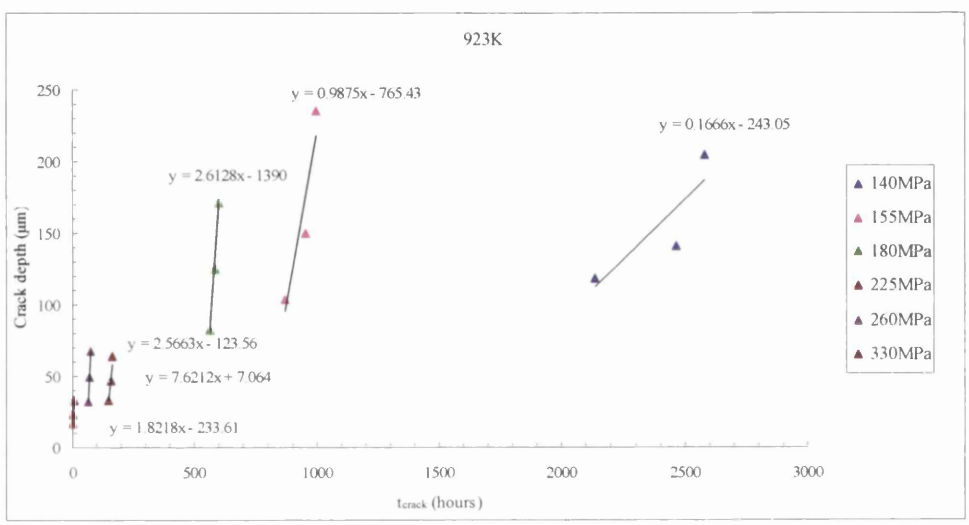
923K
Crack depth (μm)
tcrack (hours)
y = 0.9875x - 765.43
y = 0.1666x - 243.05
y = 2.6128x - 1390
y = 2.5663x - 123.56
y = 7.6212x + 7.064
y = 1.8218x - 233.61
140MPa
155MPa
180MPa
225MPa
260MPa
330MPa

(B24.5): Critical time values (at which cracks appeared) against stress.

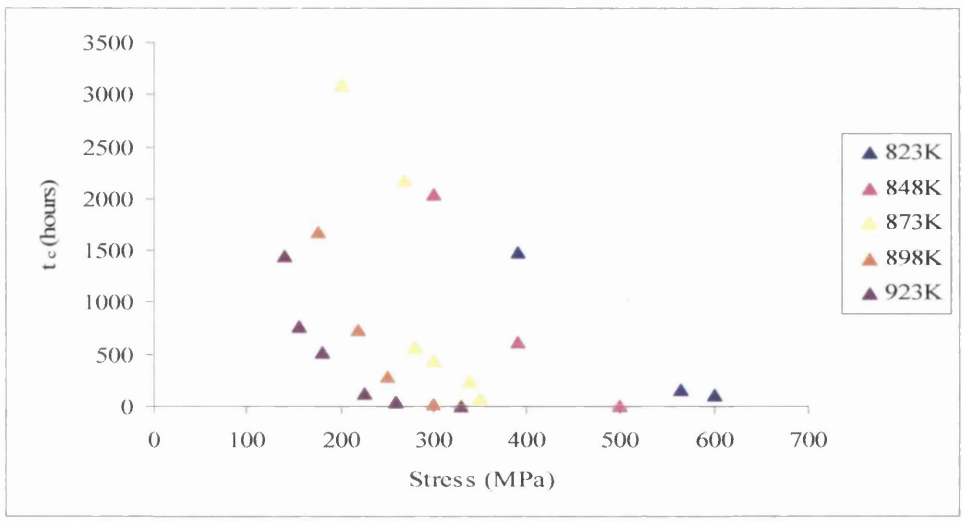

(B24.6): Critical strain values (at which cracks appeared) against stress.

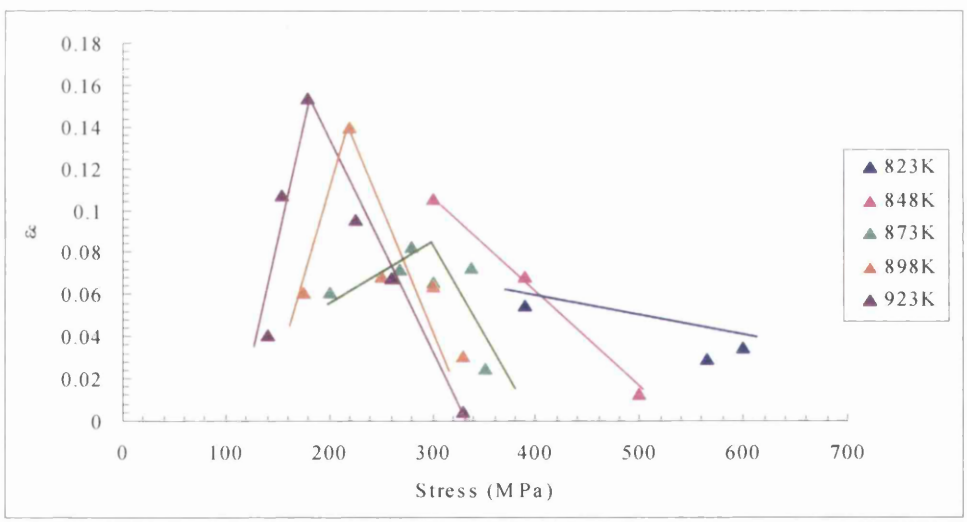

B.25 The Wilshire Technique and the Alpha-Case

(B25.1): The Wilshire predictive curves for alpha-case thicknesses < 35µm

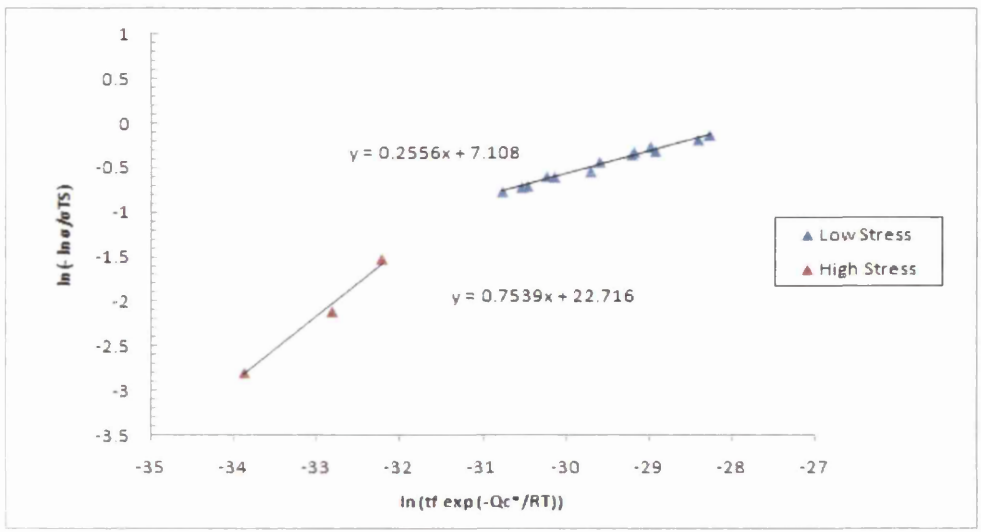

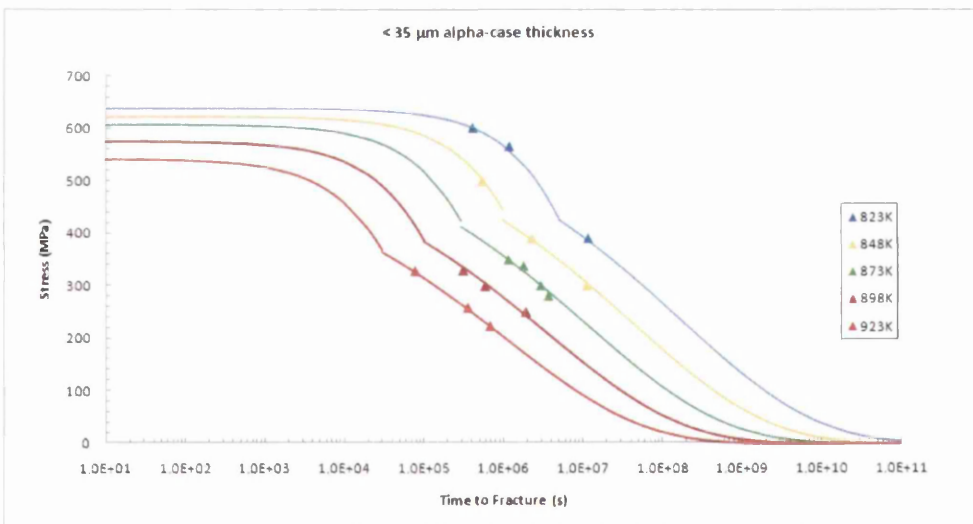

(B25.2): The Wilshire predictive curves for all alpha-case thicknesses.

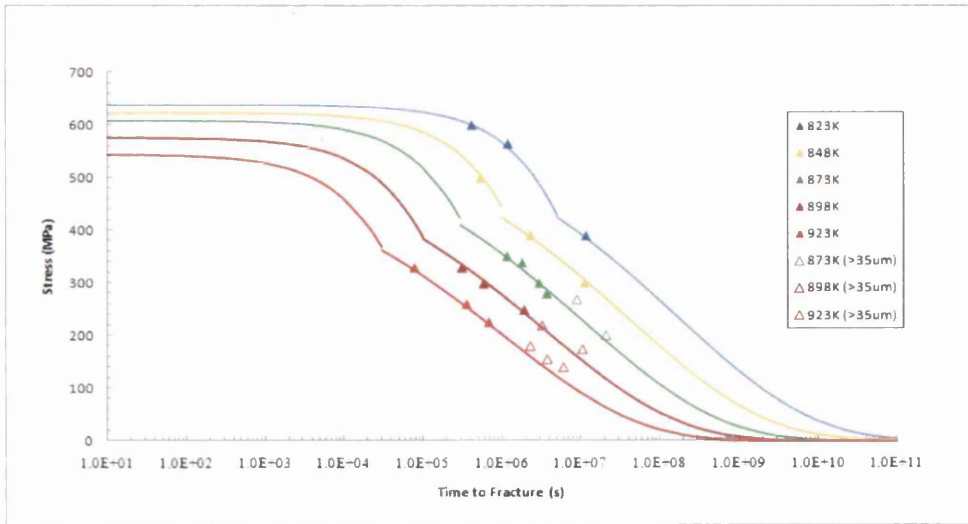

APPENDIX (C)

TABLES OF ALL ANALYSES AND RESULTS

APPENDIX (C): CONTENTS

CREEP TESTS MATRIX

Temperature (K)	σ (MPa)	Source of data	t_r (s)	t_r (hrs)
823	390	Available data	1.15E+07	3189.31562
	470	Zak	4.57E+06	1269.68942
	540	Available data	1.78E+06	493.966503
	565	Zak	1.17E+06	326.360432
	600	Available data	4.07E+05	113.161188
848	300	Available data	1.12E+07	3116.71793
	390	Available data	2.29E+06	636.352126
	420	Zak	1.54E+06	428.694444
	430	Available data	1.35E+06	375.555556
	455	Zak	1.10E+06	306.388889
	500	Zak	5.37E+05	149.175499
	570	Available data	1.78E+05	49.3966503
873	200	Available data	2.09E+07	5803.60036
	280	Available data	3.72E+06	1033.36111
	300	Available data	2.98E+06	828.888889
	350	Zak	1.17E+06	326.25
	360	Available data	9.85E+05	273.605556
	360	Available data	7.86E+05	218.296389
	360	Available data	5.32E+05	147.775
	360	Available data	5.75E+05	159.766667
	360	Available data	6.07E+05	168.669444
	360	Available data	8.49E+05	235.708333
	360	Available data	7.50E+05	208.369444
	360	Available data	7.85E+05	218.05
	360	Available data	7.05E+05	195.830556
	360	Available data	8.53E+05	236.95
	360	Available data	8.99E+05	249.647222
	360	Available data	6.80E+05	188.791389
	390	Zak	6.46E+05	179.348397
	480	Zak	1.82E+05	50.6805556
	550	Available data	5.34E+04	14.8369444
898	175	Available data	1.06E+07	2939.72222
	220	Available data	3.32E+06	921.861111
	250	Available data	1.94E+06	538.583333
	280	Zak	1.13E+06	313.5
	300	Available data	7.62E+05	211.688614
	300	Available data	5.91E+05	164.275
	330	Zak	3.13E+05	86.8055556
	400	Available data	1.11E+05	30.7916667
923	140	Available data	5.98E+06	1662.25443
	155	Available data	3.75E+06	1042.08333
	180	Available data	2.30E+06	639.305556
	225	Available data	6.96E+05	193.388889
	260	Zak	3.62E+05	100.680556
	300	Available data	1.50E+05	41.5621016
	330	Zak	7.76E+04	21.5624199

C1. THE POWER LAW ANALYSIS

T (K)	σ (MPa)	UTS (MPa)	t_f (s)	$\dot{\varepsilon}_m$ (s^{-1})	ln (t_f)	ln ($\dot{\varepsilon}_m$)	ln (σ)	1/T	σ / UTS
823	390	638	1.15E+07	6.20E-09	1.63E+01	-1.89E+01	5.9661467	1.22E-03	0.611285266
823	470	638	4.57E+06	2.08E-08	1.53E+01	-1.77E+01	6.1527327	1.22E-03	0.736677116
823	540	638	1.78E+06	3.89E-08	1.44E+01	-1.71E+01	6.2915691	1.22E-03	0.846394984
823	565	638	1.17E+06	4.46E-08	1.40E+01	-1.69E+01	6.3368257	1.22E-03	0.885579937
823	600	638	4.07E+05	9.75E-08	1.29E+01	-1.61E+01	6.3969297	1.22E-03	0.940438871
848	300	622.5	1.12E+07	5.82E-09	1.62E+01	-1.90E+01	5.7037825	1.18E-03	0.481927711
848	390	622.5	2.29E+06	1.94E-08	1.46E+01	-1.78E+01	5.9661467	1.18E-03	0.626506024
848	420	622.5	1.54E+06	5.80E-08	1.42E+01	-1.67E+01	6.0402547	1.18E-03	0.674698795
848	430	622.5	1.35E+06	6.12E-08	1.41E+01	-1.66E+01	6.0637852	1.18E-03	0.690763052
848	455	622.5	1.10E+06	7.19E-08	1.39E+01	-1.64E+01	6.1202974	1.18E-03	0.730923695
848	500	622.5	5.37E+05	1.61E-07	1.32E+01	-1.56E+01	6.2146081	1.18E-03	0.803212851
848	570	622.5	1.78E+05	3.07E-07	1.21E+01	-1.50E+01	6.3456364	1.18E-03	0.915662651
873	200	607	2.09E+07	3.56E-09	1.69E+01	-1.95E+01	5.2983174	1.15E-03	0.329489292
873	280	607	3.72E+06	2.25E-08	1.51E+01	-1.76E+01	5.6347896	1.15E-03	0.461285008
873	300	607	2.98E+06	2.91E-08	1.49E+01	-1.74E+01	5.7037825	1.15E-03	0.494233937
873	350	607	1.17E+06	7.20E-08	1.40E+01	-1.64E+01	5.8579332	1.15E-03	0.57660626
873	360	607	9.85E+05	8.96E-08	1.38E+01	-1.62E+01	5.886104	1.15E-03	0.593080725
873	360	607	7.86E+05	9.71E-08	1.36E+01	-1.61E+01	5.886104	1.15E-03	0.593080725
873	360	607	5.32E+05	1.57E-07	1.32E+01	-1.57E+01	5.886104	1.15E-03	0.593080725
873	360	607	5.75E+05	1.50E-07	1.33E+01	-1.57E+01	5.886104	1.15E-03	0.593080725
873	360	607	6.07E+05	1.37E-07	1.33E+01	-1.58E+01	5.886104	1.15E-03	0.593080725
873	360	607	8.49E+05	9.70E-08	1.37E+01	-1.61E+01	5.886104	1.15E-03	0.593080725
873	360	607	7.50E+05	9.88E-08	1.35E+01	-1.61E+01	5.886104	1.15E-03	0.593080725
873	360	607	7.85E+05	9.76E-08	1.36E+01	-1.61E+01	5.886104	1.15E-03	0.593080725
873	360	607	7.05E+05	1.00E-07	1.35E+01	-1.61E+01	5.886104	1.15E-03	0.593080725
873	360	607	8.53E+05	9.60E-08	1.37E+01	-1.62E+01	5.886104	1.15E-03	0.593080725
873	360	607	8.99E+05	9.50E-08	1.37E+01	-1.62E+01	5.886104	1.15E-03	0.593080725
873	360	607	6.80E+05	1.25E-07	1.34E+01	-1.59E+01	5.886104	1.15E-03	0.593080725
873	390	607	6.46E+05	7.74E-08	1.34E+01	-1.64E+01	5.9661467	1.15E-03	0.642504119
873	480	607	1.82E+05	4.57E-07	1.21E+01	-1.46E+01	6.1737861	1.15E-03	0.7907743
873	550	607	5.34E+04	1.55E-06	1.09E+01	-1.34E+01	6.3099183	1.15E-03	0.906095552
898	175	575	1.06E+07	7.12E-09	1.62E+01	-1.88E+01	5.164786	1.11E-03	0.304347826
898	220	575	3.32E+06	2.53E-08	1.50E+01	-1.75E+01	5.3936275	1.11E-03	0.382608696
898	250	575	1.94E+06	4.26E-08	1.45E+01	-1.70E+01	5.5214609	1.11E-03	0.434782609
898	280	575	1.13E+06	7.01E-08	1.39E+01	-1.65E+01	5.6347896	1.11E-03	0.486956522
898	300	575	7.62E+05	4.53E-07	1.35E+01	-1.46E+01	5.7037825	1.11E-03	0.52173913
898	300	575	5.91E+05	1.57E-07	1.33E+01	-1.57E+01	5.7037825	1.11E-03	0.52173913
898	330	575	3.13E+05	2.89E-07	1.27E+01	-1.51E+01	5.7990927	1.11E-03	0.573913043
898	400	575	1.11E+05	7.89E-07	1.16E+01	-1.41E+01	5.9914645	1.11E-03	0.695652174
923	140	543	5.98E+06	1.00E-08	1.56E+01	-1.84E+01	4.9416424	1.08E-03	0.257826888
923	155	543	3.75E+06	2.15E-08	1.51E+01	-1.77E+01	5.0434251	1.08E-03	0.285451197
923	180	543	2.30E+06	3.72E-08	1.46E+01	-1.71E+01	5.1929569	1.08E-03	0.331491713
923	225	543	6.96E+05	1.25E-07	1.35E+01	-1.59E+01	5.4161004	1.08E-03	0.414364641
923	260	543	3.62E+05	2.24E-07	1.28E+01	-1.53E+01	5.5606816	1.08E-03	0.478821363
923	300	543	1.50E+05	3.31E-07	1.19E+01	-1.49E+01	5.7037825	1.08E-03	0.552486188
923	330	543	7.76E+04	7.47E-07	1.13E+01	-1.41E+01	5.7990927	1.08E-03	0.607734807

C2. THE MONKMAN-GRANT ANALYSIS

T (K)	σ (MPa)	UTS (MPa)	t_f (s)	$\dot{\varepsilon}_m$ (s^{-1})	$1/t_f$ (s^{-1})	t_f (predicted) equation (2.1)	t_f (predicted) equation (2.17)	t_f (predicted) equation (2.18)
823	390	638	1.15E+07	6.20E-09	8.71E-08	1.19E+07	1.12E+07	1.11E+07
823	470	638	4.57E+06	2.08E-08	2.19E-07	3.56E+06	3.57E+06	3.51E+06
823	540	638	1.78E+06	3.89E-08	5.62E-07	1.90E+06	1.98E+06	1.93E+06
823	565	638	1.17E+06	4.46E-08	8.51E-07	1.66E+06	1.74E+06	1.70E+06
823	600	638	4.07E+05	9.75E-08	2.45E-06	7.59E+05	8.35E+05	8.05E+05
848	300	622.5	1.12E+07	5.82E-09	8.91E-08	1.27E+07	1.18E+07	1.18E+07
848	390	622.5	2.29E+06	1.94E-08	4.37E-07	3.81E+06	3.81E+06	3.75E+06
848	420	622.5	1.54E+06	5.80E-08	6.48E-07	1.28E+06	1.36E+06	1.32E+06
848	430	622.5	1.35E+06	6.12E-08	7.40E-07	1.21E+06	1.29E+06	1.26E+06
848	455	622.5	1.10E+06	7.19E-08	9.07E-07	1.03E+06	1.11E+06	1.08E+06
848	500	622.5	5.37E+05	1.61E-07	1.86E-06	4.60E+05	5.21E+05	4.99E+05
848	570	622.5	1.78E+05	3.07E-07	5.62E-06	2.41E+05	2.84E+05	2.70E+05
873	200	607	2.09E+07	3.56E-09	4.79E-08	2.08E+07	1.88E+07	1.89E+07
873	280	607	3.72E+06	2.25E-08	2.69E-07	3.29E+06	3.32E+06	3.26E+06
873	300	607	2.98E+06	2.91E-08	3.35E-07	2.54E+06	2.60E+06	2.55E+06
873	350	607	1.17E+06	7.20E-08	8.51E-07	1.03E+06	1.11E+06	1.08E+06
873	360	607	9.85E+05	8.96E-08	1.02E-06	8.26E+05	9.04E+05	8.73E+05
873	360	607	7.86E+05	9.71E-08	1.27E-06	7.62E+05	8.38E+05	8.09E+05
873	360	607	5.32E+05	1.57E-07	1.88E-06	4.71E+05	5.34E+05	5.11E+05
873	360	607	5.75E+05	1.50E-07	1.74E-06	4.93E+05	5.57E+05	5.34E+05
873	360	607	6.07E+05	1.37E-07	1.65E-06	5.40E+05	6.06E+05	5.82E+05
873	360	607	8.49E+05	9.70E-08	1.18E-06	7.63E+05	8.39E+05	8.09E+05
873	360	607	7.50E+05	9.88E-08	1.33E-06	7.49E+05	8.25E+05	7.95E+05
873	360	607	7.85E+05	9.76E-08	1.27E-06	7.58E+05	8.34E+05	8.05E+05
873	360	607	7.05E+05	1.00E-07	1.42E-06	7.40E+05	8.15E+05	7.86E+05
873	360	607	8.53E+05	9.60E-08	1.17E-06	7.71E+05	8.47E+05	8.17E+05
873	360	607	8.99E+05	9.50E-08	1.11E-06	7.79E+05	8.56E+05	8.26E+05
873	360	607	6.80E+05	1.25E-07	1.47E-06	5.92E+05	6.61E+05	6.36E+05
873	390	607	6.46E+05	7.74E-08	1.55E-06	9.56E+05	1.04E+06	1.00E+06
873	480	607	1.82E+05	4.57E-07	5.48E-06	1.62E+05	1.95E+05	1.85E+05
873	550	607	5.34E+04	1.55E-06	1.87E-05	4.77E+04	6.19E+04	5.77E+04
898	175	575	1.06E+07	7.12E-09	9.45E-08	1.04E+07	9.79E+06	9.76E+06
898	220	575	3.32E+06	2.53E-08	3.01E-07	2.92E+06	2.97E+06	2.91E+06
898	250	575	1.94E+06	4.26E-08	5.16E-07	1.74E+06	1.82E+06	1.77E+06
898	280	575	1.13E+06	7.01E-08	8.86E-07	1.06E+06	1.14E+06	1.10E+06
898	300	575	5.91E+05	1.57E-07	1.69E-06	4.71E+05	5.34E+05	5.11E+05
898	330	575	3.13E+05	2.89E-07	3.20E-06	2.56E+05	3.01E+05	2.86E+05
898	400	575	1.11E+05	7.89E-07	9.02E-06	9.38E+04	1.17E+05	1.10E+05
923	155	543	3.75E+06	2.15E-08	2.67E-07	3.44E+06	3.46E+06	3.40E+06
923	180	543	2.30E+06	3.72E-08	4.34E-07	1.99E+06	2.07E+06	2.02E+06
923	225	543	6.96E+05	1.25E-07	1.44E-06	5.92E+05	6.61E+05	6.36E+05
923	260	543	3.62E+05	2.24E-07	2.76E-06	3.30E+05	3.82E+05	3.64E+05
923	300	543	1.50E+05	3.31E-07	6.68E-06	2.24E+05	2.65E+05	2.51E+05
923	330	543	7.76E+04	7.47E-07	1.29E-05	9.91E+04	1.23E+05	1.16E+05

C3. THE LARSON-MILLER ANALYSIS

T (K)	σ (MPa)	UTS (MPa)	t_r (s)	log t_r	T (20 + log t_r)	1/T
823	390	638	1.15E+07	7.06E+00	2.23E+04	1.22E-03
823	470	638	4.57E+06	6.66E+00	2.19E+04	1.22E-03
823	540	638	1.78E+06	6.25E+00	2.16E+04	1.22E-03
823	565	638	1.17E+06	6.07E+00	2.15E+04	1.22E-03
823	600	638	4.07E+05	5.61E+00	2.11E+04	1.22E-03
848	300	622.5	1.12E+07	7.05E+00	2.29E+04	1.18E-03
848	390	622.5	2.29E+06	6.36E+00	2.24E+04	1.18E-03
848	420	622.5	1.54E+06	6.19E+00	2.22E+04	1.18E-03
848	430	622.5	1.35E+06	6.13E+00	2.22E+04	1.18E-03
848	455	622.5	1.10E+06	6.04E+00	2.21E+04	1.18E-03
848	500	622.5	5.37E+05	5.73E+00	2.18E+04	1.18E-03
848	570	622.5	1.78E+05	5.25E+00	2.14E+04	1.18E-03
873	200	607	2.09E+07	7.32E+00	2.39E+04	1.15E-03
873	280	607	3.72E+06	6.57E+00	2.32E+04	1.15E-03
873	300	607	2.98E+06	6.47E+00	2.31E+04	1.15E-03
873	350	607	1.17E+06	6.07E+00	2.28E+04	1.15E-03
873	360	607	9.85E+05	5.99E+00	2.27E+04	1.15E-03
873	360	607	7.86E+05	5.90E+00	2.26E+04	1.15E-03
873	360	607	5.32E+05	5.73E+00	2.25E+04	1.15E-03
873	360	607	5.75E+05	5.76E+00	2.25E+04	1.15E-03
873	360	607	6.07E+05	5.78E+00	2.25E+04	1.15E-03
873	360	607	8.49E+05	5.93E+00	2.26E+04	1.15E-03
873	360	607	7.50E+05	5.88E+00	2.26E+04	1.15E-03
873	360	607	7.85E+05	5.89E+00	2.26E+04	1.15E-03
873	360	607	7.05E+05	5.85E+00	2.26E+04	1.15E-03
873	360	607	8.53E+05	5.93E+00	2.26E+04	1.15E-03
873	360	607	8.99E+05	5.95E+00	2.27E+04	1.15E-03
873	360	607	6.80E+05	5.83E+00	2.26E+04	1.15E-03
873	390	607	6.46E+05	5.81E+00	2.25E+04	1.15E-03
873	480	607	1.82E+05	5.26E+00	2.21E+04	1.15E-03
873	550	607	5.34E+04	4.73E+00	2.16E+04	1.15E-03
898	175	575	1.06E+07	7.02E+00	2.43E+04	1.11E-03
898	220	575	3.32E+06	6.52E+00	2.38E+04	1.11E-03
898	250	575	1.94E+06	6.29E+00	2.36E+04	1.11E-03
898	280	575	1.13E+06	6.05E+00	2.34E+04	1.11E-03
898	300	575	7.62E+05	5.88E+00	2.32E+04	1.11E-03
898	300	575	5.91E+05	5.77E+00	2.31E+04	1.11E-03
898	330	575	3.13E+05	5.49E+00	2.29E+04	1.11E-03
898	400	575	1.11E+05	5.04E+00	2.25E+04	1.11E-03
923	140	543	5.98E+06	6.78E+00	2.47E+04	1.08E-03
923	155	543	3.75E+06	6.57E+00	2.45E+04	1.08E-03
923	180	543	2.30E+06	6.36E+00	2.43E+04	1.08E-03
923	225	543	6.96E+05	5.84E+00	2.39E+04	1.08E-03
923	260	543	3.62E+05	5.56E+00	2.36E+04	1.08E-03
923	300	543	1.50E+05	5.18E+00	2.32E+04	1.08E-03
923	330	543	7.76E+04	4.89E+00	2.30E+04	1.08E-03

C4. THE MANSON-HAFERD ANALYSIS

T (K)	σ (MPa)	UTS (MPa)	t_f (s)	log (t_f)	(log t_f - 29.713)/(1061 - T)
823	390	638	1.15E+07	7.06E+00	-9.52E-02
823	470	638	4.57E+06	6.66E+00	-9.69E-02
823	540	638	1.78E+06	6.25E+00	-9.86E-02
823	565	638	1.17E+06	6.07E+00	-9.93E-02
823	600	638	4.07E+05	5.61E+00	-1.01E-01
848	300	622.5	1.12E+07	7.05E+00	-1.06E-01
848	390	622.5	2.29E+06	6.36E+00	-1.10E-01
848	420	622.5	1.54E+06	6.19E+00	-1.10E-01
848	430	622.5	1.35E+06	6.13E+00	-1.11E-01
848	455	622.5	1.10E+06	6.04E+00	-1.11E-01
848	500	622.5	5.37E+05	5.73E+00	-1.13E-01
848	570	622.5	1.78E+05	5.25E+00	-1.15E-01
873	200	607	2.09E+07	7.32E+00	-1.19E-01
873	280	607	3.72E+06	6.57E+00	-1.23E-01
873	300	607	2.98E+06	6.47E+00	-1.24E-01
873	350	607	1.17E+06	6.07E+00	-1.26E-01
873	360	607	9.85E+05	5.99E+00	-1.26E-01
873	360	607	7.86E+05	5.90E+00	-1.27E-01
873	360	607	5.32E+05	5.73E+00	-1.28E-01
873	360	607	5.75E+05	5.76E+00	-1.27E-01
873	360	607	6.07E+05	5.78E+00	-1.27E-01
873	360	607	8.49E+05	5.93E+00	-1.27E-01
873	360	607	7.50E+05	5.88E+00	-1.27E-01
873	360	607	7.85E+05	5.89E+00	-1.27E-01
873	360	607	7.05E+05	5.85E+00	-1.27E-01
873	360	607	8.53E+05	5.93E+00	-1.27E-01
873	360	607	8.99E+05	5.95E+00	-1.26E-01
873	360	607	6.80E+05	5.83E+00	-1.27E-01
873	390	607	6.46E+05	5.81E+00	-1.27E-01
873	480	607	1.82E+05	5.26E+00	-1.30E-01
873	550	607	5.34E+04	4.73E+00	-1.33E-01
898	175	575	1.06E+07	7.02E+00	-1.39E-01
898	220	575	3.32E+06	6.52E+00	-1.42E-01
898	250	575	1.94E+06	6.29E+00	-1.44E-01
898	280	575	1.13E+06	6.05E+00	-1.45E-01
898	300	575	7.62E+05	5.88E+00	-1.46E-01
898	300	575	5.91E+05	5.77E+00	-1.47E-01
898	330	575	3.13E+05	5.49E+00	-1.49E-01
898	400	575	1.11E+05	5.04E+00	-1.51E-01
923	140	543	5.98E+06	6.78E+00	-1.66E-01
923	155	543	3.75E+06	6.57E+00	-1.68E-01
923	180	543	2.30E+06	6.36E+00	-1.69E-01
923	225	543	6.96E+05	5.84E+00	-1.73E-01
923	260	543	3.62E+05	5.56E+00	-1.75E-01
923	300	543	1.50E+05	5.18E+00	-1.78E-01
923	330	543	7.76E+04	4.89E+00	-1.80E-01

C5. THE ORR-SHERBY-DORN ANALYSIS

T (K)	σ (MPa)	UTS (MPa)	t_f (s)	log (t_f)	(20,000/T) - log t_f	1/T
823	390	638	1.15E+07	7.06E+00	1.75E+01	1.22E-03
823	470	638	4.57E+06	6.66E+00	1.79E+01	1.22E-03
823	540	638	1.78E+06	6.25E+00	1.84E+01	1.22E-03
823	565	638	1.17E+06	6.07E+00	1.85E+01	1.22E-03
823	600	638	4.07E+05	5.61E+00	1.90E+01	1.22E-03
848	300	622.5	1.12E+07	7.05E+00	1.68E+01	1.18E-03
848	390	622.5	2.29E+06	6.36E+00	1.75E+01	1.18E-03
848	420	622.5	1.54E+06	6.19E+00	1.77E+01	1.18E-03
848	430	622.5	1.35E+06	6.13E+00	1.77E+01	1.18E-03
848	455	622.5	1.10E+06	6.04E+00	1.78E+01	1.18E-03
848	500	622.5	5.37E+05	5.73E+00	1.81E+01	1.18E-03
848	570	622.5	1.78E+05	5.25E+00	1.86E+01	1.18E-03
873	200	607	2.09E+07	7.32E+00	1.59E+01	1.15E-03
873	280	607	3.72E+06	6.57E+00	1.66E+01	1.15E-03
873	300	607	2.98E+06	6.47E+00	1.67E+01	1.15E-03
873	350	607	1.17E+06	6.07E+00	1.71E+01	1.15E-03
873	360	607	9.85E+05	5.99E+00	1.72E+01	1.15E-03
873	360	607	7.86E+05	5.90E+00	1.73E+01	1.15E-03
873	360	607	5.32E+05	5.73E+00	1.75E+01	1.15E-03
873	360	607	5.75E+05	5.76E+00	1.74E+01	1.15E-03
873	360	607	6.07E+05	5.78E+00	1.74E+01	1.15E-03
873	360	607	8.49E+05	5.93E+00	1.73E+01	1.15E-03
873	360	607	7.50E+05	5.88E+00	1.73E+01	1.15E-03
873	360	607	7.85E+05	5.89E+00	1.73E+01	1.15E-03
873	360	607	7.05E+05	5.85E+00	1.73E+01	1.15E-03
873	360	607	8.53E+05	5.93E+00	1.73E+01	1.15E-03
873	360	607	8.99E+05	5.95E+00	1.72E+01	1.15E-03
873	360	607	6.80E+05	5.83E+00	1.74E+01	1.15E-03
873	390	607	6.46E+05	5.81E+00	1.74E+01	1.15E-03
873	480	607	1.82E+05	5.26E+00	1.79E+01	1.15E-03
873	550	607	5.34E+04	4.73E+00	1.85E+01	1.15E-03
898	175	575	1.06E+07	7.02E+00	1.55E+01	1.11E-03
898	220	575	3.32E+06	6.52E+00	1.60E+01	1.11E-03
898	250	575	1.94E+06	6.29E+00	1.63E+01	1.11E-03
898	280	575	1.13E+06	6.05E+00	1.65E+01	1.11E-03
898	300	575	7.62E+05	5.88E+00	1.67E+01	1.11E-03
898	300	575	5.91E+05	5.77E+00	1.68E+01	1.11E-03
898	330	575	3.13E+05	5.49E+00	1.71E+01	1.11E-03
898	400	575	1.11E+05	5.04E+00	1.75E+01	1.11E-03
923	140	543	5.98E+06	6.78E+00	1.52E+01	1.08E-03
923	155	543	3.75E+06	6.57E+00	1.54E+01	1.08E-03
923	180	543	2.30E+06	6.36E+00	1.56E+01	1.08E-03
923	225	543	6.96E+05	5.84E+00	1.61E+01	1.08E-03
923	260	543	3.62E+05	5.56E+00	1.64E+01	1.08E-03
923	300	543	1.50E+05	5.18E+00	1.68E+01	1.08E-03
923	330	543	7.76E+04	4.89E+00	1.70E+01	1.08E-03

C6. THE MANSON-SUCCOP ANALYSIS

T (K)	σ (MPa)	UTS (MPa)	t_f (s)	log (t_f)	(log t_f + 0.025 T)
823	390	638	1.15E+07	7.06E+00	2.76E+01
823	470	638	4.57E+06	6.66E+00	2.72E+01
823	540	638	1.78E+06	6.25E+00	2.68E+01
823	565	638	1.17E+06	6.07E+00	2.66E+01
823	600	638	4.07E+05	5.61E+00	2.62E+01
848	300	622.5	1.12E+07	7.05E+00	2.83E+01
848	390	622.5	2.29E+06	6.36E+00	2.76E+01
848	420	622.5	1.54E+06	6.19E+00	2.74E+01
848	430	622.5	1.35E+06	6.13E+00	2.73E+01
848	455	622.5	1.10E+06	6.04E+00	2.72E+01
848	500	622.5	5.37E+05	5.73E+00	2.69E+01
848	570	622.5	1.78E+05	5.25E+00	2.65E+01
873	200	607	2.09E+07	7.32E+00	2.91E+01
873	280	607	3.72E+06	6.57E+00	2.84E+01
873	300	607	2.98E+06	6.47E+00	2.83E+01
873	350	607	1.17E+06	6.07E+00	2.79E+01
873	360	607	9.85E+05	5.99E+00	2.78E+01
873	360	607	7.86E+05	5.90E+00	2.77E+01
873	360	607	5.32E+05	5.73E+00	2.76E+01
873	360	607	5.75E+05	5.76E+00	2.76E+01
873	360	607	6.07E+05	5.78E+00	2.76E+01
873	360	607	8.49E+05	5.93E+00	2.78E+01
873	360	607	7.50E+05	5.88E+00	2.77E+01
873	360	607	7.85E+05	5.89E+00	2.77E+01
873	360	607	7.05E+05	5.85E+00	2.77E+01
873	360	607	8.53E+05	5.93E+00	2.78E+01
873	360	607	8.99E+05	5.95E+00	2.78E+01
873	360	607	6.80E+05	5.83E+00	2.77E+01
873	390	607	6.46E+05	5.81E+00	2.76E+01
873	480	607	1.82E+05	5.26E+00	2.71E+01
873	550	607	5.34E+04	4.73E+00	2.66E+01
898	175	575	1.06E+07	7.02E+00	2.95E+01
898	220	575	3.32E+06	6.52E+00	2.90E+01
898	250	575	1.94E+06	6.29E+00	2.87E+01
898	280	575	1.13E+06	6.05E+00	2.85E+01
898	300	575	7.62E+05	5.88E+00	2.83E+01
898	300	575	5.91E+05	5.77E+00	2.82E+01
898	330	575	3.13E+05	5.49E+00	2.79E+01
898	400	575	1.11E+05	5.04E+00	2.75E+01
923	140	543	5.98E+06	6.78E+00	2.99E+01
923	155	543	3.75E+06	6.57E+00	2.96E+01
923	180	543	2.30E+06	6.36E+00	2.94E+01
923	225	543	6.96E+05	5.84E+00	2.89E+01
923	260	543	3.62E+05	5.56E+00	2.86E+01
923	300	543	1.50E+05	5.18E+00	2.83E+01
923	330	543	7.76E+04	4.89E+00	2.80E+01

C7. THE HYPERBOLIC-TANGENT ANALYSIS

T (K)	σ (MPa)	UTS (MPa)	t_f (s)	ln t_f	$\tanh^{-1}(1-2(\sigma/\sigma_{TS}))$
823	390	638	1.15E+07	1.63E+01	-2.26E-01
823	470	638	4.57E+06	1.53E+01	-5.14E-01
823	540	638	1.78E+06	1.44E+01	-8.53E-01
823	565	638	1.17E+06	1.40E+01	-1.02E+00
823	600	638	4.07E+05	1.29E+01	-1.38E+00
848	300	622.5	1.12E+07	1.62E+01	3.62E-02
848	390	622.5	2.29E+06	1.46E+01	-2.59E-01
848	420	622.5	1.54E+06	1.42E+01	-3.65E-01
848	430	622.5	1.35E+06	1.41E+01	-4.02E-01
848	455	622.5	1.10E+06	1.39E+01	-5.00E-01
848	500	622.5	5.37E+05	1.32E+01	-7.03E-01
848	570	622.5	1.78E+05	1.21E+01	-1.19E+00
873	200	607	2.09E+07	1.69E+01	3.55E-01
873	280	607	3.72E+06	1.51E+01	7.76E-02
873	300	607	2.98E+06	1.49E+01	1.15E-02
873	350	607	1.17E+06	1.40E+01	-1.54E-01
873	360	607	9.85E+05	1.38E+01	-1.88E-01
873	360	607	7.86E+05	1.36E+01	-1.88E-01
873	360	607	5.32E+05	1.32E+01	-1.88E-01
873	360	607	5.75E+05	1.33E+01	-1.88E-01
873	360	607	6.07E+05	1.33E+01	-1.88E-01
873	360	607	8.49E+05	1.37E+01	-1.88E-01
873	360	607	7.50E+05	1.35E+01	-1.88E-01
873	360	607	7.85E+05	1.36E+01	-1.88E-01
873	360	607	7.05E+05	1.35E+01	-1.88E-01
873	360	607	8.53E+05	1.37E+01	-1.88E-01
873	360	607	8.99E+05	1.37E+01	-1.88E-01
873	360	607	6.80E+05	1.34E+01	-1.88E-01
873	390	607	6.46E+05	1.34E+01	-2.93E-01
873	480	607	1.82E+05	1.21E+01	-6.65E-01
873	550	607	5.34E+04	1.09E+01	-1.13E+00
898	175	575	1.06E+07	1.62E+01	4.13E-01
898	220	575	3.32E+06	1.50E+01	2.39E-01
898	250	575	1.94E+06	1.45E+01	1.31E-01
898	280	575	1.13E+06	1.39E+01	2.61E-02
898	300	575	7.62E+05	1.35E+01	-4.35E-02
898	300	575	5.91E+05	1.33E+01	-4.35E-02
898	330	575	3.13E+05	1.27E+01	-1.49E-01
898	400	575	1.11E+05	1.16E+01	-4.13E-01
923	140	543	5.98E+06	1.56E+01	5.29E-01
923	155	543	3.75E+06	1.51E+01	4.59E-01
923	180	543	2.30E+06	1.46E+01	3.51E-01
923	225	543	6.96E+05	1.35E+01	1.73E-01
923	260	543	3.62E+05	1.28E+01	4.24E-02
923	300	543	1.50E+05	1.19E+01	-1.05E-01
923	330	543	7.76E+04	1.13E+01	-2.19E-01

C8. THE GOLDHOFF-SHERBY ANALYSIS

T (K)	σ (MPa)	UTS (MPa)	t_f (s)	(log t_f - 15.824) / (1/T - 0.0008)
823	390	638	1.15E+07	7.06E+00
823	470	638	4.57E+06	6.66E+00
823	540	638	1.78E+06	6.25E+00
823	565	638	1.17E+06	6.07E+00
823	600	638	4.07E+05	5.61E+00
848	300	622.5	1.12E+07	7.05E+00
848	390	622.5	2.29E+06	6.36E+00
848	420	622.5	1.54E+06	6.19E+00
848	430	622.5	1.35E+06	6.13E+00
848	455	622.5	1.10E+06	6.04E+00
848	500	622.5	5.37E+05	5.73E+00
848	570	622.5	1.78E+05	5.25E+00
873	200	607	2.09E+07	7.32E+00
873	280	607	3.72E+06	6.57E+00
873	300	607	2.98E+06	6.47E+00
873	350	607	1.17E+06	6.07E+00
873	360	607	9.85E+05	5.99E+00
873	360	607	7.86E+05	5.90E+00
873	360	607	5.32E+05	5.73E+00
873	360	607	5.75E+05	5.76E+00
873	360	607	6.07E+05	5.78E+00
873	360	607	8.49E+05	5.93E+00
873	360	607	7.50E+05	5.88E+00
873	360	607	7.85E+05	5.89E+00
873	360	607	7.05E+05	5.85E+00
873	360	607	8.53E+05	5.93E+00
873	360	607	8.99E+05	5.95E+00
873	360	607	6.80E+05	5.83E+00
873	390	607	6.46E+05	5.81E+00
873	480	607	1.82E+05	5.26E+00
873	550	607	5.34E+04	4.73E+00
898	175	575	1.06E+07	7.02E+00
898	220	575	3.32E+06	6.52E+00
898	250	575	1.94E+06	6.29E+00
898	280	575	1.13E+06	6.05E+00
898	300	575	7.62E+05	5.88E+00
898	300	575	5.91E+05	5.77E+00
898	330	575	3.13E+05	5.49E+00
898	400	575	1.11E+05	5.04E+00
923	140	543	5.98E+06	6.78E+00
923	155	543	3.75E+06	6.57E+00
923	180	543	2.30E+06	6.36E+00
923	225	543	6.96E+05	5.84E+00
923	260	543	3.62E+05	5.56E+00
923	300	543	1.50E+05	5.18E+00
923	330	543	7.76E+04	4.89E+00

C9. THE 4-θ EQUATION ANALYSIS

T (K)	σ (MPa)	θ_1	θ_2	θ_3	θ_4	ln (θ_1)	ln (θ_2)	ln (θ_3)	ln (θ_4)
823	390	4.64E-02	1.45E-07	4.48E-03	3.77E-07	-3.070610245	-15.74957195	-5.408432547	-14.79120819
823	470	3.90E-02	5.90E-07	4.88E-03	9.41E-07	-3.244209757	-14.34281377	-5.321805823	-13.87673227
823	540	9.50E-03	6.84E-06	1.96E-02	1.18E-06	-4.656684794	-11.8927553	-3.933971247	-13.65307728
823	565	0.014617836	5.09E-06	1.40E-02	1.67E-06	-4.225512824	-12.18853373	-4.270753978	-13.30521651
823	600	1.29E-02	1.08E-05	0.026948657	2.13393E-06	-4.349488926	-11.43293349	-3.613821831	-13.05754524
848	300	9.96E-02	6.68E-08	0.002906615	4.31589E-07	-2.306524911	-16.52190508	-5.840766098	-14.65579105
848	390	6.44E-01	3.58249E-08	0.000344242	1.79822E-06	-0.439420856	-17.14462231	-7.974166744	-13.22871396
848	420	2.75E-01	2.38E-07	1.72E-03	3.05E-06	-1.290978031	-15.25274219	-6.366549318	-12.70130352
848	430	1.83E-01	3.00E-07	1.19E-03	3.36291E-06	-1.695643672	-15.01809403	-6.733942334	-12.60270313
848	455	1.16E-01	7.14E-07	2.23E-03	3.88415E-06	-2.158053108	-14.15220431	-6.107606305	-12.45860543
848	500	4.09E-01	4.45632E-07	0.001036492	9.76391E-06	-0.89525134	-14.62377327	-6.871913071	-11.53681745
848	570	0.012244791	4.26308E-05	0.033720071	5.66694E-06	-4.402654627	-10.06293437	-3.389662043	-12.08086168
873	200	0.517515939	7.86936E-09	0.000771099	2.85768E-07	-0.658714954	-18.66028914	-7.167693208	-15.06808409
873	280	0.014916836	7.34216E-07	0.026605152	6.19827E-07	-4.205264788	-14.12446309	-3.626650406	-14.29382469
873	300	0.257408564	1.12947E-07	0.002717524	1.45635E-06	-1.357090712	-15.99635066	-5.908034195	-13.43957924
873	350	0.386895754	2.08978E-07	0.001293222	4.09465E-06	-0.949599992	-15.38103493	-6.650618226	-12.40582967
873	360	0.581993154	1.86354E-07	0.001880636	4.70037E-06	-0.541296594	-15.4956168	-6.276145344	-12.26786836
873	480	0.008401546	4.92249E-05	0.034137655	1.02904E-05	-4.779339522	-9.91911006	-3.377354242	-11.48430334
873	550	0.687649176	2.65895E-06	0.003170021	6.4805E-05	-0.37447649	-12.8375785	-5.754017011	-9.644128437
898	175	0.825511796	8.63129E-09	0.001833508	3.98E-07	-0.191751727	-18.56787155	-6.301524079	-14.73624681
898	220	0.630364985	4.77779E-08	0.00103182	1.55E-06	-0.461456286	-16.85670224	-6.876431115	-13.37596029
898	250	0.210253582	1.51196E-07	5.45E-03	1.9379E-06	-1.559440944	-15.70468648	-5.211589558	-13.15390573
898	280	0.257023247	2.16E-07	0.00991375	2.86325E-06	-1.358588744	-15.34861843	-4.613832602	-12.76355177
898	300	5.11E-01	8.58625E-07	0.004877238	1.76417E-05	-0.670581087	-13.96793312	-5.323176305	-10.9452438
898	400	0.144600796	5.02339E-06	0.010341223	2.63587E-05	-1.933778462	-12.2014052	-4.571617155	-10.54371068
923	140	0.003509547	5.80592E-06	0.029136121	1.57756E-07	-5.652268221	-12.05663172	-3.535776599	-15.66221926
923	155	0.008901718	2.69634E-06	0.01870926	6.6088E-07	-4.721510941	-12.82361501	-3.978736704	-14.22969325
923	180	0.232041521	1.42794E-07	0.004017979	1.70485E-06	-1.460838955	-15.76186175	-5.516976343	-13.28203509
923	225	0.200264529	4.77913E-07	0.007916714	4.54704E-06	-1.60811614	-14.55383647	-4.838779055	-12.30103381
923	260	0.261224797	9.272E-07	0.004590436	1.13974E-05	-1.342373953	-13.89109601	-5.383780375	-11.38212955
923	300	0.21642504	8.6505E-07	0.015236731	1.20384E-05	-1.530511028	-13.96047807	-4.184046269	-11.32740952
923	330	0.488672067	1.28862E-06	0.016633093	2.48498E-05	-0.716063634	-13.56194181	-4.096361033	-10.60266185

T (K)	σ (MPa)	t_m (using θ-method)	ε_m (using θ-method)	$\dot{\varepsilon}_m$ (using θ-method)	ε_P ($\varepsilon_m - \dot{\varepsilon}_m t_m$)	ε_P modified (only values > 0)	$t_{f\,(actual)}$	$\varepsilon_{f\,(actual)}$	ε_T ($\varepsilon_f - \varepsilon_P$)	ε_f (θ-method @ tf actual)	ε_T ($\varepsilon_{f,\theta} - \varepsilon_P$)
823	390	8.07E+05	6.70E-03	8.26E-09	3.78E-05	3.78E-05	9.20E+06	1.94E-01	1.94E-01	1.73E-01	1.73E-01
823	470	7.48E+05	1.89E-02	2.41E-08	8.89E-04	8.89E-04	3.58E+06	1.85E-01	1.84E-01	1.71E-01	1.70E-01
823	540	3.49E+05	1.86E-02	4.07E-08	4.36E-03	4.36E-03	1.50E+06	1.25E-01	1.21E-01	1.04E-01	9.97E-02
823	565	3.37E+05	2.25E-02	5.42E-08	4.25E-03	4.25E-03	1.46E+06	1.71E-01	1.67E-01	1.60E-01	1.56E-01
823	600	1.94E+05	2.51E-02	1.04E-07	4.96E-03	4.96E-03	8.00E+05	1.44E-01	1.39E-01	1.34E-01	1.30E-01
848	300	-3.97E+05	-3.14E-03	7.89E-09	-2.46E-06	0.00E+00	9.07E+06	2.25E-01	2.25E-01	1.88E-01	1.88E-01
848	390	-1.62E+05	-3.84E-03	2.37E-08	-1.16E-06	0.00E+00	3.13E+06	1.77E-01	1.77E-01	1.64E-01	1.64E-01
848	420	-8.31E+03	-5.87E-04	7.06E-08	-4.92E-09	0.00E+00	1.54E+06	3.17E-01	3.17E-01	2.72E-01	2.72E-01
848	430	5.66E+04	3.35E-03	5.90E-08	1.73E-06	1.73E-06	1.35E+06	2.07E-01	2.07E-01	1.72E-01	1.72E-01
848	455	1.22E+05	1.10E-02	8.95E-08	6.90E-05	6.90E-05	1.10E+06	2.70E-01	2.70E-01	2.22E-01	2.22E-01
848	500	-1.93E+04	-3.71E-03	1.92E-07	-1.05E-06	0.00E+00	5.01E+05	2.56E-01	2.56E-01	2.19E-01	2.19E-01
848	570	6.26E+04	2.58E-02	3.09E-07	6.43E-03	6.43E-03	2.71E+05	1.60E-01	1.54E-01	1.35E-01	1.28E-01
873	200	-2.30E+06	-9.82E-03	4.26E-09	-2.30E-05	0.00E+00	1.68E+07	1.90E-01	1.90E-01	1.57E-01	1.57E-01
873	280	-1.77E+05	-4.84E-03	2.72E-08	-1.14E-05	0.00E+00	3.72E+06	3.07E-01	3.07E-01	2.54E-01	2.54E-01
873	300	-3.59E+05	-1.17E-02	3.26E-08	-4.67E-05	0.00E+00	2.98E+06	3.44E-01	3.44E-01	2.81E-01	2.81E-01
873	350	-5.79E+04	-4.99E-03	8.60E-08	-2.53E-06	0.00E+00	1.17E+06	2.85E-01	2.85E-01	2.41E-01	2.41E-01
873	360	-1.47E+05	-1.72E-02	1.16E-07	-6.47E-05	0.00E+00	9.85E+05	3.37E-01	3.37E-01	2.88E-01	2.88E-01
873	480	2.90E+04	1.83E-02	5.73E-07	1.65E-03	1.65E-03	1.82E+05	2.24E-01	2.22E-01	1.97E-01	1.96E-01
873	550	-1.49E+04	-2.98E-02	1.98E-06	-2.43E-04	0.00E+00	5.34E+04	2.03E-01	2.03E-01	1.89E-01	1.89E-01
898	175	-3.82E+06	-2.91E-02	7.52E-09	-3.65E-04	0.00E+00	1.06E+07	2.30E-01	2.30E-01	1.94E-01	1.94E-01
898	220	-3.42E+05	-1.08E-02	3.16E-08	-1.78E-05	0.00E+00	3.32E+06	3.67E-01	3.67E-01	2.69E-01	2.69E-01
898	250	-6.94E+05	-2.73E-02	3.81E-08	-8.79E-04	0.00E+00	1.94E+06	3.59E-01	3.59E-01	2.82E-01	2.82E-01
898	280	-6.22E+05	-4.52E-02	6.82E-08	-2.73E-03	0.00E+00	1.13E+06	3.73E-01	3.73E-01	2.97E-01	2.97E-01
898	300	-7.53E+04	-3.77E-02	4.91E-07	-7.53E-04	0.00E+00	2.12E+05	3.01E-01	3.01E-01	2.85E-01	2.85E-01
898	400	-2.16E+04	-2.11E-02	9.64E-07	-2.42E-04	0.00E+00	1.11E+05	2.83E-01	2.83E-01	2.43E-01	2.43E-01
923	140	8.54E+05	7.69E-03	5.40E-09	3.07E-03	3.07E-03	9.70E+06	1.37E-01	1.34E-01	1.09E-01	1.06E-01
923	155	6.16E+05	1.66E-02	2.31E-08	2.36E-03	2.36E-03	3.75E+06	2.56E-01	2.54E-01	2.13E-01	2.11E-01
923	180	-4.89E+05	-1.91E-02	3.85E-08	-2.24E-04	0.00E+00	2.30E+06	2.73E-01	2.73E-01	2.64E-01	2.64E-01
923	225	-2.54E+05	-3.12E-02	1.19E-07	-9.41E-04	0.00E+00	6.96E+05	2.88E-01	2.88E-01	2.36E-01	2.36E-01
923	260	-7.92E+04	-2.26E-02	2.82E-07	-3.09E-04	0.00E+00	3.62E+05	4.03E-01	4.03E-01	3.56E-01	3.56E-01
923	300	-2.02E+05	-5.53E-02	2.39E-07	-6.93E-03	0.00E+00	2.32E+05	3.21E-01	3.21E-01	2.73E-01	2.73E-01
923	330	-9.71E+04	-8.03E-02	7.51E-07	-7.39E-03	0.00E+00	1.11E+05	3.63E-01	3.63E-01	3.13E-01	3.13E-01

C10. THE 6-θ EQUATION ANALYSIS

T (K)	σ (MPa)	θ_1	θ_2	θ_3	θ_4	θ_5	θ_6
823	390	1.70E+00	3.30E-09	2.78E-03	4.12E-07	2.03E-03	2.35E-05
823	470	2.29E+00	8.31E-09	1.42E-03	1.20E-06	2.41E-03	5.54E-05
823	540	3.15E+00	1.25E-08	6.45E-04	2.87E-06	3.33E-03	5.09E-05
823	565	4.47E+00	1.05E-08	1.25E-03	2.98E-06	3.97E-03	1.53E-04
823	600	5.44E+00	1.80E-08	9.48E-04	5.15E-06	4.02E-03	1.14E-04
848	300	1.91E+00	3.02E-09	2.54E-03	4.40E-07	1.35E-03	3.51E-05
848	390	3.03E+00	6.87E-09	5.31E-04	1.67E-06	9.32E-04	1.62E-04
848	420	4.73E+00	1.25E-08	1.59E-03	3.07E-06	1.50E-03	4.75E-04
848	430	6.49E+00	7.46E-09	1.10E-03	3.38E-06	1.61E-03	3.14E-04
848	455	8.62E+00	8.17E-09	1.50E-03	4.14E-06	2.26E-03	6.91E-04
848	500	9.39E+00	1.74E-08	1.13E-03	9.55E-06	1.70E-03	6.32E-04
848	570	1.19E+01	2.55E-08	7.64E-04	1.58E-05	4.95E-03	2.81E-04
873	200	2.77E+00	1.31E-09	1.01E-03	2.71E-07	1.47E-03	1.87E-05
873	280	5.04E+00	2.24E-09	1.81E-02	6.82E-07	1.49E-03	1.29E-04
873	300	5.74E+00	4.91E-09	2.19E-03	1.51E-06	4.14E-04	1.80E-04
873	350	6.49E+00	1.20E-08	1.05E-03	4.23E-06	7.06E-04	8.84E-04
873	360	6.82E+00	1.04E-08	2.37E-03	4.18E-06	3.39E-03	1.39E-04
873	360	6.69E+00	1.35E-08	7.52E-03	4.70E-06	2.42E-03	3.29E-04
873	360	6.79E+00	6.10E-09	1.20E-02	3.00E-06	2.52E-03	1.13E-04
873	360	6.84E+00	1.54E-08	3.09E-03	5.60E-06	2.61E-03	2.94E-04
873	360	7.00E+00	8.42E-09	1.00E-02	3.39E-06	2.78E-03	2.74E-04
873	360	6.62E+00	1.06E-08	7.83E-03	4.15E-06	4.00E-04	1.13E-04
873	360	6.66E+00	9.28E-09	5.31E-03	3.92E-06	2.66E-03	1.33E-04
873	360	6.94E+00	8.08E-09	7.30E-03	3.24E-06	3.24E-03	1.30E-04
873	360	7.03E+00	1.30E-08	4.81E-03	4.86E-06	2.28E-03	3.17E-04
873	360	6.74E+00	1.43E-08	4.02E-03	5.10E-06	2.13E-03	3.42E-04
873	480	1.99E+01	1.96E-08	7.02E-03	1.63E-05	2.26E-03	1.01E-03
873	550	2.41E+01	6.91E-08	3.88E-03	6.12E-05	1.12E-03	1.96E-03
898	175	6.61E+00	9.05E-10	2.87E-03	3.60E-07	1.76E-03	2.01E-05
898	220	8.90E+00	2.33E-09	3.26E-03	1.23E-06	2.37E-03	8.80E-05
898	250	1.02E+01	3.94E-10	2.41E-02	1.21E-06	1.79E-03	5.31E-05
898	280	1.62E+01	3.06E-09	1.04E-02	2.82E-06	9.39E-04	2.93E-04
898	300	1.862E+01	2.391E-08	4.068E-03	1.827E-05	1.128E-03	4.566E-07
898	400	2.20E+01	2.83E-08	1.02E-02	2.59E-05	1.84E-03	3.79E-03
923	140	3.856E+00	8.339E-10	8.960E-03	2.332E-07	2.645E-03	1.097E-05
923	155	5.028E+00	2.748E-09	6.210E-03	8.814E-07	3.093E-03	3.160E-05
923	180	6.344E+00	5.312E-09	3.098E-03	1.790E-06	2.068E-04	2.745E-04
923	225	7.525E+00	9.767E-09	1.091E-02	4.117E-06	8.699E-04	1.570E-04
923	260	8.477E+00	2.873E-08	3.665E-03	1.189E-05	1.821E-04	2.974E-03
923	300	9.267E+00	1.929E-08	1.511E-02	1.203E-05	3.799E-04	1.846E-03
923	330	1.062E+01	4.909E-08	1.921E-02	2.382E-05	1.240E-03	9.668E-03

T (K)	σ (MPa)	ln (θ_1)	ln (θ_2)	ln (θ_3)	ln (θ_4)	ln (θ_5)	ln (θ_6)
823	390	0.528608039	-19.53033395	-5.883762341	-14.7021188	-6.199809569	-10.65759937
823	470	0.82837175	-18.60600762	-6.559773092	-13.6324698	-6.029396788	-9.800606275
823	540	1.148616294	-18.19937804	-7.346210833	-12.76114469	-5.703393924	-9.884851127
823	565	1.496900524	-18.36928669	-6.68447462	-12.72368725	-5.529484749	-8.786453081
823	600	1.694049087	-17.83178923	-6.960920828	-12.17695245	-5.516483794	-9.080123276
848	300	0.649287589	-19.61680869	-5.97427604	-14.63760445	-6.605955099	-10.25740188
848	390	1.107610203	-18.79548197	-7.541571148	-13.30493164	-6.978112946	-8.72580832
848	420	1.553815927	-18.19747085	-6.446846718	-12.69417485	-6.503262706	-7.651256027
848	430	1.869547338	-18.71426453	-6.816743451	-12.59715426	-6.434081866	-8.066678415
848	455	2.153973598	-18.62258745	-6.505099786	-12.39482043	-6.093084184	-7.277148996
848	500	2.239271702	-17.86646026	-6.78121039	-11.55940376	-6.376168007	-7.367078031
848	570	2.476909733	-17.48506669	-7.176472737	-11.05738186	-5.307662259	-8.178016409
873	200	1.017894504	-20.45281733	-6.893817597	-15.12278797	-6.519530912	-10.8892695
873	280	1.6165693	-19.91747762	-4.010039237	-14.19786662	-6.511698429	-8.957855425
873	300	1.747189857	-19.1312643	-6.122029291	-13.40266809	-7.790144578	-8.623533227
873	350	1.869785086	-18.24128933	-6.856617114	-12.37288735	-7.255649186	-7.030621521
873	360	1.919854447	-18.38418881	-6.042852243	-12.38459638	-5.685651386	-8.880302488
873	360	1.901339579	-18.11962494	-4.890036976	-12.26729767	-6.025508779	-8.018311887
873	360	1.915474813	-18.91509601	-4.424996697	-12.7166956	-5.983582924	-9.091690342
873	360	1.922953213	-17.98608416	-5.779891697	-12.09187307	-5.947943441	-8.131250142
873	360	1.945295674	-18.59304364	-4.604927105	-12.59536785	-5.885859796	-8.201659436
873	360	1.890291424	-18.36168886	-4.849317823	-12.39246676	-7.823210965	-9.083930693
873	360	1.895478906	-18.49522572	-5.237233629	-12.44843803	-5.930382176	-8.921481817
873	360	1.937391368	-18.6343707	-4.919794914	-12.64006188	-5.732351337	-8.94711356
873	360	1.950803184	-18.16033582	-5.336505484	-12.23466346	-6.085569552	-8.057326593
873	360	1.907797966	-18.06292618	-5.516920773	-12.1869916	-6.15287471	-7.980894346
873	480	2.990615345	-17.74927288	-4.95877258	-11.02627113	-6.091389244	-6.894026767
873	550	3.183494446	-16.48734525	-5.551521953	-9.701510483	-6.797923789	-6.236430006
898	175	1.88798688	-20.82275026	-5.852621113	-14.83613725	-6.342376824	-10.81506574
898	220	2.18634254	-19.87837444	-5.726242428	-13.60626327	-6.045039755	-9.337634335
898	250	2.321112656	-21.65422567	-3.725837546	-13.62555176	-6.325939738	-9.842972763
898	280	2.785671705	-19.60482072	-4.567996754	-12.78039885	-6.970255338	-8.136810863
898	300	2.924239073	-17.54903891	-5.504698044	-10.91017879	-6.787488141	-14.59954021
898	400	3.092813611	-17.38180083	-4.58215518	-10.55955901	-6.299807049	-5.575285974
923	140	1.349613172	-20.9049225	-4.714991588	-15.27150831	-5.935074292	-11.42040636
923	155	1.614971961	-19.71245676	-5.081579901	-13.94179427	-5.778565336	-10.36233554
923	180	1.847433209	-19.05322649	-5.776873595	-13.2334156	-8.483731117	-8.200670072
923	225	2.018203754	-18.44430272	-4.518438113	-12.40038424	-7.047183389	-8.759573729
923	260	2.137411041	-17.36548634	-5.608811396	-11.33999003	-8.610698449	-5.817808219
923	300	2.226496461	-17.76381285	-4.192459388	-11.32834997	-7.875533759	-6.294712343
923	330	2.362286937	-16.82958519	-3.95220469	-10.64503463	-6.692251218	-4.638895055

T (K)	σ (MPa)	t_m (using θ-method)	ε_m (using θ-method)	$\dot{\varepsilon}_m$ (using θ-method)	ε_P ($\varepsilon_m - \dot{\varepsilon}_m t_m$)	ε_P modified (only values > 0)	$t_{f\ (actual)}$	$\varepsilon_{f\ (actual)}$	ε_T ($\varepsilon_f - \varepsilon_P$)	ε_f (θ-method @ tf actual)	ε_T ($\varepsilon_{f,\theta} - \varepsilon_P$)
823	390	6.400E+05	6.45E-03	7.07E-09	1.92E-03	1.92E-03	9.20E+06	1.94E-01	1.92E-01	1.73E-01	1.71E-01
823	470	2.629E+05	7.93E-03	2.13E-08	2.32E-03	2.32E-03	3.58E+06	1.85E-01	1.82E-01	1.72E-01	1.70E-01
823	540	2.474E+05	1.37E-02	4.30E-08	3.08E-03	3.08E-03	1.50E+06	1.25E-01	1.22E-01	1.09E-01	1.06E-01
823	565	1.051E+05	9.37E-03	5.21E-08	3.89E-03	3.89E-03	1.46E+06	1.71E-01	1.68E-01	1.68E-01	1.65E-01
823	600	1.172E+05	1.63E-02	1.07E-07	3.77E-03	3.77E-03	8.00E+05	1.44E-01	1.40E-01	1.39E-01	1.35E-01
848	300	4.513E+05	4.52E-03	7.14E-09	1.30E-03	1.30E-03	9.07E+06	2.25E-01	2.23E-01	1.87E-01	1.86E-01
848	390	1.024E+05	3.16E-03	2.18E-08	9.24E-04	9.24E-04	3.13E+06	1.77E-01	1.76E-01	1.63E-01	1.62E-01
848	420	3.802E+04	3.94E-03	6.46E-08	1.49E-03	1.49E-03	1.54E+06	3.17E-01	3.15E-01	2.71E-01	2.70E-01
848	430	5.581E+04	4.53E-03	5.28E-08	1.58E-03	1.58E-03	1.35E+06	2.07E-01	2.05E-01	1.72E-01	1.70E-01
848	455	2.830E+04	4.44E-03	7.74E-08	2.25E-03	2.25E-03	1.10E+06	2.70E-01	2.68E-01	2.22E-01	2.20E-01
848	500	2.622E+04	6.31E-03	1.77E-07	1.66E-03	1.66E-03	5.01E+05	2.56E-01	2.54E-01	2.18E-01	2.16E-01
848	570	4.863E+04	2.06E-02	3.29E-07	4.58E-03	4.58E-03	2.71E+05	1.60E-01	1.56E-01	1.40E-01	1.36E-01
873	200	8.476E+05	4.81E-03	3.97E-09	1.44E-03	1.44E-03	1.68E+07	1.90E-01	1.89E-01	1.57E-01	1.55E-01
873	280	1.478E+05	5.08E-03	2.50E-08	1.39E-03	1.39E-03	3.72E+06	3.07E-01	3.05E-01	2.55E-01	2.53E-01
873	300	9.038E+04	3.28E-03	3.20E-08	3.92E-04	3.92E-04	2.98E+06	3.44E-01	3.44E-01	2.81E-01	2.81E-01
873	350	2.107E+04	2.44E-03	8.25E-08	7.02E-04	7.02E-04	1.17E+06	2.85E-01	2.84E-01	2.42E-01	2.41E-01
873	360	1.070E+05	1.23E-02	8.62E-08	3.08E-03	3.08E-03	9.85E+05	3.37E-01	3.34E-01	2.16E-01	2.13E-01
873	360	5.014E+04	8.95E-03	1.35E-07	2.17E-03	2.17E-03	6.07E+05	1.81E-01	1.79E-01	1.80E-01	1.78E-01
873	360	1.363E+05	1.42E-02	9.55E-08	1.20E-03	1.20E-03	8.49E+05	1.86E-01	1.85E-01	1.78E-01	1.77E-01
873	360	5.365E+04	9.36E-03	1.29E-07	2.44E-03	2.44E-03	7.50E+05	4.11E-01	4.09E-01	2.85E-01	2.83E-01
873	360	6.322E+04	8.89E-03	1.01E-07	2.51E-03	2.51E-03	7.85E+05	1.87E-01	1.84E-01	1.82E-01	1.79E-01
873	360	5.018E+04	5.74E-03	1.10E-07	1.97E-04	1.97E-04	7.05E+05	1.89E-01	1.89E-01	1.88E-01	1.88E-01
873	360	1.110E+05	1.24E-02	9.40E-08	1.98E-03	1.98E-03	8.53E+05	2.25E-01	2.23E-01	2.01E-01	1.99E-01
873	360	1.182E+05	1.33E-02	9.07E-08	2.55E-03	2.55E-03	8.99E+05	1.86E-01	1.84E-01	1.80E-01	1.78E-01
873	360	5.157E+04	8.35E-03	1.21E-07	2.10E-03	2.10E-03	6.80E+05	2.03E-01	2.01E-01	1.90E-01	1.88E-01
873	360	4.766E+04	7.82E-03	1.22E-07	1.99E-03	1.99E-03	6.81E+05	2.05E-01	2.03E-01	1.92E-01	1.90E-01
873	480	1.652E+04	1.09E-02	5.39E-07	1.96E-03	1.96E-03	1.82E+05	2.24E-01	2.22E-01	2.03E-01	2.01E-01
873	550	7.132E+03	1.51E-02	2.03E-06	6.22E-04	6.22E-04	5.34E+04	2.03E-01	2.02E-01	1.88E-01	1.88E-01
898	175	7.858E+05	7.40E-03	7.35E-09	1.62E-03	1.62E-03	1.06E+07	2.30E-01	2.29E-01	1.92E-01	1.90E-01
898	220	1.943E+05	7.28E-03	2.58E-08	2.26E-03	2.26E-03	3.32E+06	3.67E-01	3.64E-01	2.63E-01	2.60E-01
898	250	4.900E+04	3.32E-03	4.20E-08	1.27E-03	1.27E-03	1.94E+06	3.59E-01	3.58E-01	2.37E-01	2.35E-01
898	280	6.089E+04	5.90E-03	8.43E-08	7.69E-04	7.69E-04	1.13E+06	3.73E-01	3.72E-01	2.95E-01	2.95E-01
898	300	2.000E+04	1.07E-02	5.53E-07	3.46E-04	3.46E-04	2.12E+05	3.01E-01	3.00E-01	2.85E-01	2.85E-01
898	400	5.065E+03	6.43E-03	9.26E-07	1.74E-03	1.74E-03	1.11E+05	2.83E-01	2.81E-01	2.42E-01	2.40E-01
923	140	1.863E+06	1.35E-02	6.44E-09	1.51E-03	1.51E-03	9.70E+06	1.37E-01	1.35E-01	1.11E-01	1.09E-01
923	155	4.703E+05	1.28E-02	2.21E-08	2.39E-03	2.39E-03	3.75E+06	2.56E-01	2.54E-01	2.18E-01	2.16E-01
923	180	2.000E+05	8.28E-03	4.16E-08	4.25E-05	4.25E-05	2.30E+06	2.73E-01	2.73E-01	2.65E-01	2.65E-01
923	225	4.000E+04	5.76E-03	1.27E-07	6.93E-04	6.93E-04	6.96E+05	2.88E-01	2.87E-01	2.33E-01	2.32E-01
923	260	1.000E+03	4.60E-04	3.15E-07	1.45E-04	1.45E-04	3.62E+05	4.03E-01	4.03E-01	3.57E-01	3.57E-01
923	300	9.678E+03	3.97E-03	3.83E-07	2.69E-04	2.69E-04	2.32E+05	3.21E-01	3.21E-01	2.73E-01	2.73E-01
923	330	2.206E+03	3.43E-03	1.00E-06	1.21E-03	1.21E-03	1.11E+05	3.63E-01	3.62E-01	3.12E-01	3.11E-01

C11. THE WILSHIRE TECHNIQUE ANALYSIS

T (K)	σ (MPa)	UTS (MPa)	σ/UTS	t_f (s)	$\dot{\varepsilon}_m$ (s^{-1})	ln (t_f)	ln ($\dot{\varepsilon}_m$)	1/T	t_f exp (-Qc*/RT)	$\dot{\varepsilon}_m$ exp (Qc*/RT)
823	390	638	0.6113	1.15E+07	6.20E-09	1.63E+01	-1.89E+01	1.22E-03	5.490E-14	1.296722E+12
823	470	638	0.7367	4.57E+06	2.08E-08	1.53E+01	-1.77E+01	1.22E-03	2.18547E-14	4.350292E+12
823	540	638	0.8464	1.78E+06	2.88E-08	1.44E+01	-1.74E+01	1.22E-03	8.50247E-15	6.023482E+12
823	565	638	0.8856	1.17E+06	4.46E-08	1.40E+01	-1.69E+01	1.22E-03	5.61752E-15	9.328031E+12
823	600	638	0.9404	4.07E+05	9.75E-08	1.29E+01	-1.61E+01	1.22E-03	1.9478E-15	2.039200E+13
848	300	622.5	0.4819	1.12E+07	5.82E-09	1.62E+01	-1.90E+01	1.18E-03	2.13115E-13	3.064136E+11
848	390	622.5	0.6265	2.29E+06	1.94E-08	1.46E+01	-1.78E+01	1.18E-03	4.35126E-14	1.021379E+12
848	420	622.5	0.6747	1.54E+06	5.80E-08	1.42E+01	-1.67E+01	1.18E-03	2.93133E-14	3.053607E+12
848	430	622.5	0.6908	1.35E+06	6.12E-08	1.41E+01	-1.66E+01	1.18E-03	2.56798E-14	3.222081E+12
848	455	622.5	0.7309	1.10E+06	7.19E-08	1.39E+01	-1.64E+01	1.18E-03	2.09503E-14	3.785419E+12
848	500	622.5	0.8032	5.37E+05	1.61E-07	1.32E+01	-1.56E+01	1.18E-03	1.02003E-14	8.476391E+12
848	570	622.5	0.9157	1.78E+05	3.07E-07	1.21E+01	-1.50E+01	1.18E-03	3.37765E-15	1.616306E+13
873	200	607	0.3295	2.09E+07	3.56E-09	1.69E+01	-1.95E+01	1.15E-03	1.45671E-12	5.105944E+10
873	280	607	0.4613	3.72E+06	2.25E-08	1.51E+01	-1.76E+01	1.15E-03	2.59375E-13	3.227072E+11
873	300	607	0.4942	2.98E+06	2.91E-08	1.49E+01	-1.74E+01	1.15E-03	2.08052E-13	4.173679E+11
873	350	607	0.5766	1.17E+06	7.20E-08	1.40E+01	-1.64E+01	1.15E-03	8.18893E-14	1.032663E+12
873	360	607	0.5931	9.85E+05	8.96E-08	1.38E+01	-1.62E+01	1.15E-03	6.86754E-14	1.285092E+12
873	360	607	0.5931	7.86E+05	9.71E-08	1.36E+01	-1.61E+01	1.15E-03	5.47927E-14	1.392661E+12
873	360	607	0.5931	5.32E+05	1.57E-07	1.32E+01	-1.57E+01	1.15E-03	3.70918E-14	2.251779E+12
873	360	607	0.5931	5.75E+05	1.50E-07	1.33E+01	-1.57E+01	1.15E-03	4.01017E-14	2.151381E+12
873	360	607	0.5931	6.07E+05	1.37E-07	1.33E+01	-1.58E+01	1.15E-03	4.23363E-14	1.964928E+12
873	360	607	0.5931	8.49E+05	9.70E-08	1.37E+01	-1.61E+01	1.15E-03	5.91632E-14	1.391226E+12
873	360	607	0.5931	7.50E+05	9.88E-08	1.35E+01	-1.61E+01	1.15E-03	5.23011E-14	1.417043E+12
873	360	607	0.5931	7.85E+05	9.76E-08	1.36E+01	-1.61E+01	1.15E-03	5.47309E-14	1.399832E+12
873	360	607	0.5931	7.05E+05	1.00E-07	1.35E+01	-1.61E+01	1.15E-03	4.91538E-14	1.434254E+12
873	360	607	0.5931	8.53E+05	9.60E-08	1.37E+01	-1.62E+01	1.15E-03	5.94748E-14	1.376884E+12
873	360	607	0.5931	8.99E+05	9.50E-08	1.37E+01	-1.62E+01	1.15E-03	6.26618E-14	1.362541E+12
873	360	607	0.5931	6.80E+05	1.25E-07	1.34E+01	-1.59E+01	1.15E-03	4.73869E-14	1.792818E+12
873	390	607	0.6425	6.46E+05	7.74E-08	1.34E+01	-1.64E+01	1.15E-03	4.50167E-14	1.110113E+12
873	480	607	0.7908	1.82E+05	4.57E-07	1.21E+01	-1.46E+01	1.15E-03	1.27209E-14	6.554541E+12
873	550	607	0.9061	5.34E+04	1.55E-06	1.09E+01	-1.34E+01	1.15E-03	3.7241E-15	2.223094E+13
898	175	575	0.3043	1.06E+07	7.12E-09	1.62E+01	-1.88E+01	1.11E-03	2.5194E-12	2.990835E+10
898	220	575	0.3826	3.32E+06	2.53E-08	1.50E+01	-1.75E+01	1.11E-03	7.90052E-13	1.062754E+11
898	250	575	0.4348	1.94E+06	4.26E-08	1.45E+01	-1.70E+01	1.11E-03	4.61576E-13	1.789460E+11
898	280	575	0.487	1.13E+06	7.01E-08	1.39E+01	-1.65E+01	1.11E-03	2.68675E-13	2.944628E+11
898	300	575	0.5217	7.62E+05	4.53E-07	1.35E+01	-1.46E+01	1.11E-03	1.81421E-13	1.902877E+12
898	300	575	0.5217	5.91E+05	1.57E-07	1.33E+01	-1.57E+01	1.11E-03	1.40787E-13	6.594959E+11
898	330	575	0.5739	3.13E+05	2.89E-07	1.27E+01	-1.51E+01	1.11E-03	7.43939E-14	1.213976E+12
898	400	575	0.6957	1.11E+05	7.89E-07	1.16E+01	-1.41E+01	1.11E-03	2.6389E-14	3.314282E+12
923	140	543	0.2578	5.98E+06	5.76E-09	1.56E+01	-1.90E+01	1.08E-03	4.55104E-12	7.573759E+09
923	155	543	0.2855	3.75E+06	2.15E-08	1.51E+01	-1.77E+01	1.08E-03	2.85309E-12	2.827011E+10
923	180	543	0.3315	2.30E+06	3.72E-08	1.46E+01	-1.71E+01	1.08E-03	1.75034E-12	4.891386E+10
923	225	543	0.4144	6.96E+05	1.25E-07	1.35E+01	-1.59E+01	1.08E-03	5.29474E-13	1.643611E+11
923	260	543	0.4788	3.62E+05	2.24E-07	1.28E+01	-1.53E+01	1.08E-03	2.75651E-13	2.945351E+11
923	300	543	0.5525	1.50E+05	3.31E-07	1.19E+01	-1.49E+01	1.08E-03	1.13792E-13	4.352282E+11
923	330	543	0.6077	7.76E+04	7.47E-07	1.13E+01	-1.41E+01	1.08E-03	5.90352E-14	9.822219E+11

C11.1: Time to fracture, t_f, and the minimum creep rate, $\dot{\varepsilon}_m$, analyses.

T (K)	σ (MPa)	t_f (s)	$\dot{\varepsilon}_m$ (s^{-1})	ln (t_f exp (-Qc*/RT))	ln ($\dot{\varepsilon}_m$ exp (Qc*/RT))	ln (- ln (σ/UTS))
823	390	1.15E+07	6.20E-09	-30.53332628	27.89086049	-0.708887321
823	470	4.57E+06	2.08E-08	-31.45436032	29.10126419	-1.185459934
823	540	1.78E+06	2.88E-08	-32.39842021	29.42668659	-1.791144795
823	565	1.17E+06	4.46E-08	-32.81288552	29.86404506	-2.107737711
823	600	4.07E+05	9.75E-08	-33.87207467	30.64616358	-2.79020493
848	300	1.12E+07	5.82E-09	-29.17694243	26.44820176	-0.31476396
848	390	2.29E+06	1.94E-08	-30.76572615	27.65217457	-0.760148702
848	420	1.54E+06	5.80E-08	-31.1607338	28.74734451	-0.932702377
848	430	1.35E+06	6.12E-08	-31.2930718	28.80104869	-0.994364659
848	455	1.10E+06	7.19E-08	-31.49662304	28.96217776	-1.160127515
848	500	5.37E+05	1.61E-07	-32.21635475	29.76830586	-1.518064883
848	570	1.78E+05	3.07E-07	-33.3215956	30.41374925	-2.429200258
873	200	2.09E+07	3.56E-09	-27.25483875	24.65625634	0.10455047
873	280	3.72E+06	2.25E-08	-28.98050052	26.5000111	-0.256520429
873	300	2.98E+06	2.91E-08	-29.20098639	26.75723397	-0.349917376
873	350	1.17E+06	7.20E-08	-30.13340855	27.66316191	-0.596754611
873	360	9.85E+05	8.96E-08	-30.30938501	27.88185111	-0.649274306
873	360	7.86E+05	9.71E-08	-30.53521878	27.96223717	-0.649274306
873	360	5.32E+05	1.57E-07	-30.92538166	28.4427416	-0.649274306
873	360	5.75E+05	1.50E-07	-30.84735809	28.39713109	-0.649274306
873	360	6.07E+05	1.37E-07	-30.79313165	28.30647672	-0.649274306
873	360	8.49E+05	9.70E-08	-30.45847734	27.96120677	-0.649274306
873	360	7.50E+05	9.88E-08	-30.58175982	27.9795934	-0.649274306
873	360	7.85E+05	9.76E-08	-30.53634811	27.96737328	-0.649274306
873	360	7.05E+05	1.00E-07	-30.64382273	27.99166598	-0.649274306
873	360	8.53E+05	9.60E-08	-30.45322336	27.95084398	-0.649274306
873	360	8.99E+05	9.50E-08	-30.40102369	27.94037268	-0.649274306
873	360	6.80E+05	1.25E-07	-30.68042986	28.21480953	-0.649274306
873	390	6.46E+05	7.74E-08	-30.73174224	27.73548257	-0.815581399
873	480	1.82E+05	4.57E-07	-31.99553019	29.51117918	-1.449265313
873	550	5.34E+04	1.55E-06	-33.22395219	30.732506	-2.316577402
898	175	1.06E+07	7.12E-09	-26.70700208	24.12140347	0.173603722
898	220	3.32E+06	2.53E-08	-27.86667788	25.38930014	-0.040048862
898	250	1.94E+06	4.26E-08	-28.40413022	25.91035	-0.182830739
898	280	1.13E+06	7.01E-08	-28.9452731	26.40841854	-0.329086962
898	300	7.62E+05	4.53E-07	-29.33795607	28.27438787	-0.429879376
898	300	5.91E+05	1.57E-07	-29.59153061	27.21474155	-0.429879376
898	330	3.13E+05	2.89E-07	-30.22940183	27.82492243	-0.588287495
898	400	1.11E+05	7.89E-07	-31.26582837	28.82926207	-1.013612827
923	140	5.98E+06	5.76E-09	-26.11566457	22.74795539	0.304145969
923	155	3.75E+06	2.15E-08	-26.58261743	24.06507085	0.226086579
923	180	2.30E+06	3.72E-08	-27.07121211	24.61332667	0.099078044
923	225	6.96E+05	1.25E-07	-28.2668915	25.82533165	-0.126687531
923	260	3.62E+05	2.24E-07	-28.91964194	26.40866396	-0.30594423
923	300	1.50E+05	3.31E-07	-29.80440589	26.79913629	-0.522009859
923	330	7.76E+04	7.47E-07	-30.46064265	27.6130831	-0.697121738

C11.1.1: The Wilshire kink points and the UTS and σ_{Yield} values

T (K)	UTS (MPa)	σ_{Yield} (MPa)	Wilshire curves kink points, MPa (t_f curves)	Wilshire curves kink points, MPa ($\dot{\varepsilon}_m$ curves)
823	638	520	390	383
848	622.5	508.33	380	374
873	601	500	370	360
898	575	478.33	350	340
923	543	460	330	324

C11.2: Time to 0.1% analysis

T (K)	σ (MPa)	UTS (MPa)	$t_{0.1\%}$ (s)	$\dot{\varepsilon}_m$ (s^{-1})	ln ($t_{0.1\%}$ exp (-Qc*/RT))	ln (-ln (σ/UTS))
823	390	638	1.07E+04	6.20E-09	-37.51015911	-0.708887321
823	470	638	4.10E+03	2.08E-08	-38.47083478	-1.185459934
823	540	638	1.80E+03	2.88E-08	-39.29403509	-1.791144795
823	565	638	5.75E+02	4.46E-08	-40.43444218	-2.107737711
823	600	638	2.50E+02	9.75E-08	-41.26811612	-2.79020493
848	300	622.5	1.70E+04	5.82E-09	-35.67023239	-0.31476396
848	390	622.5	2.95E+03	1.94E-08	-37.42019706	-0.760148702
848	420	622.5	1.80E+03	5.80E-08	-37.91462539	-0.932702377
848	430	622.5	1.82E+03	6.12E-08	-37.90373993	-0.994364659
848	455	622.5	1.07E+03	7.19E-08	-38.4333345	-1.160127515
848	500	622.5	4.50E+02	1.61E-07	-39.30091975	-1.518064883
848	570	622.5	1.60E+02	3.07E-07	-40.33499352	-2.429200258
873	200	607	6.17E+04	3.56E-09	-33.08037903	0.10455047
873	282	607	5.50E+03	2.25E-08	-35.49809338	-0.265761793
873	300	607	3.39E+03	2.91E-08	-35.98163625	-0.349917376
873	350	607	8.91E+02	7.20E-08	-37.3171356	-0.596754611
873	360	607	7.00E+02	8.96E-08	-37.55868129	-0.649274306
873	360	607	8.98E+02	9.71E-08	-37.30959156	-0.649274306
873	360	607	5.81E+02	1.57E-07	-37.74501087	-0.649274306
873	360	607	1.24E+03	1.50E-07	-36.98528337	-0.649274306
873	360	607	5.75E+02	1.37E-07	-37.75462677	-0.649274306
873	360	607	6.61E+02	9.70E-08	-37.61647167	-0.649274306
873	360	607	1.78E+03	9.88E-08	-36.62636008	-0.649274306
873	360	607	1.48E+03	9.76E-08	-36.81056688	-0.649274306
873	360	607	8.36E+02	1.00E-07	-37.38113302	-0.649274306
873	360	607	1.06E+03	9.60E-08	-37.14751816	-0.649274306
873	360	607	1.05E+03	9.50E-08	-37.15131323	-0.649274306
873	360	607	5.80E+02	1.25E-07	-37.74673352	-0.649274306
873	390	607	7.24E+02	7.74E-08	-37.52436826	-0.815581399
873	480	607	2.09E+02	4.57E-07	-38.76776421	-1.449265313
873	550	607	4.57E+01	1.55E-06	-40.28747037	-2.316577402
898	175	575	2.51E+04	7.12E-09	-32.75038717	0.173603722
898	220	575	6.03E+03	2.53E-08	-34.17798993	-0.040048862
898	250	575	4.47E+03	4.26E-08	-34.47732599	-0.182830739
898	280	575	1.00E+03	7.01E-08	-35.9740063	-0.329086962
898	300	575	6.31E+02	4.53E-07	-36.43452332	-0.429879376
898	300	575	6.92E+02	1.57E-07	-36.34241992	-0.429879376
898	330	575	2.50E+02	2.89E-07	-37.36030066	-0.588287495
898	400	575	1.12E+02	7.89E-07	-38.16146214	-1.013612827
923	140	543	2.35E+04	5.76E-09	-31.65552805	0.304145969
923	155	543	9.55E+03	2.15E-08	-32.55599508	0.226086579
923	180	543	6.61E+03	3.72E-08	-32.92440869	0.099078044
923	225	543	2.30E+03	1.25E-07	-33.97961935	-0.126687531
923	260	543	5.00E+02	2.24E-07	-35.50567565	-0.30594423
923	300	543	1.45E+02	3.31E-07	-36.74669995	-0.522009859
923	330	543	7.41E+01	7.47E-07	-37.41444963	-0.697121738

C11.3: Time to 0.15% analysis

T (K)	σ (MPa)	UTS (MPa)	$t_{0.15\%}$ (s)	$\dot{\varepsilon}_m$ (s^{-1})	ln ($t_{0.15\%}$ exp (-Qc^*/RT))	ln (-ln (σ/UTS))
823	390	638	2.50E+04	6.20E-09	-36.66294593	-0.708887321
823	470	638	9.00E+03	2.08E-08	-37.68459718	-1.185459934
823	540	638	5.36E+03	2.88E-08	-38.20285778	-1.791144795
823	565	638	2.51E+03	4.46E-08	-38.96078772	-2.107737711
823	600	638	1.40E+03	9.75E-08	-39.54534952	-2.79020493
848	300	622.5	4.44E+04	5.82E-09	-34.70917259	-0.31476396
848	390	622.5	4.47E+03	1.94E-08	-37.00573175	-0.760148702
848	420	622.5	3.50E+03	5.80E-08	-37.24964909	-0.932702377
848	430	622.5	2.95E+03	6.12E-08	-37.42019706	-0.994364659
848	455	622.5	2.14E+03	7.19E-08	-37.74255898	-1.160127515
848	500	622.5	1.40E+03	1.61E-07	-38.16593982	-1.518064883
848	570	622.5	4.27E+02	3.07E-07	-39.35436854	-2.429200258
873	200	607	1.62E+05	3.56E-09	-32.11329329	0.10455047
873	280	607	1.55E+04	2.25E-08	-34.46193009	-0.256520429
873	300	607	1.10E+04	2.91E-08	-34.80411108	-0.349917376
873	350	607	1.91E+03	7.20E-08	-36.55728252	-0.596754611
873	360	607	1.90E+03	8.96E-08	-36.56015246	-0.649274306
873	360	607	1.800E+03	9.71E-08	-36.61421968	-0.649274306
873	360	607	1.75E+03	1.57E-07	-36.64239056	-0.649274306
873	360	607	1.85E+03	1.50E-07	-36.58682071	-0.649274306
873	360	607	1.40E+03	1.37E-07	-36.86553411	-0.649274306
873	360	607	1.46E+03	9.70E-08	-36.82700045	-0.649274306
873	360	607	1.35E+03	9.88E-08	-36.90190176	-0.649274306
873	360	607	1.35E+03	9.76E-08	-36.90561234	-0.649274306
873	360	607	1.55E+03	1.00E-07	-36.7611741	-0.649274306
873	360	607	1.65E+03	9.60E-08	-36.70426596	-0.649274306
873	360	607	1.23E+03	9.50E-08	-36.99499218	-0.649274306
873	360	607	1.35E+03	1.25E-07	-36.90561234	-0.649274306
873	390	607	1.17E+03	7.74E-08	-37.04082539	-0.815581399
873	480	607	6.00E+02	4.57E-07	-37.71283197	-1.449265313
873	550	607	1.91E+02	1.55E-06	-38.85986762	-2.316577402
898	175	575	7.24E+04	7.12E-09	-31.69119803	0.173603722
898	220	575	1.80E+04	2.53E-08	-33.08363455	-0.040048862
898	250	575	1.30E+04	4.26E-08	-33.40905695	-0.182830739
898	280	575	3.50E+03	7.01E-08	-34.72124334	-0.329086962
898	300	575	1.23E+03	4.53E-07	-35.76677365	-0.429879376
898	300	575	1.70E+03	1.57E-07	-35.44441173	-0.429879376
898	330	575	2.00E+02	2.89E-07	-37.58344422	-0.588287495
898	400	575	1.91E+02	7.89E-07	-37.63186757	-1.013612827
923	140	543	4.80E+04	5.76E-09	-30.94132746	0.304145969
923	155	543	3.63E+04	2.15E-08	-31.22049573	0.226086579
923	180	543	2.20E+04	3.72E-08	-31.72148602	0.099078044
923	225	543	4.50E+03	1.25E-07	-33.30845107	-0.126687531
923	260	543	1.20E+03	2.24E-07	-34.63020691	-0.30594423
923	300	543	4.47E+02	3.31E-07	-35.61843325	-0.522009859
923	330	543	2.00E+02	7.47E-07	-36.42196638	-0.697121738

C11.4: Time to 0.2% analysis

T (K)	σ (MPa)	UTS (MPa)	$t_{0.2\%}$ (s)	$\dot{\varepsilon}_m$ (s^{-1})	ln ($t_{0.2\%}$ exp (-Qc^*/RT))	ln (-ln (σ/UTS))
823	390	638	5.25E+04	6.20E-09	-35.92053251	-0.708887321
823	470	638	1.82E+04	2.08E-08	-36.98056454	-1.185459934
823	540	638	5.75E+03	2.88E-08	-38.13185709	-1.791144795
823	565	638	2.34E+03	4.46E-08	-39.02986527	-2.107737711
823	600	638	8.71E+02	9.75E-08	-40.01997686	-2.79020493
848	300	622.5	1.02E+05	5.82E-09	-33.87421602	-0.31476396
848	390	622.5	1.02E+04	1.94E-08	-36.17680111	-0.760148702
848	420	622.5	6.36E+03	5.80E-08	-36.65206926	-0.932702377
848	430	622.5	5.50E+03	6.12E-08	-36.79766397	-0.994364659
848	455	622.5	3.89E+03	7.19E-08	-37.14388685	-1.160127515
848	500	622.5	2.50E+03	1.61E-07	-37.58612133	-1.518064883
848	570	622.5	4.27E+02	3.07E-07	-39.35436854	-2.429200258
873	200	607	2.82E+05	3.56E-09	-31.56067287	0.10455047
873	280	607	3.72E+04	2.25E-08	-33.58694775	-0.256520429
873	300	607	2.21E+04	2.91E-08	-34.10642874	-0.349917376
873	350	607	7.41E+03	7.20E-08	-35.19875732	-0.596754611
873	360	607	6.31E+03	8.96E-08	-35.35993827	-0.649274306
873	360	607	2.92E+03	9.71E-08	-36.13145066	-0.649274306
873	360	607	2.81E+03	1.57E-07	-36.16846606	-0.649274306
873	360	607	4.70E+03	1.50E-07	-35.65486946	-0.649274306
873	360	607	2.34E+03	1.37E-07	-36.35004986	-0.649274306
873	360	607	2.89E+03	9.70E-08	-36.14144213	-0.649274306
873	360	607	3.50E+03	9.88E-08	-35.94924338	-0.649274306
873	360	607	4.11E+03	9.76E-08	-35.78955703	-0.649274306
873	360	607	3.33E+03	1.00E-07	-36.00023597	-0.649274306
873	360	607	3.06E+03	9.60E-08	-36.0822851	-0.649274306
873	360	607	3.06E+03	9.50E-08	-36.0822851	-0.649274306
873	360	607	4.50E+03	1.25E-07	-35.69792895	-0.649274306
873	390	607	2.45E+03	7.74E-08	-36.30399816	-0.815581399
873	480	607	7.08E+02	4.57E-07	-37.54739411	-1.449265313
873	550	607	1.48E+02	1.55E-06	-39.11315198	-2.316577402
898	175	575	1.12E+05	7.12E-09	-31.25370686	0.173603722
898	220	575	3.72E+04	2.53E-08	-32.35894771	-0.040048862
898	250	575	2.31E+04	4.26E-08	-32.83417369	-0.182830739
898	280	575	9.10E+03	7.01E-08	-33.76573189	-0.329086962
898	300	575	5.13E+03	4.53E-07	-34.33917089	-0.429879376
898	300	575	3.89E+03	1.57E-07	-34.6154811	-0.429879376
898	330	575	2.09E+03	2.89E-07	-35.23717907	-0.588287495
898	400	575	4.47E+02	7.89E-07	-36.77991109	-1.013612827
923	140	543	8.01E+04	5.76E-09	-30.42925262	0.304145969
923	155	543	5.50E+04	2.15E-08	-30.80519529	0.226086579
923	180	543	3.16E+04	3.72E-08	-31.35865083	0.099078044
923	225	543	9.50E+03	1.25E-07	-32.56123667	-0.126687531
923	260	543	2.90E+03	2.24E-07	-33.74781773	-0.30594423
923	300	543	9.33E+02	3.31E-07	-34.88160602	-0.522009859
923	330	543	3.98E+02	7.47E-07	-35.73356251	-0.697121738

C11.5: Time to 0.5% analysis

T (K)	σ (MPa)	UTS (MPa)	$t_{0.5\%}$ (s)	$\dot{\varepsilon}_m$ (s^{-1})	ln ($t_{0.5\%}$ exp (-Qc^*/RT))	ln (-ln (σ/UTS))
823	390	638	4.17E+05	6.20E-09	-33.84760907	-0.708887321
823	470	638	1.24E+05	2.08E-08	-35.05984808	-1.185459934
823	540	638	5.03E+04	2.88E-08	-35.96314096	-1.791144795
823	565	638	2.94E+04	4.46E-08	-36.50123533	-2.107737711
823	600	638	1.84E+04	9.75E-08	-36.97028664	-2.79020493
848	300	622.5	5.50E+05	5.82E-09	-32.1933289	-0.31476396
848	390	622.5	7.08E+04	1.94E-08	-34.24262964	-0.760148702
848	420	622.5	4.52E+04	5.80E-08	-34.69233319	-0.932702377
848	430	622.5	4.00E+04	6.12E-08	-34.8135326	-0.994364659
848	455	622.5	2.88E+04	7.19E-08	-35.14241869	-1.160127515
848	500	622.5	1.74E+04	1.61E-07	-35.64720654	-1.518064883
848	570	622.5	4.53E+03	3.07E-07	-36.99146939	-2.429200258
873	200	607	9.77E+05	3.56E-09	-30.31727692	0.10455047
873	280	607	1.62E+05	2.25E-08	-32.11329329	-0.256520429
873	300	607	1.19E+05	2.91E-08	-32.42532281	-0.349917376
873	350	607	3.50E+04	7.20E-08	-33.64665829	-0.596754611
873	360	607	2.96E+04	8.96E-08	-33.81524602	-0.649274306
873	360	607	2.52E+04	9.71E-08	-33.97516235	-0.649274306
873	360	607	4.14E+04	1.57E-07	-33.47862885	-0.649274306
873	360	607	2.39E+04	1.50E-07	-34.0294677	-0.649274306
873	360	607	2.02E+04	1.37E-07	-34.19597727	-0.649274306
873	360	607	3.32E+04	9.70E-08	-33.70057155	-0.649274306
873	360	607	1.74E+04	9.88E-08	-34.3474345	-0.649274306
873	360	607	2.40E+04	9.76E-08	-34.02395252	-0.649274306
873	360	607	4.40E+04	1.00E-07	-33.41781672	-0.649274306
873	360	607	2.94E+04	9.60E-08	-33.82148798	-0.649274306
873	360	607	2.65E+04	9.50E-08	-33.92648558	-0.649274306
873	360	607	2.12E+04	1.25E-07	-34.15031916	-0.649274306
873	390	607	1.58E+04	7.74E-08	-34.43890424	-0.815581399
873	480	607	5.57E+03	4.57E-07	-35.48479084	-1.449265313
873	550	607	1.81E+03	1.55E-06	-36.60978509	-2.316577402
898	175	575	4.12E+05	7.12E-09	-29.95310432	0.173603722
898	220	575	1.49E+05	2.53E-08	-30.96818631	-0.040048862
898	250	575	9.58E+04	4.26E-08	-31.41224479	-0.182830739
898	280	575	4.62E+04	7.01E-08	-32.14102651	-0.329086962
898	300	575	1.79E+04	4.53E-07	-33.09116977	-0.429879376
898	300	575	2.28E+04	1.57E-07	-32.84939833	-0.429879376
898	330	575	1.05E+04	2.89E-07	-33.62536951	-0.588287495
898	400	575	3.09E+03	7.89E-07	-34.84713055	-1.013612827
923	140	543	3.26E+05	5.76E-09	-29.02613213	0.304145969
923	155	543	1.55E+05	2.15E-08	-29.76756453	0.226086579
923	180	543	9.00E+04	3.72E-08	-30.3127188	0.099078044
923	225	543	3.12E+04	1.25E-07	-31.37262333	-0.126687531
923	260	543	1.30E+04	2.24E-07	-32.24975126	-0.30594423
923	300	543	6.17E+03	3.31E-07	-32.99348625	-0.522009859
923	330	543	2.89E+03	7.47E-07	-33.75103674	-0.697121738

C11.6: Time to 0.7% analysis

T (K)	σ (MPa)	UTS (MPa)	$t_{0.7\%}$ (s)	$\dot{\varepsilon}_m$ (s^{-1})	ln ($t_{0.7\%}$ exp (-Qc^*/RT))	ln (-ln (σ/UTS))
823	390	638	6.90E+05	6.20E-09	-33.34513016	-0.708887321
823	470	638	2.10E+05	2.08E-08	-34.53471423	-1.185459934
823	540	638	9.00E+04	2.88E-08	-35.38201209	-1.791144795
823	565	638	6.00E+04	4.46E-08	-35.7874772	-2.107737711
823	600	638	3.20E+04	9.75E-08	-36.41608586	-2.79020493
848	300	622.5	8.00E+05	5.82E-09	-31.81780033	-0.31476396
848	390	622.5	1.23E+05	1.94E-08	-33.69000921	-0.760148702
848	420	622.5	7.50E+04	5.80E-08	-34.18492394	-0.932702377
848	430	622.5	6.10E+04	6.12E-08	-34.39153819	-0.994364659
848	455	622.5	5.30E+04	7.19E-08	-34.53212014	-1.160127515
848	500	622.5	2.80E+04	1.61E-07	-35.17020755	-1.518064883
848	570	622.5	9.20E+03	3.07E-07	-36.28320857	-2.429200258
873	201	607	1.51E+06	3.56E-09	-29.87978575	0.100047923
873	280	607	2.69E+05	2.25E-08	-31.60672457	-0.256520429
873	300	607	1.78E+05	2.91E-08	-32.0202228	-0.349917376
873	350	607	6.30E+04	7.20E-08	-33.05887162	-0.596754611
873	360	607	4.95E+04	8.96E-08	-33.30003368	-0.649274306
873	360	607	3.50E+04	9.71E-08	-33.64665829	-0.649274306
873	360	607	5.50E+04	1.57E-07	-33.19467316	-0.649274306
873	360	607	4.52E+04	1.50E-07	-33.39090926	-0.649274306
873	360	607	3.34E+04	1.37E-07	-33.69345045	-0.649274306
873	360	607	4.50E+04	9.70E-08	-33.39534386	-0.649274306
873	360	607	6.10E+04	9.88E-08	-33.09113248	-0.649274306
873	360	607	5.14E+04	9.76E-08	-33.26236818	-0.649274306
873	360	607	4.80E+04	1.00E-07	-33.33080534	-0.649274306
873	360	607	3.80E+04	9.60E-08	-33.56442019	-0.649274306
873	360	607	3.80E+04	9.50E-08	-33.56442019	-0.649274306
873	360	607	5.90E+04	1.25E-07	-33.12446891	-0.649274306
873	390	607	2.82E+04	7.74E-08	-33.86325796	-0.815581399
873	480	607	9.20E+03	4.57E-07	-34.98280287	-1.449265313
873	550	607	3.00E+03	1.55E-06	-36.10339406	-2.316577402
898	175	575	6.85E+05	7.12E-09	-29.44458747	0.173603722
898	220	575	2.14E+05	2.53E-08	-30.60898304	-0.040048862
898	250	575	1.45E+05	4.26E-08	-30.99727256	-0.182830739
898	280	575	7.00E+04	7.01E-08	-31.72551106	-0.329086962
898	300	575	3.39E+04	4.53E-07	-32.45105111	-0.429879376
898	300	575	4.27E+04	1.57E-07	-32.2207926	-0.429879376
898	330	575	1.51E+04	2.89E-07	-33.25695589	-0.588287495
898	400	575	5.35E+03	7.89E-07	-34.29690974	-1.013612827
923	140	543	5.62E+05	5.76E-09	-28.48041947	0.304145969
923	155	543	2.57E+05	2.15E-08	-29.2632984	0.226086579
923	180	543	1.66E+05	3.72E-08	-29.70054068	0.099078044
923	225	543	4.82E+04	1.25E-07	-30.93716945	-0.126687531
923	260	543	2.00E+04	2.24E-07	-31.8167962	-0.30594423
923	300	543	1.05E+04	3.31E-07	-32.46389168	-0.522009859
923	330	543	5.20E+03	7.47E-07	-33.16386985	-0.697121738

C11.7: Time to 1% analysis

T (K)	σ (MPa)	UTS (MPa)	$t_{1\%}$ (s)	$\dot{\varepsilon}_m$ (s^{-1})	ln ($t_{1\%}$ exp (-Qc*/RT))	ln (-ln (σ/UTS))
823	390	638	9.16E+05	6.20E-09	-33.06156471	-0.708887321
823	470	638	3.56E+05	2.08E-08	-34.00571195	-1.185459934
823	540	638	1.64E+05	2.88E-08	-34.77964094	-1.791144795
823	565	638	1.17E+05	4.46E-08	-35.12281523	-2.107737711
823	600	638	5.86E+04	9.75E-08	-35.81141135	-2.79020493
848	300	622.5	1.29E+06	5.82E-09	-31.34137242	-0.31476396
848	390	622.5	1.75E+05	1.94E-08	-33.33541111	-0.760148702
848	420	622.5	1.26E+05	5.80E-08	-33.66327708	-0.932702377
848	430	622.5	1.10E+05	6.12E-08	-33.79993369	-0.994364659
848	455	622.5	9.69E+04	7.19E-08	-33.92842299	-1.160127515
848	500	622.5	5.52E+04	1.61E-07	-34.49130883	-1.518064883
848	570	622.5	1.77E+04	3.07E-07	-35.62625192	-2.429200258
873	200	607	2.72E+06	3.56E-09	-29.29262655	0.10455047
873	280	607	4.45E+05	2.25E-08	-31.10476102	-0.256520429
873	300	607	2.96E+05	2.91E-08	-31.51002659	-0.349917376
873	350	607	1.07E+05	7.20E-08	-32.53161038	-0.596754611
873	360	607	7.82E+04	8.96E-08	-32.84277507	-0.649274306
873	360	607	5.85E+04	9.71E-08	-33.13373201	-0.649274306
873	360	607	9.16E+04	1.57E-07	-32.68467334	-0.649274306
873	360	607	5.95E+04	1.50E-07	-33.11589559	-0.649274306
873	360	607	7.61E+04	1.37E-07	-32.86994494	-0.649274306
873	360	607	8.75E+04	9.70E-08	-32.72996764	-0.649274306
873	360	607	8.47E+04	9.88E-08	-32.76286713	-0.649274306
873	360	607	8.07E+04	9.76E-08	-32.81068554	-0.649274306
873	360	607	6.33E+04	1.00E-07	-33.0536472	-0.649274306
873	360	607	6.33E+04	9.60E-08	-33.0536472	-0.649274306
873	360	607	7.97E+04	9.50E-08	-32.82314723	-0.649274306
873	360	607	8.02E+04	1.25E-07	-32.81735815	-0.649274306
873	390	607	4.03E+04	7.74E-08	-33.50635727	-0.815581399
873	480	607	1.63E+04	4.57E-07	-34.4135758	-1.449265313
873	550	607	5.12E+03	1.55E-06	-35.56947352	-2.316577402
898	175	575	1.11E+06	7.12E-09	-28.95946153	0.173603722
898	220	575	3.79E+05	2.53E-08	-30.03563935	-0.040048862
898	250	575	2.22E+05	4.26E-08	-30.56984354	-0.182830739
898	280	575	1.06E+05	7.01E-08	-31.31321221	-0.329086962
898	300	575	5.16E+04	4.53E-07	-32.02967804	-0.429879376
898	300	575	6.32E+04	1.57E-07	-31.82705055	-0.429879376
898	330	575	2.50E+04	2.89E-07	-32.75499234	-0.588287495
898	400	575	8.98E+03	7.89E-07	-33.77956337	-1.013612827
923	140	543	8.97E+05	5.76E-09	-28.01299469	0.304145969
923	155	543	4.06E+05	2.15E-08	-28.80738655	0.226086579
923	180	543	2.55E+05	3.72E-08	-29.27173562	0.099078044
923	225	543	7.34E+04	1.25E-07	-30.51702697	-0.126687531
923	260	543	3.23E+04	2.24E-07	-31.3386384	-0.30594423
923	300	543	1.42E+04	3.31E-07	-32.15995044	-0.522009859
923	330	543	6.14E+03	7.47E-07	-32.99809142	-0.697121738

C11.8: Time to 2% analysis

T (K)	σ (MPa)	UTS (MPa)	$t_{2\%}$ (s)	$\dot{\varepsilon}_m$ (s^{-1})	ln ($t_{2\%}$ exp (-Qc*/RT))	ln (-ln (σ/UTS))
823	390	638	2.14E+06	6.20E-09	-32.2142134	-0.708887321
823	470	638	8.11E+05	2.08E-08	-33.18314688	-1.185459934
823	540	638	3.89E+05	2.88E-08	-33.91916829	-1.791144795
823	565	638	3.07E+05	4.46E-08	-34.15608212	-2.107737711
823	600	638	1.41E+05	9.75E-08	-34.93126381	-2.79020493
848	300	622.5	2.69E+06	5.82E-09	-30.60454519	-0.31476396
848	390	622.5	4.27E+05	1.94E-08	-32.44661326	-0.760148702
848	420	622.5	2.85E+05	5.80E-08	-32.85087069	-0.932702377
848	430	622.5	2.61E+05	6.12E-08	-32.93977081	-0.994364659
848	455	622.5	2.19E+05	7.19E-08	-33.11436294	-1.160127515
848	500	622.5	1.20E+05	1.61E-07	-33.71303506	-1.518064883
848	570	622.5	4.68E+04	3.07E-07	-34.65629384	-2.429200258
873	200	607	5.89E+06	3.56E-09	-28.52126055	0.10455047
873	280	607	1.00E+06	2.25E-08	-30.29425107	-0.256520429
873	300	607	6.04E+05	2.91E-08	-30.79919403	-0.349917376
873	350	607	2.34E+05	7.20E-08	-31.74544668	-0.596754611
873	360	607	1.75E+05	8.96E-08	-32.03459525	-0.649274306
873	360	607	1.68E+05	9.71E-08	-32.08096927	-0.649274306
873	360	607	1.65E+05	1.57E-07	-32.09324666	-0.649274306
873	360	607	1.96E+05	1.50E-07	-31.92292277	-0.649274306
873	360	607	1.28E+05	1.37E-07	-32.35185285	-0.649274306
873	360	607	1.95E+05	9.70E-08	-31.92869915	-0.649274306
873	360	607	1.36E+05	9.88E-08	-32.28795538	-0.649274306
873	360	607	1.67E+05	9.76E-08	-32.08695098	-0.649274306
873	360	607	1.67E+05	1.00E-07	-32.08677083	-0.649274306
873	360	607	1.88E+05	9.60E-08	-31.96466054	-0.649274306
873	360	607	1.90E+05	9.50E-08	-31.95719525	-0.649274306
873	360	607	1.44E+05	1.25E-07	-32.23367331	-0.649274306
873	390	607	9.33E+04	7.74E-08	-32.66591372	-0.815581399
873	480	607	3.63E+04	4.57E-07	-33.6099736	-1.449265313
873	550	607	1.20E+04	1.55E-06	-34.71521445	-2.316577402
898	175	575	2.46E+06	7.12E-09	-28.16661827	0.173603722
898	220	575	8.51E+05	2.53E-08	-29.22743198	-0.040048862
898	250	575	4.35E+05	4.26E-08	-29.89840743	-0.182830739
898	280	575	2.17E+05	7.01E-08	-30.59535396	-0.329086962
898	300	575	1.07E+05	4.53E-07	-31.29975857	-0.429879376
898	300	575	1.35E+05	1.57E-07	-31.06950006	-0.429879376
898	330	575	5.62E+04	2.89E-07	-31.94448239	-0.588287495
898	400	575	1.97E+04	7.89E-07	-32.99140993	-1.013612827
923	140	543	1.95E+06	5.76E-09	-27.23702352	0.304145969
923	155	543	8.71E+05	2.15E-08	-28.0429283	0.226086579
923	180	543	5.00E+05	3.72E-08	-28.59852055	0.099078044
923	225	543	1.62E+05	1.25E-07	-29.72381542	-0.126687531
923	260	543	6.69E+04	2.24E-07	-30.60971822	-0.30594423
923	300	543	3.39E+04	3.31E-07	-31.28957328	-0.522009859
923	330	543	1.51E+04	7.47E-07	-32.09547806	-0.697121738

C11.9: Time to 5% analysis

T (K)	σ (MPa)	UTS (MPa)	$t_{5\%}$ (s)	$\dot{\varepsilon}_m$ (s^{-1})	ln ($t_{5\%}$ exp (-Qc^*/RT))	ln (-ln (σ/UTS))
823	390	638	5.01E+06	6.20E-09	-31.36225691	-0.708887321
823	470	638	1.88E+06	2.08E-08	-32.34114712	-1.185459934
823	540	638	9.54E+05	2.88E-08	-33.02132582	-1.791144795
823	565	638	7.57E+05	4.46E-08	-33.25243208	-2.107737711
823	600	638	4.05E+05	9.75E-08	-33.8773176	-2.79020493
848	300	622.5	6.46E+06	5.82E-09	-29.72956285	-0.31476396
848	390	622.5	9.77E+05	1.94E-08	-31.61768263	-0.760148702
848	420	622.5	6.58E+05	5.80E-08	-32.01376959	-0.932702377
848	430	622.5	6.10E+05	6.12E-08	-32.0886007	-0.994364659
848	455	622.5	5.17E+05	7.19E-08	-32.25347983	-1.160127515
848	500	622.5	2.82E+05	1.61E-07	-32.86107858	-1.518064883
848	570	622.5	1.32E+05	3.07E-07	-33.61976166	-2.429200258
873	200	607	1.38E+07	3.56E-09	-27.66930406	0.10455047
873	280	607	2.29E+06	2.25E-08	-29.46532044	-0.256520429
873	300	607	1.55E+06	2.91E-08	-29.8567599	-0.349917376
873	350	607	5.31E+05	7.20E-08	-30.92797906	-0.596754611
873	360	607	3.96E+05	8.96E-08	-31.22071841	-0.649274306
873	360	607	4.62E+05	9.71E-08	-31.06581395	-0.649274306
873	360	607	2.88E+05	1.57E-07	-31.54067915	-0.649274306
873	360	607	4.18E+05	1.50E-07	-31.16638139	-0.649274306
873	360	607	3.26E+05	1.37E-07	-31.41599893	-0.649274306
873	360	607	3.72E+05	9.70E-08	-31.28284371	-0.649274306
873	360	607	3.48E+05	9.88E-08	-31.3494591	-0.649274306
873	360	607	4.16E+05	9.76E-08	-31.17165768	-0.649274306
873	360	607	4.38E+05	1.00E-07	-31.11994727	-0.649274306
873	360	607	3.23E+05	9.60E-08	-31.42537312	-0.649274306
873	360	607	3.23E+05	9.50E-08	-31.42537622	-0.649274306
873	360	607	6.03E+05	1.25E-07	-30.80081979	-0.649274306
873	390	607	2.24E+05	7.74E-08	-31.79093138	-0.815581399
873	480	607	9.55E+04	4.57E-07	-32.64288786	-1.449265313
873	550	607	2.95E+04	1.55E-06	-33.81720626	-2.316577402
898	175	575	5.29E+06	7.12E-09	-27.40098113	0.173603722
898	220	575	1.86E+06	2.53E-08	-28.44455305	-0.040048862
898	251	575	8.68E+05	4.26E-08	-29.20791828	-0.187635127
898	280	575	5.25E+05	7.01E-08	-29.71097485	-0.329086962
898	300	575	2.95E+05	4.53E-07	-30.28662112	-0.429879376
898	300	575	2.19E+05	1.57E-07	-30.58595719	-0.429879376
898	330	575	1.23E+05	2.89E-07	-31.16160346	-0.588287495
898	400	575	4.35E+04	7.89E-07	-32.20099252	-1.013612827
923	140	543	4.68E+06	5.76E-09	-26.36204118	0.304145969
923	155	543	2.34E+06	2.15E-08	-27.05281671	0.226086579
923	180	543	1.38E+06	3.72E-08	-27.58241128	0.099078044
923	225	543	3.80E+05	1.25E-07	-28.87185893	-0.126687531
923	260	543	1.70E+05	2.24E-07	-29.67776371	-0.30594423
923	300	543	7.59E+04	3.31E-07	-30.4836685	-0.522009859
923	330	543	3.47E+04	7.47E-07	-31.26654743	-0.697121738

C11.10: Time to 7% analysis

T (K)	σ (MPa)	UTS (MPa)	$t_{7\%}$ (s)	$\dot{\varepsilon}_m$ (s^{-1})	ln ($t_{7\%}$ exp (-Qc*/RT))	ln (-ln (σ/UTS))
823	390	638	6.22E+06	6.20E-09	-31.14629657	-0.708887321
823	470	638	2.37E+06	2.08E-08	-32.11328846	-1.185459934
823	540	638	1.21E+06	2.88E-08	-32.78758691	-1.791144795
823	565	638	9.63E+05	4.46E-08	-33.01176835	-2.107737711
823	600	638	5.33E+05	9.75E-08	-33.60330033	-2.79020493
848	300	622.5	8.91E+06	5.82E-09	-29.40720094	-0.31476396
848	390	622.5	1.32E+06	1.94E-08	-31.31834657	-0.760148702
848	420	622.5	8.34E+05	5.80E-08	-31.77617866	-0.932702377
848	430	622.5	7.10E+05	6.12E-08	-31.93714709	-0.994364659
848	455	622.5	6.56E+05	7.19E-08	-32.01625127	-1.160127515
848	500	622.5	3.80E+05	1.61E-07	-32.56174252	-1.518064883
848	570	622.5	1.76E+05	3.07E-07	-33.33192806	-2.429200258
873	202	607	1.32E+07	3.56E-09	-27.71535577	0.09554751
873	280	607	3.02E+06	2.25E-08	-29.18901023	-0.256520429
873	300	607	2.04E+06	2.91E-08	-29.58044969	-0.349917376
873	350	607	6.69E+05	7.20E-08	-30.69626713	-0.596754611
873	360	607	5.00E+05	8.96E-08	-30.98739825	-0.649274306
873	360	607	3.65E+05	9.71E-08	-31.302109	-0.649274306
873	360	607	5.24E+05	1.57E-07	-30.94051466	-0.649274306
873	360	607	3.95E+05	1.50E-07	-31.22312058	-0.649274306
873	360	607	4.72E+05	1.37E-07	-31.04502736	-0.649274306
873	360	607	4.30E+05	9.70E-08	-31.13822114	-0.649274306
873	360	607	5.18E+05	9.88E-08	-30.95203111	-0.649274306
873	360	607	5.50E+05	9.76E-08	-30.89208807	-0.649274306
873	360	607	4.08E+05	1.00E-07	-31.19073917	-0.649274306
873	360	607	4.08E+05	9.60E-08	-31.19073917	-0.649274306
873	360	607	4.90E+05	9.50E-08	-31.00760096	-0.649274306
873	360	607	4.80E+05	1.25E-07	-31.02822025	-0.649274306
873	390	607	2.95E+05	7.74E-08	-31.51462117	-0.815581399
873	480	607	1.32E+05	4.57E-07	-32.32052595	-1.449265313
873	552	607	3.47E+04	1.55E-06	-33.65602531	-2.354081094
898	175	575	6.60E+06	7.12E-09	-27.17918138	0.173603722
898	220	575	2.24E+06	2.53E-08	-28.26034624	-0.040048862
898	251	575	1.20E+06	4.26E-08	-28.88204422	-0.187635127
898	280	575	7.24E+05	7.01E-08	-29.38861294	-0.329086962
898	300	575	2.85E+05	4.53E-07	-30.32137678	-0.429879376
898	300	575	3.72E+05	1.57E-07	-30.05636261	-0.429879376
898	330	575	2.00E+05	2.89E-07	-30.67806059	-0.588287495
898	406	575	5.57E+04	7.89E-07	-31.95409797	-1.055504291
923	140	543	5.25E+06	5.76E-09	-26.24691193	0.304145969
923	155	543	2.45E+06	2.15E-08	-27.00676501	0.226086579
923	180	543	1.26E+06	3.72E-08	-27.67175852	0.099078044
923	225	543	4.90E+05	1.25E-07	-28.61857457	-0.126687531
923	260	543	2.09E+05	2.24E-07	-29.47053106	-0.30594423
923	300	543	1.00E+05	3.31E-07	-30.20735829	-0.522009859
923	330	543	4.94E+04	7.47E-07	-30.9121328	-0.697121738

C11.11: Time to 10% analysis

T (K)	σ (MPa)	UTS (MPa)	$t_{10\%}$ (s)	$\dot{\varepsilon}_m$ (s^{-1})	ln ($t_{10\%}$ exp (-Qc^*/RT))	ln (-ln (σ/UTS))
823	390	638	7.48E+06	6.20E-09	-30.96227496	-0.708887321
823	470	638	2.89E+06	2.08E-08	-31.91312144	-1.185459934
823	540	638	1.43E+06	2.88E-08	-32.61436612	-1.791144795
823	565	638	1.18E+06	4.46E-08	-32.80652021	-2.107737711
823	600	638	6.79E+05	9.75E-08	-33.36131846	-2.79020493
848	300	622.5	7.25E+06	5.82E-09	-29.61390362	-0.31476396
848	390	622.5	1.86E+06	1.94E-08	-30.9729588	-0.760148702
848	420	622.5	1.04E+06	5.80E-08	-31.55582075	-0.932702377
848	430	622.5	1.11E+06	6.12E-08	-31.48867645	-0.994364659
848	455	622.5	8.09E+05	7.19E-08	-31.80627945	-1.160127515
848	500	622.5	5.01E+05	1.61E-07	-32.28543231	-1.518064883
848	570	622.5	2.27E+05	3.07E-07	-33.07781453	-2.429200258
873	200	607	1.44E+07	3.56E-09	-27.62917796	0.10455047
873	280	607	2.36E+06	2.25E-08	-29.43732825	-0.256520429
873	300	607	2.00E+06	2.91E-08	-29.60350677	-0.349917376
873	350	607	8.34E+05	7.20E-08	-30.47567703	-0.596754611
873	360	607	6.28E+05	8.96E-08	-30.75903634	-0.649274306
873	360	607	6.05E+05	9.71E-08	-30.79677789	-0.649274306
873	360	607	5.84E+05	1.57E-07	-30.83210537	-0.649274306
873	360	607	5.05E+05	1.50E-07	-30.97744792	-0.649274306
873	360	607	5.82E+05	1.37E-07	-30.8355359	-0.649274306
873	360	607	6.10E+05	9.70E-08	-30.78854739	-0.649274306
873	360	607	6.28E+05	9.88E-08	-30.75946618	-0.649274306
873	360	607	5.90E+05	9.76E-08	-30.82188381	-0.649274306
873	360	607	5.58E+05	1.00E-07	-30.87764739	-0.649274306
873	360	607	5.78E+05	9.60E-08	-30.84243248	-0.649274306
873	360	607	6.00E+05	9.50E-08	-30.80507669	-0.649274306
873	360	607	6.10E+05	1.25E-07	-30.78854739	-0.649274306
873	390	607	3.39E+05	7.74E-08	-31.37646606	-0.815581399
873	480	607	1.27E+05	4.57E-07	-32.3548316	-1.449265313
873	550	607	3.80E+04	1.55E-06	-33.56568415	-2.316577402
898	175	575	8.10E+06	7.12E-09	-26.97458451	0.173603722
898	220	575	2.25E+06	2.53E-08	-28.25372209	-0.040048862
898	250	575	1.31E+06	4.26E-08	-28.79637657	-0.182830739
898	280	575	7.01E+05	7.01E-08	-29.42117037	-0.329086962
898	300	575	3.46E+05	4.53E-07	-30.12733634	-0.429879376
898	300	575	4.47E+05	1.57E-07	-29.87215581	-0.429879376
898	330	575	1.92E+05	2.89E-07	-30.71713613	-0.588287495
898	400	575	7.08E+04	7.89E-07	-31.71454286	-1.013612827
923	140	543	5.37E+06	5.76E-09	-26.22388607	0.304145969
923	155	543	2.68E+06	2.15E-08	-26.91750223	0.226086579
923	180	543	1.55E+06	3.72E-08	-27.46497107	0.099078044
923	225	543	4.72E+05	1.25E-07	-28.65658816	-0.126687531
923	260	543	2.20E+05	2.24E-07	-29.42044757	-0.30594423
923	300	543	8.51E+04	3.31E-07	-30.36853924	-0.522009859
923	330	543	6.25E+04	7.47E-07	-30.67729792	-0.697121738

C11.12: Time to 13% analysis

T (K)	σ (MPa)	UTS (MPa)	$t_{13\%}$ (s)	$\dot{\varepsilon}_m$ (s^{-1})	ln ($t_{13\%}$ exp (-Qc^*/RT))	ln (-ln (σ/UTS))
823	390	638	8.30E+06	6.20E-09	-30.8578953	-0.708887321
823	470	638	3.80E+06	2.08E-08	-31.63856712	-1.185459934
823	540	638	2.33E+06	2.88E-08		-1.791144795
823	565	638	1.32E+06	4.46E-08	-32.6933335	-2.107737711
823	600	638	6.46E+05	9.75E-08	-33.41155765	-2.79020493
848	300	622.5	8.04E+06	5.82E-09	-29.51075022	-0.31476396
848	390	622.5	2.93E+06	1.94E-08	-30.51846053	-0.760148702
848	420	622.5	1.19E+06	5.80E-08	-31.42280652	-0.932702377
848	430	622.5	1.23E+06	6.12E-08	-31.38715492	-0.994364659
848	455	622.5	9.12E+05	7.19E-08	-31.68631165	-1.160127515
848	500	622.5	5.37E+05	1.61E-07	-32.21635475	-1.518064883
848	570	622.5	2.59E+05	3.07E-07	-32.94512078	-2.429200258
873	200	607	1.82E+07	3.56E-09	-27.39299385	0.10455047
873	280	607	2.74E+06	2.25E-08	-29.28669469	-0.256520429
873	300	607	2.27E+06	2.91E-08	-29.47244686	-0.349917376
873	350	607	9.44E+05	7.20E-08	-30.35175307	-0.596754611
873	360	607	7.26E+05	8.96E-08	-30.61401566	-0.649274306
873	360	607	7.15E+05	9.71E-08	-30.62972381	-0.649274306
873	360	607	7.04E+05	1.57E-07	-30.64522799	-0.649274306
873	360	607	6.95E+05	1.50E-07	-30.6580945	-0.649274306
873	360	607	6.82E+05	1.37E-07	-30.67697669	-0.649274306
873	360	607	7.10E+05	9.70E-08	-30.63674138	-0.649274306
873	360	607	6.98E+05	9.88E-08	-30.65378725	-0.649274306
873	360	607	6.90E+05	9.76E-08	-30.66531475	-0.649274306
873	360	607	7.08E+05	1.00E-07	-30.63956226	-0.649274306
873	360	607	7.38E+05	9.60E-08	-30.59806252	-0.649274306
873	360	607	7.40E+05	9.50E-08	-30.59535616	-0.649274306
873	360	607	6.90E+05	1.25E-07	-30.66531475	-0.649274306
873	390	607	6.03E+05	7.74E-08	-30.80081979	-0.815581399
873	480	607	1.66E+05	4.57E-07	-32.09026744	-1.449265313
873	550	607	4.45E+04	1.55E-06	-33.4075739	-2.316577402
898	175	575	9.13E+06	7.12E-09	-26.85419257	0.173603722
898	220	575	2.57E+06	2.53E-08	-28.12059568	-0.040048862
898	250	575	1.48E+06	4.26E-08	-28.6755612	-0.182830739
898	280	575	8.05E+05	7.01E-08	-29.28331311	-0.329086962
898	300	575	4.37E+05	4.53E-07	-29.89518166	-0.429879376
898	300	575	3.99E+05	1.57E-07	-29.98532061	-0.429879376
898	330	575	2.26E+05	2.89E-07	-30.55236572	-0.588287495
898	400	575	9.33E+04	7.89E-07	-31.43791367	-1.013612827
923	140	543	8.91E+06	5.76E-09	-25.71731735	0.304145969
923	155	543	3.06E+06	2.15E-08	-26.78482351	0.226086579
923	180	543	1.77E+06	3.72E-08	-27.33526365	0.099078044
923	225	543	5.40E+05	1.25E-07	-28.52188569	-0.126687531
923	260	543	2.50E+05	2.24E-07	-29.29034781	-0.30594423
923	300	543	1.00E+05	3.31E-07	-30.20735829	-0.522009859
923	330	543	7.31E+04	7.47E-07	-30.52134327	-0.697121738

C11.13: Time to 15% analysis

T (K)	σ (MPa)	UTS (MPa)	$t_{15\%}$ (s)	$\dot{\varepsilon}_m$ (s^{-1})	ln ($t_{15\%}$ exp (-Qc^*/RT))	ln (-ln (σ/UTS))
823	390	638	8.66E+06	6.20E-09	-30.81498231	-0.708887321
823	470	638	3.80E+06	2.08E-08	-31.63856712	-1.185459934
823	540	638	2.40E+06	2.88E-08	-32.09859774	-1.791144795
823	565	638	1.39E+06	4.46E-08	-32.64239144	-2.107737711
823	600	638	5.25E+05	9.75E-08	-33.6187903	-2.79020493
848	300	622.5	8.41E+06	5.82E-09	-29.46552072	-0.31476396
848	390	622.5	3.05E+06	1.94E-08	-30.48089319	-0.760148702
848	420	622.5	1.45E+06	5.80E-08	-31.22624316	-0.932702377
848	430	622.5	1.28E+06	6.12E-08	-31.34483235	-0.994364659
848	455	622.5	9.68E+05	7.19E-08	-31.62757261	-1.160127515
848	500	622.5	5.50E+05	1.61E-07	-32.1933289	-1.518064883
848	570	622.5	2.19E+05	3.07E-07	-33.11436294	-2.429200258
873	200	607	1.64E+07	3.56E-09	-27.49990086	0.10455047
873	280	607	2.93E+06	2.25E-08	-29.21778215	-0.256520429
873	300	607	2.42E+06	2.91E-08	-29.40990518	-0.349917376
873	350	607	1.00E+06	7.20E-08	-30.2905579	-0.596754611
873	360	607	7.80E+05	8.96E-08	-30.54219974	-0.649274306
873	360	607	7.55E+05	9.71E-08	-30.5752886	-0.649274306
873	360	607	7.34E+05	1.57E-07	-30.60349732	-0.649274306
873	360	607	7.35E+05	1.50E-07	-30.60213585	-0.649274306
873	360	607	7.82E+05	1.37E-07	-30.54015161	-0.649274306
873	360	607	7.10E+05	9.70E-08	-30.63674138	-0.649274306
873	360	607	7.98E+05	9.88E-08	-30.51989775	-0.649274306
873	360	607	7.70E+05	9.76E-08	-30.55561583	-0.649274306
873	360	607	7.68E+05	1.00E-07	-30.55821662	-0.649274306
873	360	607	7.48E+05	9.60E-08	-30.58460337	-0.649274306
873	360	607	7.30E+05	9.50E-08	-30.60896181	-0.649274306
873	360	607	7.50E+05	1.25E-07	-30.58193314	-0.649274306
873	390	607	6.46E+05	7.74E-08	-30.73174224	-0.815581399
873	480	607	1.59E+05	4.57E-07	-32.13499072	-1.449265313
873	550	607	4.81E+04	1.55E-06	-33.32828768	-2.316577402
898	175	575	9.63E+06	7.12E-09	-26.80116014	0.173603722
898	220	575	2.74E+06	2.53E-08	-28.05665212	-0.040048862
898	250	575	1.57E+06	4.26E-08	-28.61250382	-0.182830739
898	280	575	8.61E+05	7.01E-08	-29.21567954	-0.329086962
898	300	575	4.29E+05	4.53E-07	-29.911664	-0.429879376
898	300	575	3.47E+05	1.57E-07	-30.12544017	-0.429879376
898	330	575	2.44E+05	2.89E-07	-30.47540468	-0.588287495
898	400	575	1.02E+05	7.89E-07	-31.34581027	-1.013612827
923	140	543	3.89E+06	5.76E-09	-26.54624799	0.304145969
923	155	543	3.25E+06	2.15E-08	-26.7263336	0.226086579
923	180	543	1.89E+06	3.72E-08	-27.26587103	0.099078044
923	225	543	5.79E+05	1.25E-07	-28.45074252	-0.126687531
923	260	543	2.68E+05	2.24E-07	-29.22060909	-0.30594423
923	300	543	8.71E+04	3.31E-07	-30.34551339	-0.522009859
923	330	543	7.91E+04	7.47E-07	-30.44133531	-0.697121738

C11.14: Time to 20% analysis

T (K)	σ (MPa)	UTS (MPa)	$t_{20\%}$ (s)	$\dot{\varepsilon}_m$ (s^{-1})	ln ($t_{20\%}$ exp (-Qc^*/RT))	ln (-ln (σ/UTS))
823	390	638	---	6.20E-09	---	-0.708887321
823	470	638	---	2.08E-08	---	-1.185459934
823	540	638	---	2.88E-08	---	-1.791144795
823	565	638	---	4.46E-08	---	-2.107737711
823	600	638	---	9.75E-08	---	-2.79020493
848	300	622.5	8.97E+06	5.82E-09	-29.40123944	-0.31476396
848	390	622.5	---	1.94E-08	---	-0.760148702
848	420	622.5	1.41E+06	5.80E-08	-31.25390799	-0.932702377
848	430	622.5	1.35E+06	6.12E-08	-31.2930718	-0.994364659
848	455	622.5	1.05E+06	7.19E-08	-31.54701013	-1.160127515
848	500	622.5	4.83E+05	1.61E-07	-32.32200211	-1.518064883
848	570	622.5	---	3.07E-07	---	-2.429200258
873	200	607	---	3.56E-09	---	0.10455047
873	280	607	3.34E+06	2.25E-08	-29.08854976	-0.256520429
873	300	607	2.69E+06	2.91E-08	-29.30657034	-0.349917376
873	350	607	1.11E+06	7.20E-08	-30.19169448	-0.596754611
873	360	607	8.77E+05	8.96E-08	-30.42505476	-0.649274306
873	360	607	8.25E+05	9.71E-08	-30.48662296	-0.649274306
873	360	607	8.14E+05	1.57E-07	-30.50004598	-0.649274306
873	360	607	8.55E+05	1.50E-07	-30.45090488	-0.649274306
873	360	607	8.82E+05	1.37E-07	-30.41981429	-0.649274306
873	360	607	8.90E+05	9.70E-08	-30.41078489	-0.649274306
873	360	607	8.18E+05	9.88E-08	-30.49514401	-0.649274306
873	360	607	8.20E+05	9.76E-08	-30.49270201	-0.649274306
873	360	607	8.08E+05	1.00E-07	-30.50744429	-0.649274306
873	360	607	8.48E+05	9.60E-08	-30.45912571	-0.649274306
873	360	607	8.40E+05	9.50E-08	-30.46860446	-0.649274306
873	360	607	8.80E+05	1.25E-07	-30.42208444	-0.649274306
873	390	607	8.32E+05	7.74E-08	-30.47845788	-0.815581399
873	480	607	1.79E+05	4.57E-07	-32.01702567	-1.449265313
873	550	607	3.16E+04	1.55E-06	-33.74812871	-2.316577402
898	175	575	1.04E+07	7.12E-09	-26.72358021	0.173603722
898	220	575	3.05E+06	2.53E-08	-27.95009356	-0.040048862
898	250	575	1.74E+06	4.26E-08	-28.50984037	-0.182830739
898	280	575	9.74E+05	7.01E-08	-29.09290306	-0.329086962
898	300	575	4.37E+05	4.53E-07	-29.89518166	-0.429879376
898	300	575	4.89E+05	1.57E-07	-29.7819097	-0.429879376
898	330	575	2.83E+05	2.89E-07	-30.32877144	-0.588287495
898	400	575	1.02E+05	7.89E-07	-31.35050516	-1.013612827
923	140	543	---	5.76E-09	---	0.304145969
923	155	543	3.59E+06	2.15E-08	-26.62751275	0.226086579
923	180	543	2.11E+06	3.72E-08	-27.15590752	0.099078044
923	225	543	6.50E+05	1.25E-07	-28.33495629	-0.126687531
923	260	543	3.01E+05	2.24E-07	-29.10405701	-0.30594423
923	300	543	1.12E+05	3.31E-07	-30.09222903	-0.522009859
923	330	543	9.21E+04	7.47E-07	-30.28988157	-0.697121738

C12. THE ALPHA-CASE ANALYSIS

Test conditions	α-case depth (μm)	t_f(hrs)	α-case thickness at 1 (μm)	vertical crack depth at 1 (μm)	α-case thickness at 2 (μm)	vertical crack depth at 2 (μm)	α-case thickness at 3 (μm)	vertical crack depth at 3 (μm)
823K/390MPa	17.7	2.56E+03	11.1	53.3	8.14	69.6	5.9	102.2
823K/565MPa	9.7	4.06E+02	4.4	33.3	2.2	44.4	1.8	62.2
823K/600MPa	6	2.22E+02	2.2	17.1	1.48	25.1	1.2	38.2
848K/300MPa	32	2.52E+03	12.5	72	8.4	111	4.4	156
848K/390MPa	22	8.69E+02	7.4	42	4.89	65	3	86
848K/500MPa	5.6	1.49E+02	3	19	2	27	1.5	37
873K/200MPa	54.8	4.67E+03	32.6	90.3	24.4	129.6	19.2	204.4
873K/269MPa	45.8	2.50E+03	11.1	41.2	7.7	68.1	2.9	97
873K/280MPa	31.8	1.03E+03	14.8	51.8	11.8	68.8	9.5	86.6
873K/300MPa	26.2	8.28E+02	14.8	59.2	7.4	114.8	2.9	184.4
873K/338MPa	21.3	5.02E+02	9	28.1	4.4	56.3	3.7	62.9
873K/350MPa	17.9	3.25E+02	7.4	30.3	4.4	39.2	2.9	57.7
898K/175MPa	70.9	2.80E+03	39.2	116.3	25.1	155.5	17.7	208
898K/220MPa	42.9	9.22E+02	17	65.9	11.8	90.3	8.14	132.5
898K/250MPa	32.8	5.39E+02	17.1	34	10	41.4	4.4	56.2
898K/300MPa	15.7	1.01E+02	5.9	32.5	2.9	51.1	1.48	76.3
898K/330MPa	13.5	8.69E+01	4.44	26	2.2	34.8	2	47.4
923K/140MPa	88.9	2.69E+03	57	119.2	41.5	142.2	28.9	205.9
923K/155MPa	71.1	1.04E+03	36.2	104.4	24.4	151.1	13.3	236.3
923K/180MPa	54	6.39E+02	22.2	82.9	17.7	125.18	11.85	171.85
923K/225MPa	31.1	1.93E+02	14	33.3	8.8	47.4	7.8	64.4
923K/260MPa	25.1	1.01E+02	11.1	32.3	7.4	50.3	3.7	68.1
923K/330MPa	13.3	3.08E+01	8.88	17.7	5.18	23.3	4.44	33.3

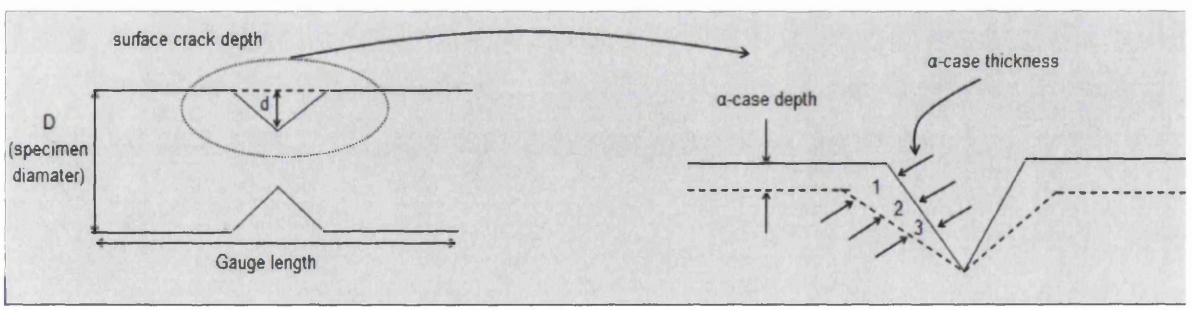

C13. Steve-Brown's Model Analysis

Actual α-case thickness:

Temperature (K)	Time (hrs)	α-case depth (μm)
848	1000	18.50
873	11	5.00
873	57	10.00
873	247	15.00
873	500	18.00
873	992	27.50
873	2371	43.75
873	4252	55.25
898	2	2.00
898	4	3.00
898	8	2.25
923	2	1.70
923	8	4.00
923	100	21.50

Predicted α-case thickness:

Temperature (K)	Time (hrs)	α-case depth (μm)
848	1000	19.5
873	11	4.5
873	57	8.4
873	247	13.8
873	500	20.7
873	992	31.5
873	2371	47.8
873	4252	59
898	2	3
898	4	4.2
898	8	5.4
923	2	4.2
923	8	7.2
923	100	19.5

Steve Brown's Model (only temperature exposure, un-tested specimens)

C14. THE ALPHA-CASE THICKNESS AND SURFACE CRACKS (MEASURED AND PREDICTED)

T (K)	σ (MPa)	α-case thickness (μm)	Time for α-case formation (hrs)	vertical crack depth (μm)	Time for crack intiation (hrs)	Normalised time (Time for crack initiation/tf)
823	390	11.1	608.5921498	53.3	1946.90785	0.76
823	390	8.14	323.5863678	69.6	2231.913632	0.87
823	390	5.9	200.6247451	102.2	2354.875255	0.92
823	565	4.4	145.6675484	33.3	259.8324516	0.64
823	565	2.2	91.08866497	44.4	314.411335	0.77
823	565	1.8	83.63573677	62.2	321.8642632	0.79
823	600	2.2	91.08866497	17.1	131.111335	0.59
823	600	1.48	78.11490828	25.1	144.0850917	0.64
823	600	1.2	73.58396951	38.2	148.6160305	0.66

T (K)	σ (MPa)	α-case thickness (μm)	Time for α-case formation (hrs)	vertical crack depth (μm)	Time for crack intiation (hrs)	Normalised time (Time for crack initiation/tf)
848	300	12.5	312.9144199	72	2206.48558	0.87
848	300	8.4	201.6975896	111	2317.70241	0.92
848	300	4.4	131.4097731	156	2387.990227	0.95
848	390	7.4	181.2101198	42	688.1898802	0.79
848	390	4.89	138.4910197	65	730.9089803	0.84
848	390	3	113.110286	86	756.289714	0.87
848	500	3	113.110286	19	36.06521302	0.24
848	500	2	101.6210878	27	47.55441115	0.32
848	500	1.5	96.32182651	37	52.85367248	0.35

T (K)	σ (MPa)	α-case thickness (μm)	Time for α-case formation (hrs)	vertical crack depth (μm)	Time for crack intiation (hrs)	Normalised time (Time for crack initiation/tf)
873	200	32.6	1057.5636	90.3	3609.0364	0.77
873	200	24.4	600.1092152	129.6	4066.490785	0.87
873	200	19.2	418.9690813	204.4	4247.630919	0.91
873	269	11.1	239.3903858	41.2	2260.609614	0.90
873	269	7.7	189.2670923	68.1	2310.732908	0.92
873	269	2.9	135.8408861	97	2364.159114	0.95
873	280	14.8	309.1299525	51.8	724.1700475	0.70
873	280	11.8	251.2541302	68.6	782.0458698	0.76
873	280	9.5	214.3343788	86.6	818.9656212	0.79
873	300	14.8	309.1299525	59.2	518.5700475	0.63
873	300	7.4	185.3840314	114.8	642.3159686	0.78
873	300	2.9	135.8408861	184.4	691.8591139	0.84
873	338	9	207.0556999	28.1	294.9443001	0.59
873	338	4.4	150.6761256	56.3	351.3238744	0.70
873	338	3.7	143.5614843	62.9	358.4385157	0.71
873	350	7.4	185.3840314	30.3	139.6159686	0.43
873	350	4.4	150.6761256	39.2	174.3238744	0.54
873	350	2.9	135.8408861	57.7	189.1591139	0.58

T (K)	σ (MPa)	α-case thickness (μm)	Time for α-case formation (hrs)	vertical crack depth (μm)	Time for crack intiation (hrs)	Normalised time (Time for crack initiation/tf)
898	175	39.2	538.402688	116.3	2261.597312	0.81
898	175	25.1	214.9999984	155.5	2585.000002	0.92
898	175	17.7	132.8030479	208	2667.196952	0.95
898	220	17	126.886663	65.9	795.313337	0.86
898	220	11.8	90.44596533	90.3	831.7540347	0.90
898	220	8.14	71.26970584	132.5	850.9302942	0.92
898	250	17.1	127.715443	34	411.084557	0.76
898	250	10	80.44430681	41.4	458.3556932	0.85
898	250	4.4	55.86744162	56.2	482.9325584	0.89
898	300	5.9	61.59853088	32.5	38.90146912	0.38
898	300	2.9	50.66956938	51.1	49.83043062	0.49
898	300	1.48	46.19527888	76.3	54.30472112	0.54
898	330	4.44	56.01311936	26	30.88688064	0.35
898	330	2.2	48.4122366	34.8	38.4877634	0.44
898	330	2	47.78595514	47.4	39.11404486	0.45

T (K)	σ (MPa)	α-case thickness (μm)	Time for α-case formation (hrs)	vertical crack depth (μm)	Time for crack intiation (hrs)	Normalised time (Time for crack initiation/tf)
923	140	57	560.2481475	119.2	2134.151852	0.79
923	140	41.5	230.0628893	142.2	2464.337111	0.91
923	140	28.9	111.5917141	205.9	2582.808286	0.95
923	155	36.2	169.6980795	104.4	871.9019205	0.83
923	155	24.4	86.18118093	151.1	955.4188191	0.92
923	155	13.3	45.56216182	236.3	996.0378382	0.95
923	180	22.2	75.95381116	82.9	563.3517444	0.88
923	180	17.7	58.65837976	125.18	580.6471758	0.91
923	180	11.85	41.92226154	171.85	597.383294	0.93
923	225	14	47.43082623	33.3	145.9580627	0.75
923	225	8.8	35.18720851	47.4	158.2016804	0.82
923	225	7.8	33.22363495	64.4	160.1652539	0.83
923	260	11.1	40.15516842	32.3	60.52538713	0.60
923	260	7.4	32.46923668	50.3	68.21131888	0.68
923	260	3.7	26.25443677	68.1	74.42611878	0.74
923	330	8.88	35.34921941	17.7	1.345675432	0.43
923	330	5.18	28.58317414	23.3	2.216825865	0.72
923	330	4.44	27.39407122	33.3	3.405928778	0.11

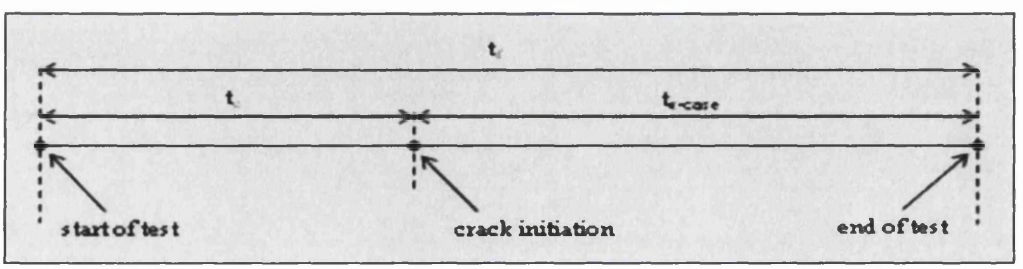

C15. THE ALPHA-CASE, SURFACE CRACKS AND THE CRITICAL TIME AND STRAIN FOR CRACKS INITIATIONS

T (K)	σ (MPa)	t_f (hours)	α-case depth at t_f (μm)	time (t) for 1st crack appearance (hours)	strain (ε) at 1st crack appearance	$t_{crack\ initiation}/t_f$	Ductility (ε_f)	$\varepsilon_{crack\ initiation}/\varepsilon_f$
823	390	2555.5	17.7	1489.2	0.055	0.582743103	0.19395	0.283578242
823	565	405.5	9.7	171.8	0.039	0.423674476	0.17146	0.227458299
823	600	222.2	6	116.3	0.051	0.52340234	0.14368	0.354955457
848	300	2519.4	32	2054.5	0.106	0.815471938	0.22467	0.471803089
848	390	869.4	22	623.8	0.069	0.717506326	0.17711	0.389588391
848	500	149.175	5.6	18.1	0.013	0.121333598	0.25598	0.050785218
873	200	4666.6	54.8	3094.5	0.061	0.663116616	0.19036	0.320445472
873	269	2500	45.8	2184.3	0.072	0.87372	0.27432	0.262467192
873	280	1033.3	31.8	583.6	0.083	0.564792413	0.30669	0.270631582
873	300	827.7	26.2	439.3	0.066	0.530747856	0.34432	0.191682156
873	338	502	21.3	242.2	0.073	0.48247012	0.37234	0.196057367
873	350	325	17.9	82.9	0.025	0.255076923	0.28455	0.087858021
898	175	2800	70.9	1690.6	0.061	0.603785714	0.23015	0.265044536
898	220	922.2	42.9	740.7	0.14	0.803188029	0.36656	0.381929289
898	250	538.8	32.8	298.8	0.069	0.554565702	0.35948	0.191943919
898	300	100.5	15.7	27.4	0.064	0.272636816	0.30068	0.212850871
898	330	86.9	13.5	18.1	0.031	0.208285386	0.28123	0.110230061
923	140	2694.4	88.9	1458.9	0.041	0.541456354	0.13671	0.299904908
923	155	1041.6	71.1	775.1	0.107	0.744143625	0.25626	0.417544681
923	180	639.306	54	532	0.154	0.832152944	0.27321	0.563668973
923	225	193.389	31.1	128.2	0.096	0.662912956	0.28813	0.333182938
923	260	100.681	25.1	48.1	0.068	0.477748655	0.40313	0.168680078
923	330	30.8	13.3	0.92	0.005	0.02987013	0.36318	0.013767278

APPENDIX (D)

MATHEMATICAL AND ANALYTICAL GUIDE

APPENDIX (D): CONTENTS

APPENDIX (D)

MATHEMATICAL & ANALYTICAL GUIDE

This appendix illustrates some of the calculations that are useful for creep predictions analysis. These calculations range from the derivation of curves from raw experimental data to the interpolation and extrapolation of creep properties using different creep predictions techniques. Many of the calculations can be obtained using simple graphical means, e.g. the minimum creep rate, $\dot{\varepsilon}_m$, can be read directly from the plot of the creep rate, $\dot{\varepsilon}$, against time, t, or strain, ε, the time to fracture, t_f, can be obtained from the end point of the strain-time plot as well as the ductility, ε_f, which represents the creep strain at fracture. The calculations and procedures presented in this appendix can be considered as a 'Mathematical Guide' for creep lifing techniques and a very useful tool for comparison purposes using the different lifing techniques based on any available creep data of any material.

D.1 The Power Law Equation

The general form of the Power Law equation is:

$$\dot{\varepsilon}_s = A\,\sigma^n \exp(-Qc/RT) \qquad \ldots\ldots\ldots\ldots (D.1^*)$$

This equation can be re-arranged in a linear form by taking the natural logarithm of both sides to give:

$$\ln \dot{\varepsilon}_s = \ln A + n \ln \sigma - (Qc/R)\, 1/T \qquad \ldots\ldots\ldots\ldots (D.2^*)$$

Now, there are two possibilities to solve this equation: at constant stress, σ, or at constant temperature, T.

- **Constant Stress:** To solve equation (D.2*) at constant stress, this equation can then be written as:

$$\ln \dot{\varepsilon}_s = -(Qc/R)\, 1/T + B \qquad \ldots\ldots\ldots\ldots (D.3^*)$$

where B is a constant equals to ($\ln A + n \ln \sigma$). Now equation (D.3*) has the linear form: ($y = mx + c$). Therefore, plotting ($\ln \dot{\varepsilon}_s$) against (1/T), at constant stress, will give a straight line of slope (-Qc/R) and an intercept of B with the y-axis, as shown in Figure (D1).

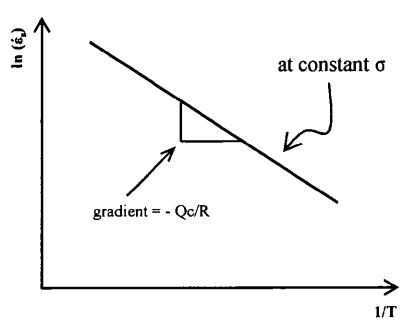

Figure (D1): The linear relationship between $\ln \dot{\varepsilon}_s$ and 1/T, at constant stress.

- **Constant Temperature:** To solve equation (D.2*) at constant temperature, this equation can then be written as:

$$\ln \dot{\varepsilon}_s = n \ln \sigma + C \qquad \ldots\ldots\ldots\ldots (D.4^*)$$

where C is a constant equals to (ln A - (Qc/R) 1/T). Now equation (D.4*) has the linear form: (y = mx + c). Therefore, plotting (ln $\dot{\varepsilon}_s$) against (ln σ), at constant temperature, will give a straight line of slope (n) and an intercept of C with the y-axis, as shown in Figure (D2).

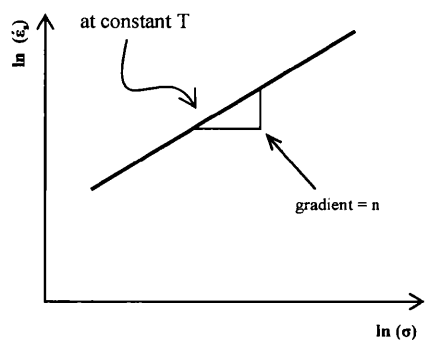

Figure (D2): The linear relationship between ln $\dot{\varepsilon}_s$ and 1/T, at constant stress.

In addition to the above, the creep rate, $\dot{\varepsilon}_s$, in equation (D.1*) can be replaced by the time to fracture, t_f, according to Monkman-Grant relationship which suggests that the product of the creep rate and the time to fracture is always constant (i.e. $t_f \dot{\varepsilon}_s = M$). Therefore, equation (D.1*) can be re-written as:

$$M/t_f = A \sigma^n \exp(-Qc/RT) \qquad \ldots\ldots\ldots\ldots (D.5^*)$$

Re-arranging equation (D.5*) will give a final form, such that:

$$t_f = D \sigma^{-n} \exp(Qc/RT) \qquad \ldots\ldots\ldots\ldots (D.6^*)$$

where D is a constant equals to M/A. This equation can be re-arranged in a linear form by taking the natural logarithm of both sides to give:

$$\ln t_f = \ln D - n \ln \sigma + (Qc/R)\ 1/T \qquad \ldots\ldots\ldots\ldots (D.7^*)$$

Now, there are two possibilities to solve this equation: at constant stress, σ, or at constant temperature, T.

- **Constant Stress:** To solve equation (D.7*) at constant stress, this equation can then be written as:

$$\ln t_f = (Qc/R)\ 1/T + E \qquad \ldots\ldots\ldots\ldots (D.8^*)$$

where E is a constant equals to (ln D - n ln σ).

Now equation (D.8*) has the linear form: (y = mx + c). Therefore, plotting (ln t_f) against (1/T), at constant stress, will give a straight line of slope (Qc/R) and an intercept of E with the y-axis, as shown in Figure (D3).

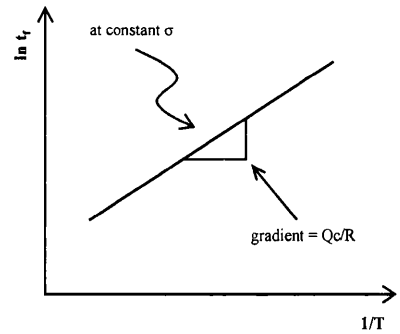

Figure (D3): The linear relationship between ln t_f and 1/T, at constant stress.

- **Constant Temperature:** To solve equation (D.7*) at constant temperature, this equation can then be written as:

$$\ln t_f = - n \ln \sigma + G \qquad \text{..... (D.9*)}$$

where G is a constant equals to (ln D + (Qc/R) 1/T). Now equation (D.9*) has the linear form: (y = mx + c). Therefore, plotting (ln t_f) against (ln σ), at constant temperature, will give a straight line of slope (-n) and an intercept of G with the y-axis, as shown in Figure (D4).

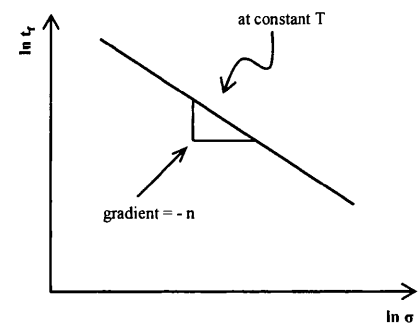

Figure (D4): The linear relationship between ln t_f and ln σ, at constant temperature.

D.2 The Monkman-Grant Equation

The general form of the Monkman-Grant equation is:

$$M = t_f \, \dot{\varepsilon}_s \qquad \text{..... (D.10*)}$$

This equation can be re-arranged in a linear form (y = mx), such that:

$$\dot{\varepsilon}_s = M/t_f \qquad \text{..... (D.11*)}$$

Plotting ($\dot{\varepsilon}_s$) against ($1/t_f$) gives a straight line of a slope equals to M and an intercept of zero, as shown in Figure (D5).

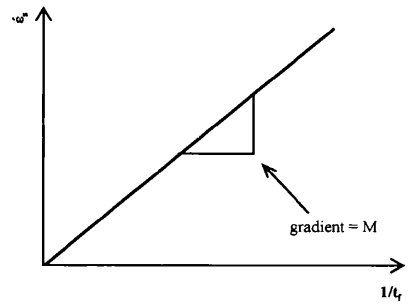

Figure (D5): The linear relationship between $\dot{\varepsilon}_s$ and $1/t_f$.

Other scholars plotted t_f against $\dot{\varepsilon}_s$, as in Figure (D6), and obtained the power relationship of the form:

$$M` = t_f \, \dot{\varepsilon}_s^{\,m} \qquad \ldots\ldots\ldots\ldots\ldots\ldots (D.12^*)$$

where in this equation, the creep rate is raised to the power m. It is worthwhile noting that the value of M` does not equal the value of M in equation (D.10*)

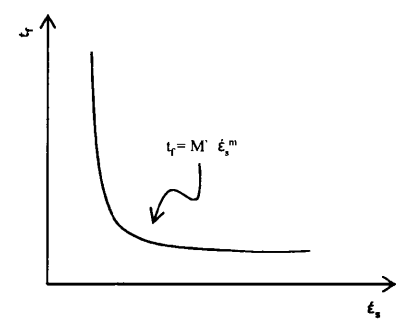

Figure (D6): The relationship between t_f and $\dot{\varepsilon}_s$.

Other Scholars plotted $\dot{\varepsilon}_s$ against t_f, i.e. by just swapping the axes as in Figure (D6), as show in Figure (D7) and obtained the form:

$$M` = \dot{\varepsilon}_s \, t_f^{\,m} \qquad \ldots\ldots\ldots\ldots\ldots\ldots (D.13^*)$$

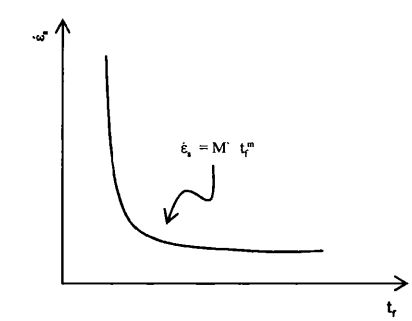

Figure (D7): The relationship between $\dot{\varepsilon}_s$ and t_f.

In this equation, the time to fracture is raised to the power m, in contrast to equation (D.12*) wherein the strain rate is raised to the power constant. Moreover, the value of m and M` in this equation are different to those in equation (D.12*).

- The power law equation (D.1*) and Monkman-Grant equation (D.12*):

In this case:

$$M`/ t_f = \dot{\varepsilon}_s^{\,m} \qquad \text{..... (D.14*)}$$

but from the power law equation, we know that: $\dot{\varepsilon}_s = A\,\sigma^n \exp(-Qc/RT)$. Therefore:

$$M`/ t_f = [A\,\sigma^n \exp(-Qc/RT)]^m \qquad \text{..... (D.15*)}$$

simplifying and re-arranging equation (D.15*) gives:

$$t_f = (M`/A^m)\,\sigma^{-m\,n} \exp(mQc/RT) \qquad \text{..... (D.16*)}$$

From equation (D.16*), plotting ln t_f against 1/T, at constant stress, gives a straight line of slope equals to mQc/R, as shown in Figure (D18).

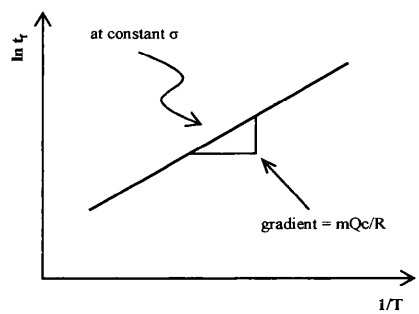

Figure (D8): The linear relationship between ln t_f and 1/T.

Alternatively, plotting ln t_f against ln σ, at constant temperature, gives a straight line of a slope equals to - m n, as shown in Figure (D9).

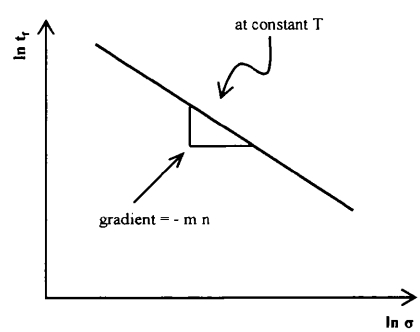

Figure (D9): The linear relationship between ln t_f and ln σ.

- The power law equation (D.1*) and Monkman-Grant equation (D.13*):

In this case:

$$M`/ t_f^{\,m} = \dot{\varepsilon}_s \qquad \text{..... (D.17*)}$$

but from the power law equation, we know that: $\dot{\varepsilon}_s = A\,\sigma^n \exp(-Qc/RT)$. Therefore:

$$M`/ t_f^{m} = A \sigma^{n} \exp(-Qc/RT) \quad \ldots\ldots\ldots\ldots (D.18^{*})$$

simplifying and re-arranging equation (D.18*) gives:

$$t_f = (M`/A)^{1/m} \sigma^{-n/m} \exp(Qc/mRT) \quad \ldots\ldots\ldots\ldots (D.19^{*})$$

From equation (D.19*), plotting ln t_f against 1/T, at constant stress, gives a straight line of slope equals to Qc/mR, as shown in Figure (D10).

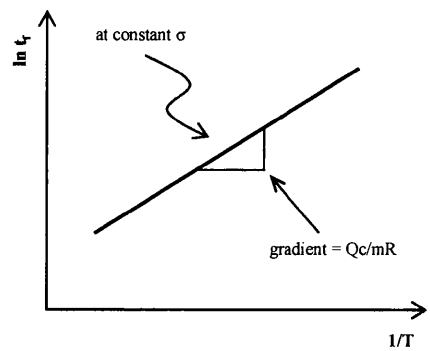

Figure (D10): The linear relationship between ln t_f and 1/T.

Alternatively, plotting ln t_f against ln σ, at constant temperature, gives a straight line of a slope equals to - n/m, as shown in Figure (D11).

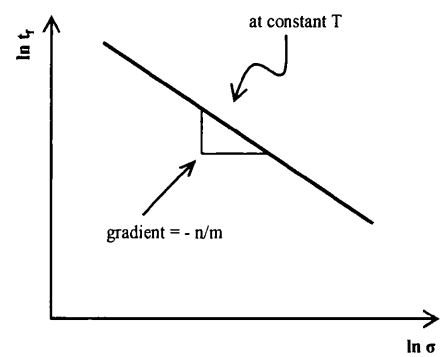

Figure (D11): The linear relationship between ln t_f and ln σ.

D.3 The Larson-Miller Equation

The general form of Larson-Miller equation is:

$$P_{LM} = T (C + \log t) \quad \ldots\ldots\ldots\ldots (D.20^{*})$$

This equation can be re-written in a linear form (y = mx + c), such that:

$$\log t = P_{LM} (1/T) - C \quad \ldots\ldots\ldots\ldots (D.21^{*})$$

Plotting (log t) against (1/T), at constant stresses, gives straight lines of a slope equals to P_{LM} and an intercept point with the y-axis equals to - C, as shown in Figure (D12).

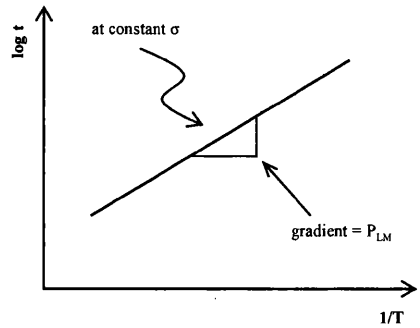

Figure (D12): The linear relationship between log t and 1/T, at constant stress, based on equation (D.21*).

The average value of C for Titanium IMI834 was around 20. Using this value, the stress was then plotted against equation (D.20*), i.e. against T (20 + log t), which superimposed all the data points onto a single curve, as shown in Figure (D13).

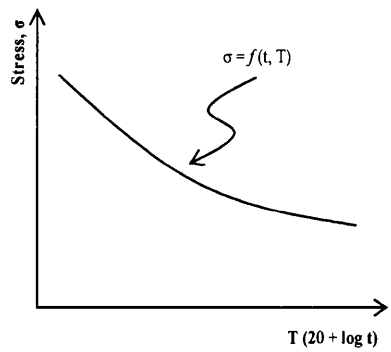

Figure (D13): Finding the relationship between stress, σ, and time, t.

The stress rupture curves (σ against t) were then obtained, at each temperature, by substituting random values of time (from 0 to, say, $1*10^{11}$ seconds). The actual creep data were then projected on those curves in order to evaluate the predictive curves capability of fitting those data.

D.4 The Manson-Haferd Equation

The general equation of Manson and Haferd is:

$$P_{MH} = (\log t - \log t_a) / (T_a - T) \quad \ldots\ldots\ldots\ldots\ldots\ldots (D.22^*)$$

This equation can be re-written in the linear form (y = mx + c), as:

$$\log t = - P_{MH}\, T + \{P_{MH}\, T_a + \log t_a\} \quad \ldots\ldots\ldots\ldots\ldots\ldots (D.23^*)$$

Plotting (log t) against (T), at constant stresses, gives a linear line with a slope of $(-P_{MH})$ and an intercept value of $(P_{MH}\, T_a + \log t_a)$, as shown in Figure (D14), where $\log t_a$ and T_a are the intercept points with the y and x axes, respectively.

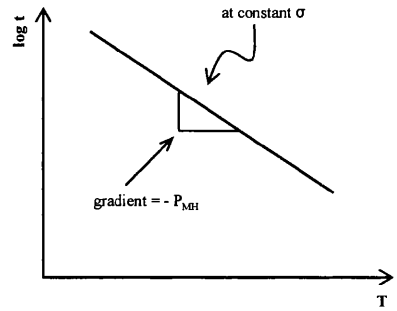

Figure (D14): The linear relationship between log t and T, at constant stress, based on equation (D.23*).

Hence, obtaining the average value of P_{MH} will help finding the value of the constant t_a and T_a. This can be done in two successive steps: firstly, the value of t_a can be calculated from Figure (D14) by substituting T_a = 0 and finding the corresponding value of log t_a and, secondly, substituting log t_a = 0 and finding the corresponding value of T_a, as shown in Figure (D15).

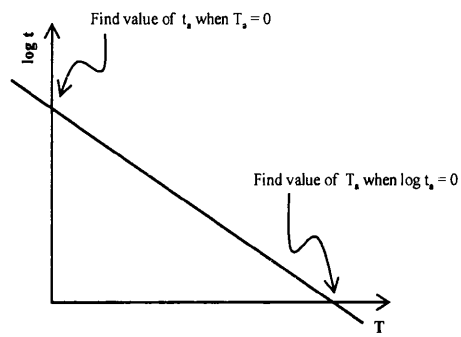

Figure (D15): Finding the value of t_a and Ta, at constant stress.

For Titanium IMI834, the calculated values of the constants were: P_{MH} = 0.025, T_a = 1061 and log t_a = 29.713. Substituting the values of t_a and T_a into equation (D22*) gives:

$$P_{MH} = (\log t - 29.713) / (1061 - T) \quad \ldots\ldots\ldots\ldots\ldots\ldots \quad (D.24^*)$$

A relationship between the stress and the time can be obtained, at each temperature, by plotting the stress, σ, against equation (D.24*), i.e. against (log t - 29.713) / (1061 - T), as shown in Figure (D16).

At this stage, the stress rupture curves (σ against t) were obtained, at each temperature, by substituting random values of time (from 0 to, say, $1*10^{11}$ seconds). The actual creep data were then projected on those curves in order to assess the accuracy of the fitting curves.

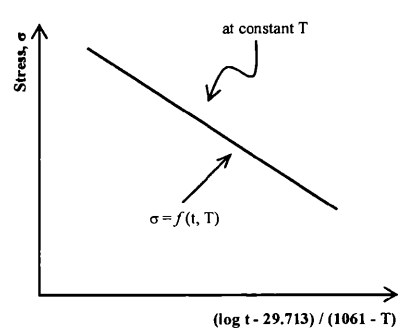

Figure (D16): Finding the relationship between stress, σ, and time, t, at each temperature, T.

D.5 The Orr-Sherby-Dorn Equation

The general form of Orr-Sherby-Dorn equation is:

$$P_{OSD} = C/T - \log t \quad \text{..... (D.25*)}$$

This equation can be re-arranged to give the linear form (y = mx + c), as:

$$\log t = C\,(1/T) - P_{OSD} \quad \text{..... (D.26*)}$$

Plotting (log t) against (1/T), at constant stresses, gives straight linear lines of a slope equals to C and an intercept with the y-axis equals to - P_{OSD}, as shown in Figure (D17).

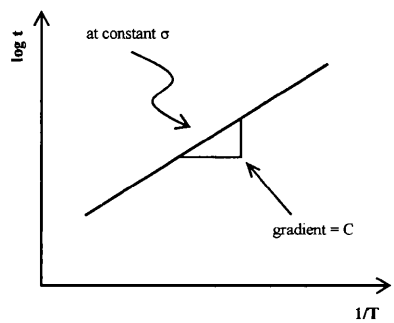

Figure (D17): The linear relationship between log t and 1/T, at constant stress, based on equation

The value of the constant C that was obtained from the analysis of Titanium IMI834 data was around 18,427 based on Figure (D17) analysis. The stress was then plotted against equation (D.25*), i.e. against (C/T - log t), by substituting 18,427 instead of C, which forced the data to be superimposed onto a single curve. However, changing the value of C gave a better fit of the data where it was observed that the best fit was achieved when the value of C was 20,000, as shown in Figure (D18).

The stress rupture curves (σ against t) were obtained, at each temperature, by substituting values of time (between 0 and, say, $1*10^{11}$ seconds). The actual creep data were then projected on those curves so as to assess the accuracy of the predictive curves.

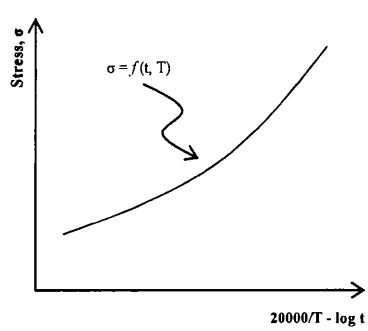

Figure (D18): Finding the relationship between stress, σ, and time, t.

D.6 The Manson-Succop Equation

The general form of Manson and Succop equation is:

$$P_{MS} = \log t + C_{MS}\, T \qquad \ldots\ldots\ldots\ldots\ldots\ldots (D.27^{*})$$

This equation can be re-arranged in a linear form (y = mx + c), such that:

$$\log t = - C_{MS}\, T + P_{MS} \qquad \ldots\ldots\ldots\ldots\ldots\ldots (D.28^{*})$$

Plotting (log t) against (T), at constant stresses, gives straight lines of a slope equals to - C_{MS} and an intercept with the y-axis equals to P_{MS}, as shown in Figure (D19).

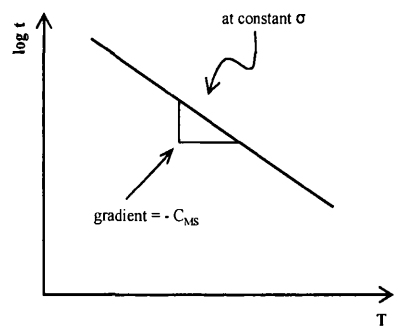

Figure (D19): The linear relationship between log t and T, at constant stress.

The average value of C_{MS} for Titanium IMI834 was around 0.025. Using this value, the stress was then plotted against equation (D.27*), i.e. against (log t + 0.025 T) which superimposed all the data points onto a single curve, as shown in Figure (D14).

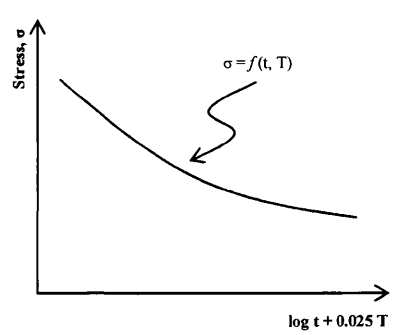

Figure (D20): Finding the relationship between stress, σ, and time, t.

The stress rupture curves (σ against t) were then obtained, at each temperature, by substituting values of time (from 0 to, say, $1*10^{11}$ seconds). The actual creep data were then projected on those curves in order to compare the predictive capability of those curves with the actual data.

D.7 The Hyperbolic -Tangent Equation

The general form of the Hyperbolic-Tangent equation is:

$$\sigma = (\sigma_{TS}/2)\,(1 - \tanh\,(k \ln\,(t/t_i))) \qquad \ldots\ldots\ldots\ldots\ldots\ldots\ (D.29^*)$$

This equation can be re-arranged in a linear form (y = mx + c), such that:

$$\tanh^{-1}\,(1 - 2\,(\sigma/\sigma_{Ts})) = k \ln t - k \ln t_i \qquad \ldots\ldots\ldots\ldots\ldots\ldots\ (D.30^*)$$

Plotting $\{\tanh^{-1}\,(1 - 2\,(\sigma/\sigma_{Ts}))\}$ against (ln t), at constant temperatures (and thus constant σ_{TS}), gives a straight line of slope k and an intercept of (k ln t_i), as shown in Figure (D21).

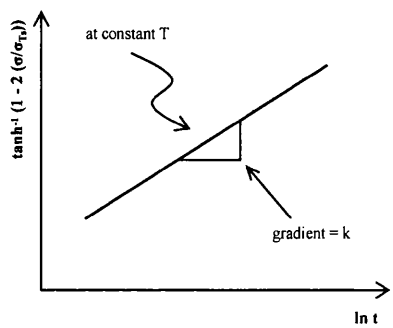

Figure (D21): The linear relationship between $\tanh^{-1}\,(1 - 2\,(\sigma/\sigma_{Ts}))$ and ln t, at constant temperatures.

From these linear plots, the value of the constant k and t_i can be calculated at each temperature. Substituting the values of these constants into equation (D.29*) gives a direct relationship between the stress, σ, and time, t, from which the stress rupture curves can be constructed.

D.8 The Goldhoff-Sherby Equation

The general equation of Goldhoff and Sherby is:

$$P_{GS} = (\log t - \log t_a) / (\,1/T - 1/T_a\,) \qquad \ldots\ldots\ldots\ldots\ldots\ldots\ (D.31^*)$$

This equation can be re-written in the linear form (y = mx + c), as:

$$\log t = P_{GS}\ 1/T + \{\ \log t_a - P_{MH}\ 1/T_a\ \} \qquad \ldots\ldots\ldots\ldots\ldots\ldots\ (D.32^*)$$

Plotting (log t) against (1/T), at constant stresses, gives a linear line with a slope of (P_{GS}) and an intercept value of (log t_a - P_{MH} $1/T_a$), as shown in Figure (D22), where log t_a and $1/T_a$ are the intercept points with the y and x axes, respectively.

Hence, obtaining the average value of P_{GS} will help finding the value of the constant log t_a and $1/T_a$. This can be done in two successive steps: firstly, the value of log t_a can be calculated from Figure (D22) by substituting $1/T_a = 0$ and finding the corresponding value of log t_a and, secondly, substituting log $t_a = 0$ and finding the corresponding value of $1/T_a$, as shown in Figure (D23).

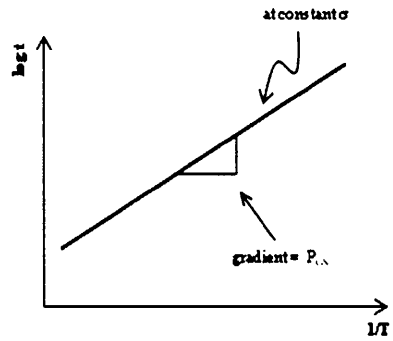

Figure (D22): The linear relationship between log t and T, at constant stress, based on equation (D.32*).

For Titanium IMI834, the calculated values of the constants were: $1/T_a = 0.0008$ and $\log t_a = 15.824$. Substituting the values of t_a and T_a into equation (D.31*) gives:

$$P_{GS} = (\log t - 15.824) / (1/T - 0.0008) \quad \ldots\ldots\ldots\ldots\ldots\ldots \quad (D.33^*)$$

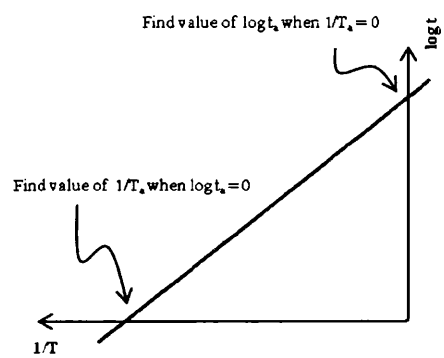

Figure (D23): Finding the value of log t_a and 1/Ta, at constant stress.

A relationship between the stress and the time can be obtained, at each temperature, by plotting the stress, σ, against equation (D.33*), i.e. against (log t – 15.824) / (1/T – 0.0008), as shown in Figure (D24).

At this stage, the stress rupture curves (σ against t) were obtained, at each temperature, by substituting random values of time (from 0 to, say, $1*10^{11}$ seconds). The actual creep data were then projected on those curves in order to assess the accuracy of the fitting curves.

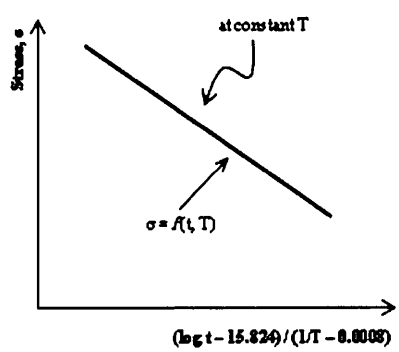

Figure (D24): Finding the relationship between stress, σ, and time, t, at each temperature, T.

D.9 The θ-Projection Equations

The general equation of this technique is the (4-θ equation) of the form:

$$\varepsilon = \theta_1[1\text{-}\exp(-\theta_2 t)] - \theta_3[1\text{-}\exp(\theta_4 t)] \quad \ldots\ldots\ldots\ldots (D.34^*)$$

where the first right hand side of this equation describes the primary creep whereas the second half is a description of the tertiary stage, as show in Figure (D25).

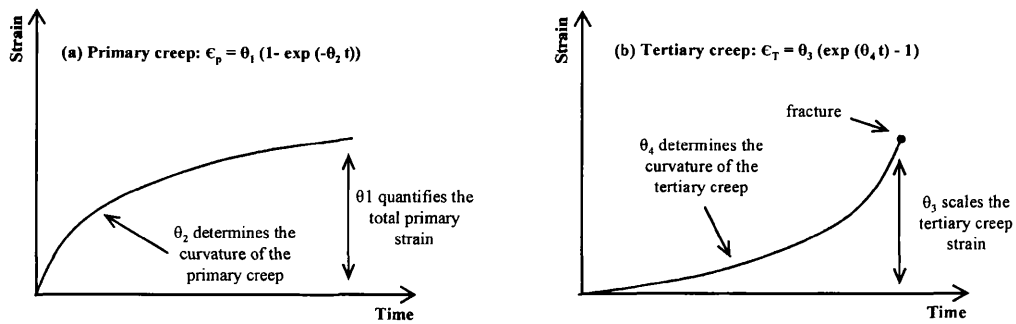

Figure (D25): The description of the: (a) primary creep, and (b) the tertiary creep, using the θ-method.

Differentiating equation (D.34*) provides the creep rate equation as:

$$d\varepsilon/dt = \dot{\varepsilon} = \theta_1 \theta_2 \exp(-\theta_2 t) + \theta_3 \theta_4 \exp(\theta_4 t) \quad \ldots\ldots\ldots\ldots (D.35^*)$$

At any point along the creep curve, equation (D.35*) provides a mean to measure the creep rate value, as shown in Figure (D26).

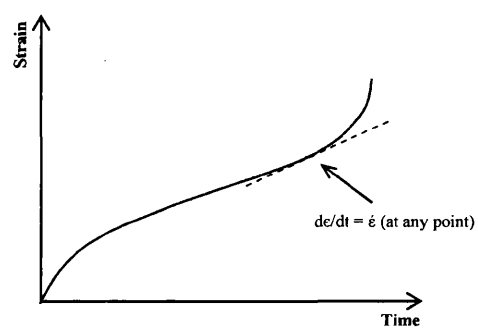

Figure (D26): Calculating the creep rate value at any point along the creep curve using equation (A.32*).

To find the minimum creep rate point, a plot of ($\dot{\varepsilon}$) against (t) provides the easiest way to read the point at which the minimum creep rate takes place, as shown in Figure (D27).

Differentiating equation (D.35*) gives:

$$d\dot{\varepsilon}/dt = -\theta_1 \theta_2^{\,2} \exp(-\theta_2 t) + \theta_3 \theta_4^{\,2} \exp(\theta_4 t) \quad \ldots\ldots\ldots\ldots (D.36^*)$$

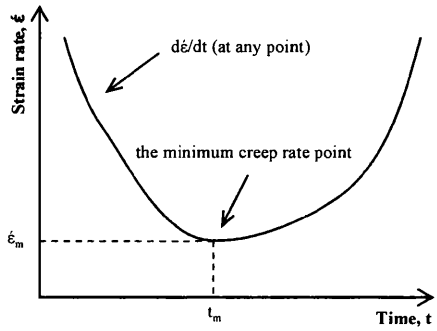

Figure (D27): Determining the minimum creep rate point.

From this equation, the minimum creep point (t_m, $\dot{\varepsilon}_m$) occurs when $d\dot{\varepsilon}/dt = 0$, which means, at $t = t_m$:

$$d\dot{\varepsilon}/dt = - \theta_1 \theta_2^{\,2} \exp(-\theta_2 t_m) + \theta_3 \theta_4^{\,2} \exp(\theta_4 t_m) = 0$$

$$\rightarrow \quad \theta_1 \theta_2^{\,2} / \exp(\theta_2 t_m) = \theta_3 \theta_4^{\,2} \exp(\theta_4 t_m)$$

$$\rightarrow \quad \theta_1 \theta_2^{\,2} / \theta_3 \theta_4^{\,2} = \exp(\theta_2 t_m) \exp(\theta_4 t_m) = \exp(\theta_2 + \theta_4)\, t_m$$

taking the natural logarithm for both sides gives:

$$\ln(\theta_1 \theta_2^{\,2} / \theta_3 \theta_4^{\,2}) = (\theta_2 + \theta_4)\, t_m$$

which gives the time at which the minimum creep rate point takes place, as:

$$t_m = (1/(\theta_2 + \theta_4)) \ln(\theta_1 \theta_2^{\,2} / \theta_3 \theta_4^{\,2}) \qquad \ldots\ldots\ldots\ldots (D.37^*)$$

At t_m, calculate ϵ_m from equation (D.34*) when $t = t_m$

At t_m, calculate $\dot{\varepsilon}_m$ from equation (D.35*) when $t = t_m$

- **<u>Calculating the primary creep (ϵ_p) and the tertiary creep (ϵ_T)</u>:**

The general creep curve can be plotted as in Figure (D28). From this figure, the primary creep can be calculated according to:

$$\epsilon_p = \epsilon_m - \dot{\varepsilon}_m t_m \qquad \ldots\ldots\ldots\ldots (D.38^*)$$

where ϵ_m and $\dot{\varepsilon}_m$ can be calculated from equation (D.34*) and (D.35*) at $t = t_m$, respectively, and t_m can be calculated from equation (D.37*).

The tertiary creep can be calculated, from the same figure, according to:

$$\epsilon_T = \epsilon_f - \epsilon_p \qquad \ldots\ldots\ldots\ldots (D.39^*)$$

where ϵ_p is calculated from equation (D.38*) and ϵ_f is either obtained from the actual creep curves at fracture (i.e. at $t = t_f$) or it can be calculated, from equation (D.34*), at $t = t_f$ (NB. in both cases, t_f is obtained directly from the actual creep curves at fracture).

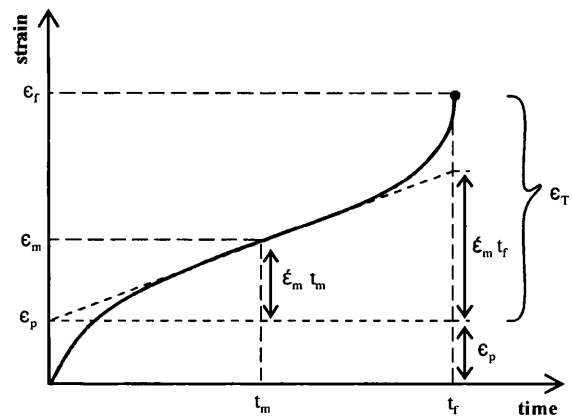

Figure (D28): The general creep curve showing the necessary strain values and the corresponding time values.

The modified form of the 4-θ method is the 6-θ of the form:

$$\varepsilon = \theta_1[1-\exp(-\theta_2 t)] - \theta_3[1-\exp(\theta_4 t)] + \theta_5[1-\exp(-\theta_6 t)] \quad \ldots\ldots\ldots\ldots (D.40^*)$$

In this equation, the first two hand right terms have the same physical meaning of equation (D.34*) whereas the third term was added to improve the fit of the primary creep. The same sequence starting from equation (D.34*) up to equation (D.39*) can be applied to equation (D.40*) in order to get the full description of the creep behaviour.

D.10 The Wilshire Equations

The general form of this equation is:

$$\sigma/\sigma_{TS} = \exp(-k_1 [t_f \exp(-Qc^*/RT)]^u) \quad \ldots\ldots\ldots\ldots (D.41^*)$$

this equation can be written in a linear form ($y = mx + c$) by taking the double-natural logarithm of both sides, such that:

$$\ln(-\ln \sigma/\sigma_{TS}) = u \ln(t_f \exp(-Qc^*/RT)) + \ln k_1 \quad \ldots\ldots\ldots\ldots (D.42^*)$$

- **The value of Qc^*:**

The value of Qc^* can be obtained by plotting ($\ln t_f$) against ($1/T$) at constant σ/σ_{TS}, unlike Qc that was obtained at constant σ, based on:

$$t_f = D^* (\sigma/\sigma_{TS})^{-n} \exp(Qc^*/RT) \quad \ldots\ldots\ldots\ldots (D.43^*)$$

this will give a straight line of slope (Qc^*/R) from which Qc^* can be calculated, as shown in Figure (D29).

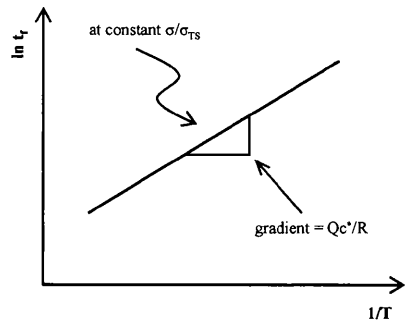

Figure (D29): The linear relationship between ln t_f and 1/T.

- **The value of k_1 and u:**

From the linearity of equation (D.42*), the value of k_1 and u can be obtained by plotting ln (-ln σ/σ_{TS}) against ln (t_f exp (-Qc*/RT)), as shown in Figure (D30).

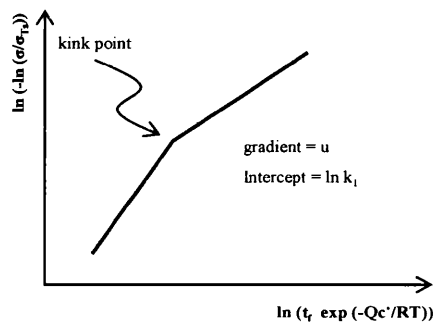

Figure (D30): The relationship between ln (-ln σ/σ_{TS}) and ln (t_f exp (-Qc*/RT)).

The slope of these plots represents the value of u whereas the intercept with the y-axis is the value of ln k_1. However, it was observed that there was always a 'kink' point in these plots which separated the data into two linear regimes, namely: the high and the low stress regimes. Based on this fact, different values of u and k_1 were obtained for these two regimes.

Accordingly, having obtained the value of Qc*, k_1 and u for the high and the low stress regimes, the stress rupture curves (stress versus the time) can be constructed from the direct relationship between the stress and the time in equation (D.41*).

The other Wilshire equation is of the form:

$$\sigma/\sigma_{TS} = \exp(-k_2 [\dot{\varepsilon}_m \exp(Qc^*/RT)]^v) \quad \ldots\ldots\ldots\ldots (D.44^*)$$

this equation can be written in a linear form (y = mx + c) by taking the double-natural logarithm of both sides, such that:

$$\ln(-\ln \sigma/\sigma_{TS}) = v \ln(\dot{\varepsilon}_m \exp(Qc^*/RT)) + \ln k_2 \quad \ldots\ldots\ldots\ldots (D.45^*)$$

- **The value of Qc^*:**

The value of Qc^* can be obtained by plotting ($\ln \dot{\varepsilon}_m$) against (1/T) at constant σ/σ_{TS}, unlike Qc that was obtained at constant σ, based on:

$$\dot{\varepsilon}_m = A^* (\sigma/\sigma_{TS})^n \exp(-Qc^*/RT) \quad \ldots\ldots\ldots\ldots\ldots\ldots (D.46^*)$$

this will give a straight line of slope ($-Qc^*/R$) from which Qc^* can be calculated, as shown in Figure (D31).

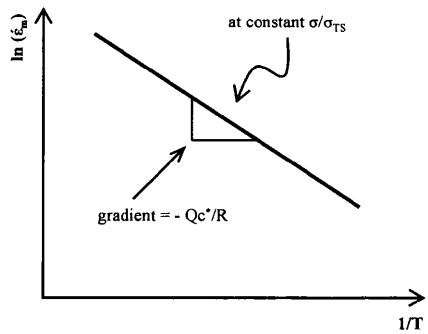

Figure (D31): The linear relationship between $\ln \dot{\varepsilon}_m$ and 1/T.

- **The value of k_2 and v:**

From the linearity of equation ($D.45^*$), the value of k_2 and v can be obtained by plotting $\ln(-\ln \sigma/\sigma_{TS})$ against $\ln(\dot{\varepsilon}_m \exp(Qc^*/RT))$, as shown in Figure (D32).

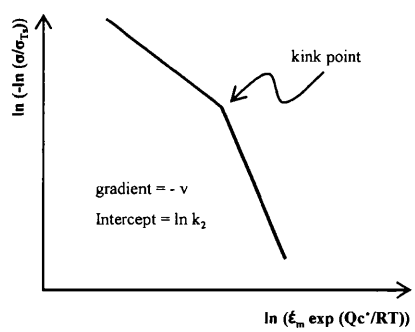

Figure (D32): The relationship between $\ln(-\ln \sigma/\sigma_{TS})$ and $\ln(\dot{\varepsilon}_m \exp(Qc^*/RT))$.

The slope of these plots represents the value of -v whereas the intercept with the y-axis is the value of $\ln k_2$. However, it was observed that there was always a 'kink' point in these plots which separated the data into two linear regimes, namely: the high and the low stress regimes. Based on this fact, different values of v and k_2 were obtained for these two regimes. Accordingly, having obtained the value of Qc^*, k_2 and v for the high and the low stress regimes, the stress rupture curves (stress versus the minimum creep rate) can be constructed from the direct relationship between the stress and the minimum creep rate in equation ($D.41^*$).

The last Wilshire equation is of the form:

$$\sigma/\sigma_{TS} = \exp(-k_3 [t_\epsilon \exp(-Qc^*/RT)]^w) \quad \ldots\ldots\ldots\ldots (D.47^*)$$

This equation can be considered as a special case of equation (D.41*) just by replacing the time to fracture, t_f, by the time required to reach a certain strain, t_ϵ. This equation can be written in a linear form ($y = mx + c$) by taking the double-natural logarithm of both sides, such that:

$$\ln(-\ln \sigma/\sigma_{TS}) = w \ln(t_\epsilon \exp(-Qc^*/RT)) + \ln k_3 \quad \ldots\ldots\ldots\ldots (D.48^*)$$

- **The value of Qc^*:**

The value of Qc^* can be obtained by either plotting ($\ln t_f$) or ($\ln \dot{\varepsilon}_m$) against ($1/T$) at constant σ/σ_{TS}, as discussed earlier in Figure (D29) and (D31), respectively.

- **The value of k_3 and w:**

From the linearity of equation (D.48*), the value of k_3 and w can be obtained by plotting $\ln(-\ln \sigma/\sigma_{TS})$ against $\ln(t_\epsilon \exp(-Qc^*/RT))$, as shown in Figure (D33).

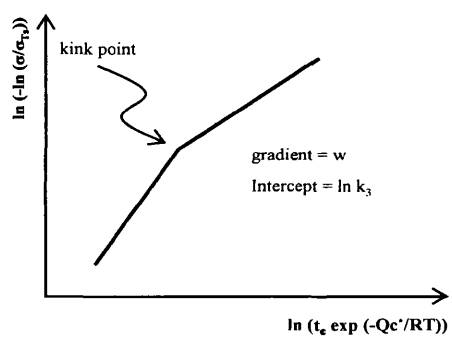

Figure (D33): The relationship between $\ln(-\ln \sigma/\sigma_{TS})$ and $\ln(t_\epsilon \exp(-Qc^*/RT))$.

The slope of these plots represents the value of w whereas the intercept with the y-axis is the value of $\ln k_3$. However, it was observed that there was always a 'kink' point in these plots which separated the data into two linear regimes, namely: the high and the low stress regimes. Based on this fact, different values of w and k_3 were obtained for these two regimes.

Accordingly, having obtained the value of Qc^*, k_3 and w for the high and the low stress regimes, the stress rupture curves (stress versus the time), for a certain strain level, can be constructed from the direct relationship between the stress and the time in equation (D.47*).

The advantage of equation (D.47*) can be summarized in that at any strain level, the time required to reach that strain level can be read directly from the creep curves at multiple stresses and temperatures and thus, the stress rupture curves can be constructed based on these readings. Similarly, equation (D.41*) presents a way

to define the end point of a creep curve. In other words, the time to fracture can be read from the creep curves at multiple stresses and temperatures alongside the corresponding strain at fracture. These values can then be entered into this equation and the stress rupture curves can be constructed accordingly. Another way of constructing the long-term predictive curves can be based on equation (D.44*) wherein the minimum creep rates are required to start the analysis. Once these values are obtained and entered into this equation, the stress versus the minimum creep rate curves can be constructed at any stress and temperature.

In conclusion, equation (D.41*) defines the end point of a creep curve whereas equation (D.47*) defines any point along the creep curve and equation (D.44*) defines the point where the minimum creep rate takes place during creep.